UNCLASSIFIED

AD NUMBER

AD478715

NEW LIMITATION CHANGE

TO

Approved for public release, distribution unlimited

FROM

Distribution authorized to U.S. Gov't. agencies and their contractors; Administrative/Operational Use; DEC 1965. Other requests shall be referred to Air Force Materials Laboratory, Attn: RTD, Wright-Patterson AFB, OH 45433.

AUTHORITY

AFML ltr 7 Dec 1972

THIS PAGE IS UNCLASSIFIED

TI AFML TR-65-418 110179

DO NOT DESTROY
RETURN TO
TECHNICAL INFORMATION LIBRARY
SEPIR

COMPOSITE CERAMIC RADOME MANUFACTURE BY MOSAIC TECHNIQUES

TECHNICAL REPORT AFML TR-65-418

December 1965

Chemical Processing Branch
Manufacturing Technology Division
Air Force Materials Laboratory
Research and Technology Division
Air Force Systems Command
Wright-Patterson Air Force Base, Ohio

MMP Project No. 7-984

This document is subject to special export controls and each transmittal to foreign governments or to foreign nationals may be made only with prior approval of the Manufacturing Technology Division

(Prepared under Contract AF 33(657)-10111 by Whittaker Corporation, Narmco Research & Development Division, San Diego, California, Rodney A. Jones and Francis A. Barr)

20050809089

Best Available Copy

NOTICES

When US Government drawings, specifications, or other data are used for any purpose other than a definitely related Government procurement operation, the Government thereby incurs no responsibility nor any obligation whatsoever; and the fact that the Government may have formulated, furnished, or in any way supplied the said drawings, specifications, or other data, is not to be regarded by implication or otherwise, as in any manner licensing the holder or any other person or corporation, or conveying any rights or permission to manufacture, use, or sell any patented invention that may in any way be related thereto.

Qualified requesters may obtain copies from DDC, Document Service Center, Camerson Station, Alexandria Virginia 22314. Orders will be expedited if placed through the librarian or other designated persons to request documents from DDC.

Do not return this copy unless return is required by security considerations, contractual obligations, or notice on a specific document.

Reproduction in whole or in part is prohibited except with the permission of the Manufacturing Technology Division. However, DDC is authorized to reproduce the document for "US Government Purposes."

DDC release to CFSTI is NOT authorized.

AFML TR-65-418

COMPOSITE CERAMIC RADOME MANUFACTURE BY MOSAIC TECHNIQUES

Rodney A. Jones
Francis A. Barr

This document is subject to special export controls and each transmittal to foreign governments or to foreign nationals may be made only with prior approval of the Manufacturing Technology Division

FOREWORD

This report covers work conducted by Narmco Research & Development Division, Whittaker Corporation, San Diego, California, under Contract AF 33(657)10111, and modifications thereto, from 1 November 1962 to 5 January 1966. A break occurred in this contract period between 31 October 1963 and 29 January 1964 due to supplemental contract negotiations. The manuscript was released in November 1965 by the authors as an RTD Technical Report.

This contract was initiated under Manufacturing Methods Project No. 7-984, "Composite Ceramic Radome Manufacture by Mosaic Techniques." Before 1 May 1964, it was accomplished under the technical direction of Dorsie C. Harleman, Chemical Engineering Branch, ASRCT, Manufacturing Technology Laboratory, Aeronautical Systems Division, Wright-Patterson Air Force Base, Ohio; after that date, work was accomplished under the technical direction of 1/Lt. Leigh E. Stamets, Chemical Processing Branch, MATC, Manufacturing Technology Division, Air Force Materials Laboratory, Wright-Patterson Air Force Base, Ohio.

The project was given Narmco internal control number MJO 338. Mr. Frank J. Filippi was Project Manager to 1 August 1964. Subsequently, it was accomplished under the supervision of Mr. Roger A. Long, Manager, Refractories Research Department, with Mr. Rodney A. Jones as Project Manager and Mr. Filippi as Engineering Consultant. Mr. Francis A. Barr, Chief, Ceramics Research, supervised the technical efforts and was a major contributor to the report preparation. Others who participated were Messrs. N. O. Brink, Project Engineer; D. W. Chamberlain, Supervisor, Engineering Test; K. Feher, Research Engineer; S. Feher, Research Engineer; W. H. Gottwald, Senior Test Engineer; V. Grinius, Research Engineer; J. Haener, PhD, Research Specialist; G. Mihelsic, Senior Design Engineer; D. S. Pratt, Senior Research Ceramist; J. Robinson, Senior Design Engineer; and J. D. Stillman, Research Ceramist. Messrs. P. G. Loefke, Senior Research Technician, and L. D. Tripp, Research Technician, also provided valuable assistance in tooling and fabrication.

This project has been accomplished as a part of the Air Force Manufacturing Methods Program, the primary objectives of which are to develop, on a timely basis, manufacturing processes, techniques, and equipment for use in the economical production of USAF materials and components. This overall program encompasses the following technical areas:

Metallurgy - Rolling, Forging, Extruding, Casting, Fiber, Powder

Chemical - Propellant, Coating, Ceramics, Graphite, Nonmetallics

Electronic - Solid State, Materials & Special Techniques, Thermionics

Fabrication - Forming, Material Removal, Joining, Components

Suggestions concerning additional manufacturing methods development required on this or other subjects will be appreciated.

This technical report has been reviewed and is approved.

Melvin E. Fields

MELVIN E. FIELDS
Colonel, USAF
Chief, Manufacturing Technology Division

ABSTRACT

COMPOSITE CERAMIC RADOME MANUFACTURE BY MOSAIC TECHNIQUES

Rodney A. Jones
and
Francis A. Barr
WHITTAKER CORPORATION
Narmco Research & Development Division

A comprehensive research and development program directed toward the fabrication of large ceramic radomes for operation at 1000°F or above, by ceramic adhesive bonding together of preformed ceramic tile segments, is described.

On the basis of a state-of-the-art review plus extensive materials selection investigations, 99.0% high-density alumina was selected as the radome body material and a magnesium aluminosilicate glass forming composition with a fusion temperature of approximately 2150°F was selected as the ceramic adhesive. Engineering design and structural investigations plus manufacturing considerations led to the choice of a double layer of staggered, overlapping, trapezoidal tiles for the radome wall construction. The mosaic tile wall, 0.221 in. thick, was capped with a monolithic alumina nose cap to form the ogive radome of approximately 31-in. diameter at the base and 8-ft height.

The fabrication techniques involving use of a differential thermal expansion firing tool concept are described, with details as to the fused silica tooling, fabrication, and use. The mosaic full-size radome and radome sections were fabricated, and were subjected to thermal and structural testing. A correlation of these test results with previous detailed thermal and structural analyses is presented.

The program results are presented and show that fabrication of large, high-strength ceramic structures by adhesive bonding mosaic techniques is feasible and provides a means of circumventing some of the serious limitations of conventional ceramic fabrication procedures for large structures. The test results also show that the analytical and design techniques which were developed can be used with reasonable confidence in the design of such composite ceramic structures.

TABLE OF CONTENTS

Section		Page
I	INTRODUCTION	1
II	STATE-OF-THE-ART REVIEW AND ANALYSIS	2
	Wetting Characteristics	7
	Compressive Shear Tests	7
	Discussion of Findings	7
	Preliminary Surface Preparation and Bond Thickness Investigation	12
	Method of Adhesive Application	14
	Results	14
III	FABRICATION AND BONDING TECHNIQUES DEVELOPMENT	16
	Segment Materials	16
	Ceramic Adhesives	29
	Composite Ceramic Technique Development	52
	Emissive Coatings	78
IV	RADOME DESIGN AND ENGINEERING CONSIDERATIONS	93
	Mosaic Segment and Joint Design	96
	Mosaic Radome Thermal and Structural Analysis	113
	Analytical Comparisons with Test Results	126
V	TOOLING	131
	Tooling Concepts	131
	Selection of Tooling Materials	133
	Truncated Tooling	145
	Full-Scale Tooling	159
VI	CERAMIC KILN CONSTRUCTION	172
	Initial Kiln Size	172
	Kiln Modification	176

TABLE OF CONTENTS (Continued)

Section		Page
VII	PARTING AGENT	181
	Oxidizing Atmosphere	181
	Reducing Atmosphere	187
	Protective Atmosphere	187
VIII	RADOME REPAIR	191
	Segment Removal	191
	Candidate Repair Adhesives	193
	Screening Tests	196
	Results and Repair of Test Panels	198
IX	EXPERIMENTAL INVESTIGATIONS INTO FABRICATION TECHNIQUES	202
	Effects of Kiln Atmospheres on Bonded Alumina Segments	202
	Pre-Oxidation	204
	Preglazed Alumina Tiles	204
	Glass Transfer Tape	204
	Flat Mosaic Alumina Panels	206
	Alumina Spacers	211
X	TRUNCATED MOSAIC BASE SECTIONS	213
	Truncated Section No. 1	214
	Truncated Section No. 2	228
	Truncated Section No. 3	229
	Truncated Section No. 4	235
	Truncated Section No. 5 (Repair of Truncated Section No. 3)	235

TABLE OF CONTENTS (Continued)

Section		Page
XI	FULL-SCALE MOSAIC RADOME FABRICATION	240
	Fabrication Procedures	242
	Radome Firing	250
XII	QUALITY ASSURANCE; DIMENSIONAL AND PROPERTY DATA	257
	Alumina Components (General)	257
	Alumina Components (Strength Properties)	260
	Alumina Components (Electrical Properties)	261
	Firing Tooling Inspection Gage	261
	Dimensional Accuracy of Fabricated Radomes	268
XIII	ENGINEERING TEST PROGRAM AND RESULTS	269
	Thermal Gradient Tests	271
	Structural Tests and Evaluation	272
XIV	SUMMARY AND CONCLUSIONS	284
	Mosaic Ceramic Radome Fabrication	284
	Firing Tooling	285
	Ceramic Adhesive Development	286
	Alumina Tile Manufacture	286
	Mosaic Radome Analysis, Design, and Test Conditions	287
	Mosaic Radome Manufacturing Feasibility and Costs	287
	APPENDIX I. Literature Review	289
	APPENDIX II. Stresses in Adhesive Joints	307
	APPENDIX III. Determination of Rhombic Segment Geometry	324
	APPENDIX IV. Geometry and Size of Radome Tiles	333

TABLE OF CONTENTS (Continued)

		Page
APPENDIX V.	Calculative Approach to Radome Tiles	342
APPENDIX VI.	Structural Analysis of Radome Base Attachment	358
APPENDIX VII.	Radome Structural Analysis	372
APPENDIX VIII.	Radome Aerodynamic Heating Analysis	388
APPENDIX IX.	Mosaic Radome Tile Stress Analysis	412
APPENDIX X.	Mosaic Radome and Affiliated Drawings	458

LIST OF ILLUSTRATIONS

Figure		Page
1	Prepared Lap Joints for Compressive Shear Tests	8
2	Lap Shear Fixture Opened to Show Lap Specimen in Place	9
3	Lap Shear Fixture as Assembled during Testing	9
4	Sheared Lap Joints Showing Wettability and Adherence of Pycerad 300 on Beryllia and Pycerad 300-A on Alumina (left)	11
5	Wetting Tests on 97.4% Alumina (left) and Stabilized Zirconia Segments Using Narmco's Pycerad Adhesives	12
6	Ceramic Segment Bodies — Loss Tangent vs Temperature at 9.375 Gc	26
7	Ceramic Segment Bodies — Dielectric Constant vs Temperature at 9.375 Gc	27
8	Mean Coefficient of Thermal Expansion vs Temperature for S1 Alumina from Room Temperature (75°F)	30
9	Mean Coefficient of Thermal Expansion vs Temperature for S6 Alumina from Room Temperature (80°F)	31
10	Mean Coefficient of Thermal Expansion vs Temperature for S7 Alumina from Room Temperature (75°F)	32
11	Mean Coefficient of Thermal Expansion vs Temperature for S4 Beryllia from 120°F	33
12	Wetting Tests of Interpace High-Temperature Adhesive (top) and Pycerad 500 (bottom)	34
13	Photomicrograph of 97.6% Alumina Segments (light) Bonded with Interpace High-Temperature Adhesive	36
14	Adhesives — Loss Tangent vs Temperature at 9.375 Gc	41
15	Adhesives — Dielectric Constant vs Temperature at 9.375 Gc	42

LIST OF ILLUSTRATIONS (Continued)

Figure		Page
16	Dielectric Constant vs Temperature at 9.375 Gc for Composite Samples and S1 Alumina Segment	45
17	Loss Tangent vs Temperature at 9.375 Gc for Composite Samples and S1 Alumina Segment	46
18	Mean Coefficient of Thermal Expansion vs Temperature from Room Temperature (80°F) for Pycerad 500 Adhesive	48
19	Mean Coefficient of Thermal Expansion vs Temperature from Room Temperature (80°F) for Pyroceram 45 Case Adhesive	49
20	Mean Coefficient of Thermal Expansion vs Temperature from Room Temperature (84°F) for Interpace Cast Adhesive	50
21	Mean Coefficient of Thermal Expansion vs Temperature from Room Temperature (80°F) for Narmcad 110 and 120	51
22	Segment Pattern for Flat Mosaic Panels	53
23	Flat Panel Holding Tool and Sleeve	54
24	Flat Panel Firing Fixture	55
25	Top View of Shim Position with Respect to Alumina Segments and Mold	57
26	Firing Curves for Panel A	59
27	Flat Panel Fracture	61
28	Close-Up of Cracked Zone	61
29	Dimensions of Panel A	62
30	Photomicrograph of Typical Joint	64
31	Firing Curves for Panel B	66
32	Flat Panel Fracture	67
33	Radome Section Female Fixture	69
34	Ring Segment Pattern	70

LIST OF ILLUSTRATIONS (Continued)

Figure		Page
35	Layup of Outer Tile Layer	72
36	Final Closure Gap	72
37	Final Layup of Ring	73
38	Layup Showing Protective Cloth	73
39	Completed Tooling Assembly	74
40	Firing Curves for Ring Segment	76
41	Alumina Ring Segments	77
42	Emissivity Test Apparatus	85
43	Total Normal Emittance Specimen (E-318)	89
44	Total Normal Emittance Specimen (E-325)	90
45	Loss Tangent and Dielectric Constant vs Temperature at 9.375 Gc for S1 Alumina with Emissive Coatings	92
46	Prototype Radome	94
47	Flight Trajectory	95
48	Required Variation for Rhomboid	98
49	Trapezoidal Geometric Variation	99
50	Test Specimen	101
51	Test Specimen	102
52	Test Specimen	103
53	Test Specimen	104
54	Test Specimen	105
55	Test Specimen	105
56	Test Specimen	106
57	Test Specimen	106

LIST OF ILLUSTRATIONS (Continued)

Figure		Page
58	Test Specimen	107
59	Test Specimen	107
60	50% Utilization of Material Strength in Directions of x and y	108
61	100% Utilization of the Tile Strength in Two Perpendicular Directions	108
62	Arrangement of Tiles	109
63	Flat, Two-Layer Trapezoidal Tiles	112
64	Ogival, Two-Layer Trapezoidal Tiles	114
65	Thermal Stress Distribution in Typical Tile Cross Section at Unit ΔT_o	115
66	Stress Concentration Factors	118
67	Stress Concentration Factors	119
68	Stress Concentration Factors	120
69	Stress Concentration Factors	121
70	Stress Concentration Factors	122
71	Stress Concentration Factors	123
72	Stress Concentration Factors	124
73	Stress Concentration Factors	125
74	Base Attachment Design	127
75	Linear Thermal Expansion	128
76	Yield Strength vs Temperature	129
77	Base Attachment Fixture	130
78	Pressure Generation by Differential Expansion	132
79	Differential Expansion Application to Mosaic Radome	134
80	Fiberfrax Bulk Fiber	144

LIST OF ILLUSTRATIONS (Continued)

Figure		Page
81	Turntable and Template Frame	146
82	Template Coordinates — Layup Tool, Mosaic Radome	147
83	Template — Layup Tool, Mosaic Radome	148
84	Initial Plaster Coating on Truncated Layup Tool	150
85	Plaster Truncated Layup Tool	150
86	Template Coordinates — Firing Tool, Mosaic Radome	151
87	Casting Mold for Truncated Firing Tool Form	153
88	Glasrock Truncated Firing Tool Form	153
89	Cross Section of Backcasting Arrangement	154
90	Plaster Mandrel and Fused-Silica Model Form	155
91	Truncated Firing Tool Separated from Plaster Core	156
92	Truncated Firing Tool Inspection Data	157
93	Firing Fixture Assembly, Mosaic Radome	159
94	Handling Device (Drawing No. NR 63-153)	161
95	Full-Scale Layup Tool Arrangement	163
96	Layup Tool with Plaster Rough Coat	164
97	Full-Scale Layup Tool	164
98	Support Foundation for Full-Scale Firing Tool Model	165
99	Firing Tool Model inside Plaster Form	166
100	Glasrock Tool Form with Handling Fixture	167
101	Removal of Tool Form from Core	167

LIST OF ILLUSTRATIONS (Continued)

Figure		Page
102	Moving Tool to Kiln Area	168
103	Full-Scale Glasrock Firing Tool Form in Kiln	168
104	Cross Section of Backcasting Arrangement for Firing Tool	170
105	Inspection Data Summary — Mosaic Radome Full-Scale Firing Tool No. 1	171
106	Base under Construction Showing Burner Blocks	173
107	Corbel Arch	174
108	Completed Kiln (Initial Size)	175
109	Sealed Burner Port Pilot and System	176
110	Module Section prior to Lining with Refractory Castable	178
111	Inside of Module Section Showing Initial Refractory Lining and Anchor Blocks	178
112	Completed Kiln Module Lining	179
113	Kiln Module	179
114	Kiln Construction Stages (Kiln Base)	180
115	Kiln Construction Stages (Installing First Module Section)	180
116	Kiln Construction Stages (Extending Hinge Post)	180
117	Kiln Construction Stages (Completed Kiln)	180
118	Method of Introducing Argon Gas around Mosaic Panel	188
119	Typical Firing Curves for Flat Mosaic Alumina Panels Using Graphite Cloth Parting Agent and Argon Gas During Entire Cycle	190
120	Portion of Mosaic Panel Removed with Diamond Blade and Router Bit	193

LIST OF ILLUSTRATIONS (Continued)

Figure		Page
121	Flame Test	197
122	Typical Open Bondlines prior to Repair	201
123	Bondlines after Repair	201
124	Narmcad "Transfer Tape"	206
125	Mosaic Panel Fired under Reducing Conditions	207
126	Mosaic Panel Fired with Nitrogen Gas and Cooled under Oxidizing Conditions	210
127	Graphite Cloth after Firing in Nitrogen Atmosphere	212
128	Alumina Panel after Firing in Nitrogen Atmosphere	212
129	Alumina Spacers Attached to Alumina Tile	212
130	Truncated Mosaic Radome Base Sections	214
131	Initial Prefitting of Tiles onto Truncated Layup Tool	215
132	Edge Coating Alumina Tiles with Narmcad Adhesives	216
133	Measuring Coating Thickness	217
134	Spray Coating Alumina Tiles	217
135	Adhesive-Coated Tiles for First Section	219
136	Final Layup of First Truncated Section	219
137	Graphite Cloth Sleeve Covering Layup Truncated Section	220
138	Handling Box	220
139	Withdrawal of Male Layup Tool	221
140	Truncated Section in Firing Tool	221
141	Cross Section of Truncated Section and Tooling Firing Arrangement	222

LIST OF ILLUSTRATIONS (Continued)

Figure		Page
142	Firing Curves for First Mosaic Truncated Section	224
143	Firing Tool and Part after Firing	226
144	Interior View of Truncated Section No. 1	226
145	Truncated Section, Firing Too, and Fiber Packing with Cover Lid	227
146	Cross Section of Modified Truncated Section and Firing Tooling Arrangement	230
147	Firing Curves for Truncated Radome Section No. 2	231
148	Truncated Firing Tool Arrangement in Kiln	233
149	Truncated Section No. 3, Showing Misaligned Attachment Tiles	233
150	Close-Up of Slipped Attachment Tile in Truncated Section No. 3	234
151	Firing Curves for Truncated Section No. 5	237
152	Truncated Radome Sections	238
153	Mosaic Radome in Final Layup Stage	247
154	Mosaic Radome, Covered with Graphite Cloth and Fiberfrax Paper, and the Firing Tooling	247
155	Mating of Firing Tool with Mosaic Radome	248
156	Position of Stainless Steel Expansion Ring with Respect to Attachment Tiles	249
157	Cross Section of Mosaic Radome and Firing Tool Arrangement	249
158	Firing Tool and Radome prior to Firing	250
159	Firing Curves for Full-Scale Mosaic Radome	251
160	Radome and Tool Assemblage after Firing	252
161	Two Views of Mosaic Radome after Removal from Kiln	253
162	Full-Scale Mosaic Radome	253

LIST OF ILLUSTRATIONS (Continued)

Figure		Page
163	Lack of Joint Closure between Nose Cap and Tiles	254
164	View of Mosaic Radome Near Nose Cap	255
165	Tile Dimensional Inspection Gages	260
166	Check Gage, Truncated Mosaic Radome Firing Tool	264
167	Check Gage, Mounting Ring and Movable Indicator Arm	265
168	Detail Check Gage Indicator Arm	265
169	Check Gage, Calibrating Head	266
170	Thermal Shock Test Setup of Truncated Mosaic Radome Section	270
171	Thermoshocked Truncated Test Specimen	272
172	Truncated Section Test Setup	275
173	Failed Truncated Radome Section	276
174	Failed Truncated Section	276
175	Photoelastic Color Pattern on Stressed Radome	279
176	Full-Scale Radome Test Setup	280
177	Full-Scale Radome after Test	281
178	Full-Scale Radome — Failure Detail	281

LIST OF TABLES

Table		Page
1	Ceramic Segment Materials Data	6
2	Shear Strength Values of Candidate Adhesives on Respective Segments	10
3	Preliminary Surface Preparation vs Shear Strength	13
4	Bondline Thickness vs Shear Strength	15
5	Segment Material Candidates	17
6	Segments Screening	18
7	Flexural Strength of Ceramic Segment Bodies	19
8	Compressive Strength of Ceramic Segment Bodies	21
9	Tensile Strength of Ceramic Segment Bodies	22
10	Ceramic Segment Bodies — Dielectric Constant Data	24
11	Ceramic Segment Bodies — Loss Tangent Data	25
12	Dielectric Constant Increase with Temperature	28
13	Electromagnetic Property Comparisons	28
14	Dielectric Constant Data for Adhesive Specimens	39
15	Loss Tangent Data for Adhesive Specimens	40
16	Dielectric Constant for Composite Samples 97.6% Alumina Segments and Adhesives	43
17	Loss Tangent Data for Composite Samples 97.6% Alumina Segments and Adhesives	44
18	Dielectric Constant Increase with Temperature	47
19	Base Glaze Compositions	79
20	Emissive Coatings — Base Glaze 1	80
21	Emissive Coatings — Base Glaze 2	81

LIST OF TABLES (Continued)

Table		Page
22	Emissive Coatings — Base Glaze 3	82
23	Emissivity Test Results	86
24	Total Normal Emittance of Coatings	87
25	Electromagnetic Properties of Emissive Coatings	91
26	Increase in Dielectric Constant with Temperature	91
27	Castable Refractory Materials	136
28	Tooling Materials Evaluation	138
29	Quality Control Data for Glasrock Fused-Silica Castable (Type S-820)	142
30	Repair Adhesive Evaluations	199
31	Reducing Firing Conditions for Flat Mosaic Alumina Panels	208
32	Thermal Expansion Characteristics of Glasrock Tool Samples and Test Bars	240
33	Specification Summary for Alumina Tiles and Nose Caps	258
34	Modulus of Rupture Test Results	262
35	Thermal Shock Test Conditions	271
36	Maximum Stresses at Station 0 (Radome Base), psi	274

SECTION I

INTRODUCTION

The mission requirements and performance characteristics of advanced aerospace vehicles and weapon systems are continually demanding more refined and efficient detection and ranging equipment. The radomes or electromagnetic windows for containing such devices must, in turn, compromise the performance of the radar equipment as little as possible, while offering aerodynamic smoothness, structural integrity, and environmental protection. Only certain ceramic materials possess the high-temperature stability, resistance to rain erosion, and electrical properties which make them even potentially suitable for meeting the severe requirements which are beyond the capabilities of conventional fiberglass-plastic materials.

Unfortunately, manufacture of one-piece or monolithic ceramic radomes in the large sizes and configurations for optimum system performance has not been proved possible and would be a most difficult task. This is due to inherent limitations of ceramic forming and sintering operations, to the nonuniform shrinkage and property variations encountered in such large components, and to the difficulties of grinding or finishing these hard and brittle materials to the required tolerances. It was postulated that one method of overcoming these limitations and fabricating large, structurally and electrically acceptable ceramic radomes was to bond together low dielectric ceramic segments or "tiles" using mosaic techniques. Suitable ceramic adhesives, possessing elevated temperature strength and stability, were available or within the state-of-the-art and no serious problems were foreseen in fabricating ceramic materials into tile segments having the required dimensional tolerances and properties; therefore, the concept appeared feasible for manufacturing technology development.

This concept was the basis for the project covered by this report — to establish the manufacturing technology know-how for fabricating composite ceramic radomes by mosaic techniques. The basic goal of the program was to demonstrate the developed manufacturing methods and processes by the fabrication and test of a large prototype radome of the configuration selected. The following design and materials goals served as guideline objectives for the program:

1. Fabrication of a bonded mosaic ceramic ogive radome of half-wave wall thickness design, having dimensions of approximately 96-in. length and 32-in. diameter at the base, and suitable for supersonic, 1000°F operating conditions

2. Deviations in contour and out-of-roundness within ±0.015 in. with mounting attachments flush to the base body surface

3. Use of a ceramic body having a loss tangent of 9375 Mc of less than 0.005 at 80°F and 0.010 at 1000°F

4. A temperature coefficient of dielectric constant within ±1% over the operating temperature range

5. Use of ceramic materials capable of effective operation over the temperature range of 85°F to 1000°F at 9375 Mc in relative humidity from zero to 100% while maintaining a 75% transmission efficiency

6. An insertion phase delay varying less than ±1 degree over the length of the radome

7. Use of a ceramic body having the following properties:

   a. Tensile strength of 30,000 psi and flexural strength of 60,000 psi

   b. A thermal expansion in the range of 3.5 to 5.0 x 10^{-6} in./in./°F over the operational temperature range

   c. An emissivity of 0.9 in the temperature range from 500°F to 1000°F

   d. A moisture absorptivity of less than 0.02%

The program, as accomplished and reported herein, covered a literature and state-of-the-art review, ceramic body and adhesive selection, radome design including structural and thermal analysis, fabrication technique development including tooling material selection plus tooling design and fabrication, ceramic tile design and procurement, and fabrication and test of several radome base sections as well as a full-scale radome.

SECTION II

STATE-OF-THE-ART REVIEW AND ANALYSIS

The initial or Phase I efforts accomplished under the program were a state-of-the-art and literature review relative to adhesives, ceramic body materials, and manufacturing practices pertinent to high-performance composite ceramic structures suitable for mosaic radome applications. A Narmco Research & Development internally conducted literature survey was supplemented by a literature review accomplished under subcontract by Battelle Memorial Institute. The references and results of these reviews are included in Appendixes I and II respectively.

An analysis of the literature and available information indicated several high-temperature inorganic compounds which might be used as adhesives. These materials, with a short description of manufacturers claims, are listed below:

1. Astroceram A&B LP (American Thermocatalytic Corporation). This cement is resistant to high temperatures and heat shock. It offers a maximum service temperature of 4400°F and does not react when in contact with metals or ceramics. The cements have excellent cohesive properties, including a Moh's hardness between 8 and 9. Chemically, the cements are insoluble in hydrochloric acid, nitric acid, phosphoric acid and sulfuric acid at room temperature. There are two basically different cements available: one can be air-dried, and the other must be fired to form a bond. Low-porosity compounds of each type are intended for vacuum sealers.

   Glass, quartz, zirconia, alumina, refractories, ceramics and metals have been bonded. The cement may also be used for potting electronic components and for thermocouple protection sheaths. Its dielectric constant is between 7 and 9 at 10^6 cps.

2. Melbond CA-100 (Melpar, Incorporated). Melbond CA-100 is a ceramic adhesive with excellent bonding strength when used with refractory materials such as ceramics. Melbond adheres well to Melfoam, dense alumina, pyrophyllite, K-30 brick, Foamsil and graphite at temperatures up to 2000°F, to dense zirconia up to 1500°F, and to Alundum, cast magnesia and cinder block to 1000°F. This cement has good electrical properties (dielectric constant below 2.5 and loss tangent below 0.04 at room temperature and 10^{10} cps), attains a high degree of mechanical strength, and does not flake or disintegrate during use.

3. Eccoceram QC (Emerson & Cuming). Eccoceram QC is a highly siliceous cement. It consists of two parts, which set up at room temperature when mixed. The product maintains its physical strength and desirable electrical properties up to 2500°F. This cement has a cohesive tensile strength of 800 psi.

4. Interpace High-Temperature Cement (International Pipe & Ceramics Corporation. This cement was specifically developed for bonding alumina laminae. Work done by Caldwell (Gladding-McBean) under Contract NOas 59-6222c in 1961 included fabrication of the laminate by assembling the required sheets with a fired cement of nepheline syenite and talc. The mixture was sprayed on each sheet and the total assembly fired to 1250°C (2280°F) on flat alumina plates. During the firing, a weight was placed on each assembly to minimize horizontal shifting of the sheets. The fired adhesive provided a strong bond, as indicated by the success of edge machining without excessive loss.

5. Pyroceram 45*and Others (Corning Glass Works). These cements are a new type of sealing glasses which, when fired, develop into a partially crystalline structure analogous to Pyroceram 9606 and 9608 which results in a devitrified glass seal that is much stronger and harder than the original glass. The strong seals are vacuum-tight and may be reheated to their firing temperature during service. Pyroceram 45 has a maximum service temperature of 700°C (1292°F) and is compatible with tungsten, molybdenum, several glasses and standard electrical ceramics (including alumina). Pyroceram has a modulus of rupture at 25°C of 10,000 psi. Its dielectric constant is 6.1 at 1 kc and its loss tangent at 25°C and 1 kc is below 0.002.

6. Pycerad 300 and Allied Compounds (Narmco Research & Development). These crystalline adhesives form a family of composite materials based on a series of refractory ceramic, liquid phase binders. These binders bond readily to refractory oxides, whether these oxides are in the form of powder or prefabricated bodies.

In like manner, an initial review of the literature and manufacturers' catalogs indicated the following materials could be of use:

Alumina

Beryllia

Magnesia

Fused silica

Glass-bonded mica and ceramplastics

Boron nitride

Zirconia

Forsterite

The literature review, however, indicated that the following materials would probably be unsatisfactory for meeting the goals of the program:

1. Magnesia. Although magnesia bodies have good electrical properties, they are difficult to sinter and fabricate. In addition, thermal expansion is higher than that desired in the program.

*Registered trademark.

2. Fused Silica. The thermal expansion of this material is much too low for the desired minimum target goal of 3.5×10^{-6} in./in./°F. Its expansion is roughly 0.3×10^{-6} in./in./°F and there is a question as to whether compatible joints could be made with present adhesives due to the expansion mismatch.

3. Glass-Bonded Mica and Ceramplastics. The maximum operating temperatures of these materials are too low. In addition, these temperature limits would prevent curing of any adhesive system over 1500°F.

4. Boron Nitride. This material is quite soft and relatively weak, and is affected by water and high humidity.

5. Forsterite. This material has good electrical properties, but its expansion is slightly higher than the goal. Its thermal shock resistance is poor.

Based on the survey, it was concluded that three materials should be considered for segments: alumina, beryllia, and zirconia. Alumina was obviously favored for selection since it is an established radome material. Beryllia, despite its toxic nature, showed excellent promise as a candidate material. Zirconia was selected because of its high-temperature strength and thermal shock resistance, although electrical property data were scarce.

Sample segments of these candidate materials were obtained from suppliers for preliminary screening tests and examinations to aid in selecting the optimum material.

Table 1 consists of composite property data for the three candidate materials.

Some preliminary laboratory testing was conducted on the candidate body materials and adhesives to provide a basis for future program decisions. The following observations were made with respect to the 1-in. x 2-in. x 1/4-in. thick tile specimens of the segment material candidates for which at least one surface was ground smooth within 0.002 in.

1. 97.6% Alumina, GMcB351. These specimens had good, uniform white color, and there was no evidence of inclusions or specks.

2. 99.5% Beryllia. Segments varied from white to dark grey; several had black specks. This was apparently caused by the vendor's hot-pressing process using graphite molds. This contamination would have to be eliminated for radome applications.

3. Stabilized Zirconia. The zirconia samples were a dense, impervious grade stabilized with magnesia to prevent deterioration caused by inversions which occurs in pure monoclinic zirconia. It can also be stabilized with calcia, but reportedly deteriorates under temperature cycling between 1000°F and 1800°F, which was within the prospective adhesive maturing range. The zirconia samples contained small white inclusions which tended to pull out during surface grinding. It was assumed that these were magnesia particles.

TABLE 1

CERAMIC SEGMENT MATERIALS DATA

(Compiled from Manufacturers' Literature)

Property	Material		
	Alumina	Beryllia	Zirconia
Purity, w/o	97.6	99.5	≈95*
Forming Process	Dry Press	Hot Press	Dry Press
Specific Gravity	3.8	3.0	5.5
Flexural Strength, psi	51,000	--	35,000
Compressive Strength, psi	330,000	180,000	245,000
Modulus of Elasticity, psi	46×10^6	53×10^6	22×10^6
Thermal Expansion, in./in./°F x 10^{-6} 70°-500°F	3.8	4.0	5.0
Thermal Conductivity @ 100°C, cal/sec-cm-°C	0.069	0.500	0.005
Vol Resistivity @ 20°C, ohms-cm	$>10^{14}$	$>10^{14}$	10^8
Dielectric Constant			
1 Mc	8.9	6.5	27
8500 Mc or 10 kmc	8.2	6.6	
Dissipation Factor			
1 Mc	0.0006	0.00015	0.0029
8500 Mc or 10 kmc	0.005	0.00059	

* MgO stabilized.

WETTING CHARACTERISTICS

A qualitative wetting test was accomplished by placing a mound of the adhesive powder on the ceramic segment surface and noting its behavior upon fusing. Good wetting was indicated if the adhesive flowed out and adhered to the surface. Poor wetting was assumed if the mound tended to contract and exhibit a large contact angle. Wetting tests could, of course, be accomplished only on those adhesives which cured by fusion rather than by air setting or moderate heating.

COMPRESSIVE SHEAR TESTS

Preliminary compatibility between the adhesives and segments was established by determining compressive shear strength on lap joints at room temperature.

The joints were prepared by joining together tile segments, allowing a 7/8-in. overlap after the adhesive was applied in slurry form to the lap areas. The adhesive powder was mixed in accordance with the vendor's specific instructions and also made into a paste slurry using isopropyl alcohol. The adhesive was evenly spread on the surface of the segments, which were then placed together to form the joint. After drying, the samples were fired to their respective firing temperatures, utilizing a refractory brick alignment jig and applying slight positive pressure.

Figure 1 shows samples which are representative of the type used for shear strength testing. Testing of the samples was performed by applying a compressive force to the sample until the bond failed in shear. Samples were tested in a jig designed specifically for testing lap joints. The testing arrangements are shown in Figures 2 and 3.

In addition to the quantitative shear strength data obtained from testing the lap joints, a visual examination of the sheared area was made to determine if failure was of an adhesive or cohesive nature.

DISCUSSION OF FINDINGS

American Thermocatalytic's Astroceram A LP and Melbond CA-100 were tested in shear at room temperature. Comparatively poor adhesion at the surface of the alumina segments was noted, and further testing was eliminated on the basis of these preliminary tests.

Emerson & Cuming's Eccoceram QC, a highly siliceous cement (consisting of a two-part system, requiring mixing of a granular powder and mobile liquid immediately before use), was also examined. Alumina segments, after being prepared according to the manufacturer's instructions, failed to adhere at room temperature, although cohesive properties of the cement were good.

Astroceram B LP cement was used with both alumina and stabilized zirconia segments. The cement required drying at 160°F for 20-30 minutes, continued drying at 500°F to 1100°F for 10 to 20 minutes and, finally, curing at 2200°F

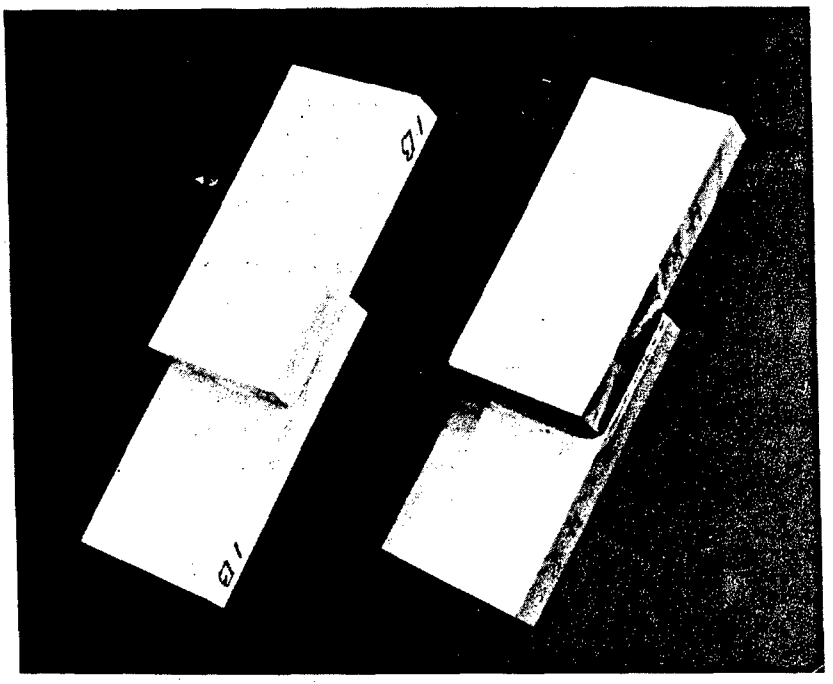


Figure 1. Prepared Lap Joints for Compressive Shear Tests. Pyroceram adhesive joining beryllia segments (left) and Pycerad 300 with stabilized zirconia

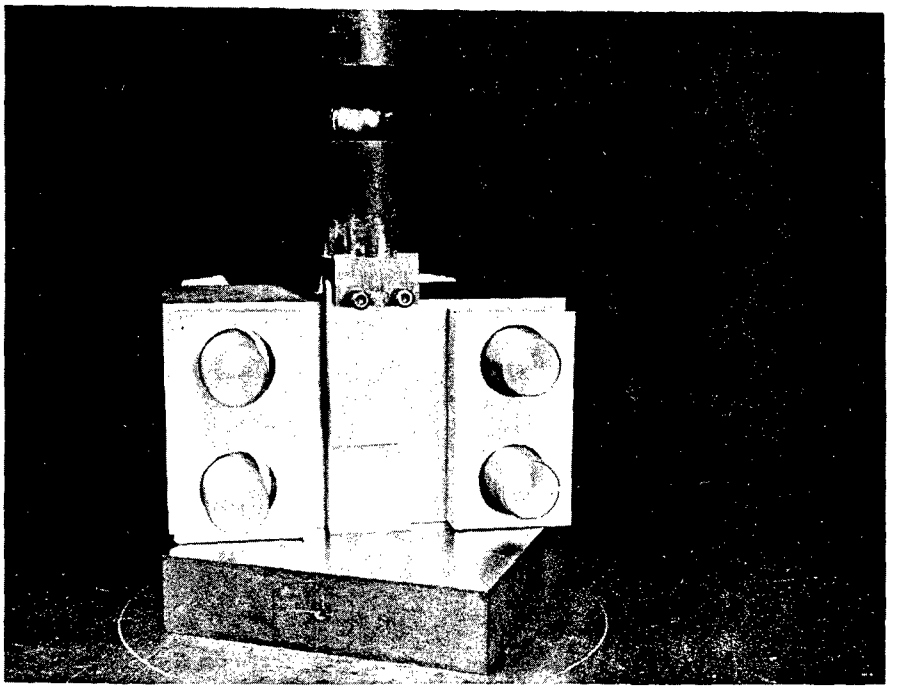


Figure 2. Lap Shear Fixture Opened to Show Lap Specimen in Place

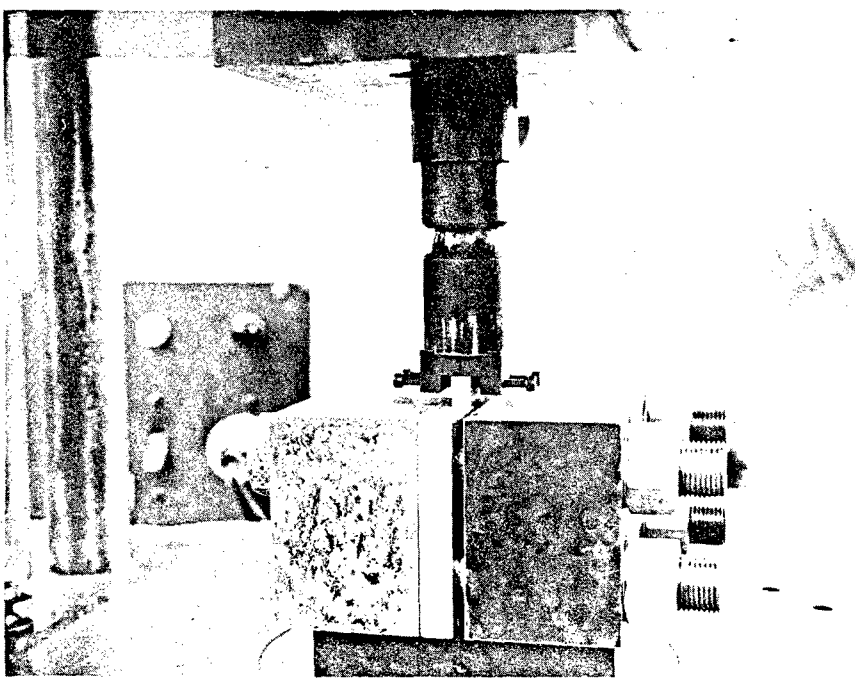


Figure 3. Lap Shear Fixture as Assembled during Testing

for 20 minutes. It failed, both cohesively and adhesively, after being cooled to room temperature under no applied load.

A communication from International Pipe and Ceramics Corporation explained preparation of the adhesive they have used in bonding alumina laminae. It consists of a mixture of nepheline syenite and talc. Upon firing to 2246°F, this adhesive forms a glassy bond with shear strength of about 4400 psi. While the room temperature strength of joints was high, the cement did not exhibit good wetting. Examination of the fusion test button indicated a large contact angle with the surface of the alumina segment.

Pyroceram 45 and Pycerad 500 along with allied adhesives showed considerable promise; hence, major emphasis was devoted to these compositions. Bonding of ceramic segments with these adhesives was accomplished in an electric furnace. Pyroceram 45 lap joints were placed in the furnace and the temperature raised to the curing temperature of 1382°F at a rate of about 20°F/minute and cured for 1 hour. They were then cooled at approximately 8°F/minute to 600°-850°F and removed for further cooling under a silica fiber blanket. Pycerad 300 and 500 joints were made in a similar manner, except the maximum temperature of 50°-100°F above the melting point (1830°F) was held for only 5 minutes.

Typical initial shear strengths obtained for testing lap joints of the various ceramic segments for Pyroceram 45 and Pycerad adhesives are shown in Table 2.

TABLE 2

SHEAR STRENGTH VALUES OF CANDIDATE ADHESIVES ON RESPECTIVE SEGMENTS

Segment Material	Pyroceram 45	Pycerad 300	Pycerad 500
Alumina	1370-7580 psi	805-1985 psi	3360 psi*
Beryllia	2360-3320 psi	Too low to test	790-3210 psi
Zirconia	1995-5110 psi	970-1170 psi	--

* Avg

Pyroceram 45 wet the surface of all segment materials quite well; Pycerad 300 wet alumina and zirconia but did not react sufficiently with beryllia to develop shear strength. However, the versatility of Pycerad systems permits ready adjustment of the basic cements to make them compatible with various oxides as noted with Pycerad 500. Figure 4 shows the wetting traits of Pycerad 300 adhesive on alumina and beryllia segments as well as the sheared lap joints. The failure mechanism was adhesive in nature.

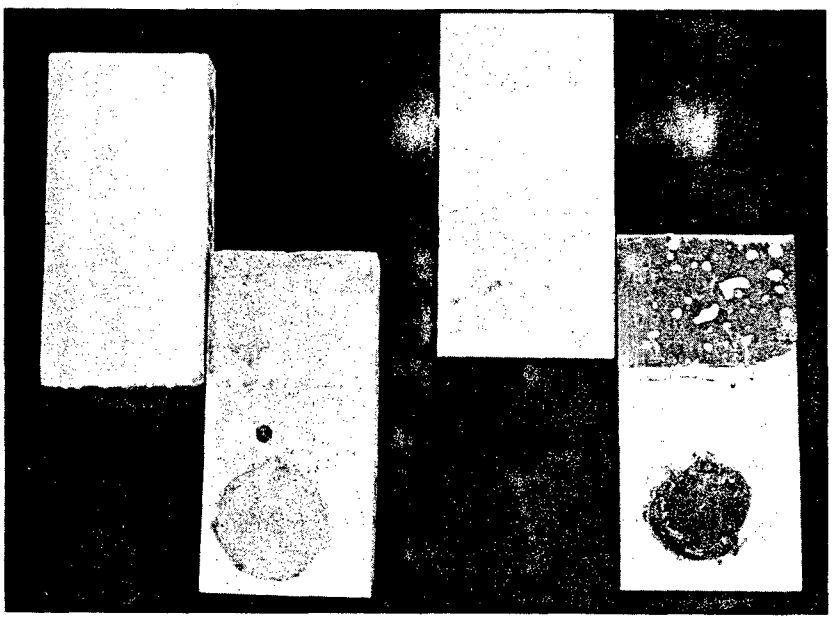


Figure 4. Sheared Lap Joints showing Wettability and Adherence of Pycerad 300 on Beryllia and Pycerad 300-A on Alumina (left)

Initial specimens were prepared without surface modification of the ceramic body or particular control of the adhesive bondline thickness. Preliminary study indicates these factors have a measurable influence on strength, so these data must be considered as approximations of strength rather than the ultimate potential of the adhesives.

The wetting of Pycerad 300 on zirconia was more pronounced than on either alumina or beryllia, as indicated in Figure 5. The fused adhesive flowed outwardly on the surface of the zirconia segment as well as along the margin of lap joints. However, this may not be a function of wettability, but due to the apparent surface porosity of the zirconia segment, it created a capillary phenomenon. This condition also may explain the wide range of strength data obtained for other adhesives when testing zirconia lap joints.

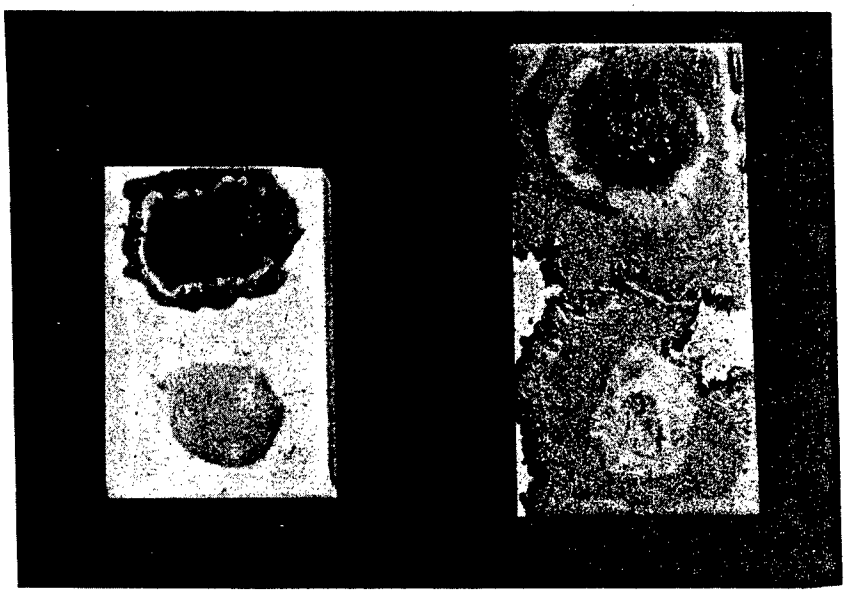


Figure 5. Wetting Tests on 97.4% Alumina (left) and Stabilized Zirconia Segments Using Narmco's Pycerad Adhesives. Wetting characteristics are shown for Pycerad 300 (upper) and Pycerad 300-A (lower)

PRELIMINARY SURFACE PREPARATION AND BOND THICKNESS INVESTIGATION

Since some of the composite samples were failing adhesively rather than cohesively, a preliminary examination of the effects of segment surface condition was made. These studies were arbitrarily confined to 97.6% alumina segments. Lap joints of Pycerad 300 and Pyroceram 45 were prepared on chemically etched, mechanically abraded, and as-received surfaces. The mechanical surfaces on which the lap joints were prepared included as-received smooth, as-received rough, fine grit sandblasted, and coarse grit sandblasted. Hydrofluoric acid (50% concentration) and a combination (one-to-one) of hydrochloric and nitric acids were used to chemically etch the smooth as-received surfaces.

After curing, the samples were tested and the shear strengths recorded (see Table 3).

TABLE 3

PRELIMINARY SURFACE PREPARATION VS SHEAR STRENGTH

Preparation	Application	Shear Strength, psi	
		Pyroceram 45	Pycerad 300
Etch HF	5 min	3484 7579	1335 1223
	10 min	2378 4067	1186 864
HNO_3 + HCl Etch	5 min	1983 2212	1083 866
	10 min	7093 1897	1143 1598
Sandblast	Coarse Grit	3678 1689	1948 1945
	Fine Grit	5683 5118	1089 1265
Unprepared Surface	Smooth	6645 6710	1741 1399
	Rough	5000 3972	1487 1707

As indicated in this table, the shear strength range was large for both Pyroceram 45 and Pycerad 300. The best method of applying these adhesives to the segments had not yet been determined and largely accounts for wide discrepancies in test data.

The Pycerad 300 adhered better to the rough side of unprepared (as-received) alumina. Sandblasted surfaces also gave fairly high strength values. The four highest shear test values were on either unprepared or sandblasted surfaces.

Pyroceram 45 tests indicated that its strength was generally independent of the method of surface preparation. The two strongest shear joints were observed on etched surfaces. The two next strongest occurred on smooth as-received surfaces. The highest Pyroceram shear joint tested was 7579 psi and the lowest was 1680 psi. Average shear strength for 16 shear joints with a

7/8-in. overlap was 4150 psi. This value, being independent of surface preparation, is believed to be a representative average of Pyroceram 45, as no high strength values were concentrated on any one prepared surface. However, the smooth surface of the segments yielded more uniform test results for the Pyroceram 45 than did the other surfaces.

Examination of the data revealed the room temperature shear strength values for Pyroceram 45 to be higher than those for Pycerad 300, but elevated temperature tests were necessary before definite evaluation of relative merits could be made.

The data were categorized into different bondline thickness groupings using 5-mil increments, and shear strengths were tabulated (see Table 4). Pyroceram 45 shows greatest strength in the 5-10 mil range, with an average shear strength of 6200 psi. The next increment showing strength is in the 10-15 mil range. Bondline thicknesses below 5 mils and above 15 mils showed a decrease in shear strength values.

METHOD OF ADHESIVE APPLICATION

It was observed that the method of spreading the adhesive onto the segment possibly was responsible for some discrepancies noted in test data. Therefore, alternate methods of applying the adhesive were studied. It seemed a spraying technique would offer decided advantages for controlling bond thickness. It was also desirable to have a vehicle or medium which would promote sufficient green strength for the adhesive in order to permit handling and joint alignment movement before firing without excess dusting.

A nitrocellulose lacquer and Pyroceram 45 suspension was prepared, having the consistency of cream for spray application. In this manner, thin coatings could be sprayed onto ceramic segments. These were rapidly dried by application of hot air. The lacquer coatings had sufficient strength to permit handling and positioning of lap joints prior to firing. There was some indication that lacquer-sprayed samples would have to be cured slowly to prevent rapid volatilization of the nitrocellulose and entrapment of gas within the adhesive.

RESULTS

It was concluded that alumina and beryllia were the most promising candidate radome segment materials, with zirconia offering some possibility. Of the ceramic adhesives screened, Pyroceram 45, Pycerad, and the Interpace compositions were considered most suitable for further study.

TABLE 4

BONDLINE THICKNESS VS SHEAR STRENGTH

Material	Bondline Thickness, mils				
	1	1-5	5-10	10-15	15
Pycerad 300	1083	1223	866	1986	1399
Shear Strength, psi	968	864	1598	1300	1335
	--	1143	1948	--	--
	--	1089	1945	--	--
	--	1487	1265	--	--
	--	1080	1741	--	--
	--	--	1707	--	--
	--	--	805	--	--
Avg	1025	1148	1484	1243	1367
Pyroceram 45	1897	1372	3484	4067	2212
Shear Strength, psi	--	5118	7579	1983	2378
	--	3678	7093	5000	--
	--	--	6645	6710	--
	--	--	--	5683	--
	--	--	--	1689	--
Avg	1897	3056	6200	4189	2295

SECTION III

FABRICATION AND BONDING TECHNIQUES DEVELOPMENT

The preliminary screening data indicated that alumina and possibly beryllia and zirconia were suitable as segment materials for the desired radome application, and that there were several high-temperature ceramic adhesives which were promising as segment binding agents. Work was therefore continued to evaluate and select the best combination and to develop techniques for making the desired composite mosaic radome.

SEGMENT MATERIALS

Various grades of alumina and beryllia were investigated. Zirconia samples were obtained only for testing dielectric constant and loss tangent, since the literature indicated rather poor electrical properties for this material. The fabricated ceramic bodies listed in Table 5 were obtained. (Hereafter these specimens are referred to by the Narmco code number given in this table.)

Dimensional Reproducibility

The segments employed were basically of two dimensional types. Those used for screening, such as lap shear joints, were ordered against a normal tolerance as supplied by the manufacturer. These in general consisted of 1-in. x 2-in. rectangles of 1/4-in. thickness, the latter being the critical dimension. The other type of segment material ordered consisted of those specimens required for specific electrical, mechanical, and thermal tests. These latter samples were ordered to certain specifications and tolerances usually within ±0.001 in.

In addition to checking the segments for dimensional accuracy, they were also checked for density as a further quality control procedure. In all cases, the density of the segments received agreed well with values published in the manufacturer's literature.

Table 6 shows the results of checking the screening segments for dimensional accuracy as well as the delivery time required for the various types. Of all the segments received, only one type was not suitable for making lap shear samples. The remaining segments all had uniform thickness tolerances within the range from ±0.0005 in. to ±0.003 in.

Flexural Strength

Flexural strength of the segment materials was measured using a two-point loading method on samples cut to 0.25 in. x 1.0 in. x 4.5 in. The results obtained were compared, whenever possible, to the manufacturer's published values or other published data. The results are shown in Table 7.

TABLE 5

SEGMENT MATERIAL CANDIDATES

Narmco Code	Source	Specimen Designation	Composition, w/o
S1	International Pipe & Ceramic Co.	GMcB 351	97.6 Al_2O_3
S2	International Pipe & Ceramic Co.	GMcB 352	99.0 Al_2O_3
S3	Western Gold & Platinum Co.	AL 300	97.6 Al_2O_3
S4	The Beryllium Corp.	Berylco	99.7 BeO (Hot pressed)
S5	National Beryllia Corp.	Zirox	≈95 ZrO_2
S6	Western Gold & Platinum Co.	AL 995	99.5 Al_2O_3
S7	American Lava Corp.	AlSiMag 614	96 Al_2O_3
S8	W. P. Keith Co. (McDanel)	AP 35	99.0 Al_2O_3
S9	National Beryllia Corp.	Berlox	99.5 BeO (Sintered)
S10	Corning Glass Works	Pyroceram 9606	

TABLE 6

SEGMENTS SCREENING

Material	Sample Size, in.	Delivery Time, Weeks	Thickness, in.			Width, in.			Length, in.		
			Range	Tolerance		Range	Tolerance		Range	Tolerance	
				Specified	Received		Specified	Received		Specified	Received
S7	1/4 x 1 x 2	7	0.251-0.253	±0.005	±0.001	0.982-0.989	±0.01	±0.004	2.006-2.017	±0.02	±0.006
S1	↓	2	0.267-0.273	Nominal	±0.0025	0.991-1.017	Nominal	±0.013	2.009-2.021	Nominal	±0.006
S1	↓	2-1/2	0.250-0.256	↓	±0.0030	0.999-1.013	↓	±0.007	2.021-1.998	↓	±0.01
S6	3/8 x 2 x 2	3	0.372-0.375	↓	±0.0015	2.002-2.007	↓	±0.0025	2.003-2.009	↓	±0.003
S8	1/4 x 1-3/4 x 1-3/4	7	Samples all warped and not suitable for use								
S9	1/4 x 1 x 2	7	0.251-0.252	±0.005	±0.0005	1.006-1.009	±0.005	±0.0015	1.995-1.997	±0.005	±0.001
S4	↓	5-1/2	0.248-0.250	±0.005	±0.001	1.003-1.004	±0.005	±0.0005	2.001-2.003	±0.005	±0.001
S10	↓	4	0.248-0.252	Nominal	±0.002	0.997-1.004	Nominal	±0.0035	2.00-2.60	Nominal	±0.30

TABLE 7

FLEXURAL STRENGTH OF CERAMIC SEGMENT BODIES

Material	No. of Samples Tested	Data Source	Flexural Strength, psi			
			RT		1000°F	
			Range	Avg	Range	Avg
S1 Alumina	6	Narmco	26,210 – 34,520	29,660	17,210 – 23,620	20,520
	--	Manufacturer	--	51,000	--	--
S3 Alumina	4	Narmco	28,420 – 30,410	29,415	24,850 – 25,250	25,050
	--	Manufacturer	--	46,000	--	--
S4 Beryllia	6	Narmco	17,020 – 25,050	20,540	6,660 – 13,080	9,245
	--	Manufacturer	--	30,000	--	--
S6 Alumina	4	Narmco	28,460 – 28,960	28,710	23,420 – 25,340	24,380
	--	Manufacturer	--	62,000	--	--

Only room temperature flexural strength data were available from the manufacturer's literature for the particular alumina ceramics tested. Narmco's test data are considerably lower than the reported values. This may be due to testing procedures employed and also to the shape of test samples. A general review of the ceramic literature did not reveal much data for flexural strength at 1000°F for alumina ceramics. However, one reference showed good agreement with Narmco's flexural strength data. The reference reported the average flexural strength of a 99.8% sintered alumina body to be 30,000 psi at room temperature and 22,000 psi at 1830°F.*

The flexural strength of the beryllia body was also lower at room temperature than that reported in the manufacturer's literature. However, the manufacturer reported the flexural strength to be almost inversely proportional to grain size, with strength dropping from 38,000 psi for a 20-μ grain diameter to 10,000 psi for a 100-μ diameter grain size. A variation in particle size may be the cause of room temperature discrepancies since, as in the past, this particular type of hot-pressed beryllia has shown severe variation in color. This indicates possible directional properties, probably due to temperature gradients exsiting in the hot pressing mold. No manufacturer's data were listed for high-temperature flexural strength for the beryllia, which had a density of > 2.95 gm/cc, although a value of 17,000 psi was reported for a low-density beryllia approximately 2.75 gm/cc by the same manufacturer at 1110°F. The same reference used for alumina* showed fair correlation with Narmco data, as a figure of 20,000 psi was given for the room temperature flexural strength, while 10,000 psi was noted for a 99.8% sintered beryllia body 1832°F.

Compressive Strength

Compressive strength was determined by observing the compressive load necessary to produce failure in test specimens measuring 0.250 in. x 0.250 in. x 1.0 in., whose ends were parallel and perpendicular to their longitudinal axis. The results are given in Table 8.

In general, the room temperature data obtained for the various alumina ceramics tested were in fair agreement with the manufacturers' published values. As was the case for the flexural tests, the differences that existed were probably due to sample shape and method of testing. The values shown for the S1 material have considerable spread, since these were the initial specimens tested. The low value for this material is probably not realistic.

While no high-temperature test data were given by the manufacturers of the individual alumina bodies, a comparison can be made to sintered alumina in general. It has been shown that a pure sintered alumina decreases from a compressive strength of 420,000 psi at room temperature to approximately 202,000 psi at 1000°F. Therefore, it appears that Narmco's high-temperature values are realistic.

---

* W. D. Kingery, Property Measurements at High Temperatures, New York, John Wiley & Sons, Inc., 1959, pp. 44-45.

TABLE 8

COMPRESSIVE STRENGTH OF CERAMIC SEGMENT BODIES

Material	No. of Samples Tested	Data Source	Compressive Strength, psi			
			RT		1000°F	
			Range	Avg	Range	Avg
S1 Alumina	6	Narmco	159,360 – 258,960	203,155	207,110 – 220,720	215,915
		Manufacturer	--	250,000	--	--
				330,000		
S3 Alumina	4	Narmco	208,940 – 232,520	220,940	166,660 – 185,780	176,220
		Manufacturer	--	>250,000	--	--
S4 Beryllia	9	Narmco	95,310 – 132,810	115,670	53,750 – 64,450	58,230
		Manufacturer	--	180,000	--	70,000
S6 Alumina	4	Narmco	239,020 – 256,910	247,910	171,430 – 171,660	171,545
		Manufacturer	--	>300,000	--	--

While the manufacturer of the hot-pressed beryllia claimed a room temperature compressive strength of 180,000 psi, Narmco's average of 115,670 psi agrees quite favorably to the published value of 114,000 psi for sintered beryllia having a density of 2.9 gm/cc (as compared to 2.95 gm/cc for the hot-pressed material). Again, Narmco's value of 58,230 psi at 1000°F approximates the published compressive strength of 70,000 psi for dense sintered beryllia. However, it was noted during compression testing that the beryllia segments showed directional fracture when tested at 1000°F, with much powdering of the beryllia occurring. The surfaces also appeared corroded. This might have been caused by the contaminating carbon reacting with water (contained in the cement), which produced an effect similar to water vapor attack at high temperature.

Tensile Strength

As mentioned previously, only the S1 alumina was tested for tensile strength. This test was performed on tensile specimens approximately 6.0-in. long with ends of 0.5-in. diameter and the center portion necked-down to 0.25-in. diameter for a length of 2.5 in., with the midpoint of this length machined to 0.1875-in. diameter. The values measured for tensile strength are shown in Table 9.

TABLE 9

TENSILE STRENGTH OF CERAMIC SEGMENT BODIES

Temp	No. Tested	Tensile Strength, psi	
		Range	Avg
RT	2	22,130 - 29,800	25,965
1000°F	2	13,840 - 17,390	15,615

No data were listed by the manufacturers for tensile strength, either at room temperature or at elevated temperatures. A review of the literature revealed, as expected, a considerable range of values for this property. This is probably due to the introduction of bending moments in most tensile tests. The following ranges were tabulated for 96-98w/o alumina bodies:

Temperature	Tensile Strength, psi
Room temperature	21,000 - 37,400
1500°-2000°F	14,000 - 33,900

While Narmco's 1000°F data are on the low side, it appears that test results are characteristic of the tensile strength of alumina ceramics.

Electromagnetic Properties

Dielectric constant and loss tangent of ceramic segment bodies were determined by Melpar, Inc. on samples submitted by Narmco. At least two or three specimens were tested to check reproducibility. Results of tests are shown in Tables 10 and 11, and in Figures 6 and 7.

The charts and graphs show the individual properties for each segment sample, and also the average value for dielectric constant and loss tangent at each particular temperature. As the graph indicates, the S2 material had the lowest loss tangent values at all temperatures. The S3 body had loss tangent values approaching those of the S2 alumina material, while being significantly lower than the equivalent S1 body. The S4 beryllia segments showed a considerable spread in loss tangent values, more than likely caused by carbon contamination as previously noted and discussed. Another interesting aspect of the S4 beryllia material is the decrease observed for the loss tangent from room temperature to 500°F. This may be a result of slight moisture pickup due to capillarity and/or porosity. The same phenomenon also occurred in the S5 zirconia segments, which were slightly porous. As expected, the zirconia segments had very high loss tangent values at both room temperature and elevated temperatures.

All three alumina bodies had similar dielectric constant values throughout the temperature range, and also showed the same slope for their dielectric constant vs temperature curves. The S4 beryllia body, although lower in actual values, also had a similar curve. Two of the three zirconia segments tested showed a slight decrease in their dielectric constant from room temperature to 500°F. However, their overall increase was higher than for any of the other materials tested. Table 12 shows the average percentage increase in dielectric constant from room temperature to 1000°F and 1200°F, respectively, for each material.

The S6 alumina showed surprisingly high loss tangent values for an alumina ceramic of this percentage. In fact, at elevated temperatures, this body was higher in loss tangent than the same manufacturer's 97.6% alumina body (No. S3). The S6 alumina segments also showed a wide discrepancy in loss tangent values at 1200°F, measuring 0.0024 (for one sample) and 0.0055. This may have been caused by some foreign impurity within the body.

A direct comparison of Narmco's measured electromagnetic properties with those reported by the manufacturer is not possible since the frequencies used are different and their method of testing unknown. Table 13 compares Melpar results with those reported by the manufacturers.

Except for the dielectric constant values, there appears to be fair agreement with the manufacturer's data for the various alumina bodies tested. There is a noticeable difference between loss tangent values obtained and those reported by the manufacturer for the S4 beryllia segments. Narmco values are approximately one order of magnitude higher than those given by beryllia ceramic manufacturers. A review of the literature has revealed that the accepted loss tangent value range for beryllia ceramics at high frequencies, 8.5 - 10.0 Gc, is approximately 0.0001 - 0.0006.

TABLE 10

CERAMIC SEGMENT BODIES - DIELECTRIC CONSTANT DATA

(Frequency 9.375 Gc)

Temp. °F	International Pipe & Ceramics GMcB 351 – 97.6% Al_2O_3		Western Gold & Platinum Co. AL 300 – 97.6% Al_2O_3			International Pipe & Ceramics GMcB 352 – 99.0% Al_2O_3		The Beryllium Corp. Berylco – 99.7% BeO		National Beryllia Corp. Zirox – 95% ZrO_2			Western Gold & Platinum AL 995 – 99.5% Al_2O_3	
	Dielectric Constant		Dielectric Constant			Dielectric Constant		Dielectric Constant		Dielectric Constant			Dielectric Constant	
	S1-1	S1-2	S3-1	S3-2	S3-3	S2-1	S2-2	S4-1	S4-2	S5-1	S5-2	S5-3	S6-1	S6-2
RT	8.24	8.25	8.34	8.27	8.29	8.40	8.40	6.43 6.43	6.45 6.47	10.87	10.59	11.25	8.75	8.85
Av.	8.24		8.30			8.40		6.44			10.90		8.80	
500°	8.42	8.43	8.54	8.44	8.47	8.59	8.57	6.62	6.64	11.67	10.25	10.42	8.94	9.03
Av.	8.42		8.48			8.58		6.63				10.78	8.98	
1000°	8.73	8.72	8.82	8.74	8.74	8.90	8.86	6.87	6.91	12.92	11.33	11.60	9.27	9.36
Av.	8.72		8.76			8.88		6.89			11.95		9.31	
1200°	8.82	8.83	8.92	8.86	8.87	9.02	8.97	6.86	6.90	13.75	12.06	12.43	9.41	9.54
Av.	8.82		8.88			8.99		6.88			12.75		9.47	

TABLE 11

CERAMIC SEGMENT BODIES - LOSS TANGENT DATA

(Frequency 9.375 Gc)

Temp. °F	International Pipe & Ceramics GMcB 351 — 97.6% Al_2O_3		Western Gold & Platinum Co. AL 300 — 97.6% Al_2O_3			International Pipe & Ceramics GMcB 352 — 99.0% Al_2O_3		The Beryllium Corp Berylco — 99.7% BeO		National Beryllia Corp. Zirox — 95% ZrO_2			Western Gold & Platinum AL 995 — 99.5% Al_2O_3	
	Loss Tangent		Loss Tangent			Loss Tangent		Loss Tangent		Loss Tangent			Loss Tangent	
	S1-1	S1-2	S3-1	S3-2	S3-3	S2-1	S2-2	S4-1	S4-2	S5-1	S5-2	S5-3	S6-1	S6-2
RT	0.0007	0.0007	0.0006	0.0005	0.0006	0.0003	0.0003	0.0029 0.0031	0.0023 0.0018	0.0297	0.0345	0.1064	0.0004	0.0006
Av.	0.0007		0.00056			0.0003		0.00252		0.0568			0.0005	
500°	0.0011	0.0016	0.0007	0.0007	0.0009	0.0004	0.0004	0.0018	0.0012	0.0201	0.0200	0.0194	0.0008	0.0009
Av.	0.00135		0.00076			0.0004		0.0015		.0198			0.00085	
1000°	0.0026	0.0024	0.0010	0.0010	0.0009	0.0007	0.0006	0.0023	0.0020	0.0481	0.0445	0.0573	0.0016	0.0019
Av.	0.0025		0.00096			0.00065		0.00215		0.0499			0.00175	
1200°	0.0036	0.0033	0.0013	0.0012	0.0012	0.0008	0.0008	0.0085	0.0021	0.0791	0.0757	0.0917	0.0024	0.0055
Av.	0.00345		0.00123			0.0008		0.0053		0.0822			0.00395	

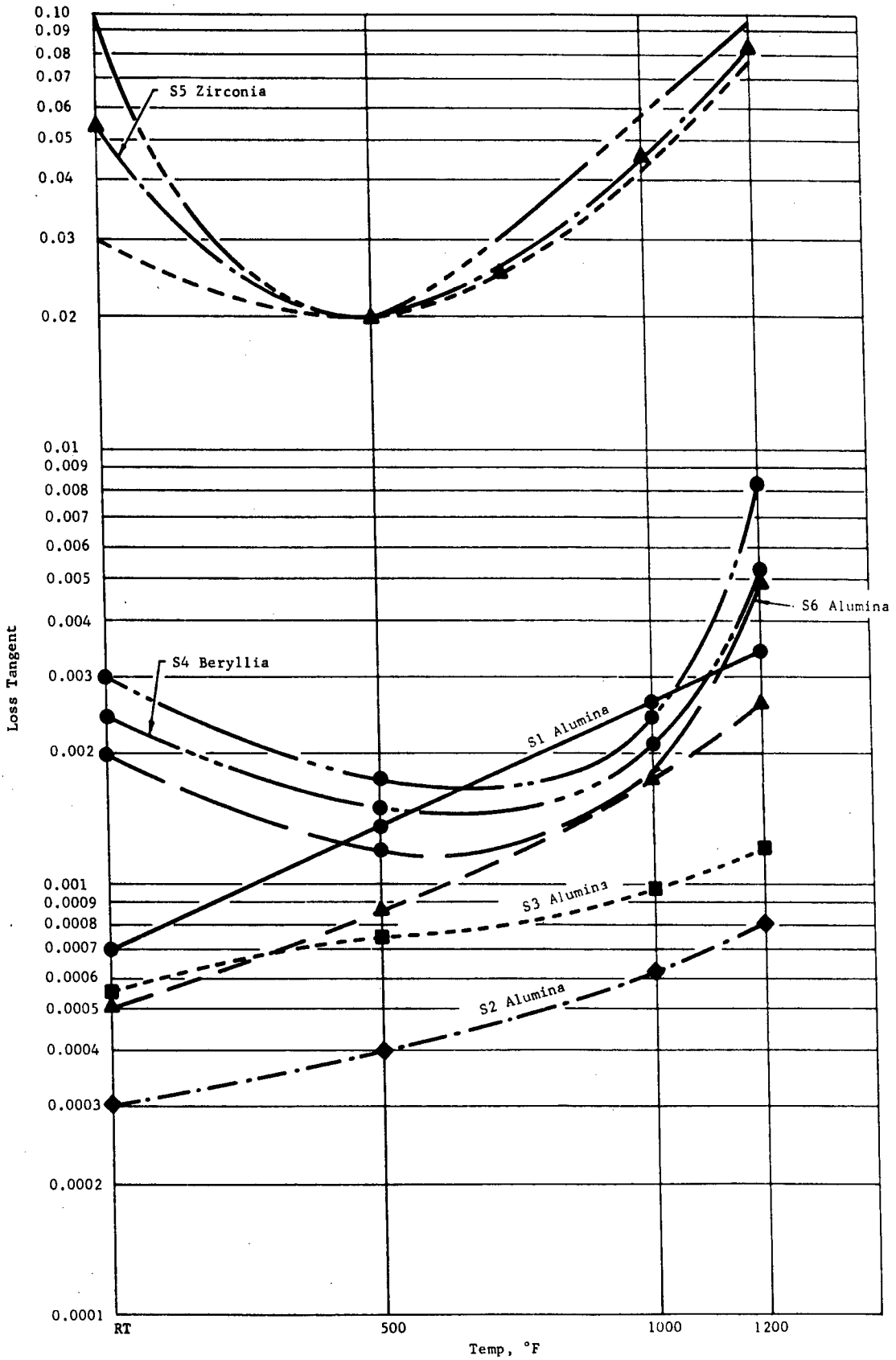


Figure 6. Ceramic Segment Bodies — Loss Tangent vs Temperature at 9.375 Gc

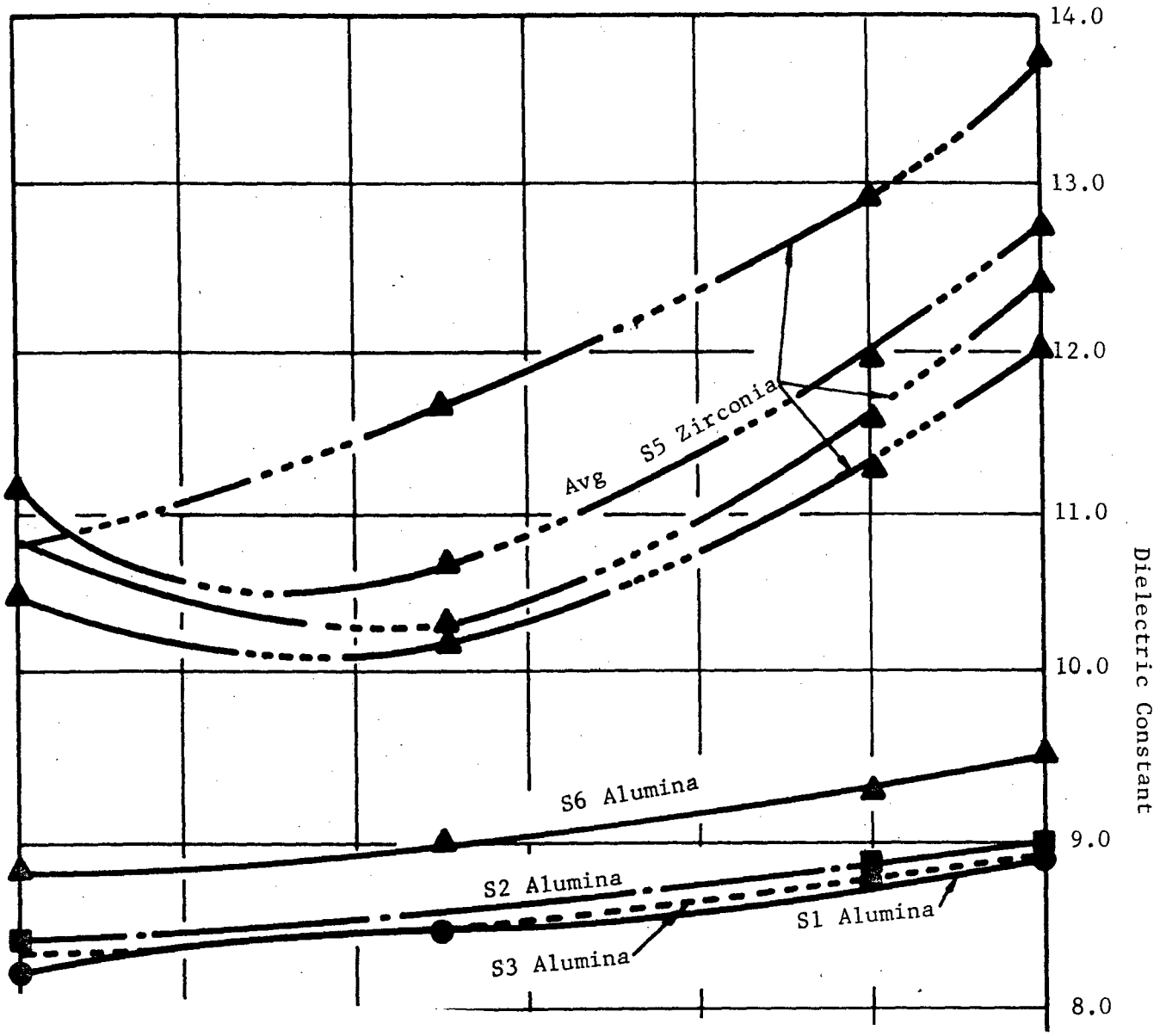

14.0
13.0
12.0
11.0
10.0
9.0
8.0
Dielectric Constant
Avg
S5 Zirconia
S6 Alumina
S2 Alumina
S1 Alumina
S3 Alumina

TABLE 12

DIELECTRIC CONSTANT INCREASE WITH TEMPERATURE

Material	% Dielectric Constant Increase	
	1000°F	1200°F
S1 Alumina	5.82	7.04
S3 Alumina	5.54	7.00
S2 Alumina	5.71	7.02
S4 Beryllia	7.00	7.00
S5 Zirconia	9.70	17.0
S6 Alumina	5.80	7.62

TABLE 13

ELECTROMAGNETIC PROPERTY COMPARISONS

Material	Data Source	Frequency, Gc	RT		1000°F	
			Dielectric Constant	Loss Tangent	Dielectric Constant	Loss Tangent
S1 Alumina	Manufacturer	8.5	8.20	0.0005	--	--
	Melpar	9.375	8.24	0.0007	--	--
S2 Alumina	Manufacturer	8.5	9.20	0.0002	--	--
	Melpar	9.375	8.40	0.0003	--	--
S3 Alumina	Manufacturer	8.5	9.04	0.00045	9.45	0.00072
	Melpar	9.375	8.30	0.00056	8.76	0.00096
S4 Beryllia	Manufacturer	10.0	6.6	0.00059	--	--
	Melpar	9.375	6.44	0.00252	--	--
S6 Alumina	Manufacturer	8.5	9.37	0.00009	9.82	0.00025
	Melpar	9.375	8.80	0.0005	9.31	0.00175

Thermal Expansion

Thermal expansion data were obtained by the quartz dilatometer method. Figure 8 shows two tests performed on S1 alumina. The curves are in reasonable agreement with each other, and may be compared directly to the adhesives curves.* Figures 9 and 10 show data on S6 alumina and S7 alumina respectively. A comparison between these grades of alumina shows that there is no measurable difference in expansion at these purity levels.

Figure 11 graphs the expansion of S4 beryllia. Although this material was not selected for further use, the graph is included for comparative purposes.

CERAMIC ADHESIVES

Evaluation of candidate adhesive compositions was continued to determine compatibility with segment materials and to obtain necessary property data and the effects of use conditions on the properties. In addition to candidate adhesives previously selected (Pyroceram 45, Pycerad 300 and 500, and the Interpace compositions), another ceramic adhesive was introduced into the program on the basis of some promising results obtained under a Corporate-sponsored research program. This was the Narmcad series of high-temperature adhesives which are essentially magnesium aluminosilicate glasses that have varying amounts of boric oxide additions to adjust the maturing temperature and other characteristics. Preliminary room temperature compression lap shear strength of the more promising adhesives with alumina segments was found to be as follows:

Adhesive	Avg Shear Strength, psi
Pyroceram 45	4,450
Interpace	4,125
Pycerad 500	3,360
Narmcad 105	6,120
Narmcad 110	11,200

On the basis of this lap shear strength data, these adhesives were selected for further evaluation.

Wetting Characteristics

Qualitative wetting tests were performed on the candidate adhesives in contact with segment materials employing the previously described "button" technique. A hemispherical mound of the produced adhesive was placed on the segment surfaces and its characteristics observed on heating to the fusion or maturing temperature. Wetting was demonstrated if the contact angle was less than 90 degrees. All the final candidate adhesives (Pycerad 500, Interpace, Pyroceram 45, and the Narmcad compositions) exhibited wetting as illustrated by Figure 12. The Pycerad adhesive spread readily with a low contact angle

* See Figures 19 through 21.

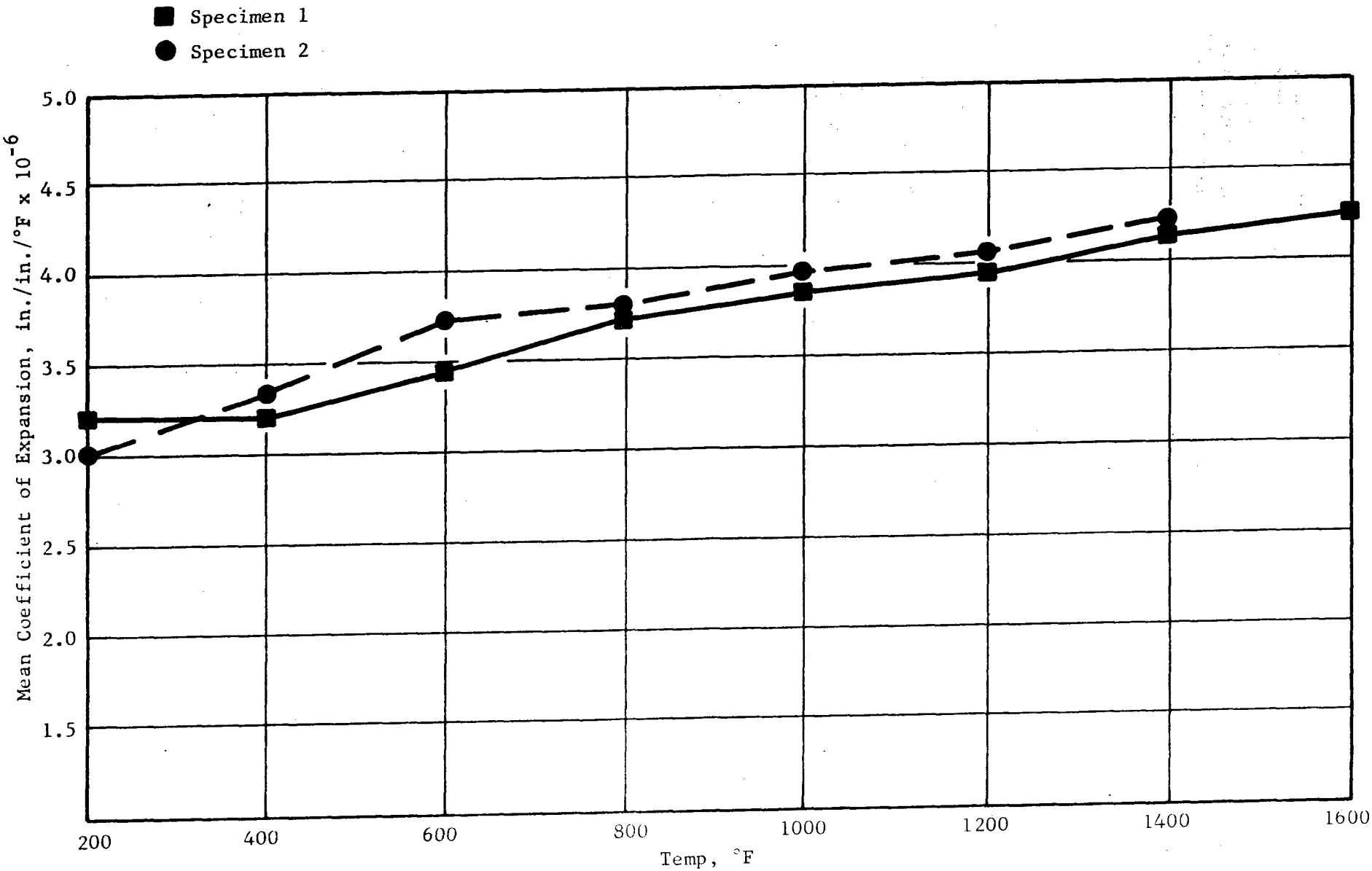


Figure 8. Mean Coefficient of Thermal Expansion vs Temperature for S1 Alumina from Room Temperature (75°F)

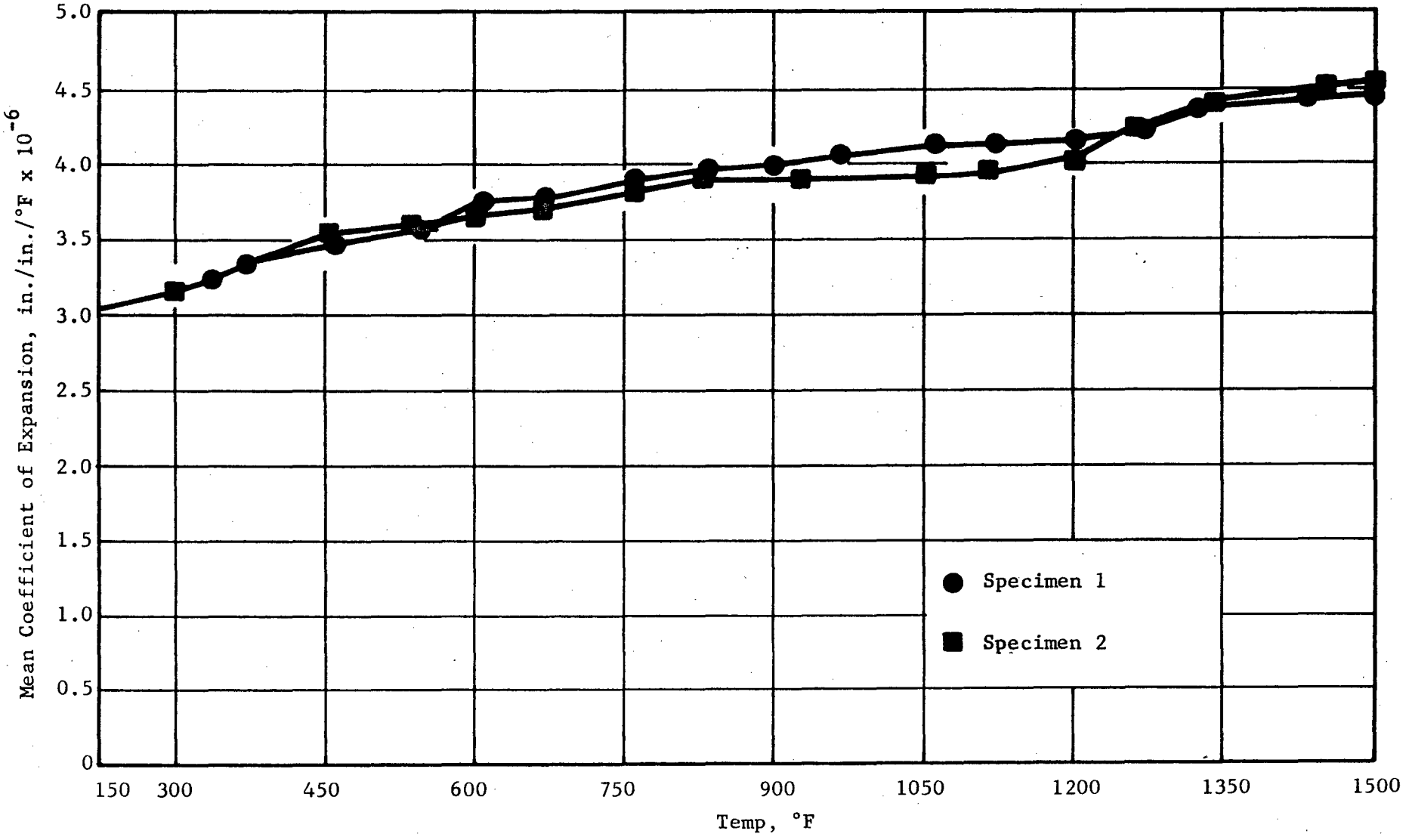


Figure 9. Mean Coefficient of Thermal Expansion vs Temperature for S6 Alumina from Room Temperature (80°F)

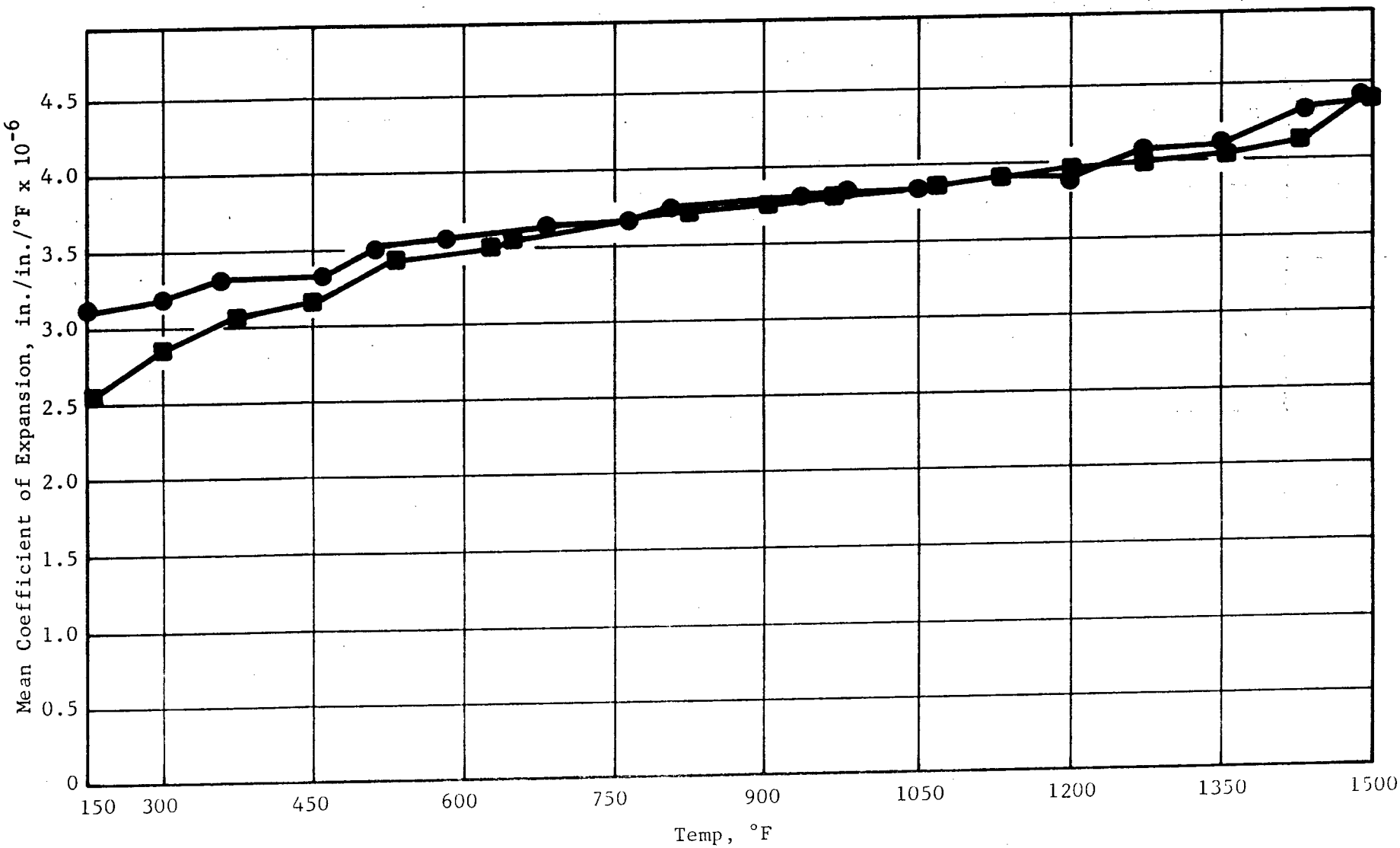


Figure 10. Mean Coefficient of Thermal Expansion vs Temperature for S7 Alumina from Room Temperature (75°F)

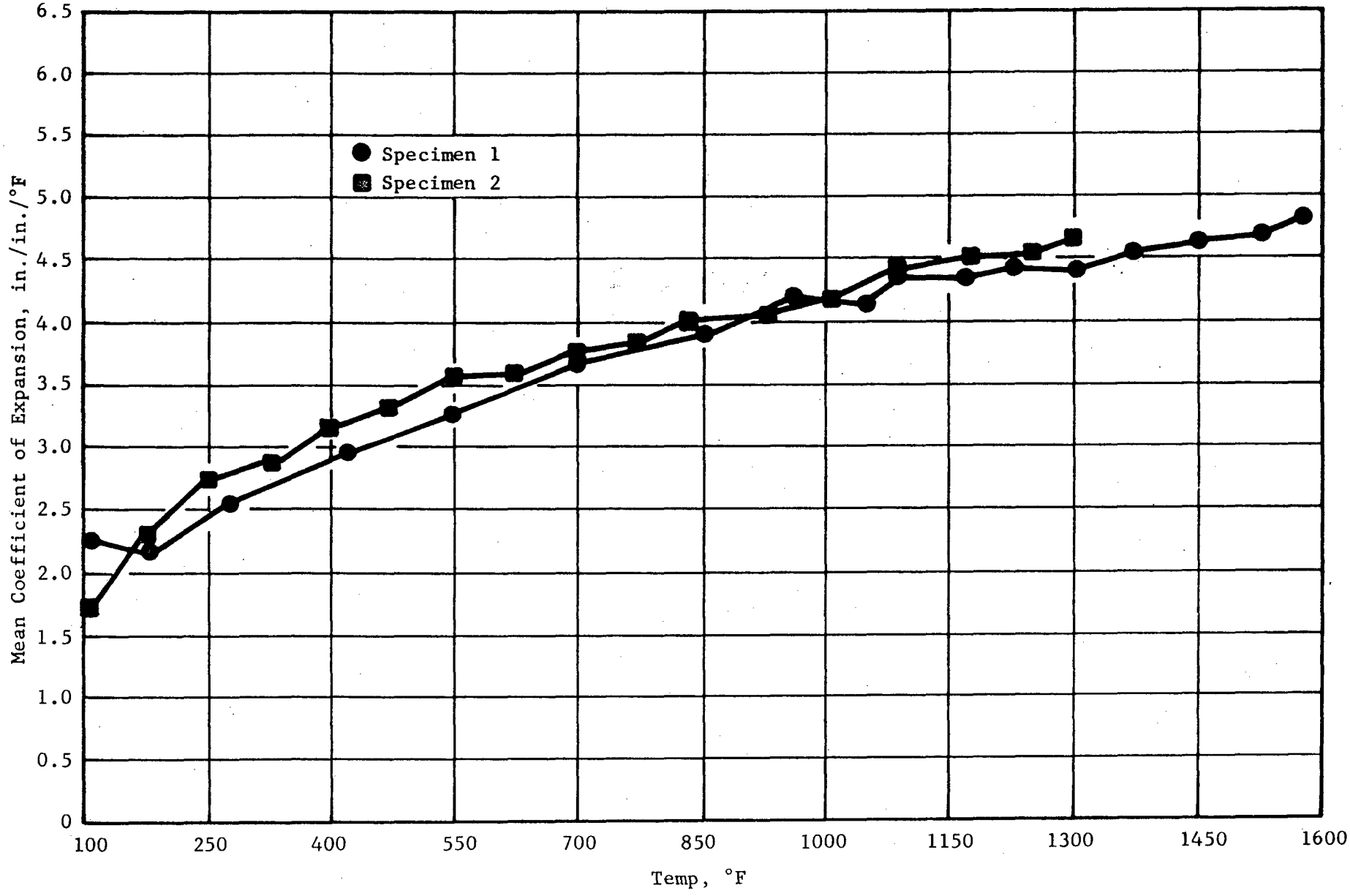


Figure 11. Mean Coefficient of Thermal Expansion vs Temperature for S4 Beryllia from 120°F

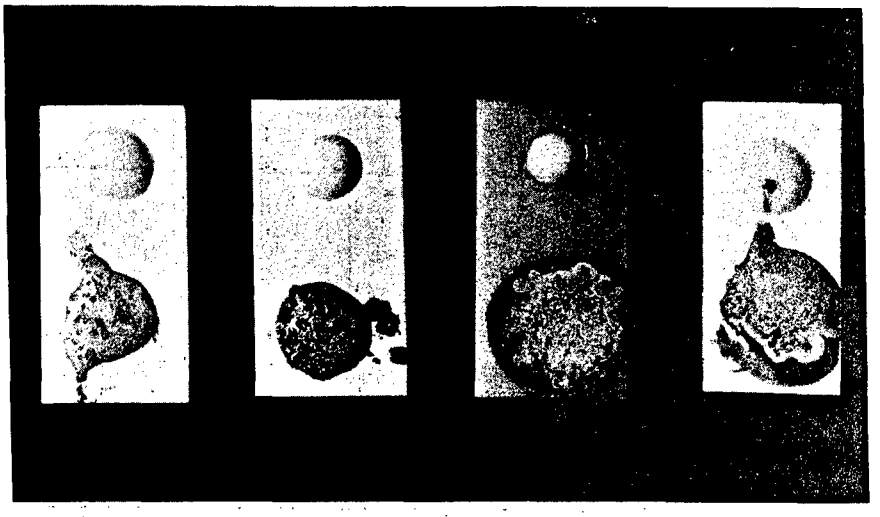


Figure 12. Wetting Tests of Interpace High-Temperature Adhesive (top) and Pycerad 500 (bottom). Left to right: 96.0% alumina, sintered beryllia, hot-pressed beryllia, and 99.5% alumina segments

(< 5 degrees). The Pycerad 500 showed greater spread on the S4 beryllia segments than on the S9 beryllia specimens, probably a result of different manufacturing methods. The S4 beryllia segments were produced by hot pressing while the S9 beryllia segments were made by sintering techniques. The S4 specimens were gray in color, indicating possible contamination from carbon molds. In addition, the density of the S4 beryllia specimens was slightly higher, ranging from 2.95 to 3.00 gm/cc, while that of the S9 beryllia specimens ranged from 2.85 to 2.90 gm/cc. The Interpace adhesive adhered to all segments with an approximate contact angle of 60 to 70 degrees. Similar characteristics were observed for the Narmcad adhesives.

Polished sections of the contact interfaces between the various adhesives and alumina segments were prepared to observe penetration and reaction. No significant differences were noted in any case when examined under reflected light at 300X magnification using a Unitron U-11 microscope. A representative photomicrograph of the adhesive-segment interface is shown in Figure 13. Good contact and wetting was indicated in all cases with no evidence of adhesive penetration or reaction (except in the case of Pyroceram 45, where there was evidence of a very slight reaction).

Lap Shear Strengths

Compressive lap shear strength was used as a basic screening test for comparing the various ceramic adhesives. The test specimens were prepared by coating the segment tiles with the adhesives in a slurry form followed by drying and firing. The following vehicle binder combinations were used to facilitate adhesive application and promote green strength: Narmcad and Pyroceram 45 with amylacetate and nitrocellulose; Pycerad 500 with liquid latex; and Interpace with water. After coating the tile faying surfaces with the desired thickness of adhesive, the two surfaces were placed together under slight pressure and fired to the adhesive maturing temperatures.

Numerous lap shear tests were made with different adhesive – segment combinations, to determine strength properties and the effects of bondline thickness, surface preparation, and firing conditions. Since these were screening tests, the following summarizations are considered adequate for report purposes:

1. Pyroceram 45. An average shear value of 4450 psi at room temperature and 4280 psi at 1000°F was obtained on 97.6% alumina, and very similar results were obtained on 99.5% alumina. Slightly lower values with a wider scatter were obtained with beryllia segments.

2. Pycerad 500. Joint strengths with 97.6% alumina ranged from 1420 psi to 4380 psi with a wide scatter and no significant difference at room temperature and 1000°F. Lower strengths were obtained with beryllia segments. It was also noted that joints prepared with this adhesive were sensitive to thermal shock failure, which indicated excessive thermal expansion differences between adhesive and bodies.

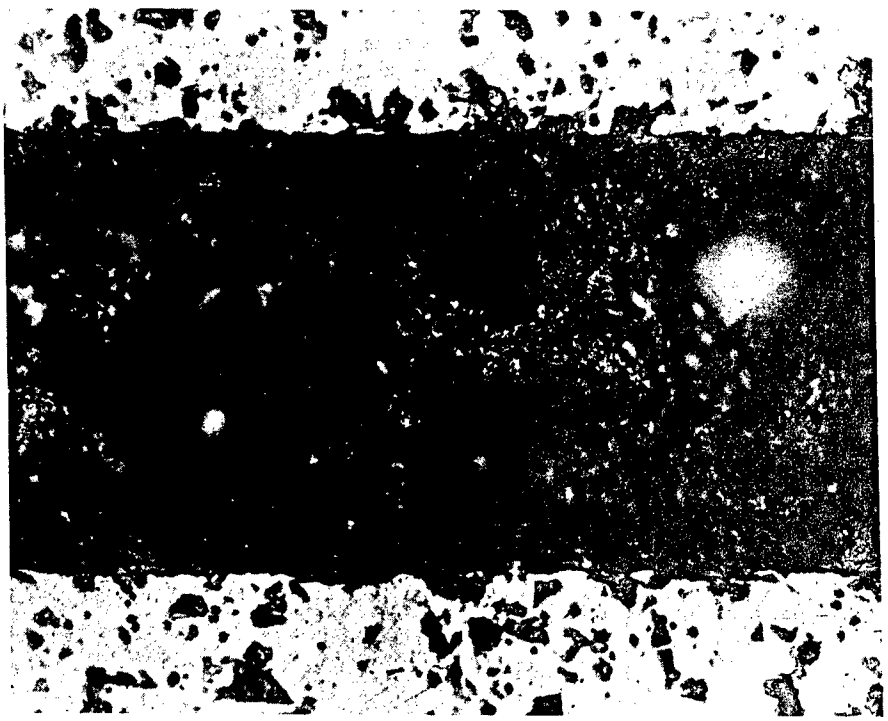


Figure 13. Photomicrograph of 97.6% Alumina Segments (light) Bonded with Interpace High-Temperature Adhesive. Dark spots in alumina are voids (Magnification 300X in reflected light)

3. Interpace High-Temperature Adhesive. This adhesive gave strengths ranging from 2430 psi to 8750 psi on 97.6% alumina. Other alumina and beryllia lap joints gave similar or higher values, and there was little or no loss of strength at 1000°F. The joint strength results obtained were more consistent than with the two previous adhesives.

4. Narmcad Adhesives. These adhesives gave consistently higher joint strengths with all alumina bodies than did the other adhesives; hence they received priority in this program. They also performed well with beryllia; however, at this point in the program, it appeared that alumina segments would be the tile material selected. Therefore, most of the Narmcad testing was done with alumina tile segments. The average room temperature lap shear strength of Narmcad 105 on 97.6% alumina was 6,120 psi and that of Narmcad 110 was above 10,000 psi.

The latter adhesive (Narmcad 110) was so markedly superior in strength that its selection for the radome application was indicated, providing its other properties were satisfactory.

Environmental Effects

Candidate adhesive-bonded specimens were then screened for their ability to withstand the effects of various environments such as moisture, fungus, and chemicals. The negligible water absorption of the promising bodies and adhesives, plus the known resistance of most such ceramic materials to water and chemicals to which they might be exposed in a radome application, indicated that this should not be a problem area; this was verified through tests. Glassy adhesives containing silicates are subject to solution by hydrofluoric acid while the alumina segments are more resistant. This was investigated in a qualitative manner since it offered a possibility of removing broken or partially bonded segments for repair of a mosaic radome structure. (The feasibility of this application was later demonstrated.)

Effects of Firing Conditions

Firing time and temperature variations were used to determine the applicability of the selected ceramic adhesives to these variables. As would be expected in the case of vitreous or glassy adhesives such as Interpace and the Narmcad 110 compositions, the firing range was wide. Sag tests and melting experiments with these glasses indicated that they had similar firing ranges, with approximately 1800°F being required for initial softening. Good fusion and wetting required a temperature of at least 2150°F for Narmcad 110 and one slightly higher for the Interpace adhesive. The viscosities of both are high, and reaction with alumina segments was not significant; thus, firing temperatures of 2350°F were considered to present no problems. The sag tests employed to determine adhesive softening temperatures consisted of observing the temperature at which a previously fired specimen (0.320 in. x 0.370 in. x 1.25 in.) sagged under its own weight when supported on alumina knife edges 1 in. apart. On the basis of numerous bonding experiments and tests, a normal firing temperature for the Narmcad 110 composition was selected as 2200°±50°F for at least 30 minutes.

Monolithic Sample Preparation

Solid specimens of the candidate adhesives were required for accomplishing various mechanical, physical, and electromagnetic tests. These were prepared by cold pressing the powdered frit adhesives then sintering them to zero porosity in graphite molds. The adhesive samples thus produced were then cut and ground into the following specimens for use in the indicated tests:

Test	Specimen Dimensions, in.
Sag Test (Softening Temperature)	0.320 x 0.370 x 1.25
Dielectric Constant and Loss Tangent	0.030 x 0.340 x 0.890 (all ±0.001)
Thermal Expansion	0.250 x 0.300 x 2.0
Others	As required

Electromagnetic Properties

Monolithic test specimens of the adhesive compositions were prepared as previously described and submitted to Melpar, Incorporated for dielectric constant and loss tangent determinations. These properties were measured at a frequency of 9.375 Gc at room temperature, 500°F, 1000°F, and 1200°F. The results of these tests are given in Tables 14 and 15 and Figures 14 and 15.

Electromagnetic data were also obtained on body – adhesive composite specimens to determine the effects of the adhesive bondlines on these properties. The specimens, 0.330 in. x 0.340 in. x 0.890 in., were cut from bonded segments so that two were available for each test: one with the bond surface perpendicular to the 0.340-in. side and the other parallel to this side.

The composite specimens were made up using the S1 alumina as the segment material, with samples made from each of the following adhesives: Pyroceram 45, Interpace, Narmcad 110, and Narmcad 120. The main objective was to determine the effect of a relatively high loss tangent material in the bondline on the overall property of the composite structure. In order to include all possibilities of the bondline position in actual use in a radome, samples were made to allow measuring loss tangent both perpendicular and parallel to the bondline.

Tables 16 and 17, and Figures 16 and 17 show the individual properties for composites made with each individual adhesive. Also shown are the average loss tangent and dielectric constant values for the S1 alumina segment material.

All adhesives gave values very similar to one another, regardless of prior results obtained on monolithic samples of these adhesives. The results from the Interpace and Narmcad 110 adhesives were quite encouraging in view of the very high loss tangent values that were measured on the monolithic samples for these two adhesives. Of the three adhesives used to make the

TABLE 14

DIELECTRIC CONSTANT DATA FOR ADHESIVE SPECIMENS

(Frequency 9.375 Gc)

Temp	Pycerad 500		Pyroceram 45		Interpace		Narmcad 110	Narmcad 120
	Specimen Code							
	A1-1	A1-2	A2-1	A2-2	A3-1	A3-2	A4-1	A5-1
RT	6.07	6.14	5.21	5.25	5.28	5.67	5.86	6.17
Avg	6.10		5.23		5.47			
500°F	6.04	6.07	5.29	5.33	5.83	6.23	6.21	6.49
Avg	6.05		5.31		6.03			
1000°F	6.10	6.14	5.57	5.58	6.52	6.94	6.79	7.14
Avg	6.12		5.57		6.73			
1200°F	6.25	6.27	5.73	5.73	6.52	6.80	6.93	7.16
Avg	6.26		5.73		6.66			
	% Increase with Temp							
To 500°F	-0.82		1.53		10.24		5.97	5.18
To 1000°F	0.33		6.50		23.04		15.88	15.70
To 1200°F	2.62		9.56		21.76		18.28	16.03

TABLE 15

LOSS TANGENT DATA FOR ADHESIVE SPECIMENS

(Frequency 9.375 Gc)

Temp	Pycerad 500		Pyroceram 45		Interpace		Narmcad 110	Narmcad 120
	Specimen Code							
	A1-1	A1-2	A2-1	A2-2	A3-1	A3-2	A4-1	A5-1
RT	0.0078	0.0021	0.0029	0.0049	0.0204	0.0220	0.0154	0.0135
Avg	0.0049		0.0039		0.0212			
500°F	0.0096	0.0022	0.0025	0.0057	0.0414	0.0421	0.0346	0.0269
Avg	0.0059		0.0041		0.0418			
1000°F	0.0112	0.0047	0.0023	0.0044	0.1275	0.1282	0.0815	0.0704
Avg	0.0079		0.0033		0.1328			
1200°F	0.0126	0.0118	0.0024	0.0044	0.2508	0.2807	0.2360	0.2646
Avg	0.0122		0.0034		0.2657			

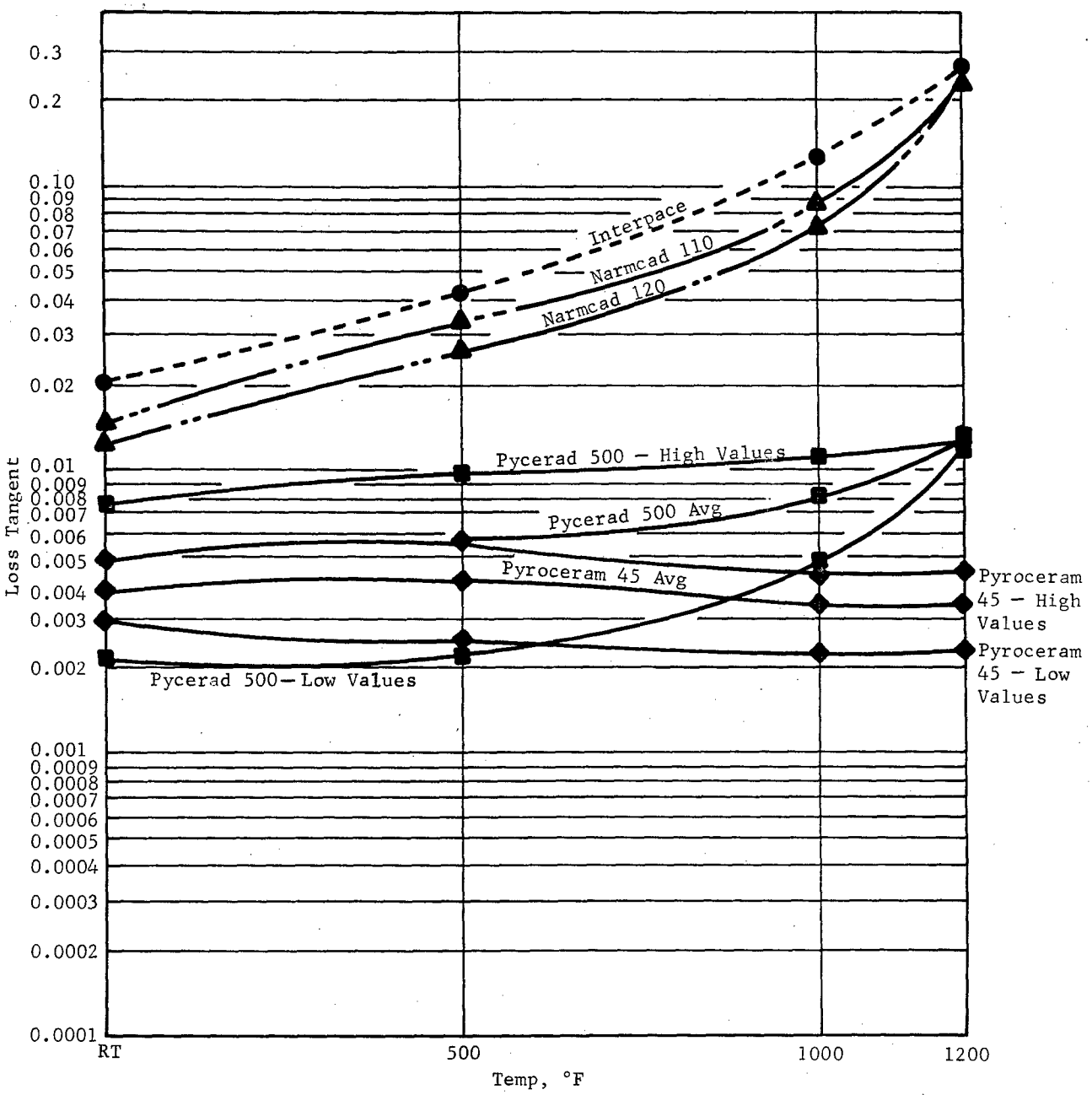


Figure 14. Adhesives — Loss Tangent vs Temperature at 9.375 Gc

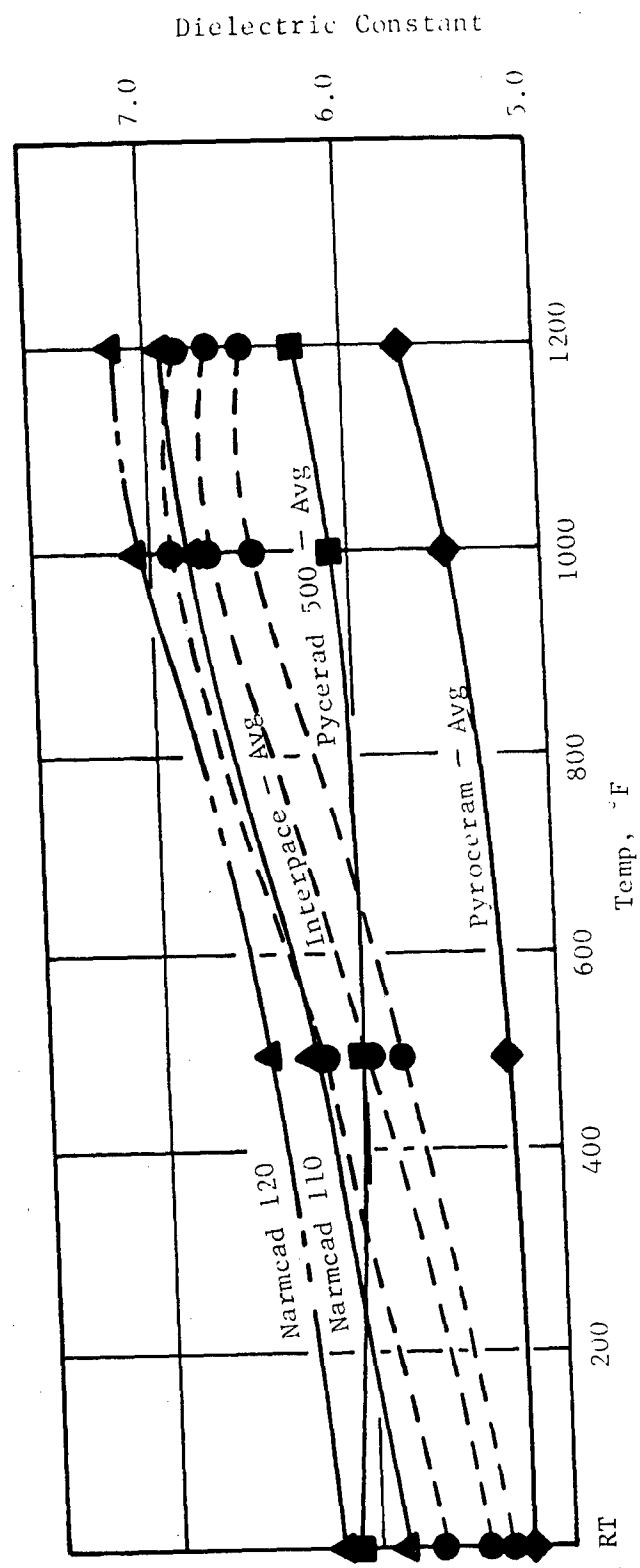


Figure 15. Adhesives — Dielectric Constant vs Temperature at 9.375 Gc

TABLE 16

DIELECTRIC CONSTANT FOR COMPOSITE SAMPLES
97.6% ALUMINA SEGMENTS AND ADHESIVES

(Frequency, 0.375 Gc; Measured Perpendicular
and Parallel to Bondline)

Temp, °F	S1 Alumina Dielectric Constant	Pyroceram 45		Interpace		Narmcad 110	
		Dielectric Constant					
		S1A2-1 Perpendicular	S1A2-2 Parallel	S1A3-1 Perpendicular	S1A3-2 Parallel	S1A4-1 Perpendicular	S1A4-2 Parallel
RT	8.24	8.25	8.42	8.38	8.37	8.26	8.30
500	8.42	8.41	8.67	8.56	8.54	8.41	8.44
1000	8.72	8.71	8.92	8.88	8.84	8.70	8.76
1200	8.82	8.85	9.07	9.00	8.97	8.81	8.89

TABLE 17

LOSS TANGENT DATA FOR COMPOSITE SAMPLES
97.6% ALUMINA SEGMENTS AND ADHESIVES

(Frequency, 9.375 Gc; Measured Perpendicular and Parallel to Bondline)

Temp, °F	S1 Alumina Loss Tangent	Pyroceram 45		Interpace		Narmcad 110	
		Loss Tangent					
		S1A2-1 Perpendicular	S1A2-2 Parallel	S1A3-1 Perpendicular	S1A3-2 Parallel	S1A4-1 Perpendicular	S1A4-2 Parallel
RT	0.0007	0.0005	0.0007	0.0009	0.0008	0.0009	0.0012
500	0.0015	0.0009	0.0011	0.0015	0.0013	0.0015	0.0019
1000	0.0025	0.0015	0.0017	0.0034	0.0029	0.0032	0.0045
1200	0.00345	0.0020	0.0025	0.0049	0.0041	0.0048	0.0068

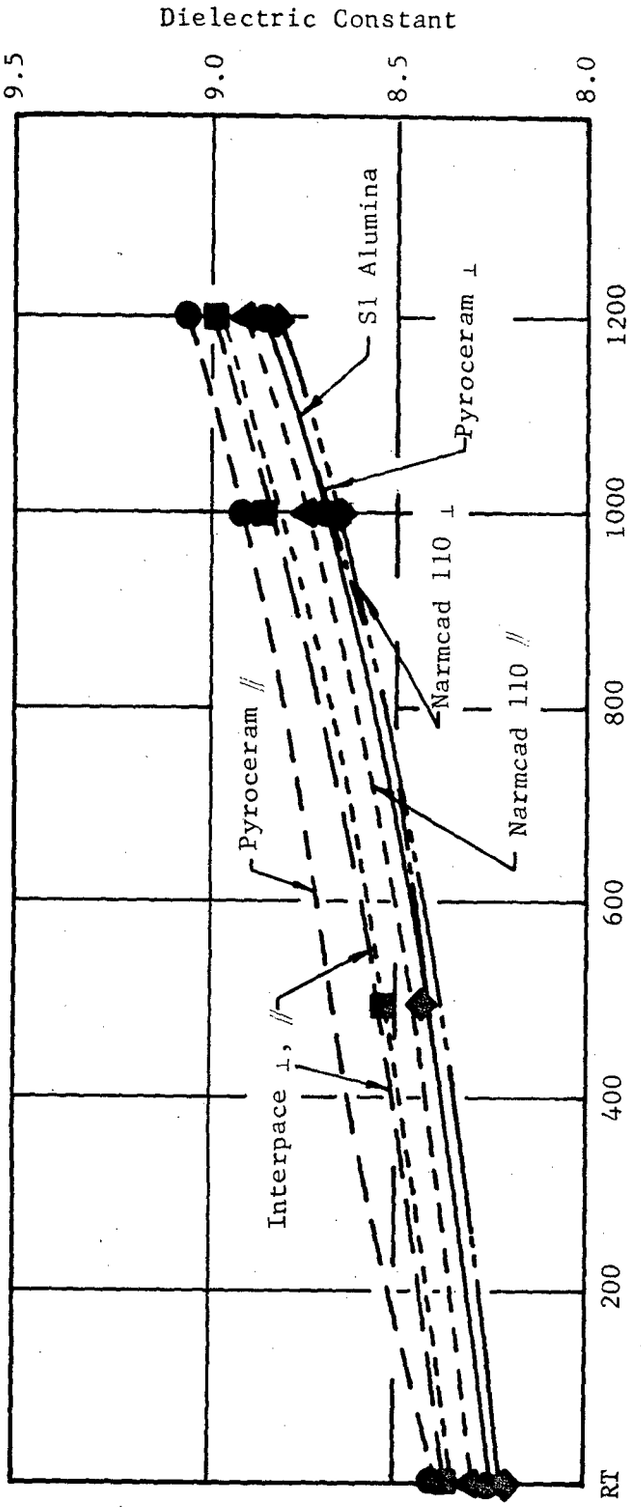


Figure 16. Dielectric Constant vs Temperature at 9.375 Gc for Composite Samples and S1 Alumina Segment

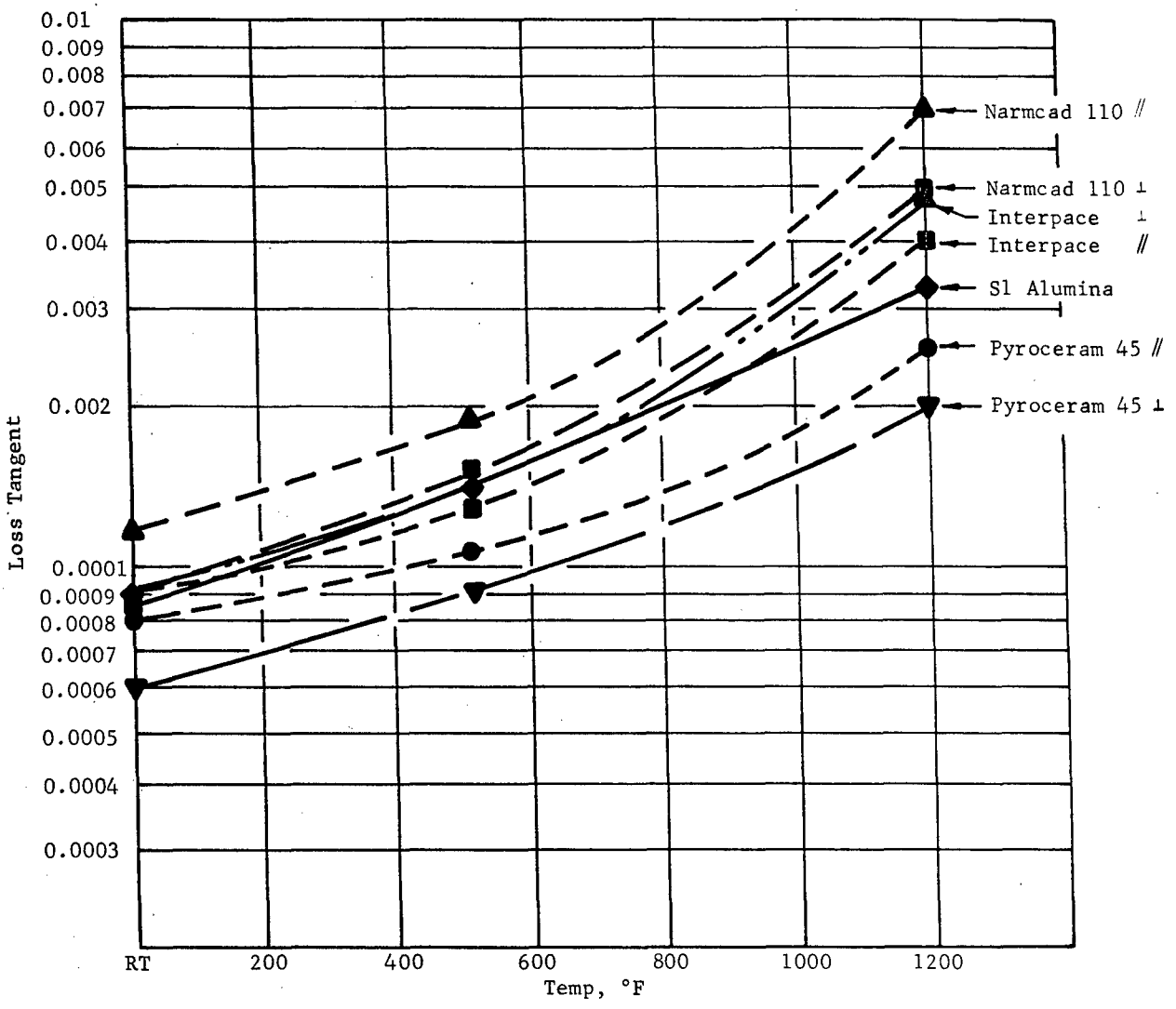


Figure 17. Loss Tangent vs Temperature at 9.375 Gc for Composite Samples and S1 Alumina Segment

composite samples, only the Narmcad 110 showed any significant change in loss tangent with change in the position of the bondline. Higher loss tangent values for the Narmcad composite were obtained when tested parallel to the bondline, indicating the possibility of a definite maximum bondline thickness at which the loss tangent would be detrimental. Since the loss tangent values obtained for all composite samples were well within the program goals of 0.005 at room temperature and 0.010 at 1000°F, it was believed that this would not be a problem in actual radome construction. In addition, it was not anticipated that bondline thickness in an actual mosaic radome would be much greater than the 5-7 mil bondline employed in these composite test samples. While the composite samples made with the Pyroceram 45 adhesive measured lower in loss tangent than the actual segment values, this was not believed to be significant, as it was probably due to segment compositional variance rather than the effect of the adhesive.

The effects of the adhesives on the dielectric constant of the bondline were all quite similar, and closely matched that of the segment material. It was thought that the relatively high percentage increase of dielectric constant with temperature exhibited by monolithic samples of the Interpace and Narmcad 110 adhesives (16%-23% at 1000°F) might be detrimental when used in a composite structure. However, the results showed that all composite samples had dielectric constant increases similar to each other and also to the base segment material itself. Table 18 shows the percent increase in dielectric constant, from room temperature to 1000°F and 1200°F, for each composite samples as well as for the S1 alumina segment material.

TABLE 18

DIELECTRIC CONSTANT INCREASE WITH TEMPERATURE

Specimen	% Dielectric Constant Increase	
	1000°F	1200°F
S1 Alumina	5.82	7.04
Pyroceram 45 (Measured Perpendicular)	5.58	7.27
Pyroceram 45 (Measured Parallel)	5.93	7.71
Interpace (Measured Perpendicular)	5.98	7.41
Interpace (Measured Parallel)	5.62	7.18
Narmcad 110 (Measured Perpendicular)	5.33	6.66
Narmcad 110 (Measured Parallel)	5.54	7.12

Thermal Expansion

Thermal expansion properties of the adhesive candidate materials was determined in a standard fused quartz dilatometer using the previously described sintered or cast specimens. The results are plotted in Figures 18 through 21. These results showed that the Pycerad 500 and the Pyroceram 45

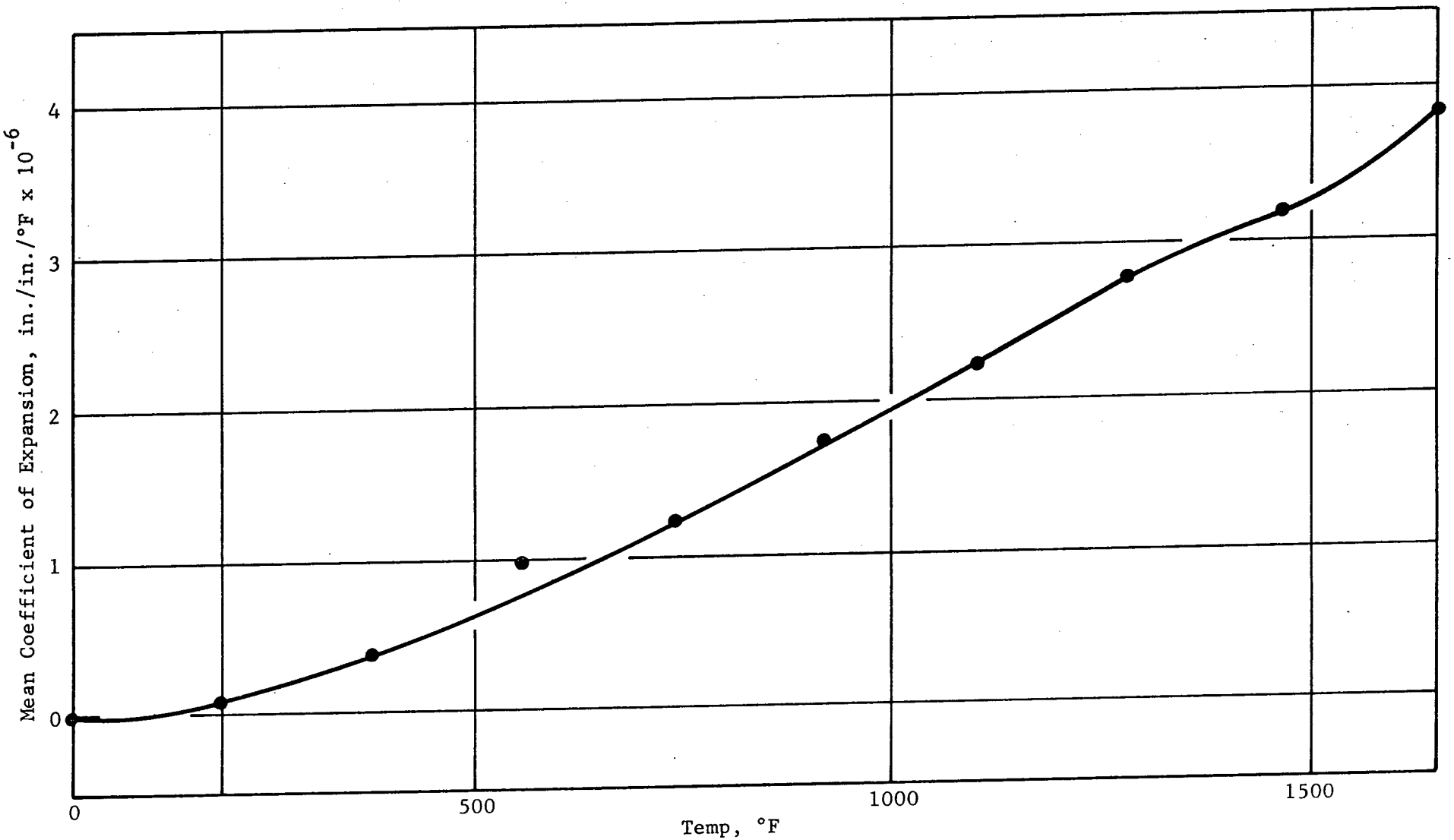


Figure 18. Mean Coefficient of Thermal Expansion vs Temperature from Room Temperature (80°F) for Pycerad 500 Adhesive

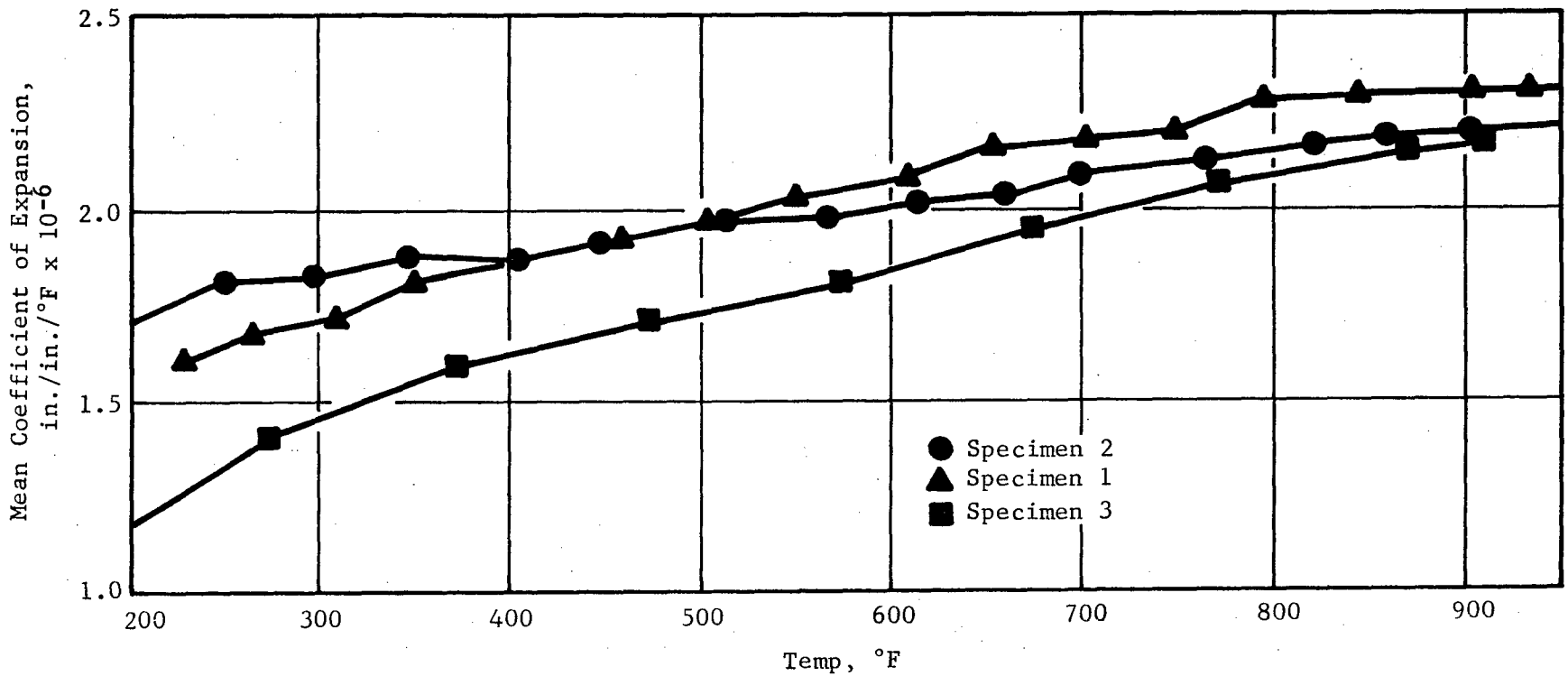


Figure 19. Mean Coefficient of Thermal Expansion vs Temperature from Room Temperature (80°F) for Pyroceram 45 Cast Adhesive

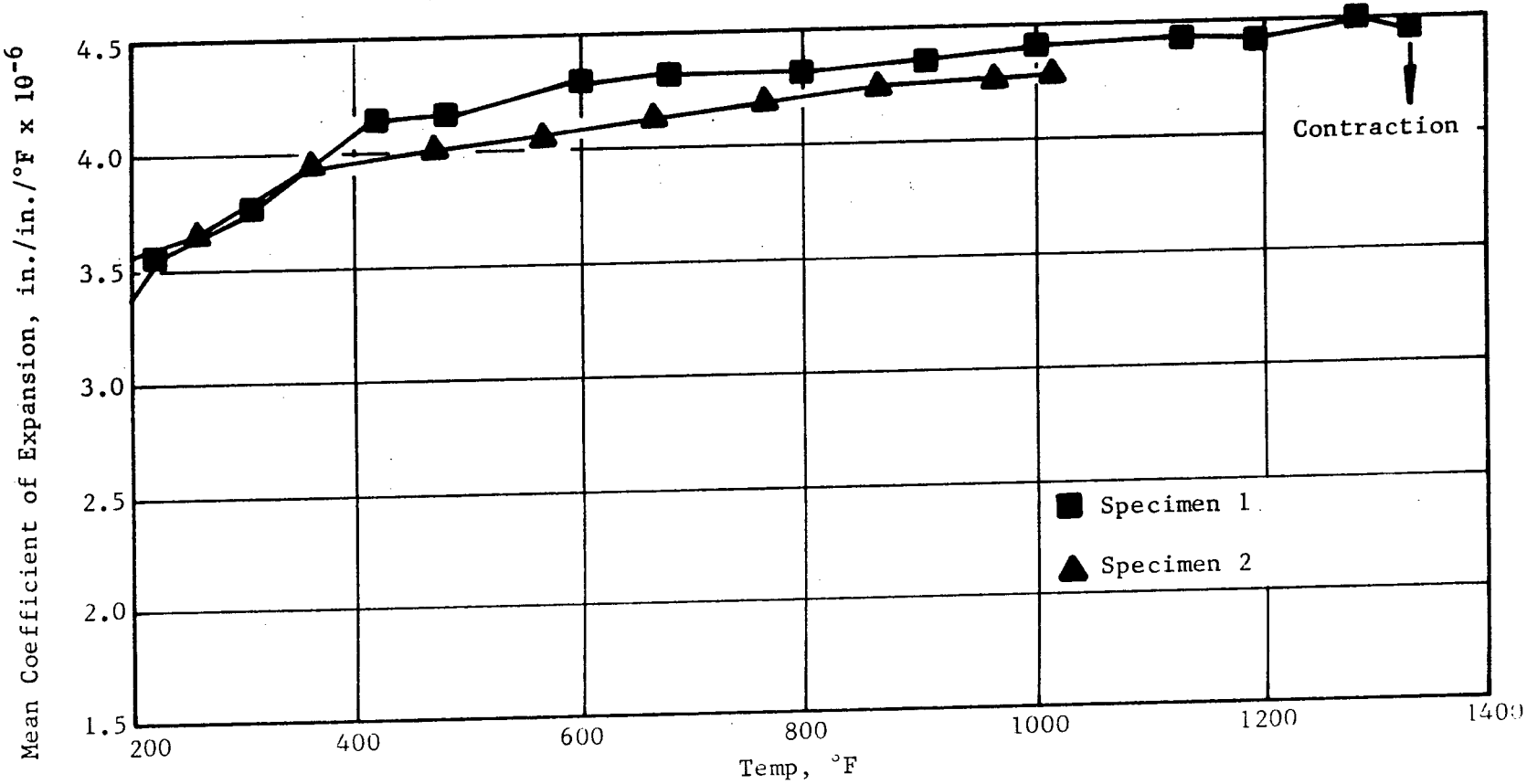


Figure 20. Mean Coefficient of Thermal Expansion vs Temperature from Room Temperature (84°F) for Interpace Cast Adhesive

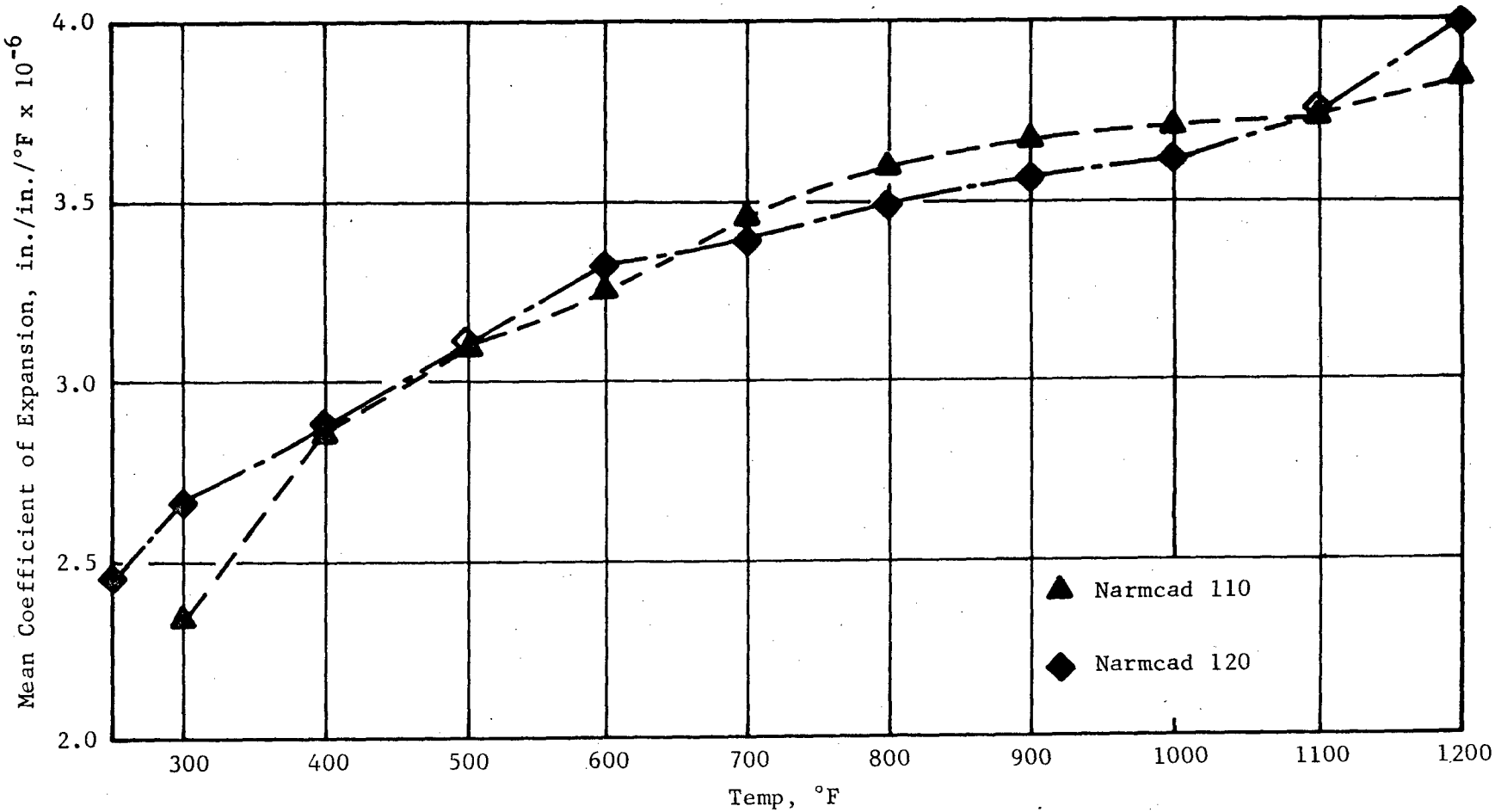


Figure 21. Mean Coefficient of Thermal Expansion vs Temperature from Room Temperature (80°F) for Narmcad 110 and 120

adhesives exhibit coefficients of thermal expansion appreciably lower than that of the alumina tile materials; therefore, they were not considered suitable for this application. On the other hand, the expansion of both the Interpace and the Narmcad adhesives closely approximated that of alumina and was considered to be more suitable for this radome fabrication.

COMPOSITE CERAMIC TECHNIQUE DEVELOPMENT

The conclusion derived from the foregoing work on candidate segment materials and adhesives for the composite ceramic radome application was that 97%-99% purity alumina tile segments and Narmcad 110 ceramic adhesive were the logical choices.

The next step, then, was to develop techniques and the know-how for utilizing these materials in the fabrication of close-tolerance composite mosaic structures.

Flat Panel Fabrication

An overall size of 16 in. x 16 in. was chosen for the flat panel that would utilize S1 4-in. x 4-in. alumina tiles, in keeping with the contemplated segment size. The approach taken utilized a staggered, double-layer configuration with butt joints. Tiles were ordered 0.108 in. thick to allow the double layer with included adhesive to meet the thickness requirements of a half-wave wall radome. All the 97.6% alumina tiles were ordered and received having a tolerance of ±0.001 in. for the 0.108-in. x 4.00-in. x 4.00-in. size required. The actual pattern of the double-layered panel was as shown in Figure 22. In addition to the 4-in. x 4-in. tiles, several were cut to 1 in. x 2 in. x 3 in., or 2 in. x 4 in. (all ±0.001 in.), to allow proper staggering of all adhesive joints.

Glasrock castable, a fused-silica refractory cement, was chosen as the mold material for firing the panel as a result of Narmco's investigations of the various castable candidates for possible tooling mandrels and fixtures for production of ceramic mosaic radomes. The low expansion of this material serves the requirement for a thermal expansion differential between the tool and bonded segments, causing closing of bondlines to a predetermined thickness. Since a mosaic radome in production would be fired in a vertical position, the design of the mold was made to allow simulation of the anticipated firing condition while still allowing simple layup procedures to be employed. The firing mold for the flat panels consisted of three parts: a female section for laying-up the segments into the desired panel; a male part to hold the parts in alignment; and a sleeve into which the tapered, assembled male and female portions were placed to allow firing in a vertical position. Figure 23 shows the dimensions of the various mold parts while Figure 24 illustrates the final parts after casting and curing. The overall area of the mold was made larger than the desired panel so that controlled burnout shims could be used in attempting to control the bondline thickness.

The adhesive employed for bonding was Narmcad 110. Preparation of this glassy-type adhesive for application to the 97.6% alumina tiles was accomplished by grinding the prepared mix to a -325 mesh particle size, and blending

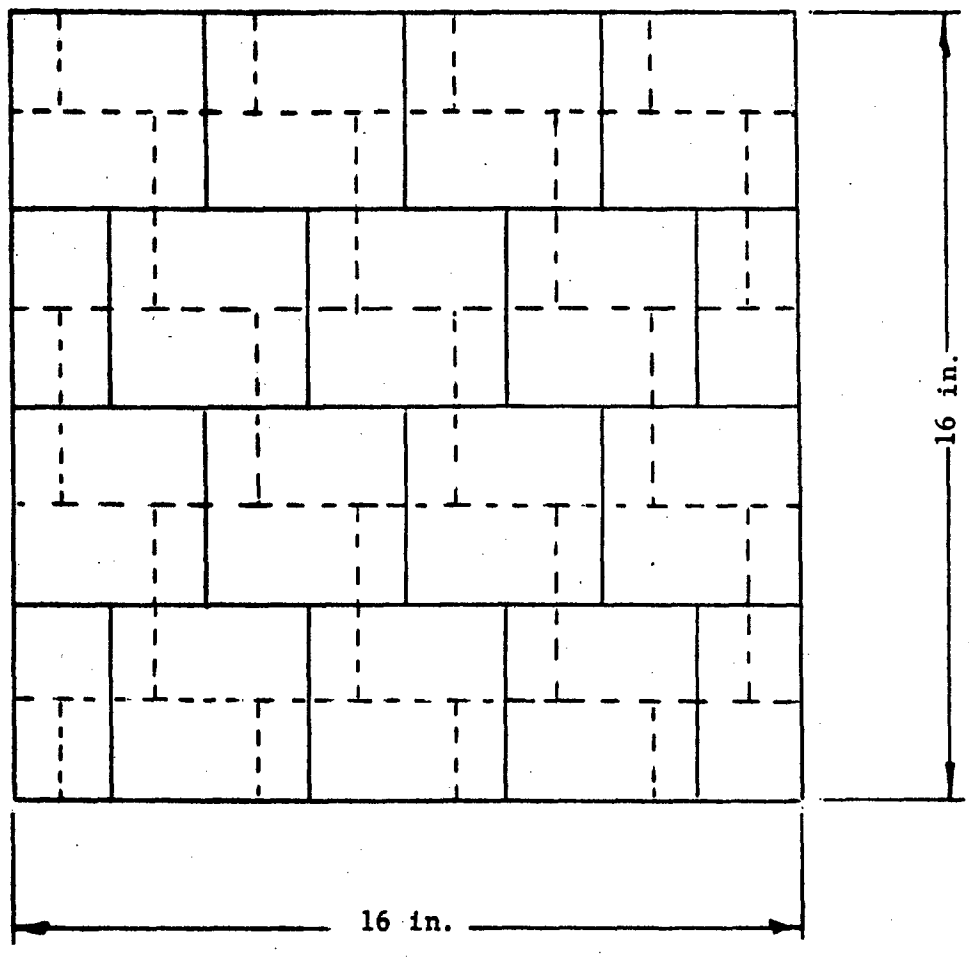


Figure 22. Segment Pattern for Flat Mosaic Panels

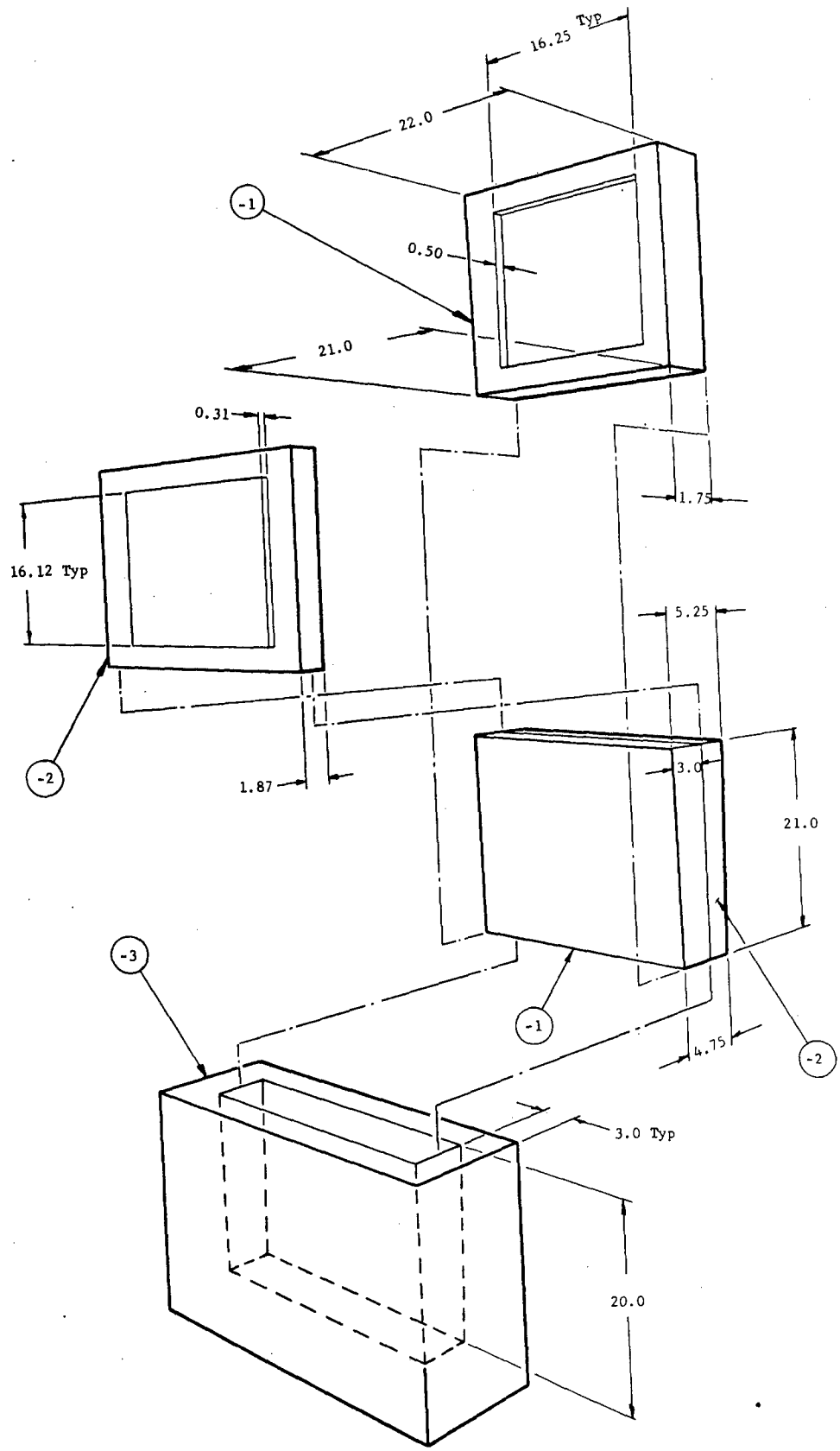
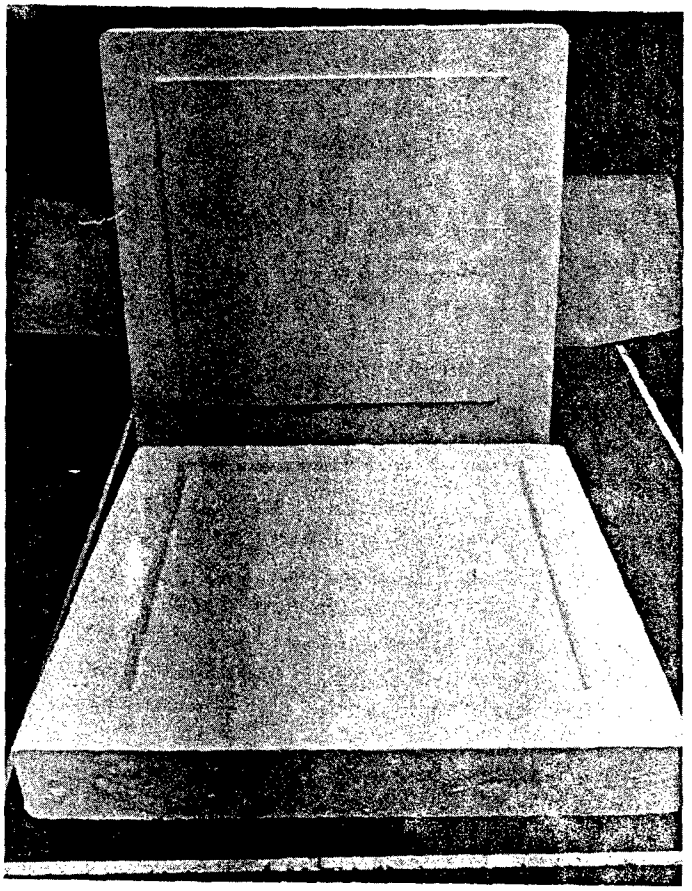
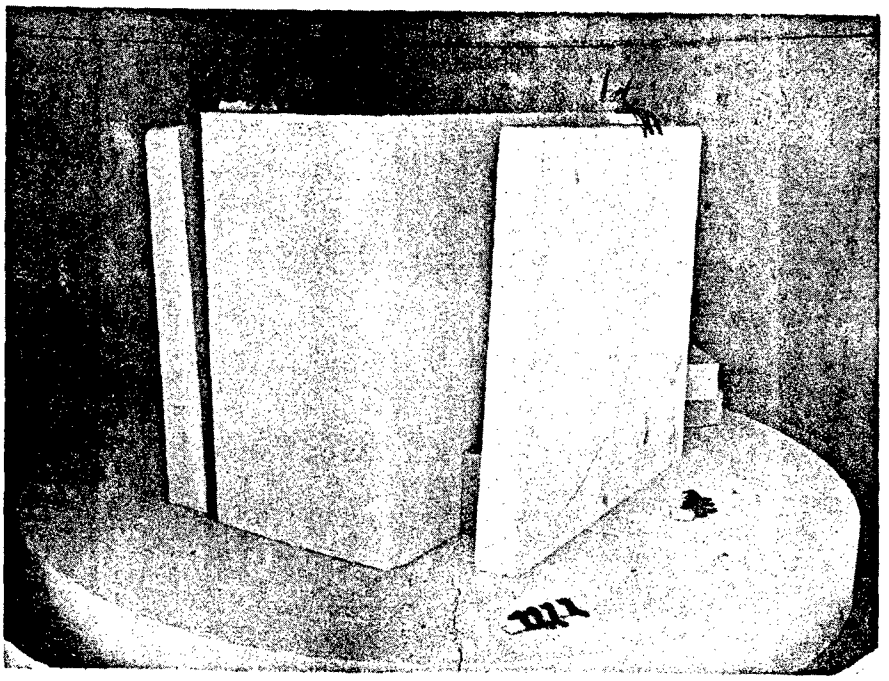


Figure 23. Flat Panel Holding Tool and Sleeve



(a)



(b)

Figure 24. Flat Panel Firing Fixture

with a nitrocellulose solution to a consistency suitable for spraying. The approximate solids content of the prepared adhesive slurry was 40%-45%. A Binks Model 18V spray gun was employed for spraying the adhesive onto the tiles. All alumina tiles were ultrasonically cleaned prior to spraying.

After air drying, the spray-coated alumina tiles could be handled without the adhesive flaking or rubbing off. It is apparent that the use of nitrocellulose as a temporary bond for the inorganic Narmcad adhesive facilitates handling and assembly of a production-size mosaic radome.

Flat Panel A

A 6-8 mil thick coating was sprayed onto the faces and edges of the individual tiles. When butted together, the total unfired bondline adhesive thickness was 12-16 mils. The mold faces in contact with the tiles and each other were coated with a 5-mil layer of boron nitride powder prior to the lay-up of the tiles. Narmco's preliminary studies indicated that boron nitride showed promise as a parting agent for the Narmcad adhesive and prevented seizure of the alumina tile to the fused silica castable.

The first layer of coated tiles was laid up horizontally in the female mold with the adhesive face of the tiles pointing upward. The second layer was than placed with the adhesive face of the tiles positioned downward so that adjacent adhesive faces were in contact with each other. The tiles were placed according to the desired pattern, with two of the outside edges of the formed panel in contact with the sides of the female mold. The remaining two gaps between the edges of the panel and mold were taken up with a burnout shim thickness, calculated for closing bondlines to a predetermined thickness, and with a liquid castable fused-silica slip. The actual arrangement is depicted in Figure 25. The shims were made of wood to allow burning-out, and formed the desired gap that would account for the differential expansion between the tiles and mold wall. The shim thickness used for this particular experiment was calculated from the following analysis:

Linear Thermal Expansion Coefficient of Alumina and Adhesive Composites	$\approx 4.3 \times 10^{-6}/°F$
Linear Thermal Expansion of Coefficient of Glasrock Mold	$\approx 0.3 \times 10^{-6}/°F$
Differential Thermal Expansion Coefficient α	$\approx 4.0 \times 10^{-6}/°F$

The change in length of the 16-in. panel length can then be calculated from the following formula:

$$L_t = L_o(1 + \alpha\Delta T)$$

where L_t = length of part at firing temperature
L_o = length of part at room temperature
α = thermal expansion differential
ΔT = firing temperature minus room temperature

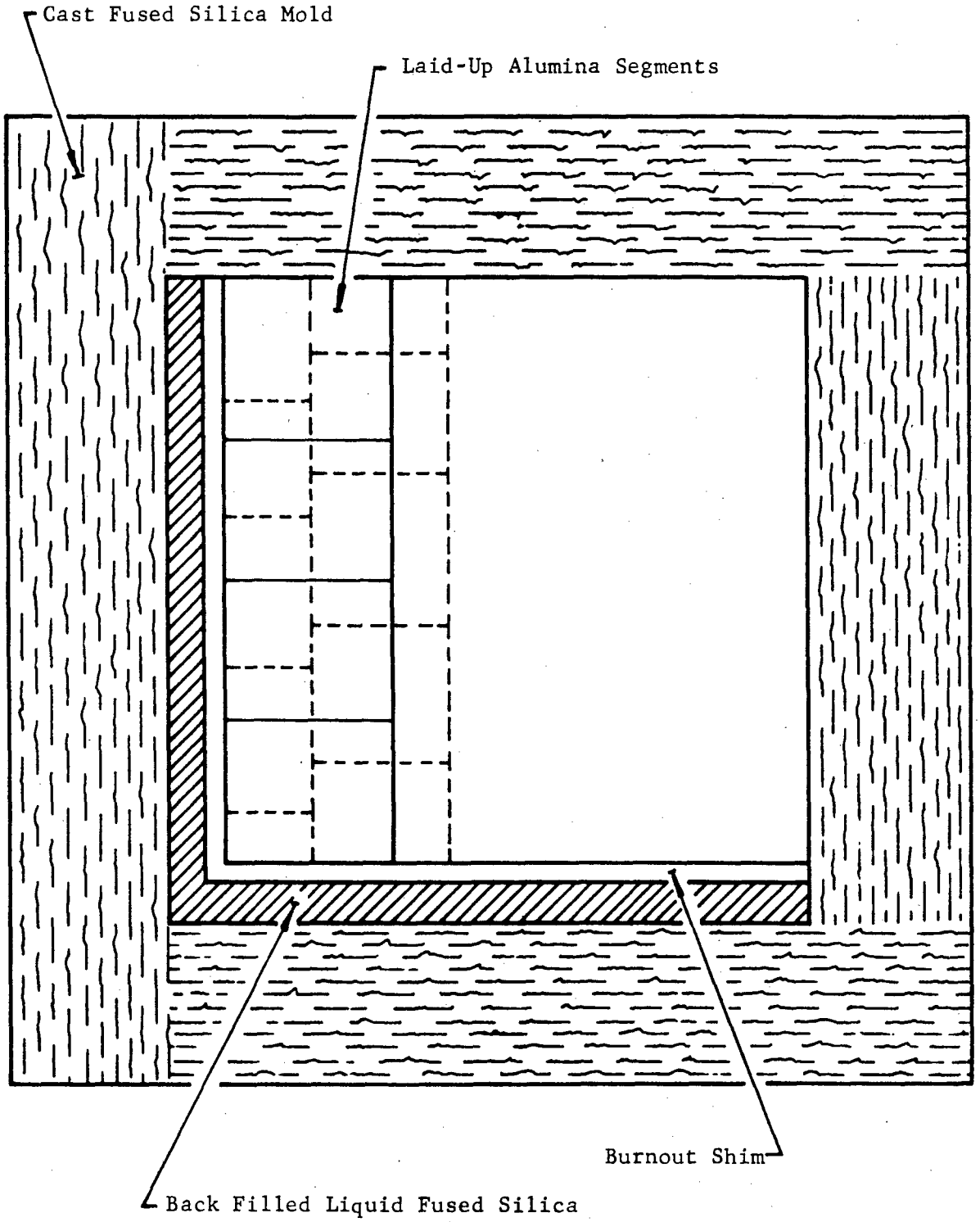


Figure 25. Top View of Shim Position with Respect to Alumina Segments and Mold

Assuming a firing temperature of 2250°F,

$$L_t = 16(1 + 4.0 \times 10^{-6} \times 2170°F)$$

$$= 16.138 \text{ in.} \quad \text{or increase in length} = 0.138 \text{ in.}$$

If the joints are to be closed to a bondline thickness of 0.006 in., the total amount to be closed will be four joints x 0.006 in. = 0.024 in. Therefore, the shim thickness desired would be

$$\begin{array}{r} 0.138 \text{ in.} \\ \underline{- \ 0.024 \text{ in.}} \\ 0.114 \text{ in.} \end{array}$$

If bondlines were closed flushed (total unfired bondline separation = 0.012 in.), then total thickness would be four joints x 0.012 in. = 0.048 in., or

$$\begin{array}{r} 0.138 \text{ in.} \\ \underline{- \ 0.048 \text{ in.}} \\ 0.090 \text{ in.} \end{array}$$

An arbitrary closing of between 0.006 and 0.012 in. per joint was assumed. This required a shim of approximately 0.100 in. This was the shim thickness used in the first firing and was machined from wood to 0.100 ±0.005 in.

After the tiles were positioned and the shims incorporated, the male lid was placed in position, and the entire assembly slipped into the fused silica sleeve. Again, a coating of boron nitride powder was used on the exterior surfaces of the mold parts and inside the sleeve to facilitate positioning and removal of the fixture. The complete tooling fixture was then loaded into the furnace in a vertical position to simulate conditions anticipated during firing of a mosaic radome.

Firing of the part was monitored by thermocouples and pyrometric cones. Although a thermocouple was located at the midpoint of the interior of the male mold portion, this thermocouple broke during the run, and only exterior firing temperatures were recorded beyond this point. Pyrometric cones were employed to determine the combined effects of temperature and time (sometimes called "heat work" in the firing of ceramics). These indicate the progress of firing, through the use of a series of cones, and are observed during firing. In addition, cones can be used to determine the degree of uniformity of firing treatment in various sections of the furnace through the use of a number of suitably located plaques of cones. They also provide a means to qualitatively check the thermocouple calibration.

Figure 26 is a graph of the firing curve employed during this particular run. The dotted line is an extrapolation of the inside temperature of the mold, or expected part temperature. The furnace was shut off when the extrapolated curve reached a temperature of 2300°F. At this point, the furnace

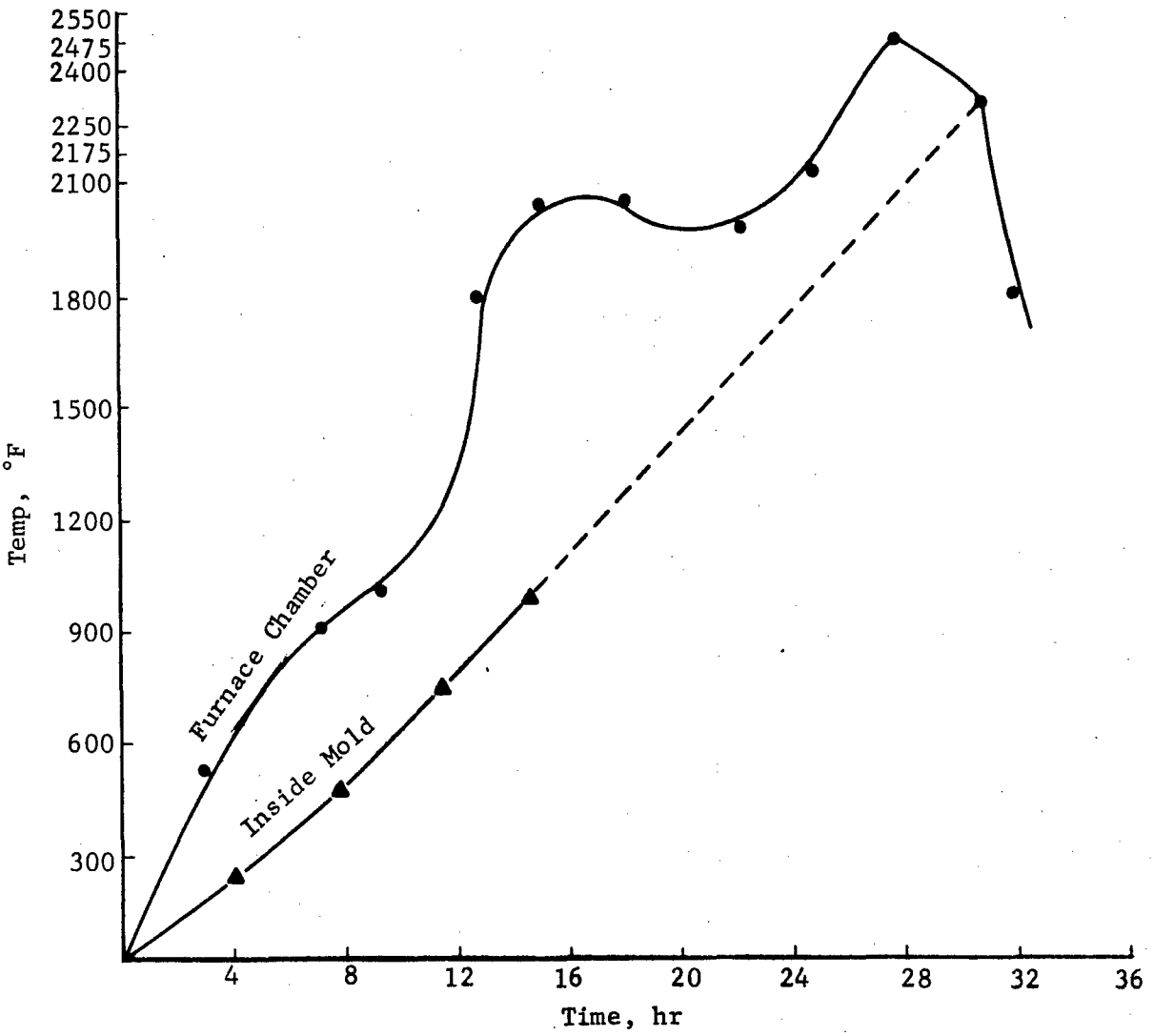


Figure 26. Firing Curves for Panel A

chamber temperature had been above 2250°F to 2300°F for a 5-6 hour period. No attempt was made to control the cooling rate, as the relatively large mass of the fused silica firing tool was considered sufficient to control slow cooling of the part due to this material's low thermal conductivity.

The male and female portions of the mold were removed from the sleeve after it was cooled to room temperature. Removing the inner portions from the sleeve was difficult, however, and mechanical force had to be exerted by tapping the mold through a "knock-out" hole located in the bottom of the sleeve. This difficulty was caused by corners of the mold adhering to the bottom of the sleeve. This may have been due to oxidation of the boron nitride to boron oxide and formation of a glassy phase. Figure 27 shows the panel as it appeared upon removal from the mold. The panel was cracked into three parts. Slight adherence to the fixture was noted along the edges, the faces being free from seizure. Examination of the faces of the mold revealed that the male portion was not quite flat but slightly concave after firing. It is not known whether the observed cracks in the panel were from adherence of the part to the mold or from a bending moment existing from the combination of the mechanical blows required to free the sleeve and the concave mold surface. However, as will be discussed on page 63, bonding to the mold was probably the main cause of the cracking. Upon cooling, the part was not free to contract and failed under tension. A close-up of the cracked zone is shown in Figure 28.

Except for the previously described cracks, the individual tiles were satisfactorily aligned and bonded together. The panel was flat and free from warpage. All tiles were evidently well bonded, with the adhesive showing its usual good wetting characteristics. As a control procedure, several lap shear samples were prepared and fired simultaneously in the gas-fired furnace. These specimens compared favorably with previous test specimens utilizing Narmcad adhesive. The tiles within the individual layers were well aligned, but some misalignment of the layers was noted. Edges extended approximately 0.020-0.030 in. beyond one another. This condition may have been caused by adherence of individual layers to the side of the mold, or by faulty positioning of shims and inadequate back filling of the void space with castable during the layup process. Another condition noted was that a few bondlines were relatively large, probably due to the slight seizure of the part to the mold, which prevented contraction of the joints during the cooling period. These particular joints are described later on.

Examination of the individual joints showed that the shim thickness used for control of the pressure was too small, since bondlines were thinner than the desired 0.006 in. Bondlines were examined and measured both optically and by a dimensional analysis of the final bonded panel. A study of the diagrams in Figure 29 will simplify discussion of the various dimensions. Figure 29(a) shows the various tiles and their position in the first layer, while Figure 29(b) shows the second layer of tiles which are superimposed in the bonded panel over the first layer. The spaces between segments show the bondline thicknesses between each tile prior to firing. The dimensions marked B are the cumulative length dimensions of the individual tiles without adhesive, prior to firing, while those marked A were the overall dimensions of the layers after firing and include the adhesive bondline thickness. By subtracting the two dimensions and dividing by the number of joints, an approximation of the average bondline's width can be made. These results are also indicated in the diagrams in Figure 29. As mentioned previously, several joints were

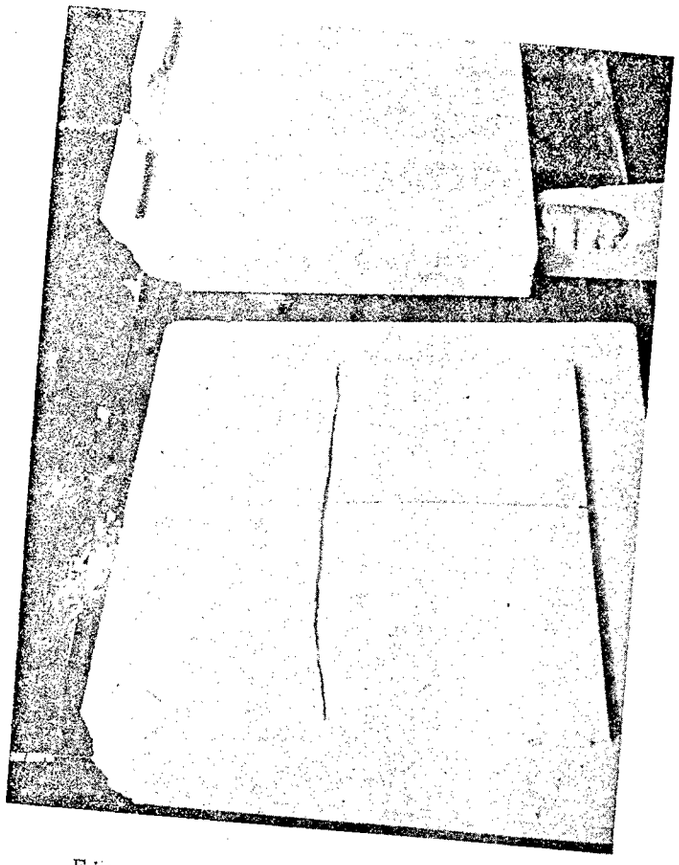


Figure 27. Flat Panel Fracture

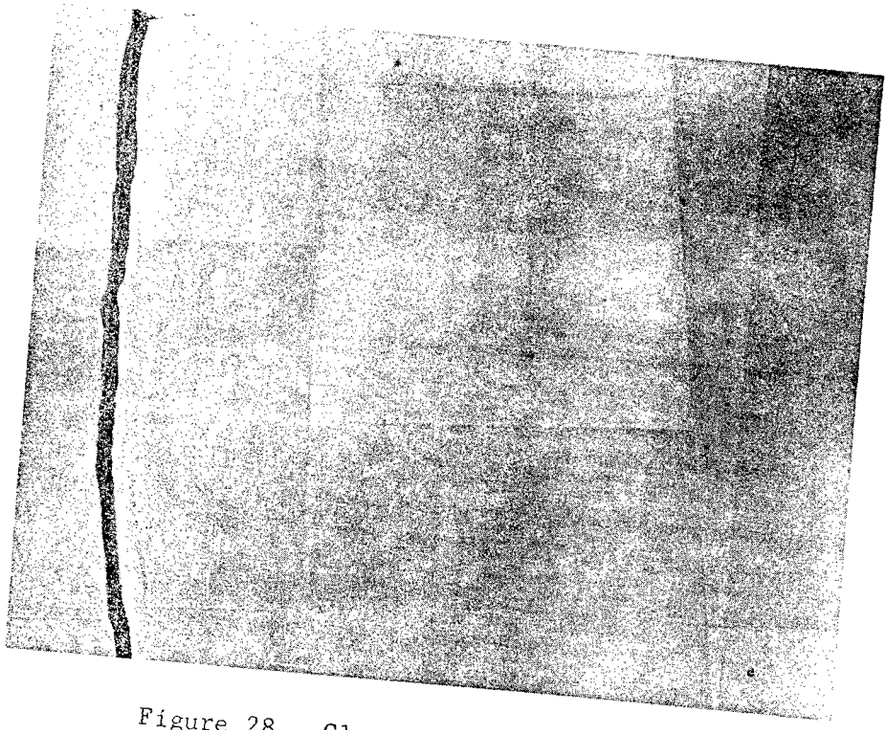
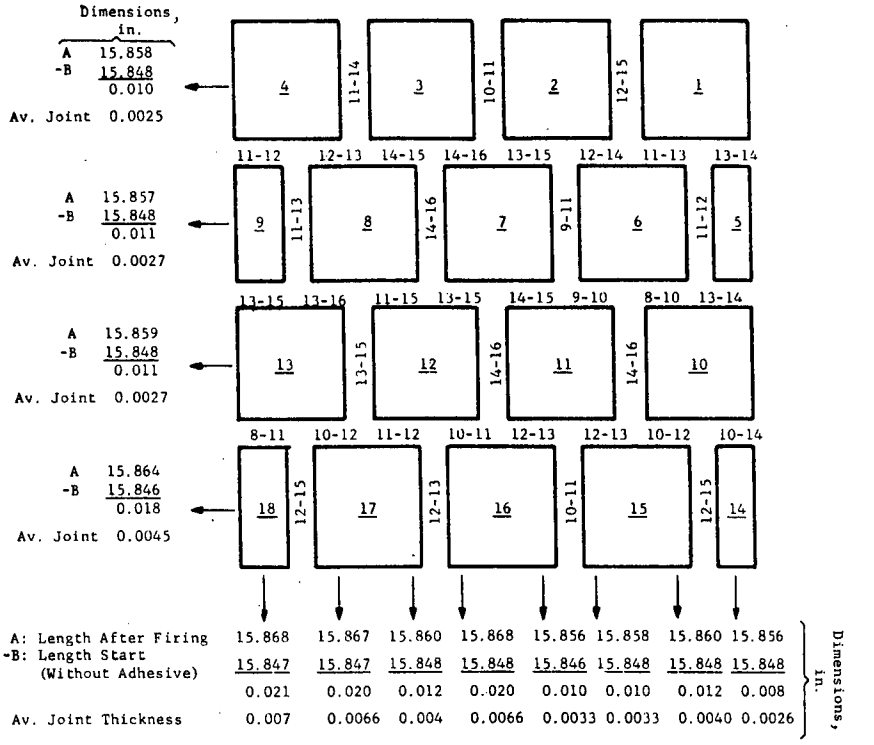
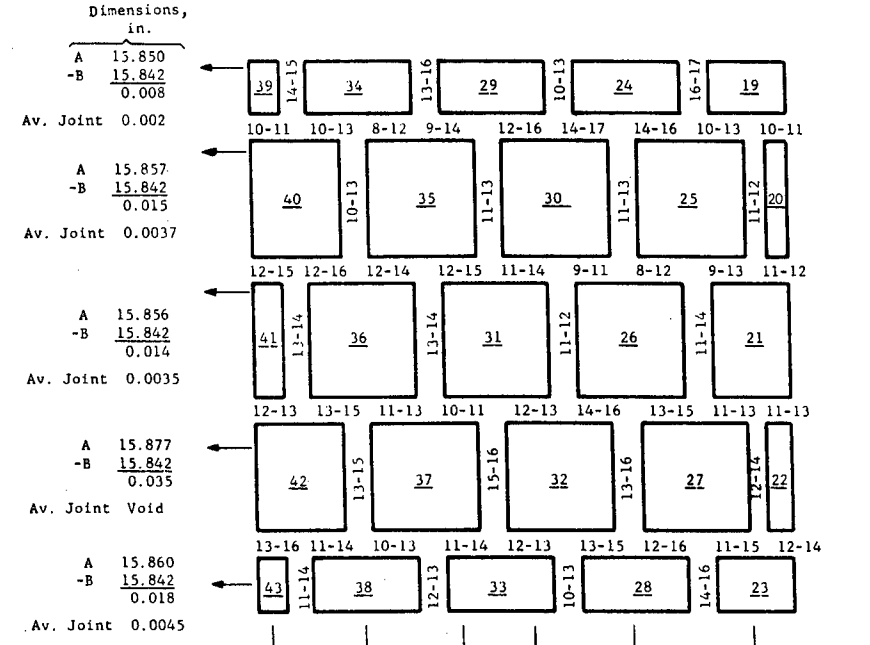


Figure 28. Close-Up of Cracked Zone



(a) First Layer



(b) Second Layer

NOTE: All measurements given between segments are in mils.

Figure 29. Dimensions of Panel A

relatively large, and dimensions including these joints would show a relatively large average bondline thickness. The joints which were relatively wide existed between the following numbered tiles:

8-13
9-13
34-40
39-40
35-36
41-42
22-27

The average bondline thickness, excluding the oversized joints, varied approximately from 0.002 in. to 0.004 in.

A number of individual joints were examined microscopically and the bondline thickness measured. The measured values for the different joint locations are listed below:

Joint	Bondline Width, in.
7-8	0.0004 - 0.0006
8-9	0.0012
8-12	0.0006
7-12	0.0012 - 0.0014
12-16	0.0006 - 0.0008
12-17	0.0006 - 0.0008
16-17	0.0012
17-18	0.0012
36-37	0.0016
37-42	0.0004 - 0.0006
37-38	0.0008
31-36	0.0027 - 0.0030
33-38	0.0008
31-37	0.001 - 0.0012

These measurements revealed that many of the bondlines were very thin, indicating excessive pressure from the firing tool. However, microscopic examinations showed that the thickness within an individual joint was quite uniform. Figure 30 is a photomicrograph of a representative joint between two of the alumina tiles.

Panel thickness after firing ranged from 0.222 in. to 0.226 in., with the average thickness calculated as 0.224 in. Therefore, based on the original 0.108 ±0.001 in. thickness of the alumina tiles, the interlayer bondline thickness was approximately 7 to 10 mils with an average thickness of 8 mils.

Flat Panel B

The second panel was of the same general construction as described for Panel A; however this panel was to be fired in a horizontal position in an attempt to promote more bonding between layers. Therefore, only the male and female portions of the silica mold were used, and the sleeve was eliminated. the S1 alumina tiles were coated with Narmcad adhesive as previously discussed, with coating thicknesses similar to those for Panel A.

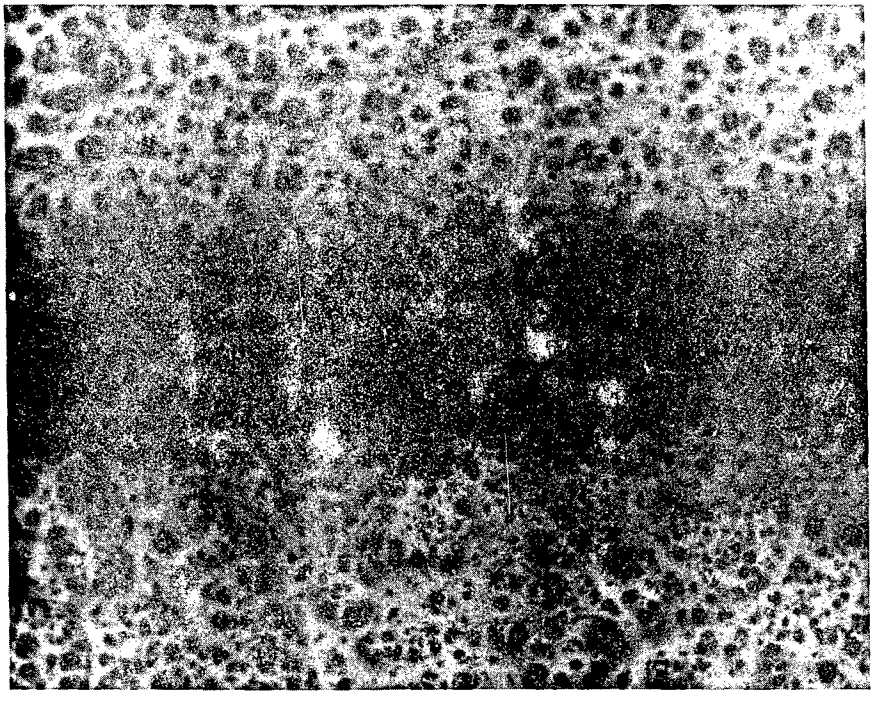


Figure 30. Photomicrograph of Typical Joint
(Magnification 150X)

The major difference in the layup procedure was that a thicker shim was used to increase the average bondline width of the fired panel. The burnout shim employed in Panel B measured approximately 0.122 in. This constituted an increase of approximately 0.020 in., which theoretically would increase each joint by approximately 0.005 in. from that obtained for bondlines in Panel A. Another change from the first panel was that graphite cloth was used on the top surface of the panel; i.e., between the top panel and the lid of the mold. It was believed that a resilient member such as graphite cloth would transmit pressure uniformly during the firing cycle. Previous experiments on parting agents had shown graphite cloth to be satisfactory when protected from oxidation.

The bottom portion of the mold was coated again, with boron nitride as a parting agent, as were the entire faces of the mold including that portion in contact with the graphite cloth. To prevent excess graphite oxidation, a dead air space was created by sealing the mold halves with Fiberfrax (mullite) batting. Temperature measurement of the part was made with a platinum-platinum – 10% rhodium thermocouple located midway in the female portion of the mold.

Figure 31 shows the heating curves employed for this firing and indicates the relationship of the exterior furnace chamber to that existing in the interior of the mold by the part.

The firing rate of the furnace was approximately 100°-125°F/hour up to 2100°F, at which point the rate was decreased to approximately 40°-50°F/hour until a furnace temperature of 2400°F was reached. As was expected, and as shown by the firing curves, the inside mold or part temperature lagged behind approximately 300°F. The actual firing rate of the part was also calculated to be 100°-125°F/hour up to a temperature of 1800°F. From 1800°F to the final part temperature of 2150°F, a rate of approximately 30°F/hour was employed. After soaking at peak temperature for approximately 1 hour, the part was cooled at approximately 75°F/hour to 1200°-1300°F.

After cooling to room temperature, the mold was disassembled. Figure 32 shows the condition of the panel and mold after firing. The black discoloration outlines residual dust of graphite cloth used as a parting agent. The panel was cracked through the tiles and also through bondlines into three pieces. This was evidently caused from severe bonding of the part, especially to the bottom of the mold. The adherence was caused by gravity flow of the adhesive onto the horizontal mold area, and possibly by decomposition of the boron nitride parting agent to boron oxide. It was theorized that the boron nitride failed as a parting agent due to a greater total heat effect than encountered in the first panel. This is evident in light of the fact that Panel B did not contain the large, protective, fused-silica sleeve as did Panel A. Another reason could have been that due to the presence of the sleeve in Panel A, a tighter seal was obtained. As a result, oxidation of the boron nitride was not as severe, as evidenced by the fact that portions of the boron nitride coating was intact after Panel A was fired and cooled. It can be concluded that the boron nitride in Panel B converted to a glass former, boron oxide, and caused excessive seizure between the panel and the mold. The top surface of the panel was relatively free from adhesion to the mold, with approximately 60% of the graphite cloth intact after firing and functioning as a parting medium.

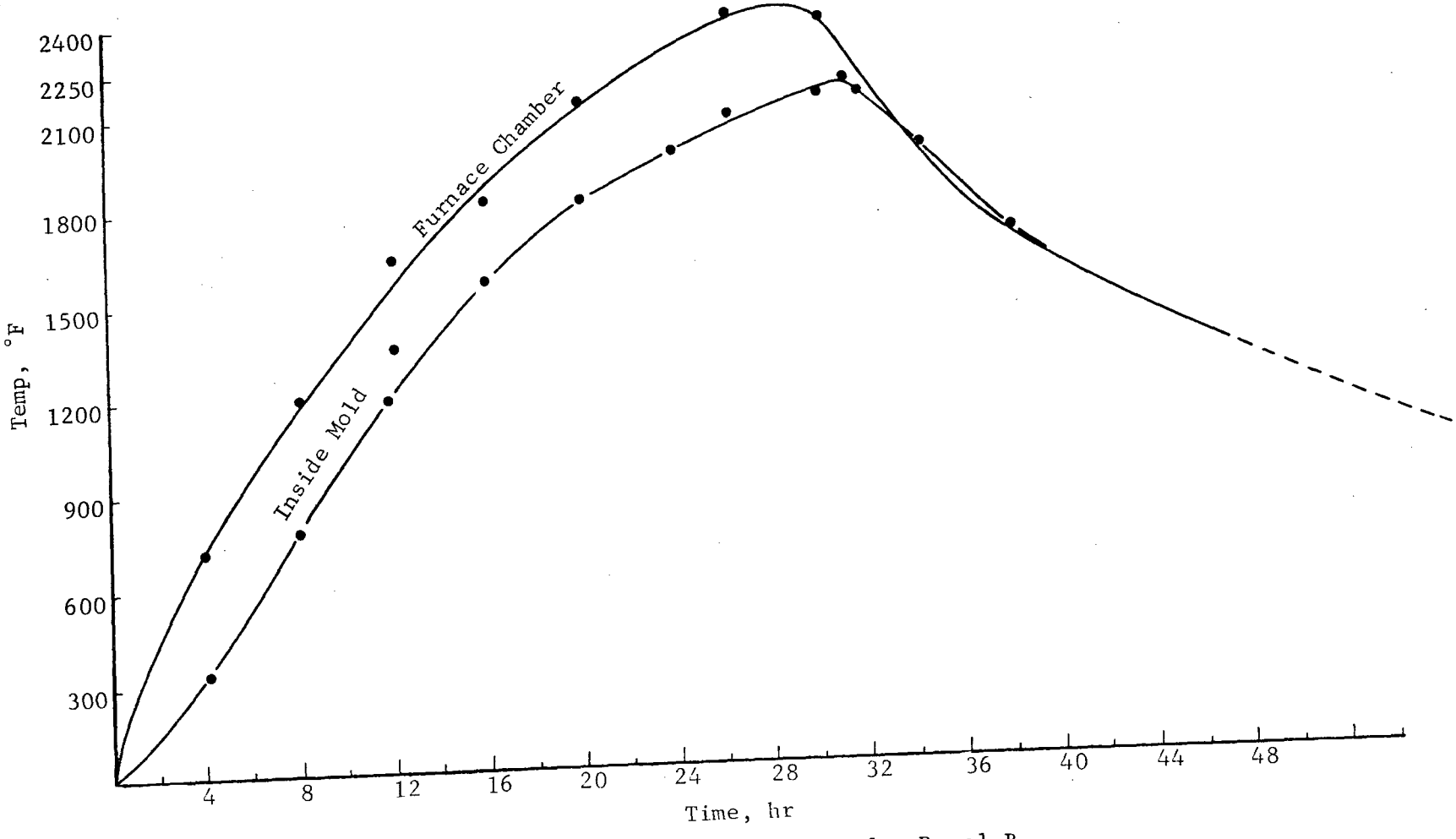


Figure 31. Firing Curves for Panel B

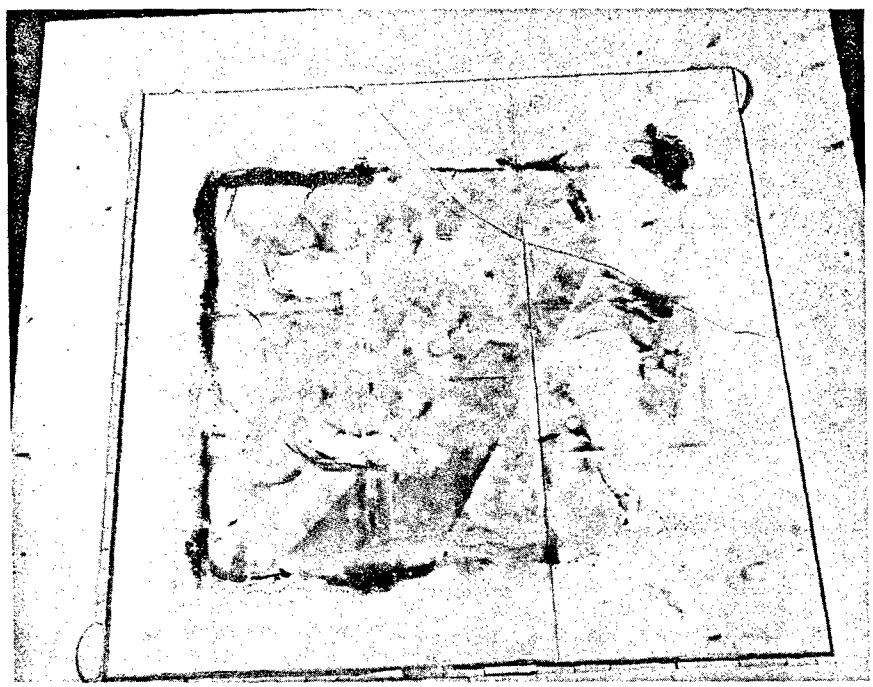


Figure 32. Flat Panel Fracture

Due to the severe seizure, dimensional analysis of this panel was difficult to perform. Many joints were relatively large, and the interlayer thickness varied considerably due to the inability of the panel to properly contract during cooling. However, there was some indication that the use of the thicker shim tended to yield the approximate desired increase in the bondlines. A measurement through several sections where joints were relatively intact gave these results:

Cumulative dimension of tiles before firing:	15.912 in.
Dimension of panel after firing:	15.932 in.
Increase due to four bondlines:	0.020 in.
Average bondline width:	0.005 in.

In addition, much better alignment of the individual layers was obtained, as edges of the fired panel were flush. This was due in part to more precise back-filling methods and closer dimensional control of the burnout shim.

The thickness of the panel varied considerably, ranging from 0.222 in. to 0.232 in., or an interlayer bond thickness of 6-16 mils. Since the sprayed-on raw adhesive bondline was only approximately 10-14 mils to start, it is readily apparent that considerable pulling apart of the layers occurred.

Alumina Ring Segment Fabrication

A firing was also made of an alumina segment ring having the approximate diameter of the proposed radome base. Again, a double layer of individual alumina tiles was employed to simulate the actual production model. Since the scope and task of this phase did not permit purchasing of curved tiles to fit the desired radii, flat tiles 1/8 in. x 1 in. x 2 in. were used for the ring assembly, and were assembled longitudinally around the inner diameter of a cast fused-silica mold to a height of approximately 6 in.

Figure 33 shows the configuration and dimensions of the female mold. The wall thickness was approximately 3 in., while the overall dimensions were 10 in. high with a bottom outside diameter of 34 in. and a top outside diameter of 34-3/4 in., the mold being tapered similarly to the final proposed ogival-shaped radome. The inside working dimensions of the mold were 8 in. high with a bottom inside diameter of 31 in. and a top inside diameter of 31-3/4 in. A complete staggering of all joints could not be obtained due to the tile shape and excessive machining that would have had to be performed; therefore, the 1/8-in. x 1-in. x 2-in. tiles were laid up in a configuration as shown in Figure 34 with alternate tiles of the bottom end of each layer being cut to 1/8 in. x 1 in. x 1 in.

The tiles were coated with Narmcad adhesive, using multiple-tile spraying techniques to coat the required edges and faces. Approximately 500 tiles were employed for assembly of the desired ring segment. Tiles were sprayed with adhesive to an approximate prefired bondline thickness of 15-20 mils for individual joints, while the interlayer prefired thickness of the bondline was approximately 20-25 mils. Bondlines were deliberately made thick in an effort to compensate for the fact that the flat tiles against the tapered, curved section would cause gaps between tiles.

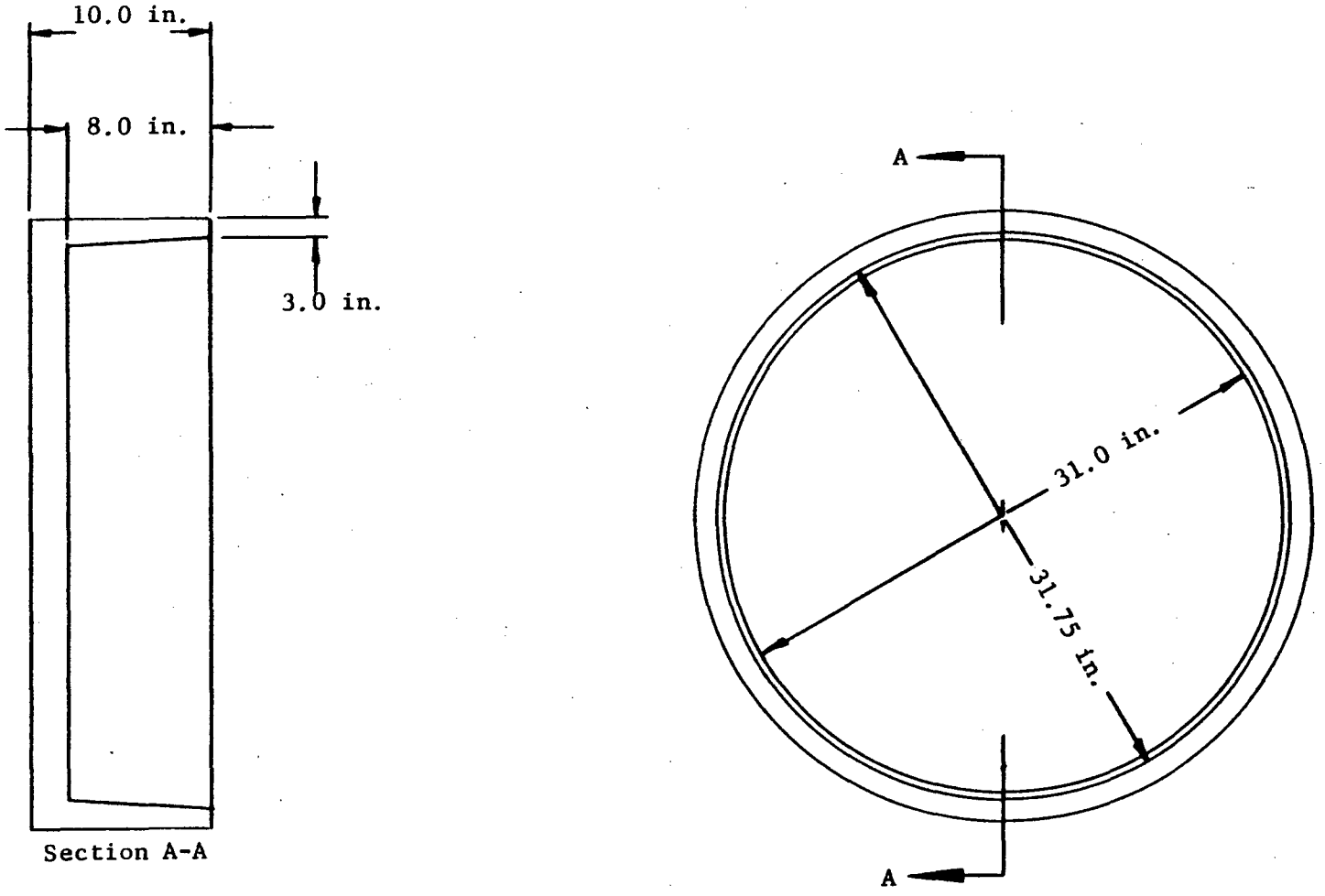


Figure 33. Radome Section Female Fixture

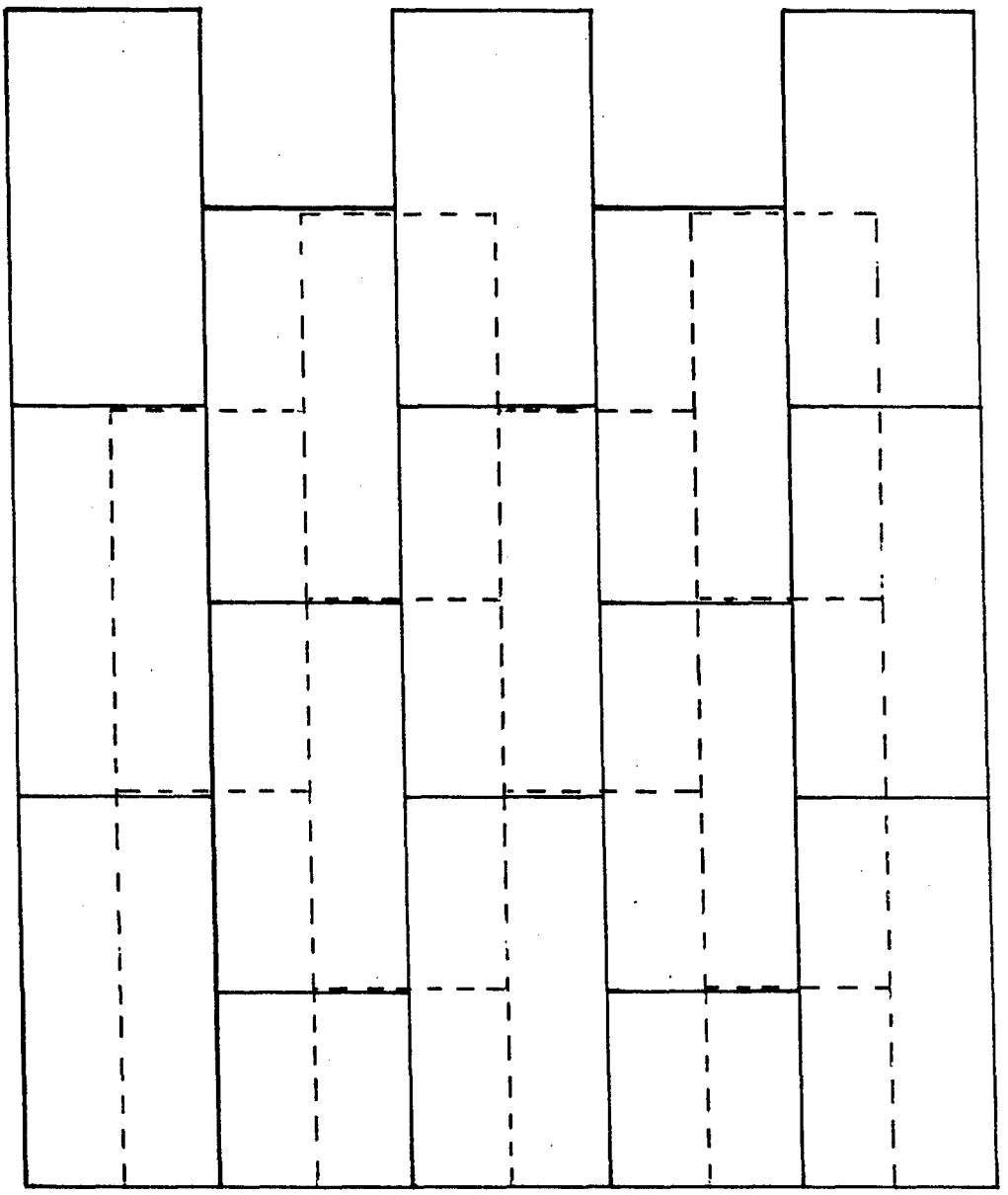


Figure 34. Ring Segment Pattern

Figure 35 shows the layup method used for the first, or outer, layer of tiles. Prior to tile assembly, the mold was given a 5-mil coating of boron nitride powder, using a nitrocellulose binder.

Numerous rows of double-backed masking tape were positioned around the inner diameter of the mold as illustrated in Figure 35. The use of the masking tape allowed the tiles to be firmly positioned in the mold and placed in close contact with each other. Final closing of the layers was accomplished by cutting key-shaped alumina tiles to fit the resulting gap shown in Figure 36. Where noticeable gaps occurred between tile joints, a "grouting" method was used to fill the space with Narmcad adhesive. The second or inner layer was positioned with respect to the first by using a small spot of rubber cement on the coated face to adhere individual tiles to their adjacent member. Figure 37 illustrates the final configuration of the laid-up alumina segment ring. A layer of quartz cloth was placed over the tile assembly (Figure 38).

Next, a 24-in. OD 321 stainless steel ring 0.060 in. thick was positioned in the center of the mold, and the annular space between ring and tiles filled with zircon sand. The high-temperature quartz cloth protected adhesive bondlines from direct contact with the sand.

Figure 39 shows the complete assembly and positioning of the thermocouple. In theory, the metal ring expands, exerting pressure on the sand which transmits pressure to the tiles and prevents inner buckling during firing. The actual closing of the bondlines was to be accomplished by the approximate differential expansion of $4.0 \times 10^{-6}/°F$ existing between the bonded alumina ring and fused-silica mold. This was calculated as follows:

Assuming the ring to be of 32-in. diameter, the change in length occurring at a firing temperature of 2250°F is

$$L_t = L_o (1 + \alpha \Delta T)$$

$$= 32 (1 + 4.0 \times 10^{-6} \times 2170°F)$$

$$L_t = 32.278 \text{ in.}$$

or increase in diametral length = 0.278 in.

Assuming a prefired adhesive gap of 0.018 in. between tiles and 100 joints along the circumference,

$$\text{Total gap thickness} = 0.0018 \times 100 = 1.8 \text{ in.}$$

or

$$\frac{1.8}{\pi} = \frac{1.8}{3.14} = 0.573\text{-in. total diametral gap}$$

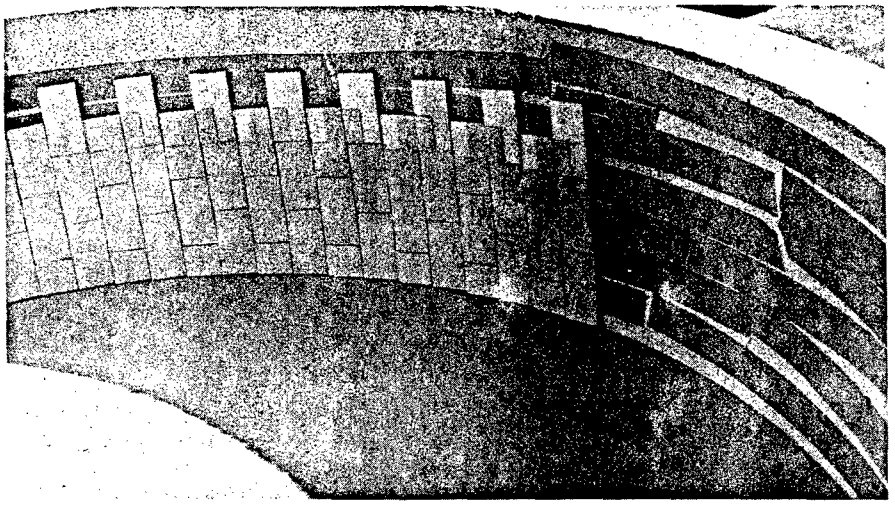


Figure 35. Layup of Outer Tile Layer

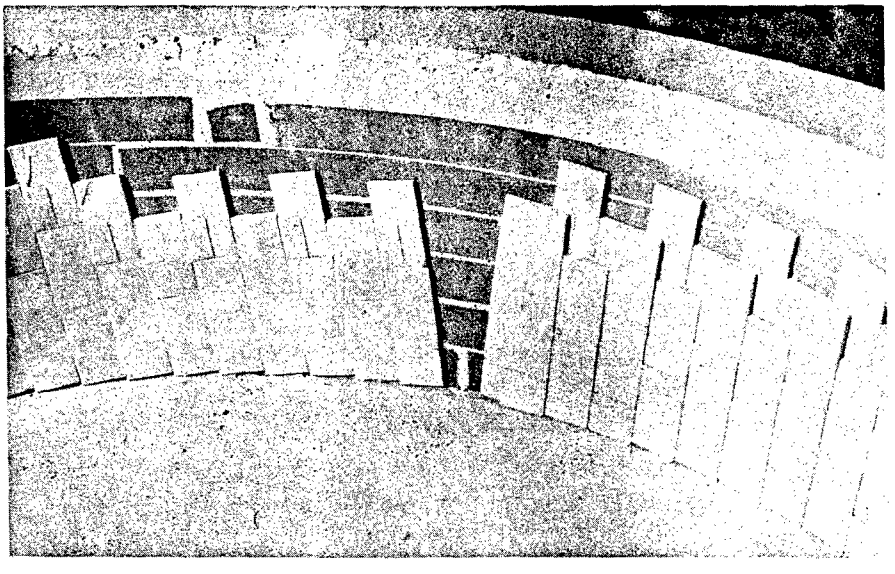


Figure 36. Final Closure Gap

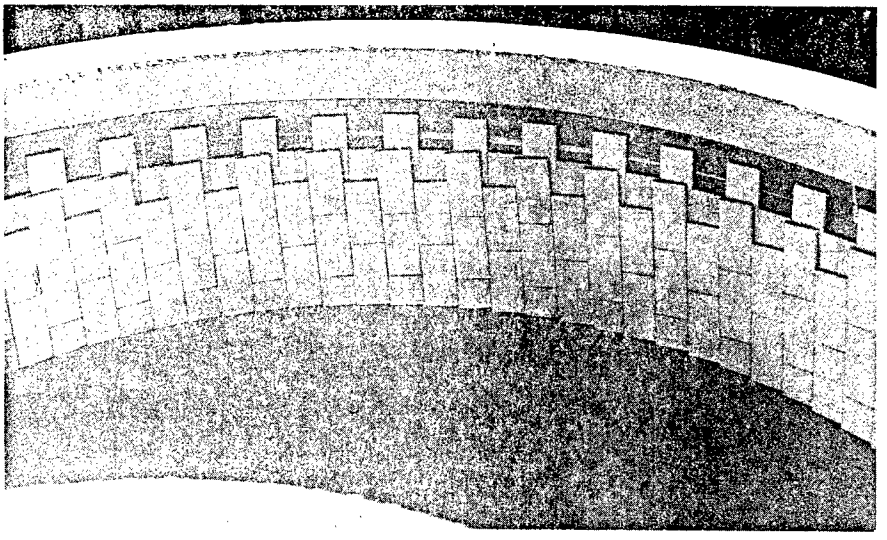


Figure 37. Final Layup of Ring

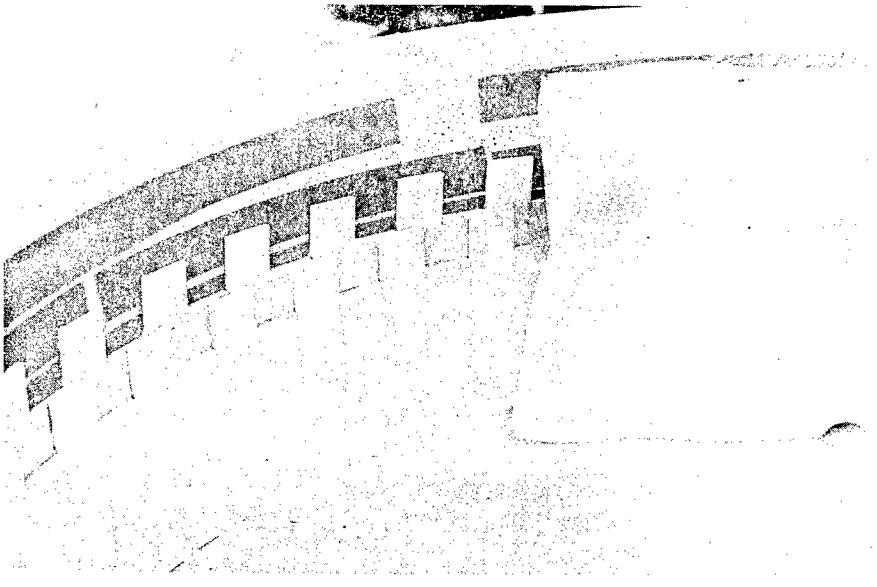


Figure 38. Layup Showing Protective Cloth

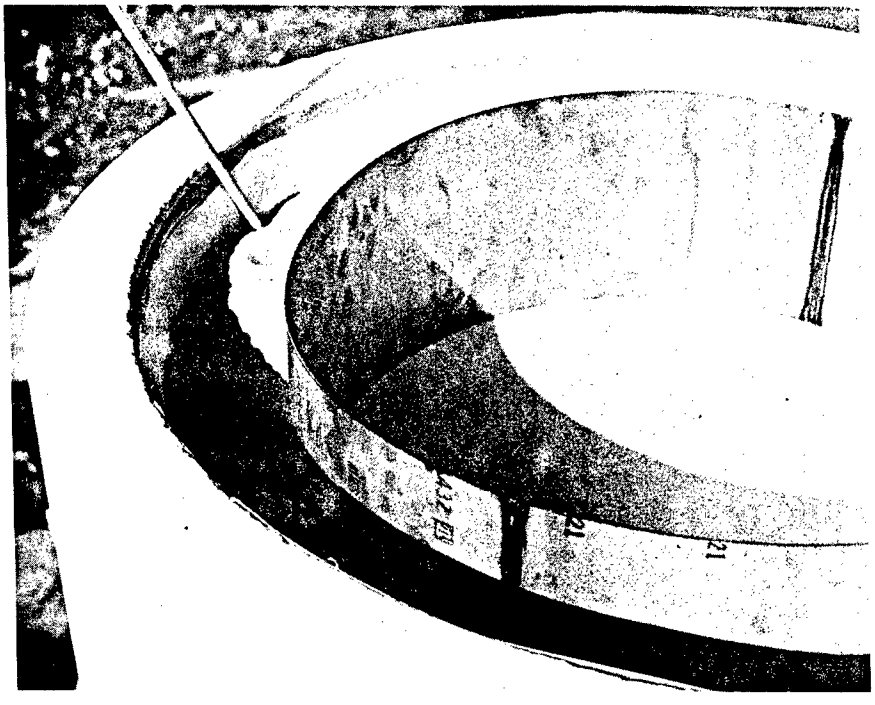


Figure 39. Completed Tooling Assembly

Thus

$$\begin{array}{r} 0.573 \text{ in.} \\ -\ 0.278 \text{ in.} \\ \hline 0.295 \text{ in. resulting diametral gap after firing} \end{array}$$

or $0.295 \text{ in.} \times \pi = 0.93\text{-in. circumferential gap distance}$

Individual bondline thickness equals

$$\frac{0.93 \text{ in.}}{100} = 0.0093 \text{ in.}$$

In theory, the joints would each be closed to 9.3 mils.

The mold was positioned in the furnace as assembled and the actual ring temperature and outside chamber temperature monitored. Figure 40 shows the heating curves determined for this firing. The furnace temperature was slowly raised to 1100°F at approximately 60°-70°F/hour in order to assure burnout of all organic matter used in the tile assembly as well as the nitrocellulose binder in the Narmcad adhesive. A peak furnace temperature of 2480°F was inadvertently obtained that was approximately 100°F higher than desired.

The firing rate from 1100°F to 2480°F was approximately 150°F/hour. In general, the mold or part temperature lagged approximately 2 or 3 hours behind the outer chamber. The heating rate for the part was calculated to be approximately 100°F/hour from 900°F, with a peak temperature of 2280°F being recorded at the part location. Since the part temperature was above the desired 2150°F, the soaking period was eliminated and cooling commenced at a rate of approximately 60°F/hour.

The firing was unsuccessful. The results showed that the sand was too fine to shift and relieve excessive pressure and tended to pack together. Consequently, the pressure exerted by the metal ring was very high, breaking the female fixture below the end firing temperature. This breakage was observed visually during the furnace operation at a chamber temperature of approximately 1800°F.

After the metal ring was disassembled and the sand removed, it was observed that fixture failure permitted the part to overexpand, opening gaps through the expanding action of the metal ring. Again, despite liberal application of the parting agent, localized adhesion between part and fixture occurred at various locations. The quartz cloth was intact after firing but had reacted with the exposed bondlines of the segment ring. As a result of the part seizure to the mold, failure occurred within the segment ring. This failure was quite severe. During cooling, the adherence caused tensile failure in the ring every 3 to 5 in. along the periphery. Figure 41 shows typical sections of the fired ring. All cracks were from top to bottom of the overall 6-in. high ring, with no evidence of failure occurring radially. While the bondline gaps differed considerably, all tile faces were relatively flush with each other (both on the inner and outer faces) and followed the curvature of the fixture. The joints

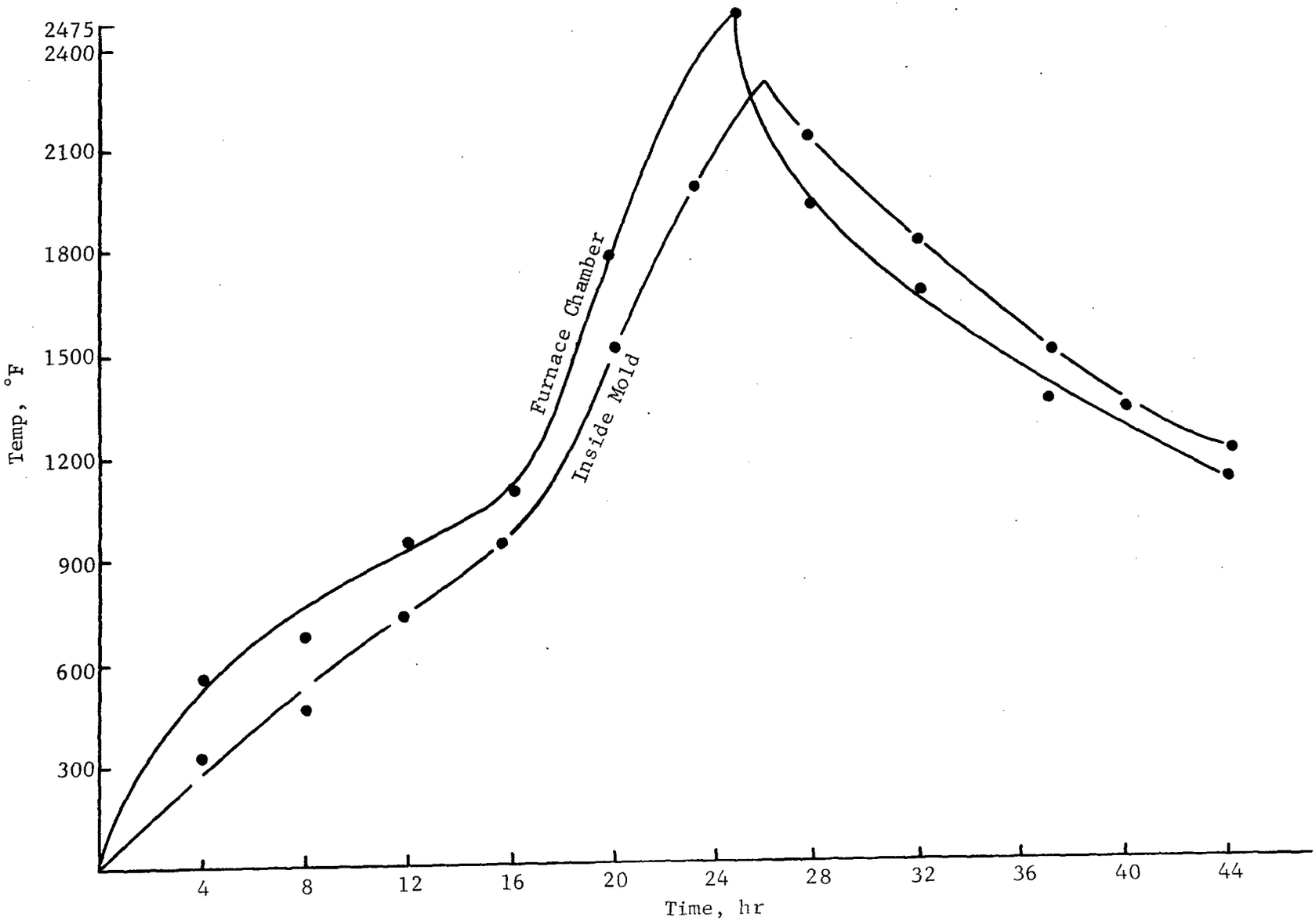


Figure 40. Firing Curves for Ring Segment

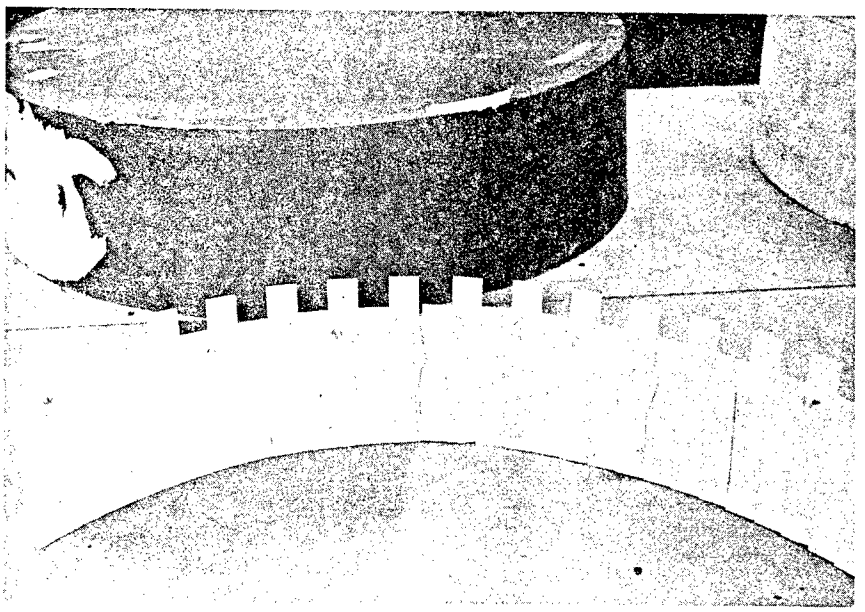


Figure 41. Alumina Ring Segments

on the outer curved surface (i.e., the tile layer in contact with the wall of the fixture) were significantly larger than those of the inner surface, being approximately 0.03 - 0.04 in. in width from the combined effects of excess temperature and fixture breakage. In addition, major portions of the adhesive had been drained out of all the bondlines both horizontally and vertically on the outer curved surface. The joints on the inner surface appeared to be well bonded and filled with the cured Narmcad adhesive. The majority of the joints on the inner surface were well aligned, and measured approximately 0.010 - 0.015 in. in width. This strongly indicated that the concept of gap closure by differential expansion was applicable to a production process.

The conclusions obtained from the ring segment fabrication were that the tile joint closure by the differential expansion concept appeared practical but that sand and quarts cloth were not suitable as internal fill material and parting medium respectively.

EMISSIVE COATINGS

One of the goals of the mosaic radome program was a ceramic material having a total normal emissivity of 0.90 at 1000°F. The reason for this was to increase the rate of heat loss (emission) of the radome under high-speed, aerodynamic heating conditions and thus, in effect, raise its performance limits insofar as thermal considerations are concerned. The alumina tiles being used for the radome normally have an emissivity of from approximately 0.40 to 0.60, depending on smoothness and surface finish. It was concluded that the best method for raising the emissivity with a minimum effect on desirable electromagnetic properties was to glaze or stain the tiles with a thin, highly emissive coating.

The approach was to formulate a series of glaze compositions for alumina to which high emissivity materials could be added. Such materials consist, in general, of the transition metal coloring oxides. An acceptable coating must be able to withstand adhesive curing temperatures if it is to be applied to the tiles prior to assembly, which would appear to be desirable. Several base glaze compositions, known to be suitable for alumina bodies, were selected for investigation. These compositions, which mature in the range from 2000°F to 2500°F, are shown in Table 19.

After the base glazes were mixed and ground, the desired coatings were formulated by adding the high-emissivity oxides.

The blended emissive coatings were than mixed with water to a consistency satisfactory for spraying onto the alumina test specimens. The alumina panels employed were 99% alumina, measuring approximately 0.25 in. x 1.75 in. x 1.75 in. Various thicknesses of the coatings were applied, and finishes varied from bright (glossy) to dull (matte). From the results of the emissive tests, it was established that the bright-finish coatings were difficult to test because of their high reflectivity. Therefore, the majority of coatings tested had either matte or semi-matte finishes. In addition, the use of matte or stain surface coatings would be more practical, since thickness buildup would be at a minimum and would not require holding close tolerances. The actual coatings formulated and applied to the alumina segments are described in Tables 20 through 22.

TABLE 19

BASE GLAZE COMPOSITIONS

Raw Material	Base Glaze, w/o		
	1	2	3
Frit #71	34.5		
Frit #44		49.0	
Frit #14			46.1
Feldspar ($Na_2O \cdot Al_2O_3 \cdot 6SiO_2$)	19.5	19.0	13.1
Silica (SiO_2)	23.0	16.0	16.3
Zinc Oxide (ZnO)	7.0	5.0	3.7
E. P. Kaolin ($Al_2O_3 \cdot 2SiO_2 \cdot 2H_2O$)	7.0	6.0	4.2
Calcium Carbonate ($CaCo_3$)	9.0	5.0	3.7
Zircon ($ZrSiO_4$)			12.9

Frit Compositions *

14		44		71	
SiO_2	46.15w/o	PbO	38.40w/o	PbO	71.00w/o
B_2O_3	23.25w/o	SiO_2	32.76w/o	SiO_2	24.96w/o
CaO	20.2w/o	ZnO	8.40w/o	Al_2O_3	2.35w/o
NaKO	10.4w/o	B_2O_3	7.98w/o	NaKO	1.69w/o
		Al_2O_3	5.36w/o		
		CaO	5.00w/o		
		NaKO	2.10w/o		

* The O. Hommel Co., Frit Compositions.

TABLE 20

EMISSIVE COATINGS — BASE GLAZE 1

Coating No.	Thickness, mils	Firing Temp	Color and (Finish)	Composition, pbw						Total Normal Emissivity (E_{tn})
				BG 1	Co_2O_3	Cr_2O_3	CeO_2 #217*	CeO_2 #210B†	MnO_2	
E-111	7-10	2100°F	Blue-green (Glossy)	100.0	5.0	5.0				0.90
E-112	10-15	2100°F	Blue-black (Glossy)						5.0	
E-113	---	Not Fired	---						10.0	
E-114	5-7	2000°F	Cream (Glossy)				10.0			0.72
E-115	5-7	2000°F	Salmon (Glossy)					10.0		
E-116	2-3	2350°F	Blue-green (Matte)	33.3	33.3	33.3				0.77
E-117	2-3	2350°F	Yellow-Orange (Matte)	33.3				66.6		0.58

* #217 = 99.9%+ purity.

† #210B = 94%-97% purity.

TABLE 21

EMISSIVE COATINGS — BASE GLAZE 2

Coating No.	Thickness, mils	Firing Temp	Color and (Finish)	Composition, pbw						Total Normal Emissivity (E_{tn})
				BG 2	Co_2O_3	Cr_2O_3	CeO_2 #217	CeO_2 #210B	MnO_2	
E-211	10-15	2100°F	Blue-green (Glossy)	100.0	5.0	5.0				0.77
E-212	10-15	2100°F	Blue (Glossy)						5.0	0.84
E-213	--	Not Fired	--						10.0	
E-214	5-7	2000°F	Yellow (Glossy)				10.0			
E-215	5-7	2000°F	Salmon (Glossy)					10.0		

TABLE 22

EMISSIVE COATINGS — BASE GLAZE 3

Coating No.	Thickness, mils	Firing Temp, °F	Color and (Finish)	Composition, pbw									Total Normal Emissivity (Etn)
				BG 3	Co_2O_3	Cr_2O_3	CeO_2 #217	CeO_2 #210B	MnO_2	Fe_2O_3	NiO	$Li_2O \cdot Al_2O_3 \cdot SiO_2$	
E-311	75	2100	Blue-green (Bloated)	100.0	5.0	5.0							
E-312	10-15	2100	Blue (Glossy-Crawled)						5.0				
E-313	---	Not Fired	---						10.0				
E-314	5-7	2100	Yellow-tan (Semi-Glossy)				10.0						
E-315		2100	Tan (Semi-Glossy)					10.0					
E-316		2000	Blue-black (Glossy)		5.0				10.0			6.5	
E-317	2-4		Blue-black (Semi-Matte)		10.0			5.0					0.60
E-318	5-7		Black (Matte)	40.0	20.0				40.0				0.84
E-319	3-5		Blue-black (Semi-Glossy)	62.5	12.5				25.0				
E-320			Blue-black (Semi-Glossy)	77.0	7.7				15.3				
E-321		2100	Blue-black (Semi-Matte)	80.5	6.5				13.0				
E-322	2-3	2350	Black (Matte)	33.3		33.3				33.3			0.71
E-323			Blue-black (Semi-Matte)	50.0	50.0								0.69
E-324			Blue-black (Matte)	33.3	33.3						33.3		0.80
E-325			Blue-black (Matte)	50.0	25.0						25.0		0.86
E-326			Black (Matte)	33.3						33.3	33.3		0.83
E-327			Black (Matte)	33.3					33.3	33.3			0.82

Emissivity Screening Tests

The emissivity of fourteen of the coated alumina segments was determined, using the apparatus and procedures established for a quick screening test. The objective was to use this equipment primarily to screen out the best emissive coatings, and then have the selections further tested to determine their actual total normal emissivity. A specimen of graphite was used as a standard, with the emissivity of the samples calculated on the basis of the graphite having a total normal emissivity of 1.00 at 1000°F. Using this approach, the uncoated alumina segments were calculated to have a total normal emissivity of 0.59. A review of available literature revealed values of 0.2 to 0.7 obtained for the total normal emissivity of high-alumina ceramics. (The 0.2 value was for a highly polished surface.) The majority of values were from 0.35 to 0.60. The literature also revealed that total normal emissivity for unpolished graphites were from 0.80 to 0.90. Therefore, if the emissivity values were recalculated on this basis, a range of 0.47 to 0.53 would be obtained for the uncoated alumina segments. Since this was primarily a screening test, the emissivity of the coatings was determined using a value of 1.0 for the graphite standard.

In order to determine their total normal emissivities, the fourteen segments were tested at approximately 900°-1150°F. Compositions of the coatings with measured emissivities $\left(E_{tn} \right)$ are shown in Tables 20 through 22.

The coatings evaluations made with Base Glaze 1 showed that the glossy surfaces had higher emissivity than the matte finishes. Coatings E-111 and E-116 were quite similar except that the oxides in E-116 increased to give a matte finish. Coatings E-111 measured 0.90, while E-116 had an emissivity of 0.77. The same conditions were noted for coatings E-114 and E-117, where the latter contained the higher colorant oxide percentage to give the dull surface. The glossy coating (E-114) had an emissivity of 0.72, while the matte coating (E-117) measured 0.58.

The highest emissivity values for coatings made with Base Glaze 1 were obtained from the blue-green colored coatings (E-111 and E-116), which were made with cobalt and chromium oxide. The yellow or salmon-colored coatings compounded from ceria (E-114 and E-117) were lower in emissivity.

Only two coatings made with Base Glaze 2 were satisfactory for testing emissivity. Both were glossy, and blue to blue-green in color. Of the two, the E-212 coating (containing cobalt oxide and manganese dioxide as colorants) had the highest emissivity (0.84). The E-211 coating (containing cobalt and chromium oxide) measured 0.77 for total normal emissivity.

The majority of the emissive coatings tested were those made from Base Glaze 3. These, in general, had the best fit to the alumina segments. In this group, all of the coatings measured were blue-black to black in color. They also showed increased emissivity for the matte or stained surfaces rather than for the glossy or bright finishes. (This is shown by comparing coating E-317 to E-318: while both were compounded with cobalt oxide and manganese dioxide, E-318 had the higher percentage, giving a matte finish. The E-318 had an emissive value of 0.84, compared to 0.60 for E-317.)

The use of cobalt oxide alone as an additive to Base Glaze 3 did not produce a high emissive coating (illustrated by coating E-323, which measured 0.69). However, when used in combination with either manganese dioxide or nickel oxide, as in E-318 and E-324, respective values of 0.84 and 0.80 were obtained for total normal emissivity. It was also found that coatings using ferric oxide with either nickel oxide or manganese oxide had relatively high emissive values (measuring 0.83 for the E-326 coating, and 0.82 for the E-327 finish).

The best of the thin (0.002 - 0.003 in. thick) matte, Base Glaze 3 coatings was E-325, having an emissivity of 0.86. This coating was similar in composition to E-325, containing both cobalt and nickel oxide; however, the base glaze percentage was increased. This should also tend to promote better electromagnetic properties since cobalt and nickel oxide do not usually have low loss properties.

Since this screening test was employed strictly to determine which coatings would yield high emissive values, further testing was planned for the best indicated coatings. These were tested by an approved outside source to give a true quantitative value of the total normal emissivity. Alumina segments measuring 0.25 in. x 1.5 in. x 2.0 in. were therefore coated and tested with coatings of the E-318 and E-325 compositions.

Test Apparatus

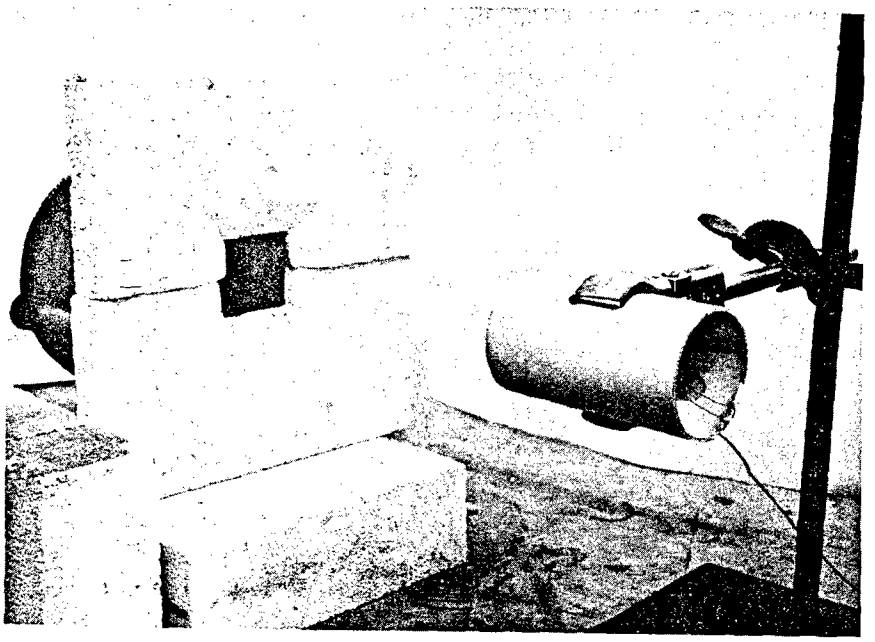
The purpose of these tests was to evaluate candidate emissive coatings. The method chosen provided a basis for comparison between the relative emissivity of each specimen at a surface temperature of approximately 1000°F.

Commercially available thermopiles are normally made for use at temperatures above 1000°F, and were not sensitive enough to obtain a reasonable millivolt output at the desired test temperature. Therefore, a 40-junction iron-constantan thermopile was fabricated. The assembly consisted of a 2.0-in. diameter x 4.0-in. steel tube. A laminated plastic ring at the center of the cylinder supported the thermocouple junctions. Both ends were closed; one end with Plexiglas, and the viewing end with cellophane. The cold junctions were located on the periphery of the ring, and were painted white. The hot junctions were directed radially toward the center, and presented a black target area of approximately 1.0-in. diameter. Since the cold junctions were exposed to the same thermal environment as the hot junctions, any extraneous effects due to conduction or convection were eliminated, leaving only the effect of thermal radiation on the white and black junctions. See Figure 42(b).

The 1.75-in. x 1.75-in. x 0.25-in. alumina specimens were held horizontally in a magnesium oxide frame. The back side of these specimens contacted a commercial-type hot plate which provided (approximately) the desired surface temperature. The specimen surface temperature was measured by a thermocouple bonded to one corner of the front surface. A photograph of the test setup is shown in Figure 42(a).

The output from the thermopile and surface temperature thermocouple was recorded on a 2-channel Varian recorder. A period of approximately 1/2 hour or more was required to achieve equilibrium.

(a)



(b)

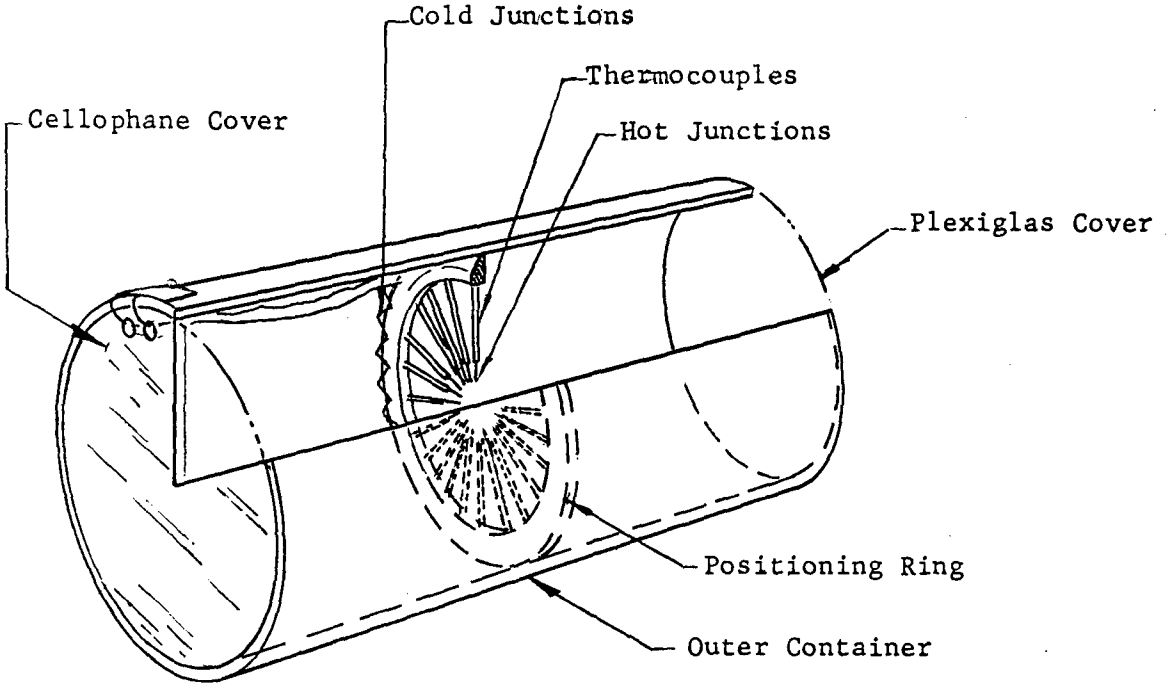


Figure 42. Emissivity Test Apparatus

A graphite calibration specimen was run first for each series of tests, and the thermopile output from this specimen was arbitrarily assigned a value of 1.0. The emissivities of the test specimens that followed were then assumed to be the ratios of the calibration output to the individual specimen output. The thermopile output level varied from day to day, depending on a number of conditions. This variation is not believed to have influenced the overall results, however.

Test results are shown in Table 23. Note that the specimen surface temperatures vary from 886°F to 1183°F. Surface temperatures of the graphite specimens were within a narrower range (from 1026°F to 1153°F). Although no correction for surface temperature differences has been made in the table, this effect is a source of error, and should be considered in evaluating the test results. In particular, those specimens with surface temperatures lower than 1000°F undoubtedly have emissivities slightly higher than the results indicated.

TABLE 23

EMISSIVITY TEST RESULTS

Specimen	Surface Temp, °F	Millivolt Ratio	ϵ
E-111	1183	6.10 to 6.80	0.90
E-325	910	2.90 to 3.37	0.86
E-318	1090	2.60 to 3.10	0.84
E-212	1137	5.70 to 6.80	0.84
E-326	954	2.80 to 3.37	0.83
E-327	1053	3.10 to 3.78	0.82
E-324	949	2.70 to 3.37	0.80
E-116	886	2.60 to 3.37	0.77
E-211	1026	2.90 to 3.76	0.77
E-322	1077	2.66 to 3.78	0.71
E-323	1050	2.60 to 3.78	0.69
E-317	1101	2.25 to 3.76	0.60
Uncoated	1168	4.00 to 6.80	0.59
E-117	1069	2.20 to 3.78	0.58

Total Normal Emittance

As a result of emissive screening tests performed earlier by Narmco, two glaze-type coatings were selected for further testing to give a true quantitative value. The coatings selected were E-318 and E-325, which consisted of the following compositions:

E-318		E-325	
Base Glaze 3	40.0	Base Glaze 3	50.0
Co_2O_3	20.0	Co_2O_3	25.0
MnO_2	40.0	NiO	25.0

These coatings were applied to 97.6% alumina segments 1/4 in. thick, 1-1/2 in. wide, and 2 in. long with a coating thickness of approximately 3 mils after firing at 2100°F. Samples were submitted to Melpar, Incorporated for determination of total normal emittance over a temperature range from approximately 1000°F to 1500°F.

A blackbody comparison technique was used to measure the total normal emittance in the temperature range from 300°F to 3000°F. A blackbody constructed of Inconel 702, with a theoretical blackness of 0.995, was used as the standard. The sample under test was heated in a second furnace. The temperatures of the blackbody and sample surface were maintained within 0.1°C through the use of a series opposition thermocouple. The characteristics of the blackbody radiation in the temperature range of this test were such that peak radiation occurred at 3.6 μ for the lowest temperature, and at 2.5 μ for the upper temperature limit. In this temperature range, 95% to 98% of the blackbody radiation was contained in the wavelength region of 1 to 15 μ. Based on this analysis, a KRS-5 window was used in conjunction with an Eply total radiation thermopile as a detector. Once equilibrium was reached, the detector was allowed to view the sample and the blackbody alternately through a water-cooled baffle system. The ratio of the two readings represents the normal total emittance. This measurement had a probable error of ±3.5%. Table 24 shows the results obtained for the two coatings.

TABLE 24

TOTAL NORMAL EMITTANCE OF COATINGS

Sample E-318		Sample E-325	
Temp, °F	E_{tn}	Temp, °F	E_{tn}
1085	0.93	1017	0.88
1173	0.92	1113	0.90
1325	0.91	1330	0.91
1491	0.90	1515	0.87

There were no visible signs of glaze deterioration resulting from temperature cycling. Both samples were each subjected to 72-hour heat period. The samples incurred some surface abrasion from insertion into the testing apparatus and other preparations preliminary to testing. However, the test area in all cases was not affected by the above processes. Figures 43 and 44 show the graphic representations of emittance vs temperature for both coatings.

As can be seen from the presented data, coating E-318 satisfied the contractual goal of an emittance of 0.90 at 1000°F, while coating E-325 was quite close to this goal.

Electromagnetic Properties

The effect of emissive coatings on the loss tangent and dielectric constant of 96.7% alumina segments was determined. The evaluation was made by applying and firing a thin layer (2-3 mils) of the emissive coating onto the alumina electromagnetic test specimens. Only one surface of the alumina segment was coated, with electromagnetic values being measured in a direction perpendicular to the coated surface. The emissive coatings evaluated were E-318 and E-325, which were found to have relatively high total normal emissivity values, 0.84 and 0.86 respectively, based on Narmco's preliminary screening tests. These coatings were the same coatings reported in the previous section.

The coated samples were measured at the usual frequency of 9.375 Gc and at room temperature and elevated temperature.

Table 25 shows the values obtained for the alumina samples with the emissive coatings, and their comparison with the uncoated S1 alumina body.

The percent increase of the dielectric constant with temperature was also calculated for the emissive coated samples and compared with the standard S1 alumina body (see Table 26).

The loss tangents of all three samples were quite similar at all temperatures to 1000°F (Figure 45) with the values reported considered to be similar, since the S1 alumina specimen value was determined at an earlier date. Above 1000°F, the loss tangent for the E-318 increased rapidly to a value of 0.0167 at 1200°F. This same general increase was also noted in the change of dielectric constant with temperature for the E-318 composition. However, the E-325 coated sample appeared to be quite stable over the entire temperature range, and was considered to be a more suitable coating.

Application of such a coating to a complete mosaic radome was not planned, since the additional technical information to be gained did not appear to justify the additional time and cost required.

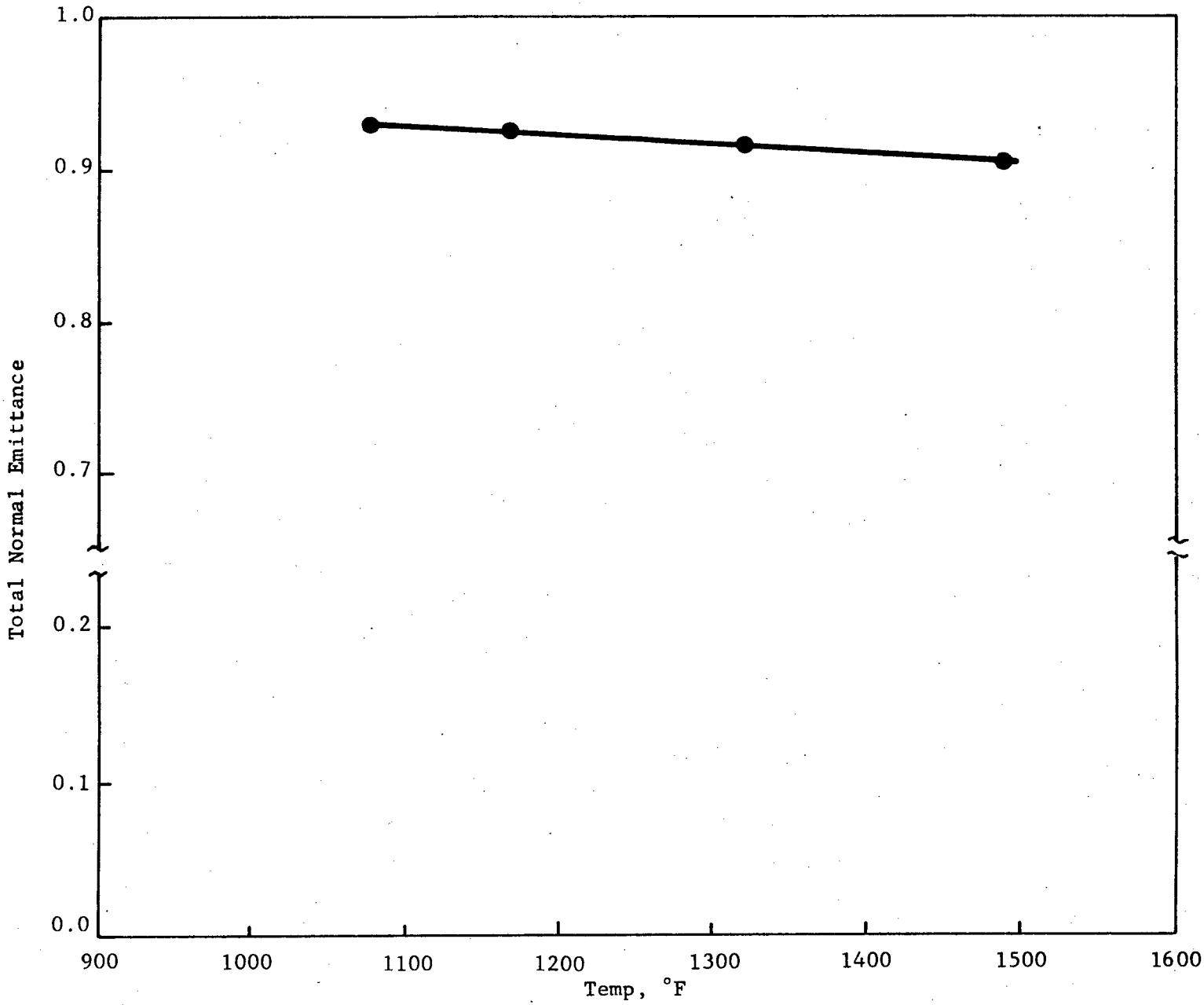


Figure 43. Total Normal Emittance Specimen (E-318)

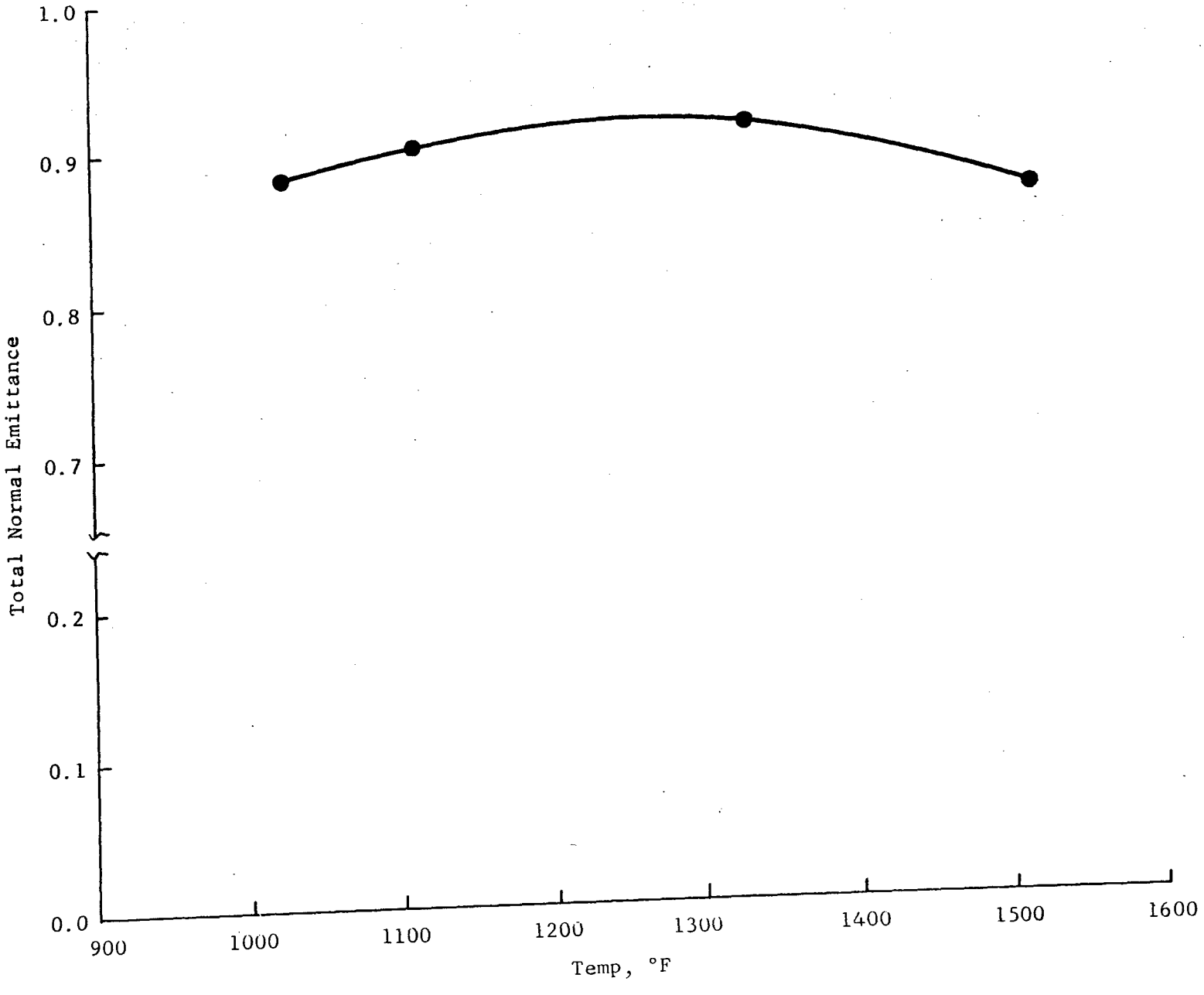


Figure 44. Total Normal Emittance Specimen (E-325)

TABLE 25

ELECTROMAGNETIC PROPERTIES OF EMISSIVE COATINGS

Temp, °F	S1 Alumina		Coating E-318		Coating E-325	
	Dielectric Constant	Loss Tangent	Dielectric Constant	Loss Tangent	Dielectric Constant	Loss Tangent
RT	8.24	0.007	8.47	0.0007	8.34	0.0006
500	8.42	0.00135	8.69	0.0013	8.59	0.0012
1000	8.72	0.0025	9.03	0.0029	8.88	0.0026
1200	8.82	0.00345	10.59	0.0167	9.01	0.0038

TABLE 26

INCREASE IN DIELECTRIC CONSTANT
WITH TEMPERATURE

Sample	% Increase		
	500°F	1000°F	1200°F
S1 Alumina	2.18	5.82	7.04
E-318	2.60	6.61	25.03
E-325	3.00	6.47	8.03

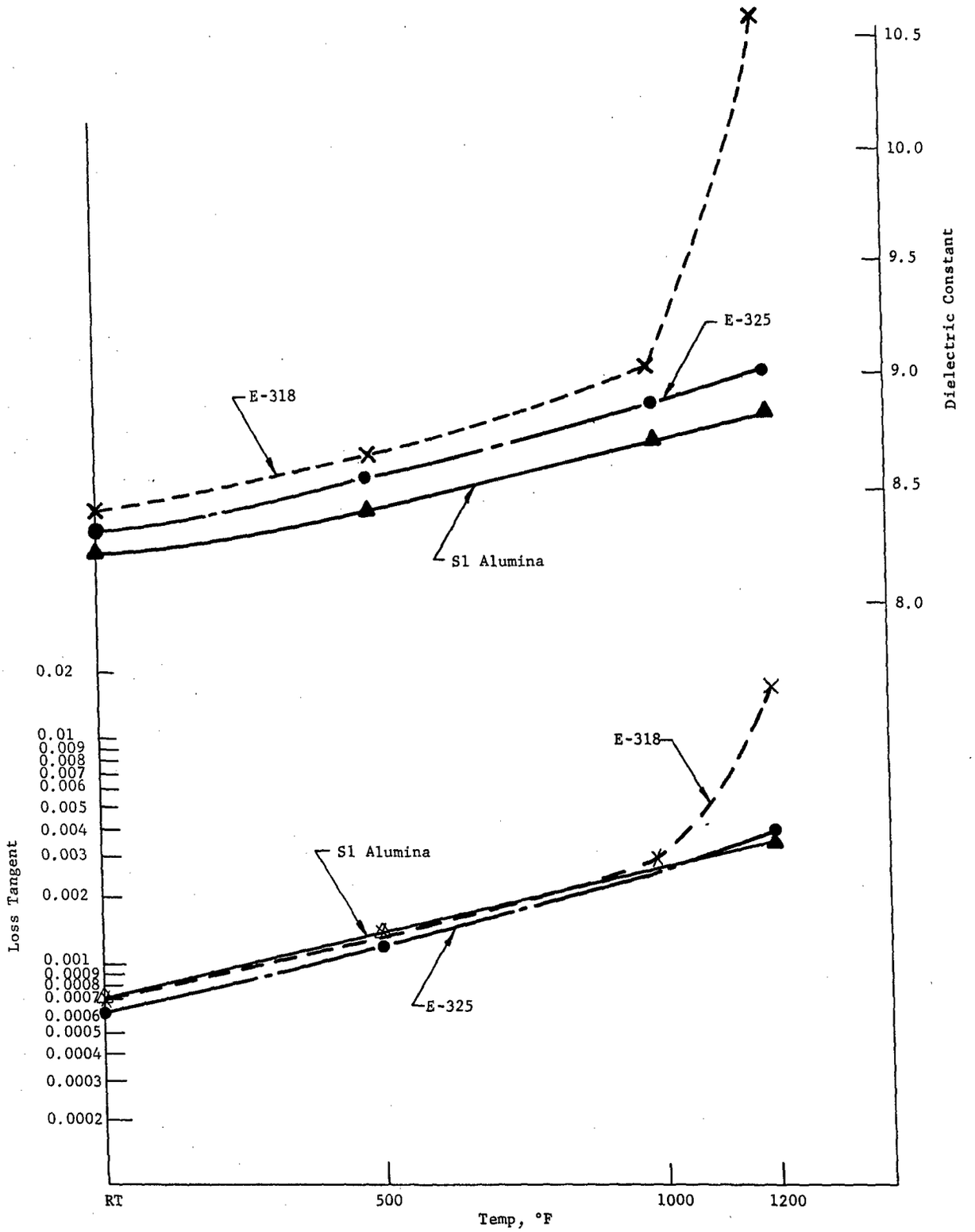


Figure 45. Loss Tangent and Dielectric Constant vs Temperature at 9.375 Gc for S1 Alumina with Emissive Coatings

SECTION IV

RADOME DESIGN AND ENGINEERING CONSIDERATIONS

The goal of the program was to fabricate a large ceramic radome of the general ogive configuration shown in Figure 46, utilizing ceramic mosaic tile construction. The ceramic body material objective was a loss tangent of less than 0.005 at room temperature and 0.010 at 1000°F, measured at 10 kmc. Another objective was that the dielectric constant remain uniform within 1% over this temperature range. In addition to these electrical characteristics, the ceramic wall material had to demonstrate sufficient strength and resistance to heat and thermal shock to withstand Mach 5 operation at a 100,000-ft altitude under assumed flight profile conditions as shown in Figure 47. Provisions for attaching the radome to a test fixture (and vehicle) were also required. A survey of potential ceramic tile fabricators indicated that in order to obtain the desired uniformity in properties by the conventional pressing and sintering techniques, the maximum tile size would have to be no greater than approximately 8 in. on the longest dimension (or 16 to 20 $in.^2$ area). The maximum size would be determined by practical considerations of handling, layup, and lap joint design.

The above considerations clearly indicated that the mosaic radome designing would encompass several areas including thermal and structural analyses, tile size and configuration, joint type, plus base attachment techniques.

It should be noted at this point that a mutual understanding was established between Narmco and the Contracting Agency with respect to two significant design parameters:

1. The tip of the ogive-shaped radome would be terminated in a one-piece or monolithic conical nose cap with a nose radius of 2 in. and made of the same material as the ceramic tiles.

2. The maximum design temperature of 1000°F would apply slightly aft of the aerodynamic transition point which would be the approximate location of the joint between the mosaic tile structure and the monolithic nose cap. (Under corresponding aerodynamic heating conditions, a stagnation temperature approaching 1500°F would be generated at the nose tip.)

In addition to the design of the full-size ogival mosaic ceramic radome having a base diameter of 31.70 in., a length of 26.0 in., and requiring 90 different alumina tile configurations, two truncated base sections of this radome were also designed for use in developing the fabrication learning curve and for testing purposes. The complete radome assembly required a total of 834 tiles plus a conical alumina nose cap. The two truncated section designs were identical to the basic radome except that they were truncated after six and four rows of tiles from the base and employed 264 and 180 tiles respectively. Due to modification in program plans, only truncated sections of the longer design were fabricated. These were approximately 20 in. high, and were made with both the plain tiles and with the special attachment tiles in the base ring.

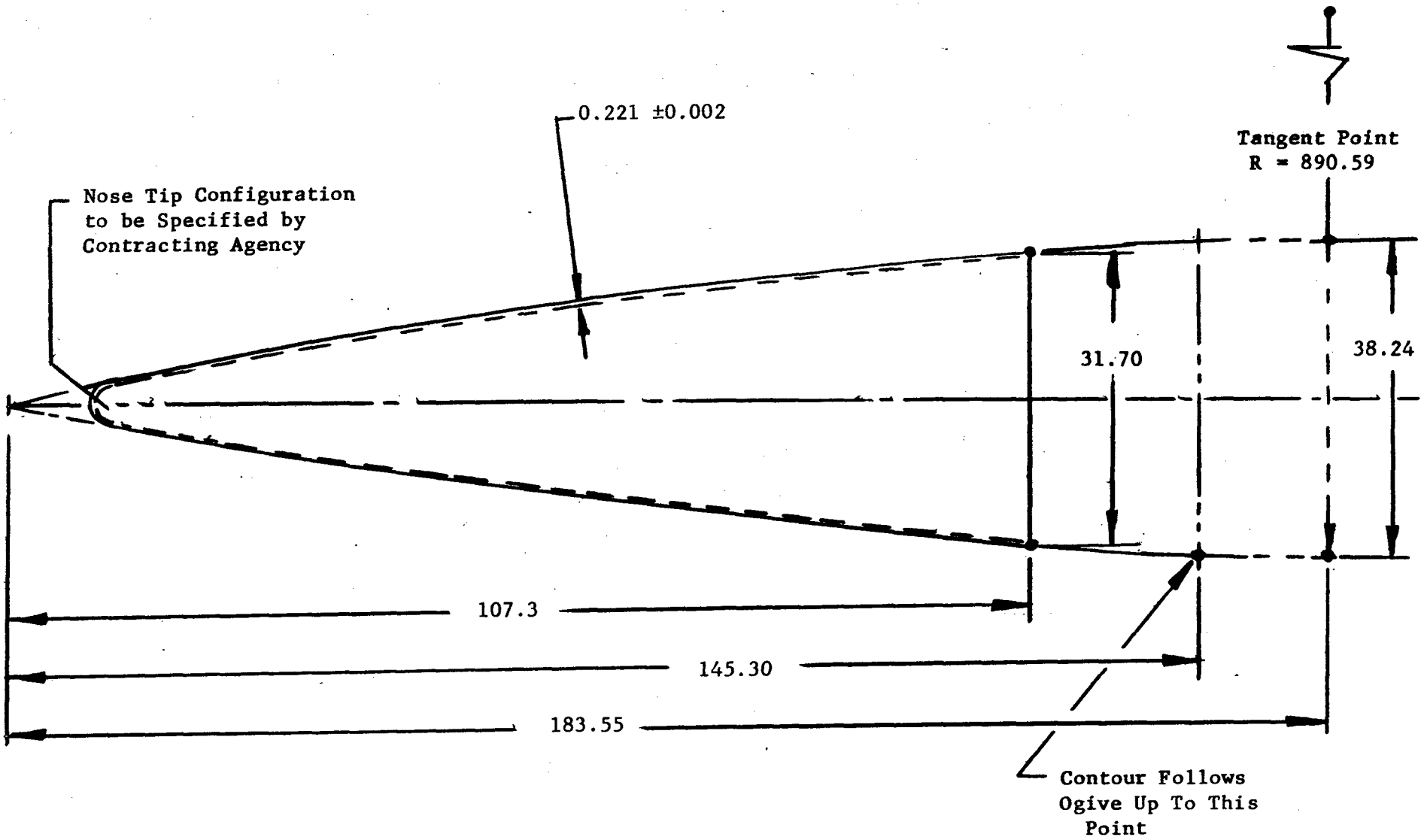


Figure 46. Prototype Radome
(Fineness Ratio 4.8:1)

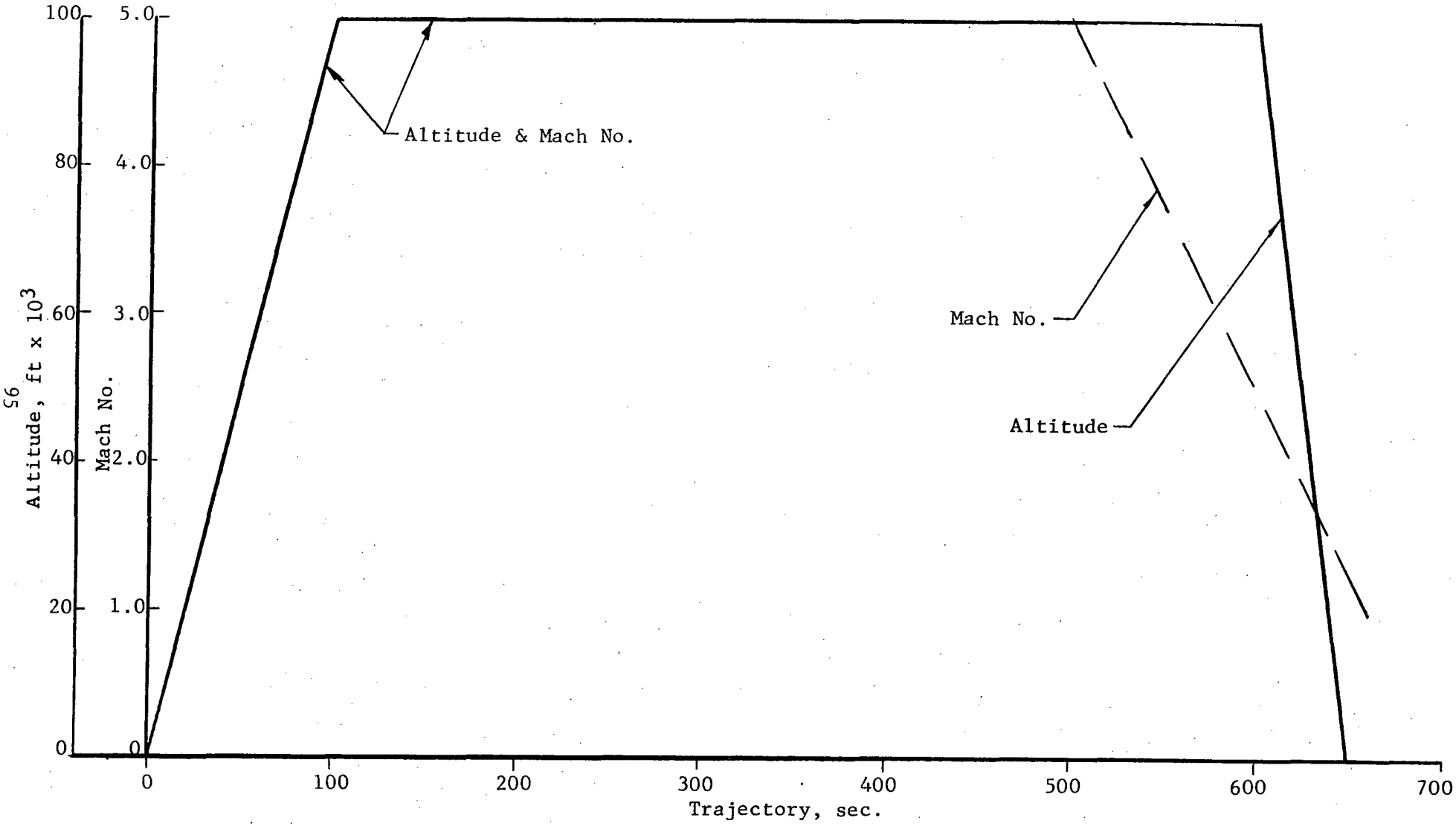


Figure 47. Flight Trajectory

The radome design is shown in Narmco Drawings Nos. NR 63-044, NR 63-045, and NR 63-046 (see Appendix X). The geometry and size of tiles were established by the method described in Appendix IV and the mathematics method used in defining the various tiles and nose caps is presented in Appendix V.

The selection of the size and number of tiles comprising the radomes was made partially on the basis of economics. It was found that a tile of approximately 16-20 sq in. was the upper limit as far as producibility is concerned and it was similarly noted that a smaller tile would cost approximately the same. Therefore, the radome was designed starting with tiles of approximately 16 sq in. of outer surface area, and tapering down (because of the ogival configuration) to tiles of about 9 sq in. of area. At this point (about 62 in. from the base), the use of 16 sq in. tiles was resumed.

All tiles were straight in the longitudinal direction and curved in the radial direction with a nominal thickness of 0.108 in., thus forming conical sections. This was done for machining and grinding reasons.

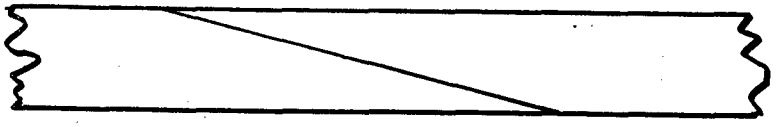
The nose cap, having a length of 14.32 in. and a base diameter of 10.13 in., had a top radius of 2 in. and a uniform thickness of 0.221 in. Again, a conical rather than an ogival shape was used for machining and grinding ease.

MOSAIC SEGMENT AND JOINT DESIGN

The mosaic segments that form a cone or ogive radome can have a variety of shapes which are dependent on such criteria as loading conditions, method of joining to adjacent tiles, and fabrication limitations.

In the case of a mosaic radome, the adhesive properties presently impose stress limitations. The design must properly utilize adhesive properties, particularly when the shear strength is very attactive compared to the tensile strength. Obviously, transmission of tensile loads under these conditions, is best performed by placing the joint in shear.

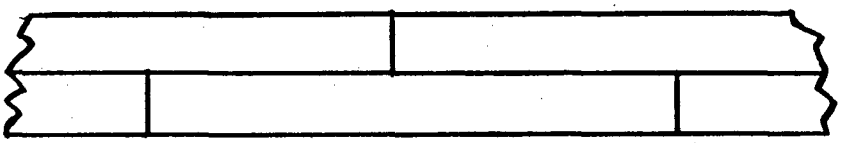
A very efficient joint from a theoretical standpoint is the scarf, as illustrated below:



Scarf Joint

Overlap length is relatively large for this application, however, and voids of any magnitude tend to produce serious stress concentrations.

A theoretically less efficient joint is the two-layer lap joint. The efficiency of this joint may be improved, if desired, by scarfing the segments; however, the butt joints as shown are simple to fabricate and assemble.



Lap Joint

Methods for analyzing stresses in these joints are presented in Appendix II.

A very efficient structural segment shape, assuming that all bonds are perfect, is that of a rhombus. Appendix III presents a geometric study of the rhombic configuration. However, stress concentrations cannot be analyzed effectively, whether inherent in the design or arising from fabrication defects and joint voids.

A less efficient shape is the square or trapezoid. The stress concentrations in this type of composite intuitively appear to be less significant, and a means of comparing rhombic and trapezoidal configurations was established using experimental techniques. It was determined that a trapezoidal segment was slightly more efficient than a rhombic segment. Based on the empirical data, a trapezoidal-shaped tile was selected as the tile design for this program. Analysis of the loads indicated a double layer is satisfactory from a stress standpoint, so the preliminary radome double-wall design was selected.

This selection also proved to be more practical from a fabrication standpoint. Some voids can be tolerated, tile shapes are simpler and more economical, and segment assembly is facilitated. During the stress analysis, the edge condition comparison between scarf and lap showed the strength contribution was slight for the scarf over the butt joint, so the butt joint was selected because the added expense of using the scarf appeared totally unwarranted. Also during the stress analysis, it was assumed that all the structural load was carried by the lap or shear portion of the lap joint.

Utilizing the analysis outlined in Appendix II, it can be shown that the scarf joint is optimum for shear transfer. It can be concluded that by rotating the scarf 90 degrees and viewing the radome surface, a rhomboid with maximum joint efficiency in the longitudinal direction and lesser efficiency in the circumferential direction will be obtained. A double layer arranged in a diagonal direction would give more stress concentration with butt edges than with scarfed edges as mentioned previously. For a conical or ogival radome, the rhombic shapes of the tiles would be as shown in Figure 48. This rhomboid would prove difficult to shape, especially since "B" must be shorter than "A" to form a cone or an ogive.

Similarly, the trapezoidal shapes would be as shown in Figure 49. Comparison of these two shapes was made by testing a series of 60 specimens. Tiles were shaped to simulate load conditions expected in the radome, and

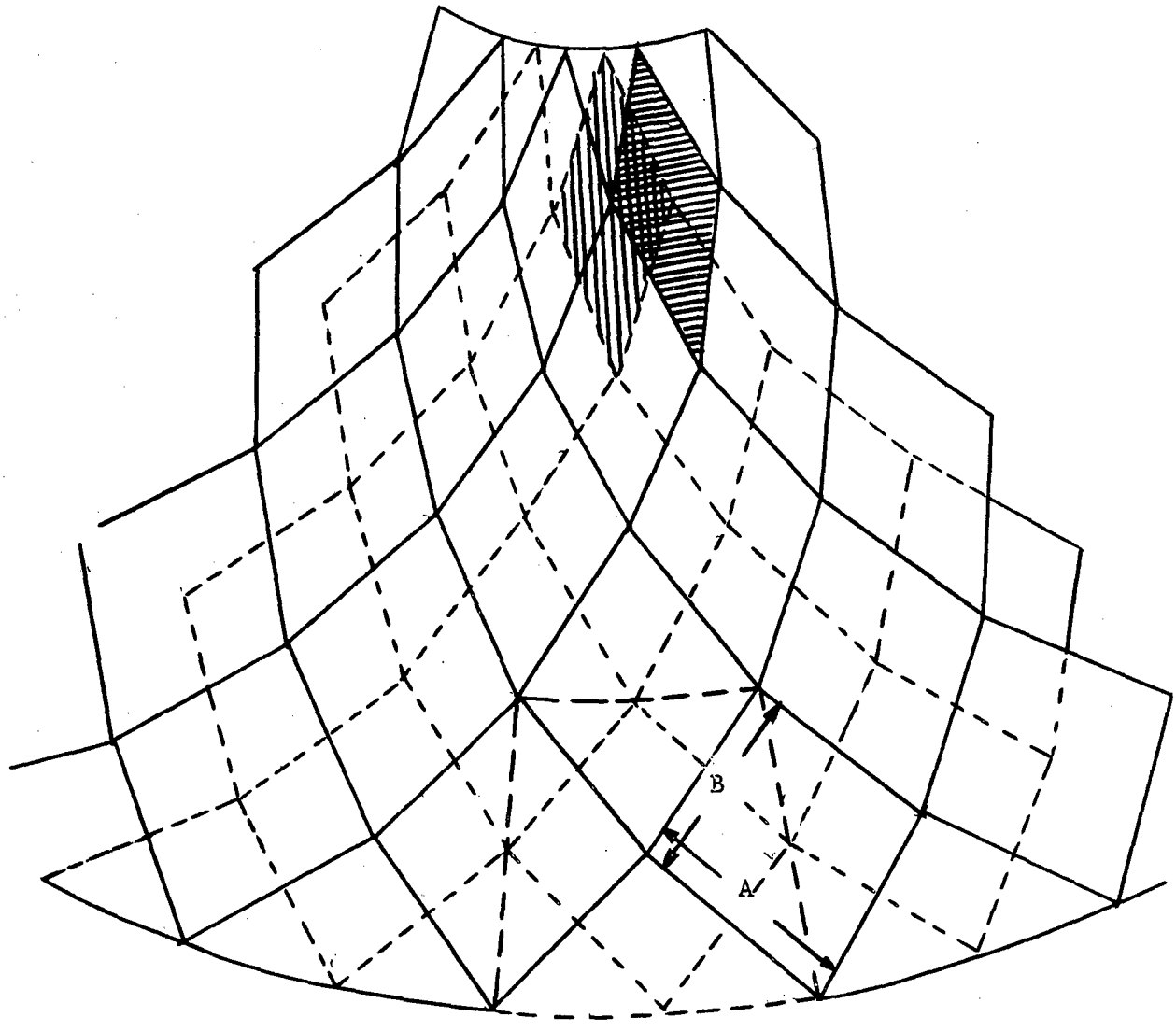


Figure 48. Required Variation for Rhomboid

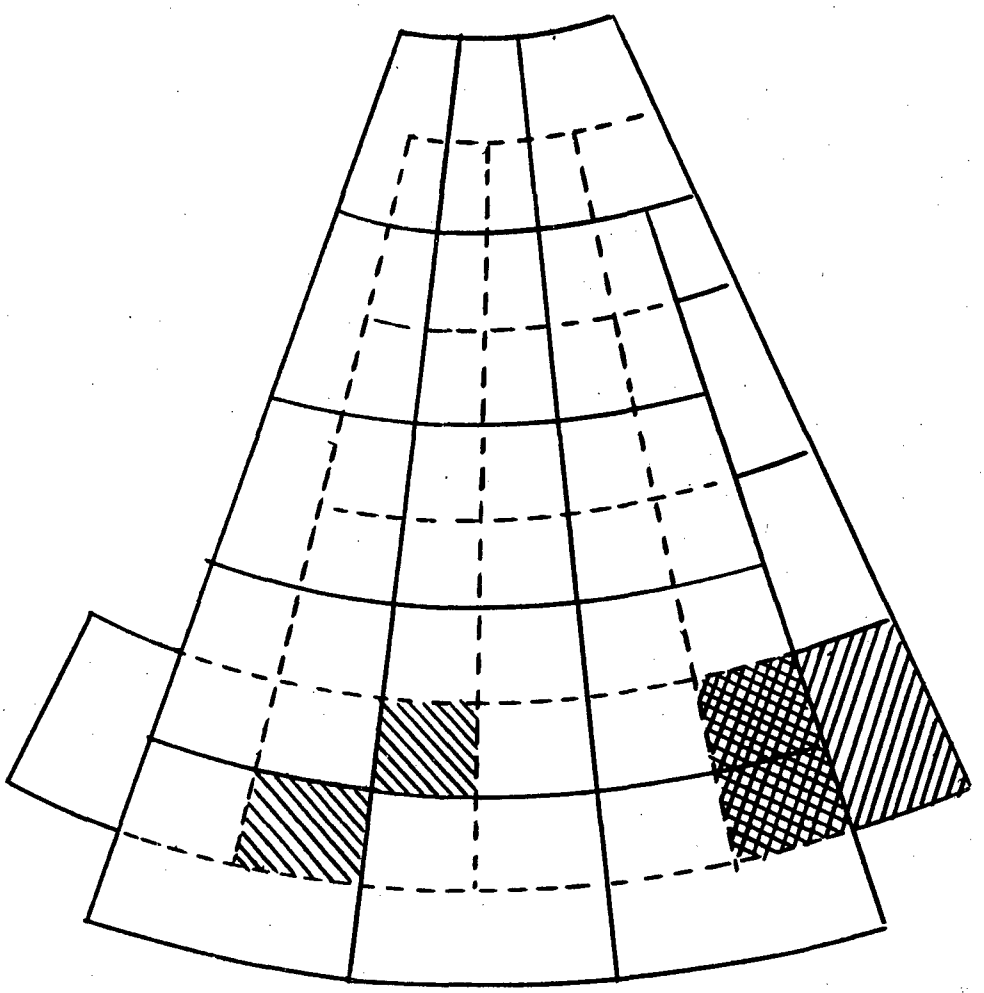


Figure 49. Trapezoidal Geometric Variation

bonding was done with a brittle adhesive. Common industrial tile and an organic resin were used to simulate the expected composite. Figures 50 through 55 show the variety of test specimens tested, and Figures 56 through 59 are photographs of actual failures.

From the tests performed with various tile materials and adhesives, no significant advantage of rhomboid overlapping could be found. The samples shown in Figure 56 failed at 500 to 600 psi while those shown in Figure 57 failed at 900 to 1000 psi.

The samples shown in Figures 58 and 59 were designed to fail in the bond. The average failing stress of the rhombic joint was 1323 psi and 1565 psi for the trapezoidal joint.

The failure stress of the bonded area is reduced by increasing the overall depth of both rhombic and trapezoidal shapes. Sufficient tests have been completed to establish a functional relationship, but for preliminary purposes, only relative results for comparison of the rhombic and trapezoidal joints are needed.

The construction of a radome utilizing mosaic techniques required an efficient arrangement of the tiles. Comparison of two layers of uniformly distributed tiles, Figures 60 and 61, shows that 50% of the material strength is utilized in the trapezoidal tiles in both major axes, and 100% utilization is realized in the diagonal direction for the rhombic tiles.

The staggered arrangement of the tiles in Figure 62 furnishes 75% material utilization in the "y" direction and 50% in the lateral direction; it will be shown that this satisfies the structural requirements of the radome.

To fully utilize the strength of the tile material, the bond should not fail prior to the tile. A reasonable failing shear stress of the adhesive in an overlapped alumina bond is assumed to be

$$\sigma_{adh} = 4000 \text{ psi}$$

The ultimate tensile stress of the alumina tile material can also be approximated as

$$\sigma_T = 25{,}000 \text{ psi}$$

For the tile arrangement shown in Figure 60, where 50% of the tile material strength is used, the following relationship exists; the failing force transmitted through the tiles has to be equal to the failing force transmitted through the adhesive.

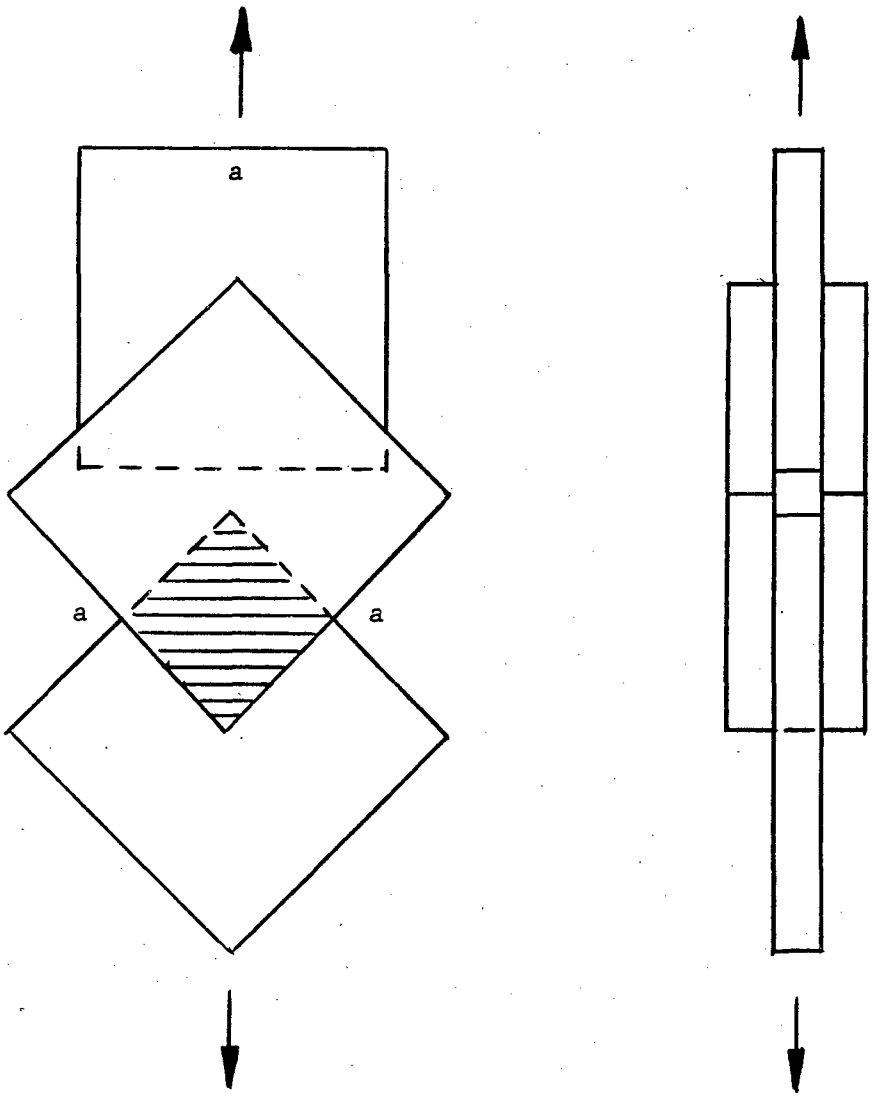


Figure 50. Test Specimen

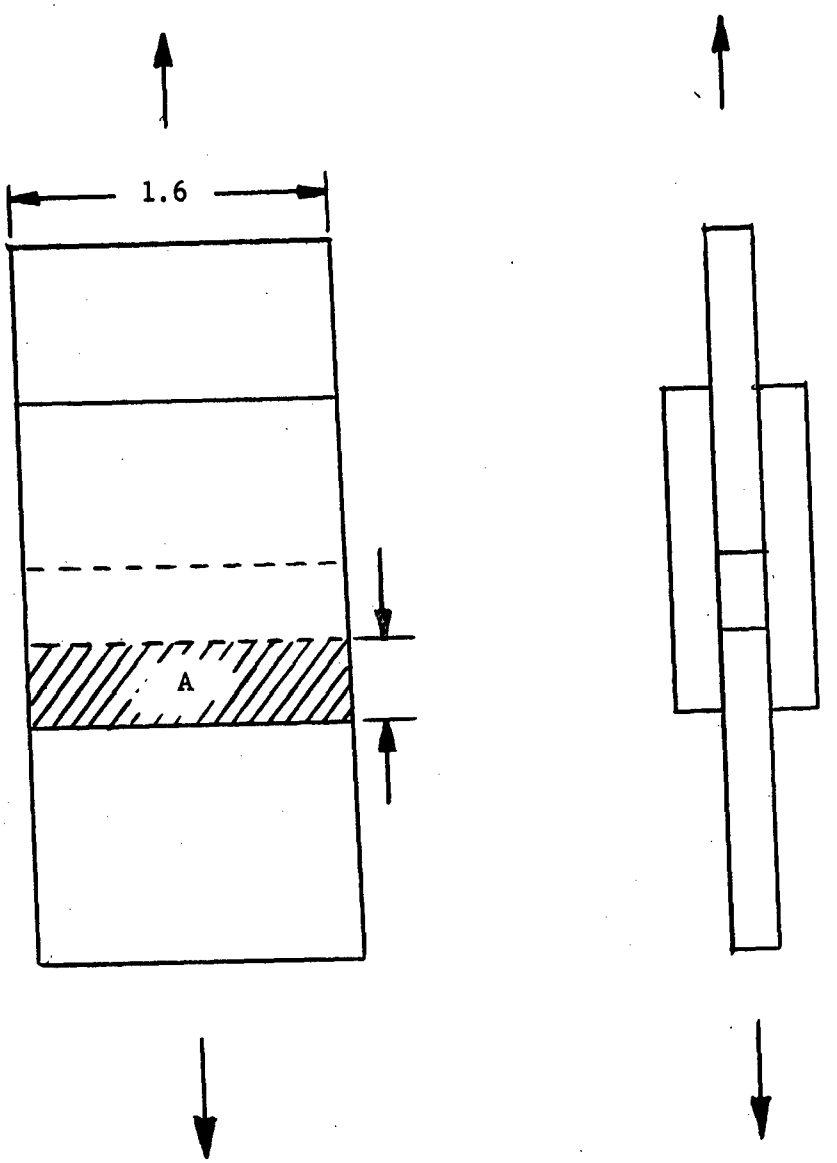
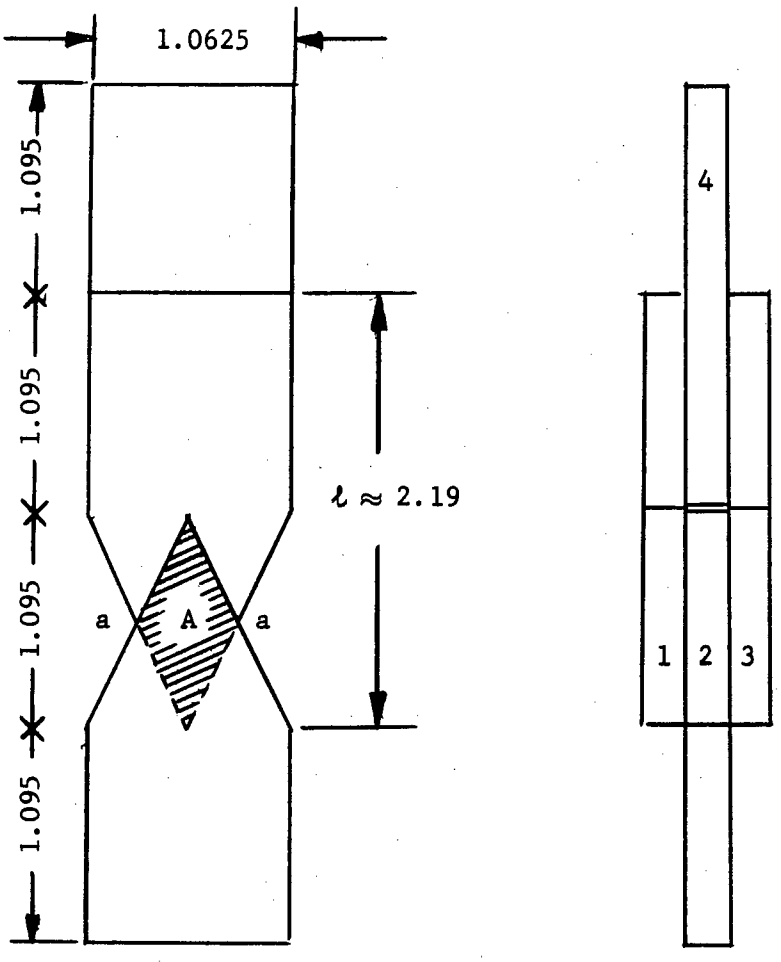


Figure 51. Test Specimen



$$A = 0.291 \text{ in.}^2$$

Figure 52. Test Specimen

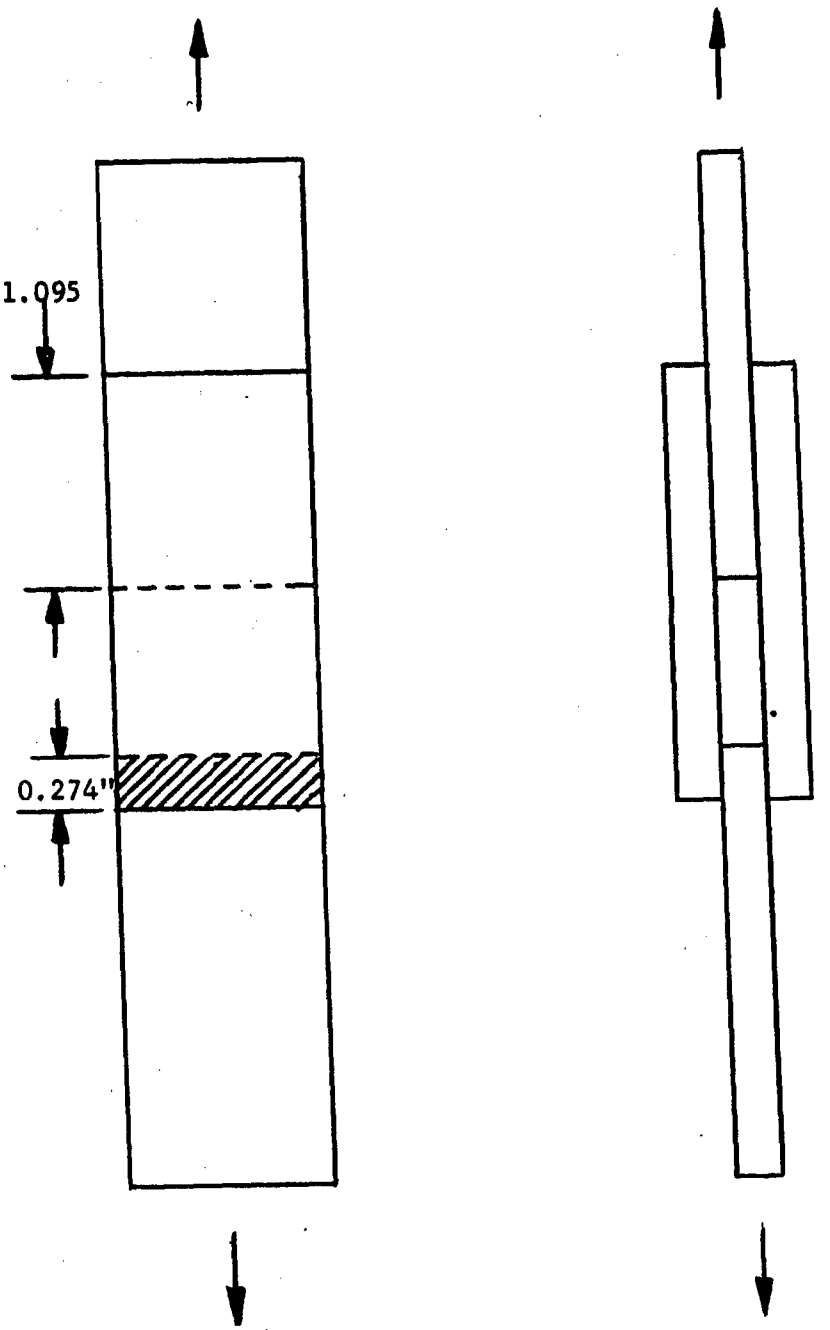


Figure 53. Test Specimen

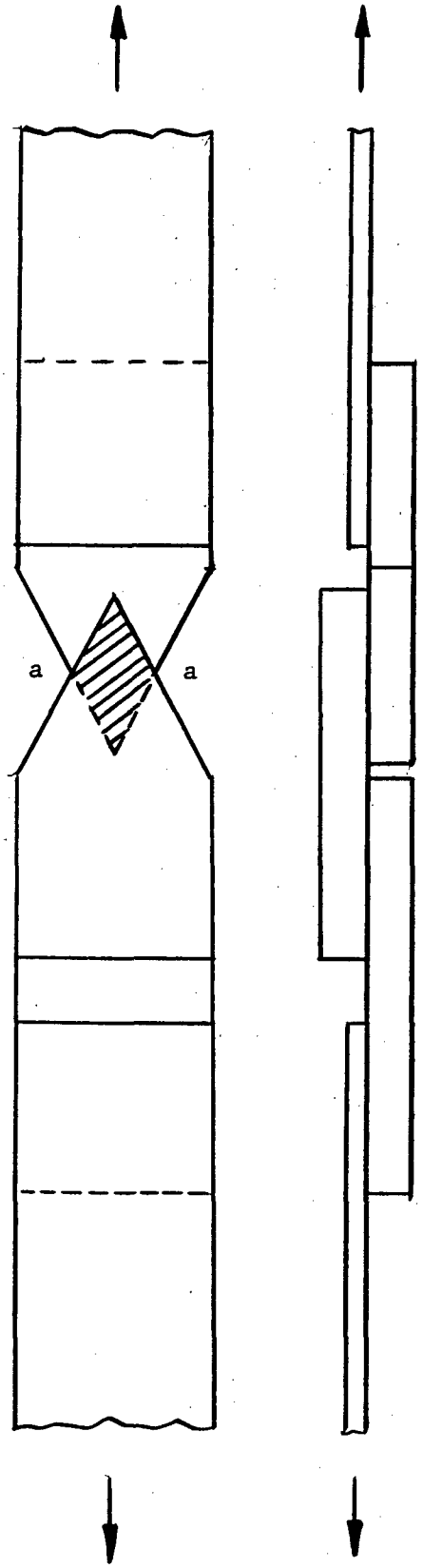


Figure 54. Test Specimen

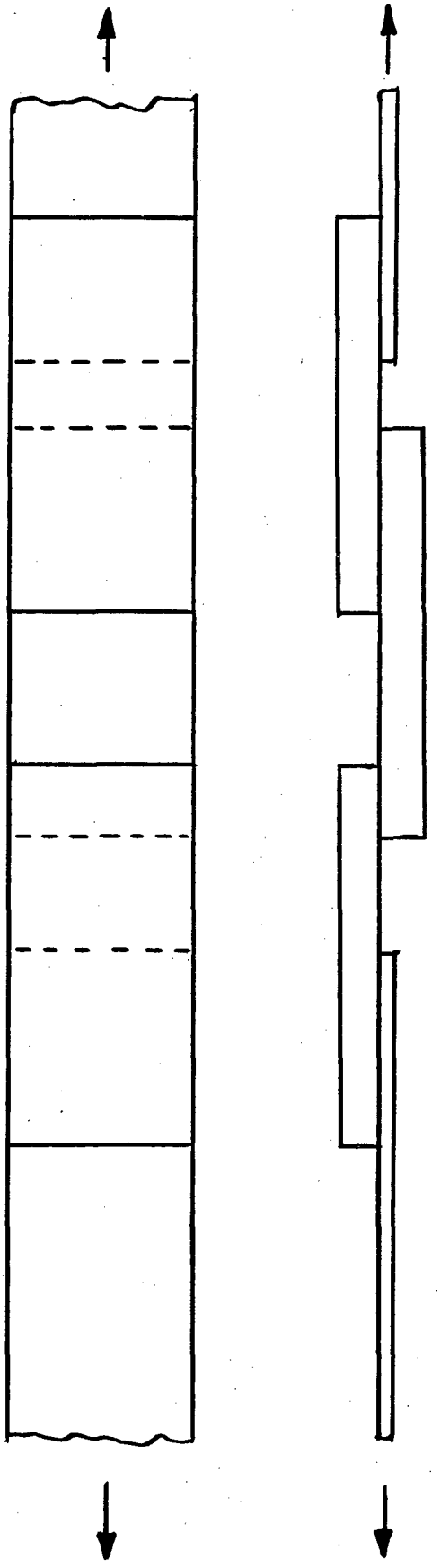


Figure 55. Test Specimen

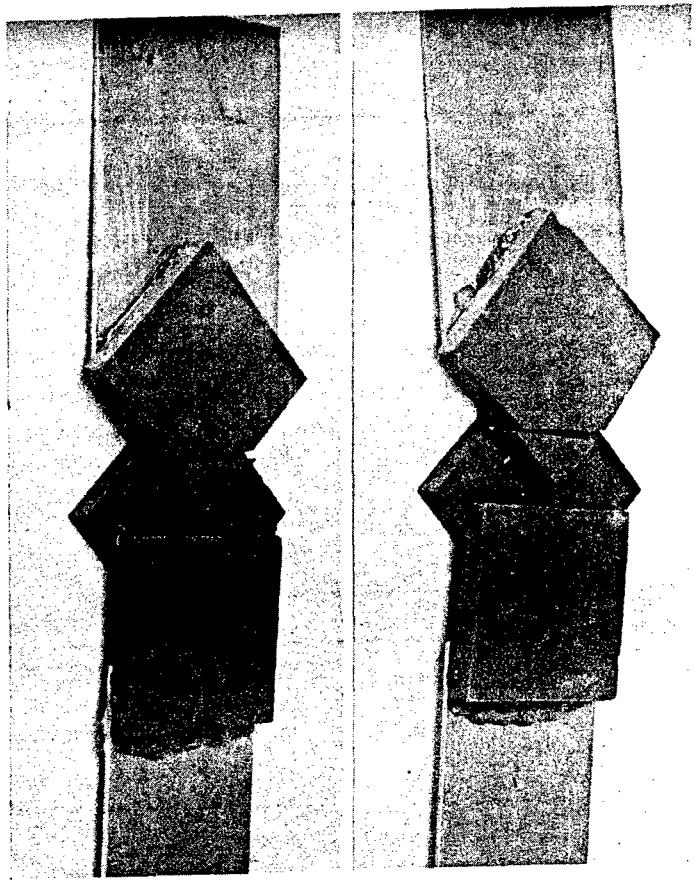


Figure 56. Test Specimens

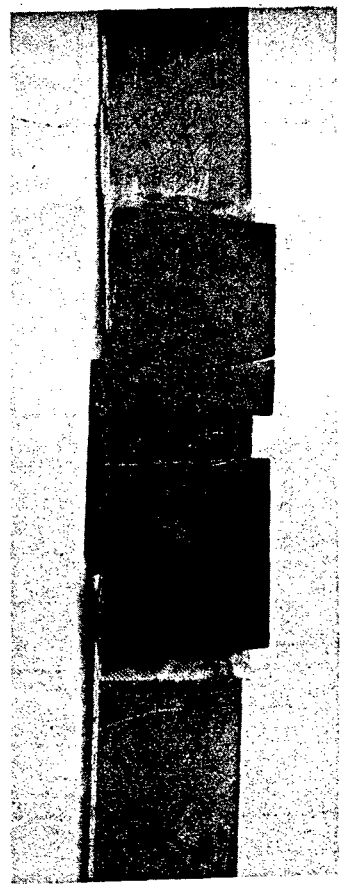


Figure 57. Test Specimens

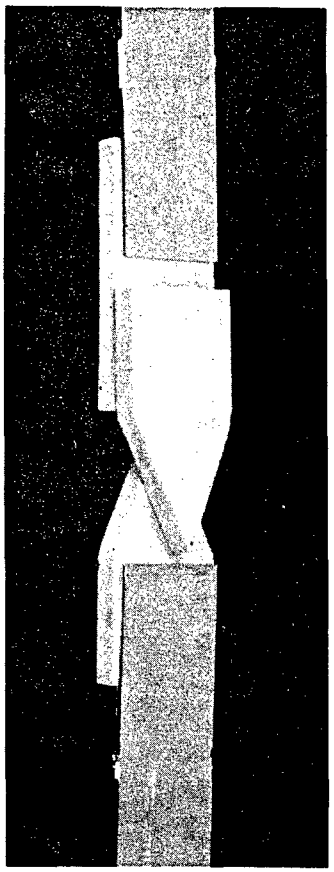


Figure 58. Test Specimen

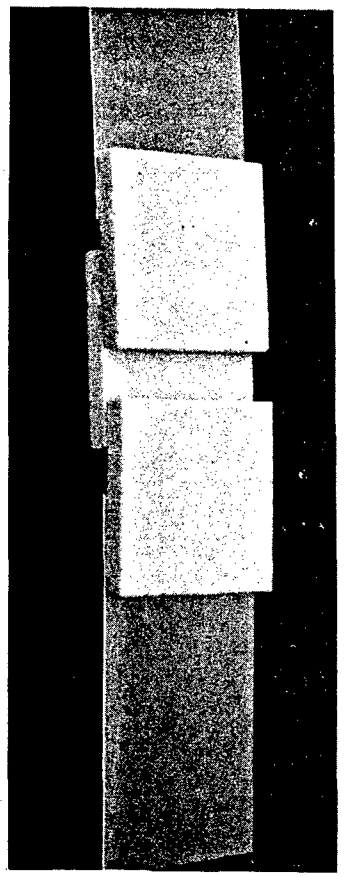


Figure 59. Test Specimen

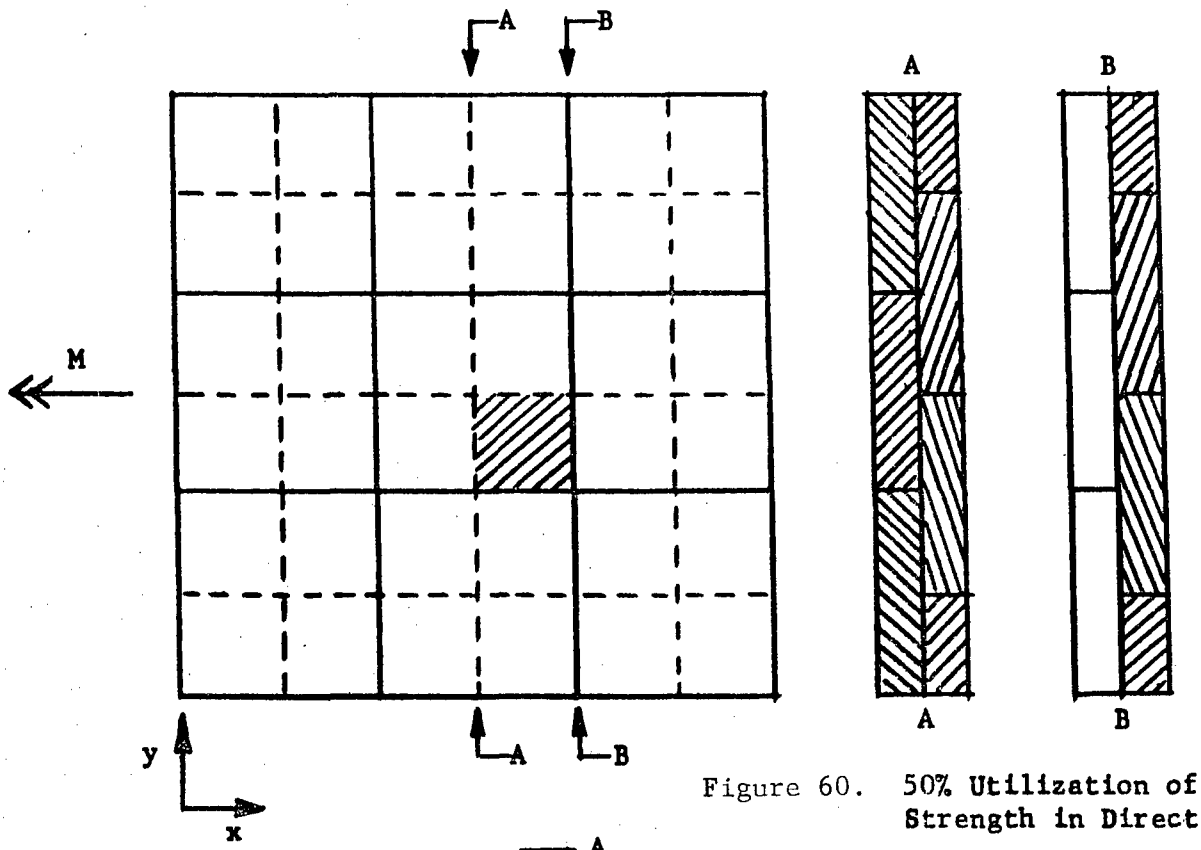


Figure 60. 50% Utilization of Material Strength in Directions of x and y

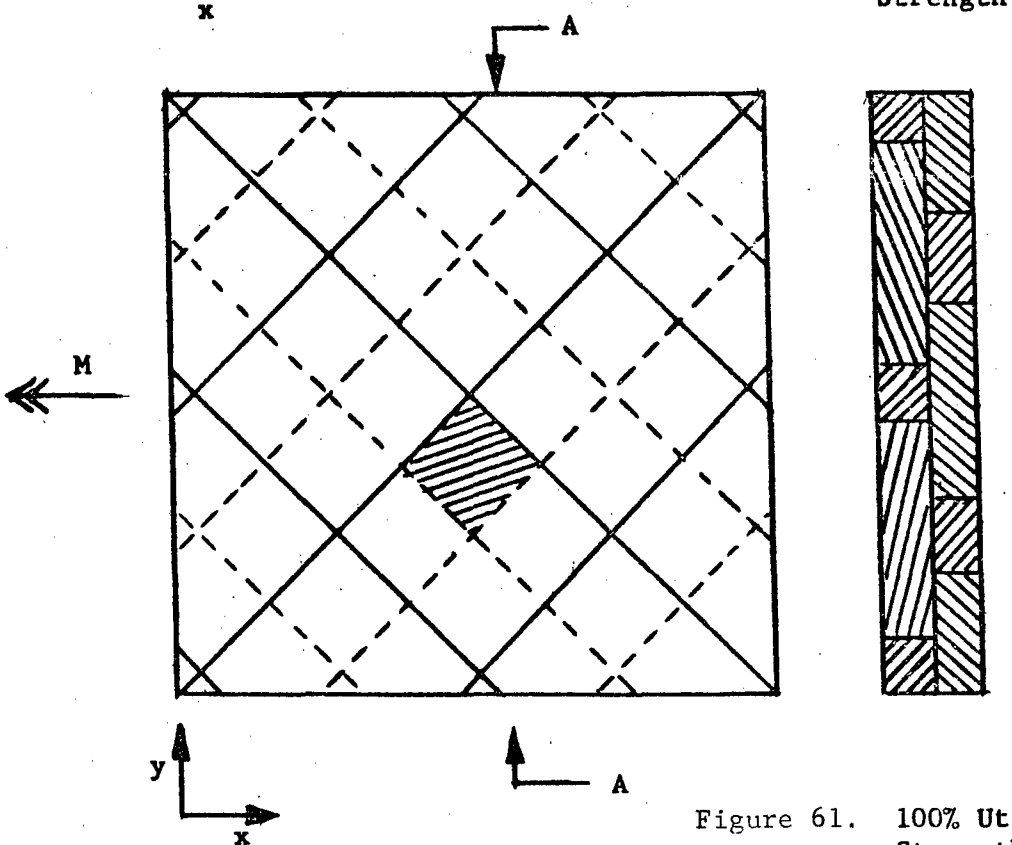
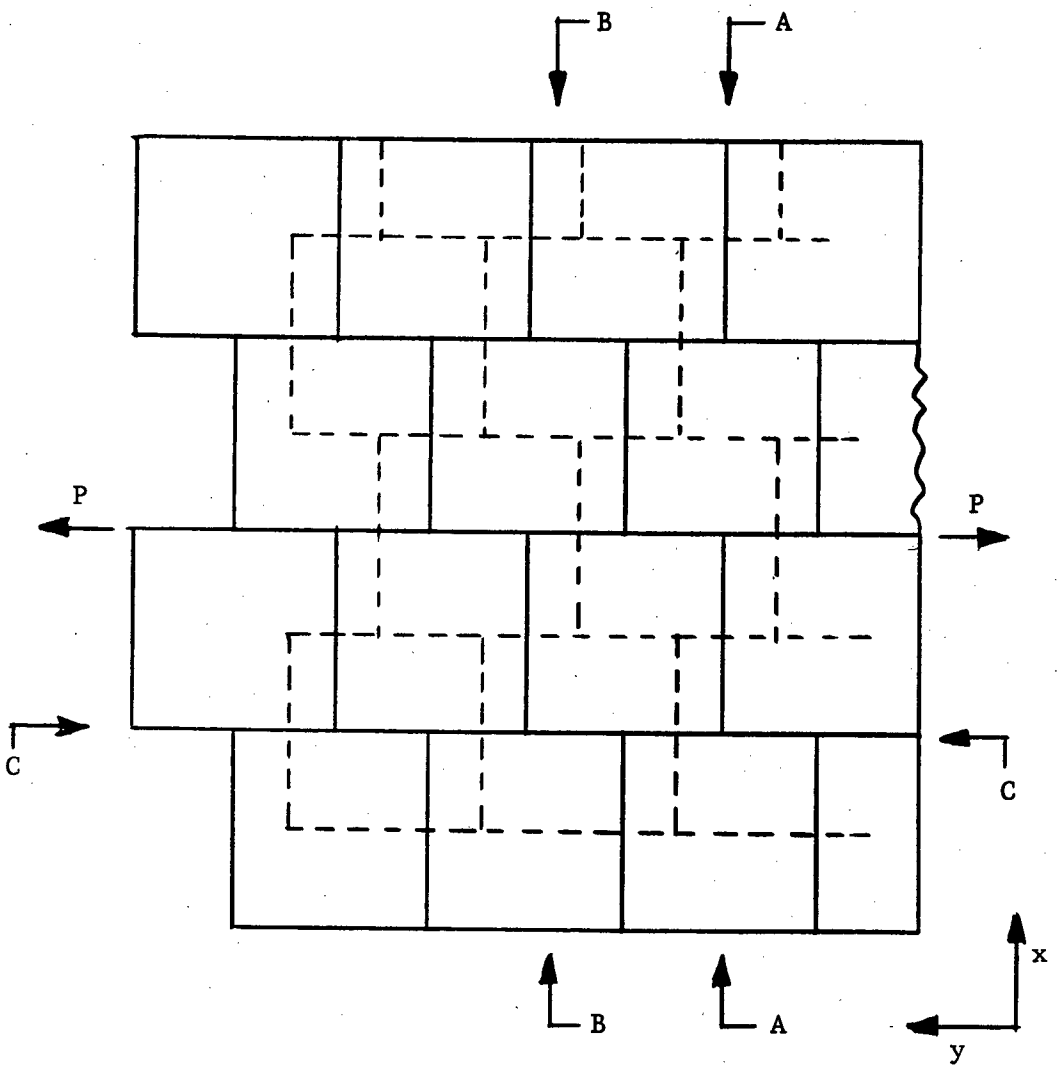
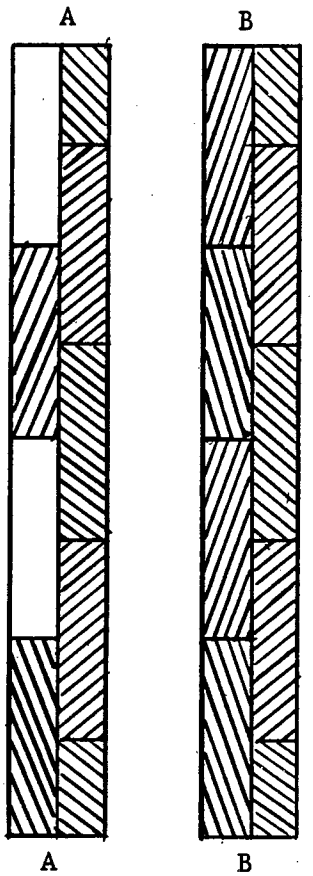
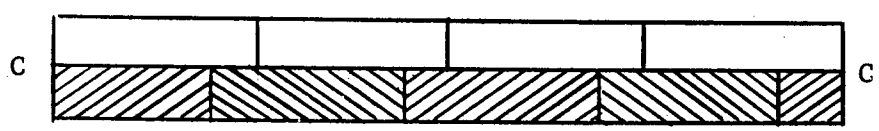


Figure 61. 100% Utilization of the Tile Strength in Two Perpendicular Directions



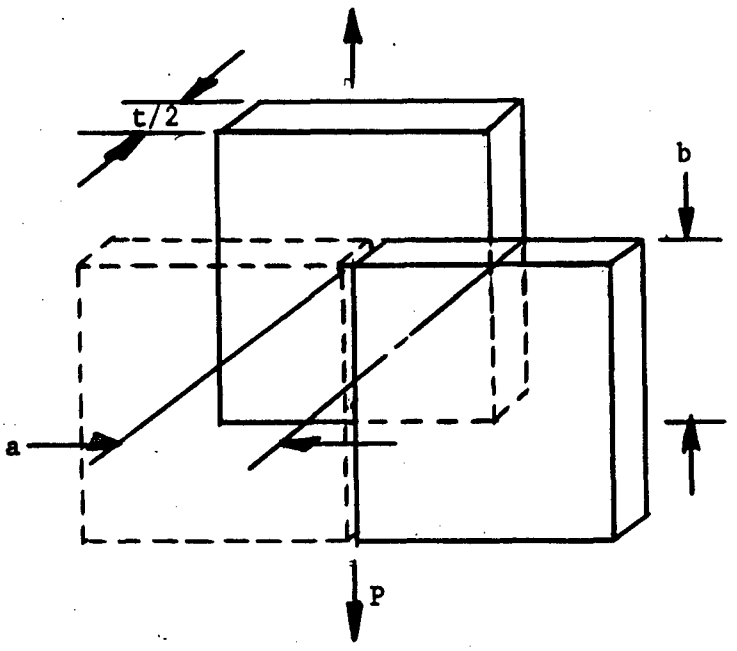


The weakest cross section is along one of the joints like A-A. The utilization of the tile strength is 75% in"y" direction.



Lateral direction - 50% of tile strength used

Figure 62. Arrangement of Tiles



Trapezoidal Tile

From the above sketch,

$$P = \sigma_T \, a \, \frac{t}{2} = \sigma_S \, a \, b$$

Force per length

$$P = \sigma_T \, \frac{t}{2} = \sigma_S \, b$$

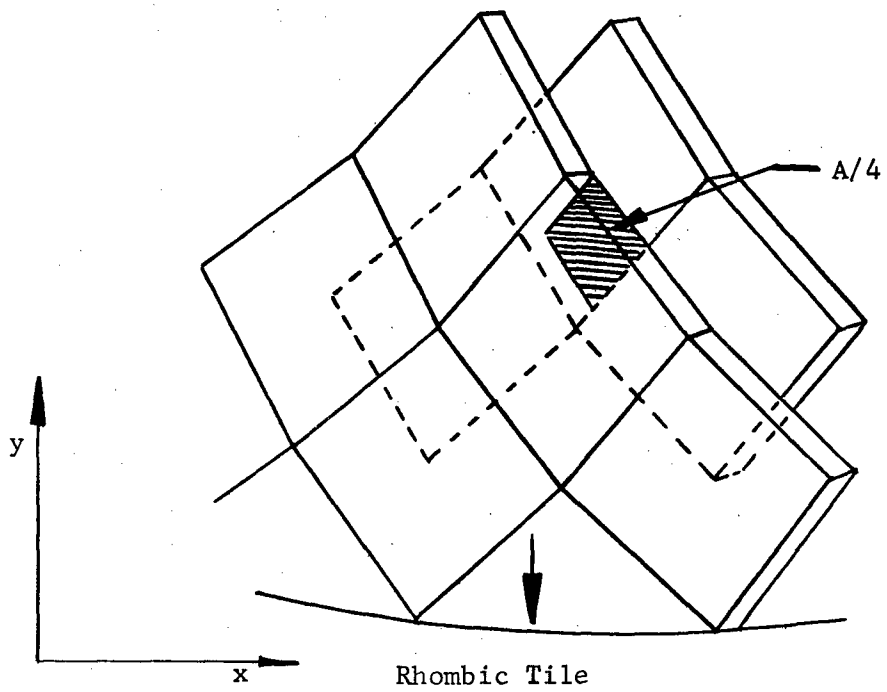
The minimum overlap depth is

$$b = \frac{\sigma_T}{\sigma_S} \, \frac{t}{2} = \frac{25{,}000}{4{,}000} \, \frac{0.221}{2} = 0.69 \text{ in.}$$

The 0.69-in. overlap should be easily maintained, particularly at the base or root section of the radome where the structural loads are highest and the tile dimensions largest.

The effective shear area is then equal to the total tile area. Since the total wall thickness "t" is given and is constant for the entire radome, the overlap area can be determined. This is also the limitation for the

minimum tile dimension. It is estimated that the minimum overlap of a rhombic tile is twice that of a trapezoidal tile. From this preliminary estimation for rhombic orientation



Rhombic Tile

the minimum tile area is obtained:

$$A = \left(\frac{\sigma_{tensile}}{\sigma_S}\right) t = \frac{25,000}{4,000} 0.221 = 1.325 \text{ in.}^2$$

It should be pointed out that the tensile strength of rhombic tiles in double layers is twice as strong in tension as the unstaggered trapezoidal arrangement of Figure 60.

Assuming a staggered, two-layer, trapezoidal configuration of tiles (Figure 63), there is, in the staggered direction, a 75% utilization of the tile strength if the minimum overlapping depth is not smaller than

$$b = \frac{\sigma_T}{\sigma_S} 0.75 \, t$$

$$= \frac{25,000}{4,000} 0.75 \times 0.221 = 1.035 \text{ in.}$$

The overlapping area must have a minimum mean depth of 1.035 in.

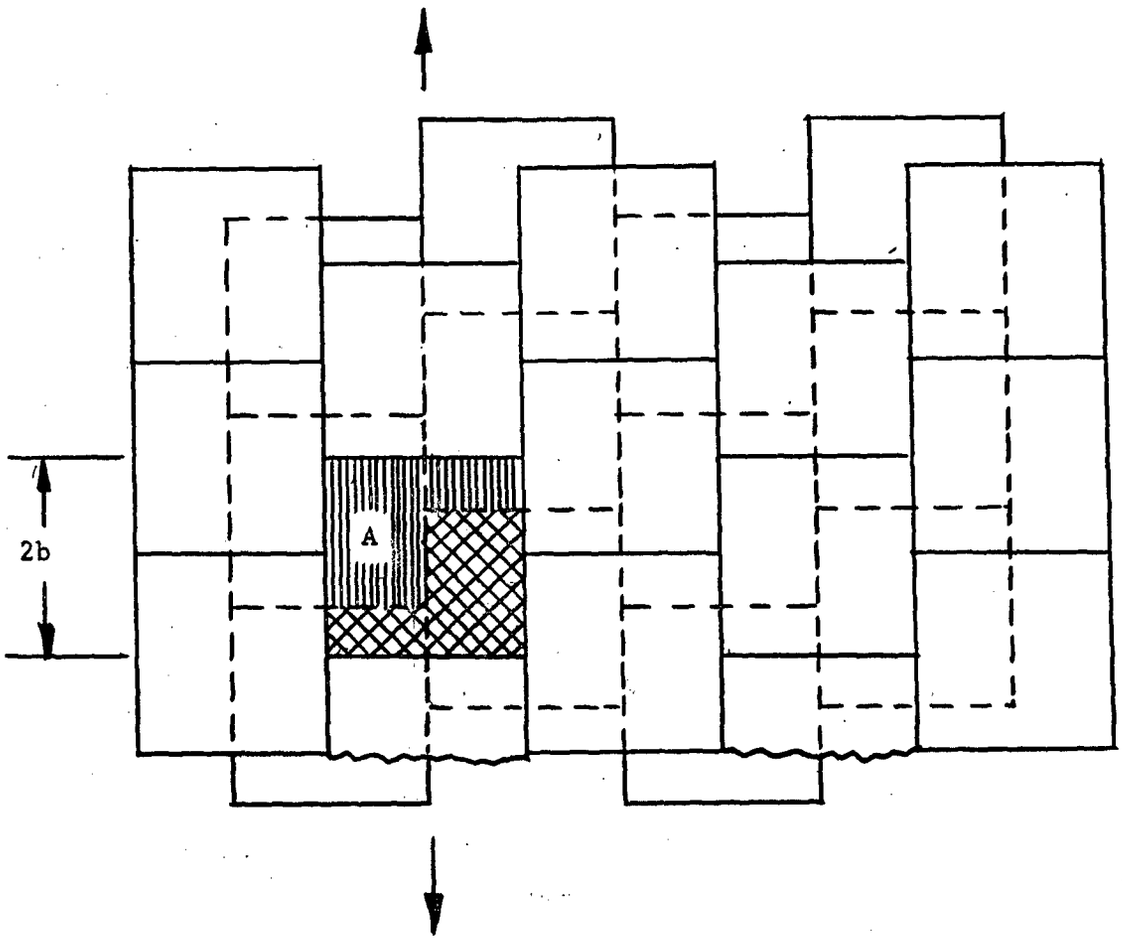


Figure 63. Flat, Two-Layer Trapezoidal Tiles

These analyses indicated that the configuration having each tile staggered in the meridional direction (as shown in Figure 64) would be optimum for this radome application.

MOSAIC RADOME THERMAL AND STRUCTURAL ANALYSIS

Engineering design and analysis of the composite mosaic ceramic radome concept was an essential part of the overall radome development program. In the early phases of the program, it became apparent that beyond the demonstration of manufacturing feasibility it was equally important to establish operational capabilities of the mosaic structure from the thermostructural viewpoint.

An arbitrary flight trajectory (Figure 47) was selected to serve as a basis for establishing of thermal and structural design loads representative of typical future environmental requirements of aerospace vehicles.

Thermal Analysis

An aerodynamic heating analysis was performed for the ogive shape radome under the selected trajectory conditions. The results of the boundary layer heat transfer calculations were used as imput data in a numerical two-dimensional thermal analyzer program, solving the transient heat transfer in the radome wall.

The results of this thermal analysis gave a complete temperature history of the radome wall. For the Mach 5 at 100,000-ft trajectory investigated, the maximum temperature reached by the ceramic radome structure was calculated to be 1400°F at the stagnation point. Surface temperature of points along the ogive were found to be significantly lower, ranging from approximately 1000°F at the first tile joint to approximately 400°F at the attachment section.

The maximum thermal gradients obtained in the numerical computation were 45°F at the stagnation point, reached at the end of the severe acceleration and climb phase of the trajectory, and 30°F in the mosaic tile section of the radome during the rapid deceleration and descent to sea level. Results of the analysis are delineated in Appendix VIII.

The relatively low calculated surface temperatures and moderate thermal gradients across the wall thickness indicated that the selected flight trajectory would not fully demonstrate the expected operational capabilities of the mosaic ceramic radome from the thermostructural viewpoint. In order to allow a general evaluation of the structure under similar but possibly more severe conditions, the thermal stress computations were carried out for several temperature profile approximations using a normalized unit thermal gradient value in addition to the actual computed thermal gradient case. For the particular trajectory under consideration, the highest thermal stress levels were obtained for a quadratic temperature profile approximation, which is in close agreement with the computed temperature distribution in the composite tile wall during rapid cooling. The distribution of the principle stresses in a typical tile section for this condition is shown in Figure 65. A detailed description of the computer analysis technique used in the thermal stress computations is given in Appendix VIII with results for several other temperature profile conditions.

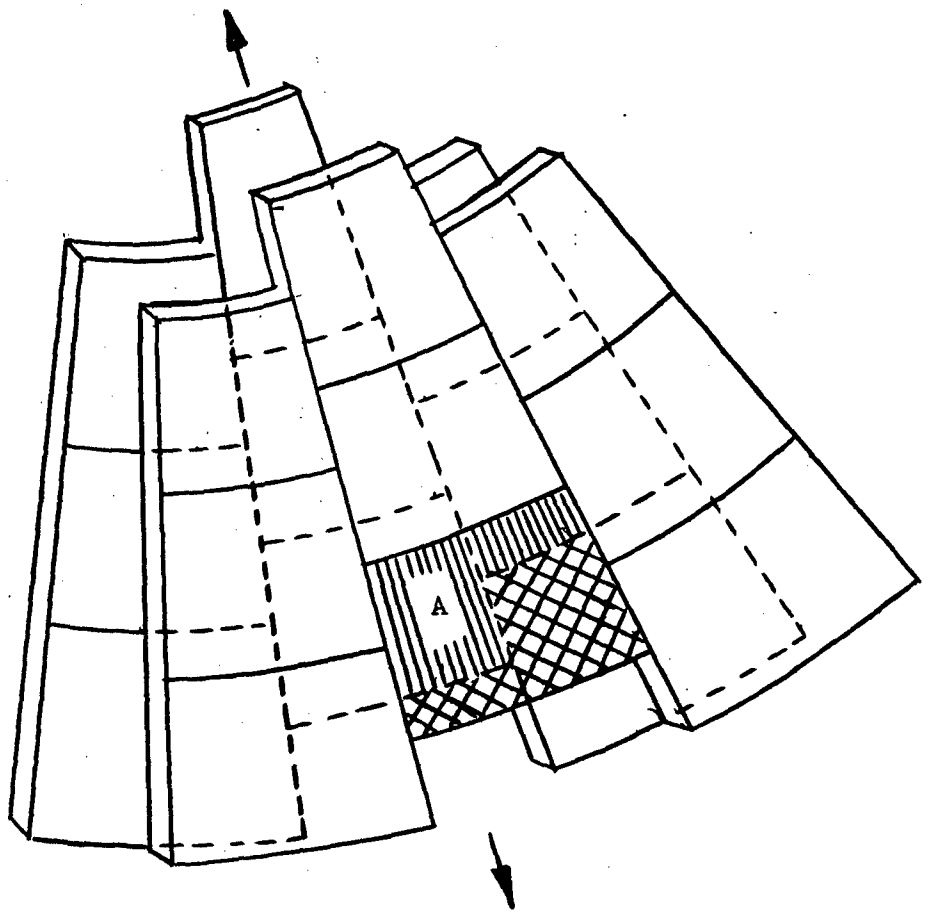
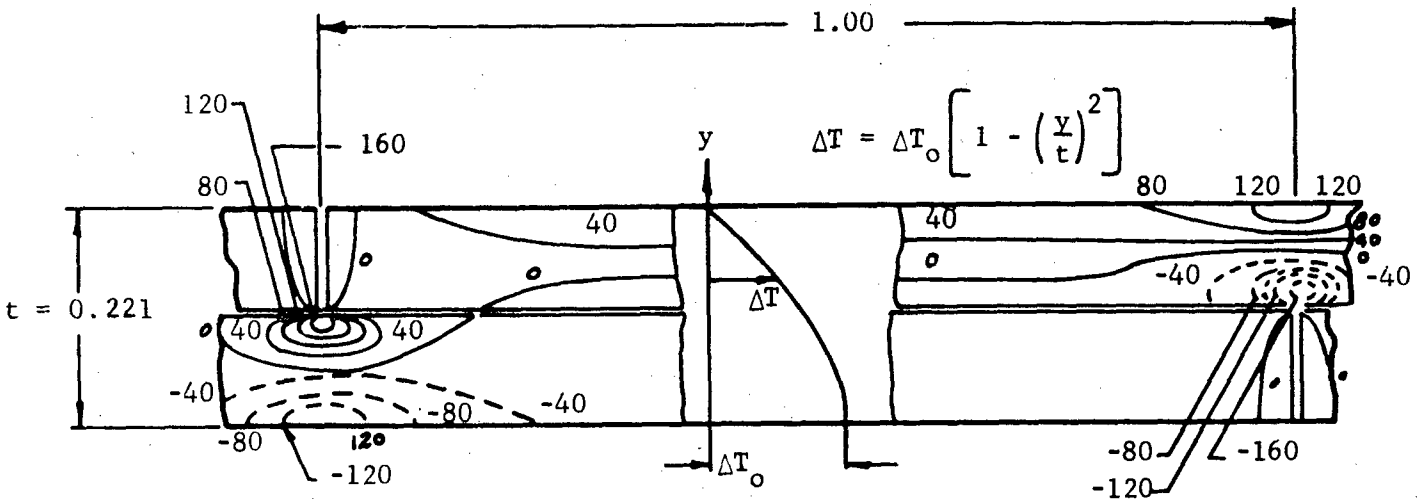
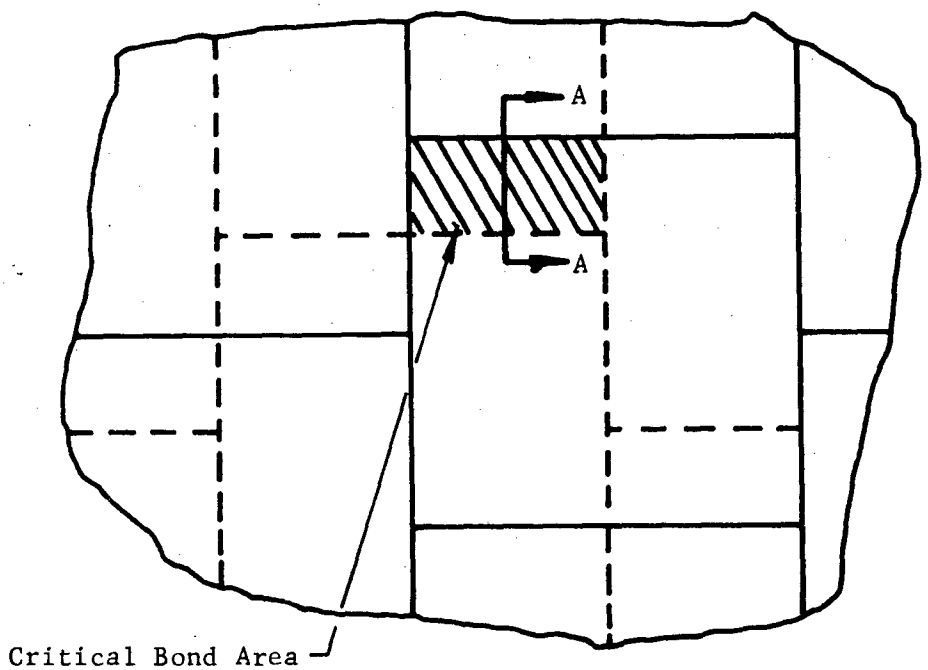


Figure 64. Ogival, Two-Layer Trapezoidal Tiles



SECTION A-A
(Rotated 90°)



NOTE: Numerical values of stresses in psi

Figure 65. Thermal Stress Distribution in Typical Tile Cross Section at Unit ΔT_o

Based on the stress distribution shown in Figure 65, it is easily seen that the maximum thermal gradient of 30°F calculated for the mosaic section of the radome would result in a maximum tensile stress level of

$$\sigma_T = 166 \frac{psi}{°F} \times 30°F = 5000 \text{ psi}$$

The alumina tile material has an ultimate tensile strength of at least 15,000 psi at 1000°F, therefore it is estimated that the mosaic radome structure could withstand a thermal gradient of approximately 90°F across its wall thickness.

This result supports the speculation that the trajectory used in this analysis does not fully demonstrate the operational capabilities of the mosaic radome. Based on the thermal analysis, it is estimated that a composite mosaic radome could operate under the assumed trajectory conditions at temperatures well above 1000°F.

Structural Analysis and Stress Concentration Considerations

The ogive shape of the radome does not lend itself to straightforward methods of structural analysis. Due to its ogival shape, the shell cannot be analyzed as a single truncated cone. The shell structure can be approximated by a series of separate conical shells, and a spherical tip cap.

In the early stages of the program, various methods of analysis were considered. The choice narrowed to two methods for obtaining the stress distribution in the shell. The first method was a combination of the hoopring and membrane theories, and the second a pure membrane analysis, with a modification required to obtain the hoop and longitudinal bending moments at the boundaries of the truncated cones. Due to the geometry and the loading (the radome has an axisymmetric geometry, load, and temperature distribution), the second method was chosen as the most practical and is described in Appendix VII.

A computer analysis as described in Appendix IX was programmed in order to establish, in some detail, the distribution of stresses within the individual tile used in the construction of the mosaic radome. The objectives of the analysis were twofold: first, to obtain information regarding stress concentration effects near the tile junctures; and second, to establish the distribution of loads across the bond holding the tile together. Two types of loading were considered in the analysis, one being analogous to a pressure loading of the radome and the other a thermal gradient across the thickness of the tile.

Besides the thermal gradient obtained from the Lockheed "Thermal Analyzer Program" (Reference Appendix VIII), thermal loading conditions were applied simply to generate stress influence coefficients for linear, quadratic, and quardic thermal distributions across the section with the idea that these distributions might be superimposed in various proportions in order to gain insight into other thermal loadings which might be present in future radome studies.

The results of the computer analysis were summarized as stress concentration factors for an individual tile for a prescribed number of loading conditions. The advantage of this approach is that the computer results can be combined with the previously mentioned membrane analysis, and the margins of safety for the radome can be obtained for the given stress concentrations and loadings without having to perform a computer run for every loading condition or radome geometry in the case the dimensions of the radome are changed.

The stress concentration factors are presented in graphic form in Figures 66 through 73. These curves were obtained from the computer results reported in Appendix IX. The stress concentration factors shown in the curves were to be applied to any stresses produced by the static tests or calculated for the dynamic pressure distribution.

An important factor to be noted regarding the computer analysis evaluation is the assumption that the butt joints between tiles were adhesive-free and all loads were carried between overlapping tiles through shear in the adhesive. The assumed absence of adhesive in the butt joints would increase the magnitude of the stress concentration factor, therefore making the computer analysis slightly conservative.

At the onset of the analysis, there was doubt as to whether or not the small temperature drop across the tile thickness would produce significant stresses. The analysis indicated that axial stresses near the tile joints in the order of 4000 psi (including stress concentration factor) may exist due to thermal gradients. Apparently thermal effects, from even small temperature drops across the tile, play a quite significant role in the total stress picture.

The magnitude of the stresses (due to a uniform external dynamic pressure) obtained from the membrane analysis is relatively small. The hoop stress at the base of the radome is approximately 1200 psi, and is 600 psi near the tip at the first row of tiles. The axial stresses are also rather small, varying from about 250 psi at the tip to 115 psi at the base. The hoop and axial stresses have to be magnified by the appropriate stress concentration factor, and then combined with the applicable thermal stress to obtain a realistic margin of safety.

The computer analysis produced considerable information as to stress magnifications in the vicinity of tile boundaries and indicated that they could possibly approach 10 in the axial direction. The analysis, of course, yielded no information as to design allowables for this type of ceramic structure.

Base Attachment

A difficult problem associated with any ceramic electromagnetic window is that it must be attached to a metallic base structure. This problem becomes especially critical in the case of the mosaic ceramic radome where (1) service temperatures eliminate the possibility of using an organic adhesive or a resilient, stress-distribution interface material; (2) the large size and brittleness of the ceramic would dictate an "impossible" match of expansion coefficients and control of concentricities for the use of a ceramic-to-metal braze; and (3) operational requirements call for an attachment fixture flush with the outer surface of the ceramic radome base.

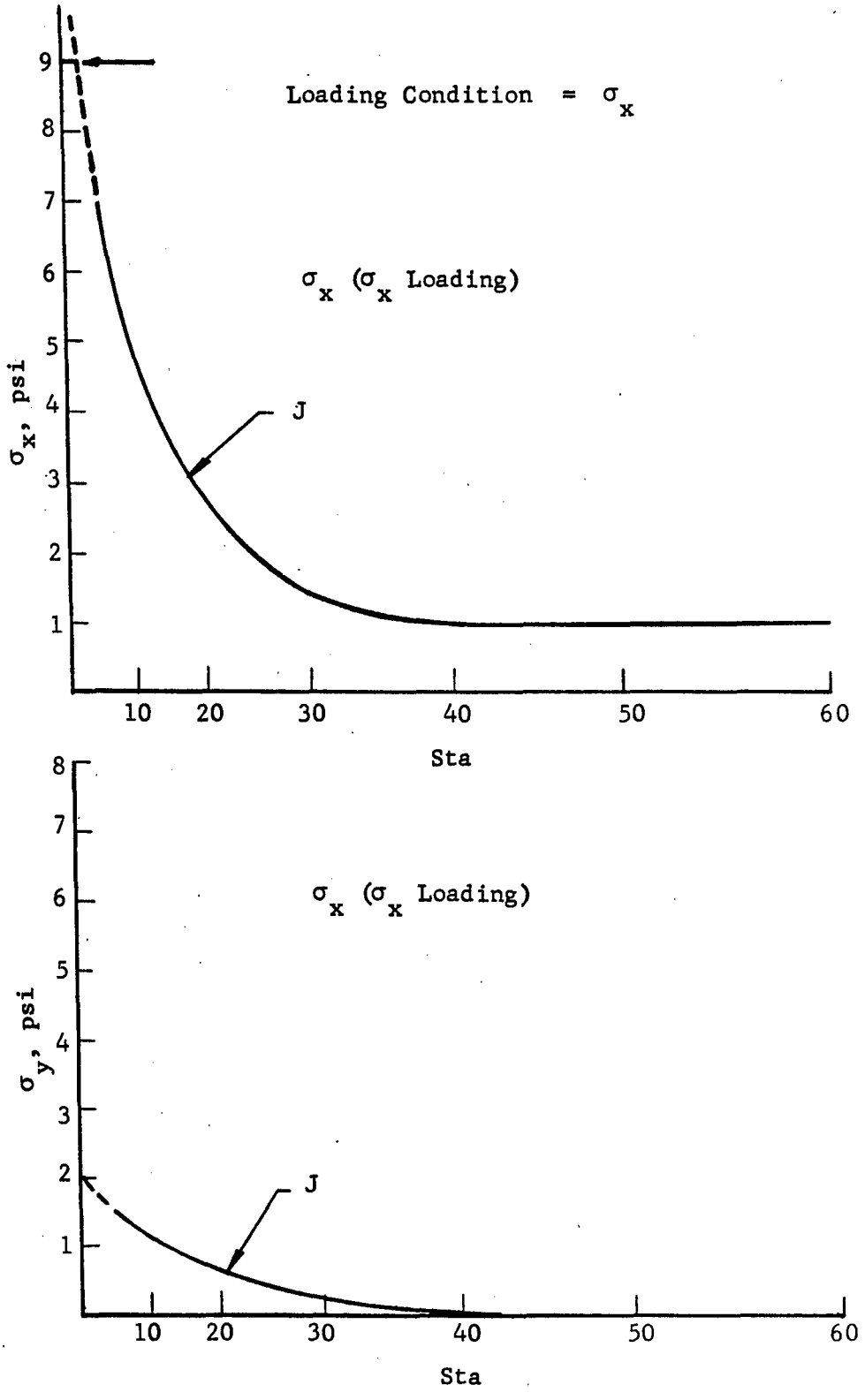


Figure 66. Stress Concentration Factors

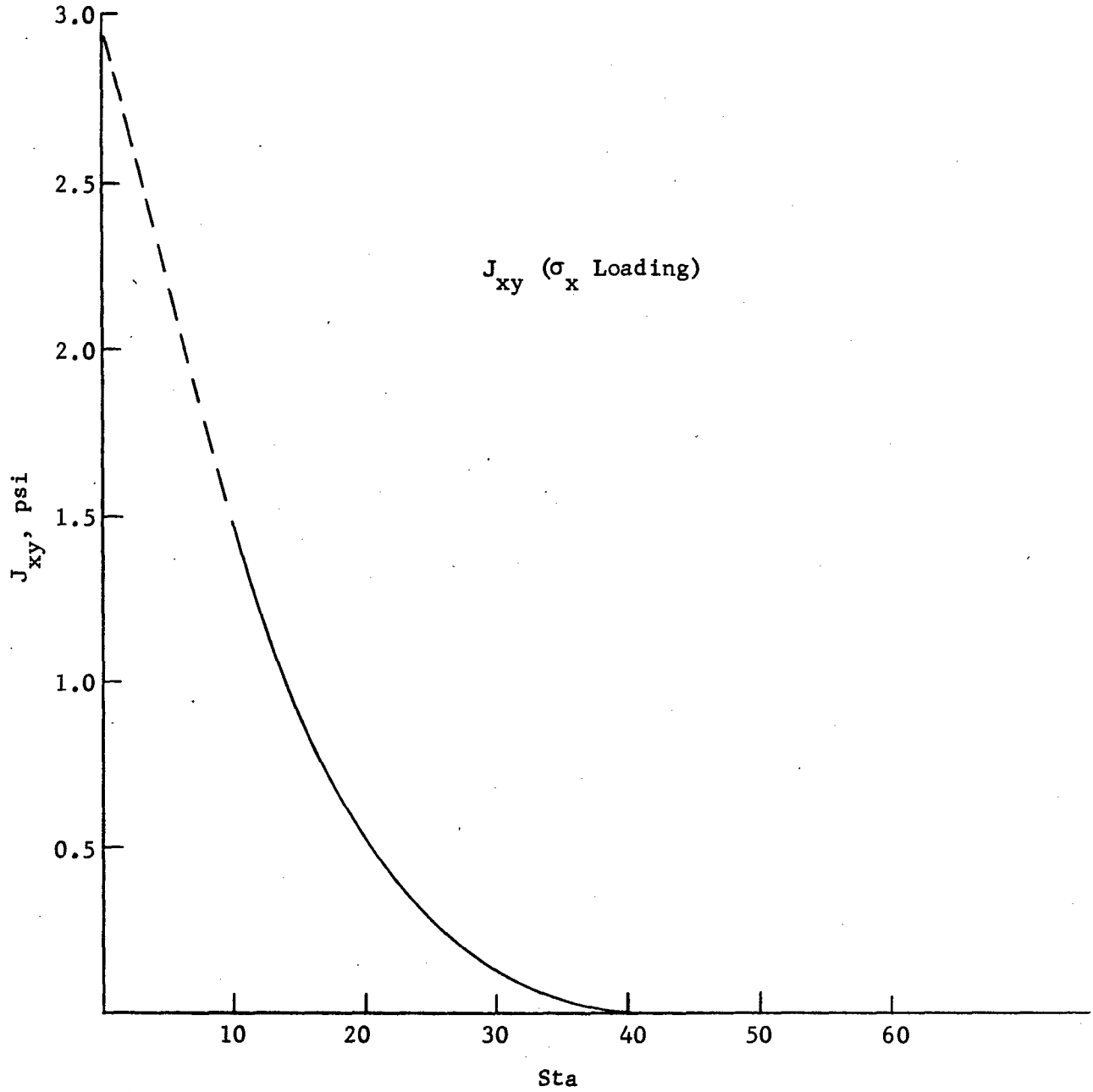


Figure 67. Stress Concentration Factors

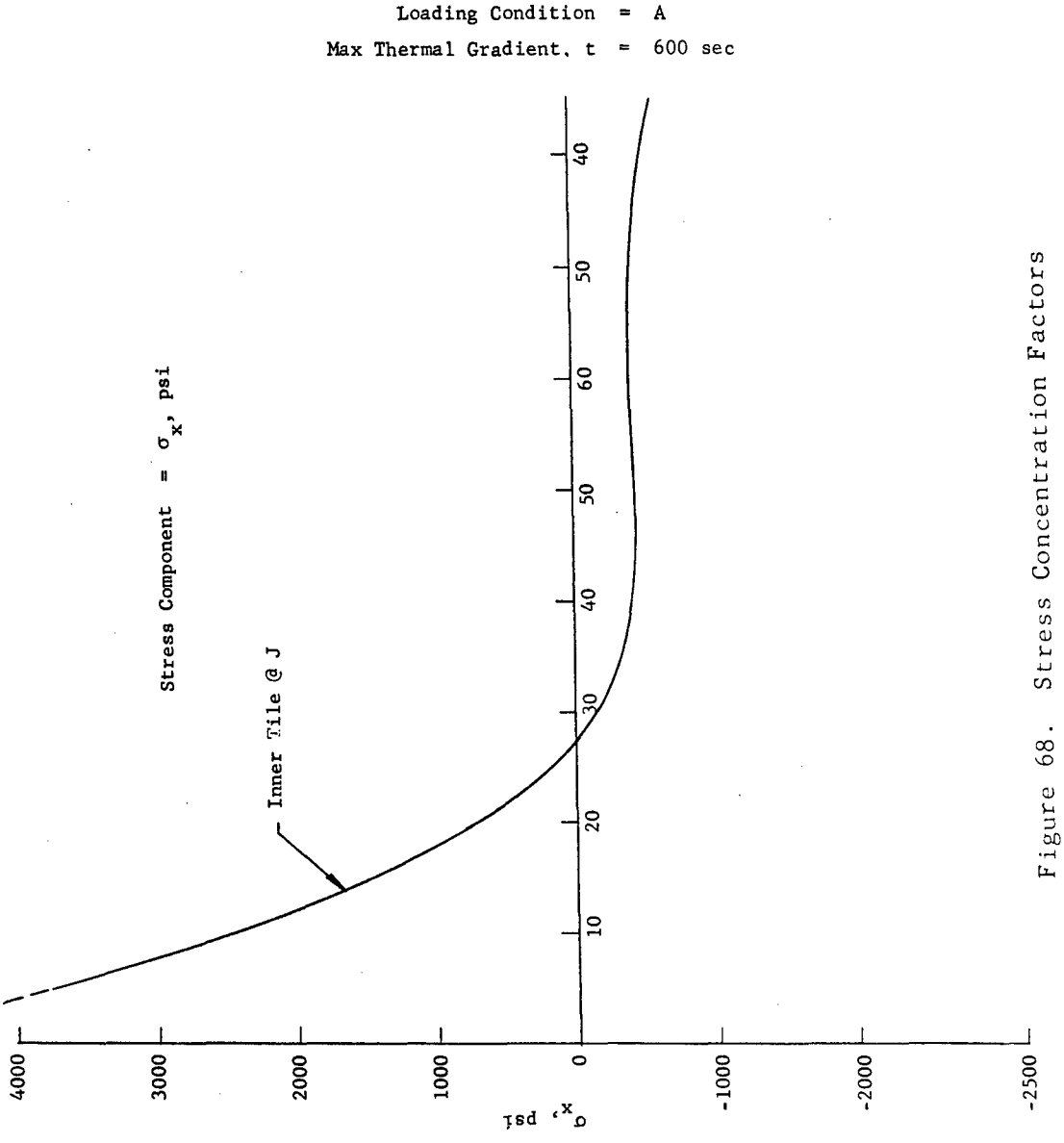


Figure 68. Stress Concentration Factors

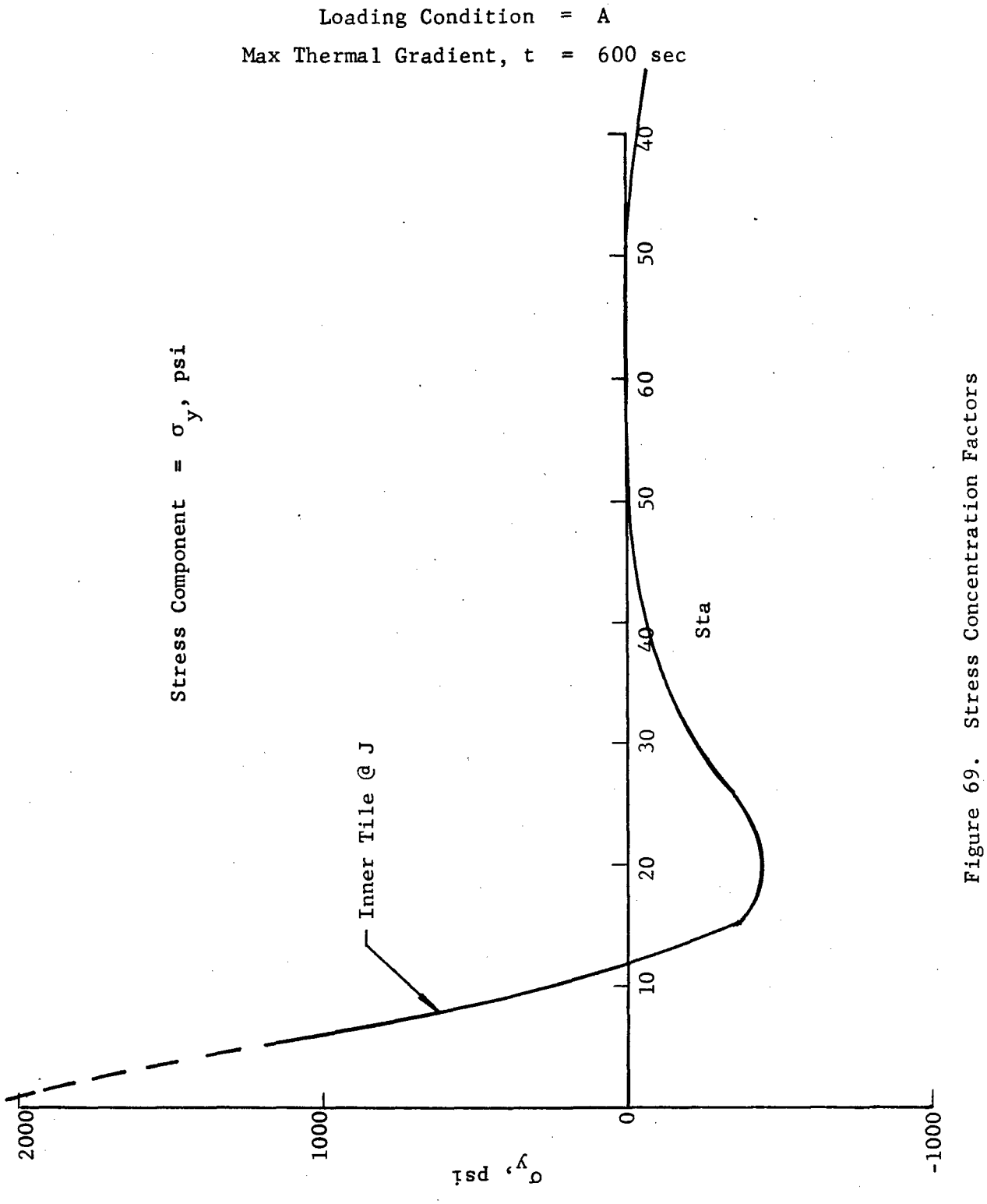


Figure 69. Stress Concentration Factors

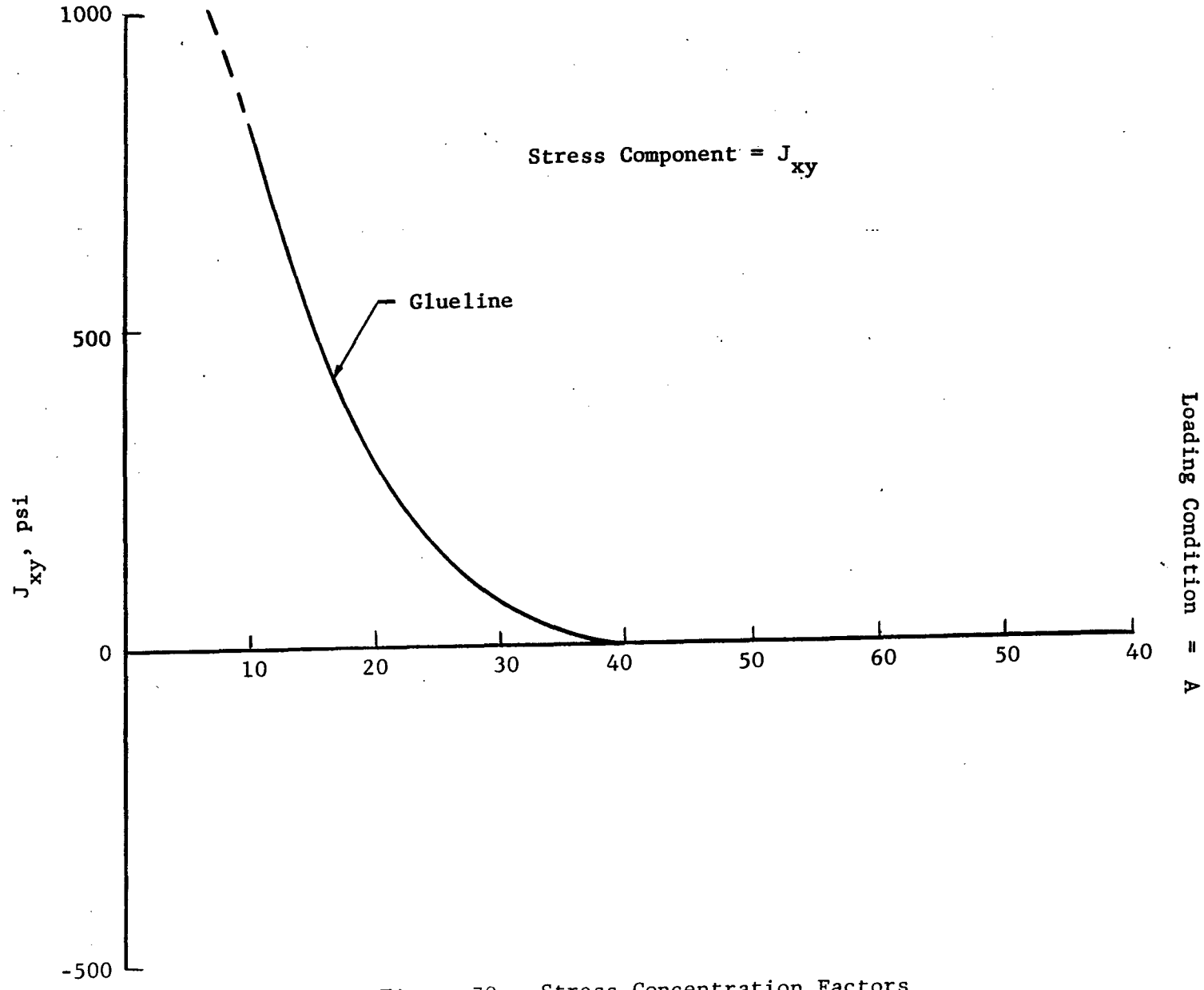


Figure 70. Stress Concentration Factors

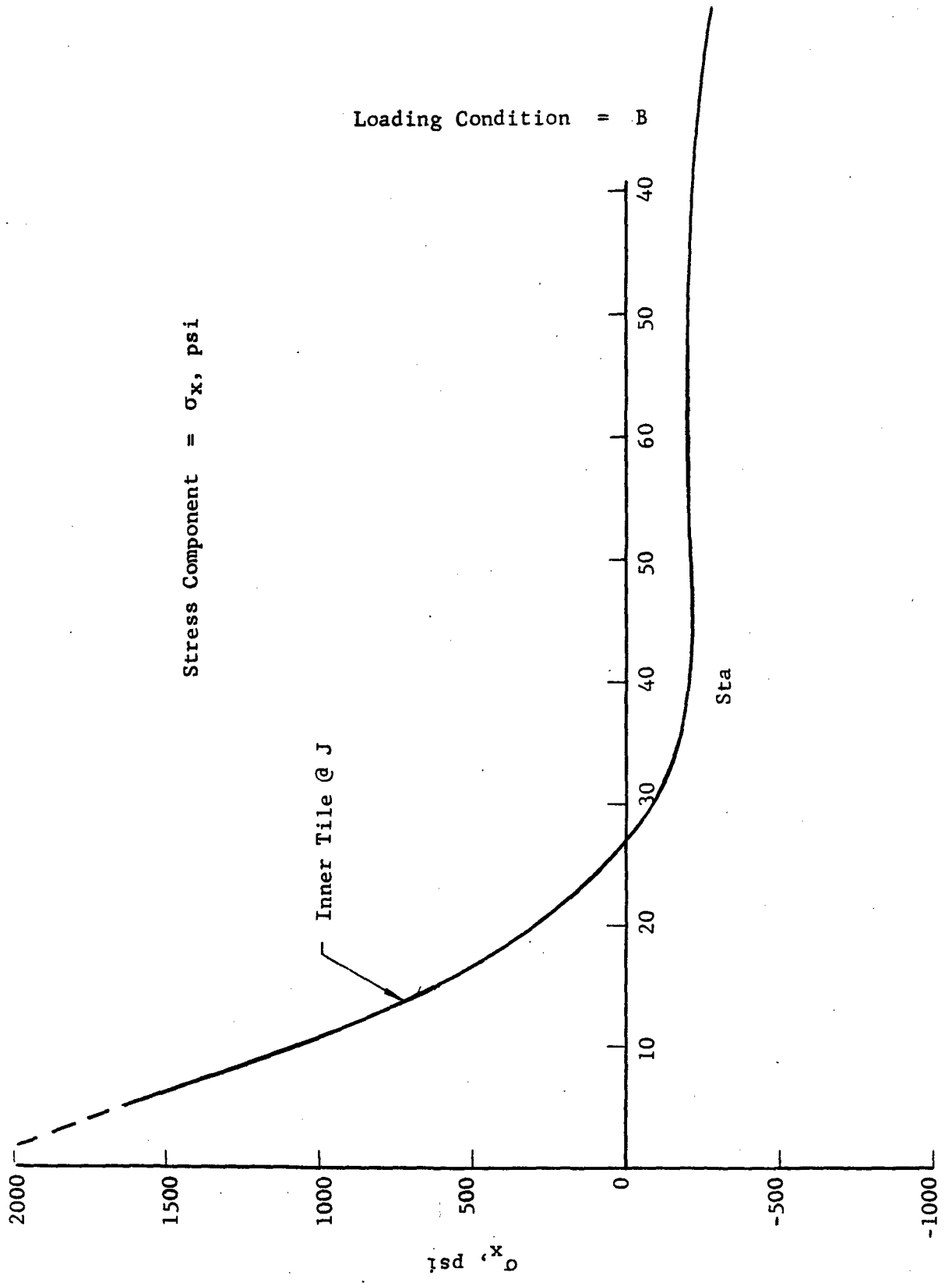


Figure 71. Stress Concentration Factors

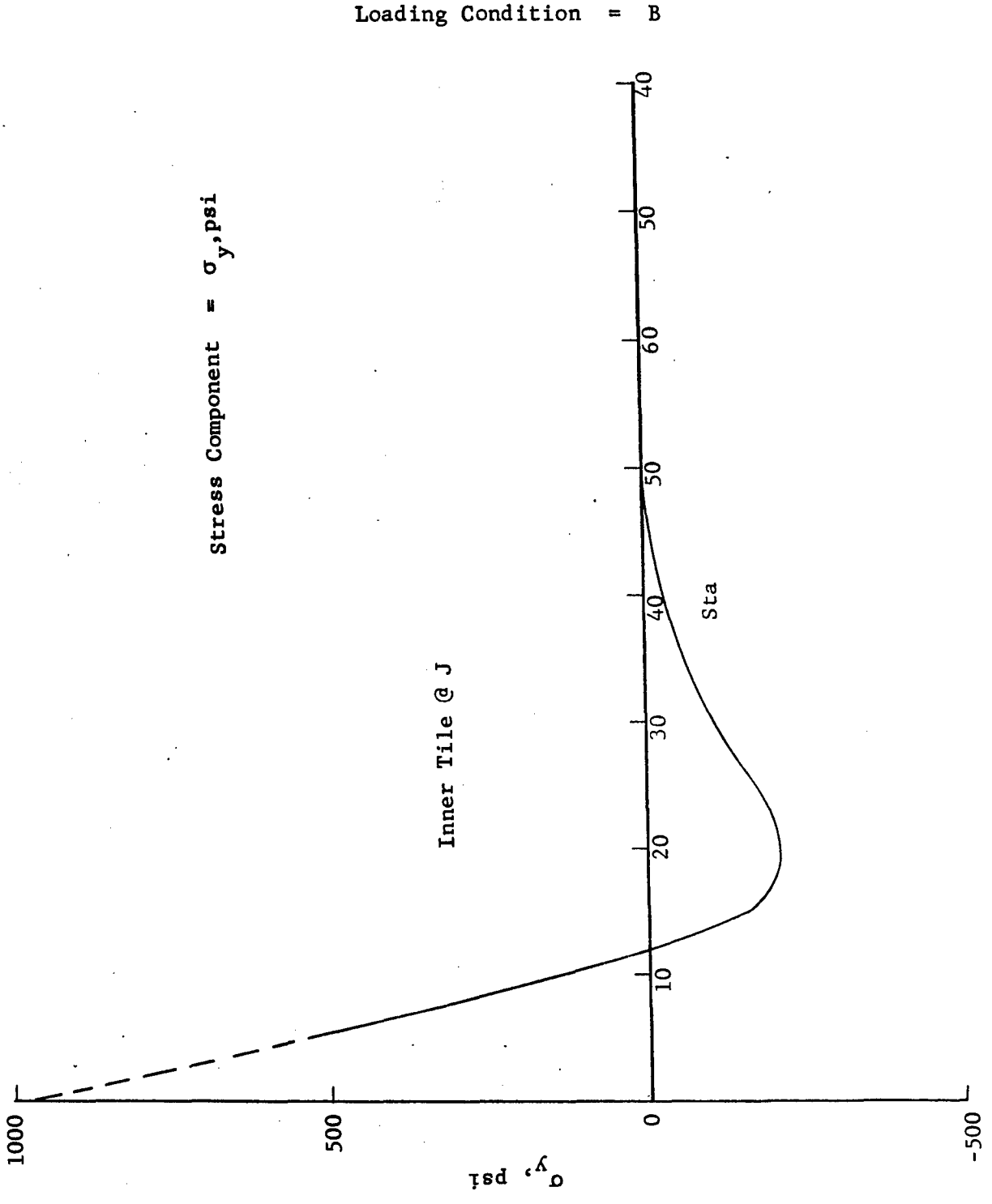


Figure 72. Stress Concentration Factors

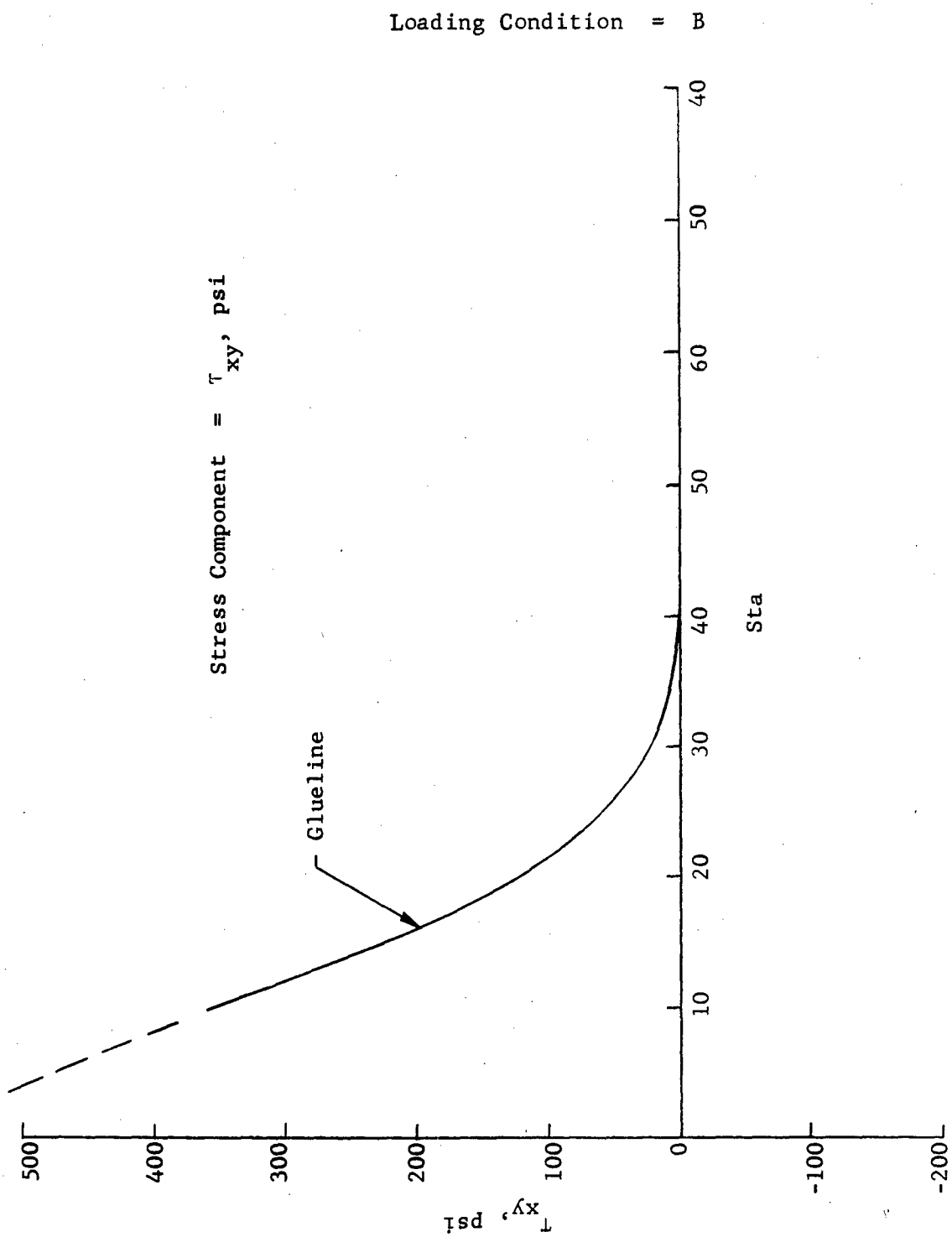


Figure 73. Stress Concentration Factors

Analytical and design considerations (see Appendix VI) resulted in the attachment concept illustrated in Figure 74. It consists of 24 attachment fixtures of Kovar alloy, which has a coefficient of thermal expansion slightly lower than that of the alumina tile. A separate fixture section for each base tile would allow for minor dimensional variations, and the copper shims would promote stress equalization over the tile-to-metal surfaces. A thickened "shoulder" section on the base tiles was to be placed in a desired state of compression by Kovar wire windings on the outside circumference of the metal fixtures. Finally, a large measure of thermal and mechanical stress isolation between the radome and vehicle or test stand structure was to be achieved by a semifloating mounting design which would accommodate considerable concentricity mismatch. The engineering design drawing for this attachment design is included as Narmco Drawing NR 63-061 in Appendix X.

Thermal expansion characteristics of candidate base attachment materials and yield strength vs temperature for the selected materials are shown in Figures 75 and 76 respectively. The 24 Kovar outer attachment segments and 24 stainless steel inner segments were manufactured by the Arrowsmith Tool and Manufacturing Corporation (San Diego, California). These attachment fixtures are shown assembled on the full-scale radome in Figure 77. Figure 77(a) shows an overall view of the assembly, while 77(b) is a close-up showing the three-layer Kovar wire winding that would ensure a tight compression fit of the outer attachment fixtures to the base tiles. Bolts rather than studs were used for the assembly as a matter of convenience. It should be noted that the use of studs would eliminate the need for exposed nuts on the outer surface; however, this was not considered essential for the test purposes comtemplated.

ANALYTICAL COMPARISONS WITH TEST RESULTS

Although test results are delineated in Section XIII, the results are reviewed here for direct comparison with the analytical and design predictions. Both the truncated and the full-scale section failed in the tile array of the ogive structure beyond the attachment, as predicted. The failing stresses with the application of the tile joint concentration factor of 9 (reference Figure 66) were 15,660 psi (truncated test) and 12,015 psi (full-scale radome test). The tile joint closure in the full-scale radome was not as good as in the truncated section; this strength variation is not unusual for brittle ceramic materials. The results were considered representative of an excellent comparison with the predicted stress level of 15,000 psi obtained by analytical techniques developed under this contract.

The test completely supported the attachment design philosophy in that not only was failure achieved near the predicted level in the conical section but the stress concentration in the attachment was reduced by a factor of 3. This was demonstrated by the apparent stress level (stress level before superimposing a stress concentration factor) in the attachment area of 3,560 psi, compared to the failure section (1,335 psi). This indicated that ceramic radome attachments utilizing the design techniques presented in this section can be used with confidence. Also, the thermal test supported the analytical approach presented in this section very satisfactorily. The analytical predictions indicated that the structure could withstand gradients up to 90°F. The tests indicate capabilities of withstanding thermal gradients in excess of 100°F. In general, the results indicate this analytical approach can be used for predicting thermal effects.

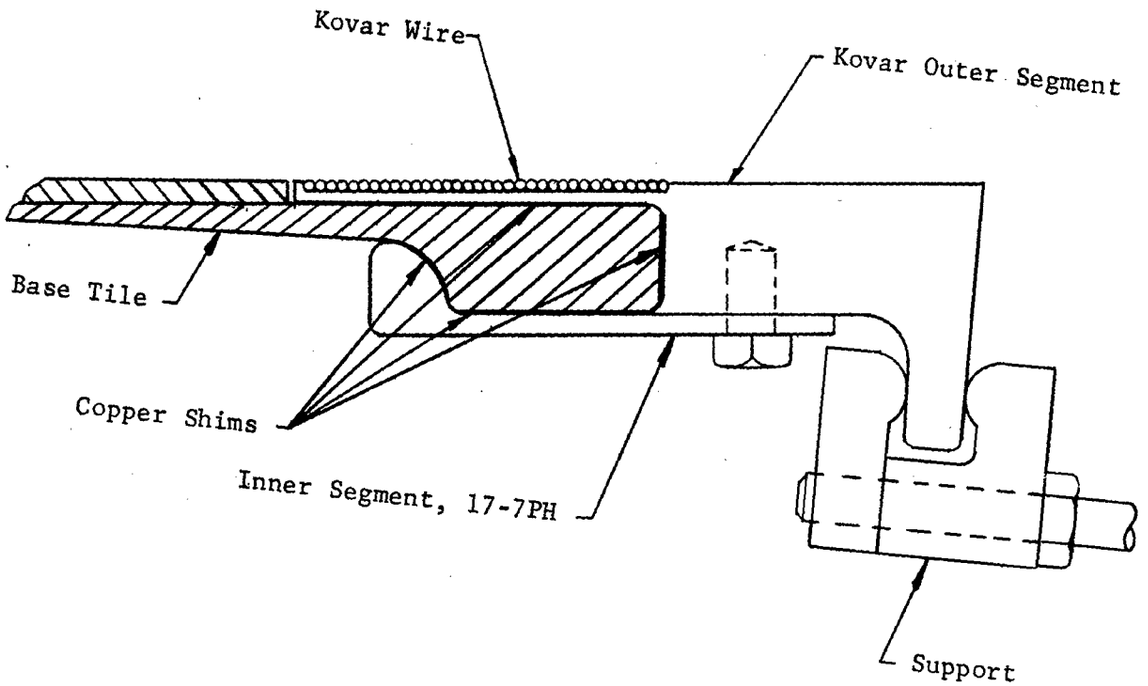


Figure 74. Base Attachment Design

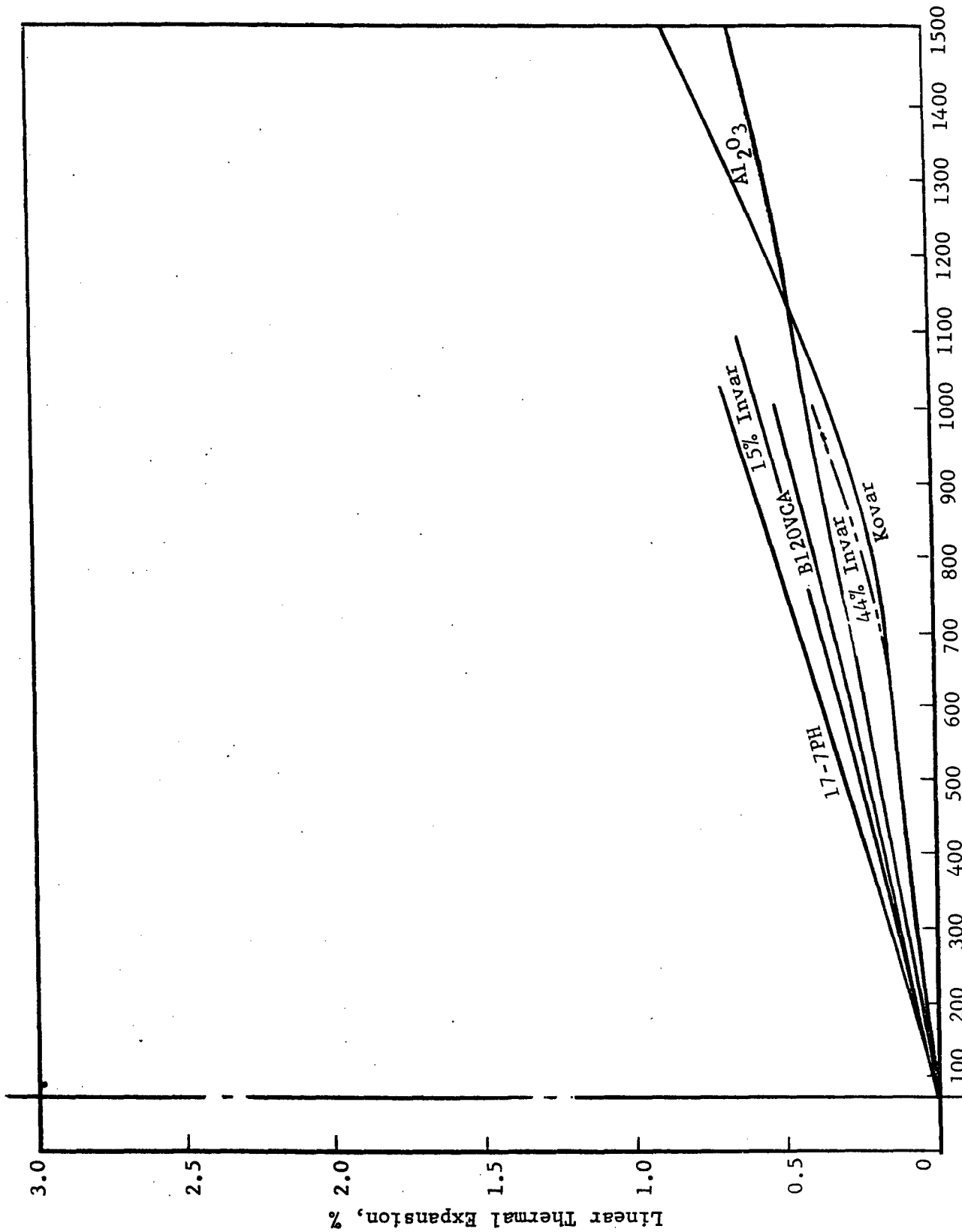


Figure 75. Linear Thermal Expansion

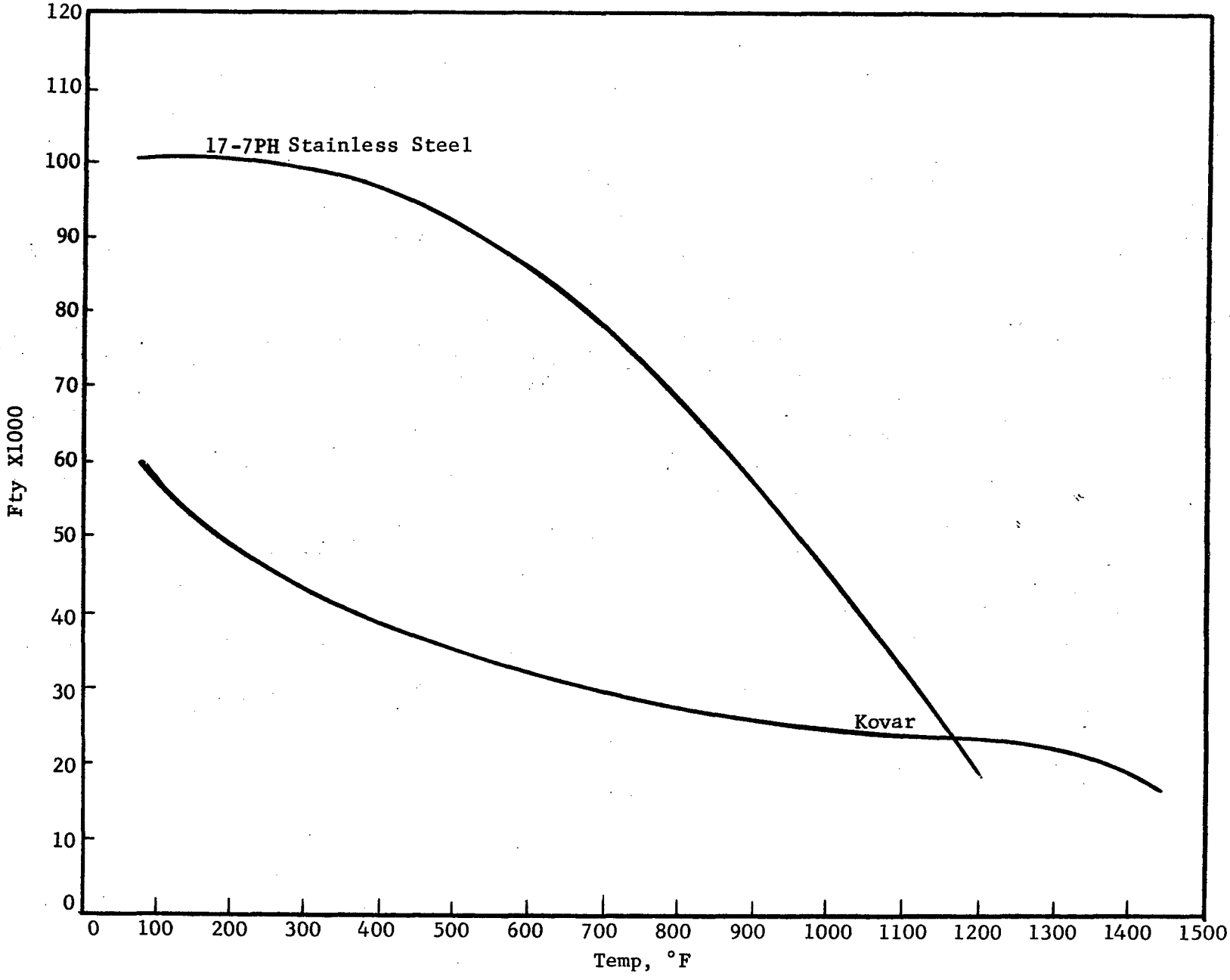
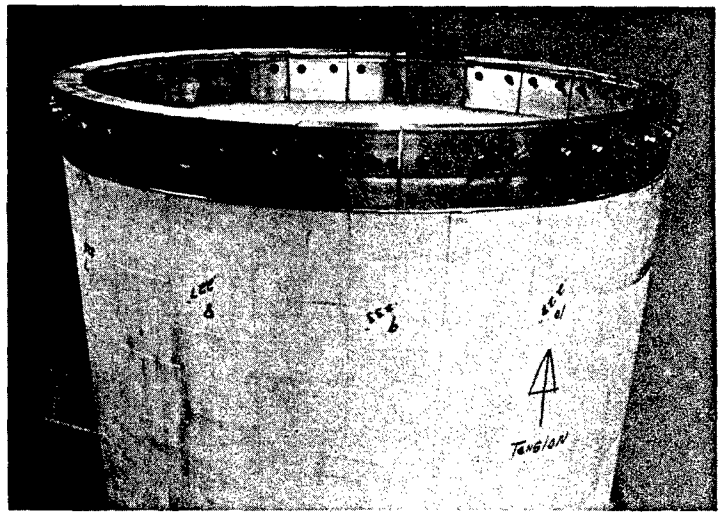
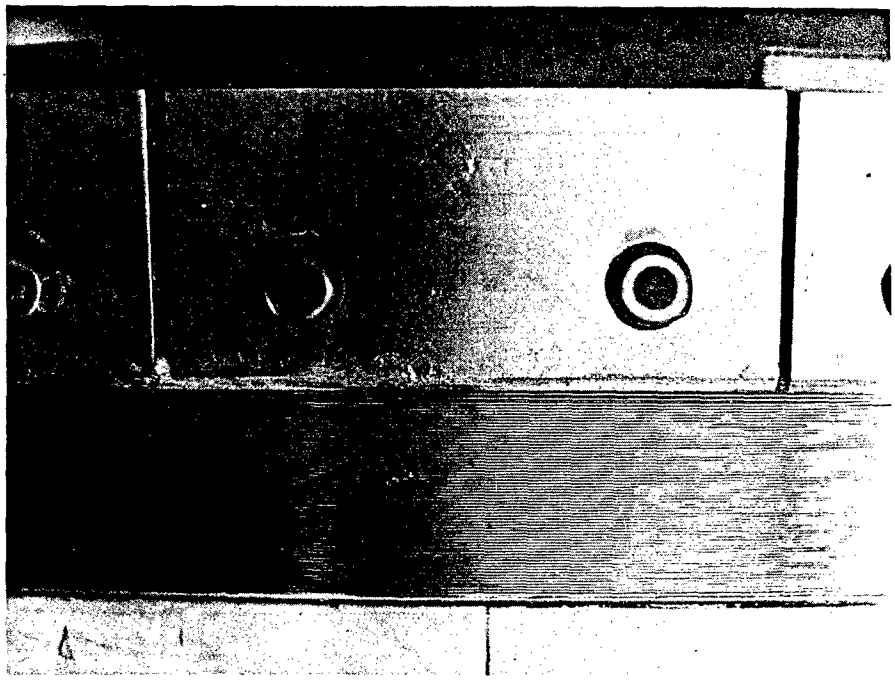


Figure 76. Yield Strength vs Temperature



(a)



(b)

Figure 77. Base Attachment Fixture

SECTION V

TOOLING

TOOLING CONCEPTS

The successful fabrication of a mosaic radome structure was predicated on the tooling techniques involved, and especially the hot or firing tooling. In order to produce a full-size mosaic radome, the firing tooling had to perform as follows:

1. Provide axial and circumferential contact pressures for the faying joints of the ceramic segments

2. Limit movement in the axial and circumferential directions to a predetermined distance to prevent squeezing-out of all adhesive which results in "starved" joints

3. Prevent compressive buckling of the composite structure from applied axial and compressive loading

4. Hold the outer radome surface to a tolerance within aerodynamic and/or practical fabrication standards

5. In a two-layer composite, provide surface contact pressure between layers (radial pressure), in addition to other pressures

6. Retain shape within part tolerance levels, and maintain adequate strength at all temperatures

7. Exhibit reproducible thermal expansion and elastic properties over a reasonable number of cycles

8. Provide a mechanism or material for the prevention of any joining of part and tool

9. Provide environmental resistance to factors influencing tool accuracy, such as erosive oxidation or reduction

10. Provide relative ease of assembly of the components in fabricating the composite structure

The tooling concept chosen and developed during the course of the program was based on a simple and practical tooling philosophy: a tool whose function is governed by a basic, natural law or property is uncomplicated and reliable. In general, Narmco utilized a tooling concept based on the differential thermal expansion between the part (radome) and the tooling material in order to provide necessary bonding pressures and gap closure at firing temperature. A somewhat simplified presentation on the application of this technique is shown in Figure 78. By a proper adjustment of variables, pressures are kept within the elastic limits of fixture and part. Pressures beyond the elastic limits cause permanent deformation or breakage, usually in the fixture. Thus, careful engineering design was mandatory with this concept.

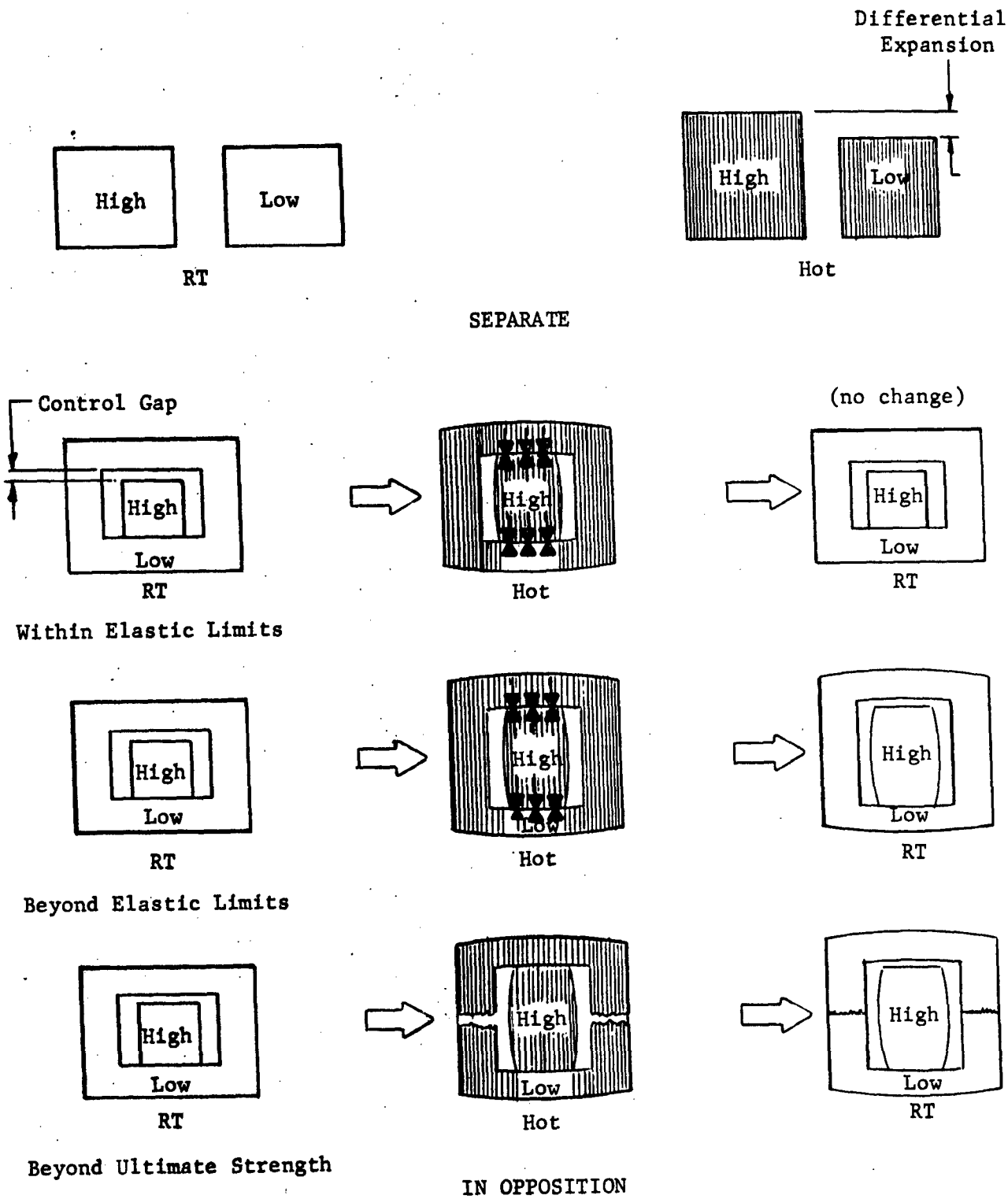


Figure 78. Pressure Generation by Differential Expansion

Figure 79 illustrates a typical application of the principle to a radome cross section. The mosaic radome assembly can be envisioned as being entrapped in a female cavity of a lesser expansion material. As the fixture and part are heated, the individual, higher expansion segments contact the fixture. Continued temperature rise forces the segments together, and closes the gaps to a predetermined distance where adhesive curing occurs. Upon cooling, the adhesive rapidly gains strength, preventing segment separation. The higher expansion (and therefore higher contraction) of the part effectively separates the bonded assembly from the fixture. These actions, properly regulated, provide for the axial and circumferential pressure requirement.

Obviously, the concept would only be practical when thermal expansion differences were reasonably mismatched. A great expansion difference becomes difficult to control, while a small variation simply does not completely perform the desired function.

Considerations were also made for providing radial pressures necessary to close the interface between the layers, while at the same time preventing internal buckling of the mosaic structure and relieving any localized pressures encountered due to contraction of the radome upon cooling. In this respect, in keeping with the overall tooling philosophy of using a positive but simple tooling technique, it was decided that a crushable- or resilient-type material would be desirable for filling the inside of the assembled radome during firing. The selected material would have to have enough packing resiliency or expansion during heating to follow and apply slight positive pressure to the walls of the mosaic structure. If high-pressure areas were developed on heating or cooling, the material would crush or have enough resiliency to relieve the stress. Materials such as hollow ceramic spheres, refractory grog, metal honeycomb, and fibrous materials were potential candidates.

In essence, the tooling required for producing the mosaic radome was to consist of two basic tools:

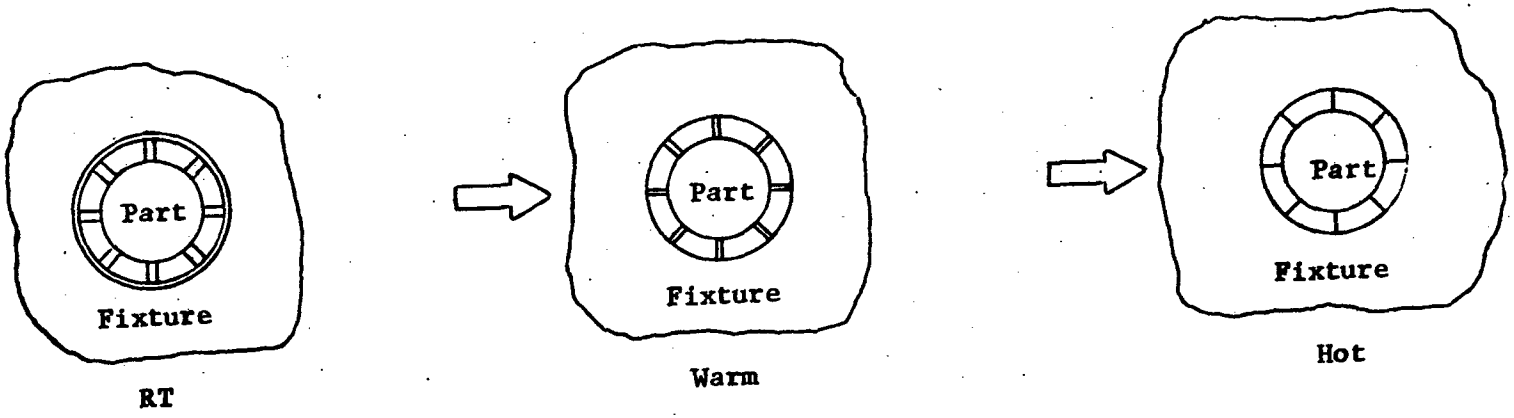
1. A male layup tool upon which the individual ceramic tiles were to be assembled.

2. A female firing tool which was to be slipped over the layup assembly and the entire assemblage inverted. After insertion, the layup tool was to be removed and the interior filled with the desired core material.

SELECTION OF TOOLING MATERIALS

The choice of material for the layup tool was quite straightforward, with plaster being chosen. Actual types will be discussed in a later section. Plaster could be readily fabricated to the desired tolerances, was economical, and had the desired structural properties.

Materials studied and investigated for the firing tooling were based on using either the lower temperature (1400°F) Pyroceram 45 adhesive or the higher temperature (2300°F) Interpace adhesives for bonding the alumina tiles. Therefore, two different expansion ranges of tooling materials were investigated. These consisted of the range for materials having little or a very



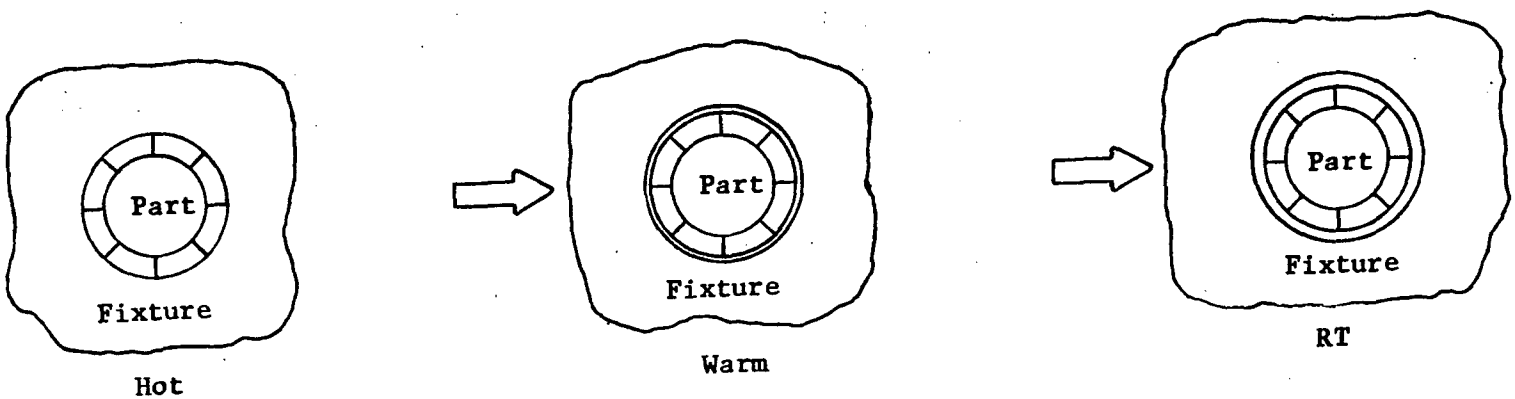


Figure 79. Differential Expansion Application to Mosaic Radome

low coefficient of thermal expansion; and the range of those having a positive expansion, but less than that of the bonded alumina segments.

It was determined that two general types of refractory castable materials met the expansion requirements while have adequate mechanical strength and temperature endurance. These consisted of fused-silica based castables with a thermal expansion coefficient of approximately 0.30 x 10^{-6}/°F, and either mullite or silicon carbide based castables with expansion coefficients in the range of 2.6-2.9 x 10^{-6}/°F. In addition, the use of graphite was also considered for the tool for the following reasons: it could be fabricated to close tolerances, it was available in large sizes, it was mechanically strong, and had a coefficient of thermal expansion from 1.4 x 10^{-6}/°F (parallel to grain orientation) to 2.1 x 10^{-6}/°F (perpendicular to grain). It was recognized that while the castables investigated were all resistant to oxidation, the use of graphite would require the proper protective atmosphere during the firing operation. As will be discussed later, however, the effect of the molten adhesives on the tool material dictated the use of a lubricant or parting agent that also required protective atmosphere.

The refractory castable materials investigated are listed in Table 27 and indicate the properties determined by their respective manufacturer. It was felt that the values published by the manufacturers were representative of the strength and expansion characteristics; therefore, no confirmation tests were performed. In addition, literature has shown confirmation of these properties by other investigators.

The major effort of this investigation was devoted toward determining the effect of the molten adhesives on the various candidate tool materials. Slabs approximately 0.5 in. x 2.0 in. x 4.5 in. were either ram- or slip-cast for each material, using "Smooth-on-FMC" polysulfide rubber molds. In all cases, the manufacturer's recommended mixing and preparation instructions were followed. All specimens were allowed to air dry completely before removal. All but the Carbofrax cement cured at temperatures slightly higher than 220°F. (The Carbofrax instructions specified heating to above the desired end-use temperature for vitrification of the bond.)

In order to determine the compatibility of the tooling materials with the adhesives, it was decided to qualitatively determine the amount of sticking or attack of the molten adhesive to the tool material. This was accomplished in the following manner:

1. The adhesives utilized were in direct contact with the tooling material.

2. An open face of the alumina segment was coated.

3. A typical lap joint between two alumina segments was tested.

It was felt that these conditions would simulate actual fabricating techniques where excess adhesive from exposed joints might be in direct contact with the tooling. In addition to evaluating the tooling materials in direct contact with the adhesives and joints, it was also recognized that special lubricants or parting agents might be needed to prevent seizure of the part to the tool;

TABLE 27

CASTABLE REFRACTORY MATERIALS

Source	Type	Max. Temp, °F	Coefficient of Expansion, RT — 1900°F	Modulus of Rupture, psi
Glasrock Castable Glasrock Products, Inc.	Dry fused silica	2000	0.30×10^{-6}	300-500
Glasrock Cement Glasrock Products, Inc.	Wet fused silica			300-500
Masrock Glasrock Products, Inc.	Liquid castable fused silica			1000-3000
Ampco Sil #2023	Dry fused silica, hydraulic setting		0.68×10^{-6}	800-1100 (unfired) 400-600 (fired @ 2000°F for 5 hr)
Plicast 34-R	Dry alumina	2600-3000	2.9×10^{-6}	400-500
Plicast K-L	Silica hydraulic setting	3000	2.9×10^{-6}	1100-1200
Carbofrax #6 Cement The Carborundum Co.	Dry silicon carbide	2900	2.6×10^{-6}	1000

therefore, several materials were investigated for possible use as parting media. These included

1. Boron Nitride Powder
2. Synthetic Mica Powder
3. Fel-Pro-C-100 Hi-Temp Compound (Molybdenum disulfide base)
4. Dexsan-Activated Carbon Web Paper
5. Pyrolytic Graphite Flake (-20 mesh)
6. Graphite Cloth (#181 weave)

The above materials were applied to the castable slabs either as a powder or, in the case of the carbon paper and graphite cloth, between the slab and adhesive samples. The experiments containing the carbon paper, graphite flakes, and graphite cloth were run using a protective argon atmosphere. (In addition, a more extensive investigation or parting agents for preventing seizure between the radome and tool was performed and is discussed in Section VII.)

Although it was previously established that Pycerad 500 did not have satisfactory "all-around" properties for the program, it was nevertheless tested for compatibility with the tooling materials since its reaction would be representative of any future, successfully developed ceramic adhesives.

In order to establish some criteria for rating the various tooling and parting materials, the following arbitrary rating system was devised for the qualitative test:

Rating No.	Description
1	No adherence between adhesive and tooling or parting material
2	No adherence, but reaction of adhesive with tooling or parting material
3	Slight adherence to tooling or parting material
4	Slight adherence and reaction of adhesive with tooling or parting material
5	Complete adherence (sticking) between adhesive and tooling or parting material

The results of the tests performed are summarized in Table 28 and in the subsequent text.

1. Pyroceram 45 showed the least sticking and reaction with the tooling and parting materials. This was as expected, since vertical firing of prepared lap joints indicated that the Pyroceram 45 had very high viscosity with little or no drainage of the adhesive

TABLE 28

TOOLING MATERIALS EVALUATION

Tooling Material	Parting Compound	Pyroceram #45 (1400°F)		Interpace (2300°F)		Pycerad 500 (1940°F)	
		Direct Contact	Joint	Direct Contact	Joint	Direct Contact	Joint
Carbofrax #6 Cement	None	5	1	5	3	4-5	4-5
	Synthetic Mica	1	1	3	3	4-5	4-5
	Boron Nitride	1	1	2	2	4-5	4-5
	Fel-Pro-C-100	2	1	5	5	4-5	4-5
	Carbon Paper	2	1	2	2	2	2
	Graphite Flake	2	1	2	2	2	2
	Graphite Cloth	1	1	2	2	2	2
Glasrock Castable	None	2	1	5	5	4-5	4-5
	Synthetic Mica	1	1	5	5	4-5	4-5
	Boron Nitride	1	1	2	2	4-5	4-5
	Fel-Pro-C-100	2	1	3	5	4-5	4-5
	Carbon Paper	1	1	2	2	2	2
	Graphite Flake	1	1	2	2	4	1
	Graphite Cloth	1	1	2	2	2	2
Glasrock Cement	None	1	1	5	5	4-5	4-5
	Synthetic Mica	1	1	5	3	4-5	4-5
	Boron Nitride	1	1	3	3	4-5	4-5
	Fel-Pro-C-100	2	1	4	4	4-5	4-5
	Carbon Paper	2	2	2	2	2	2
	Graphite Flake	3		4	2	4	3
	Graphite Cloth	1	1	1-2	1-2	2	2
Masrock Liquid Castable	None	1	1	5	5	4-5	4-5
	Synthetic Mica	1	1	5	5	4-5	4-5
	Boron Nitride	1	1	2	3	4-5	4-5
	Fel-Pro-C-100	3	1	5	5	4-5	4-5
	Carbon Paper	1	1	2	2	2	2
	Graphite Flake	2	1	2	2	4	2
	Graphite Cloth	1	1	2	2	2	2
Ampco Sil #2023	None	1	1	5	5	4-5	4-5
	Synthetic Mica	1	1	5	5	4-5	4-5
	Boron Nitride	1	1	2	2	4-5	4-5
	Fel-Pro-C-100	3	1	5	5	4-5	4-5
	Carbon Paper	1	1	2	2	2	2
	Graphite Flake	2	1	2	2	3-4	3-4
	Graphite Cloth	1	1	2	2	2	2
Plicast 34R & K-L	None	3	1	5	5	4-5	4-5
	Synthetic Mica	1	1	5	5	4-5	4-5
	Boron Nitride	1	1	3	3	4-5	4-5
	Fel-Pro-C-100	3	1	5	5	4-5	4-5
	Carbon Paper	2	1	2	2	2	2
	Graphite Flake	1	1	2	2	3-4	3
	Graphite Cloth	1	1	2	2	2	2
Graphite		2	1	2	2	Did not adhere; but severe reaction occurred	

from the joint. Firing of the Interpace adhesive vertical joints showed some drainage, but the amount was not excessive. Pycerad 500 was quite fluid and had considerable drainage.

2. Pyroceram 45 adhered only to Carbofrax and Plicast castables. This condition existed only when direct contact was made, since the joint specimens were free after firing. In most cases, the use of a parting medium eliminated the sticking to these castables. However, sticking still occurred when the Fel-Pro-C-100 compound and graphite flakes were used. (It was determined that in this particular experiment, full protection from the argon atmosphere was not obtained. Therefore, some oxidation of the flakes occurred, allowing reaction between the flake and Pyroceram 45.)

3. As expected, Pyroceram 45 showed no evidence of adhering to the graphite slab, except for a slight reaction when placed in direct contact. This reaction did not diffuse through Pyroceram 45, and was limited to the surface. Similar results were produced when Pyroceram 45 was in direct contact with graphite flakes and carbon paper. No reaction was noted when graphite cloth was used as the parting material. Of all the graphite and carbon compounds investigated, only the carbon paper showed any reaction toward joint specimens. Therefore, it was not expected that the electrical properties of a Pyroceram 45-bonded mosaic radome would be adversely affected from graphite reaction.

4. The Interpace adhesive stuck to all the refractory castables tested whenever a parting compound was not employed. This was true not only of direct contact, but also of the lap joint samples. Of the nongraphite-type parting materials, only the boron nitride showed any promise of preventing sticking between the part and the tool. The graphite cloth gave the best results of the carbonaceous materials, although some reaction of graphite with the Interpace was observed. This was also the case when the Interpace was fired in contact with a graphite slab. However, it is known (from melting and casting experiments in graphite molds) that this is primarily a reaction, and does not diffuse throughout the Interpace adhesive. Therefore, no pronounced changes in electrical properties should occur. Subsequent testing of the Narmcad adhesives showed similar results.

5. Results from Pycerad 500 adhesive confirmed previous known reactions of this type of ceramic eutectic. In all cases, its affinity for numerous refractory oxides, silicates, carbides, etc. caused it to stick and react with all the tooling and parting materials, particularly with those fired under oxidizing conditions. Where the graphite or carbon-based parting materials were used, sticking was eliminated by the use of carbon paper or graphite cloth. The graphite cloth was preferred, since both the carbon paper and graphite flakes had a tendency to oxidize at this temperature unless totally protected by argon. However, as shown when in direct contact, the graphite or carbon reacts with and diffuses throughout Pycerad 500. This is most obvious when Pycerad 500 is

fired directly on a graphite slab. Such reactions would more than likely be detrimental to the dielectric properties of the system.

Glasrock castable, a fused-silica refractory, was initially selected as the firing tool material. This selection was based in part on its properties, availability, cost, and its ability to be readily formed into intricate shapes. In addition, its overall reaction behavior with the various candidate adhesives was a determing factor in this selection. Proofing of the general concept was established by assembling and firing flat mosaic alumina panels using Glasrock firing fixtures. During the course of the program, considerable properties data were obtained for the Glasrock castable as a result of quality control measures undertaken to ensure adequacy of the full-size firing tool with respect to strength for both handling and actual firing of the radome. The S-820 type material employed was determined as representative of a technical grade of the Glasrock castable which has been processed through their quality control checks for special applications requiring rigid property controls. The following tests were performed by Narmco in order to establish a baseline against which future quality control data could be checked.

1. Density of Casting. Various shapes were cast using the recommended 16w/o addition of water, cured and dried at 180°F, and density calculated from weight and volume.

2. Bulk Density of Powder. This was accomplished by using a constant weight of 300 g of the dry powdered samples and measuring the volume it occupied in a graduated cylinder under standard conditions for each test.

3. Particle Size. The samples used for the powdered bulk density were sieved through a standard set of screens using a Cenco-Meinzer sieve shaker. Screen sizes consisted of 60, 100, 150, 250, and 325 mesh.

4. Drying Shrinkage. The sample material was mixed with 16w/o water, blended, and placed in 10-1/2.in. x 5-1/4 in. x 3/8-in. molds. The samples were cured under a plastic sheet for 24 hours and then cured at room temperature for 24 hours. The dried slab was then cut into 5-1/4 in. x 1-in. x 3/8-in. segments with a diamond saw. The samples were then dried at 180°F for 18 hours and measured to obtain the total drying shrinkage.

5. Firing Shrinkage. Additional segments of the above size were fired at 2000°F for 1 hour. The samples were remeasured and compared to their dry length to obtain the firing shrinkage.

6. Modulus of Rupture. Samples of both the dried and fired segments were tested by quarter- and single-joint loading using a 4-in. span. No significant difference was observed between the single- and two-point loading. In addition, modulus of rupture measurements were made on the material after casting into standard 9-in. brick straights. These tests will be discussed further.

Table 29 lists the results obtained for the various tests as well as a comparison with the manufacturer's reported data.

The results of the tests showed good agreement from one bag of material to the next, as well as general agreement with the manufacturer's data except for modulus of rupture. Narmco's initial testing for modulus of rupture (using a 4-in. span and 3/8-in. x 1-in. x 5-1/4 in. specimens) yielded values approximately 60%-70% of the manufacturer's data. During the final phase of the quality control check, the manufacturer informed Narmco that they checked the modulus of rupture per ASTM Specification C-133-51, which employs a standard 9-in. x 4-1/2 in. x 2-1/2 in. brick shape as the test specimen. Therefore, test bricks were cast and dried at 180°F for 24 hours. These bricks were tested by Testing Engineers, Incorporated (San Diego, California). The average value of 920 psi was slightly higher than the initial test data, but still represented only approximately 75% of the reported strength. It was determined that as long as the material were consistent in properties, the lower strength values would not significantly effect the handling or performance of the tooling. One possible explanation for the differences occurring in modulus of rupture values was thought to be in the purity of water used in preparing the castable. Variation in the pH and/or soluble salts in water has been known to have an effect on other ceramic casting processes. Therefore, test brick specimens were cast using deionized water and compared to bricks processed with normal tap water. The results indicated that modulus of rupture values approaching 1020-1050 psi were obtained from using deionized water, representing an increase of about approximately 100 psi over using tapwater.

A significant aspect relative to the use of fused silica tooling was the consideration of the inversion of fused silica to the higher expanding cristobalite crystalline form. Some cristobalite formation was to be expected, since this is a well-recognized but sluggish silica transformation which can occur as low as about 1900°F. The inversion rate is influenced by such factors as grain size, composition, and furnace atmosphere, but ordinarily does not become very significant below 2200°-2300°F. At the time of tooling material selection, it was anticipated that time required at peak temperature during firing of a radome would be relatively short, and any slight increase in expansion experienced in the Glasrock tool over that assumed in making the dimensional calculations could be compensated for. Further considerations and investigations of cristobalite formation from the Glasrock castable are presented in Section X.

Based on its properties, ready availability, and cost, Narmco decided that bulk Fiberfrax fiber material offered the most promise for initial use for producing the desired radial pressure to close the interfacial joints between tile layers. This material, produced by Carborundum Company as Fiberfrax bulk fiber, is described by the manufacturer as being comprised of aluminosilicate fibers that can withstand both continuous use temperatures up to 2300°F and extreme thermal shock. It is a lightweight material having low thermal conductivity, and can be readily packed to higher densities. Fiberfrax can be handled easily and has excellent resiliency which makes it ideal as a packing material for expansion joints, crevices, enclosures, and spaces

TABLE 29

QUALITY CONTROL DATA FOR GLASROCK FUSED-SILICA CASTABLE (TYPE S-820)

Property	Manufacturer's Typical Data	Narmco Test Data					
Density of cast specimens	115-118 lb/ft^3	118-122 lb/ft^3					
Bulk density of powder	--	94 lb/ft^3					
Particle size (screen analysis)	Proprietary	w/o Retained on Sieve					
		60 mesh	100	150	250	325	Pan
		46.1	34.8	4.9	9.7	2.5	2.0
Shrinkage Dried @ 180°F Fired @ 2000°F	 0.15% max. 0.35% max.	 0.12% Avg 0.39% Avg					
Modulus of rupture Dried @ 180°F Fired @ 2000°F	 1250 psi min.* 1050 psi min.*	 Avg 920 psi* and Avg 720 psi** Avg 710 psi**					

* Tested per ASTM C-133-51 using standard 9-in. brick straight

** Test specimen 3/8 in. x 1 in. x 5-1/2 in.; span, 4 in.

where movement must be accommodated. The following list indicates a few of its physical properties:

Color	White
Bulk Density as Shipped (Approximate)	3-4 lb/cu ft
Recommended Packing Density	6 lb/cu ft or greater
Recommended Continuous Use Temperature	Up to 2300°F
Melting Point	Above 3200°F

Figure 80 shows the Fiberfrax bulk fiber as-received.

Initial experiments with this material consisted of observing its deformation or compressibility under various pressures in order to ascertain whether it was sufficiently resilient for the desired purposes. In addition, some indication of its packing ability and springback under various loading conditions was established. To determine compressibility, a cylinder of known volume and area and open at one end, was packed with the Fiberfrax to the recommended packing density of 6 lb/cu ft (0.1 g/cc). Pressure was then applied by means of a weighted plunger and compressibility observed. Recovery (springback) was also measured when the pressure was released. (The percent compressibility is based on the initial length of the Fiberfrax column.)

The following results were obtained:

Pressure, psi (lb/sq ft)	Compressibility, %
0.2 (30)	5
0.4 (60)	15
0.6 (90)	25
0.8 (115)	35
1.0 (145)	40
1.2 (175)	45
1.4 (205)	50

The above data indicated that the bulk fiber material would readily deform under relatively low loading pressures. It was also noted during the course of investigation that the Fiberfrax had significant recovery once the pressure was removed. This was observed particularly at low pressures of 0.2-0.6 psi where the percentage of recovery ranged from 25% to 66%.

As a result of the aforementioned experiments, some indication of the degree of compaction that would be suitable for use in the interior of the radome during firing was obtained. A packing density corresponding to approximately 9.5 lb/cu ft appeared to be adequate. Further use of this bulk material for applying the desired radial pressure is described in Sections X and XI.

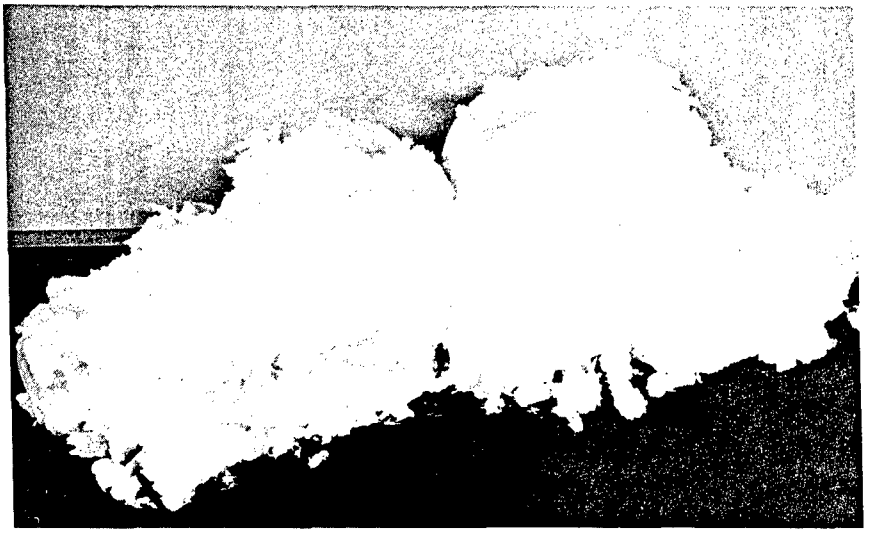


Figure 80. Fiberfrax Bulk Fiber

TRUNCATED TOOLING

The tooling required to produce the lower base radome sections was fabricated similarly to tooling required for the full-scale radome and consisted of three basic units:

1. A layup tool faced with hard plaster which was built to the inside contour of the radome section

2. A plaster model formed to the outside contour of the radome existing at the firing temperature, based on the differential expansion between the part and firing tool material

3. A firing tool which was cast of fused silica from the model

To generate the truncated layup tool and firing tool model, a turntable and template system was employed for sweeping the plaster to final tolerance. A Model FT2 turntable, manufactured by Aronson Machine Company (Arcade, New York) having a 42-in. diameter base and capable of operating at speeds of 0-5 rpm while supporting over 2500 lb was used for both truncated and full-scale tooling. The basic turntable was further modified by attaching a 42-in. diameter x 1-in. thick aluminum bed plate, and also a stanchion on which the sweeping template for the lower base sections was supported. Figure 81 shows the basic modified unit as well as a welded pipe structure attached to the bed plate. The welded structure served as the support and foundation around which plaster models were built-up to form the layup and firing tools required for the lower base sections of the radome.

The following sections describe the activities performed in producing the truncated plaster layup tool and fused-silica firing tool.

Layup Tool (Lower Base Sections)

The development of this form was quite straightforward, except for dimensional tolerances required, and involved producing a plaster truncated form to final dimensions to fit the inside contour of the base radome with allowances made to accommodate the unfired Narmcad adhesive joint widths of 0.0013 in. The sweeping template was fabricated from calculated coordinates to a layout tolerance of ±0.0005, and final cutting tolerance on coordinate dimensions of ±0.0015. The coordinates as well as the template shape are shown in Figures 82 and 83.

The layup tool male form was built up of plaster to within 1/4 in. of the surface. The surface coat was "swept on" using a mixture of 75% plaster and 25% Hydromite. The surface produced by this mixture was considerably harder and more abrasion resistant than that produced by high-strength gypsum cements. Hydromite is a two-component material manufactured by US Gypsum Company and consists of a water-compatible resin and plaster. Upon mixing, the plaster forms an initial set in approximately 1 hour. After 24 hours, the resin component sets to a hard, dense finish. The 75/25 plaster-to-Hydromite ratio was established by a series of tests consisting of slump time, pot life, and hardness.

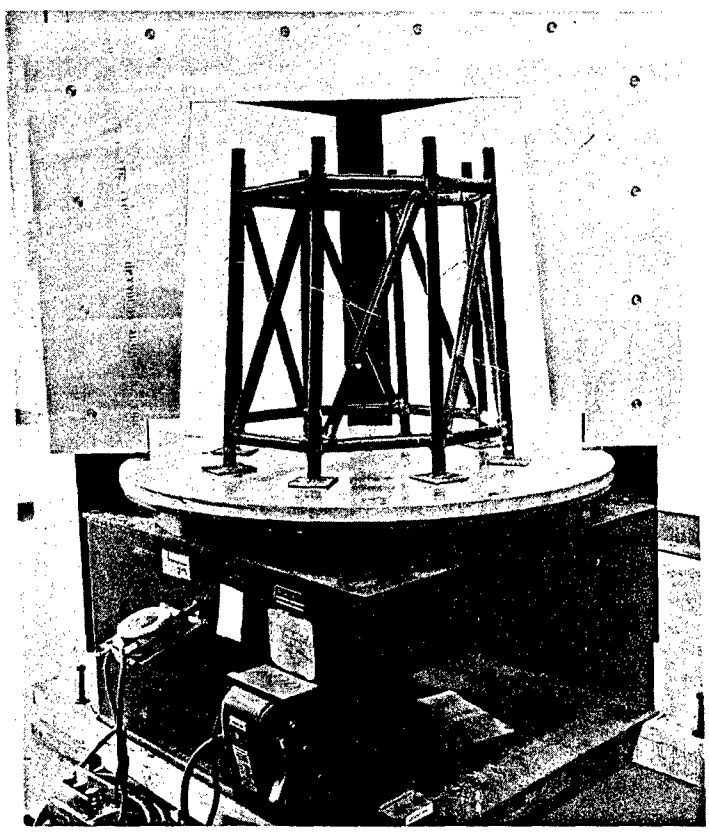


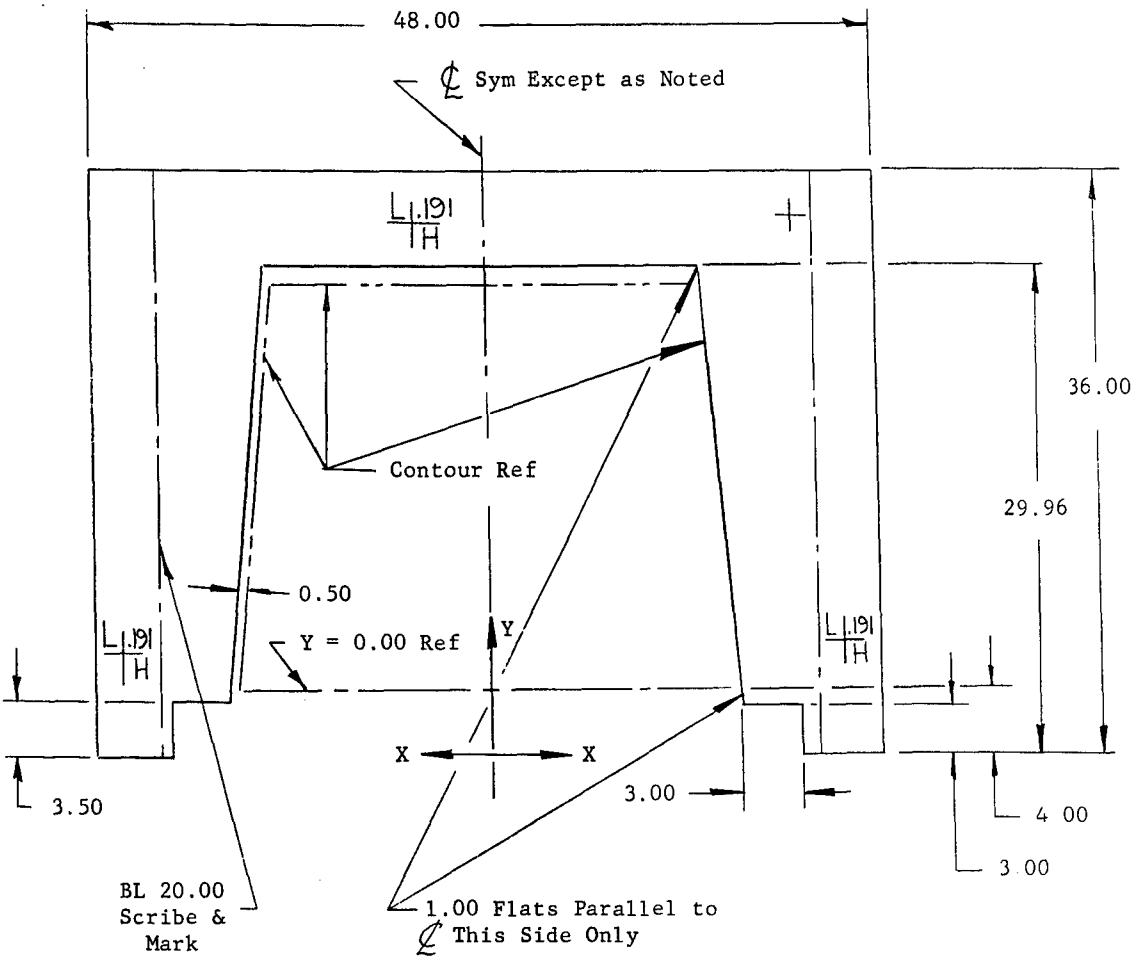
Figure 81. Turntable and Template Frame

Layup Tool Coordinates			
Point	Tile No.	X	Y
A	-107 & -149	15.655	0.00
B	-151	15.393	3.001
C	-109	15.213	4.990
D	-153	15.028	6.998
E	-111	14.839	8.988
F	-155	14.644	10.993
G	-113	14.446	12.986
H	-157	14.243	14.986
I	-115	14.036	16.978
J	-159	13.824	18.977
K	-117	13.607	20.968
L	-161	13.387	22.968
M	-119	13.161	24.957

Layout tolerance on coordinate dimensions ±0.0005

Cutting tolerance on coordinate dimensions ±0.0015

Figure 82. Template Coordinates — Layup Tool, Mosaic Radome



Locate (3) Locating Holes Approx. as Shown

Material - 0.064 Sheet Steel to be Furnished by Narmco

Figure 83. Template — Layup Tool, Mosaic Radome

Figure 84 shows the welded pipe structure with expanded metal lath covering and the initial rough coat of plaster, while Figure 85 depicts the finished truncated plaster layup tool.

Firing Tool (Lower Base Section)

The coordinates for the tuncated firing tool plaster model were calculated to fit the outside contour of the part at firing temperatures based on the differential expansion between the part and fused silica tool. The coordinates were also calculated to include the thickness of graphite cloth used as a parting agent during the firing operation. Figure 86 lists the coordinates established for the firing tool template. The overall shape of the template was similar to that shown for the layup tool and was fabricated to the same tolerances by Fansteel/Torrance, Incorporated (a subsidiary of Fansteel Metallurgical Corporation).

During the course of the program, three truncated firing tools were fabricated. The basic steps involved in the fabrication of these items were essentially those developed during the production of the first section; however, there were certain minor modifications, which are discussed in Section X. Therefore, the procedures involved for the first tool are discussed in detail in the following paragraph.

In producing the first truncated firing tool, the plaster layup tool was also used as the core from which the basic Glasrock fused-silica tool shape could be cast. (Subsequently, an additional oversize plaster core was fabricated for the additional truncated firing tools.)

The basic objective was to produce a fused-silica tool whose inside dimensions fit the outside contour of the radome shape at firing temperature (approximately 2150°F), based on the differential expansion between the part and the fused silica. To avoid the necessity of machining the inside contour of the Glasrock tool, the initial fused-silica section was made with a slightly oversize inside diameter, then fired to produce its reported nominal firing shrinkage of 0.35%. After firing, the final desired internal dimensions were obtained by casting a thin face coat of Glasrock slurry against the fired surface. The slight amount of additional drying and firing shrinkage in the nominal face coat thickness of approximately 1/4-in. were within acceptable tolerance limits. The surface crazing associated with this surface coat shrinkage did not affect the utility of the tool. The two Glasrock materials used in the double-firing technique differed. The castable, used in the major portion of the tool, was hydraulic setting, containing fused-silica grain and a small percentage of calcium aluminate. The slurry used in casting the thin interface was composed of fine, fused-silica grains suspended in a water-base medium. While composition information was not available, the setting characteristics of the slurry indicated that it probably contains colloidal silica as a binder for increasing dry strength.

After applying a polyvinyl chloride parting agent to the finished plaster layup tool (to facilitate its subsequent removal), an extra layer of plaster was swept onto it to define the oversize inside diameter of the Glasrock firing tool. A plaster mold was made to form the outside diameter of the Glasrock firing tool and incorporated with the inside diameter to form a mold

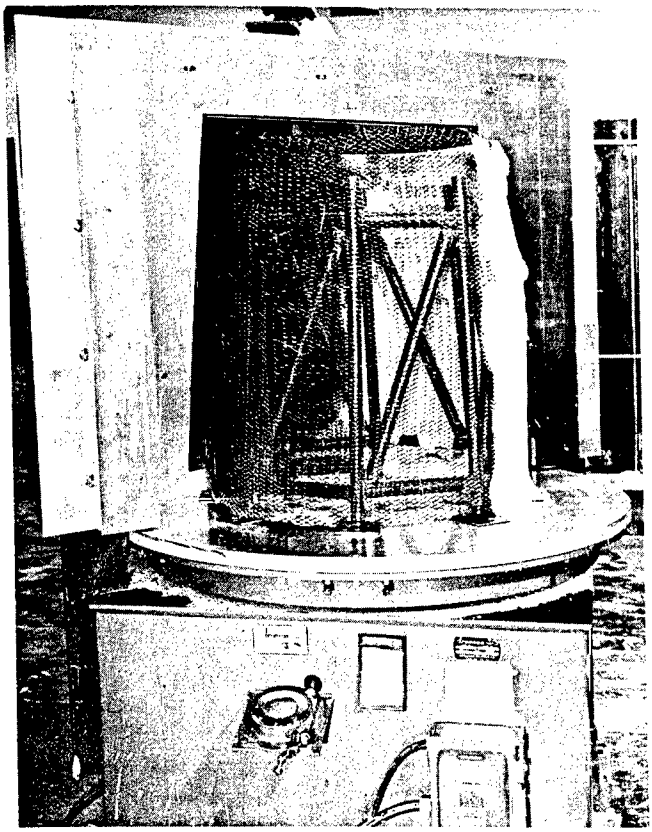


Figure 84. Initial Plaster Coating on Truncated Layup Tool

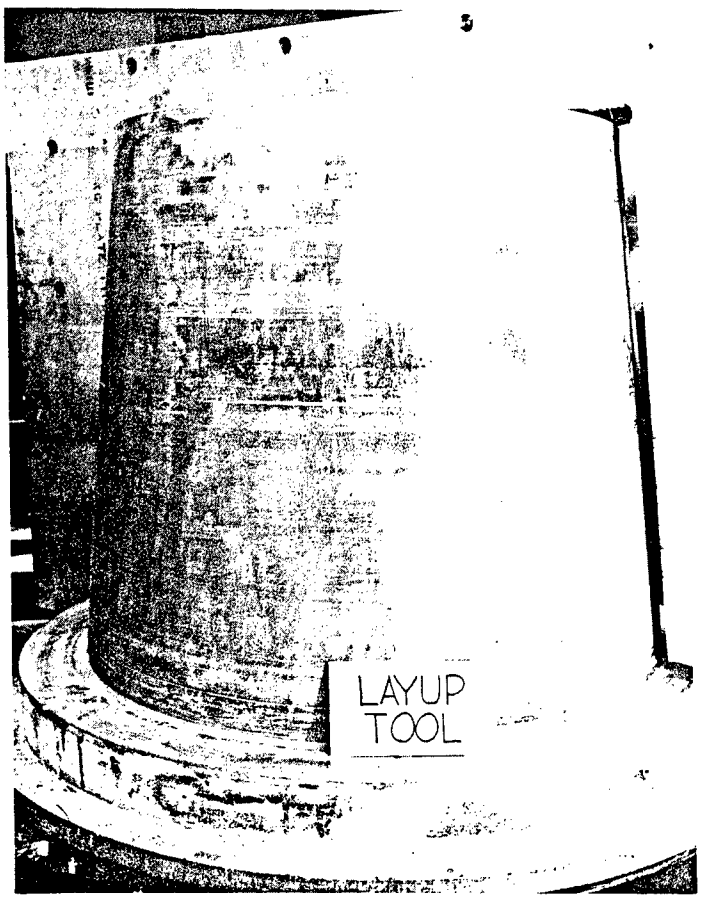


Figure 85. Plaster Truncated Layup Tool

Firing Tool Coordinates			
Point	Tile No.	X	Y
AA	-7 & -51	16.001	0.00
BB	-53	15.825	2.012
CC	- 9	15.646	4.027
DD	-55	15.461	6.038
EE	-11	15.272	8.051
FF	-57	15.079	10.063
GG	-13	14.881	12.074
HH	-59	14.679	14.085
II	-15	14.472	16.095
JJ	-61	14.260	18.105
KK	-17	14.044	20.115
LL	-63	13.824	22.125
MM	-19	13.598	24.132

Layout tolerance on coordinate dimensions ±0.0005

Cutting tolerance on coordinate dimensions ±0.0015

Figure 86. Template Coordinates — Firing Tool, Mosaic Radome

for casting the final basic shape. Figure 87 shows the rough inside and outside diameter of the truncated firing tool. Fused silica Glasrock Castable Type S-820 was cast into the annular space. Upon setting and drying, the outside plaster shell was removed and the cast part slipped off the inside form. The Glasrock firing tool shape produced as shown in Figure 88 had a wall thickness of approximately 3 in. with a slightly oversize inside diameter.

To obtain the final internal dimensions required, a plaster male model of the true surface was fabricated and centered in the Glasrock form, leaving an annular space of about 1/4 in. which was to be backcast with Glasrock slurry. This would result in a thin face coat against the fired surface. A sketch of the entire backcasting arrangement is shown in Figure 89. During the backcasting operation, a major problem area was revealed which was essentially one of seizure or sticking between the male core and the final dried cast shape; this prevented removal of the finished truncated firing tool. While Narmco's normal parting agent, sprayable polyvinyl chloride plastic, performed satisfactorily for separating the main Glasrock castable form during its initial removal, it did not function as a release agent for the slurry used in the face coat. Therefore, a series of screening tests and experiments were performed on various release agents in order to devise a solution allowing positive release of the cast tool from the plaster model.

Preliminary screening tests were devised which simulated the final truncated part on a small scale; i.e., a plaster core of approximately 2-in. diameter by 2-in. height around which the slurry could be cast against a containing ring of fired Glasrock castable. The plaster core was coated with the particular release agent being investigated and then assembled with the miniature Glasrock shell. By this technique, it was possible to perform approximately 60 screening tests on various release agents of the following types:

1. Silicones (Greases, sprays, and oils)
2. Teflon (Air and low-temperature curing sprays)
3. Stearates (Aerosol sprays and solutions of calcium and zinc stearate and stearic acid)
4. Waxes (Used by themselves and in combination with other release agents)
5. Lacquer
6. Keltex solution
7. Boron nitride powder
8. Molybdenum disulfide aerosol sprays
9. Graphite (Powder and aerosol sprays)

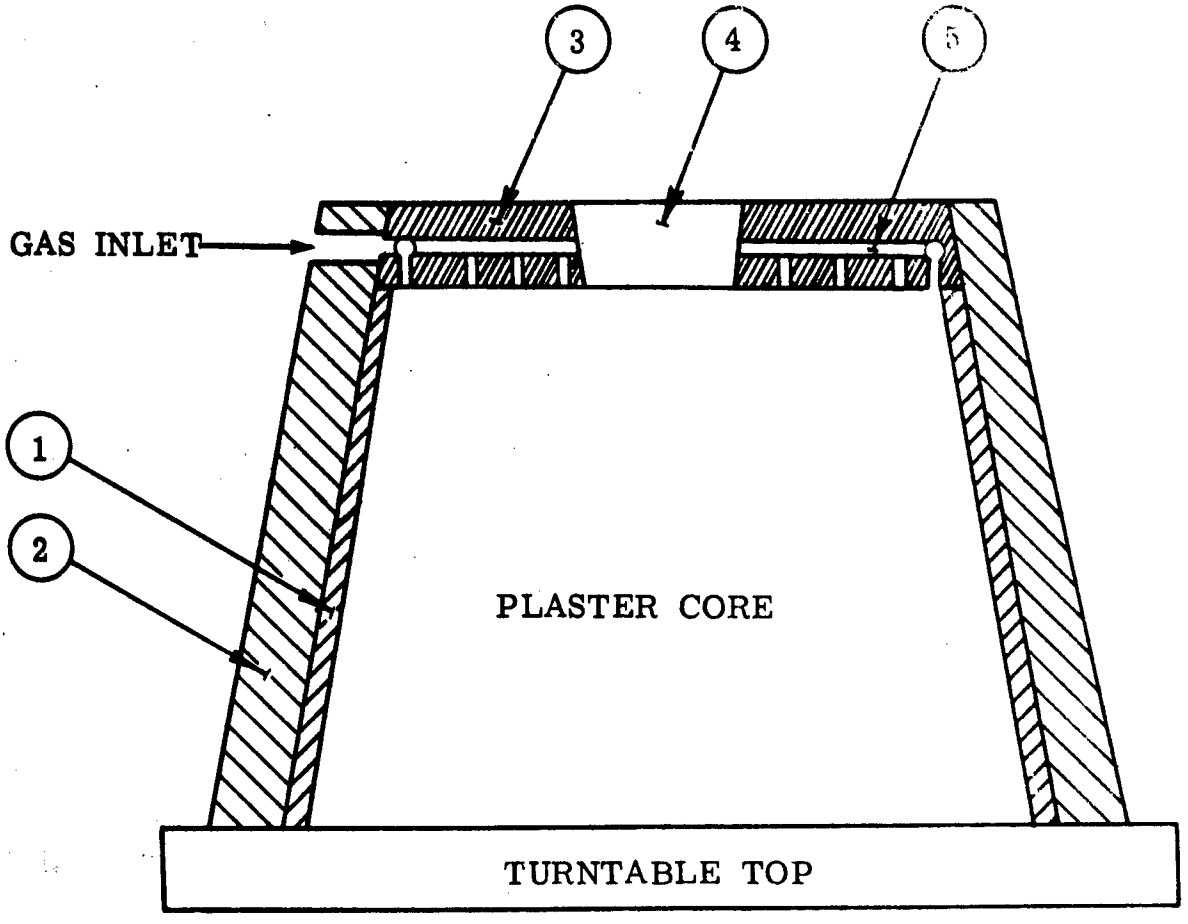
Only those release agents that showed no evidence of seizure on the miniature scale were further evaluated. Final screening of successful candidate release agents was performed using a simulated one-third scale model test as illustrated in Figure 90.



Figure 87. Casting Mold for Trucated Firing Tool Form



Figure 88. Glasrock Truncated Firing Tool



1. BACKCAST SPACE (GLASROCK SLURRY)
2. GLASROCK FORM
3. BOTTOM CAST FROM GLASROCK CASTABLE AFTER BACK CASTING HAS SET
4. CAVITY IN BOTTOM FOR QUALITY CONTROL TOOLING MEASUREMENTS
5. MANIFOLD SYSTEM TO DISTRIBUTE N_2 TO EDGE OF TILE AND GRAPHITE PARTING CLOTH

Figure 89. Cross Section of Backcasting Arrangement



Figure 90. Plaster Mandrel and Fused-Silica Model Form

The plaster mandrel was coated with the candidate release agent and centered within the fused-silica model, and backcast with Glasrock slurry. After the slurry had set and thoroughly dried, the plaster mandrel was manually removed (when possible) and examined for adhesion between it and the slurry. Of the various release agents studied, only a specially prepared slurry of graphite powder and Keltex solution gave a positive release for all tests.

Based on the successful screening results obtained with the graphite release agent, the male plaster model of the truncated firing tool was coated to an approximate 10-mil thickness of the slurry. As will be discussed later, this resulted in the final cast truncated firing tools being oversized, but there was a possibility for compensation by using extra graphite cloth during the firing of the radome part. After coating the male core with graphite slurry and centering it within the Glasrock shell, the final internal face was back-cast with Glasrock slurry. The bottom section containing a nitrogen gas manifold system was then cast with the regular Glasrock material. To ensure complete drying and curing, the complete tool was dried at 125°-150°F for a period of approximately 240 hours. After drying, the plaster core was removed from the tool without any evidence of seizure as shown in Figure 91. The tool was subsequently inverted for dimensional inspection.

Initial inspection of the first truncated firing tool revealed two hairline cracks approximately 10 in. long extending completely through the walls on opposite sides of the bottom portion. In order to reduce the possibility of these cracks propagating during firing of the base radome section, a Glasrock reinforcement ring approximately 3 in. thick was prepared and fired, then cemented around the bottom one-third of the tool. The cracking of the initial truncated firing tool was believed to have resulted primarily from the rough handling associated with the previously reported difficulties in the core removal after backcasting the working surface. Subsequent truncated firing tools were produced free from cracks using improved drying and curing techniques recommended by the manufacturer during the course of the program and reported under full-scale tooling. Dimensional inspection of the interior of the truncated firing tools was accomplished in Section XII. Using this inspection fixture, internal working dimensions of the tool could be checked to an accuracy of approximately ±0.002 in.

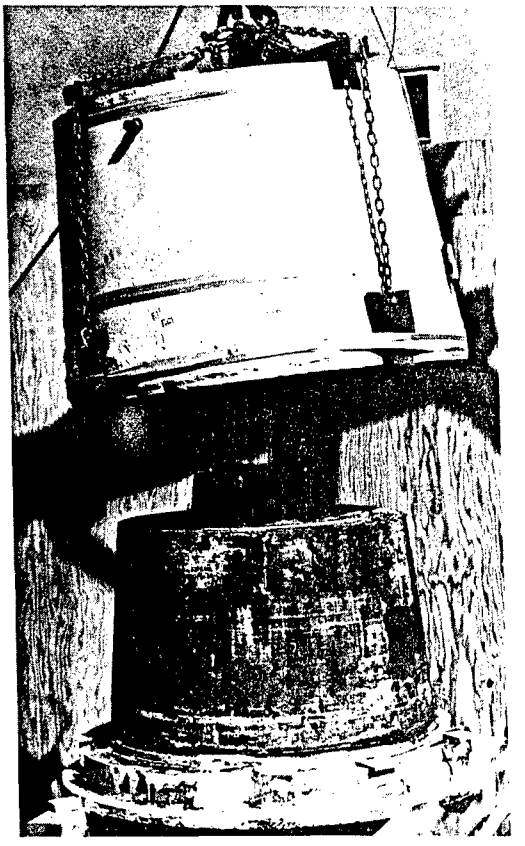
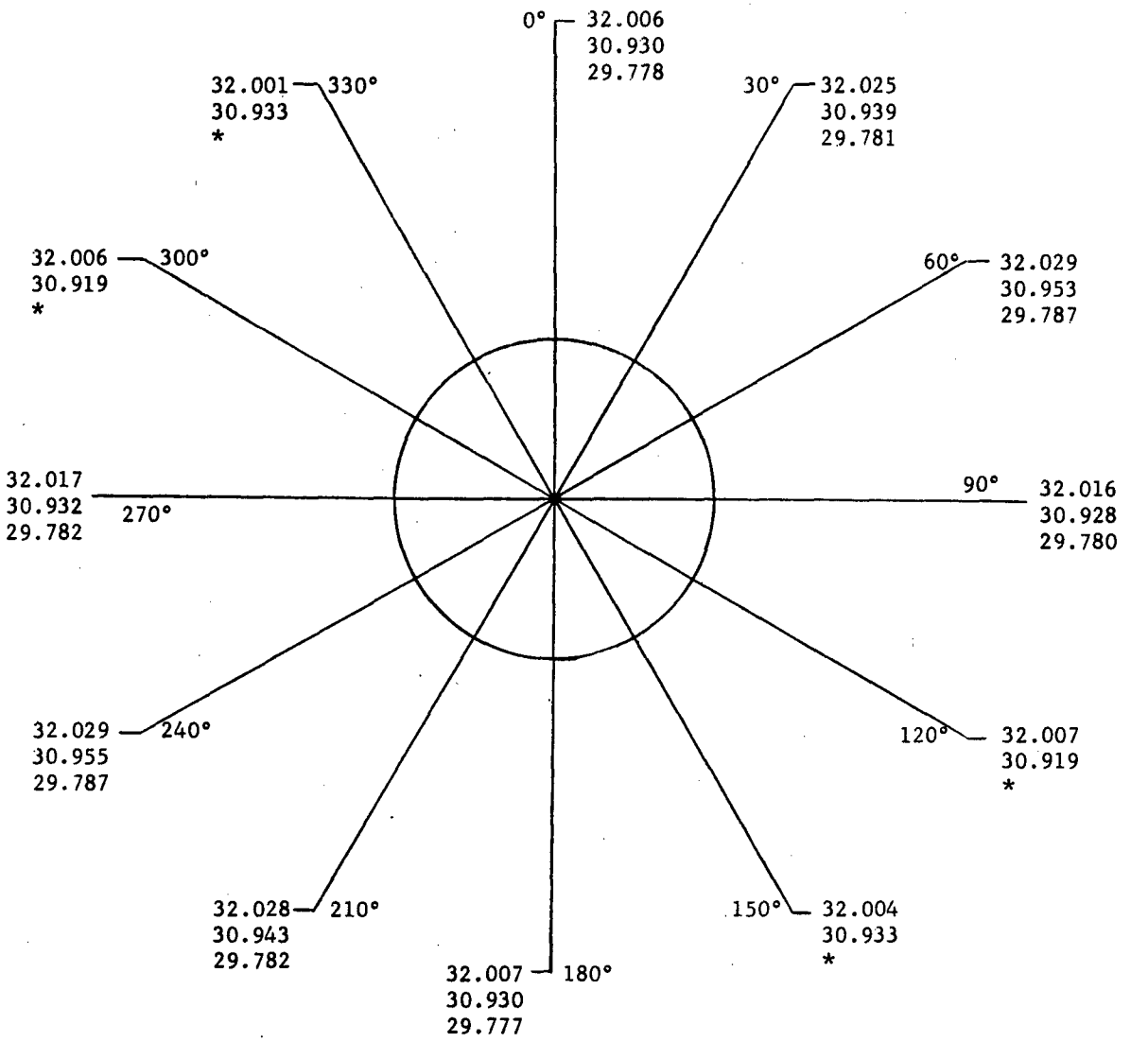


Figure 91. Truncated Firing Tool Separated from Plaster Core

Final inspection of the truncated firing tools was performed against the coordinates previously established and listed for the truncated firing tool template. These dimensions were originally calculated to include the nominal compressed thickness of one layer of graphite cloth within the final working dimensions of the truncated tool. As previously mentioned, the plaster model core used for final casting had to be coated with a layer of graphite powder approximately 7-10 mils to ensure a satisfactory release of the final tool. Thus, the final inside dimensions of the firing tool would be oversize in diameter by approximately 15-20 mils. This dimensional oversize could be compensated for by the addition of another layer of graphite cloth to ensure proper butt joint thickness within the fired base section. Figure 92 shows the inspection data obtained for measuring three stations at 30-degree increments. The inspection data revealed the tool to be oversize as expected; i.e., within the range of 0.012-in. to 0.020-in. diameter. Since compensation was possible, as previously explained, the truncated firing tool was determined acceptable.

Station	Required Dia., ±0.010 in.	Max. Dia., in.	Min. Dia., in.	Av. Dia., in.
0	32.002	32.029	32.001	32.014
6.038	30.922	30.955	30.919	30.935
12.074	29.762	29.787	29.777	29.782



* Bad surface prevented readings (subsequently repaired)

Figure 92. Truncated Firing Tool Inspection Data

Additional truncated firing tools produced during the program were similarly oversized. Their final dimensions and compensations are discussed in a later section during their use in fabricating mosaic base sections of the radome.

FULL-SCALE TOOLING

The principles involved in the fabrication of the truncated tooling were found to be satisfactory and were employed in the design of the full-scale tooling. Once again, three basic tools were involved: a plaster male layup tool, a plaster male model for the firing tool, and a cast Glasrock fused-silica firing tool.

Design of Full-Scale Tooling

A list of detail and assembly drawings of the tools and components that have been prepared is as follows:

NR 63-092R	Template layup tool full mosaic radome
NR 63-093R	Template firing tool full mosaic radome
NR 63-105	Firing tool Glasrock full mosaic radome
NR 63-104	Layup tool plaster full mosaic radome
NR 63-114	Firing fixture assembly mosaic radome (Figure 93)

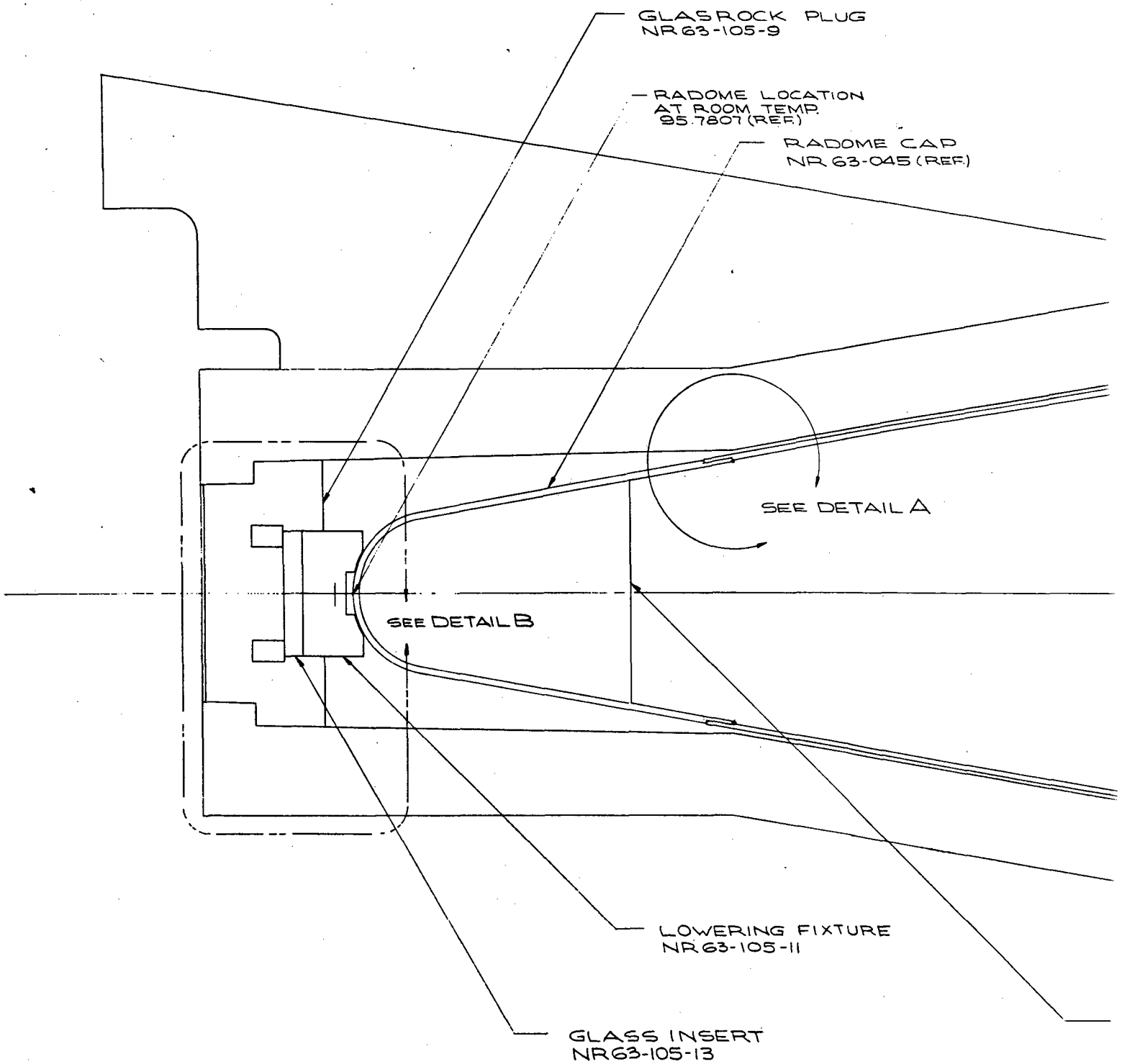
Although the various Narmco drawing numbers are listed as a matter of record, only the firing fixture assembly drawing (NR 63-114) is considered essential for inclusion in the main text of this report. All others are included in Appendix X. The following lists the more significant aspects of the tooling design.

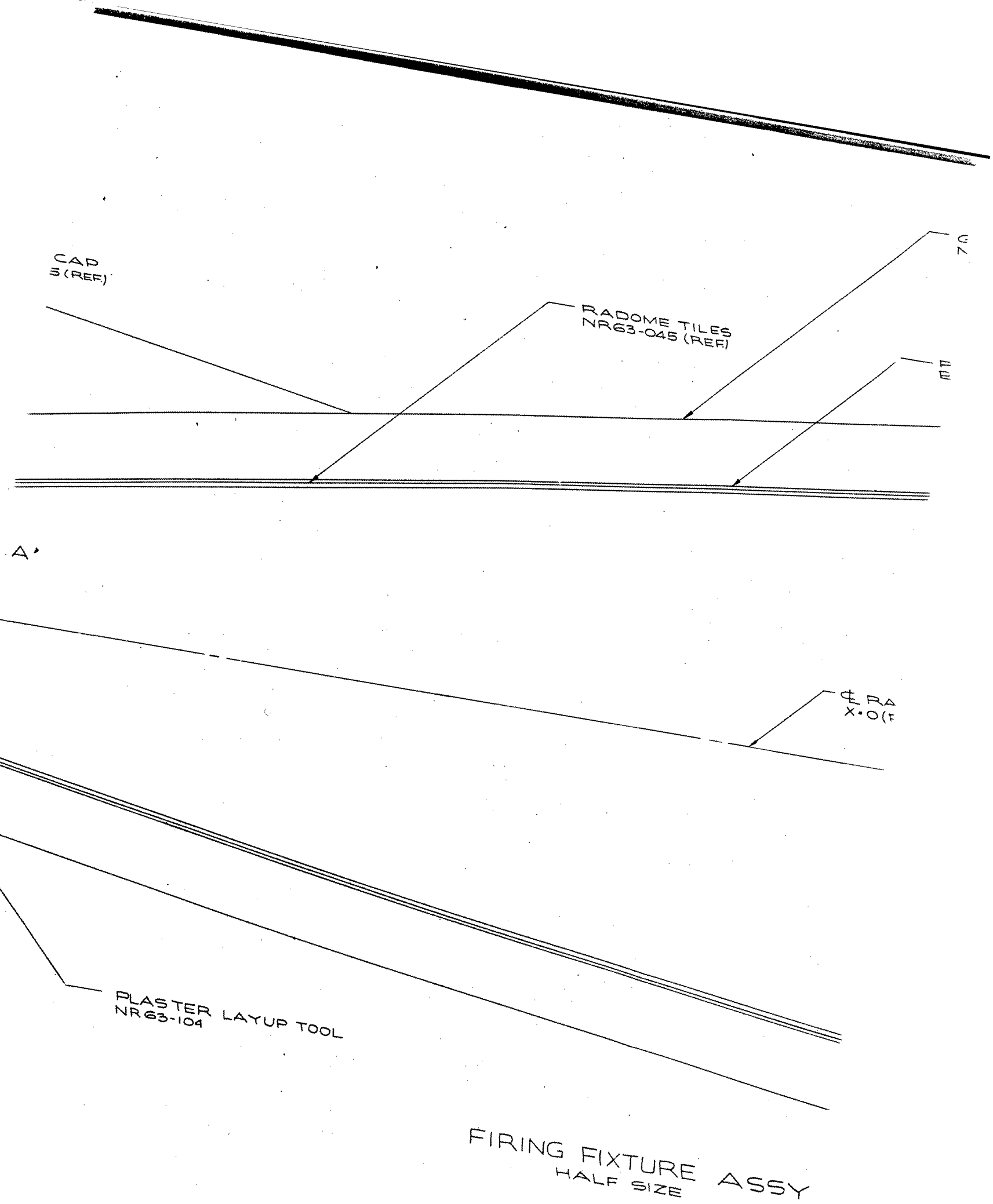
The layup tool (NR 63-104) was to be used directly to support and locate the tiles. It had a stand-out flange below the base tile that supported and also located the firing tool on the final assembly.

The upper end of the layup tool extended into the cavity of the nose cap to assure its proper location and support, prior to firing. The thickness of plaster on the tool was kept to a minimum to assure lighter weight and easier handling. (See Figure 93.)

The female firing tool assembly (NR 63-105) consisted of four parts: the Glasrock firing tool, a removable plug, the lowering fixture, and a composite insert.

The female firing tool (NR 63 105-7) had a final inside contour established by the coordinate system. During firing, it would be inverted and supported by three fins that were an integral part of the tool.


GLASROCK PLUG
NR63-105-9
RADOME LOCATION
AT ROOM TEMP.
95.7807 (REF.)
RADOME CAP
NR63-045 (REF.)
SEE DETAIL A
SEE DETAIL B
LOWERING FIXTURE
NR63-105-11
GLASS INSERT
NR63-105-13



FIRING FIXTURE ASSY
HALF SIZE

Figure 93.

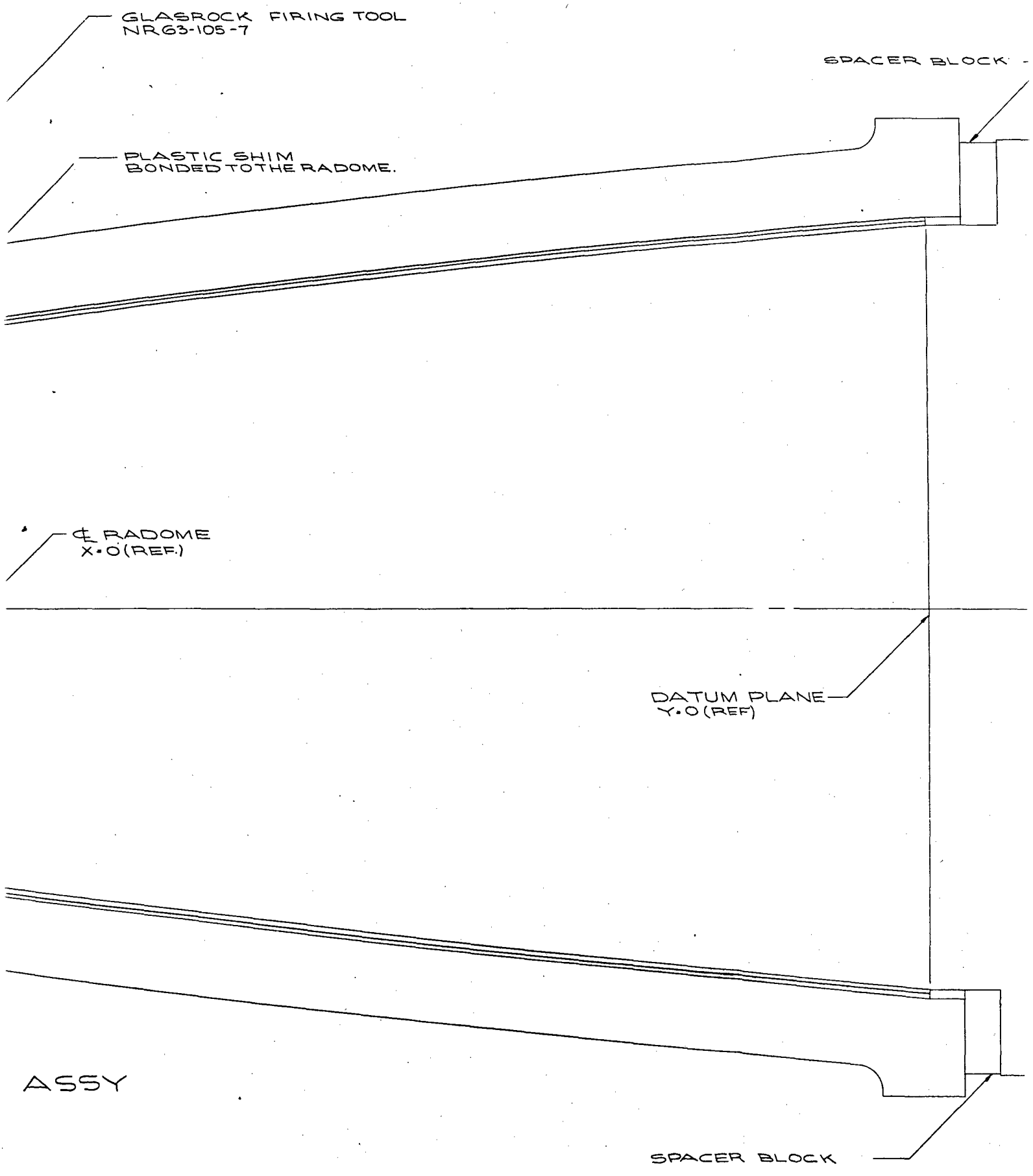
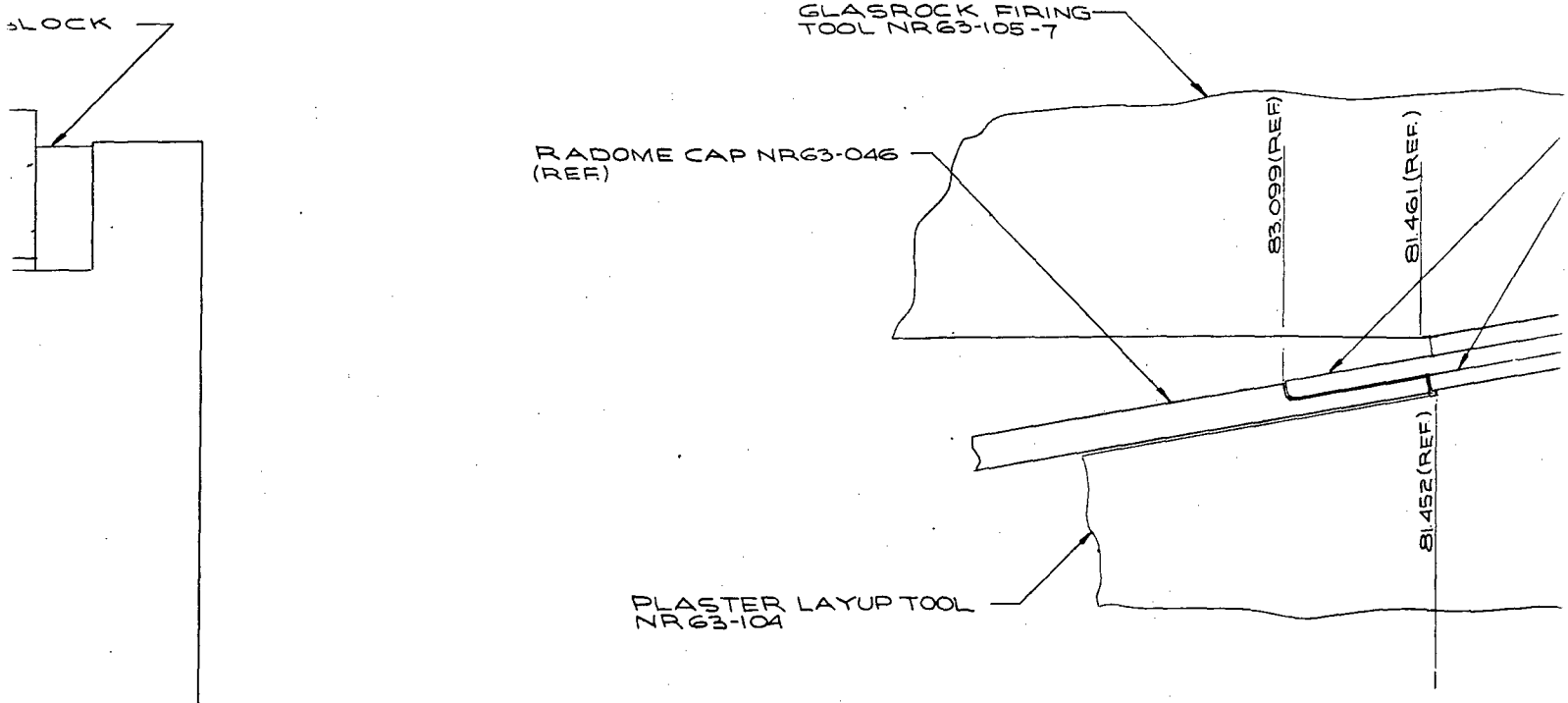
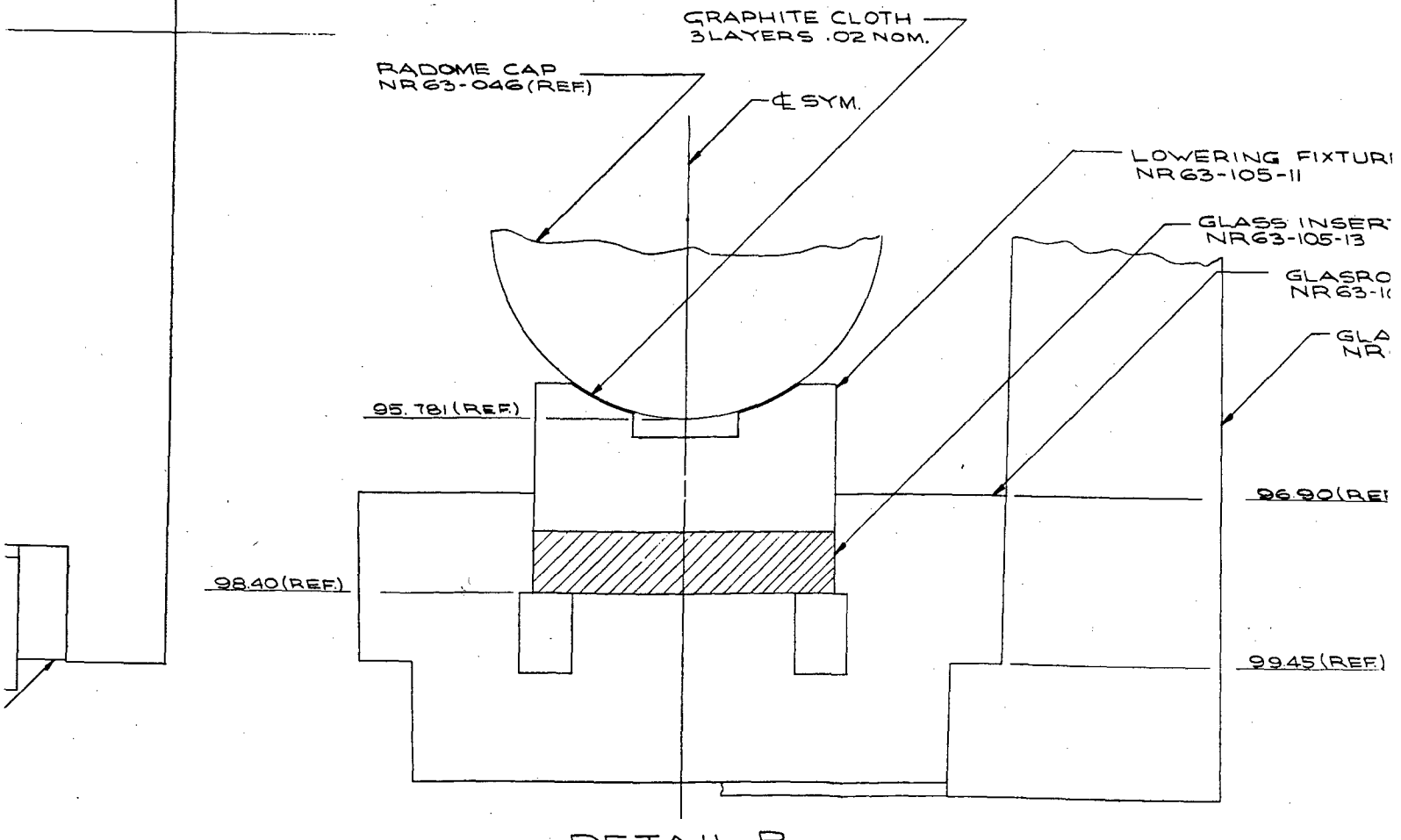


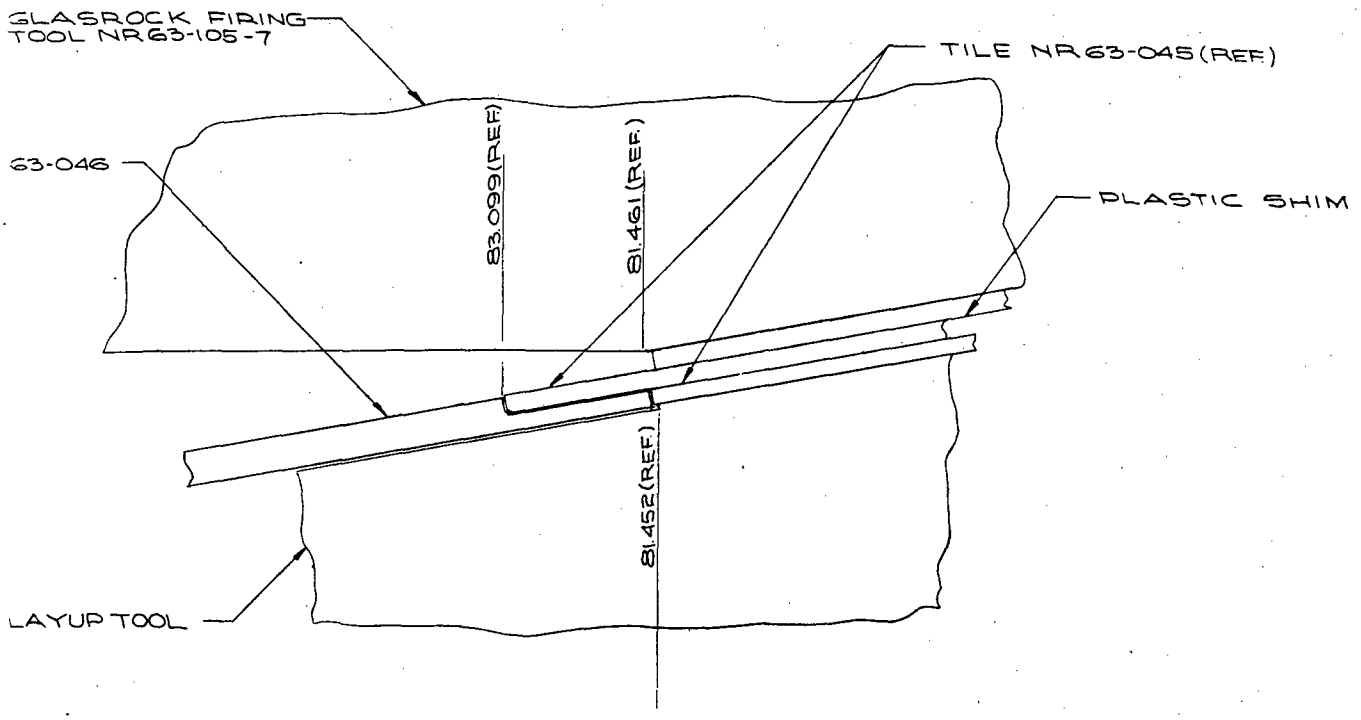
Figure 93. Firing Fixture Assembly, Mosaic Radome



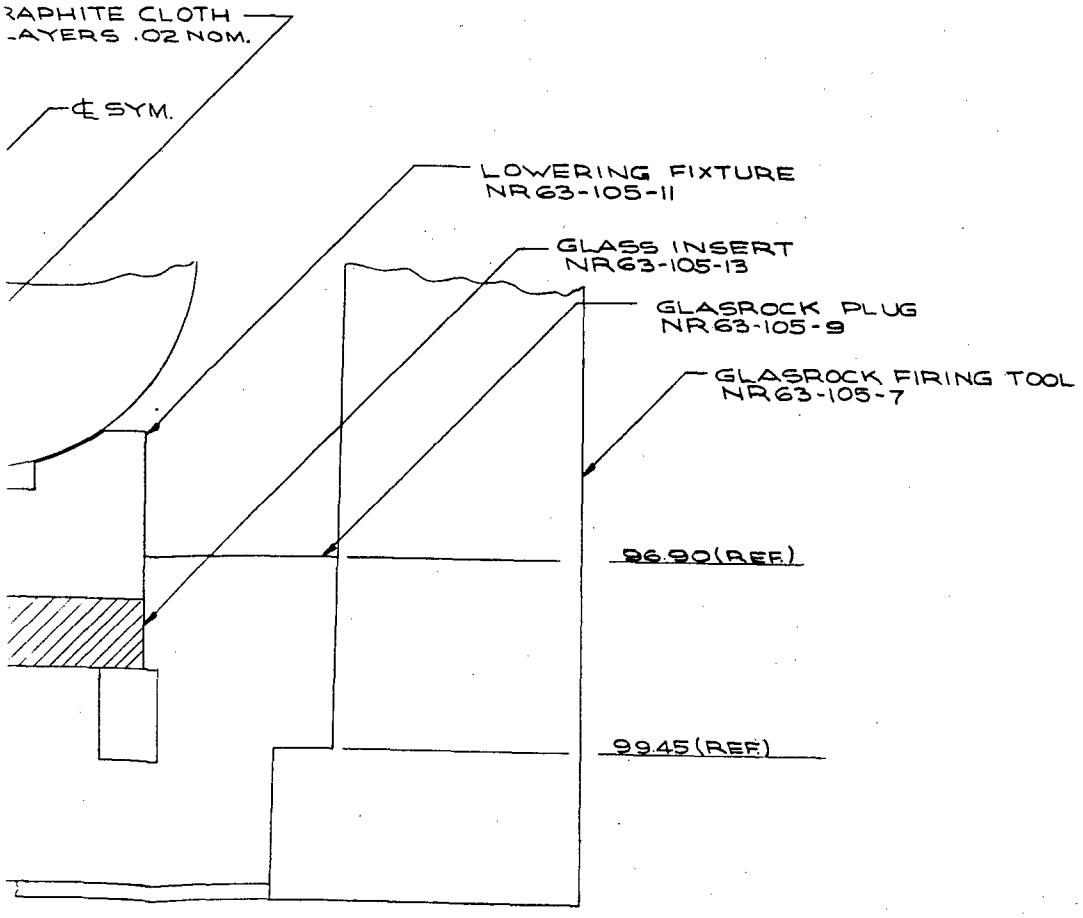
DETAIL A
TWICE SIZE



DETAIL B
FULL SIZE



DETAIL A
TWICE SIZE



L B
ZE

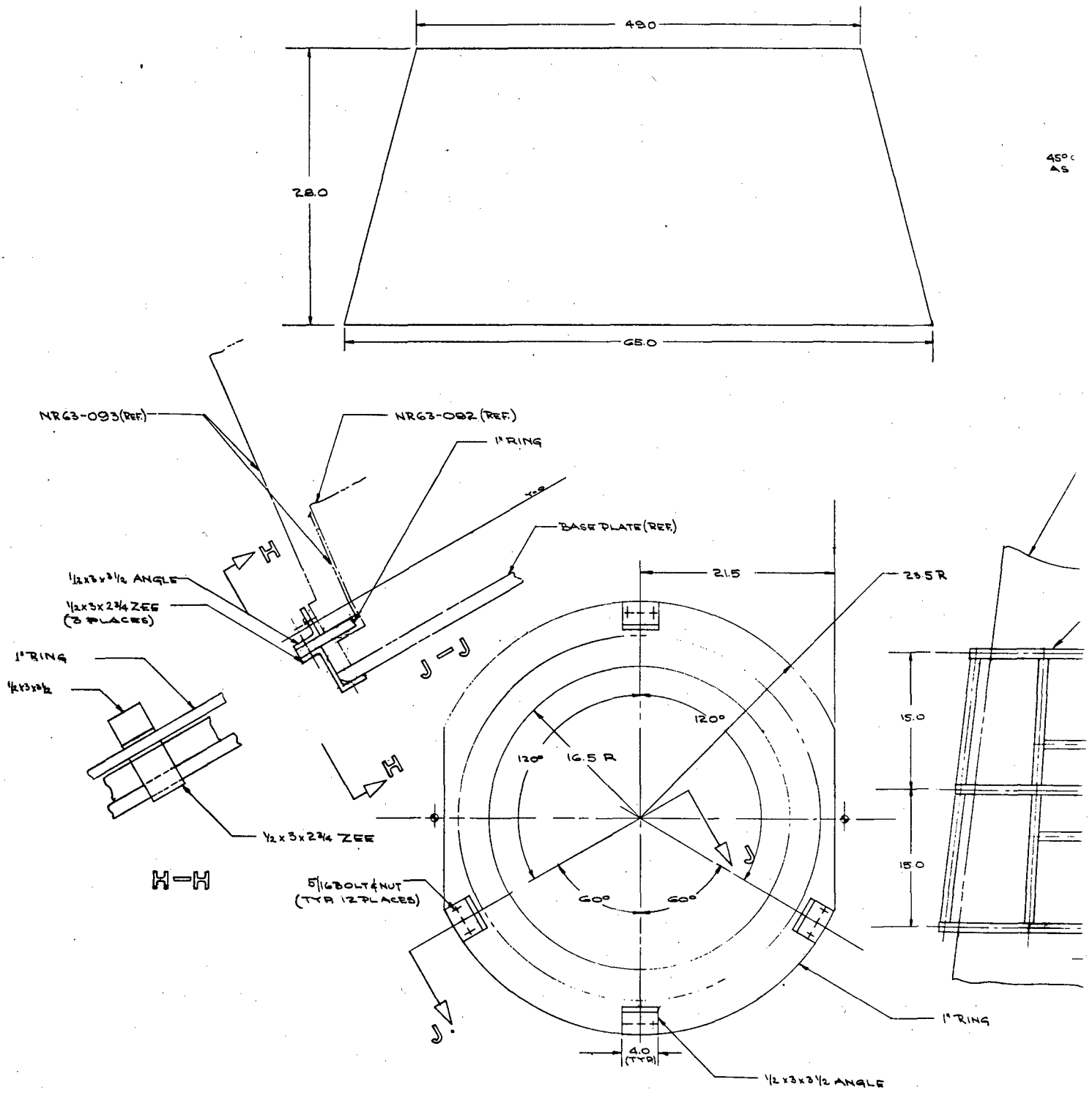
The Glasrock plug (NR 63 105-9) would close the firing tool and support the radome through the lowering fixture. It could be removed and used for subsequent firings.

To avoid point loading on the nose cap, a lowering fixture (NR 63 105-11) was designed that would assure a more even load distribution during all firing stages. Two concepts were considered for the final lowering fixture design. The first allowed the radome to rest on a holding fixture at the bottom of the firing tool. However, corresponding points on the radome and the inverted firing tool were consequently offset by the amount of expected differential thermal expansion. During firing, this would conceivably result in an interference between the radome and the tool before firing temperature was reached. The selected concept had an independent support that was to allow gradual lowering of the radome during its firing. As the temperature increased, a glass sandwich insert plate controlled the lowering of the radome at approximately the same rate as required by the predetermined differential thermal expansion. The lowering fixture that supports the radome would retract and force the insert deeper into the Glasrock plug. At maximum firing temperature, the radome would fit to the exact contour of the firing tool with the lowering fixture being fully retracted. The insert was designed to have several layers of different softening point glasses, the compositions of which are described in the radome fabrication section.

A handling device was also designed, as shown in Figure 94 (drawing NR 63-153), to permit handling and positioning of the full-scale firing tool as required. This device was to be used for handling and inverting the assembled firing tool, layup tool, and alumina tiles prior to firing of the radome. In fact, the requirement for inverting the entire assembly largely dictated the handling fixture design. Under the planned fabrication procedures, the alumina tiles with the unfired adhesive material on the faying surfaces were laid up on the layup tool in a basedown position. After implacement of the graphite cloth parting material and the plastic positioning shims as discussed in Section XI, the female firing tool was lowered into position over the tiles. The entire assembly was then inverted and the male layup tool removed. Note from the drawing that the handling fixture was designed to permit this rotation to be accomplished smoothly about the center of gravity.

Layup Tool

A support foundation for the plaster layup tool was assembled and constructed from welded pipe and expanded metal lath. This in turn was mounted onto the turntable. In order to assure rigidity and stability of the templates during plaster sweeping operations, a template-mounting structure was designed and fabricated for securing the template to the turntable. This structure was approximately 12 ft high and was fabricated from welded iron pipe. The arrangement for the layup tool prior to sweeping with plaster is shown in Figure 95. As shown in the illustration, rigid template backup plates were mounted on the backup plates with adjustable lugs. Templates for the layup tool and firing tool model were again fabricated by Fansteel/Torrance to the specifications and tolerances listed in their respective drawings, NR 63-092R and NR 63-093R. Final precise positioning of the template with respect to the tool was accomplished by using a transit level. The initial rough coat


49.0
28.0
65.0
45° c
AS
NRG3-093(REF.)
NRG3-092 (REF.)
1" RING
BASE PLATE (REF.)
1/2x3x3 1/2 ANGLE
1/2x3x2 3/4 ZEE
(3 PLACES)
H
J-J
1" RING
1/2x3x3 1/2
H-H
1/2 x 3 x 2 3/4 ZEE
5/16 BOLT & NUT
(TYP 12 PLACES)
21.5
28.5 R
120°
120°
16.5 R
60°
60°
J
J
15.0
15.0
1" RING
4.0
(TYP)
1/2 x 3 x 3 1/2 ANGLE

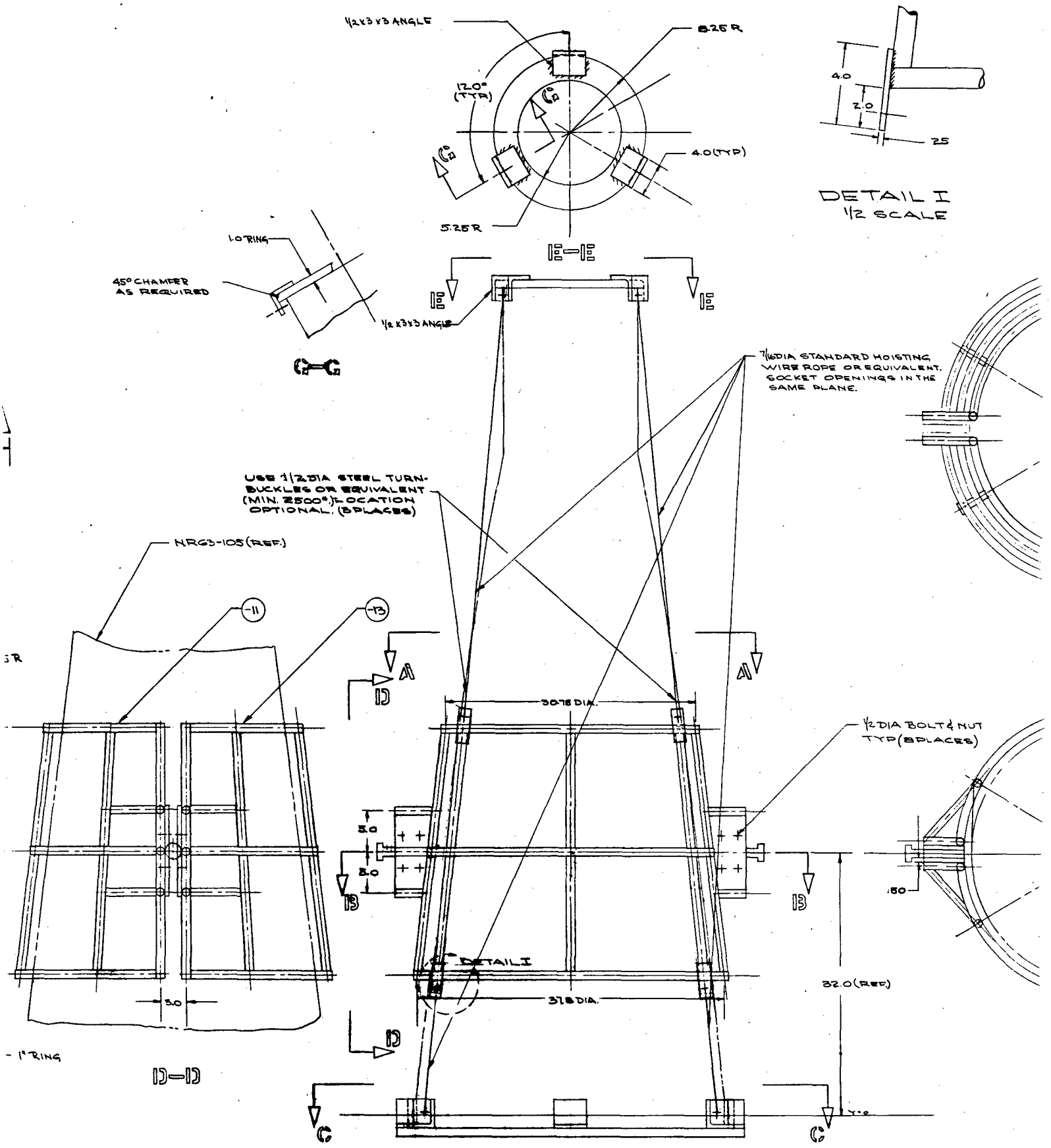
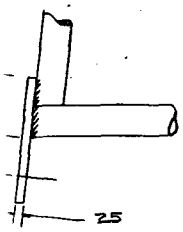
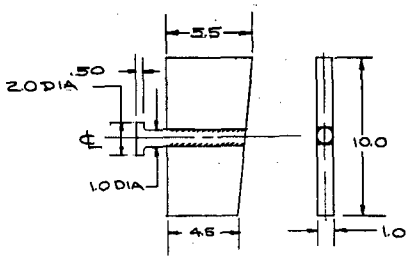


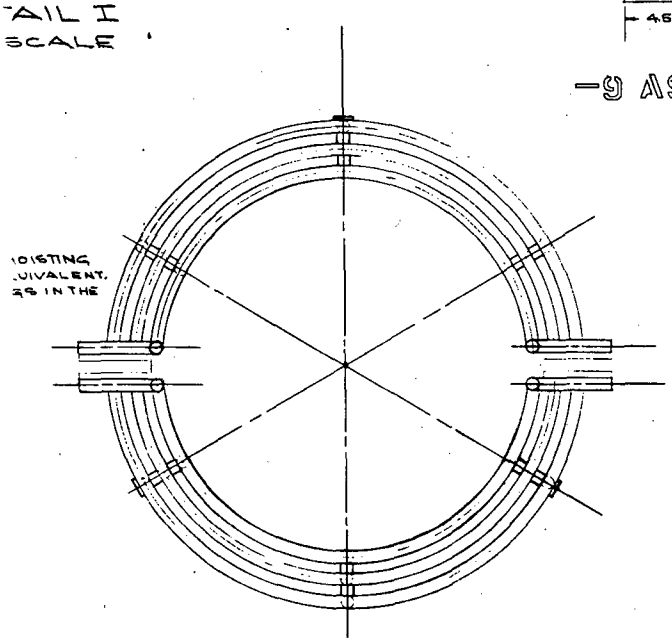
Figure 94. Handling Device (Drawing No. NR 63-153)



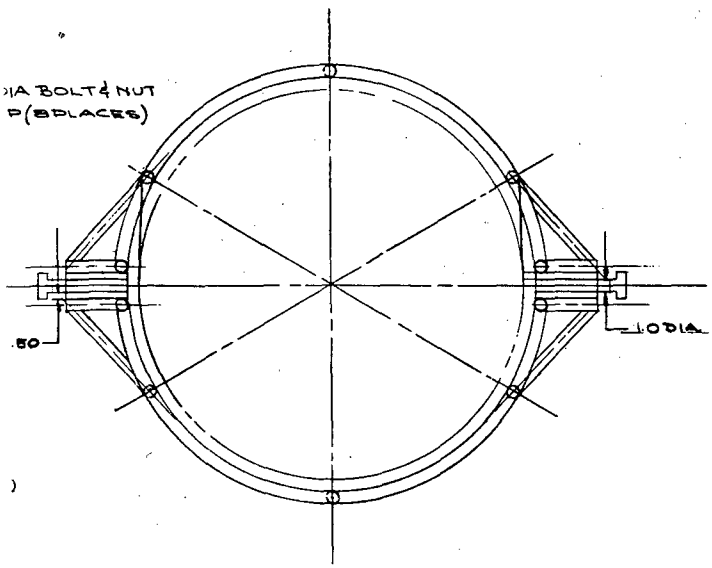
AIL I
SCALE



-9 ASSY



A - A



B - B

3			WIRE ROPE 7/16 DIA STANDARD
3			TURNBUCKLE 1/2 DIA STEEL
3			WIRE ROPE 7/16 DIA STANDARD
1			CANVAS BELT
3			ZEE SECTION 1/2 x 3 x 2 1/4 STEEL 12.0 LONG
3			ANGLE 1/2 x 3 x 3 STEEL x 12.0" LONG
3			ANGLE 1/2 x 3 x 3 1/2 STEEL x 16.0" LONG
1			TOP RING 1.0" STEEL PLATE 16.6 DIA
1			BASE RING 1.0" STEEL PLATE 47.0 DIA
1		-13	PIPE ASSY. 1 1/4" DIA STD ST PIPE 28 FT. LG
1		-11	PIPE ASSY. 1 1/4" DIA STD. ST. PIPE 30 FT. LONG
2		-8	WELD ASSY
-1	DWG. NO	OPP SHN	PART NAME
REQUIREMENTS PER ASSEMBLY		DASH NO	

MANUFACTURING TOLERANCES ARE UNLESS OTHERWISE NOTED
FRACTIONS ± .031
DECIMALS .XX ± .010
.XXX ± .005
ANGLES ± 1/2 DEG
ALL MACHINED SURFACES & AS NOTED REF. MIL STD

DESIGN K. Fehr 2/6
STRESS
PROCESS
TOOLING
CHECK J.L. Rowe 2/6
WEIGHT
APPROVED W.A. Jones
HEAT TREAT
FINISH

Whittaker
NARMCO
RESEARCH & DEVELOPMENT
DIVISION
3540 Aero Court
San Diego, California 92123

THIS DWG DASH NO | NEXT ASSEMBLY | NO REQD

TITLE HANDLING DEVICE-
RADOME ASSY.

SCALE 1/4 = 1'-0" W.O. 338-108
DWG NO NRG3-153
SIZE D
SHEET 1 OF 1

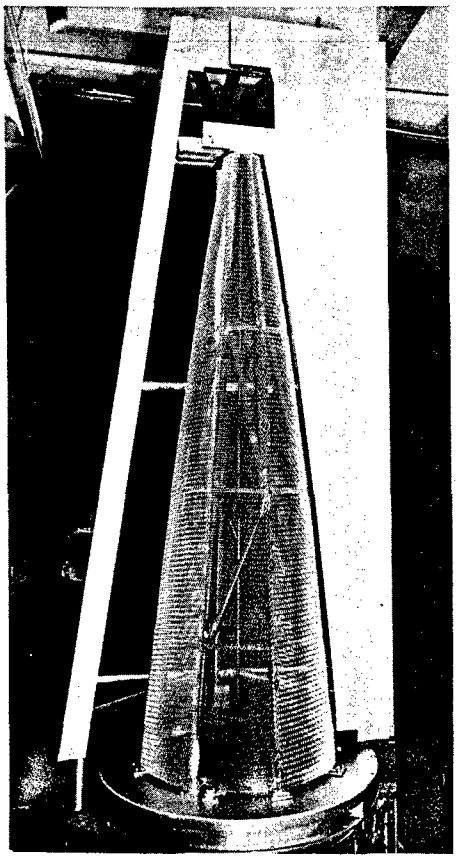


Figure 95. Full-Scale Layup Tool Arrangement

of plaster built up on the support foundation is shown in Figure 96, while Figure 97 illustrates the finished full-scale plaster layup tool. Inspection of the finished layup tool was performed at the top and bottom stations in accordance with the coordinates listed in Drawing NR 63-104. The following results were obtained:

Top Station:	Required Diameter	8.206 ±0.005 in.
	Actual Diameter	8.207 in.
Bottom Station:	Required Diameter	31.310 ±0.005 in.
	Actual Diameter	31.307 in.

Therefore, based on the inspection results, the full-scale layup tool was satisfactory for use in fabricating full-size mosaic radomes.

Firing Tool

The support foundation used for sweeping the male plaster model used for final casting of the firing tool is depicted in Figure 98. Once again, plaster was built up on this form and swept to final dimensions using the firing tool

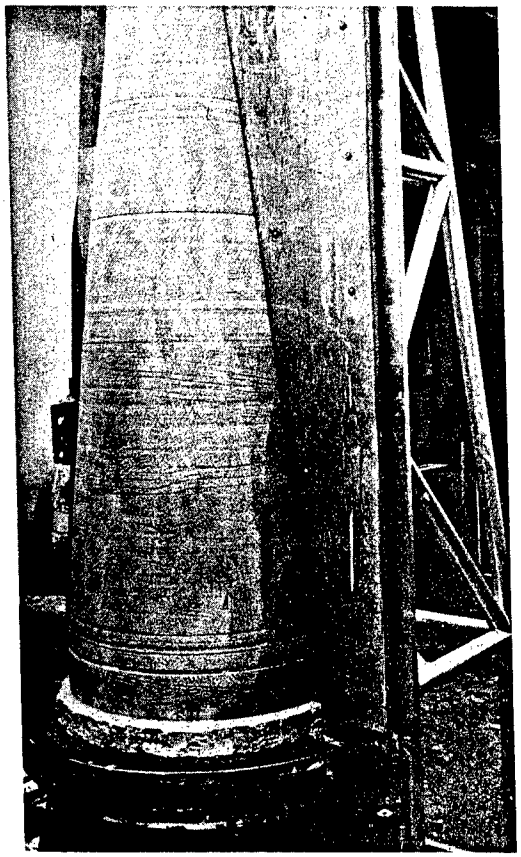


Figure 96. Layup Tool with Plaster Rough Coat

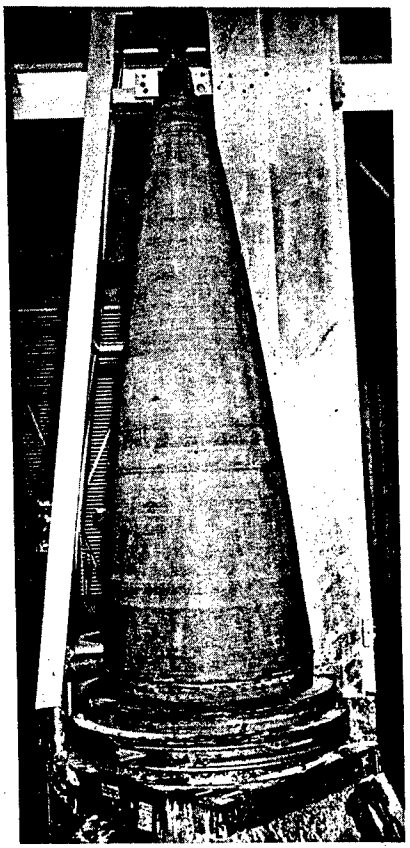


Figure 97. Full-Scale Layup Tool

template. The final plaster model produced for the interior surface of the firing tool is shown in Figure 99, centrally located in the plaster mold. In addition to serving as the core around which the final surface was backcast, an additional removable layer of plaster was built up around it to serve as the male mold for casting the initial, oversized Glasrock tool form. The casting of this tool form also included the use of an outer metal-pipe reinforced, plaster casting mold which defined the outer profile of the firing tool. Figure 99 shows the mold arrangement used for casting the initial Glasrock form. Using this casting mold setup, the firing tool form was cast from the top using approximately 1 ton of Glasrock castable material. Wet mixing was accomplished by using three power cement mixers (thoroughly cleaned prior to use) each of one-third yard capacity. Mixing and casting of the form was accomplished within 1 hour, as recommended for the Glasrock S-820 castable.

The entire mold assembly was vibrated during casting operation to aid in densification. Previous experiments utilizing vibration in the casting of Glasrock 9-in. bricks had shown an increase in flexural strength of about 100 psi (approximately 13%) above the dried strength of conventionally cast specimens. Visual examination of vibrated samples also indicated further elimination of entrapped air bubbles.

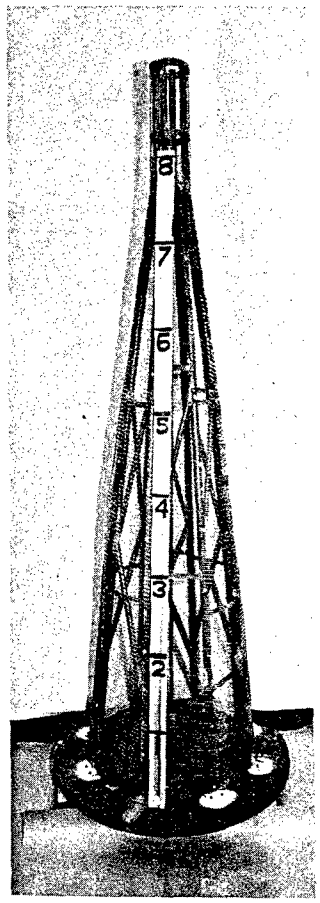


Figure 98. Support Foundation for Full-Scale Firing Tool Model

The full-scale cast form was removed from the mold 24 hours after air drying (as recommended by Glasrock Products, Incorporated). Removal and handling of this large structure was a major undertaking and initially required the use of a large crane in conjunction with the specially-designed handling fixture previously described. (Subsequently, in-house handling facilities were established by using a 2-ton capacity "A" frame and 2-ton electric hoist placed around the roof opening above the tooling fabrication area. This, combined with a fork truck for transporting to and from the kiln area, provided handling and lifting capacity.)

Figure 100 shows the cast tool after the mold halves were removed and the handling device positioned and secured to the tool form. Figure 101 shows the Glasrock tool form being lifted and removed from the plaster core, while Figure 102 depicts the crane transporting the tool to the kiln area. Figure 103 shows the part located in the kiln before drying and final shrinkage firing.

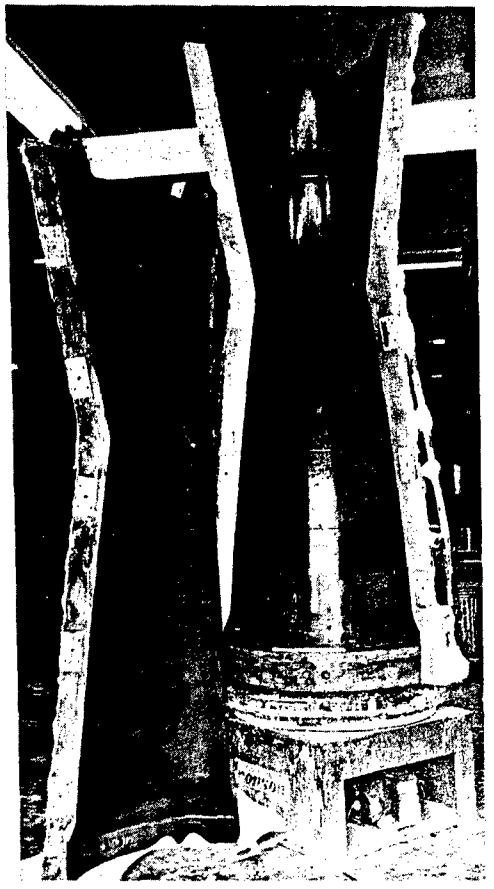


Figure 99. Firing Tool Model inside Plaster Form

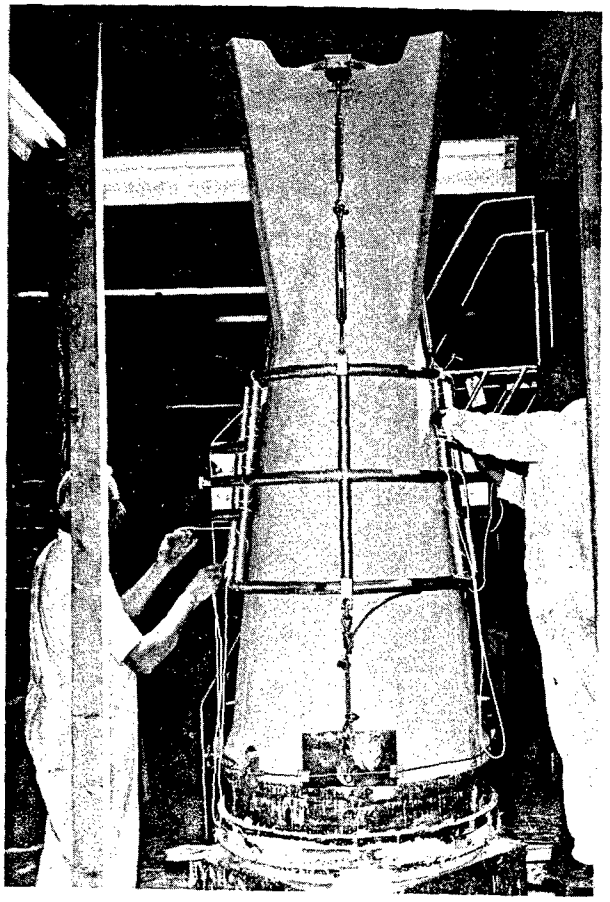


Figure 100. Glasrock Tool Form with Handling Fixture

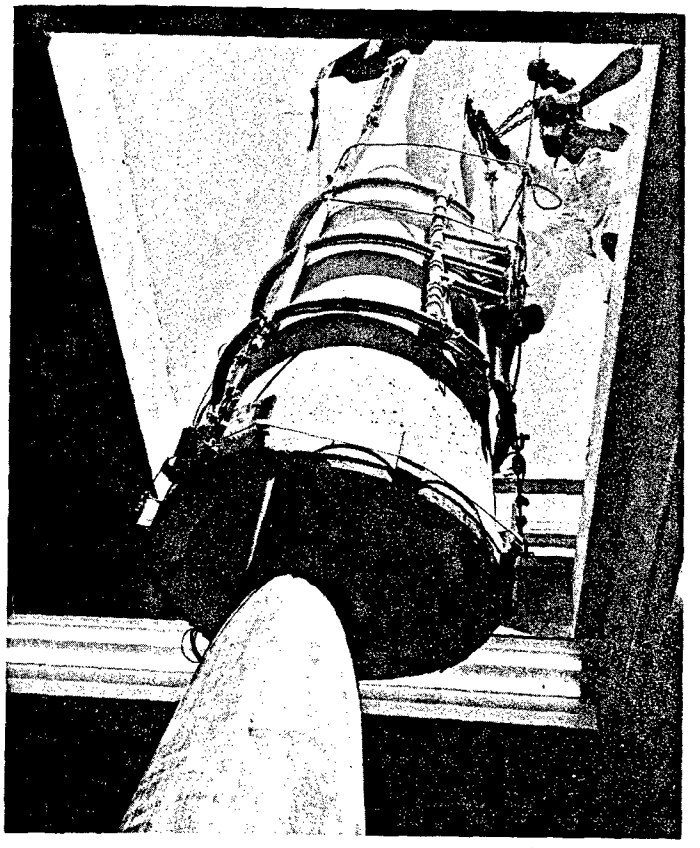


Figure 101. Removal of Tool Form from Core



Figure 102. Moving Tool to Kiln Area

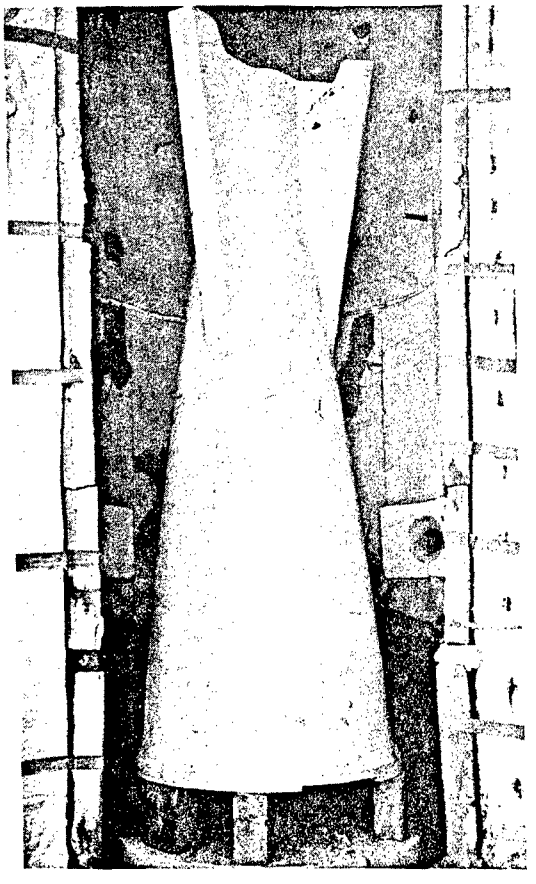


Figure 103. Full-Scale Glasrock Firing Tool Form in Kiln

Drying and firing was accomplished according to the manufacturer's recommended schedule as follows:

Hold at approximately 200°F for 72 hours.

Hold at 350°-400°F for 24 hours.

Raise the temperature to approximately 850°F and hold for 36 hours.

Raise temperature 100°F per hour to approximately 1950°F and hold for 2 hours.

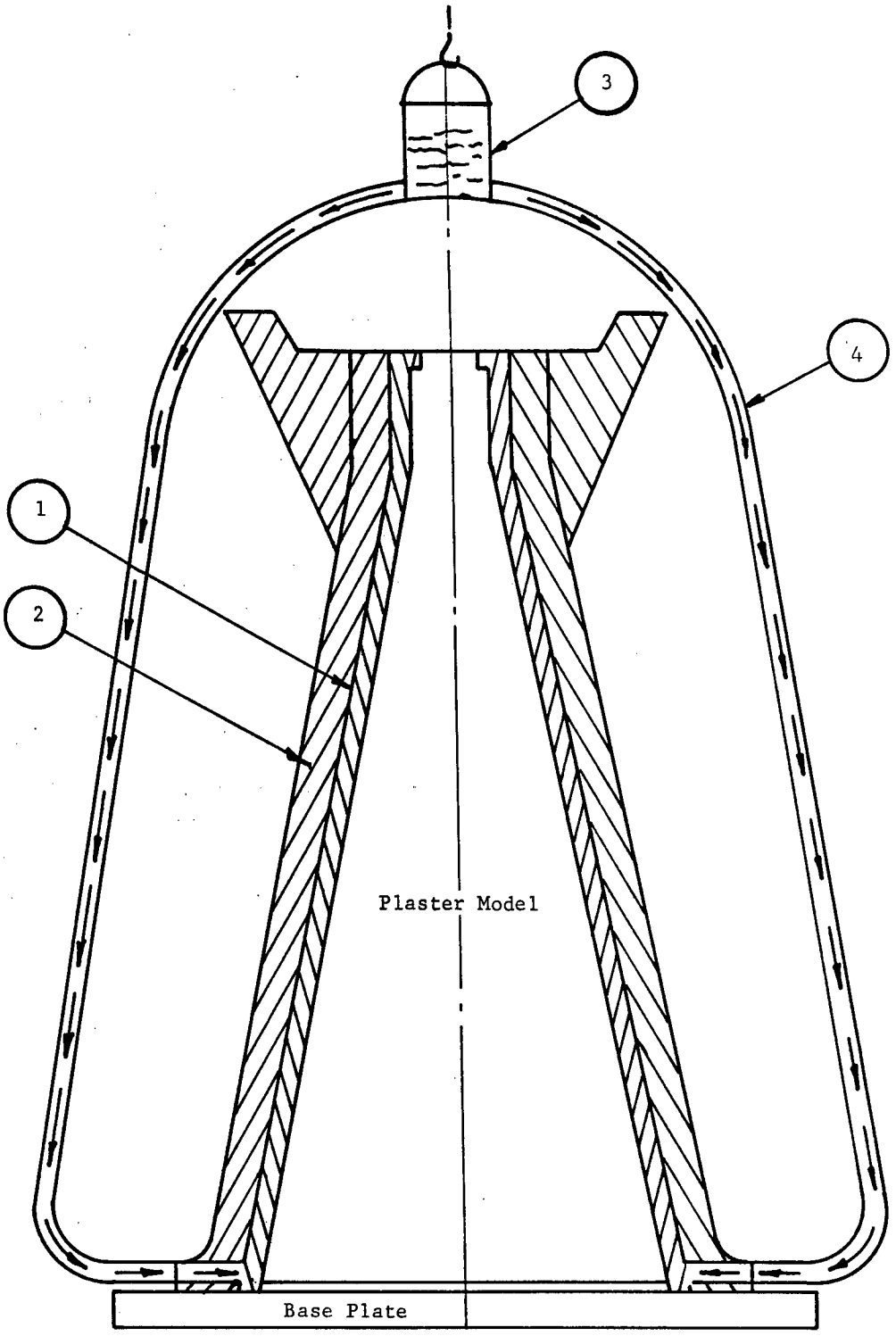
Cool the part to ambient air temperature before removal from kiln.

Drying and prefiring of the full-scale Glasrock tool form was accomplished satisfactorily. The form was free from cracks and no distortion of the tool was observed, thus indicating uniform firing conditions.

The fired Glasrock cast form was removed from the kiln and repositioned around the male plaster core model. The plaster core was sprayed with a slurry of graphite powder and Keltex solution to act as a parting agent to facilitate release of the final backcast firing tool. Backcasting of the face coat was performed using the specially prepared Glasrock slurry and pressure casting from the mold bottom. Three equally spaced inlets were used and positively fed from a reservoir approximately 5 ft above the top of the casting mold using plastic tubing. Approximately 25 gallons were required to obtain the final approximate 1/4-in. face coat thickness. Figure 104 depicts a sketch of the arrangement employed for backcasting to final dimension. The backcast firing tool was air-dried and force-dried at 125°-150°F using infrared lamps for a total time period of 3 weeks in order to assure complete curing and setting of the Glasrock slurry.

Separation of the cast firing tool from the plaster core was accomplished without difficulty as the graphite parting agent performed as expected. The handling fixture was fastened to the tool and the entire assembly raised and inverted. This allowed the male plaster core to be subsequently lifted out and removed from the cast tool using the "A" frame and hoist. Visual examination of the cast inner surface showed that there was a casting void starting at a point about 3 ft down from the base end and extending to the neck with largest width measuring approximately 10-12 in. It appeared that the defect was caused by the slurry casting (drying) into the graphite model surface simultaneously with normal drying through the Glasrock form. This resulted in premature setting of the slurry in this area leaving an interior void which failed to fill under the casting pressure. Repair of this void area was made by consecutively building up layers of Glasrock slurry by manual techniques using appropriate templates matching the contour of the tool at this area.

Inspection of the full-scale firing tool using techniques established for the truncated tools revealed that the tool was slightly oversize but correctable by using additional layers of graphite cloth and Fiberfrax paper. The inspection data are shown in Figure 105.



(1) Backcast Space Glasrock Slurry
(2) Glasrock Tool Form
(3) Glasrock Casting Slurry Container
(4) Casting, Manifold System — 3 platic tubes @ 120 degrees each

Figure 104. Cross Section of Backcasting Arrangement for Firing Tool

	Sta	Dia, in.				Deviation	
		Required (±0.010)	Max.	Min.	Avg	Avg	Range
Ⓐ	2.012	31.650	31.732	31.722	31.725	0.077	0.072 – 0.082
Ⓑ	6.038	301922	31.010	30.981	30.992	0.074	0.059 – 0.088
Ⓒ	12.074	29.762	29.861	29.839	29.847	0.088	0.077 – 0.099

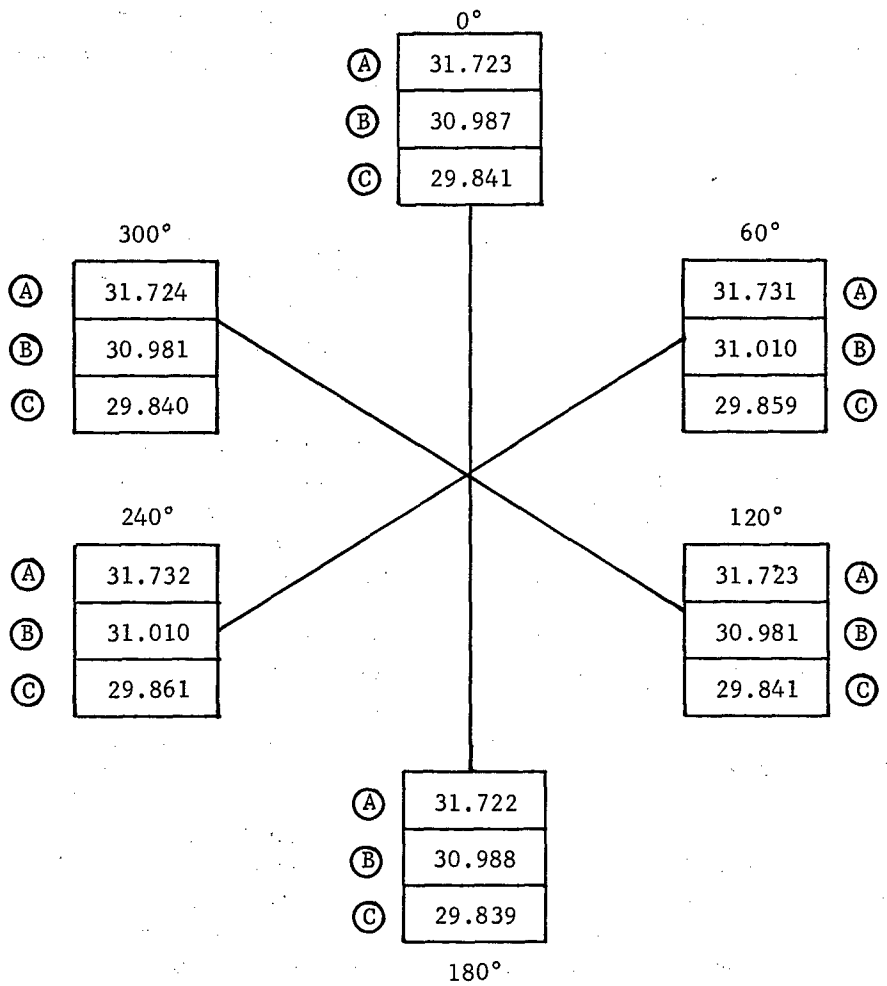


Figure 105. Inspection Data Summary – Mosaic Radome Full-Scale Firing Tool No. 1

SECTION VI

CERAMIC KILN CONSTRUCTION

The size of the final mosaic radome dictated the use of a large ceramic kiln capable of firing up to temperatures of 2500°F. In addition, the firing of test panels and truncated mosaic sections also had to be performed under comparable conditions. Because the anticipated size of the test articles and their supporting fixtures were larger than could be accommodated by most commercially available laboratory kilns, it was decided that the most satisfactory course would be to undertake the construction of a kiln designed to meet the specific problems at hand. Based on economic considerations, it was decided that a round modular natural gas-fired kiln would best meet the needs of the program. The construction of the kiln was performed during various stages of the program. Because of its modular design, the size was increased periodically as the project progressed. The construction and use of the kiln through its various modifications and stages is described in the following sections.

INITIAL KILN SIZE

To permit moving with a minimum of damage to the refractory lining, the kiln was designed to be enclosed in a metal shell sufficiently rigid to permit lifting. To eliminate the need for bag walls, the burner ports were designed to introduce the flame into the kiln tangentially to the lining (Figure 106).

Basically, the initial structure consisted of three units: (1) the combustion chamber, which included the bottom, the burner blocks and the side walls, and the hearth and its supports; (2) the firing chamber which incorporated the door; and finally (3) the crown. Each of these units will be described in detail in the subsequent paragraphs.

The shell for each of the units was constructed separately and bolted together from the outside. The door was hinged on a large pipe set in the floor. With the exception of the crown, the entire kiln was a monolithic construction employing hydraulic casting cements. Both refractory cements and firebrick were used in the crown.

The combustion chamber was housed in a steel container 20 in. high inside and 76 in. in diameter lined on the walls with 1-in. x 6-in. fiberglass insulation board. This base was mounted on two sets of transverse I-beams arranged to permit lifting by a fork truck. The refractory lining was constructed in two sections: the floor, and the vertical wall. The floor was built-up in three layers of castables, becoming more dense and more heat resistant as each layer progresses toward the interior. The first (bottom) layer was a low-cost, low-temperature, high-strength cement, covering the entire bottom of the "pan" to a depth of 5 in. The second layer was a high-temperature (3000°F) insulating castable covering the first layer to a depth

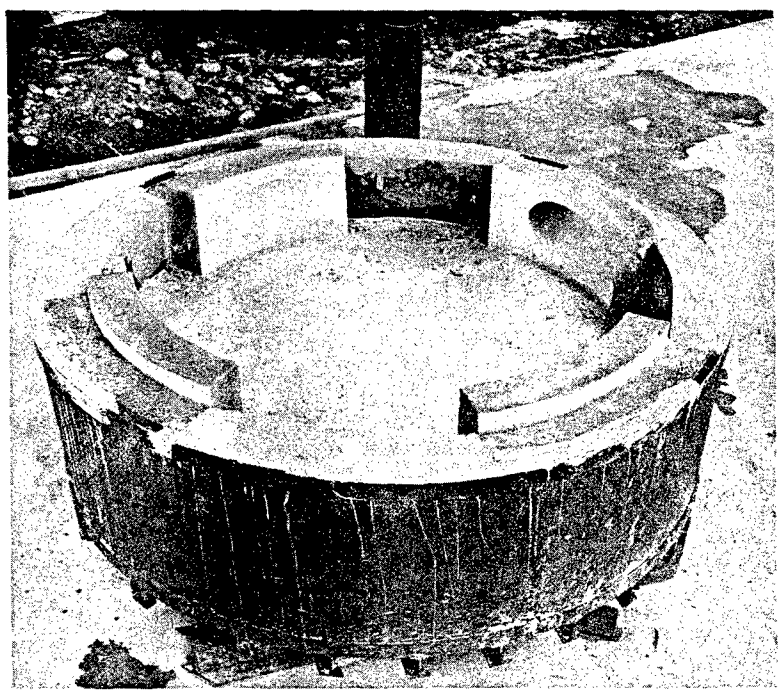


Figure 106. Base under Construction
Showing Burner Blocks

of 2 in. in the center 56 in., and 5 in. high in the wall area. The center 56 in. x 3 in. was filled with a high-density (3200°F) alumina castable. On this floor were placed the four-burner blocks (tuyeres) that had been previously cast from high-density alumina. The spaces between the tuyeres were filled with insulating castable, 4-1/2 in. of 2200°F castable next to the fiberglass block, backed up with 4-1/2 in. of 3000°F refractory on the inside.

The firing chamber was constructed of 2200°F and 3000°F insulating castable, supported by the inturned flange of a 1/2-in. x 4-in. x 4-in. angle. Sheet metal was used for the forms. One-half inch plywood spacers were positioned around the door opening to allow clearance. These were left in place until the kiln was completed.

The crown consisted of a 3000°F refractory castable ring 6 in. high and 9 in. thick, resting on the inturned flange of a 1/2-in. x 4-in. x 4-in. angle formed into a circle. On this ceramic "beam" was supported a Corbel arch (Figure 107) formed of 2200°F and 3000°F insulating firebrick. The exhaust port was 13 in. in diameter, formed of high-temperature arch brick on end and tapered 3 degrees to match a similar taper in the top four tiers of brick. This formed, in effect, a hollow keystone. The fiberglass block insulation was eliminated in the top three tiers and the space was filled with a castable refractory to transfer the thrust directly to the structure of the shell.

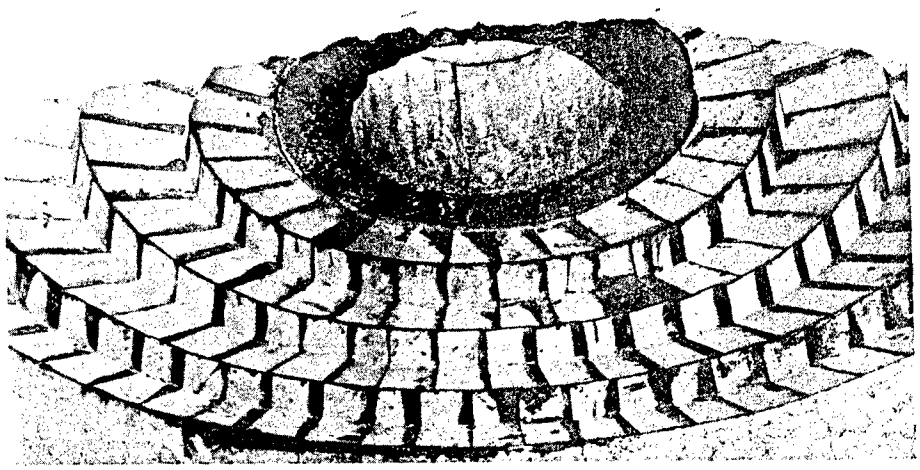


Figure 107. Corbel Arch

The floor, which was cast at the same time as the walls and separated from them with plywood strips, was attached to the hinge-post which supported the weight of the door from a cap on the upper end, and was connected to the hinge with tie rods. While appearing to be a bit cumbersome, it provided an easily operable closure which could be altered to accommodate a door 10-12 ft in height as the need arose.

Heat was supplied by four burners each mounted on individual air/gas mixing tubes. The blower could deliver 400 cfh of air at 8-oz pressure to the nozzles. Gas enters the mixing tubes at 5-oz pressure. The system as originally planned was capable of producing 2,160,000 Btu/hour. However, these burner nozzles did not have sufficient turn-down capacity at the lower temperatures. Smaller nozzles were substituted, each rated from 90,000 to 650,000 Btu/hour, whereas the larger were rated from 150,000 to 1,200,000 Btu/hour each.

Each burner port was provided with an inspirator pilot operating from the high-pressure (5 psi) side of the gas inlet system. The four pilots provided sufficient heat to raise the kiln temperature to approximately 1200°F at 100°F/hour.

All joints between pours were either separated with one or more layers of polyethylene film or sprayed with not less than five coats of polyvinyl chloride. The fiberglass block insulation between the shell and the refractory lining was sprayed with a sufficient number of coats of polyvinyl chloride to insure against penetration of water from the refractory cements during fabrication.

Figure 108 shows the kiln in its initial stage.

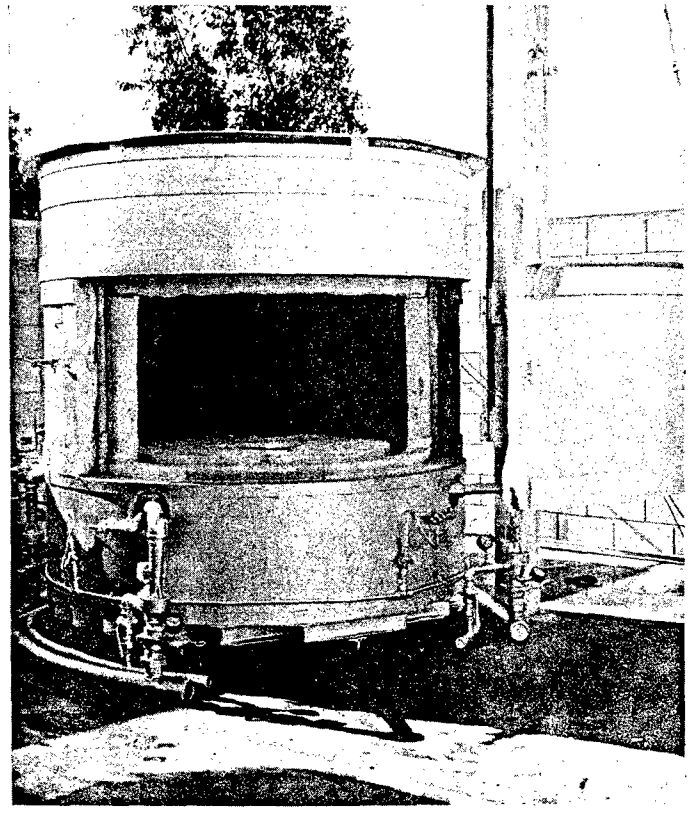


Figure 108. Completed Kiln (Initial Size)

KILN MODIFICATION

During the course of the program, the need for obtaining a reducing or neutral kiln atmosphere arose. This required replacing the original open burners with sealed burners to exclude secondary air from the kiln. The sealing of the burner parts necessitated the installation of spark-ignited pilots as shown in Figure 109. Subsequent operation of the kiln using sealed burners indicated the necessity of having a pilot flame monitoring in order to prevent accidental blow-out of the flame. This system was installed and constantly observed the pilot flame completely shut off the gas flow if the flame was extinguished for any reason. As part of the kiln atmosphere control system, and air/gas proportioning valve was installed in conjunction with a flowmeter to indicate the rate of gas consumption. This gave accurate control of the ratio between the gas and air admitted to the kiln and permitted mixtures as rich as five parts air to one part gas, and as lean as fifteen parts air to one part gas. A 10-to-1 ratio is considered to be approximately normal for combustion efficiency. The flowmeter installed on the gasline between the proportioning valve and burner mixing tubes permitted calculation of the amount of air from the ratio between the two.

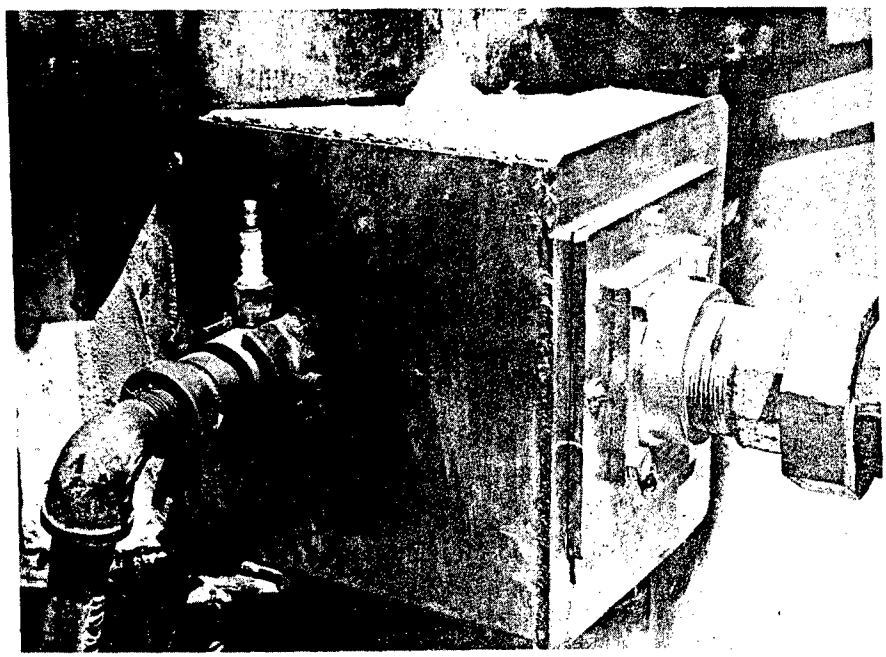


Figure 109. Sealed Burner Port Pilot and System

The main work performed under this task during the program was in connection with increasing the size of the initial kiln to accommodate the full-size radomes. This effort was centered on completing two additional module sections required for extending the height of the kiln. These two modules, both 56 in. high were of the same general construction as the original kiln. They both consisted of steel cylindrical shells which were lined with an outer layer of a 2200°F refractory castable and an inner layer of a 3000°F service castable. One module unit was designed to incorporate the additional two burners required for heating the extended kiln. Figure 110 shows the general construction involved for obtaining the required lining of this module. The illustration shows a layer of fiberglass block taped to the steel shell and cardboard cartons used to form the holes for locating the required anchor blocks. As illustrated, a sheet metal form was used in order to case the first lining against the shell and around the burner block. Figure 111 shows a portion of the initial lining and the ceramic anchor blocks to the outside steel shell. Figures 112 and 113 show the final 3000°F cast lining and the overall shape of a completed module.

Basically, the extension consisted of adding two module sections (both 56 in. high) to the existing kiln shell and replacing the crown on top of the two additions. As previously discussed, one module was designed to incorporate two additional burners, giving a total of six burners on the full-size kiln. Figures 114 through 117 show some of the various construction stages involved in extending the kiln and the hinge post required for accomodating the enlarged door area.

The two additional burners were installed and connected to the existing combustion system. The initial drying-out period for the extended kiln was performed concurrently with final securing of individual sections to each other. An initial dummy firing of the full-size kiln was also accomplished to a temperature of 2100°F. This firing was primarily for the purpose of removing all chemically combined water from the kiln lining. It was apparent that no difficulty would be encountered in obtaining the required radome firing temperature using the six available burners. Heating of the kiln was regulated by controlling the temperature of the kiln chamber through use of a protected platinum-platinum–10% rhodium thermocouple connected to a programmed controller. Trial dummy firings indicated that the temperature gradients existing in the kiln chamber would be well within the ±50°F temperature tolerance required to cure the selected Narmcad adhesive. The completed kiln was operated satisfactorily to approximately 2400°F, however it is estimated that it would be suitable for 2700°-2800°F operation.



Figure 110. Module Section prior to Lining with Refractory Castable



Figure 111. Inside of Module Section Showing Initial Refractory Lining and Anchor Blocks

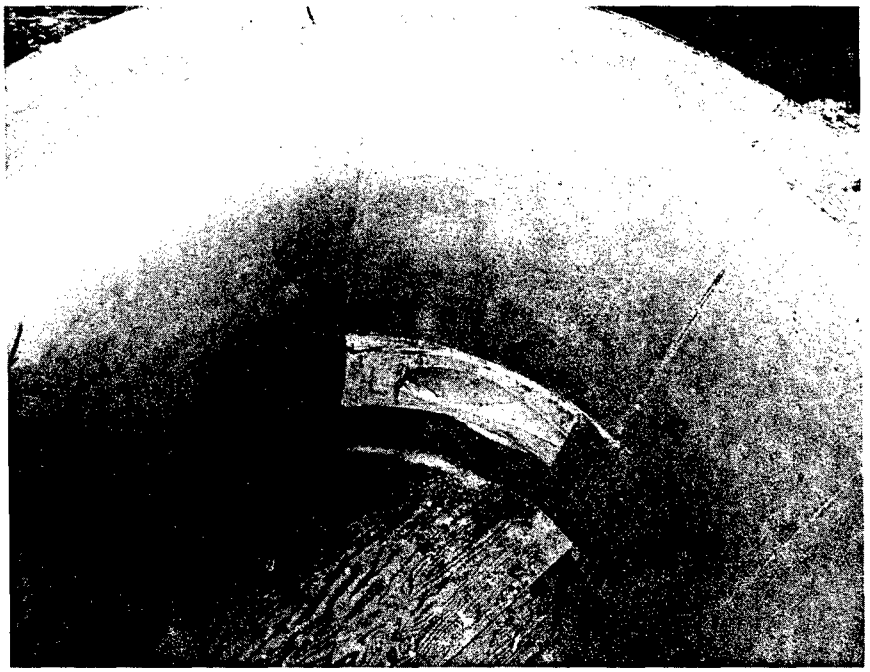


Figure 112. Completed Kiln Module Lining

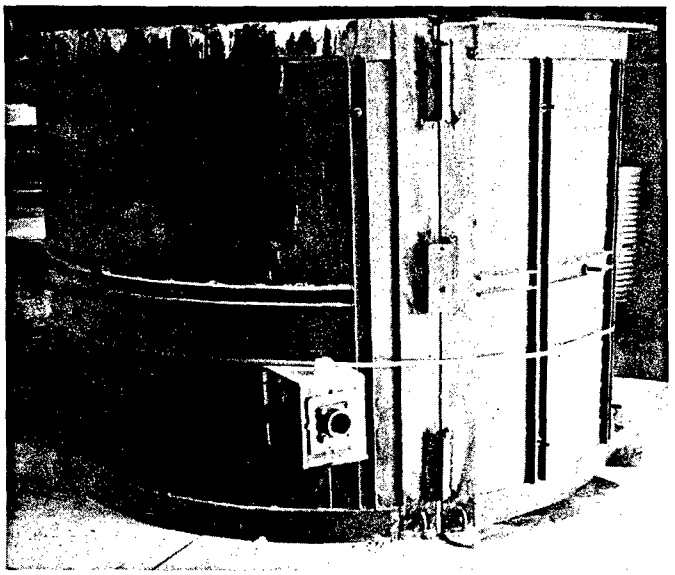


Figure 113. Kiln Module



Figure 114. Kiln Construction Stages (Kiln Base)

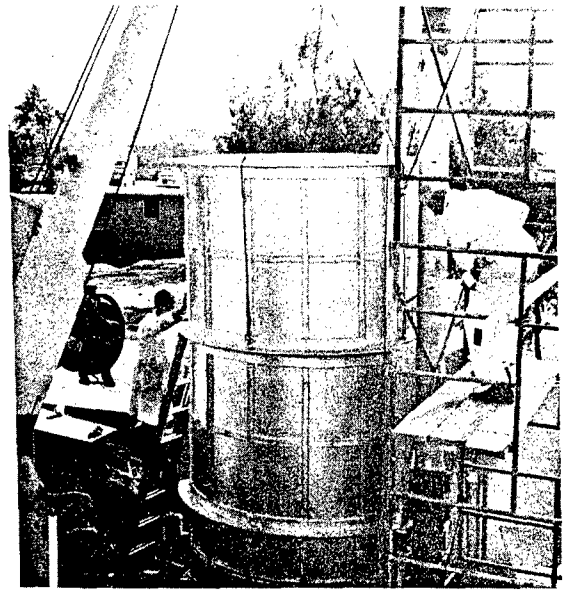


Figure 115. Kiln Construction Stages (Installing First Module Section)

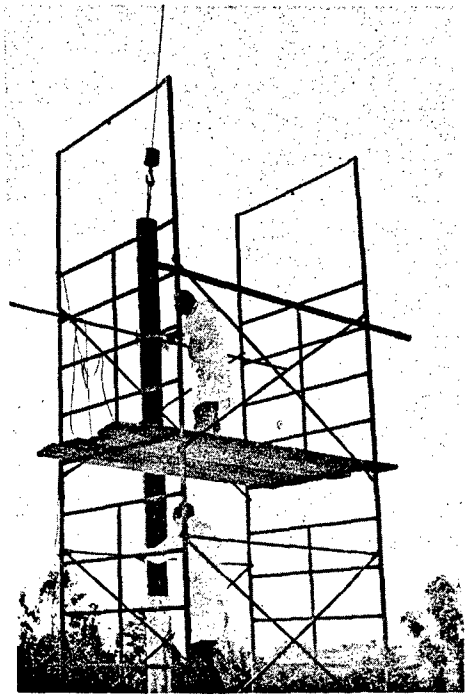


Figure 116. Kiln Construction Stages (Extending Hinge Post)

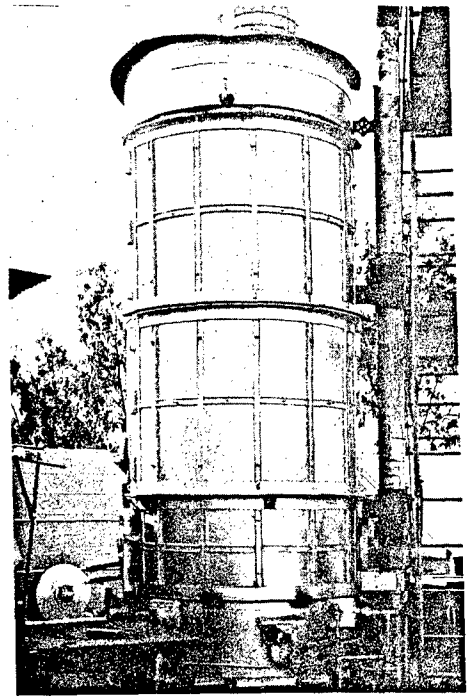


Figure 117. Kiln Construction Stages (Completed Kiln)

SECTION VII

PARTING AGENT

One of the immediate problem areas revealed during the firing of the initial flat mosaic alumina panels was the importance of utilizing a parting agent material that would prevent seizure between the part (radome) and the firing tool. Sufficient reaction occurred between the viscous glassy Narmcad adhesive and the fused-silica Glasrock firing fixture to result in adhesion between the panel and tool which upon cooling prevented full contraction of the panel and caused subsequent tensile failure. The use of boron nitride as a parting agent as previously described in Section V did not prove entirely satisfactory. Under the normal oxidizing conditions of the gas-fired kiln at temperatures of 2200°F, significant breakdown of the boron nitride to boron oxide occured with resulting glass formation, causing additional seizure between the panel and the mold. Furthermore, the use of graphite cloth under these conditions was not satisfactory due to partial oxidation of the cloth. Therefore, since successful fabrication of the mosaic radome depends upon nonsticking of the Narmcad adhesive to the tooling material, studies were performed in the following areas in an effort to devise a fabricating technique which would prevent seizure of the part to the firing fixture.

OXIDIZING ATMOSPHERE

The initial phase of the parting agent task involved investigating possible high-temperature inorganic materials that could be employed under the original existing oxidizing conditions of the gas-fired kiln. If successful, the desirability and ease of using the kiln without excessive modification was obviously preferable.

A screening test was employed which allowed relatively rapid evaluation of the candidate materials for use as a parting agent with the fused-silica tooling material. In general, it consisted on coating two slabs approximately 1/2 in. x 2 in. x 4 in. of the fused silica Glasrock refractory castable material with the desired parting agent and sandwiching bonded alumina-Narmcad segments between the two coated surfaces. The parting agents were applied either by spraying or painting, using a nitrocellulose slurry of fine powder, or as a sheet or mat form when the material was available in this form. The alumina segments, 1/4 in. x 1 in. x 2 in., were coated with the Narmcad adhesive and laid up in an overlapping manner similar to the desired mosaic pattern. In addition, one outer surface of the tiles was coated with the Narmcad so that the adhesive would be in direct contact with the parting agent when sandwiched between the tooling slabs. It was felt this represented the most severe condition that might be encountered during an actual firing of a mosaic radome.

The sandwiches were heated in air using electric kilns to 2150°F for 1 hour, and visually examined for sticking and seizure. The results were compared to those originally obtained using boron nitride, and if satisfactory,

reheated to 2300°F and again examined. It was planned to further evaluate the most promising compounds by utilizing them as a parting agent for firing large, flat, mosaic panels.

The materials investigated and results obtained are given below.

1. Silicon Nitride. Silicon nitride is a refractory material having high oxidation resistance, with suggested applications being coatings, mold washes, slurries, and mortar. It was reported to have excellent corrosion resistance to molten aluminum, zinc, lead, and tin, plus resistance to a variety of corrosive media. Its sublimation point of 3452°F was significantly high to make it attractive as a possible parting agent.

Using -325 mesh silicon nitride coatings of 0.005 in. and 0.015 in. thick were applied to the fused silica slabs. At temperatures of 2150°F, the silicon nitride bonded to the exposed Narmcad adhesive where direct contact was made. Although total seizure to the fused silica was slight, it was nevertheless enough to cause sticking on an extended run. The adhesion was also increased with a thinner coating of silicon nitride.

2. Calcium Fluoride. This material had a melting point of 2320°-2530°F and, upon heating, decrepitated. It was investigated as a possible parting agent since it reportedly has high-temperature lubricating properties when used as a dry film lubricant.

It was applied as -325 powder using both calcined and uncalcined forms. It was thought that calcining might be beneficial in preventing excess fluxing of the adhesive due to loss of fluorine from the calcium fluoride. However, both types showed severe reaction with the adhesive at 2150°F which resulted in bonding of tiles to the fused-silica material.

3. Silicon Carbide. This compound was of interest due to its slow rate of oxidation in air and the fact that it is reported to be serviceable to 2800°-3000°F.

The results of using -325 mesh silicon carbide in an 0.015-in. layer showed reaction and bonding with the adhesive. While seizure to the fused-silica slab at 2150°-2300°F was slight, enough penetration of the Narmcad through the silicon carbide occurred which would allow seizure of the part to the tooling mandrel.

4. Tungsten Disulfide. This compound was investigated even though it was known to oxidize starting at 950°F. In reply to a request for a high-temperature parting agent, one manufacturer (Bemol, Inc.) recommended its use since the main concern was how long it would be exposed to open air at the peak temperature. Tungsten disulfide, when exposed at 1350°F for 5 minutes, still leaves a film capable of lubricating. It was estimated that at 2150°F the lubricating film would be destroyed in about 1 minute. It was suggested that

even though the tungsten disulfide film was destroyed, the resulting tungsten oxide formed might prove to be a satisfactory release agent.

The results of using an 0.015-in. layer of -325 mesh tungsten disulfide proved negative. Oxidation of the tungsten disulfide allowed reaction with the Narmcad causing severe sticking to the fused silica slab.

5. Molybdenum Disulfide. This compound was investigated on the same premises discussed in the use of tungsten disulfide. Micronized molybdenum disulfide approximately 5-10 μ particle size, was used to build up a 0.015-in. coating on the fused silica slabs. Again, the reaction of the oxidized molybdenum disulfide (to the oxide form) with the Narmcad caused extreme seizure of the alumina segments to the slab at 2150°F.

6. Type 505 (White Lubricating Paste). This material was suggested as a possible high-temperature lubricant by Alpha-Molykote Corporation. It was described as a paste containing a blend of white inorganic solid lubricants containing no free metals. The solids were described as lubricating up to 2200°F, preventing galling and seizing as well as providing excellent corrosion protection. Above 2200°F, this compound was reported to chemically change, but not very rapidly, forming an asbestos-type material which might conceivably serve as a parting agent.

The paste was applied to the fused-silica slabs in an approximate 0.010-in. layer. The results, after heating to 2150°F, showed severe sticking of the alumina segments to the slabs. In fact, observations showed deep reaction into the fused-silica slab with approximately 1/8 in. of the slab being pulled out when the alumina segments were pried off.

7. Pyrophyllite. This material was selected because of its two-dimensional, layerlike sheet structure offering the possibility of serving as a barrier between the part and tooling mandrel. It is very soft, having a Moh's hardness between 1 and 2.

The pyrophyllite used to apply an 0.015-in. coating to the fused-silica slabs was micronized -325 mesh calcined powder. The material was calcined at 1500°-1600°F prior to use to remove the chemically combined water. The experiments with pyrophyllite showed some indication that it might serve as a parting agent, since the coating was intact after heating to 2150°F. Although showing promise, it was not as effective as the boron nitride material under similar conditions. Several small areas existed where the pyrophyllite had bonded to the Narmcad, and also where the Narmcad had penetrated the pyrophyllite coating causing seizure between alumina tiles and fused silica.

8. Fluorphlogopite. This compound, which is synthetic mica, is another material characterized by a layerlike sheet structure having a melting point of approximately 2500°F. The investigations consisted of using a 0.015-in. coating deposited from nominal -200 mesh synthetic mica flakes. After heating to 2150°F, small areas of sticking occurred between the tiles and fused silica. Examination revealed most of the seizure to be reaction between the synthetic mica and Narmcad adhesive with only slight reaction with the fused silica. However, the overall results were considered to be negative since, over a large area and extended time period, the condition would be aggravated.

9. Built-Up Natural Mica Plate (Amber Mica). This material consisted of an inorganic-bonded sheet mica insulation built up from mica splittings. The sheet used for the experiment was 0.015-in. thick and consisted of the higher temperature phlogopite form of mica.

After heating to 2150°F, the material showed severe embrittlement from the loss of chemically combined water. Although it did not melt and flow, the embrittlement over a large curved area would allow cracking and subsequent penetration of adhesive.

10. Synthetic Mica Paper. This material consisted of platelets of synthetic mica of the general formula $X.Mg_2.Li.Si_4.O_{10}.F_2$ (where X is Li or Na) laid down as a sheet on standard paper-making equipment without the use of binders. Its melting point was reported to be greater than 1800°F.

The results of using a 0.005-in. sheet as a barrier and parting agent at 2150°F indicated this temperature to be borderline for fusion of the material. Although only slight sticking to the fused silica occurred, the paper melted and bonded to the alumina tiles. It was also quite brittle and may have lost fluorine from its structure, which, in either case, could cause difficulty over a large area and long-firing cycle. Thus, it was concluded that this material was not suitable as a parting agent.

11. Type 302 Stainless Stock (3-mil Shim Stock). One approach investigated as a possible means of preventing sticking of the Narmcad adhesive to the fused-silica tooling mandrel was the use of a metal foil as a barrier between the part and tool. While it was anticipated that the metal would bond to the alumina tiles, the overall part would be free to contract upon cooling without failure, since the foil would prevent direct seizure to the tool. If bonding of foil to the alumina tiles occurred, an etching or grinding operation was envisioned for removal.

The initial experiment consisted of using a 3-mil thickness of 302 stainless steel between the fused-silica slab and bonded alumina segments. It was noted that after firing to 2150°F, oxidation of the steel occurred, allowing sufficient penetration of the Narmcad and adherence to the fused silica. In addition, the steel was strongly bonded to the alumina segments.

12. Metallized Mylar Film. Several manufacturers of metallized plastic films were contacted regarding a tape, film, or sheeting similar to aluminum-coated Mylar tapes in which the metal could withstand air temperatures up to 2300°F. The approach was to be similar to the use of the metal barrier previously explained. In use, the tape or film would be placed between the part and mandrel, and, upon heating, the organic plastic would burn off, leaving the metal in place as a barrier and parting agent.

Out of eight concerns contacted as possible suppliers of high-temperature metallized foil or plastic, only one could supply a material for possible use. A chromium-metallized Mylar, 1 mil thick, was obtained from Coating-Products, Incorporated, and was investigated using both a single and double layer of material. Results after firing to 2150°F were similar in both cases. No visible evidence of chromium remained after firing. Although seizure was not severe (it consisted of a series of pinpoint contacts), it was nevertheless considered to be detrimental for any large-scale use.

13. Asbestos Paper. One of the fibrous-type materials investigated as a possible barrier for preventing penetration of the Narmcad adhesive (and the resulting seizure of the part to the mold) was common asbestos insulating paper. It was anticipated the asbestos sheet would bond the tiles but would prevent bleed-through of the adhesive to the tooling material, preventing overall seizure. Depending upon type of asbestos, the fusion point varies from 2180°F to 2770°F, with the most common type, chrysotile ($3MgO.2SiO_2.H_2O$), melting at 2770°F.

The paper employed for this experiment was 0.020 in. thick, and was placed between the bonded alumina segments and the fused-silica slab. The results were entirely negative since, after heating to 2150°F, it was observed that the Narmcad had penetrated through the asbestos, causing extreme seizure.

14. Potassium Titanate Fibrous Material. This material, produced by DuPont as Tipersul fibrous insulation, is available in paper and sheet form. It has the chemical composition $K_2.Ti_6.O_{13}$ and a reported temperature resistance of up to 2200°F. Among the manufacturer's suggested applications was possible use as a dry lubricant. It was investigated for Narmco's use as a possible barrier material preventing penetration of the adhesive through to the tooling fixture.

After firing to 2150°F, the results showed that potassium titanate paper, approximately 0.030-in. thick, was not satisfactory for Narmco's use. Not only did the Narmcad penetrate the paper, but it also reacted with the potassium titanate, causing severe bonding of the part to the fused silica slab.

15. Ammonium Zirconyl Carbonate. This material, which was suggested as a possible parting agent for use under the normal oxidizing conditions of the gas-fired kiln, consists of a clear solution of ammonium zirconyl carbonate. The solid which can be crystallized from this solution has an approximate formula $(NH_4)_3.ZrOH\ (CO_3)_3.2H_2O$. Upon heating, the solution breaks down to form zirconium oxide.

The coated panel, as suggested, was heated to 500°-600°F before being placed in direct contact with alumina tiles coated with Narmcad adhesive. After firing the panel and tiles to 2200°F and cooling, the alumina tiles were observed to be securely bonded to the fused-silica castable.

16. Fiberfrax Ceramic Fiber. This material, produced by Carborundum, was available in loose fibers, paper, board, block, and mat or blanket form. Its composition consisted of high-purity alumina and silica, with small additions of modifiers such as soda, borax, or zirconia. It was reported to have temperature resistance up to 2300°F and higher for short intervals. It was investigated for use as a possible fibrous barrier material in which event, even if bonding to tiles occurred, removal would be easy as long as it prevented bleedthrough of the adhesive to the mandrel.

The results of the screening tests were quite promising. Using Fiberfrax mat approximately 0.035 in. thick, no seizure between bonded alumina segments and the fused silica slab was observed after firing to 2150°F. No penetration of Narmcad through the mat was noted, while only slight bonding to the alumina segments occurred. The segments could be removed from the Fiberfrax without undue pulling apart of the mat. Bondlines also were filled with adhesive after firing at 2150°F. Based on these initial results, further screening tests were performed using Fiberfrax mat at temperatures up to 2300°F. Again, the results were encouraging with no seizure of segments to the fused-silica slab. Even at this temperature, no penetration of the Narmcad adhesive through the Fiberfrax could be found. In addition, reaction between the adhesive and Fiberfrax at the segment interface was not severe, with bonding still slight and no apparent loss of adhesive from the bondlines.

Since the use of Fiberfrax proved successful on the screening test, it was decided to further evaluate this material as a parting agent for a "mosaic" flat panel fired under similar conditions to those planned for the final mosaic radome. In general, the chief concern over the use of this fibrous mat was the possibility of drawing out the adhesive from the bondlines over the extended time period. A flat panel similar to those previously described was fabricated with the Fiberfrax mat positioned on the face of the female mold, and the first layer of coated tiles laid-up horizontally with the adhesive face up. The second layer

was positioned with the adhesive face down so that adhacent faces were in contact. Another layer of Fiberfrax mat was placed over the top layer of tiles, and the male tooling lid placed in position to close the entire assembly.

After firing to 2200°F, soaking for 1 hour, and cooling to room temperature, the firing tool was disassembled. The cracked panel confirmed original thoughts about the use of the Fiberfrax material as a parting agent. The results were entirely negative since, with the extended time period, the Fiberfrax acted as a sponge and pulled the Narmcad adhesive from the exposed bondlines. In addition, the firing cycle proved long enough to allow penetration of the adhesive through the mat, causing severe seizure between the part and firing fixture, with the result being a tensile failure of the panel upon cooling.

17. Graphite Cloth. Since all attempts to use various inorganic materials as parting agents under the normal oxidizing conditions of the kiln were negative, efforts were concentrated on using graphite cloth; this required a protective atmosphere to prevent oxidation of the cloth during the firing cycle. Various neutral, reducing, and inert atmospheres experiments were conducted to verify the suitability of graphite cloth.

REDUCING ATMOSPHERE

Initial experiments were performed on a laboratory scale to obtain reducing conditions. Natural gas was burned in a Fisher burner and the combustion gas was introduced into a Globar-heated ceramic tube containing Narmcad-bonded alumina segments. The results indicated sufficient protection of graphite cloth was obtained at temperatures up to 2150°F under an atmosphere containing 7%-8% carbon dioxide and 1/2%-1% oxygen. Subsequent fabrication of flat, mosaic panels as described in Section IX showed that controlling the required reducing atmosphere would be critical for firing the full-scale radome and that a protective atmosphere would be easier to employ.

PROTECTIVE ATMOSPHERE

The initial laboratory-scale experiments showed that argon gas would protect the graphite cloth. A successful method for protecting the cloth from oxidation was devised which allowed the evaluation of its use as a parting agent for flat mosaic panels. The results, in general, showed that when properly protected by argon atmosphere, the graphite cloth would serve as a satisfactory parting agent. This method involved modification of the individual mold halves of the panel firing tool to allow argon gas to be introduced directly onto the graphite cloth during the firing cycle (see Figure 118). The assembled firing fixture had to be muffled to prevent any localized oxidation produced from the turbulent atmosphere of the kiln. This was accomplished by sealing the joint between the top and bottom mold halves with Fiberfrax mat, placing a refractory brick muffle wall around the assembly, and then packing the open area with more Fiberfrax matting.

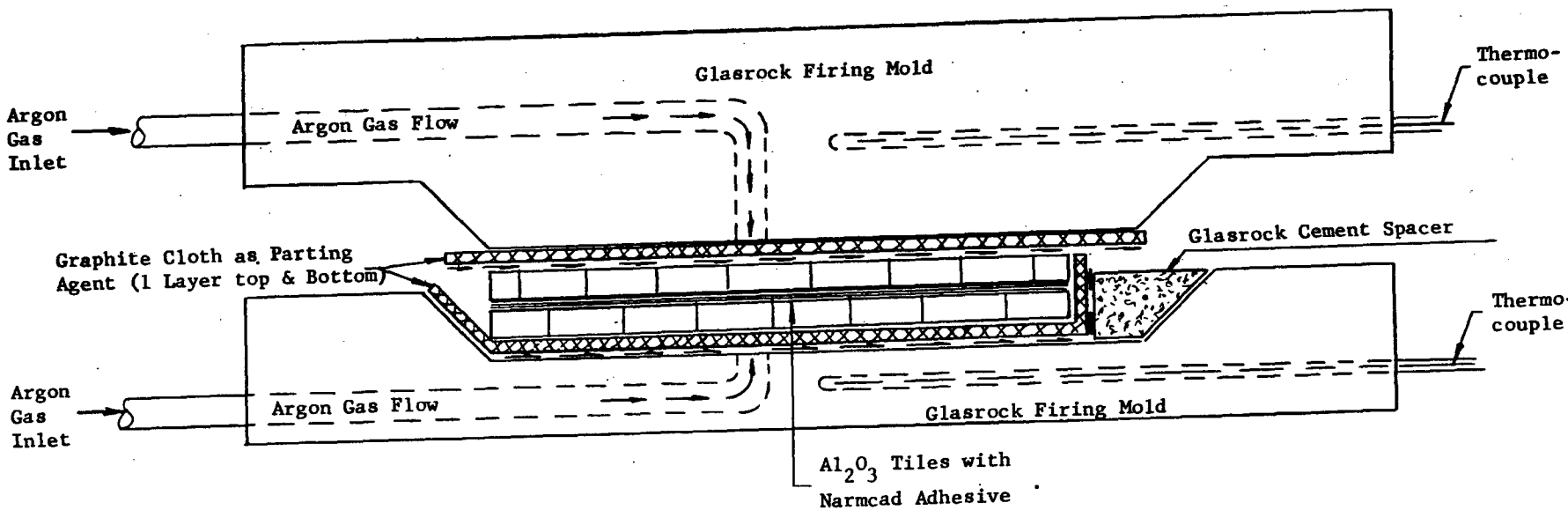


Figure 118. Method of Introducing Argon Gas around Mosaic Panel

Figure 119 shows typical heating curves employed and the results of a successful firing of an 8-in. x 8-in. alumina mosaic panel, using argon gas to protect the graphite cloth. There was no evidence of seizure between the part and the fused silica firing fixture. All individual alumina tiles were free of cracks, and good bonding was obtained in both layers. The effectiveness of the graphite cloth was further demonstrated since several joints showed where excessive Narmcad adhesive had been forced out during the firing, but did not react nor bond to the fused silica.

The initial firing of a panel, using argon to protect the graphite cloth, was made with a flow rate of 20 cfh during the entire firing cycle. Although this rate was satisfactory for producing an intact panel, it nevertheless resulted in considerable oxidation of the graphite cloth. Examination revealed that only approximately 10% of the graphite cloth remained on the top half of the panel after firing, while 60% was left on the bottom portion of the mold. Better protection of the graphite cloth was obtained by increasing the flowrate of argon gas to 60 cfh during the firing cycle. This rate resulted in approximately 80% retention of the graphite cloth on the top half, and almost 100% on the bottom portion of the mold. The protection provided by the argon gas was significant when considering the oxidation of graphite cloth in still air at various temperatures. The following data, reported by National Carbon Company, shows loss in weight per time period at various temperatures:

Temp, °F	Hours to Lose 1% Weight
510	10,000
680	100
920	1.0
1292	0.01

Considering the success of the experiments previously described graphite cloth was selected as the parting agent for preventing seizure between the radome and the firing tool. Studies of available graphite cloth indicated that a type similar to National Carbon Company's Grade WCB was adequate for production use. This grade was plain weave type with the following properties:

Weight (oz/sq yd)	7.3
Gauge, in.	0.023
Count, yarns/in. – warp	27
– fill	24
Filaments/Yarn Bundle	1440
Filament Diameter, in.	0.0003
Permeability, cfm air/sq ft (at 0.5 in. H_2O ΔP)	120

Further investigation concerning the use of graphite cloth as a high temperature parting agent are described in Section IX.

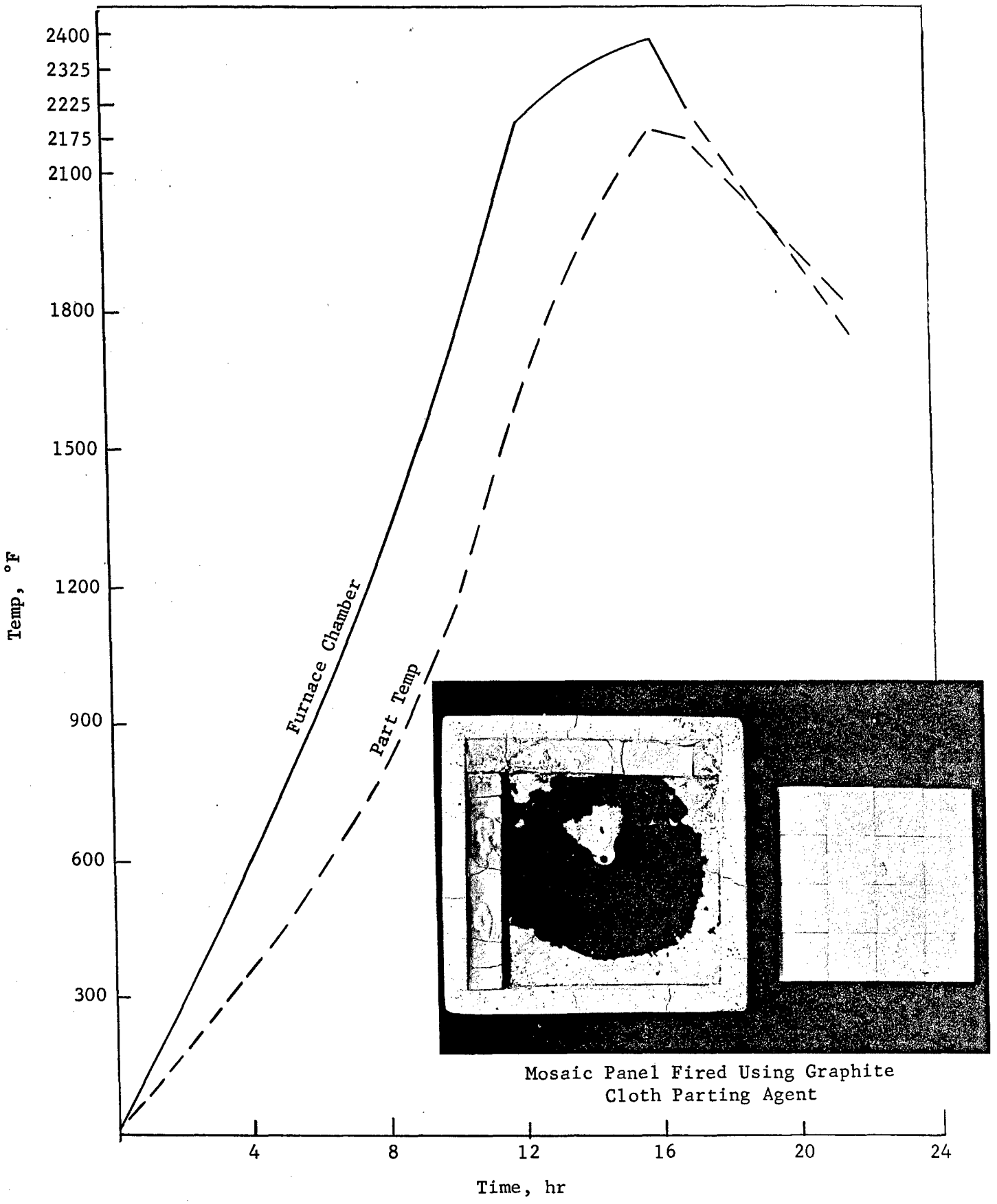


Figure 119. Typical Firing Curves for Flat Mosaic Alumina Panels Using Graphite Cloth Parting Agent and Argon Gas During Entire Cycle

SECTION VIII

RADOME REPAIR

A decided advantage offered by the fabrication of radomes by mosaic techniques was the potential for repair. Procedures for repairing a mosaic-type construction were investigated during the early stages of the program and involved the use of flat, mosaic, alumina panels. Flat test panels were fabricated to simulate conditions that might be encountered in repairing large mosaic radomes. Investigations were performed covering both repair in the field and at the factory level. The repair techniques developed during this program are described in the following paragraphs. Since considerable overlapping of experimental procedures was involved, regardless of whether the repair was of the factory or field type, the results in general are reported concurrently except where indicated.

An application of repair procedures developed during these investigations will also be discussed in Section X in which a truncated mosaic radome section was repaired and refired.

SEGMENT REMOVAL

Different methods of removing individual alumina tiles from double-layer flat mosaic panels were investigated under simulated conditions that might be encountered in repairing mosaic radomes. These consisted essentially of mechanical methods, although localized thermal shocking and chemical attack techniques were also studied. The following discussion describes the activities and results obtained for the various segment removal methods explored.

Airbrasive Unit

A Model C, single jet Airbrasive unit (manufactured by S. S. White Industrial Division, New York) was investigated as a possible tool for cutting and removing damaged tile sections. This type of equipment has been successfully used in various industries for cutting, shaping, drilling, deburring, and abrading a wide variety of hard, brittle materials such as germanium, silicon, mica, glass, and ceramics. Finely graded abrasive particles, usually alumina or silicon carbide, are gas-propelled at supersonic speeds through a small, precise nozzle to produce a cool, shockless cutting action. There is no contact between the tool and the work, with little or no heat generation. A high order of accuracy is claimed by the manufacturer. The Airbrasive unit was found to be satisfactory for removing the Narmcad adhesive from the bondline at a rapid rate, as well as for slight enlargment and shaping of the bondline area. However, it was not effective for cutting through the alumina tiles. Both 50-μ alumina abrasive powder and 400-grit silicon carbide were tried unsuccessfully for cutting through and removal of alumina tile. Cutting time was excessive and, in addition, the abrasive stream obviously could not be directed into the interface between tile layers.

The alumina and silicon carbide abrasive powders were evaluated in the S. S. White unit by cutting back and forth on a line across an 1/8-in. x 2-in. alumina tile for 30 minutes and by continuously abrading one spot for 5 minutes. The silicon carbide grit produced a groove 5 to 10 mils deep, while the alumina powder only cut 2 mils in depth. The continuous abrasion produced a spot 50 mils deep with silicon carbide grit, while a corresponding spot made by alumina was only 2 mils deep. Neither was considered adequate for complete tile removal.

Ultrasonic Machining

Ultrasonic grinding has also proved successful in shaping brittle materials. The process involves a tool and workpiece with a slurry of abrasive grit. Cutting is done by the abrasive grains driven into the workpiece by linear oscillation of the tool. A transducer converts electrical energy into mechanical energy which causes the tool to oscillate at ultrasonic frequencies. The effectiveness of removing alumina tiles by ultrasonic machining was demonstrated for Narmco by the Nova Engineering Company (La Mesa, California). A 1000-watt Sheffield "Cavitron" unit (Sheffield Corp., Dayton, Ohio) was employed to cut a disk approximately 1/2-in. diameter out of a 1/8-in. alumina tile within 15 minutes.

Narmco was advised that a semiportable, ultrasonic unit could be manufactured. Such a unit would mount the cutting tool on a moveable arm system, with flexible power and abrasive slurry leads permitting machining on the actual radome. Since the cost of such units were outside the scope of the program, no further investigations were made.

Diamond-Edged Cutting Blades and Bits

Of all the segment removal methods explored, the best results were obtained using a diamond-edged circular saw blade mounted in an air-operated hand drill in conjunction with diamond-coated router bits. This method also appeared to be the most practical and economical.

The particular blade employed was a 4-in. diameter x 0.035-in. thick Di-Met Rimlock. An air drill motor was selected as the power source for safety and speed control. The diamond cutting edge must be lubricated with water to prevent over-heating of the alumina tile and the blade; thus, spray from the rotating blade would constitute a safety hazard around an electric motor drill. In addition, the type of blade employed required operation at 2000-2500 sfm, which could be regulated by the air pressure but could not be obtained with Narmco's available electric hand drills. Some degree of skill and control of cutting was developed by personnel using this technique with the result that cuts could be made through alumina tiles in straight lines and to controlled depths. While the circular diamond blade could be used for straight incisions, it could not cut into corners without cutting across the corresponding perpendicular cut line required for tile removal. To overcome this condition, it was determined that the material remaining at a corner, formed by two perpendicular cuts, could be removed by using an 0.118-in. diameter diamond-coated router bit. The router bit was mounted in a high-speed, electrical motor suitably protected from water spray.

Figure 120 shows the type of diamond blade and router used for removing a portion of several cracked tiles from one layer of a flat mosaic alumina panel. Three cuts were made through the top layer and then the individual, cut segments were broken loose using slight mechanical tapping with hammer and punch. By tapping on the edge of the segments, the adhesive parted on the interface without damage to the rest of the panel. Hopefully, removal could be further facilitated by using a multiple series of criss-cross cuts to leave relatively small squares or rectangular segments which could be removed by mechanical tapping. The cutout area shown, is approximately 1 in. x 4 in., and encompasses several of the 2-in. x 2-in. tiles comprising the panel.

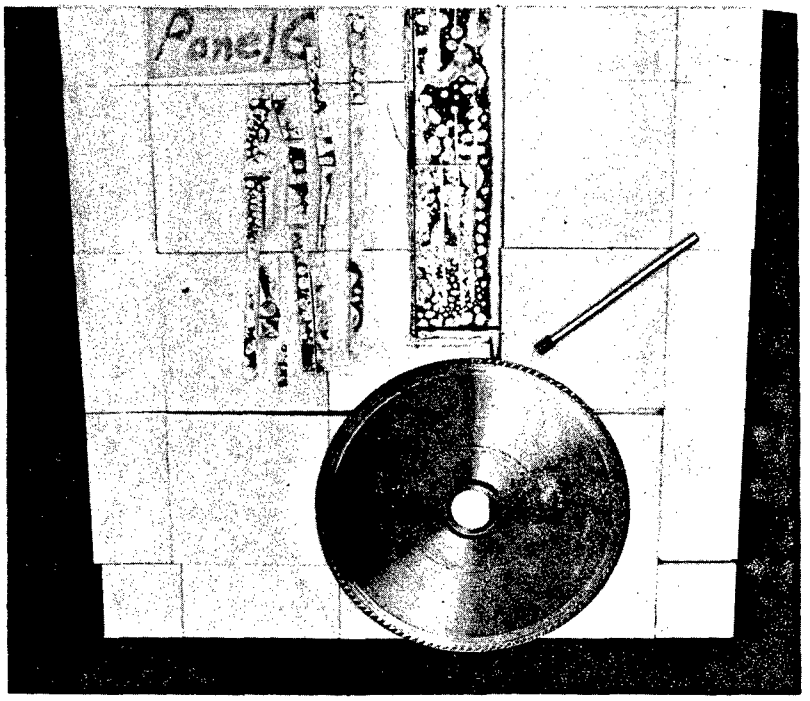


Figure 120. Portion of Mosaic Panel Removed with Diamond Blade and Router Bit

Chemical Attack

The use of hydrofluoric acid to selectively etch out the glassy bondline without significant attack on alumina tiles was also investigated, using wax "dams" to contain the acid over the desired removal area. The results of these experiments showed that directional control of etching was difficult after the acid had reacted and etched out the glassy butt joints and started migrating along the tile interface, there was no easy way that could be found to control the acid flow. Some degree of control might be obtained by first removing the surface bondlines using a mechanical method, and drilling a series of small holes through the tile layer to the interface bondline and then filling the holes with HF acid. In view of the

success obtained by using a diamond-edge blade, however, no further study was made for acid removal technique except as used for removal of a base attachment tile in a truncated radome section (see Section X).

Thermal Shocking

Tile removal by thermal shock was not satisfactory. In one approach, the adhesive was removed from the surface bondlines around a cracked tile and then an oxyacetylene torch was used to heat the surface of the exposed tile. After heating to approximately 500°F, the tile was quenched by placing dry ice in contact with the surface. A modification of this method consisted of criss-crossing the damaged tile with a series of cuts prior to thermal shocking. In both cases, uncontrolled thermal stresses cracked the remaining undamaged area of the test panel.

Another approach for thermal shocking employed the use of exothermic heating patches placed over the area to be removed. The exothermic systems, developed by Narmco, consist of active metals and oxides mixed in stoichiometric proportion which, upon ignition, release large amounts of heat energy in a relatively short time. Typical temperature rise time, measured through a thin metal panel, shows a rate of 1800°-3000°F/minute.

A 2700 Btu rated exotherm package was employed for Narmco's experiments with and without dry-ice quenching for further thermal shock. Again, thermal gradients were such that the original undamaged areas of the panel were severely cracked in many places.

CANDIDATE REPAIR ADHESIVES

It was anticipated that the majority of factory repairs would be of a structural nature, and thus would involve using the original Narmcad adhesive and refiring in existing heating facilities. The nonstructural repairs could be made with a lower curing adhesive at the factory level. In the field, low-temperature or cold-setting adhesives would be mandatory, since, at best, only limited heating facilities would be available for field repairs.

The following low-temperature inorganic compounds were selected and evaluated during this program.

Metlbond Type CA-100 Ceramic Adhesive

This type of adhesive, produced by Melpar, Inc., was originally investigated for possible use as the adhesive for actual bonding of the ceramic segments into the radome shape. As previously described this adhesive was found to be unsatisfactory for this use; however, it had potential for nonstructural repairs, especially in the field, since it required only a 250°F curing temperature. It was reported to have a maximum service temperature of 2600°F after curing. In addition to the low curing aspects, its electromagnetic properties were satisfactory for repair with a dielectric constant of 1.9 and loss tangent less than 0.002 at room temperature.

Astroceram A-LP High-Temperature Cement

Again, this type of material was originally evaluated, unsuccessfully, as the main adhesive for bonding the radome. It was thought that Type A-LP (Low Porosity) manufactured by American Thermocatalytic Corporation (Mineola, New York) might be suitable as a repair adhesive since it could be air dried, although curing at 1100°F was required for full strength. Maximum service temperature for Astroceram A-LP was reported to be 4400°F. In addition, its shrinkage is relatively low, ranging from 1% to 4%.

Sauereisen Cements (Various Types)

These cements, produced by Sauereisen Cements Company (Pittsburgh, Pennsylvania), are air-setting type compounds or require only a minimum heat cure of 150°-200°F, and resist temperature up to 2500°F. There are a wide variety of types for various applications such as electric resistors, low expansion, electrical, acid-resistant, and high-temperature resistant cements. Some were reported to have shrinkages less than 2%. The more attractive types were selected for repair use.

Pyroceram Brand Low-Temperature Thermal Setting Cements

Two types, 89 and 95, as produced by Corning Glass Works (Corning, New York), were evaluated as possible repair adhesives. Both these sealing glasses develop a partially crystalline structure which results in a devitrified glass upon heating. Both types require only a relatively low-temperature firing of approximately 850°F. The thermal expansion of Pyroceram 89 more closely matches that of the alumina segments and is recommended for sealing materials in the thermal expansion range of 4.44 to 5.11 x 10^{-6} in./in./°F. The Pyroceram 95 had a higher expansion and was recommended for sealing materials with a thermal expansion range of 5.0 to 6.12 x 10^{-6} in./in./°F.

Sodium Silicate and Ceramic Powder

A cement formulated from approximately 40w/o sodium silicate (water glass) and 60w/o low soda alumina -325 mesh powder was also evaluated as a possible air-setting repair adhesive.

Phosphate-Bonded Composition

A review of several of the low-curing ($\approx$ 800°F) phosphate-type binders was also made for possible use as a repair adhesive. The particular type selected was described by Marquardt Corporation in their program "Development and Evaluation of Insulating-Type Ceramic Coatings."* This type, designated

* ADC Technical Report 59-102, Nov 1959.

P-56, consisted of the following:

Constituents	Parts by Weight
Alumina – 48 mesh	50
Alumina – 325 mesh	45
Red Label Clay	5
Magnesium Trisilicate	2
Phosphoric Acid, 85%	10
Water	8

Epoxy Adhesive

An available epoxy adhesive, produced by Epoxy Coatings Co. (San Francisco, California) and classified as Helor Hi-Water concrete adhesive, was also evaluated as a nonstructural repair adhesive. This is a commercially available cement for permanently affixing anchor bolts, pipes, studs, hinges, etc. to concrete or masonry, and reportedly is absolutely unaffected by moisture or temperature change besides being free from cracking or shrinkage tendencies.

A temperature endurance of 450°F was reported by the manufacturer for short periods with the following physical properties of the cured adhesive being claimed:

Compressive Strength	9850 psi
Tensile Strength	1080 psi
Flexural Strength	1855 psi
Shrinkage Tests after 3 days	0.00063 in./in.
Shrinkage Tests after 4 days	0.00065 in./in.

SCREENING TESTS

The candidate adhesives investigated for nonstructural repairs either for the factory or field were screened for their ability to withstand various operating conditions such as handling, high humidity, thermal shock, and thermal stability. These tests are described below.

Thermal Shock

Alumina tiles 1/8 in. x 2 in. x 2 in. bonded together with the candidate adhesive were heated to 150°F, 200°F, 250°F, 300°F, 350°F, and 400°F for 5 minutes at each temperature, and then removed and cooled to room temperature at a normal rate. Each temperature was repeated for five cycles before going to the next higher temperature. Visual observation was made of any separation due to thermal shock at the end of each cycle.

Water Solubility

Bonded tiles were soaked in water at room temperature for periods up to 168 hours. At the end of each 24 hours, they were removed and examined for strength retention.

Porosity (Percent Water Absorption)

Bonded tiles were boiled in water for 6 hours and their percent water absorption calculated based on their original dry weight.

Flame Test

Three alumina tiles 1/8 in. x 2 in. x 2 in. were bonded together in such a manner to simulate the overlapping of tiles in the final radome pattern. One layer consisted of two tiles with a butt joint while the third tile was placed equally over the joint. The bonded test specimen was positioned in a refractory brick holder and a propane hand torch flame adjusted to impinge on the butt joint as shown in Figure 121. The torch-to-tile distance was adjusted to give a 500°F reading on a thermocouple placed on the surface of the sample. After holding the tile at 500°F for 1 minute, the torch was moved in to give 1000°F for 1 minute and then finally adjusted to a temperature of 1500°F for 1 minute. After final heating at 1500°F, the samples were removed from the holder and allowed to cool to room temperature before being retested for a total of five cycles or to failure.

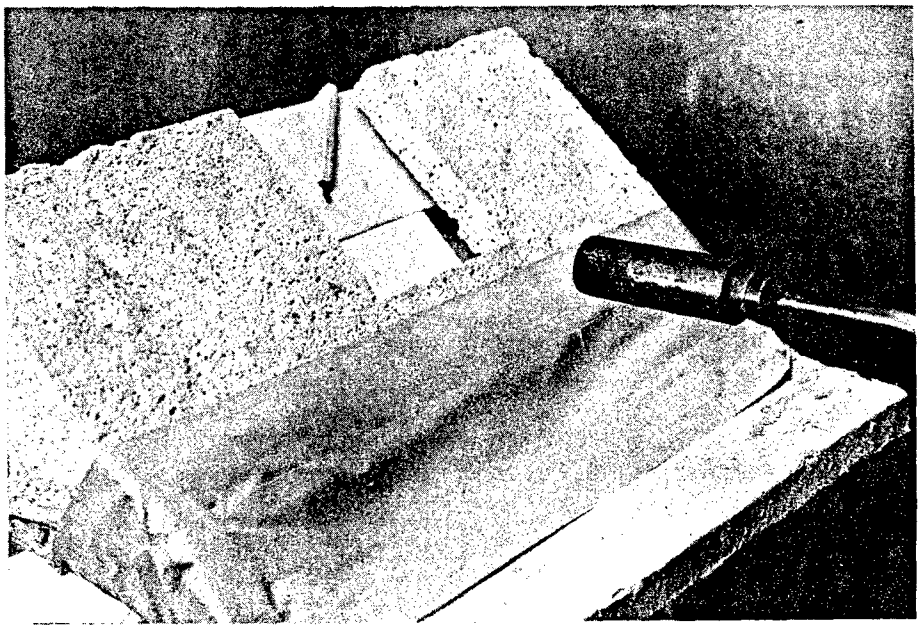


Figure 121. Flame Test

RESULTS AND REPAIR OF TEST PANELS

The results of the various tests performed on the candidate repair adhesives are listed in Table 30. Narmcad 110 was also included in all tests as a standard to serve as a basis for comparison. These results indicated that only the following candidate adhesives satisfactorily met and passed all screening tests:

Pyroceram 89

P-56 Phosphate Binder

Helor Hi-Water Epoxy Adhesive

The above three adhesives were further evaluated for shear strength using compressive lap shear samples fabricated from 1/4 in. x 1 in x 2 in. alumina segments. The following average shear strength values were obtained:

Pyroceram 89	2600 psi
Helor Hi-Water Epoxy	3500 psi
P-56 Phosphate Binder	480 psi

The conclusion, from the results obtained, is that any of the above adhesives could be employed for nonstructural repair depending upon the type and degree of repair required. Each one would have specific advantages and disadvantages.

Pyroceram 89 has a low loss tangent and a relatively high dielectric constant (approximately 20), although its use in a thin, bondline-type repair would probably be acceptable. In addition to a high density of 6.3 g/cc, considerable shrinkage occurred during heating. Its use was demonstrated in repairing a flat panel, although considerable shrinkage occurred on initial repair and multiple firings were required for complete filling and smoothing. Narmco anticipates that Pyroceram 89 could be used for factory repair where heating facilities are available for obtaining the required temperature of approximately 850°F. This adhesive could also be employed in the field where heating devices were available. The Pyroceram 89 could be cured by such devices as electric tapes, gas torches, or by radiant heat from a bank of quartz lamps, providing sufficient care is taken to prevent damaging thermal stresses.

The use of the P-56 type of phosphate binder would have to be limited to strictly nonstructual applications for aerodynamic smoothing and bridging of bondline void areas, due to its relatively low shear strength. However, its main advantage would be in repairing areas where maximum temperature resistance would be required. Although curing temperatures of only about 850°F are required, the material is capable of withstanding temperatures approaching 2500°F. Again, field repairs would require availability of heating devices previously discussed.

The epoxy type of adhesive would be satisfactory for field repairs where no heating facilities were available, since it requires only 8-12 hours setting time above 60°F for use. This adhesive continues to increase in strength

TABLE 30

REPAIR ADHESIVE EVALUATIONS

Cure Temp, °F	Adhesive	Flame Test*	Thermal Shock	Water Solubility	% Water Absorption
1100	Astroceram A-LP	Fell apart after 2nd cycle (500°F) Fell apart after 2nd cycle (1500°F)	OK	OK	0.5%
250	Melbond CA-100	OK Fell apart after 2nd cycle		Fell apart in 12 hr	Fell apart in 2 hr
2150	Narmcad 110	OK		OK	0%
800-850	Pyroceram 89			OK	0%
RT	Sodium silicate & Alumina cement			Fell apart in 24 hr	Fell apart in 2 hr
	Sauereisen P-1	Fell apart after 4th cycle		Fell apart in 32 hr	Fell apart in 1 hr
	Sauereisen P-6	Cracked on 4th cycle (1000°F)		Fell apart in 30 hr	
	Sauereisen P-8	Fell apart after 1st cycle	Fell apart after 3rd cycle (250°F) Fell apart after 3rd cycle (250°F)	Fell apart in 3 hr	
	Sauereisen P-29	Blew up on 2nd cycle (1000°F)	Fell apart after 2nd cycle (250°F)		0%
	Sauereisen P-30	Fell apart after 1st cycle	OK		Fell apart in 15 min
	Sauereisen DW-30	Fell apart after 1st cycle			Fell apart in 15 min
	Sauereisen DW-31	Blew up on 1st cycle (1000°F)			0.2% loss
	Sauereisen DW-33	Fell apart after 3rd cycle			Fell apart in 4 hr
	Sauereisen DW-74	Blew up on 3rd cycle (1500°F)	Fell apart after 1st cycle (350°F) Fell apart after 1st cycle (350°F)		Fell apart in 1 hr
	Sauereisen DW-78	Fell apart after 1st cycle	Fell apart after 3rd cycle (350°F) Fell apart after 3rd cycle (350°F)	Fell apart in 26 hr	Fell apart in 3 hr
800-850	Pyroceram 95	Cracked backup tile when going from 500°-1000°F (both samples)	OK	OK	0%
850	P56 phosphate binder	OK			0.1%
RT	Epoxy adhesive				0.2%

* 2 samples

for 2-3 days, and the time of initial set can be greatly reduced in cold weather by applying some external heat source. It possesses relatively high strength and unexpected temperature resistance for an organic material and its electrical properties should be satisfactory for thin bondline type repairs.

Figures 122 and 123 show the type of repairs made with both the phosphate and epoxy-type adhesives.

A mosaic panel was also structurally repaired using Narmcad adhesive to simulate a factory repair. The repair was made without adulteration, using original segments and adhesive as well as repeating the original firing cycle to a temperature of 2200°F. Initially, a flat panel was fired with the center top layer segment void of adhesive to assume the appearance of a defect that might be encountered during a radome firing. A repeat firing was made with the void segment recoated with Narmcad adhesive and the entire panel reheated to the original peak temperature of 2150°-2200°F. Visual observation of the "repaired panel," revealed no apparent change in adherence of the originally bonded segments, with the patched area also similar in appearance. This procedure was subsequently employed for repairing and refiring a fabricated truncated radome section, reference Section X.

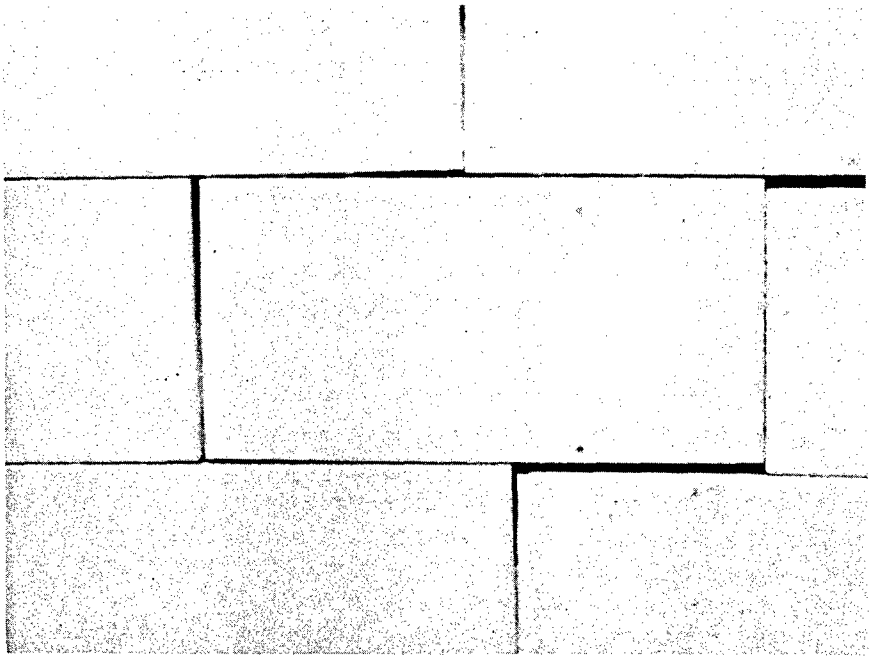


Figure 122. Typical Open Bondlines prior to Repair

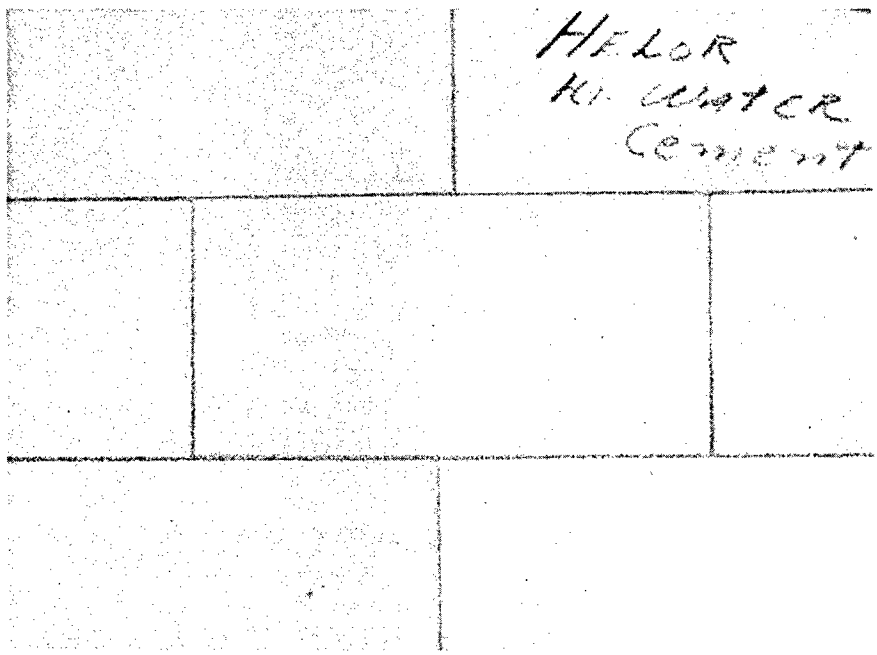


Figure 123. Bondlines after Repair

SECTION IX

EXPERIMENTAL INVESTIGATIONS INTO FABRICATION TECHNIQUES

Prior to full-scale assembly of individual, curved, alumina tiles into truncated base sections of the full-scale, ogival radome, a number of studies and investigations were conducted to establish final radome fabrication procedures. Proofing of these concepts was obtained by fabricating flat, mosaic, alumina panels. This section describes the investigations and results obtained.

EFFECT OF KILN ATMOSPHERES ON BONDED ALUMINA SEGMENTS

The major effect of using a reducing or neutral firing atmosphere appeared to be on the decomposition of the nitrocellulose binder employed with the Narmcad adhesive. The binder was used to provide green strength for handling purposes as well as acting as a vehicle to allow tiles to be coated by spraying, dipping, and painting techniques. Original firings with Narmcad were performed in a normal oxidizing atmosphere (prior to use of graphite cloth), and the carbonaceous material contained in the binder had been burned off duing the firing cycle.

Several Narmcad-bonded alumina tiles were fired in the laboratory-simulated reducing atmosphere previously described. Peak temperature obtained was 2150°F with a carbon dioxide content of approximately 6-1/2% to 7-1/2%, and 1/2% of oxygen. After firing, the bonded tiles were split to examine the interfacial fired adhesive layer. Visual examination showed that the Narmcad has fused and flowed out, and was unaffected by the atmosphere since neither darkening nor discoloration was noted. The amount of oxygen present in the simulated atmosphere was sufficient to permit most of the carbon to be burned off. However, an abnormal bubble structure was contained in the glassy adhesive, indicating entrapment of gas.

Visual examination of bonded alumina tiles fired in an argon protective atmosphere showed the Narmcad to be dark grey in color with a significant increase of gas entrapment within the interfacial bondline resulting in a bubble structure. As expected, the deposite of carbonaceous material had a detrimental effect on the strength of the adhesive. Lap shear samples tested for compressive shear strength showed a close relationship to the amount of visible carbon present in the adhesives. Values of lap shear specimens (with nitrocellulose) fired in an argon atmosphere retained only 20%-40% of the original strength of Narmcad fired under oxidizing conditions.

Substitution of nitrogen for argon did not eliminate the condition. Changes were made in the organic binder and firing cycle, and the results were observed. Initial changes consisted of using different green strength binders in the Narmcad adhesive.

The following is a description of the materials that were tried.

1. Methocel MC (Dow Chemical Company), a dimethyl ether of cellulose in powder form, is a water-soluble, gumlike material used primarily as a thickening agent. Approximately ½w/o was added to the Narmcad, and a sprayable slurry was made by adding water. The green strength was much less than that of nitrocellulose, although with care, the tiles could be handled.

2. Vee-gum Tee (R. T. Vanderbilt Company) is a complex colloidal magnesium – aluminum silicate powder that is used as a suspending agent and surface hardener for glazes. This material was of interest since its composition was very similar to that of Narmcad, which is essentially a modified magnesium – aluminum silicate. Again, a ½w/o addition to the Narmcad was employed, with very little green strength being obtained from the sprayable slurry.

3. Krylon Crystal-Clear solution (Krylon, Incorporated) is a standard pressure spray coating containing 6.27% nonvolatile acrylic ester resin and 93.73% volatile material. This solution was mixed with the adhesive to give approximately 27 parts nonvolatiles to 100 parts adhesive. Good green strength was obtained with this material.

4. Vitta Corporation's glass transfer tape is made from a process whereby powdered glass can be laid down in controlled thickness upon a plastic carrier film. (Narmco's original interest in this process was to have Narmco adhesive prepared on such a transfer tape as a possible method for applying the adhesive to the individual alumina tiles.) Experimental samples of Narmcad adhesive on a transfer tape were prepared and evaluated, as discussed in a later section. A decision was also made to evaluate the effect of the argon atmosphere on the transfer tape during firing.

Sample alumina tile layups of the above green strength binders were made and fired in an argon atmosphere using the normal firing cycle and peak temperature of 2200°F. Results of these firings showed that the Methocel, Vee-gum, and Krylon acrylic binders all volatized from the Narmcad adhesive without any visible trace of carbonaceous deposit; however, the bubble formation still remained. The Vitta tape binder system left a great deal of residue. Later information from Vitta Corporation revealed that the tape had to be fired under oxidizing conditions up to 750°F in order to fully burn out their organic binder system.

PRE-OXIDATION

Investigations were made into the use of an oxidation burnout period prior to introducing the argon atmosphere. Both nitrocellulose and glass transfer tape were studied under such conditions. These were fired up to 750°-800°F under normal oxidizing atmosphere, held for 30 minutes and then cooled. At the end of this initial cycle, no weight loss was recorded for the graphite cloth, indicating that the oxidation period was not detrimental to use of the cloth as a parting agent. The samples were then refired in an argon atmosphere up to 2200°F. The results showed that the carbon had been volatilized from both green-strength binders without any discoloration or evidence of carbon residue. A fine bubble structure was noted for the sample using the plastic carrier tape. These preliminary results indicate that use of a preliminary oxidation period was satisfactory for final firing of bonded mosaic alumina radomes.

PREGLAZED ALUMINA TILES

Another alternative considered for eliminating the carbon residue was preglazing the alumina tiles prior to actual layup into the radome shape. This method involved coating the tiles with the Narmcad adhesive with a nitrocellulose vehicle for spraying, followed by a glazing operation. Glazing could be accomplished by firing individual, coated tiles under normal oxidizing conditions either to the final cure temperature of 2200°F, or to a somewhat lower temperature, but probably above 1800°F. The preglazing step would be time consuming, but would allow the use of an inert gas atmosphere and would also provide coated tiles with considerable green strength for assembly and handling.

Preliminary experiments consisted of preglazing 1-in. x 2-in. alumina segments at 2150°F. After preglazing, the segments were assembled together to form lap shear test specimens, and refired to effect the final bond at 2200°F under normal oxidizing conditions. Test results showed preglazed smaples to have acceptable shear strength, being similar to normally prepared lap shear samples. In addition, the interfacial layer was found relatively free from detrimental bubble structure. However, subsequent investigations showed that the pre-oxidation concept would be satisfactory, and preglazing techniques were not further explored.

GLASS TRANSFER TAPE

A tape transfer method was considered as a possible technique for coating alumina tiles with a uniform layer of Narmcad adhesive, since it offered the possibility of closer production control than spraying techniques using a nitrocellulose vehicle. The technique developed and produced by the Vitta Corporation consists of glass transfer tapes, designed for coating of a desired surface with a glass layer. Applications to date by this company have included substrates for thin, evaporated films, protective coatings, microencapsulations, glass-to-glass or glass-to-metal seals, etc. The glass

transfer tapes consist, basically, of a glass frit layer attached to a plastic carrier film, which can be supplied in roll form. The carrier is a thin, flexible material of uniform thickness and serves to protect the glass layer until transfer is completed. The glass frit layer is reportedly capable of being prepared from any desired glass frit material. The thickness of the frit layer can generally be varied between 0.0008 in. and 0.005 in. with other thicknesses available. Standard widths of 8 in. are available. The powdered frit layer is generally coated with an adhesive (organic) layer. For transfer of the glass layer, the adhesive layer is activated by pressure. The adhesive layer, in turn, is protected by a release paper which must be removed prior to application.

The manufacturer listed several advantages as compared to other commonly employed liquid suspension-type techniques:

1. "The thickness and density of the glass layer is determined prior to application and can always be closely controlled."

2. "The thickness of the glass layer can be reduced to extremely low values, if required."

3. "Waste of expensive glass material is eliminated, and the layer can be placed on the desired surface with the most stringent accuracy."

4. "Application of the glass layer for any shape, surface type ('O.D.', strip, etc.), or pattern is very simple; the glass layer is simply pressed over the desired surface. Automation of the technique is simple and easy to design and perform."*

The Narmcad adhesive formed on transfer tape is illustrated in Figure 124. This material was evaluated as received and fired under normal oxidizing conditions, in addition to the previously described investigation conducted with argon gas, etc. The Narmcad tape, as received, measured 6.2 and 6.8 mils in thickness.

After firing alumina tiles coated with the tape to 2200°F, the final adhesive thickness was 3 mils. Anticipated bondlines on a fabricated radome would thus total approximately 6 mils from the shrinkage alone. This would not allow sufficient leeway for closure of joints from differential expansion.

* Narmcad powder was sent to Vitta Corporation to determine if the adhesive could be formed onto a transfer tape, and to perform a preliminary evaluation of applying it to alumina tiles. Their findings indicated that it could be formed onto tape and applied to alumina tiles.

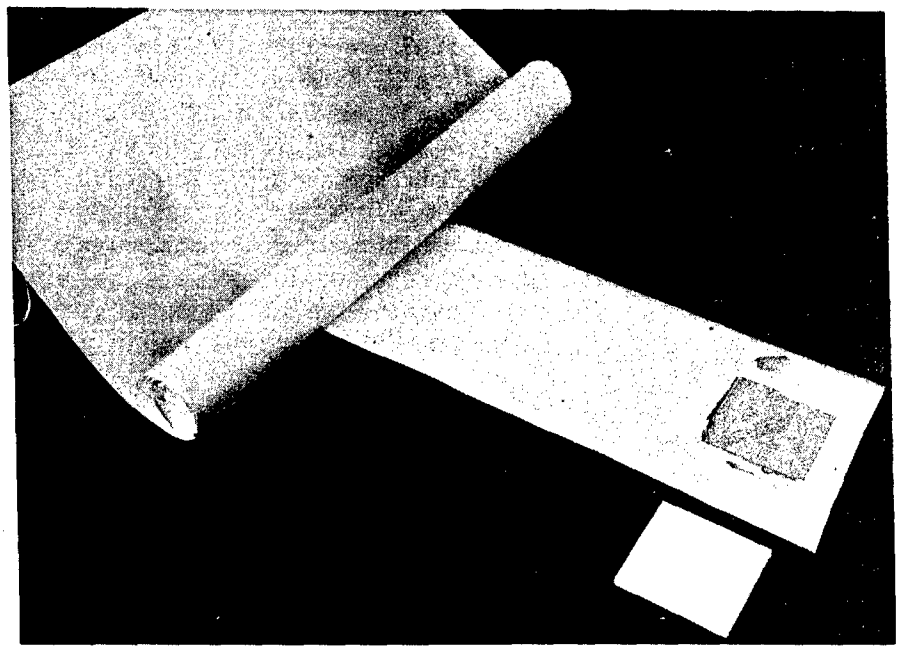


Figure 124. Narmcad "Transfer Tape"

A preferred transfer tape thickness would be on the order of 7-8 mils, allowing some excess to be squeezed out of the joints or into void areas during firing of a radome. Lap shear evaluation of the strength obtained from specimens fired with the Narmcad transfer tape indicated that satisfactory strengths could be obtained by this technique.

The use of transfer tape method for applying the Narmcad to the alumina tiles was eliminated as a candidate procedure for radome fabrication; since it contained a considerable amount of organic material which, as previously discussed, resulted in a fine bubble structure in the adhesive interface between tiles. This condition was more pronounced using the transfer tape than with other green-strength binders. In addition, while the glass transfer tape technique could be controlled precisely to one specific thickness, it was noted that the tape would not stick to itself. Thus, if thinner or thicker coatings were necessary on certain tiles during fabrication, a separate supply of transfer tape would be required for each thickness. It was therefore concluded that the use of a nitrocellulose solution as green-strength binder for spray coating or dip coating of an adhesive slurry, was the preferred approach.

FLAT MOSAIC ALUMINA PANELS

Additional flat mosaic alumina panels were fabricated in order to determine the feasibility of firing in a reducing atmosphere for protection of the graphite cloth using the truncated-size, gas-fired kiln. Panel sizes were approximately 8 in. x 8 in. and consisted of two layers of 1/8-in. x 2-in. x 2-in. alumina tiles. The individual tiles were spray-coated on all faying surfaces with Narmcad 110 adhesive powder using nitrocellulous solution as a vehicle and as a green strength binder.

In order to obtain "still" atmosphere conditions, all firings of panels under reducing conditions were performed by placing the firing tool containing the panels in a refractory muffle and sealing it off with fiber-frax matting.

A successful panel was produced by firing under reducing conditions. Figure 125 shows the finished mosaic alumina panel, while Table 31 lists the conditions existing during the firing. As previously discussed, a pre-oxidation burnout period was employed up to 800°F in order to volatilize any organic matter from the green-strength binder employed in the Narmcad adhesive, thus preventing discoloration and contamination of the bondlines. As can be seen from the data in the Table reducing conditions were maintained only through the initial portion of the cooling period (down to 1800°F), due to difficulty in maintaining a reducing atmosphere while lowering temperature. Furthermore, reducing conditions were not required below 1800°F, since at this temperature, the Narmcad had solidified to the point that no further seizure would occur between the adhesive and the mold material. As was expected, the graphite cloth was not intact after the firing. A visual examination of the fired panel indicated that the graphite cloth was present during the critical period in which the Narmcad was fluid and being squeezed out of joints. This was evident from the fact that the imprint of the graphite cloth could be seen on those bondlines from which excessive adhesive had been squeezed.

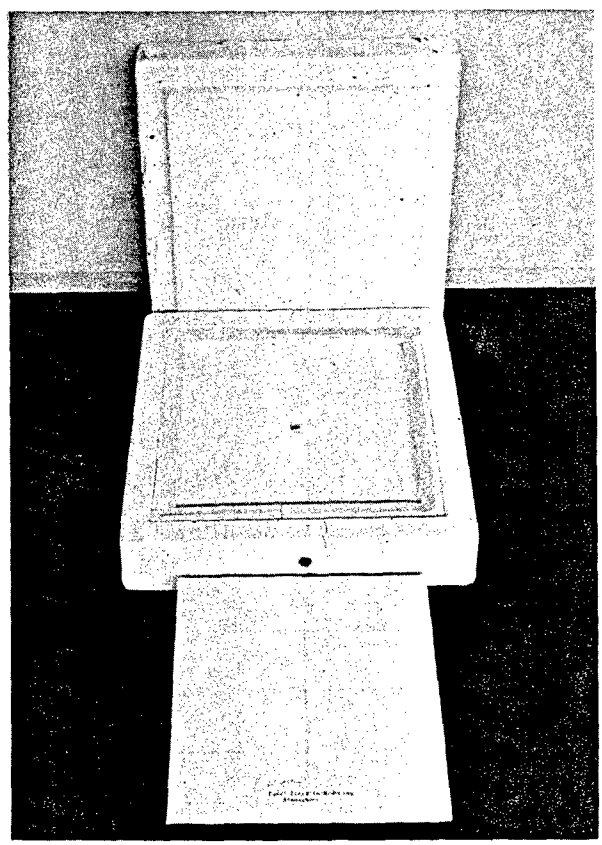


Figure 125. Mosaic Panel Fired under Reducing Conditions

TABLE 31

REDUCING FIRING CONDITIONS FOR FLAT MOSAIC ALUMINA PANELS

Time, hr	Temp, °F		Gas Flow Rate, cfh	% Oxygen	% Carbon Dioxide	Remarks
	Furnace Chamber	Part				
Start			--	High	--	Pilots only
2	815	340	--	High	--	Pilots only
8	820	780		14.0	4 0	Preoxidation period
10	1120	790	125	0.0	11.5	Main burners on
12	1360	840	300	0.0	10.0	
14	1680	940	800	0.0	9.5	
16	2080	1200	1500	1 0	8.0	
18	2210	1530	↓	1.5	5.5	
20	2200	1770		0.5	5.5	
22	2200	2000		<0.5	5.0	
24	2200	2060		0.5	5.5	
26	2100	>2100	1125	<0 5	4.5	
27	1895	2055	150	0	4.5	
30	1900	1985	--	0.5	11.0	Main burners off; pilots only
34	1890	1900	--	0	12.0	Attempting to cool under reducing atm.
36	1890	1875	--	0 5	10.0	
38	1880	1855	--	1.0	11.0	
40	1810	1830	--	1.0	11.0	
42	1760	1780	--	1.0	10.5	
43	1750	1770	--	1.0	11.0	
44	1740	--	--	High	--	Pilots off - standard; air cooling
55	1000	--				

In order to verify and establish that the graphite cloth was present during the heatup and initial cooling period, another flat panel was assembled and fired. The setup was similar to the previously described panel, except argon gas was introduced as a protective atmosphere after the panel was initially cooled to 1800°F under reducing conditions. The standard pre-oxidation burnout period at 800°F was employed, then the firing was continued to peak temperature and cooled to 1800°F under reducing atmosphere. This was followed by introducing argon into the mold (as previously shown in Figure 118) to protect the graphite cloth from oxidation during the cooldown period and provide an indication of the presence of graphite during the critical fusion period. A successful panel was produced and showed no evidence of seizure between it and the fused-silica mold. The results, however, were inconclusive, since again no graphite cloth was left after firing. The apparent reason for burnout of the graphite cloth appeared to be the fact that reproducibility of reducing conditions was not obtained. At one point in this firing, the oxygen content of the combustion products fluctuated for some unknown reason from 1% to 3% for a 1/2-hour period. This was thought to be sufficient to allow oxidation of the graphite cloth.

Although satisfactory panels were produced under reducing conditions, it was evident that controlling the required atmosphere for protection of the graphite cloth would be difficult in the full-size radome, especially in view of the physical size of the kiln. In view of these factors, it was decided that a protective inert gas atmosphere would be easier to employ and offer more positive protection of the graphite cloth parting agent.

As previously discussed, argon gas was successfully employed for protection of the graphite cloth. However, its use for truncated and full-scale radomes was considered to be quite costly and therefore the use of nitrogen gas was investigated in test panel firings. Test panels were fabricated as previously described with nitrogen introduced into the firing mold similar to the method used for argon shown in Figure 118. Prior to introduction of the nitrogen gas, a pre-oxidation burnout period at 800°F was employed to volatilize and/or oxidize any carbonaceous material from the nitrocellulose binder to prevent contamination of the final fused-adhesive bondline. There was no adverse effect from this pre-oxidation period on the graphite cloth.

The results of firing test panels showed that nitrogen was extremely effective in providing the necessary oxidation protection for the graphite cloth parting agent. An important aspect of the investigation was the fact that enough protection of the graphite cloth was obtained even when the nitrogen was turned off at the start of the cooling cycle when the panel temperature was 2150°F. As expected, after cooling from peak temperature under normal kiln atmosphere conditions, very little of the graphite cloth was left intact. Figure 126 shows the test panel and amount of graphite cloth remaining after cooling under oxidizing conditions. A visual examination of the fired panel indicated that the bulk of the graphite cloth was present during the critical period in which the Narmcad was fluid. This was evident from the fact the imprint of the cloth could be seen on those bondlines from which excessive adhesive had been squeezed. The panel after firing was free from cracks with no evidence of seizure between it and the fused-silica mold.

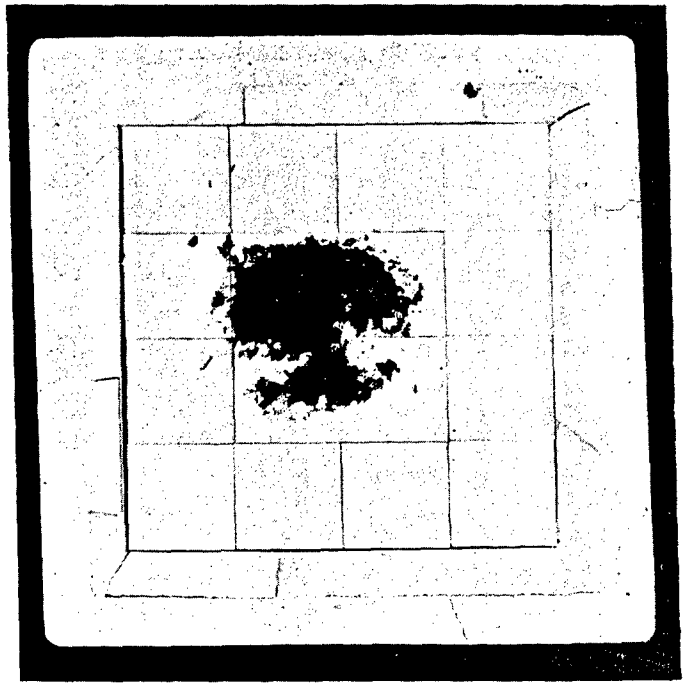


Figure 126. Mosaic Panel Fired with Nitrogen Gas and Cooled under Oxidizing Conditions

Additional proof of the protection provided by the use of nitrogen was obtained in a panel that was fired using nitrogen during the complete cycle down to room temperature. The peak temperature of the part ranged from 2150°-2200°F, with heating and cooling rates similar to panels previously described. A flow rate of 60 cfh was maintained for the nitrogen atmosphere from the end of the pre-oxidation period through the complete heating and cooling cycles. The amount of protection provided by the nitrogen can be seen from Figures 127 and 128 which illustrate the condition of the graphite cloth after firing. It was estimated that more than 95% of the original cloth was still intact, thus providing complete separation between the part and firing mold (tool). Therefore, nitrogen gas was selected for the protective atmosphere in the fabrication of truncated mosaic radome sections and the full-scale radome.

ALUMINA SPACERS

In order to assure uniformity of the bondline thickness in the final radome and truncated sections, it was planned to incorporate alumina spacers within each individual joint. The alumina spacers were 0.006 in. thick, ±0.001 in., and had a nominal size of 0.090 in. x 0.250 in. They were used in order to prevent any bondlines from closing to less than 6 mils due to possible localized pressure effects during firing. Thus, the spacers would stop closure at a specific point and cause other bondlines to take up the pressure.

A technique for attaching the spacers to the edge of the alumina tiles was developed during the fabrication of flat panels. The technique allowed the spacers to be attached directly to the tiles during application of the Narmcad adhesive. It consisted initially of spraying an approximate 1-mil thickness of Narmcad slurry onto the edge of the tile. While still wet, the spacers were placed on the sprayed coating. Sufficient strength was obtained from the nitrocellulose solution in the slurry to hold the spacers in place. After drying, the edge was again sprayed with adhesive covering the spacers to the desired green state thickness. Thus, when two tiles were butted together, the green state bondline was approximately 13 mils thick and contained the 6-mil spacers. Figure 129 shows an alumina tile with the spacers positioned on the initial layer of 110 adhesive.

A standard test panel was fabricated and fired using the 6-mil spacers between bondlines. The results indicated that the bondlines in the mosaic radome would close to a uniform thickness. Optical examination of the joints within the test panel showed all had closed tightly against the alumina spacers resulting in a uniform bondline thickness of approximately 6 mils. All spacers had remained stationary in their initial position, indicating little movement within the adhesive during the fusion stage at maximum fluidity.

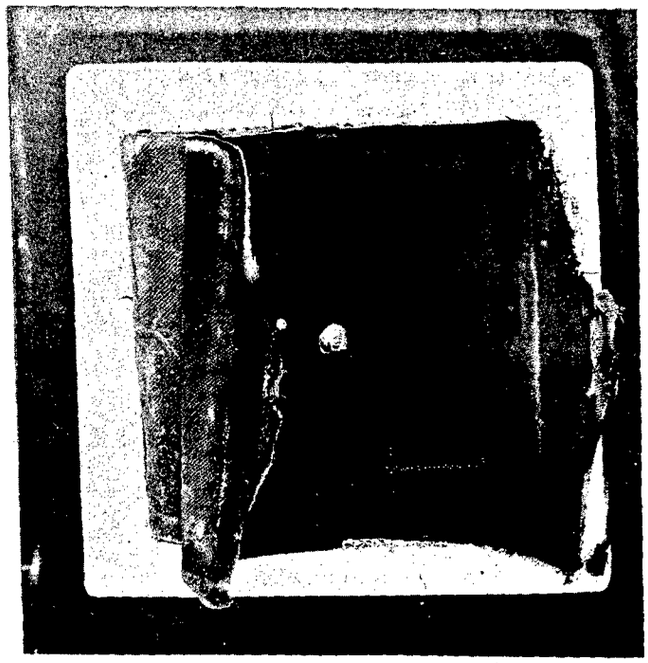


Figure 127. Graphite Cloth after Firing in Nitrogen Atmosphere

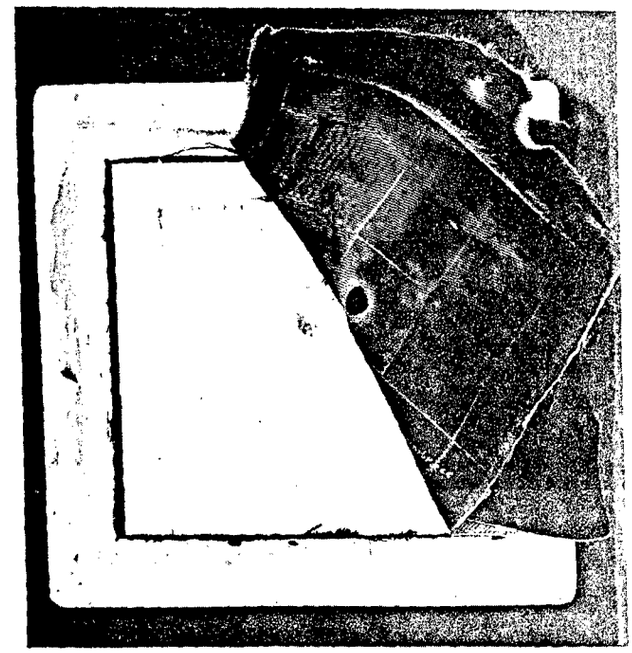


Figure 128. Alumina Panel after Firing in Nitrogen Atmosphere

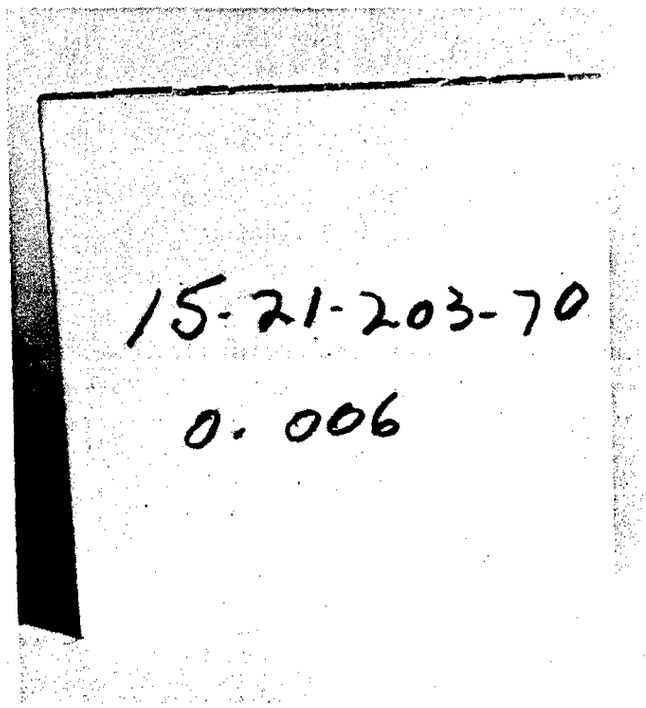


Figure 129. Alumina Spacers Attached to Alumina Tile

SECTION X

TRUNCATED MOSAIC BASE SECTIONS

Since the development of a large composite ceramic radome by mosaic techniques represented a radical departure from the state-of-the-art, it was decided to initially fabricate truncated sections of the full-scale radome in order to verify the techniques developed in the prefabrication task. The truncated sections were to be fabricated from the same size alumina tiles as in the final radome; thus, the lower sections were of the same diameter as the base of the radome, but were truncated at a height of approximately 20 in. The initial fabricated truncated sections contained standard section tiles for the internal base ring rather than the special -193 and -195 base attachment tiles with a shoulder for mating with the attachment fixture. Their fabrication served the following purposes:

1. Verifying the fabrication and differential expansion tooling techniques and initiating the fabrication learning curve

2. Providing demonstration articles and preliminary test assemblies for determining the structural properties of the mosaic assembly and verifying the structural and thermal analyses and design criteria

The final truncated sections fabricated during the program contained the special attachment tiles and served the multiple purposes of:

1. Developing the learning curve and techniques for layup, assembly, and firing of mosaic radome structures

2. Providing experimental items for developing techniques of assembling the base attachment fixtures with the radome structure

3. Providing test items for determining the design adequacy and structural characteristics of the ceramic radome-base attachment assembly

During the course of the program, four truncated base sections were fabricated as illustrated in Figure 130. As will be later described, one base section was repaired and refired. The results of fabricating the first base section were considered to be a qualified success and indicated the general feasibility of the fabrication approach. Subsequent truncated section fabrication showed continued improvement in both techniques and parts produced. Experience during the fabrication of the base sections showed that prolonged firing periods were detrimental for holding dimensional tolerances of final radomes due to transformation of the fused-silica tooling material to a crystalline phase (cristobalite) having a higher thermal expansion. The implications of this problem, the corrective steps which it necessitated, as well as the results of the base section fabrication efforts are discussed in the subsequent paragraphs.

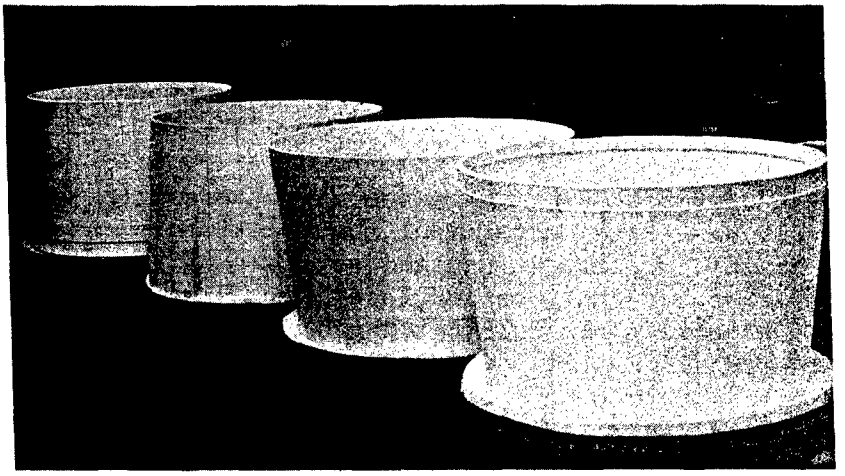


Figure 130. Truncated Mosaic Radome Base Sections

TRUNCATED SECTION NO. 1

The activities performed on the first truncated section are described in detail, since subsequent base sections were similarly fabricated except where noted.

Prefitting

The initial base section contained 264 tiles and was truncated with five rings of tiles (or at a height of approximately 20 in.) with standard section tiles for the internal base ring rather than the special attachment tiles. The top row of tiles used in this base section were cut flush in order that the truncated end would present a uniform rather than a castle-top profile, thereby facilitating fabrication techniques.

The identity (by dash number) of the specific tiles involved in the first truncated section is indicated below in relative position in the inner and outer layers:

	Outer Layer	Inner Layer
Top Row	-15 & -61 -59	-115 & -159 -157
(Declining Order)	-13 & -59 -57	-113 & -157 -155
	-11 & -57 -55	-111 & -155 -153
	- 9 & -55 -53	-109 & -153 -151
Bottom Row	- 7 & -53 -51	-107 & -151 -149

The tiles cut and their respective final reduced lengths were -61 (1.977 in.), -115 (2.997 in.), and -159 (0.994 in.).

Initial fabrication procedures consisted of prefitting the tiles of both layers to the truncated male layup tool, as shown in Figure 131, prior to actual coating with the Narmcad adhesive. The prefitting operation served as a final check of the tile dimensions as well as the functioning of the layup tool. To simulate the green-state thickness of the Narmcad adhesive, alumina spacers 0.013 ±0.001 in. thick were placed between each joint and in the interfacial layer. No significant problems were apparent with the fit or layup of the inner layer of tiles against the tool.

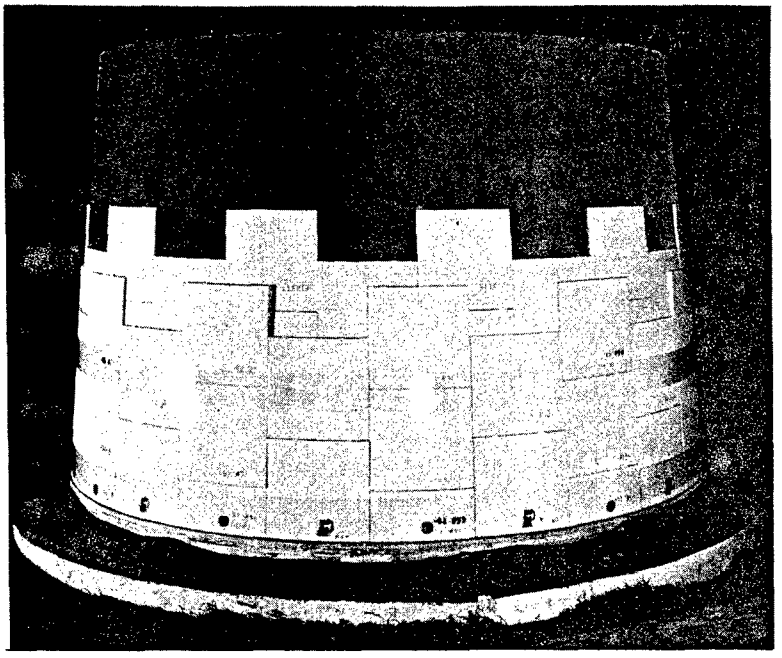


Figure 131. Initial Prefitting of Tiles onto Truncated Layup Tool

Adhesive Application

After the prefitting operation, the tiles were removed and thoroughly cleaned, using a chlorinated mild abrasive cleanser followed by a water rinse and a final cleaning in acetone solvent. Subsequent handling of the cleaned tiles was performed using white cotton gloves. To facilitate handling and storing of the individual tiles during the coating operation, a series of wooden racks were constructed, with one rack for each row of tiles per layer. Thus, after coating, the tiles could be stored in their proper layup order.

Coating of the tiles with Narmcad adhesive was accomplished using both dipping and spraying techniques. As previously established, a nitrocellulose solution was used to form a slurry with the dry Narmcad powder based on a solids content of approximately 40% by weight. Figure 132 demonstrates the dipping technique employed to coat the edges of the individual tiles. With

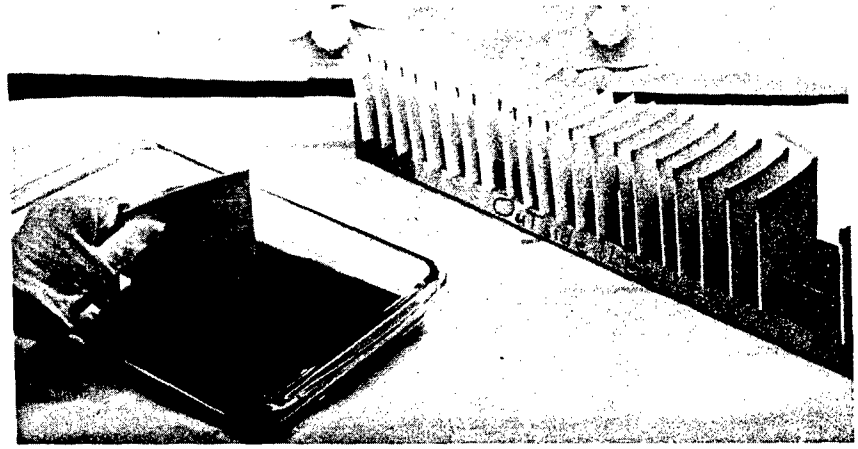


Figure 132. Edge Coating Alumina Tiles with Narmcad Adhesive

experience, the desired thickness could be built up. The thickness of all edges for the inner layer of tiles was controlled between 6-1/2 and 7-1/2 mils, thereby resulting in final assembled inner layer butt joints of approximately 13-14 mils prior to firing. Constant monitoring of the thickness applied during dipping was checked by hand micrometers, as shown in Figure 133. The edges of the outer layer of tiles were also coated by dipping, except an extra thickness of adhesive was built up on all vertical butt joints to ensure a tight fit of the outer layer in the final layup. Thus, the vertical edges of each tile were coated with 8-9 mils, giving approximately 17 mils of unfired adhesive in the vertical butt joints. The horizontal edges of the outer layer tiles were coated to give final joints of 13 mils similar to the inner layer tile joints.

The 6-mil alumina spacer shims were also incorporated and attached to the tiles during the edge coating operation. These were employed within each individual butt joint to prevent any bondline from closing during firing to less than the calculated 6 mils (which could result from possible localized pressure effects). This ensured a minimum uniform fired joint thickness. Shims were placed on each edge surface of the tiles so as to give two shims per joint when the tiles were laid up. A simple and effective technique of placing the alumina spacers consisted of scraping away a small section of dried adhesive then recoating with a thin layer of adhesive slurry to which the spacers were stuck. Upon drying, sufficient strength was obtained from the nitrocellulose solution in the slurry to hold the spacer in place. After drying, a final holding coating was painted over the spacer to the desired green state thickness.

Figure 134 depicts the spraying technique used to apply the Narmcad adhesive slurry to the interfacial surfaces of the alumina tiles. The tiles were positioned on wooden racks designed so that each tile would lie flat during spraying. In order to minimize the number of spraying operations and to facilitate layup, the interfacial adhesive coating was applied only to outer layer tiles. In other words, the total desired interfacial thickness of 13-1/2 mils was applied entirely to the inside faying surface of the outer tiles. This procedure had previously proved satisfactory on flat panel tests.

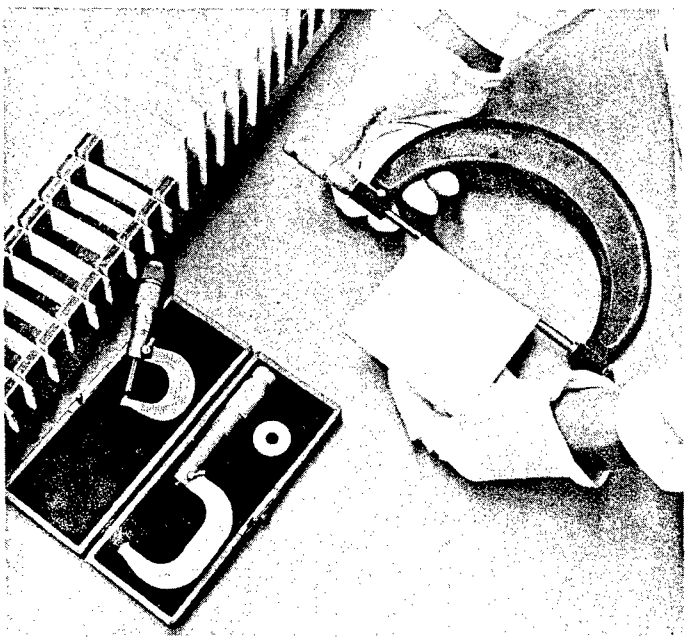


Figure 133. Measuring Coating Thickness

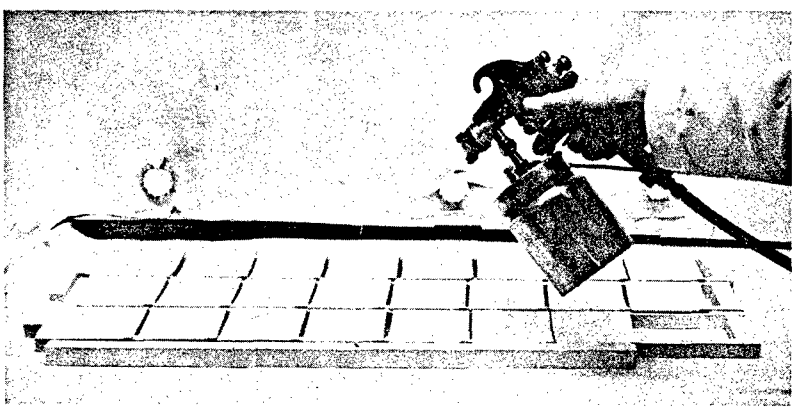


Figure 134. Spray Coating Alumina Tiles

Layup and Handling

Figure 135 shows the 264 tiles for the first truncated section after being coated with the powdered adhesive. Tiles were assembled onto the layup tool in the previously established two-layer pattern with no difficulty. In order to secure the two layers of tiles in the laid-up position and to prevent movement during inversion and tool withdrawal, a small amount of nitrocellulose-based Du-Co cement was used between the inner and outer tile layers. This cement had been found to be compatible with the green Narmcad adhesive, as well as having burnout characteristics similar to those of the nitrocellulose solution used in the Narmcad adhesive. Figure 136 illustrates the tiles laid up in final arrangement prior to assembly with the truncated firing tool.

The laid-up tiles were covered with a sleeve of two layers of the graphite cloth parting agent. At the same time, 24 narrow plastic (Plexiglas) shims were secured onto the graphite cloth as shown in Figure 137. These served two purposes: to guide the firing tool during assembly, and to fill the annular space between the assembled tiles and wall of the firing tool to prevent any shifting of the tiles during handling and inverting of the assemblage. Plastic shims were chosen since they would be completely burned out during the pre-oxidation period. At this stage, the truncated firing tool was lowered over the assembled tiles using an A-frame and electric joist to assure smooth handling. No difficulties were encountered during this operation. After the firing tool was positioned over the tiles, the completed assembly was encased and secured in a special handling box as shown in Figure 138. The handling box was then raised and the entire frame rotated to invert the truncated section and tool assemblage, thus allowing the male tool to be withdrawn as per Figure 139. Again, this operation was accomplished without any binding or difficulty.

Examination of the assembled alumina tiles after removal of the layup tool revealed that none of the tiles had moved or separated, and the complete truncated section was correctly positioned in the firing tool as shown in Figure 140. At this point, the inside of the assembled truncated section was covered with graphite separator cloth and the interior filled with bulk Fiberfrax fiber material. Approximately 75 lb of the bulk fiber material was packed into the interior, corresponding to a packing density of approximately 9-10 lb/cu ft quantity, previously estimated as suitable for providing adequate radial pressure. A Glasrock cover lid and a separate Glasrock pressure ring was then installed as shown in Figure 141, which illustrates the complete arrangement prior to firing. The purpose of the pressure ring was to apply axial pressure in order to assure closure of all horizontal joints within the mosaic section. As previously described, the initial truncated firing tool required a Glasrock reinforcement ring as depicted in the cross-sectional sketch because of the crack which occurred in the tool during the tool firing cycle.

Firing

The entire tooling and part assemblage as shown in Figure 141 was placed in the gas-fired kiln with temperature of the tool and part monitored by a series of chromel-alumel thermocouples. Five thermocouples were located in the wall of the tool within 1/2 in. of the part. They were placed in a spiral

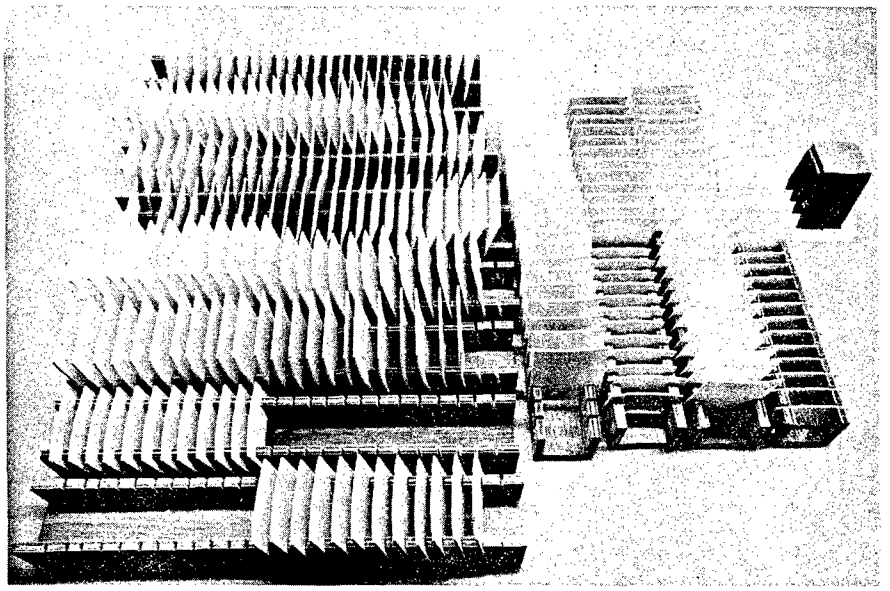


Figure 135. Adhesive-Coated Tiles for First Section

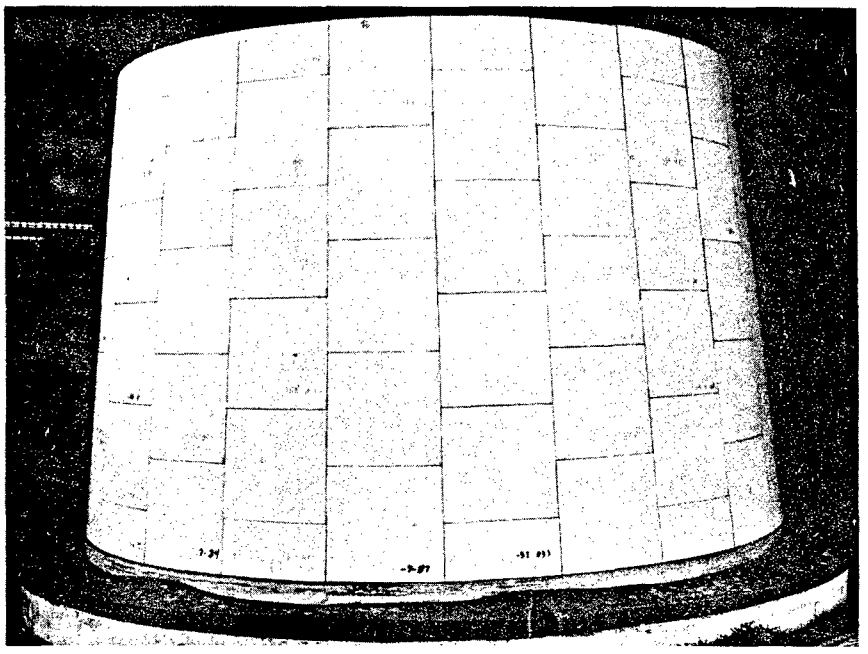


Figure 136. Final Layup of First Truncated Section

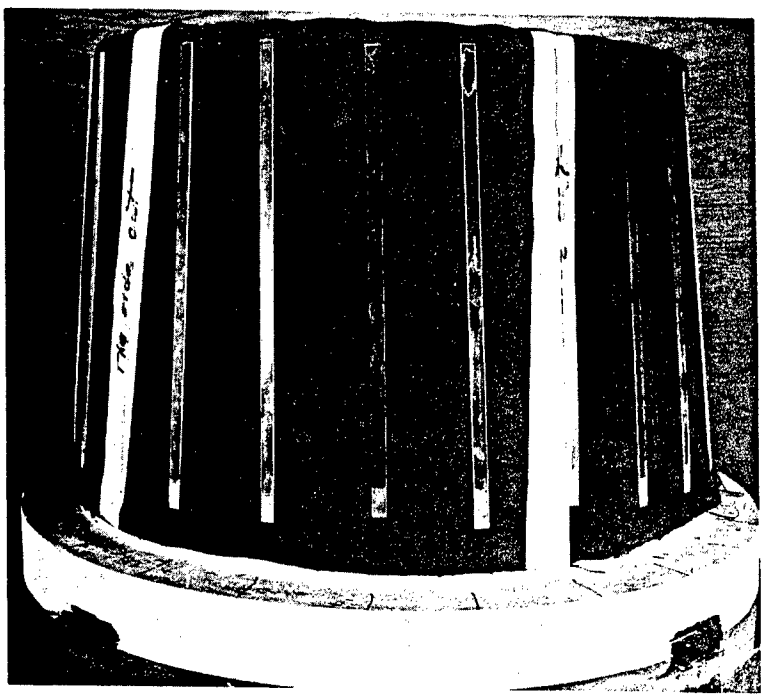


Figure 137. Graphite Cloth Sleeve Covering Layup Truncated Section

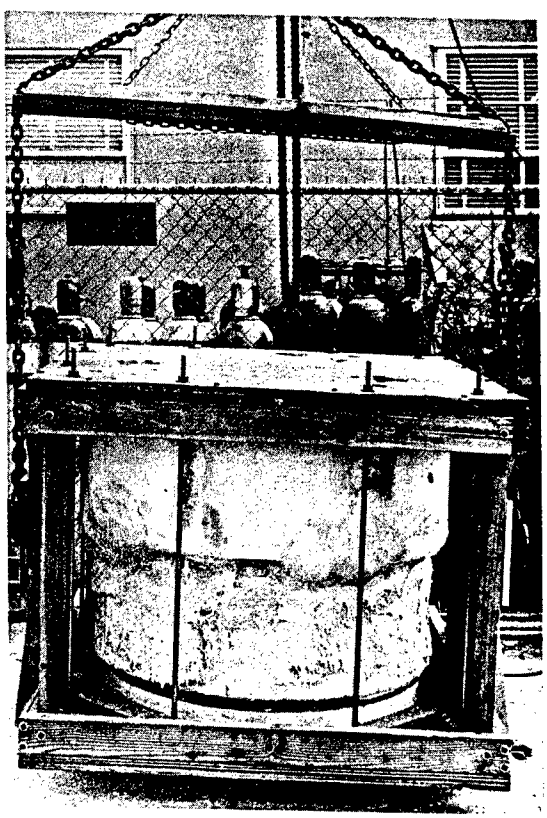


Figure 138. Handling Box



Figure 139. Withdrawal of Male Layup Tool

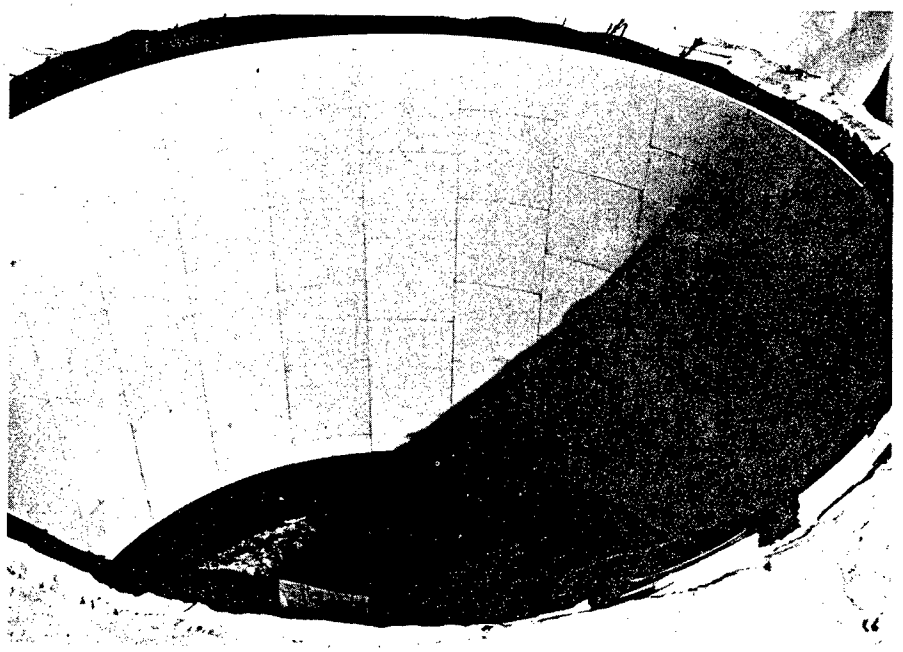


Figure 140. Truncated Section in Firing Tool

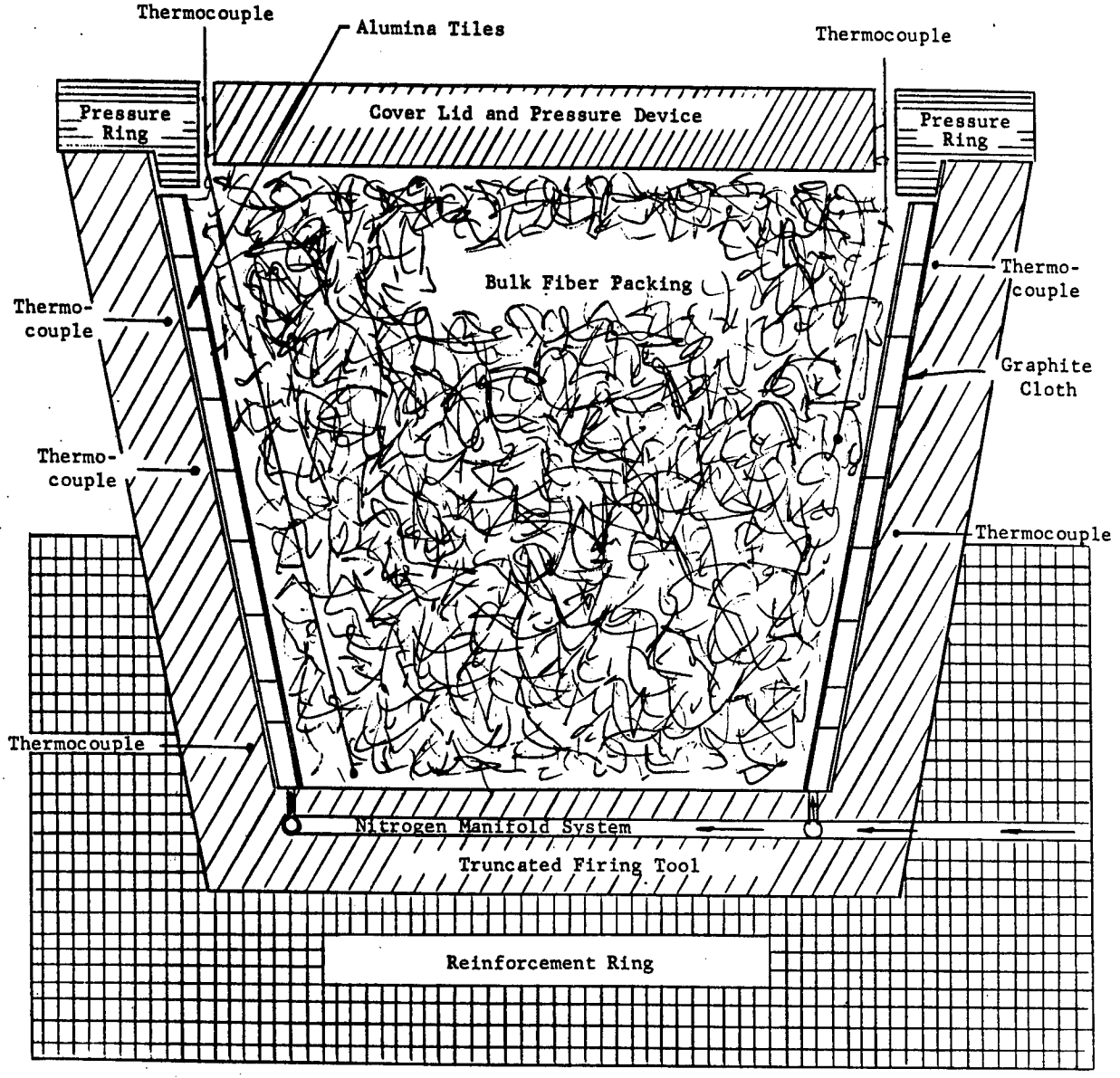


Figure 141. Cross Section of Truncated Section and Tooling Firing Arrangement

arrangement around the periphery and located approximately 3 to 4 in. apart in height. Two thermocouples were placed within the Fiberfrax inside the tool cavity and located next to the wall of the mosaic section on the bottom and center portion. A stainless steel pipe covered and wrapped with Fiberfrax paper and cement was used to introduce nitrogen into the tool manifold. This allowed the gas to flow evenly around the circumference and provided the protective atmosphere required to prevent oxidation of the graphite cloth parting agent.

Figure 142 shows the heating and cooling curves obtained for the part and tool during the firing of the first truncated mosaic base section. Initial heating to approximately 700°F was deliberately slow in order to remove any residual moisture that may have been retained in the tool as well as to thoroughly dry out the kiln. The part temperature was raised to 800°F for 5 hours to allow complete burnout of the nitrocellulose contained in the Narmcad adhesive, thereby preventing any deposition of carbonaceous residue in final fired bondlines.

After the preheat period, nitrogen gas was introduced into the manifold at a rate of 120 cfh under 30-psi pressure for 1 hour in order to thoroughly purge the system before increasing the temperature. The rate of nitrogen flow was maintained as firing proceeded at approximately 25°-50°F/hour until the part temperature reached 2200°±50°F. This temperature was held for approximately 6 hours.

Cooling of the first truncated section was at a rate of approximately 25°-50°F/hour. The nitrogen flow was reduced to 50 cfh at 1500°F in order to minimize any possibility of thermal shocking the mosaic structure. The protective atmosphere was maintained until the kiln and part temperature were about 600°F and 800°F respectively, then cooling was continued under the furnace atmosphere environment to ambient conditions before removal from the kiln. The nitrogen atmosphere was only maintained during cooling in order to determine its effectiveness in protecting the graphite cloth at the higher temperatures.

The only problem encountered during the firing cycle was loss of chromel-alumel thermocouples at various stages of heating and cooling. At about 1900°F, during the heating cycle, the thermocouples located in the tool wall became inoperable and no EMF output was recorded. The two chromel-alumel thermocouples located in the interior of the tool were lost during the cooling cycle at temperatures of 1600°F and 1000°F respectively. These couples are susceptible to deterioration under neutral or reducing atmospheres, and it was thought that this may have caused the failures. Since the thermocouples located in the tool wall were of a smaller gage than those contained in the interior, they would be expected to fail first, which did occur. Thermocouples used in future firings were encased in protection tubes to eliminate this problem.

Results

The results of firing the first truncated section were considered to be a qualified success, since the radome came out in one piece with reasonably well bonded joints and only one vertical crack. Therefore, feasibility of

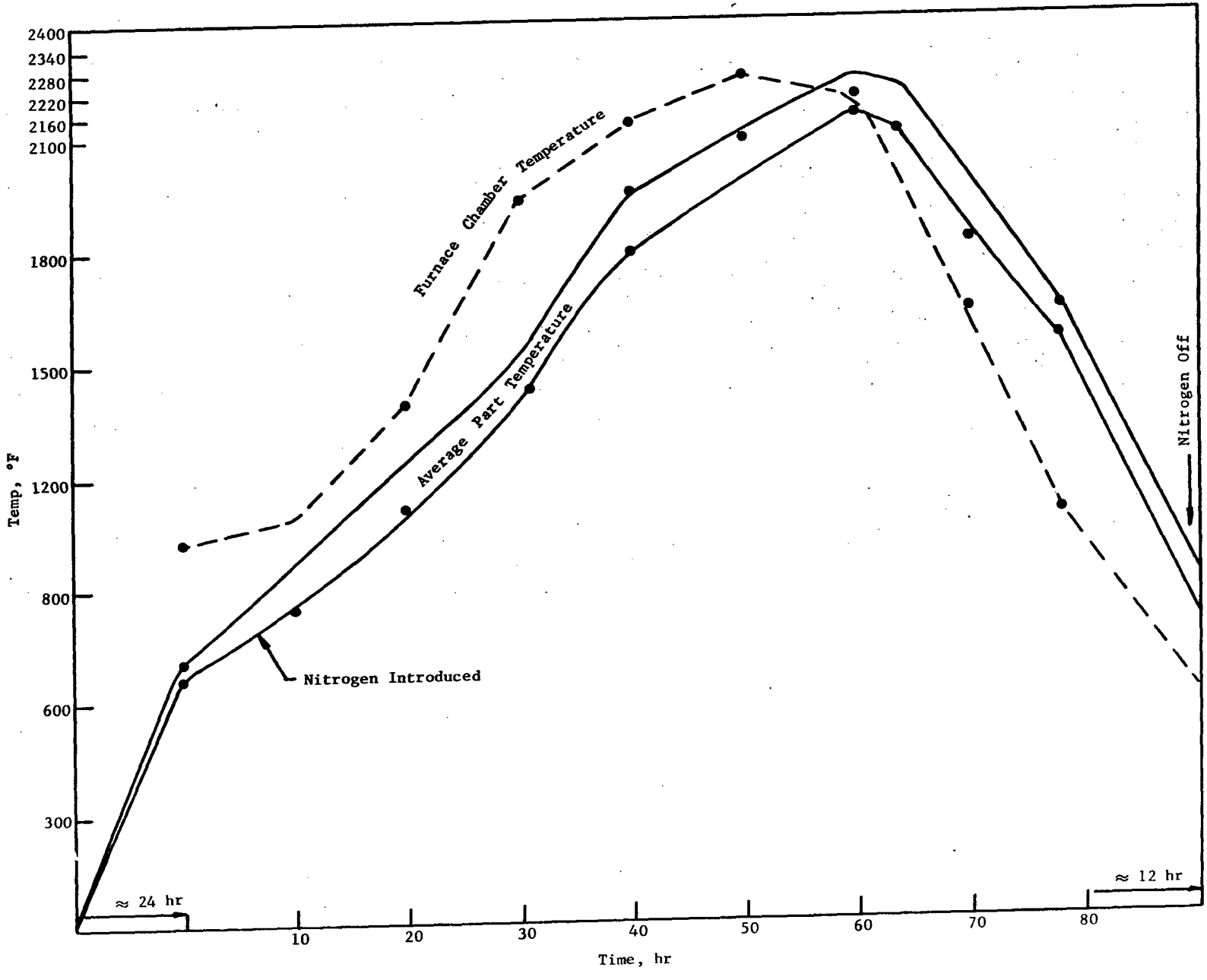


Figure 142. Firing Curves for First Mosaic Truncated Section

fabricating structures by the mosaic technique using a differential expansion tooling concept was demonstrated.

Figure 143 depicts the firing tool and part immediately after removal from the kiln. The Glasrock cover, which rested on the bulk fiber packing so that a compressive force would be applied, slumped and canted approximately 6 in. on one side and about 3 in. on the other side. This movement was not experienced on the prefabrication tests under the same loading condition of about 0.5 psi on the bulk fiber packing. The extra slumping was probably due to the extended time-temperature heat effect experienced in firing the truncated section. The effect of the lid travel under the applied loading was an 8- to 10-in. compression of the bulk fiber. This compression might have been slightly greater had the lid not been eventually restrained by the tapered wall of the truncated section. The result of this compression loading was a change in density of the packed fiber material from 9-10 lb/cu ft to about 15 lb/cu ft. Another effect of the lid travel was to expose the upper portion of the truncated part to the kiln atmosphere, which resulted in a loss of graphite cloth due to oxidation above the lid surface.

The results of firing also showed that the previously noted cracks in the firing tool had propagated through the entire wall sections approximately 180 degrees apart, including one side of the reinforcing ring. The tool cracks opened to approximately 0.8-0.9 in. at the ends opposite the constraining ring; however, the ring did serve to prevent complete separation of the tool. As will be further discussed, the enlargement of the firing tool naturally caused an oversize condition in the final truncated section. However, the individual tiles maintained a fairly close basic alignment, considering the cracking and spreading of the holding tool.

Figure 144 depicts the interior of the tool and part after the lid and bulk fiber packing have been removed. A vertical crack was observed through the wall of the base section. Subsequent analysis revealed this to be a tensile type failure. This was caused by the inability of the part to freely contract upon cooling due to pressure of the lid, which was canted and wedged against the inside tile surfaces. In addition, a hard, nonresilient crust approximately 1/2 in. thick had formed on the top and bottom of the compressed Fiberfrax packing which also prevented free contraction of the part. Thus, it was concluded that the part was sufficiently restrained from contracting upon cooling and this caused the observed vertical crack failure. When initially observed, the vertical crack was about 0.090-0.125 in. wide. Subsequent removal of the lid and Fiberfrax permitted the section to spring back to a gap of about 0.040 in. The location of this failure was about halfway between the two major cracks in the tool, and diametrically opposite the point where the cover lid wedged against the tiles.

Prior to actual removal of the part from the tool, the crack was repaired with an epoxy adhesive (Helor HiWater) previously investigated and found promising as a candidate repair adhesive. The purpose was to give structural integrity to the truncated section and minimize any strain placed on it during removal from the firing tool. Removal of the fired base section was relatively easy since the graphite cloth prevented adhesion or seizure between the Narmcad adhesive and firing tool. The protective atmosphere of nitrogen provided sufficient protection below the cover lid to preserve all the graphite cloth. In fact, close examination of the section above the lid, where oxidation of

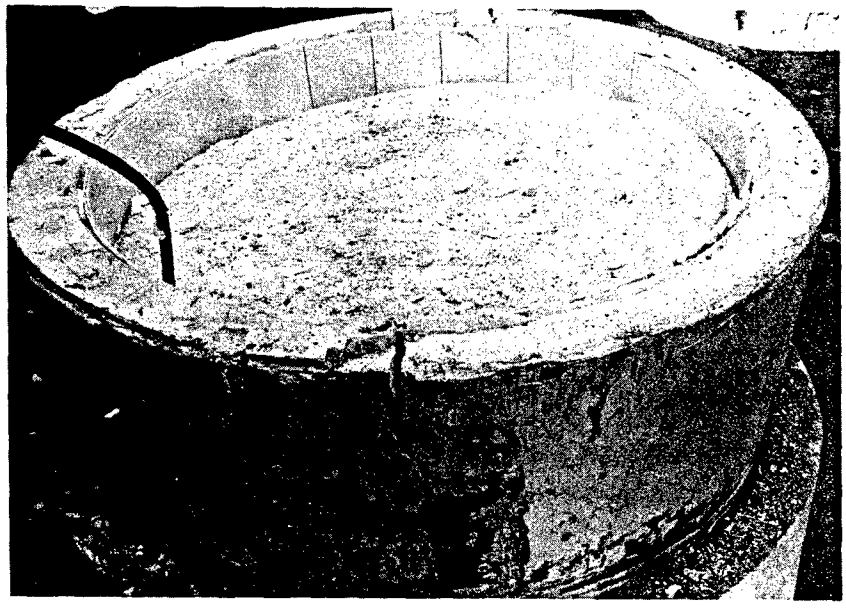


Figure 143. Firing Tool and Part after Firing

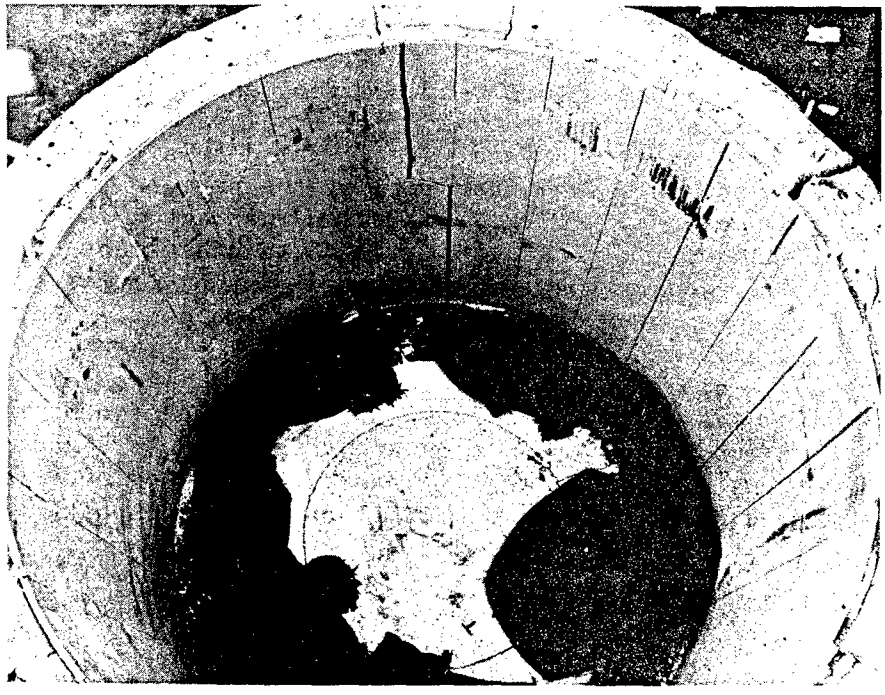


Figure 144. Interior View of Truncated Section No. 1

the graphite occurred, revealed that the graphite cloth was present during the critical period (i.e., when the Narmcad was fluid and being squeezed out of joints), since the imprint of the cloth was seen on those bondlines.

Figure 145 shows the truncated section, firing tool, compressed bulk fiber packing, and a portion of the cover lid after removing the mosaic base section from the tool.



Figure 145. Truncated Section, Firing Tool, and Fiber Packing with Cover Lid

As expected, inspection of the truncated section revealed that vertical butt joints were considerably larger than desired due to the oversize condition the tool caused by the cracking and ranged from a relatively tight fit of 0.008 in. to gaps of about 0.250 in. However, it was apparent that the interfacial bonding between layers except for one outer tile was good. The tile in question was located in the outer layer and in the top row of the final fabricated section or, conversely, on the bottom during actual firing. There was no evidence of bonding for this tile, and visual examination indicated that the Narmcad adhesive had never reached the sintering temperature range. Subsequent study of the position of this tile within the tool showed that this tile had been located directly above the inlet opening of the nitrogen gas manifold. Therefore, in all probability, it was constantly being cooled by the incoming nitrogen. This was the only area so affected and measured approximately 2 in. x 4 in., indicating that the nitrogen gas became sufficiently heated in the remaining portion of the manifold so that normal fusing of the Narmcad adhesive in the rest of the section was not prevented. In order to correct this condition, a coiled inlet pipe was designed which allowed preheating of the nitrogen in the furnace chamber before its entry into the tool manifold.

While an accurate dimensional analysis of the final fired truncated section was not feasible (because of cracking and firing tool enlargement), several measurements were made and general observations noted. The interfacial bonding between tile layers appeared to be quite good, indicating satisfactory lateral pressure. Measurements of the fired truncated part showed a thickness of 0.224 in. to 0.237 in., with an average of approximately 0.227 in.

Although the horizontal joints from bottom to top of the section were relatively tight, the overall height was about 0.050 in. to 0.060 in. longer than theoretical. This resulted in an average horizontal bondline approximately 0.010 in. wider than desired. Examination showed that the horizontal joints at the base of the section (or located near the top of the tool during firing) were somewhat wider than those near the top. This indicated that insufficient pressure was obtained in the vertical direction to obtain full closure of joints during firing. A simple, revised pressure ring was designed and used for subsequent sections which overcame this difficulty.

From the results obtained on the first truncated section, it was apparent that the main cause for off-tolerance bondlines as well as cracking of the part was one of tool function. However, the results verified the general principles of the differential thermal expansion tooling concept which was considered an important milestone event.

TRUNCATED SECTION NO. 2

This section, containing standard section tiles for the internal base ring rather than the special attachment tiles, was fabricated using a new truncated firing tool. Except where noted, all tiles were laid up and prepared for firing by techniques similar to those described for the first section.

The firing tool was free from any cracks and thus did not require an additional reinforcement ring. A slight oversize condition of the tool was compensated for by using additional layers of graphite cloth and Fiberfrax paper as a sleeve or shim around the mosaic section. Calculations showed that acceptable bondlines of approximately 7 mils should be produced from the combined tooling and shimming dimensions. Modifications were also made in the firing tool assembly to correct problems encountered in firing Truncated Section No. 1. These were as follows:

1. The Glasrock tool cover or pressure lid was designed with a flange to provide a positive stop after compressing the Fiberfrax packing approximately 1 in. during the firing. This prevented overcompression of the Fiberfrax and canting of the lid inside the radome section.

2. The top and bottom surfaces of the Fiberfrax packing inside the tool were designed to be, respectively, slightly above and below the top and bottom of the tile section. This permitted free contraction of the radome section upon cooling even though stiff surface "skins" developed on the top and bottom of the Fiberfrax, as occurred when firing Section No. 1.

3. In order to eliminate the jet-cooling effect of the nitrogen gas introduced into the tool during firing, approximately 36 in. of the stainless steel inlet pipe was bent into a coil and located outside the tooling within the kiln to serve as a nitrogen preheater. Also, no manifold ports were positioned adjacent to the inlet pipe to further reduce the possibility of direct cool gas impingement on the alumina tiles.

Figure 146 shows the general firing arrangement for the second truncated section, while Figure 147 depicts the heating and cooling curves obtained during firing.

Section No. 2 was fired at tooling temperatures of 2150°F to 2330°F as measured within the wall of the tool. These temperatures were maintained for 4-5 hours. The interior master thermocouple located with the bulk Fiberfrax recorded 2150°F for 1-2 hours. The part, after firing, was in near-perfect condition. Visual inspection indicated all tiles were well bonded and, with few minor exceptions, the butt joints were uniformly closed with excess adhesive being squeezed out as planned. The preheating obtained by the nitrogen gas worked as planned with all tiles indicating full bonding between the layers. Radome thickness measurements, made where possible with a micrometer caliper, gave an average value of about 0.227 in. versus the 0.222 in. desired. Circumference measurements with a steel tape indicated it to be slightly oversize by about 3-4 mils per vertical butt joint between tiles. Some unevenness (less than 1/16 in.) was evident between tiles ends at the truncated end (lower end during firing) of the section. This was caused by a slight nonuniformity which developed in the base plug of the firing tool.

While the firing tool performed as required, the level of the bulk Fiberfrax after firing was approximately 1-2 in. below the pressure ring. This indicated that a packing density of 11-12 lb/cu ft as compared to 9-10 lb/cu ft was required to completely fill the interior of the part during the firing cycle. Future truncated sections were prepared with Fiberfrax prepacked to this density level.

It was also observed that the graphite cloth remained intact after firing even though the nitrogen protective atmosphere was turned off during cooling at 1800°F, indicating additional oxidation protection was provided by the tightness of the tooling.

In summary, the problems encountered in firing the first truncated section were corrected by the changes outlined resulting in a successful part. Subsequent testing of this section, as described in Section XIII, confirmed the structural fidelity of the unit.

TRUNCATED SECTION NO. 3

This was the first truncated section that contained the special attachment tiles for the internal base ring. The internal "shoulder" on these tiles prevented their layup before removal of the male layup tool. Therefore, the section was laid up initially with plain end tiles; then, after the tool had been inverted and the male layup tool removed, the plain tiles were removed and replaced with base attachment tiles. The tool interior was then packed with bulk Fiberfrax to a density of about 11.5 lb/cu ft. No difficulty was

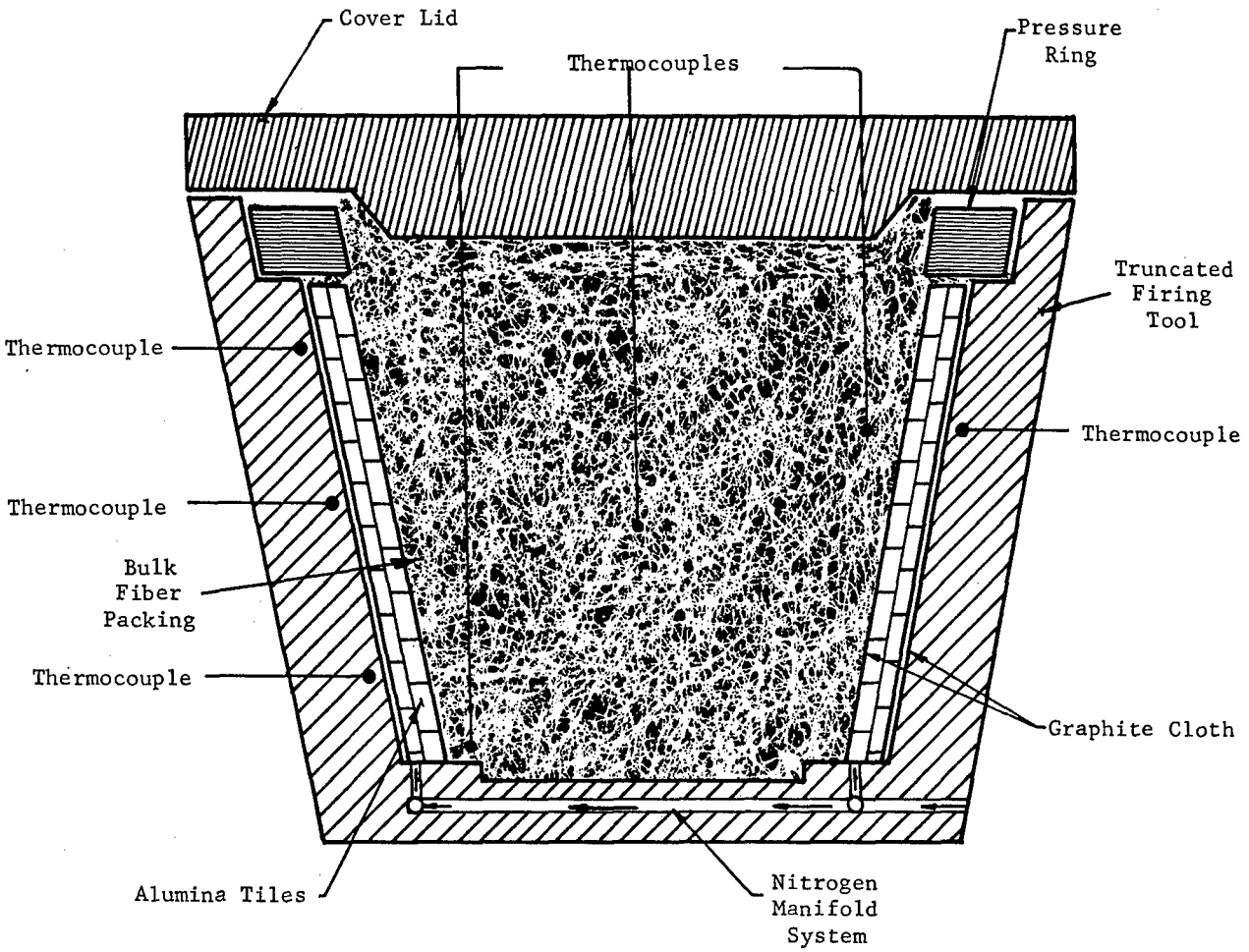


Figure 146. Cross Section of Modified Truncated Section and Firing Tooling Arrangement

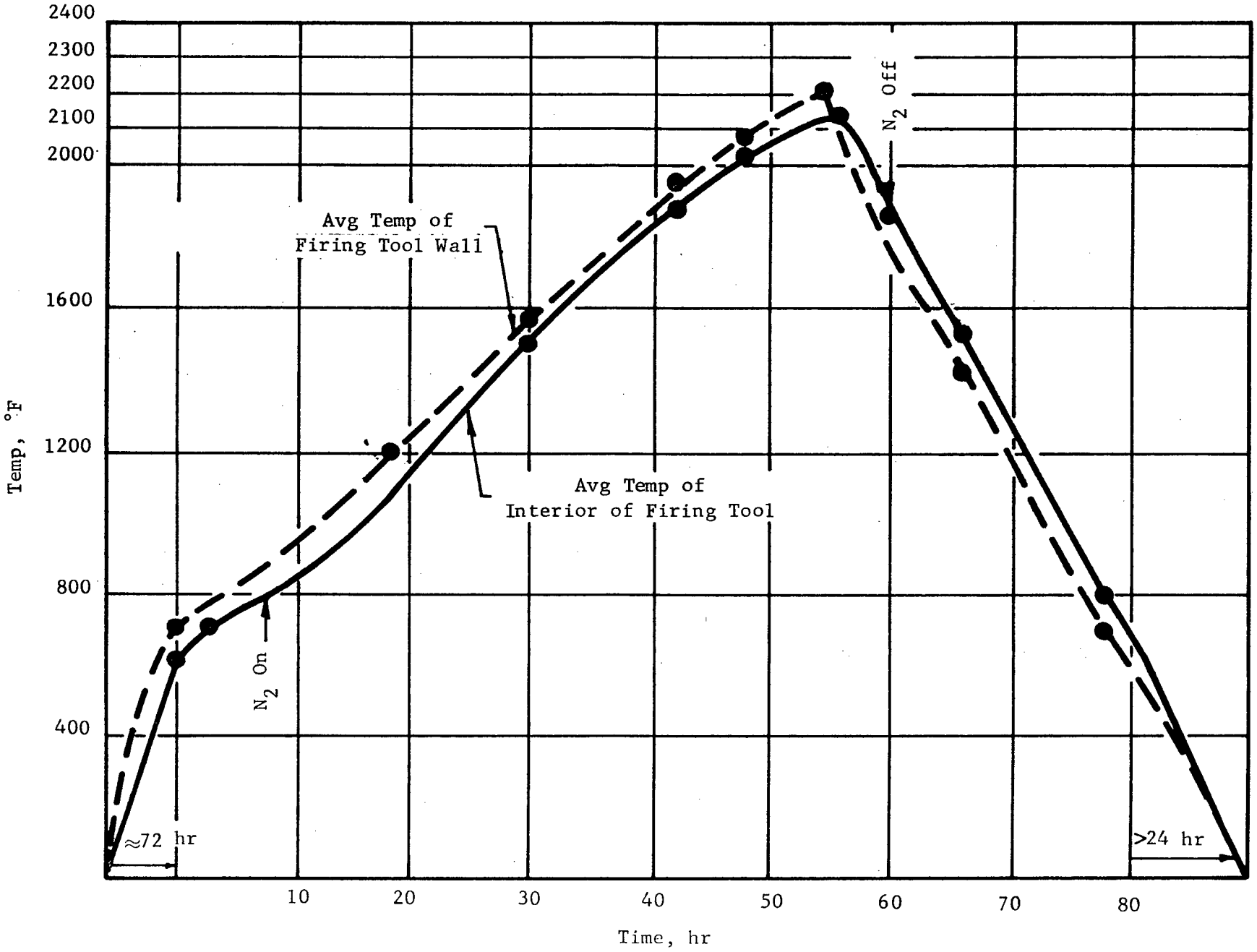


Figure 147. Firing Curves for Truncated Radome Section No. 2

encountered in placing and positioning the attachment tiles. In addition, dummy sections were cut from spare tiles to serve as backup support between the attachment tiles and the firing tool. These dummy tile sections also served to transfer pressure from the Glasrock tool to the outer layer of tiles.

The truncated firing tool and lid arrangement used for fabricating the second radome section was reemployed for firing the third truncated section. Figure 148 depicts the firing tool arrangement for heating in the gas-fired kiln. Again, the same amount of additional graphite cloth and Fiberfrax paper was used to compensate for its oversize condition. During its first use cycle, the Glasrock firing tool had developed a hairline vertical crack, approximately 10 in. in length, on the outer surface at the base. This crack appeared to have resulted from stresses caused by the nitrogen gas inlet hole and the expansion of the stainless steel inlet pipe. The crack caused no loss of dimensional tolerance, and it was determined unlikely that it would extend further in a subsequent firing; therefore, the tool was considered reusable. The nitrogen inlet tube was, however, relocated so that it would pass up through the base plug of the tool rather than through the wall. A Glasrock base plate was also cast on the bottom of the tool to prevent the slight shifting of the base plug that had occurred.

The firing of the third truncated section required a longer period to level out individual thermocouple readings within desired temperature ranges, possibly due to the extra mass of the Glasrock base plate. As a result, the temperature within the wall of the tool was held between 2150°F and 2300°F for a period of 8-12 hours, and the interior temperature within the bulk Fiberfrax ranged between 2150°F and 2250°F for approximately 5 hours.

The third truncated section came out well bonded, but with evidence of oversize internal firing tool dimensions as indicated by some of the vertical butt joints between tiles being incompletely closed. Subsequent measurements indicated that the part was approximately 0.075 in. to 0.085 in. larger in diameter than desired. Since the same tool and dimensional control was employed as for the second truncated section, this immediately suggested the probability that sufficient cristobalite inversion of the fused silica (Glasrock) had occurred in the two use cycles of this tool to increase its coefficient of expansion and hence its dimensions, at maximum firing temperature, above tolerance limits. This will be discussed further under fabrication of Truncated Section No. 5.

In addition to the above-noted oversized condition, some of the base attachment tiles as shown in Figure 149 were not firmly forced out against the outer layer of tiles. In fact, one tile had slipped down a few inches onto the inside of the part as shown in Figure 150 with lateral bonding only obtained (for the particular tile) on the indicated cross-hatched area. From their appearance, it was obvious that not enough lateral pressure was obtained from the Fiberfrax packing at this particular level. Therefore, as discussed in the next section, corrective measures were taken in an attempt to increase the radial pressure at the attachment tile level.



Figure 148. Truncated Firing Tool Arrangement in Kiln

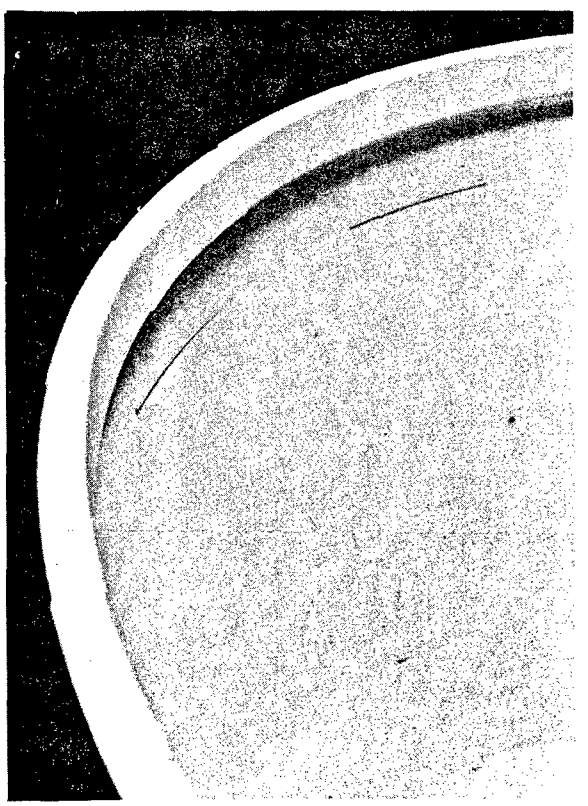


Figure 149. Truncated Section No. 3, Showing Misaligned Attachment Tiles

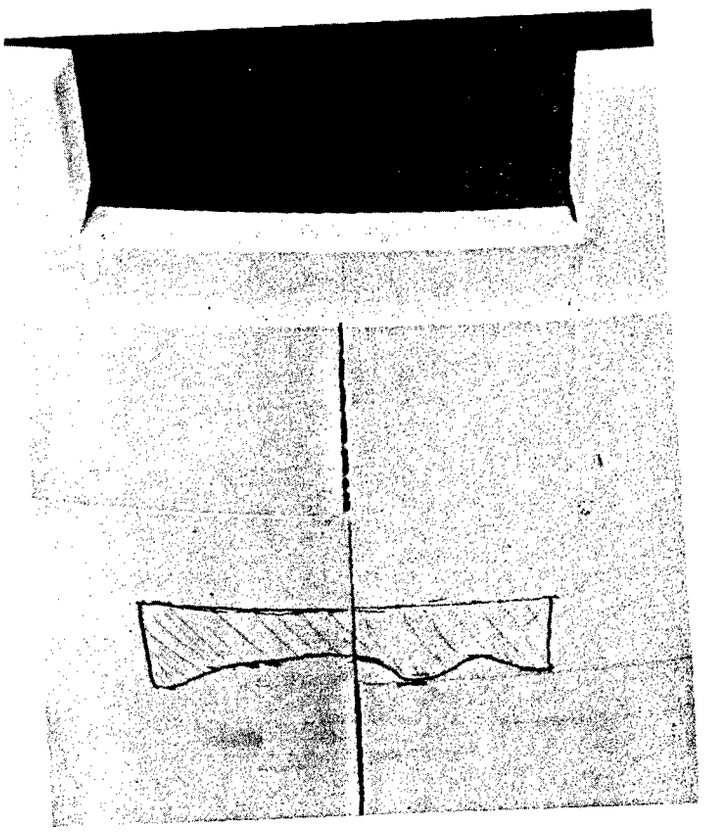


Figure 150. Close-Up of Slipped Attachment Tile in Truncated Section No. 3

TRUNCATED SECTION NO. 4

This truncated section was the second attempt at producing a radome section containing the special base attachment tiles. A new Glasrock firing tool was used. In order to obtain more internal lateral pressure on the base attachment tiles during firing, a 3-in. high ring of Glasrock was placed on the top of the firing tool to support the Glasrock cover and permit a "head" of Fiberfrax packing inside the section. As this was the initial firing of the tool, no extra dimensional compensation was provided for cristobalite conversion as only a minimum amount of change was expected during the planned firing time. Thus, the only dimensional compensation (using graphite cloth and Fiberfrax paper) was for adjusting the slightly oversize firing tool to desired dimensional tolerance. This dimensional compensation was calculated to produce the design butt joint widths of 5-6 mils.

The firing cycle was modified to reduce the time above 2100°F to a minimum in order to decrease the tendency of cristobalite formation in the Glasrock tool. As a result, the wall temperature of the tool was held between 2100°F and 2170°F for a period of only 4-5 hours, while the interior temperature within the bulk Fiberfrax varied from 2100°F to 2150°F for a 2-4 hour period.

The results were considered satisfactory, in that dimensional control was fully achieved. The top and bottom section diameters, as determined from tape measurements of the circumference and optical joint width measurements, were only +0.010 in. to +0.015 in. and -0.001 in. to -0.002 in. respectively, from the desired diameters. The average wall thickness of the part was 0.222 in. and ranged from 0.219 in. to 0.226 in. based on a series of micrometer measurements taken near the plain (small) end of the radome section. However, it was observed that the lateral faying surface closure of the base attachment tiles to the outer tiles was still less than required. This condition indicated the need for greater pressure against these tiles during firing than could be obtained from the packed bulk Fiberfrax. The method devised to obtain increased lateral pressure is described in conjunction with the investigations performed in producing the fifth truncated section.

TRUNCATED SECTION NO. 5 (REPAIR OF TRUNCATED SECTION NO. 3)

The fifth firing of a truncated section was performed with the following objective in mind:

1. Repair of a defective, previously fired radome section
2. Attainment of greater outward pressure between the faying surfaces of the attachment tiles and the outer layer of tiles through use of an internally located stainless steel expansion ring
3. Reuse of a firing tool by compensating for the dimensional changes associated with cristobalite formation in the fused-silica tool material

These three objective areas are discussed in detail in the following paragraphs.

Objective 1 – Repair and Refire of Section No. 3 (Now Designated No. 5)

As previously discussed, the results of firing Truncated Section No. 3 were not satisfactory in that the tile butt joints were not completely closed, it was oversize in circumferential dimensions, and some of the base attachment tiles were not completely forced out and bonded to the outer ring of tiles. One, in fact, had slipped a few inches out of position and was only partially bonded. To prepare this section for rework, the incorrectly positioned tile was removed by the use of hydrofluoric acid, previously found in the radome repair studies to effectively dissolve the siliceous Narmcad adhesive without attacking the alumina tiles. After removing the tile, it was recoated with adhesive slurry and replaced in the proper position. In addition, all open bondlines including interfacial joints between attachment tiles and outer tiles were grouted with Narmcad adhesive.

The section was then covered with graphite cloth parting material and Fiberfrax paper layers in the normal manner before insertion into the Glasrock tool for refiring. In this case, assembly of the part and the tool involved two considerations which departed from previous procedures. These resulted from the necessity of obtaining greater internal outward radial pressure on the attachment tiles than could be achieved with bulk Fiberfrax packing alone, and the requirement for a dimensional compensation for the increased expansion in a previously used tool due to cristobalite formation.

The refired cycle employed as shown in Figure 151 was similar to that used for Truncated Section No. 4. The average wall temperature of the tool during firing ranged from 2100°F to 2150°F for a 3-4 hour period, while the average temperature of the interior bulk Fiberfrax was 2100°-2130°F for 3 hours.

In general, the results of the refire were very favorable. The replaced attachment tile was well positioned and bonded, the tile butt joints were properly closed, and dimensions as determined by circumferential tape measurements were within print and as desired. Greater internal outward radial pressure was achieved on the attachment tiles, and at least 80%-85% of their faying surfaces appeared to be well bonded. Figure 152 shows this successful truncated section in comparison with the plain second truncated section previously described.

Tape measurements around the circumference at the attachment tile level gave a diameter of Section No. 5 only 0.002 in. larger than nominal. Optical measurement of these butt joints gave an average of 6 mils with a range of from 5 to 10 mils. Wall thickness of this section averaged 0.229 in.

An adverse effect, attributed to the use of extra layers of graphite cloth and Fiberfrax paper for tool expansion compensation, was a uniform vertical mismatch of about 1/4 in. between the inner and outer tile levels. During insertion of the bonded section into the tool for refiring, the bulk of the required cloth and paper shimming prevented the part from bottoming in the tool by about 3/8 in. Experience from firing green-state truncated sections indicated that axial (vertical) pressure during firing was sufficient to cause the parts to settle into place. In this case, however, the outer layer tiles hung from frictional drag on the bulky shim materials, while the inner layer was free to settle into place once the adhesive became molten.

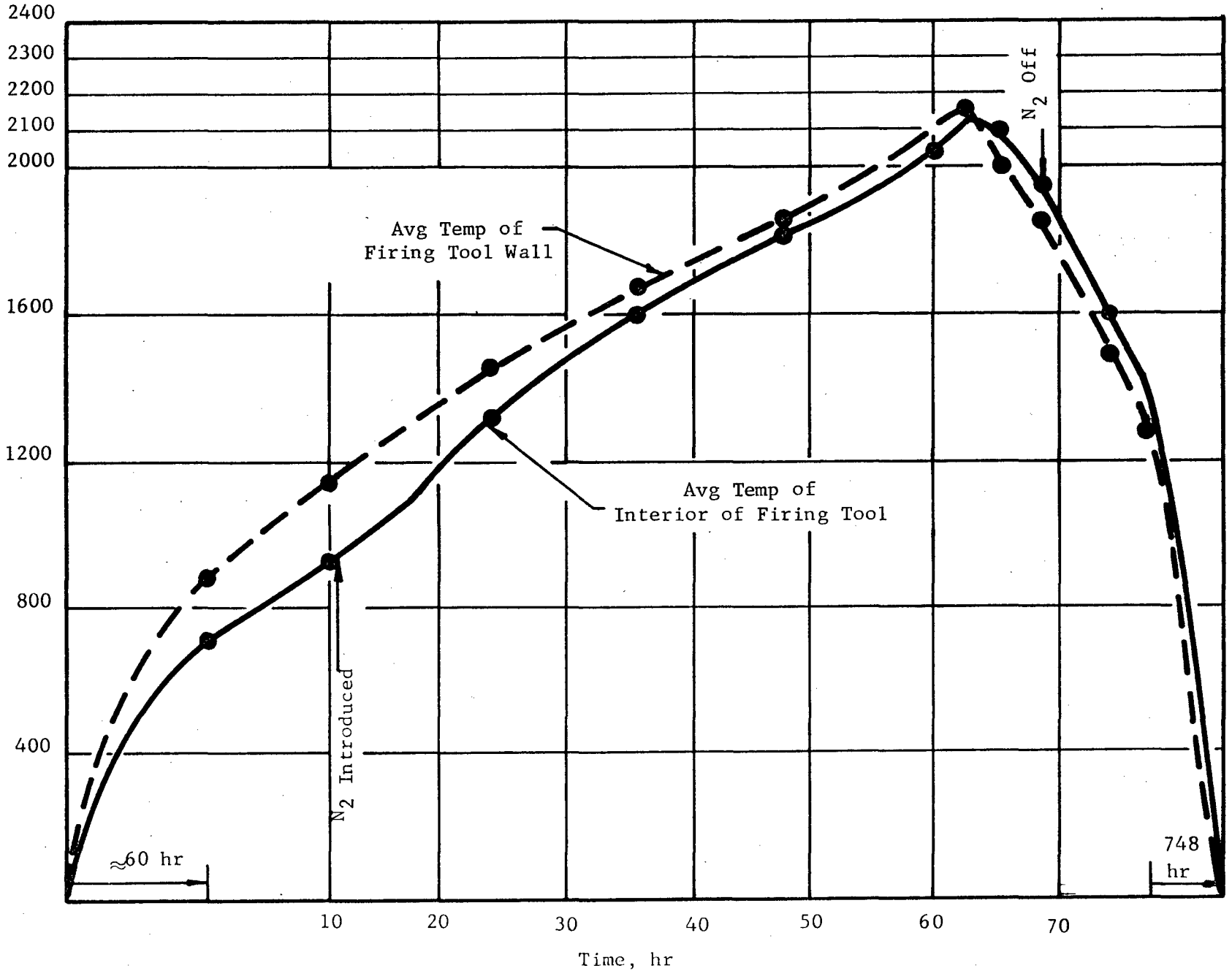


Figure 151. Firing Curves for Truncated Section No. 5

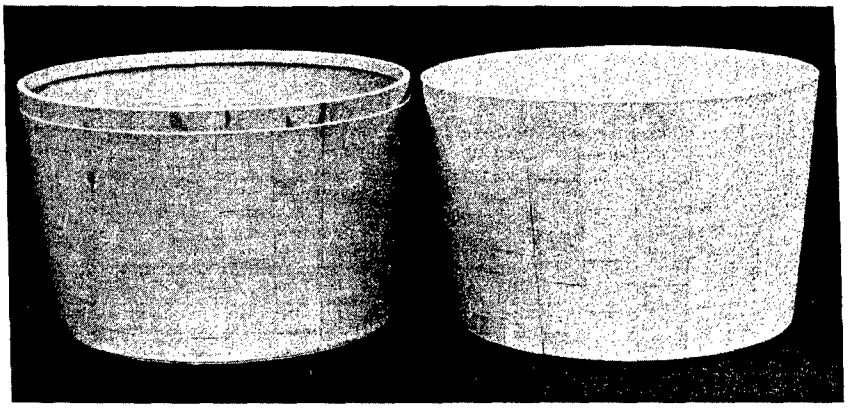


Figure 152. Truncated Radome Sections (Left, with attachment tile; right, plain tiles)

The resulting step between tile layers at the truncated end of the section and the slight dimensional deviations resulting from this mismatch did not detract from the originally planned structural testing of this action. All lateral butt joints between tiles were 6-8 mils, as desired. Inside vertical joints were also closed to this desired degree; however, the outside vertical joints were slightly wider (9-11 mils), as would be expected due to the fact that these tiles expanded into a slightly higher and correspondingly larger portion of the tool than originally intended.

Objective 2 — Stainless Steel Expansion Ring

Although bulk Fiberfrax packing inside the radome sections during firing appeared to exert sufficient radial pressure against the standard tiles to obtain good bonding, this pressure was determined to be inadequate for the heavier base attachment tiles, as previously discussed. In order to obtain more positive pressure against the attachment tiles and obtain a thinner bondline, a relatively high expansion 18-8 stainless steel expansion ring was employed inside the part for the refire operation. This expansion ring was 1/8 in. thick, 26-1/2 in. OD, and 3 in. wide and was similar to the ring shown in Figure 156 under Section XI. It was suspended from the Glasrock tool pressure ring by steel straps and was positioned vertically just below the thick flange sections of the attachment tiles. The annular space of 1-1/2 in. between the ring and the radome tiles was filled with semicompressed bulk Fiberfrax packing. The total cavity inside the part was also packed with Fiberfrax in the usual manner.

It was calculated that at maximum firing temperature, the outside diameter of the steel ring would increase about 1/4 in. because of thermal expansion, thus applying pressure through the precompressed Fiberfrax to both the long and short attachment tiles just below their thick flanged sections.

This approach was considered successful; however, even more pressure than achieved appeared desirable in the fabricating of the full-scale radome by making the ring slightly larger in diameter and by precompressing the Fiberfrax more firmly between the ring and attachment tiles.

Objective 3 — Cristobalite Formation in Glasrock Tooling

Reuse of the firing tool previously employed for firing Section No. 4 was desirable in refiring Section No. 3. In addition to containing an unknown amount of cristobalite with the resulting higher coefficient of thermal expansion, this tool had two diametrically opposed hairline cracks extending from the bottom approximately one-third the height of the tool. Although such cracking had occurred in each of the truncated tools, they did not show a tendency to extend or open up during subsequent firing. In this case, however, a reinforcement shell of Glasrock approximately 3 in. thick was cast around the lower two-thirds of the tool as a reinforcement to provide a more positive support. This reinforcement shell cracked during firing, and whether it proved beneficial is unknown. However, the cracks in the tool did not extend or open up; thus, overall performance was satisfactory in this respect.

A most important consideration in the proper functioning of the radome firing tooling is that its total thermal expansion at maximum firing temperature must be known and must be relatively low compared to that of the alumina radome tiles. Fused silica meets this requirement; however, it was recognized that at the planned firing temperature of about 2150°F, some cristobalite formation could be expected. The original assumption was that any slight increase in expansion of the tool material over that on which the tool dimensional calculations were based, could be compensated for by the use of additional thicknesses of graphite cloth and/or Fiberfrax paper between the part and the tool. As will be discussed subsequently, this still appears to be entirely feasible for at least several tool use cycles once sufficient expansion and cristobalite rate formation data are obtained under actual tool use and radome firing conditions.

The dimensional problem which developed in the case of Section No. 3 resulted from the unexpectedly large and sudden tooling expansion increase. In retrospect, this undoubtedly resulted from the duration of time at temperatures above approximately 2100°F which accrued for this tool during its second firing cycle. The following data were obtained from the firing curves for Truncated Sections Nos. 2 and 3, which utilized the same firing tool:

	First Firing	Second Firing
Approximate hours above 2100°F:	5-9	15-21
Approximate hours above 2200°F:	1	5-8

In order to obtain factual data for predicting dimensional compensation required for the reuse of a firing tool, the percent thermal expansion was measured for several thermally treated samples of the Glasrock tooling material. Samples were cut from the tool used for firing Truncated Sections Nos. 2 and 3, and also from the tool used in firing Section No. 4. Thermal expansion measurements were also obtained on unfired Glasrock material as well as on control samples of Glasrock which had been heated in an electric kiln at 2300°F for 52 hours. In addition, the expansion was determined for small specimens of Glasrock which had been cast and fired for the first time during the firing of Truncated Section No. 4. Table 32 summarizes the thermal expansion coefficients calculated for the different samples. Also included are handbook expansion data for cristobalite and the measured expansion for prefired Glasrock.

TABLE 32

THERMAL EXPANSION CHARACTERISTICS
OF GLASROCK TOOL SAMPLES AND TEST BARS

Sample Description	Linear Coefficient of Thermal Expansion x 10^{-6} in./in./°F		
	Measured RT – 800°F	Measured RT – 1600°F	Estimated RT – 2200°F
Tool No. 2 (3 firings ≈20-25 hr >2100°F)			
Sample A	2.30	1.68	≈1.45
Sample B	2.64	1.83	
Tool No. 3 (1 firing ≈4-5 hr >2100°F)			
Sample A	2.29	1.72	≈1.30
Sample B	2.38	1.65	
Test Bar Fired 4-5 hr >2100°F	1.02	0.73	≈0.59
Test Bar Fired 52 hr @ 2300°F (Electric kiln)	6.51	4.34	≈3.00
Cristobalite (Handbook values)	23.3	12.0	≈8.70
Fused-Silica Castable (Prefired @ 1900°F)	--	0.422	≈0.422

Since expansion data could be determined to only 1600°F (because of equipment limitations), an extrapolation of the total expansions to the required use temperature of 2200°F was made on the basis of the fairly flat fused-silica expansion curve in this temperature range.

These data indicate that most of the transformation (at least that which is effective in increasing the expansion) apparently occurs during the first firing use cycle of the tool. A possible explanation for the lower thermal expansion of the once-fired test specimens (in comparison with that for correspondingly fired tool samples) may be that appreciable amounts of contaminating elements were concentrated near the large tool surfaces due to leaching action during casting and drying. Certain contaminants such as calcium ions do promote cristobalite formation.

In determining the amount of extra graphite cloth and/or Fiberfrax paper required to compensate for tool dimensional changes during reuse, an optional correction of only two-thirds of the theoretical was employed. This was done for several reasons. First, there were indications that the average tool expansion was slightly less than indicated by samples cut from the surface due to the above-mentioned effects of contaminants and the probability that outer portions of the tool received a greater total heat effect than interior portions. Secondly, a lesser degree of compensation was considered more desirable than overcompensation to preclude the chance of excessive pressure and possible buckling or cracking. Finally, there was a limit to the amount of uncompressed shimming which could be physically accommodated in the annular space between the part and tool.

From the results obtained in refiring Truncated Radome Section No. 3 (designated No. 5), in which good dimensional control was achieved, it was apparent that rework of such radomes was feasible and that necessary compensation factors for cristobalite formation and expansion increase in the Glasrock tooling could be determined and applied. Although a significant amount of the fused silica in Glasrock tooling is converted to the higher expansion cristobalite form during the radome firing cycle, fused-silica tooling could be employed for firing cycles at least as high as 2150°F providing the time at top temperatures is minimized, and the extent of expansion change with time-at-temperature is determined and compensations made for the dimensional effects.

SECTION XI

FULL-SCALE MOSAIC RADOME FABRICATION

As a result of fabricating the truncated radome sections, techniques were established which could be readily used or slightly modified to produce a full-size mosaic radome. In this respect, preparation of the alumina tiles and assembly on the plaster layup tool was quite similar to procedures previously explained in Section X. A total of 834 tiles, plus the monolithic nose cap, was required.

The following represents a detailed outline of the fabrication procedures and check-off list employed during the various stages of assembly and firing of the full-scale radome. It is included herein to serve as a guide for the various activities involved.

FABRICATION PROCEDURES

Step 1 — Final Tooling Preparation Prior to Mating with Part

1. Position nitrogen inlet opening on bottom of tool.
2. Assemble Glasrock plug and lowering plate with glass-type sandwich insert.
3. Lower entire insert assemblage into tool and secure by means of wooden dowel pins.
4. Check and prefit Glasrock extension ring, pressure ring, and cover lid.

Step 2 — Layup of Mosaic Radome

1. Install catch basket for "dropped" tiles.
2. Coat layup tool with boron nitride for positive release after inverting.
3. Use cotton gloves for handling tiles.
4. Secure alternate levels of tiles with cellophane tape and Duco cement.
   a. Position tiles by following specially prepared, circular layup chart
   b. Grout butt joints of inner tile level with Narmcad adhesive during layup and wipe away excess with acetone.
   c. Periodically inspect (visually) layup for correct tile position, adhesive thickness, tightness, etc.

5. Prepare nose cap.

   a. Apply an additional thin layer of Narmcad adhesive to the outside of flanged area.

   b. Give particular attention to securing the outer layer of tiles to the nose cap.

6. Final-grout and clean outer layer of tiles.

7. Place two graphite sleeves over layup including nose cap joint area.

8. Attach and fasten 24 plastic shims over the graphite cloth with rubber cement.

9. Attach and fasten plastic shims over nose cap for protection.

10. Fasten required amount of Fiberfrax paper between plastic shims to graphite cloth.

Step 3 — Assembly (Mating) of Tooling over Laid-Up Mosaic Radome

1. Move laid-up tiles under "A" frame next to previously positioned firing tool.

2. Install handling device onto firing tool.

3. Lift firing tool and lower over layup assembly.

   a. Periodically check position of firing tool with respect to top of nose cap by means of a graduated lowering pin.

   b. Extend turnover system and attach "Z" angles to bottom of layup tool.

4. Raise and invert complete assemblage and lower to floor.

5. Attach eyebolts and chain to bottom of layup tool and pull out layup tool.

6. Place layup tool in holder.

Step 4 — Final Preparation of Tool and Radome with Attachment Tiles and Interior Sleeves and Packing

1. Visually check inner tile layer.

2. Insert graphite sock to cover entire inside area including nose cone.

3. Pack with bulk Fiberfrax to desired packing density of approximately 15 lb/cu ft using the following method:

   a. Insert dummies for positioning of final interior thermocouples.

   b. Pack Fiberfrax to within one tile level of top ring.

4. Replace plain end tiles with special attachment tiles.

   a. Remove all inner layer tiles of -107 and -149 and replace with -195 and -193 attachment tiles.

   b. Remove all outer layer tiles -7 and replace with -95 tiles; remove all outer layer tiles -51; no replacement.

   c. Before positioning -193 and -195 tiles, apply an extra thin coating of Narmcad adhesive to area in contact with outer tile layer.

5. Install 12 backup tiles (covered with graphite cloth) and 24 backup alumina shims between attachment tiles and wall of firing tool.

6. Wrap 28-in. diameter steel expansion ring with approximately 1-in. thick layer of compressed (taped) Fiberfrax batting.

   a. Position covered steel expansion ring with top edge approximately 1/4 in. below flange of attachment tile.

   b. Secure steel ring and straps to Glasrock vertical pressure ring.

7. Insert Glasrock extension ring and finish packing with Fiberfrax.

8. Place on cover lid with holes drilled to match up with thermocouples and top nitrogen inlet.

9. Accomplish final hookup and checkout for lifting by a forktruck to kiln area.

Step 5 — Preparation of Firing Tool Assemblage and Kiln for Firing Cycle

1. Lift assemblage and set on foam rubber cushion in front of kiln.

2. Remove lifting and handling device.

3. Final-seal the cover and extension ring with Fiberfrax matting.

4. Lift completed assemblage and place into kiln by forktruck.

5. Place additional brick support under tool.

6. Position assemblage and level on hearth.

7. Provide thermocouple holes through the kiln and into the tool wall. Locate holes at approximate 1-ft levels.

8. Install eight wall thermocouples in steel protection tubes.

9. Install eight interior thermocouples with steel protection tubes and bring thermocouples up through top of kiln.

10. Install nitrogen steel tube inlets at the top and bottom; bottom to have preheating coil length of about 38 in.

11. Seal and close door.

12. Connect thermocouple extension lead wires and hook up to program scanner and automatic switchover device.

Step 6 — Firing of Mosaic Radome Assemblage

1. Allow an initial heatup period to approximately 600°F in approximately 24 hours.

2. Allow a pre-oxidation period of approximately 24 hours at 800°-850°F.

3. Connect nitrogen inlet systems at flow rate of about 50 cfh.

4. Use a heating rate of approximately 25°F/hour.

5. Keep all wall and interior thermocouples at 2150°±50°F for 4-5 hours.

6. Cool assemblage at a rate of <50°F/hour until interior temperature reaches 1800°-1900°F.

7. At 1800°-1900°F, turn off nitrogen gas and shut down kiln.

Step 7 — Radome Removal

1. Cool the kiln to ambient temperatures before opening.

2. Remove assemblage from kiln by forktruck to "A" frame.

3. Install handling and turnover device on assemblage.

4. Lift firing tool and radome assemblage and lay down horizontally.

5. Remove Fiberfrax bulk fiber.

6. Remove radome.

Figure 153 depicts the radome after the final layup was completed on the male layup tool. No major problems were encountered during the layup except (as previously noted with the truncated sections) that the last vertical butt joint of all rows resulted in an oversize gap condition. An analysis of the situation revealed that this condition was to be expected, since the layup tool was designed to fit only the inside diameter of the truncated section. Therefore, the circumference of the final outside layer would increase by a factor of π times each 0.001 in. increase in diameter, or 0.00314 in. Thus, with the interlayer thickness of 0.013 in. for green adhesive or shims, the diameter to the inside of the outer layer is increased 2 x 0.007 in., or 0.014 in. This results in a circumferential increase of 0.044 in., which would show up in the final gap. This, along with the lack of an exact fit between the layers due to the straight rather than ogival longitudinal shape of the tiles, accounts for the observed gap.

This condition was more severe at the top end of the layup, but was not considered excessive. In order to assure a tight fit in the layup and to decrease the possibility of starved butt joints, additional Narmcad adhesive was grouted into these areas. To compensate for the previously described oversize condition of the firing tool, the laid-up radome was covered with one additional layer of graphite cloth and two layers of Fiberfrax paper. This provided the necessary dimensional compensation for the firing tool which as previously described was approximately 0.080 in. oversize on its inside diameter. During the course of the program, it was ascertained that the nominal 0.020-in. thick graphite cloth compressed to 0.010 in. during firing and nominal 0.028-in. thick Fiberfrax paper compressed to 0.015 in. Thus, one additional layer of graphite cloth and two layers of Fiberfrax paper gave the necessary shimming. As this represented the initial firing of the tool, no additional compensation was provided for cristobalite formation within the fused-silica tool.

After covering with the required graphite cloth, Fiberfrax paper, and strips of 0.080-in. thick Plexiglas (to assure a tight fit in the firing tool and prevent tile movement), the laid-up mosaic radome was moved next to the firing tool as shown in Figure 154 for final mating. Prior to mating, the firing tool was fitted with the Glasrock interior parts required for lowering the radome during firing. These parts consisted of the Glasrock plug and lowering fixture with a glass insert and were made in accordance with the design previously shown in Figure 93. The glass insert was made up of various low-melting glass powders approximately 0.750-in. thick, which would gradually soften and compress during firing, thus permitting the mosaic radome to fit the contour of the firing tool. Controlled lowering was considered desirable in order to retain the individual tiles in a relatively static position with respect to the tool, regardless of the differential thermal expansion. The selected powders were pressed into wafers about 0.100 in. thick and sandwiched together with the lower melting materials on the bottom (during firing), as indicated below:

Magnesium Aluminosilicate Glass	2000°-2200°F
Narmcad 120	1700°-2100°F
E-Glass	1500°-1700°F
Narmcad 130	1300°-1600°F
Lead Silicate Composition	1040°F
Lead Borate Composition	850°F
Plexiglas	400°-600°F

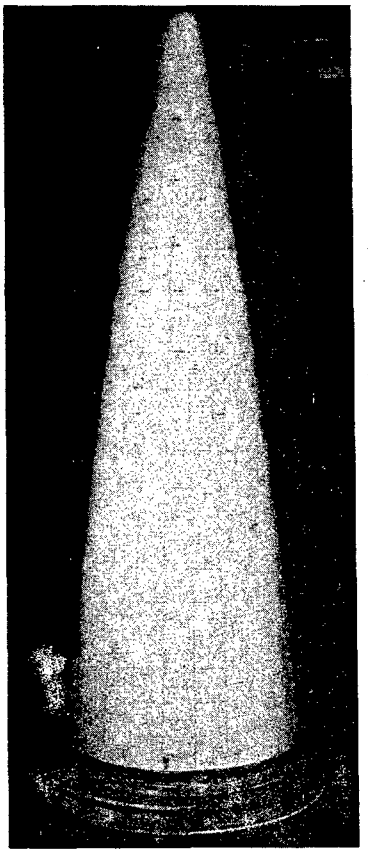


Figure 153. Mosaic Radome in Final Layup Stage

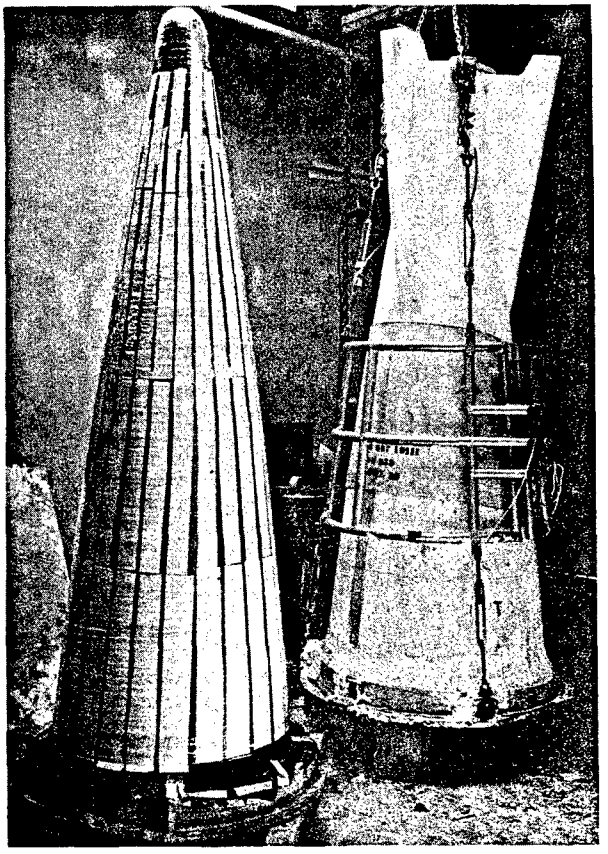


Figure 154. Mosaic Radome, Covered with Graphite Cloth and Fiberfrax Paper, and the Firing Tooling

Previous investigations of the above sandwich compositions had shown that inserts would smoothly compress during the firing cycle and, theoretically, allow a gradual lowering of the radome. The entire lowering system was assembled and joined together with plastic cement and a wooden pin. It was then lowered to the bottom shoulder of the firing tool where it was held in place by drilling three holes through the tool and inserting 1/4-in. wooden dowels. At the same time, a nitrogen inlet hole was drilled just above the lowering fixture.

As shown in Figure 155, the firing tool was lifted up by means of a hoist and "A" frame, and was lowered over the assembled mosaic radome. No problems were encountered, and the firing tool and bottom portion of the layup tool were secured together by "Z" angles. The entire assemblage was lifted and inverted, allowing the layup tool to be subsequently withdrawn. Again, this operation was accomplished without any binding or difficulty, and visual examination of the assembled, unfired mosaic radome revealed that all tiles were secure; and the complete assembly was correctly positioned within the firing tool.

A graphite cloth sock was placed within the interior of the positioned mosaic radome to prevent bulk Fiberfrax packing from absorbing and sticking to the Narmcad adhesive within the butt joints during firing. In order to obtain slightly more radial pressure than produced on the truncated sections, the bulk Fiberfrax packing density was increased to about 15 lb/cu ft. Concurrently with the packing operation, eight dummy thermocouple rods within a plastic sleeve were positioned in the radome interior. In addition, a nitrogen inlet pipe extended down to the nose cap area. After packing, the dummy couples were removed from the plastic tubing and the final thermocouples inserted after the tool and part assemblage was positioned in the kiln. As was the case with the truncated sections containing the special attachment tiles, the Fiberfrax was packed to within one level of the part end, allowing the plain layup tiles to be removed and replaced with the attachment tiles while using plain tile sections as backup support between the wall of the tool and attachment tiles. At the same time, the stainless steel attachment ring was positioned. To produce a greater lateral pressure against the attachment tiles than that obtained with the truncated section, the steel ring was increased from a diameter of 26-1/2 in. to 28 in., thus decreasing the annular space between it and the radome to about 3/4 in. Additionally,

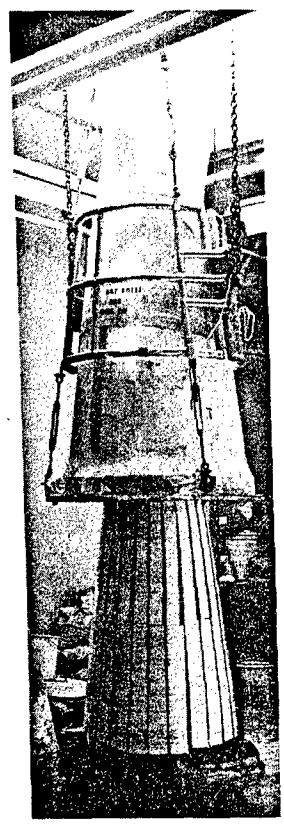


Figure 155. Mating of Firing Tool with Mosaic Radome

Fiberfrax matting was precompressed by wrapping it firmly around the expansion ring as shown in Figure 156. This, combined with the expansion of the ring during heating, exerted positive pressure on all attachment tiles so that closure was obtained between these and the outer layer of tiles.



Figure 156. Position of Stainless Steel Expansion Ring with Respect to Attachment Tiles

Final preparation of the part and tool involved positioning the Glasrock extension ring, pressure ring, and cover lid while completing the Fiberfrax packing operation, as illustrated by Figure 157.

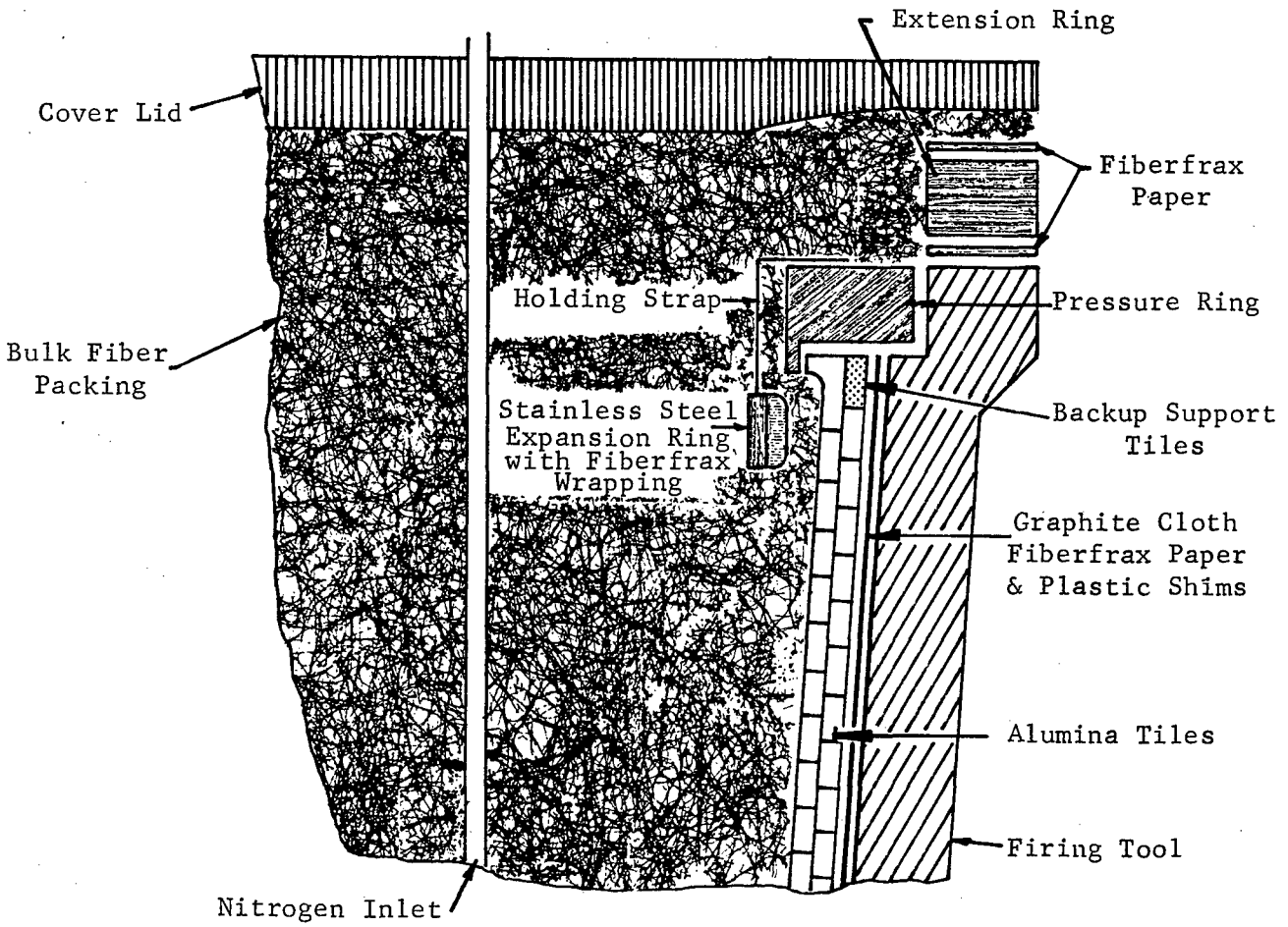


Figure. 157. Cross Section of Mosaic Radome and Firing Tool Arrangement

Figure 158 shows the firing tool containing the mosaic radome before it was loaded into the kiln. After the tool was positioned in the kiln, the required thermocouple connections were made. A total of eight chromel-alumel thermocouples, spirally positioned inside the part at approximately 1-ft vertical intervals and 1 in. from the radome tiles, extended out through the top of the kiln. Eight thermocouples were similarly positioned within the wall of the firing tool about 1 in. from the part, with leads extending through the kiln wall. Four thermocouples were located in the kiln chamber to monitor temperature along with the platinum-platinum − 10% rhodium controller thermocouple. All thermocouples were recorded automatically on a Barber Coleman strip chart recorder, using a program thermocouple scanner in conjunction with an automatic switchover device. At the same time, final hookup of the two nitrogen inlets was accomplished, thus providing for atmosphere protection of the graphite cloth around the interior and exterior of the assembled radome tiles.

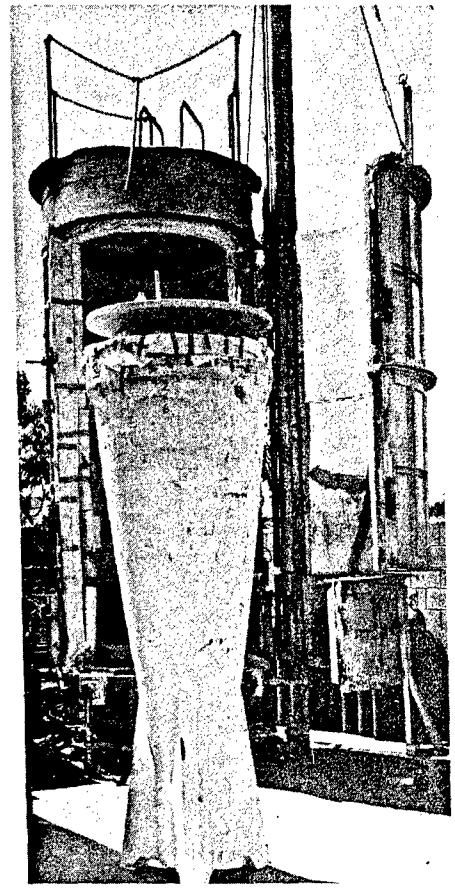


Figure 158. Firing Tool and Radome Prior to Firing

RADOME FIRING

Firing of the full-scale radome was accomplished in accordance with the heating and cooling curves depicted in Figure 159. After an initial heatup to 800°-950°F, a pre-oxidation period of about 32 hours was employed to allow burnout of all organic matter such as the nitrocellulose adhesive binder, and Plexiglas shims. Nitrogen gas was introduced after the pre-oxidation period at a rate of 50 cfh to both the interior and outer portion of the radome for graphite cloth protection. After allowing the entire systems to be purged with nitrogen for 2 hours, the temperature was increased. A programmed heating rate for the kiln chamber was adjusted to give a temperature rise of approximately 20-25°F/hour in the wall and interior of the firing tool.

As was to be expected, there was a temperature lag of 5-7 hours between the interior of the part and the wall of the firing tool. In order to compensate for this lag and to minimize possible cristobalite inversion of the tool, the average temperature of the tool interior was increased to approximately 2150°F and held for about 2 hours. This kept the wall temperature between 2150°F and 2250°F for a period of approximately 8 hours. After the soaking period, temperature of both the wall and interior was reduced at a rate of 30°-40°F/hour until all thermocouples were below 1900°F, at which point the nitrogen and the kiln were turned off. The part was then allowed to cool to ambient temperatures under the normal cooling of the kiln. This resulted in a cooling rate for the part of approximately 30°-50°F/hour from 1900°F to ambient conditions.

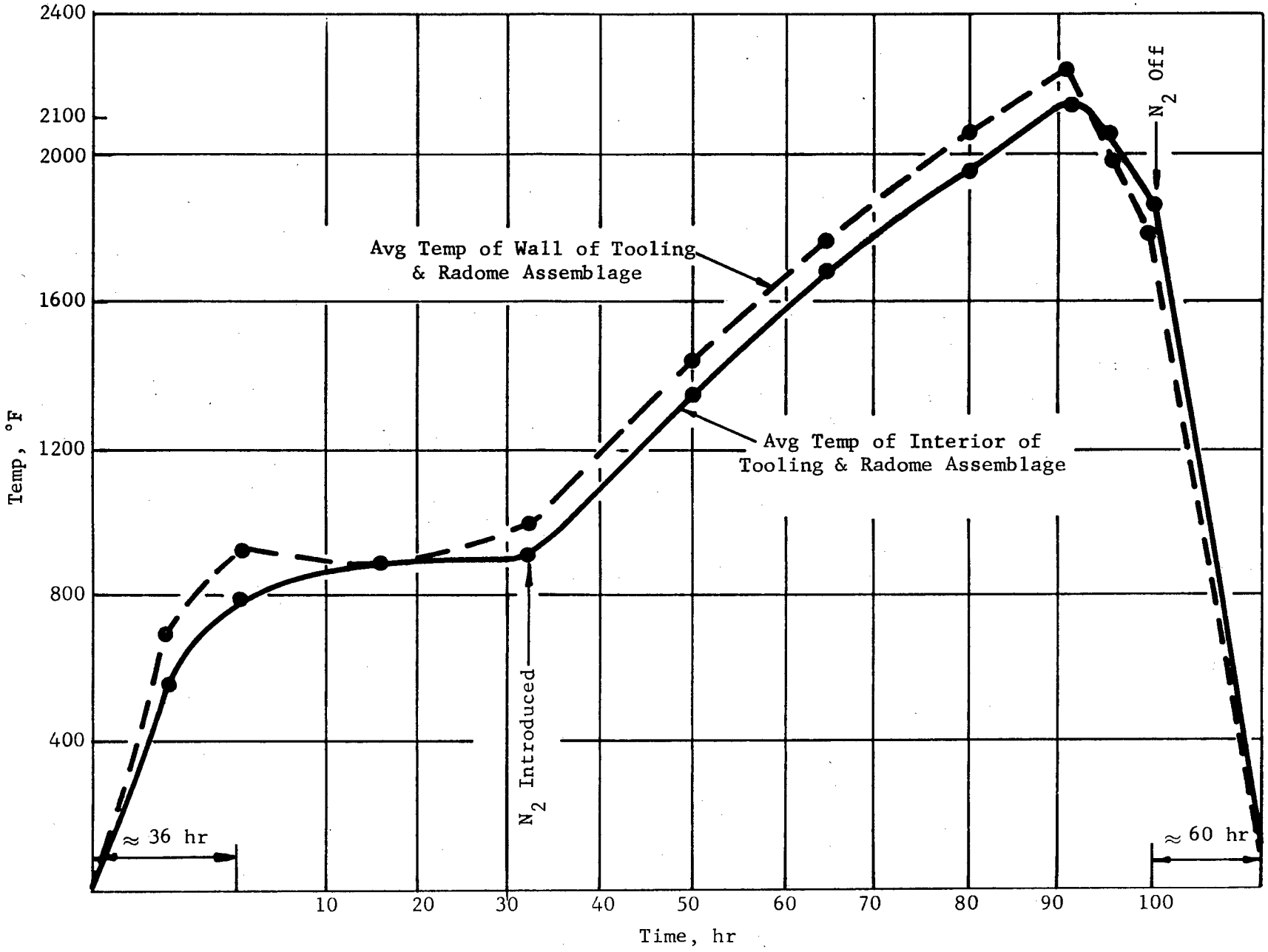


Figure 159. Firing Curves for Full-Scale Mosaic Radome

Figure 160, which depicts the tool and radome assemblage after the firing cycle, shows that the cover lid bottomed as desired. Visual inspection of the tool revealed only three hairline cracks around the periphery of its base inside of the fins and extending vertically for about 4-6 in. Based on the overall condition of the tool, it was considered to be reusable for future firings. The tool and radome assemblage was removed by a forktruck and the handling device connected to allow it to be placed in a horizontal position using the "A" frame and electric hoist.

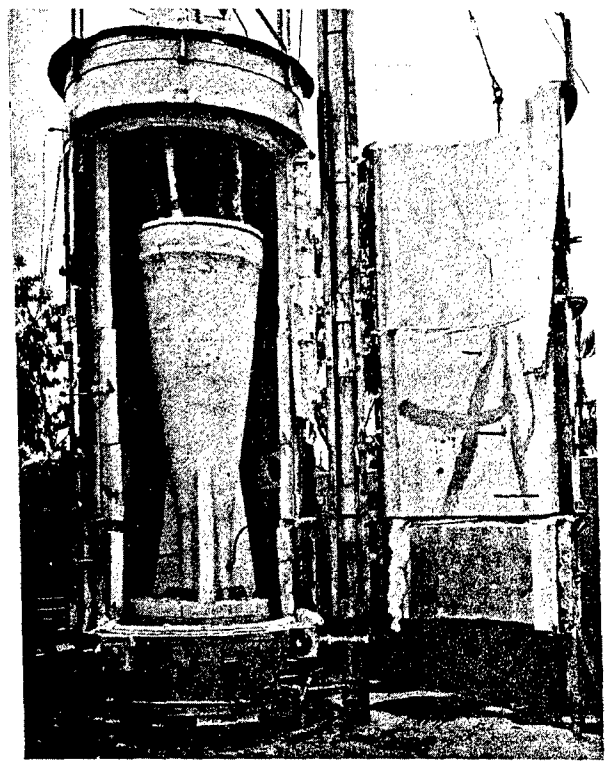


Figure 160. Radome and Tool Assemblage after Firing

Removal of the fired mosaic radome from the tool proceeded without major problems. Figure 161 shows two views of the full-size radome after its removal. Figure 162 shows a vertical view. Upon removing the compressed Fiberfrax packing from the interior, it was noted that the graphite cloth still remained intact. In fact, as indicated by the four dark streaks in the interior of the radome, it was concluded that little or no oxidation occurred in the interior bottom portion during firing.

The dark streaks coincided with the position of masking tape used for fastening the graphite sock to the part during the tool and part preparation. Evidently, the mass and tightness of Fiberfrax used was sufficient to prevent adequate access of oxygen (air) over this area even during the pre-oxidation period. This resulted in some of the inside butt joint adhesive being discolored from carbon residue left from incomplete burnoff of the nitrocellulose binder. This condition did not extend through to the outside of the radome where it was evident that satisfactory binder burnout occurred during the pre-oxidation firing period. This would provide the necessary oxygen for burnout of any carbonaceous materila and would not affect the graphite cloth provided the temperature is kept below 800°-900-F.

An examination of the attachment tiles showed that the stainless steel expansion ring concept had provided more lateral pressure than experienced during firing of truncated sections. This resulted in a uniform lateral faying surface closure between the base attachment tiles and the outer layer of tiles. No visible interfacial gaps were apparent, and all except one of the attachment tiles were well aligned vertically and butt joints sufficiently closed. The misalignment of this one tile was approximately 1/16 in.

While sufficient lateral pressure was obtained for closing of the attachment tiles to the outer tile layer, measurements of the wall thickness of the radome near its base showed that it ranged from 0.225 in. to 0.238 in., with an average of 0.231 in. as compared to the desired goal of 0.222 in. This

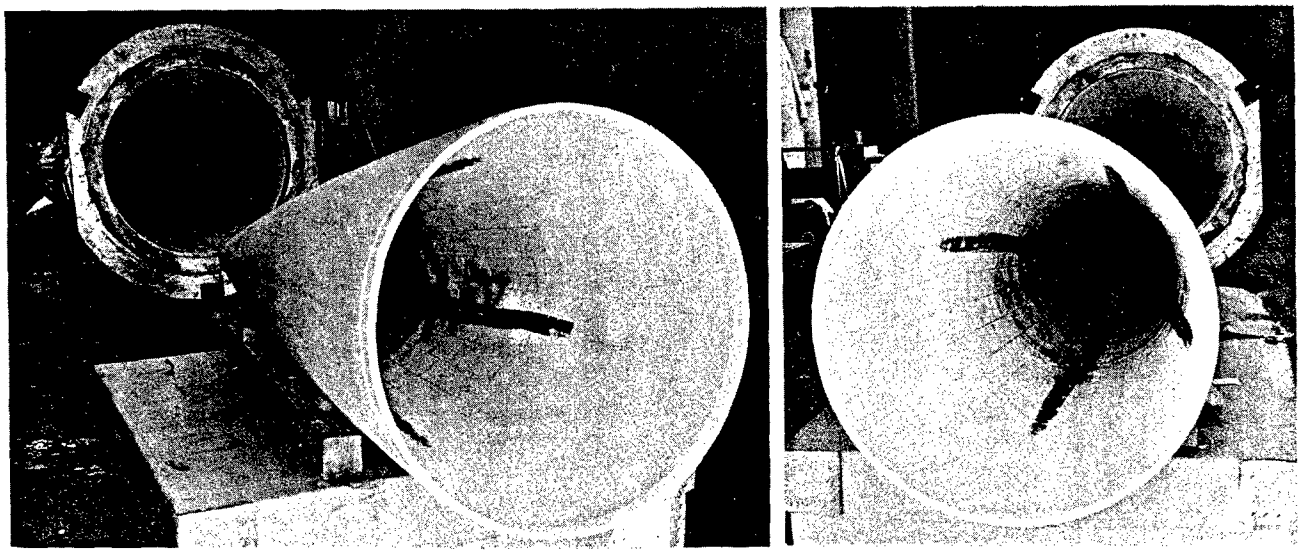


Figure 161. Two Views of Mosaic Radome after Removal from Kiln

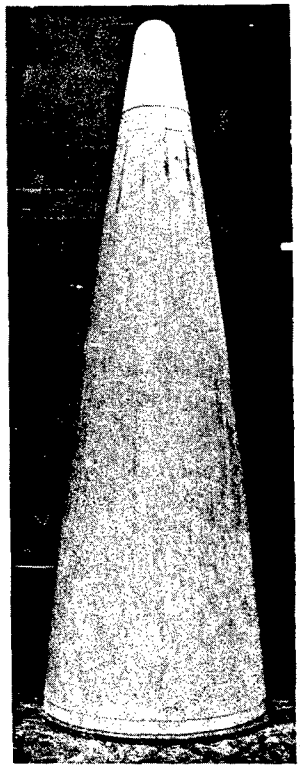


Figure 162. Full-Scale Mosaic Radome

would indicate that more radial pressure than generated by the Fiberfrax system would be desirable. However, some of the additional thickness may have resulted from an excess of Narmcad adhesive employed on these tiles, and the relatively low pressures involved may have been insufficient to squeeze out excess adhesive and thereby reduce bondlines to the desired thickness.

Another condition observed in the final radome was that the outer layer of tiles obviously hung up from frictional drag on the graphite cloth and did not mate with the nose cap. As shown in Figure 163, this resulted in a gap of approximately 3/8 in. to 1/2 in. between the nose cap and outer tile layer.

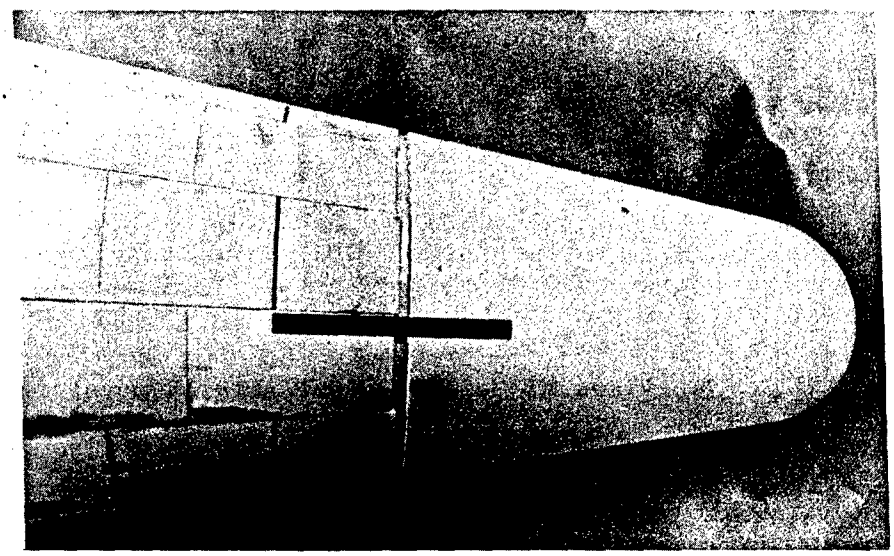


Figure 163. Lack of Joint Closure between Nose Cap and Tiles

The inner layer of tiles was free to settle into place once the adhesive was molten as evidenced by the tight bondline between the nose cap rim and tiles. Inspection of the lowering fixture mechanism indicated that it performed as expected and was not the cause of the mismatch. All of the glass sandwich insert plate had melted and flowed into the reservoir opening built into the Glasrock plug. Subsequent consideration of this problem has indicated that in all probability, the tooling would perform more satisfactorily if a lowering fixture were not used. The geometry of the assembly and the positive vertical expansion force on the tiles during heating is considered enough to minimize any effects of frictional drag and ensure uniform joint closure. The overall effect of the mismatch was to produce a radome oversized in radial dimensions since the individual tile levels were expanding into a slightly higher and correspondingly larger portion of the firing tool than was desired. Tape measurements around the circumference at the attachment tile level gave a diameter approximately 0.040 in. larger than nominal. Optical measurements of the attachment tile butt joints showed them ranging from 0.005 in. to 0.020 in., with an average bondline thickness of 0.011 in. Subsequent measurement of other butt joints at different tile levels indicated the radome to be oversize in diameter by approximately 0.035 - 0.045 in.

Although the radome gave indications of free removal from the firing tool, subsequent examination of the part and tool revealed indications of possible slight seizure during the firing cycle. A circumferential hairline crack developed, extending intermittently halfway around the radome approximately 15 in. from the nose cap joint. It was in this area that excess Narmcad adhesive was applied during the layup stage. As can be seen from Figure 164, the excess adhesive was squeezed out of the bondline during firing. Examination of the interior of the firing tool at this location showed that some of the excess adhesive had been forced through the graphite cloth pores and the Fiberfrax paper, with the result that considerable remnants of the Fiberfrax paper were found bonded to the wall of the tool. While the seizure was minimal, it probably was sufficient to prevent free contraction of the part during cooling, thus causing the tensile failure in the axial direction. In addition to the above and due to the relatively large amount of adhesive forced out of the bondlines onto the radome surface, a wedging action occurred, on cooling, between the part and tool. This effect combined with the frictional drag may have resulted in undue stress on the part at this particular location.

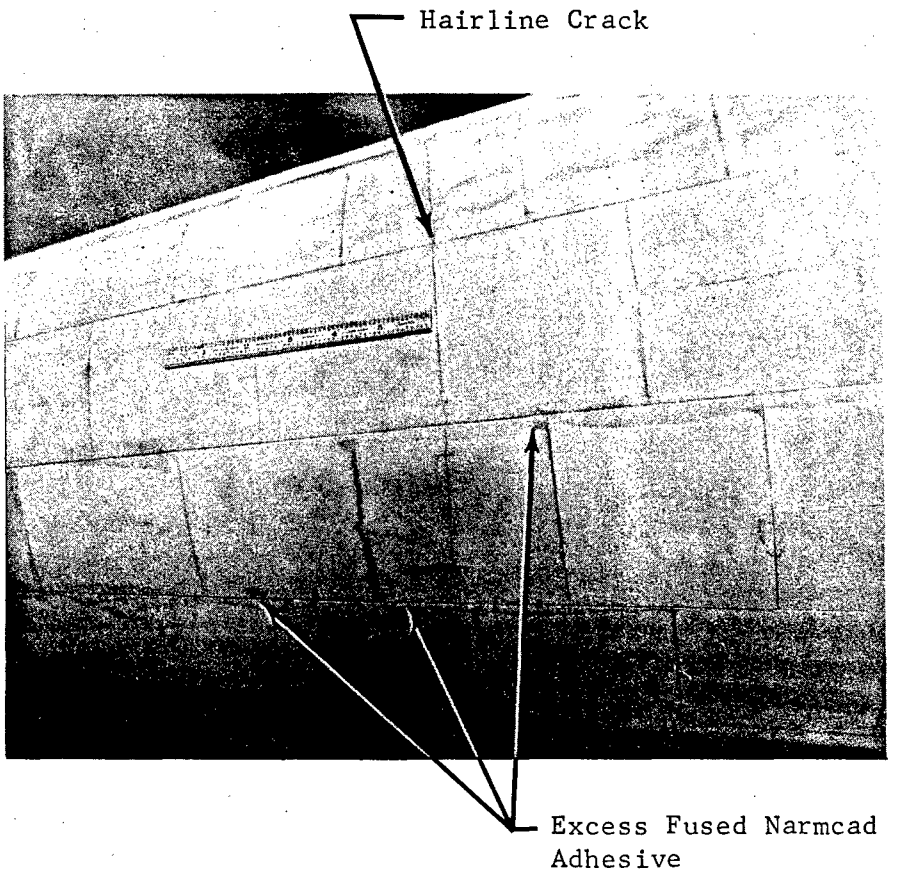


Figure 164. View of Mosaic Radome Near Nose Cap

The aforementioned defects existing in the initial mosaic radome were not thought to constitute cause for any major change in the manufacturing procedures for future radome fabrication. The difficulties appeared to be readily correctable using existing tooling and auxiliary materials. In this respect, Narmco anticipated that a completely satisfactory mosaic radome could be made if the following manufacturing corrections were made:

1. Decrease or eliminate the excess Narmcad adhesive applied during the layup stage, so that the possibility of seizure during firing would be eliminated.

2. Eliminate the glass sandwich insert plate used to lower the radome during firing. This would allow the mosaic radome to expand upward to the correct position corresponding to the tooling coordinates at firing temperatures and would eliminate the possibility of tile hang up due to friction during a lowering operation.

3. Introduce air or oxygen into the interior of the bulk Fiberfrax packed radome during the pre-oxidation firing period. This would allow complete burnout of all organic matter and prevent discoloration of interior bondlines.

4. Closely control adhesive application thickness on interfacial surfaces.

5. Increase the Fiberfrax packing in order to obtain closer control of the finished wall thickness of the fired radome.

SECTION XII

QUALITY ASSURANCE; DIMENSIONAL AND PROPERTY DATA

The primary function of the quality assurance effort under this program was to provide assurance that manufactured parts, materials, manufacturing processes, tools, and gages met applicable requirements as provided by engineering drawings, specifications, purchase orders, and contractual commitments. A major portion of this effort was concerned with inspection and quality control of the alumina tiles and other ceramic radome components which were purchased from the Coors Porcelain Company (Golden, Colorado). The Narmco specifications for these components, plus pertinent data on the delivered materials and methods of testing and inspection, are included in this section of the report. Another major quality assurance effort included tooling inspection and measurement plus dimensional inspection of finished radomes and sections. The results of these inspections are included as appropriate under Section V, Tooling; and Sections X and XI; Truncated and Full-Scale Radome Fabrication, with basic techniques and equipment being described in this section.

ALUMINA COMPONENTS (GENERAL)

As a result of detailed evaluation and design considerations, dimensions and tolerance criteria plus material properties and other required specifications were established to provide the basis for procuring the alumina tiles and nose caps for the mosaic ceramic radome program. These dimensions along with material properties (including electrical requirements) were incorporated into Narmco Drawings NR 63-044, NR 63-045, and NR 63-046, which are included in Appendix X. The more significant specification requirements which governed the procurement and inspection of these alumina ceramic components are summarized in Table 33. Procurement of the ceramic components was made from Coors on the overall basis of ability to meet the specifications, delivery schedules, and costs. The actual material used in filling the order was Coors AD 99 Grade alumina, which is nominal 99% alumina, thus exceeding the specification requirement in regard to purity.

The contract with the alumina components supplier provided for Government (Department of the Navy) inspection and acceptance at source (per Narmco specifications). Because this was a manufacturing technology program, however, it was considered desirable to determine the overall practical feasibility of the tile requirements as specified. Therefore, some inspection was performed by Narmco to obtain first-hand information on the state-of-the-art of manufacturing and finishing such ceramic items.

The specifications to which the tiles were procured were purposely made precise to reflect desired goals. Since no experience existed as to exactly which dimensional and visual quality factors were mandatory, a Materials Review Board (MRB) procedure was established to exercise engineering judgment as to the acceptability of those tiles which varied slightly from the specification. Thus, the purpose of the MRB was to ensure that usable tiles were

TABLE 33

SPECIFICATION SUMMARY FOR ALUMINA TILES AND NOSE CAPS

Item	Specification
Material	Sintered alumina, 97.6% min. purity
Flexural Strength, MOR	40,000 psi @ RT & 1000°F, min.
Specific Gravity	3.75 gm/cc min.
Dye Penetration	10 mil max. per ASTM D116-61
Loss Tangent @ RT	0.0007 max. @ 9.375 kmc
Dielectric Constant @ RT	Shall not vary more than 0.2 from nominal (Acceptable range: 9.2 min. – 9.4 max.)
Color & Texture	Uniform, free from spots & specks
Surface Defects (Pits, chips, etc.)	Area: 0.020 in. x 0.020 in. max. Depth: 0.020 in. max. Less than 1 per 2 sq in.
Edge Defects	0.005 in. max.
Cracks	None
Tile Thickness, in.	0.108 ±0.001
Tile Length, in.	Tolerance ±0.0015
Tile Chords, in.	Tolerance ±0.0015
Tile Radii, in.	Tolerance ±0.050 (in general)

not scrapped and that the goals of the overall mosaic program were not knowingly compromised. The following tile quality assurance items are recorded herein:

1. The first shipment of 40 tiles was used to establish inspection procedures and guidelines, and was subjected to a 100% visual and dimensional inspection by Narmco. Nineteen required MRB disposition and four were rejected and returned for replacement.

2. Dimensional quality improved markedly in subsequent shipments but some chips, pits, and cracks were observed. The level of confidence was such that of the first 13 shipments (895 tiles), approximately 10% were dimensionally inspected and 100% visually inspected.

3. Of the first 584 tiles received (through the tenth lot shipment), 42 required MRB action. Nine of these tiles were returned for replacement (these figures include the first shipment of tiles in Item 1. above).

4. Cost considerations dictated that Narmco tile inspection activities be held to a minimum. The next eight shipments were therefore inspected on a sampling plan, whereby 1% were visually and dimensionally inspected and, if a discrepancy were noted, then 10% were inspected. One of these lots required the 10% inspection level. When 1432 tiles had been received, 153 required MRB disposition.

5. Of the total of 4148 alumina tile segments, two alumina nose caps, and 16,400 alumina spacer shims (5,100 of 0.013-in. thickness, and 11,300 of 0.006-in. thickness) delivered, MRB action was required on 334 tiles and one nose cap. Of these, only 26 tiles were rejected as being outside acceptable specification limits.

As a result of the Narmco inspection and mosaic radome fabrication experience, it was concluded that while the original ceramic component specification criteria were capable of being fulfilled by the supplier, some relaxation was permissable and desirable in the interest of cost and time considerations. In actuality, tile quality and dimensional tolerances as delivered by the supplier were considered good, and the acceptable deviations from specifications were extremely small and in all cases within the following envelope criteria:

Characteristic	Specification Tolerance, in.	Material Review Board Envelope Criteria, in.
Thickness	±0.001	+0.001, -0.002
C^1 Chord	±0.0015	+0.0015, -0.003
C^2 Chord	±0.0015	+0.0015, -0.003
Height	±0.0015	+0.0015, -0.003
Pits and Chips	(Minor, depending on location, number, etc.)	

A set of inspection gages (W-101 and W-102) were designed and procured by Coors for measuring the two chord dimensions and the lengths of the alumina tile segments. One set of these gages (Figure 165) was obtained by Narmco for in-house inspection use. Thickness measurements were made with a micrometer caliper. The radii of curvature of the tiles were determined at source by Government inspection of the grinding setup.

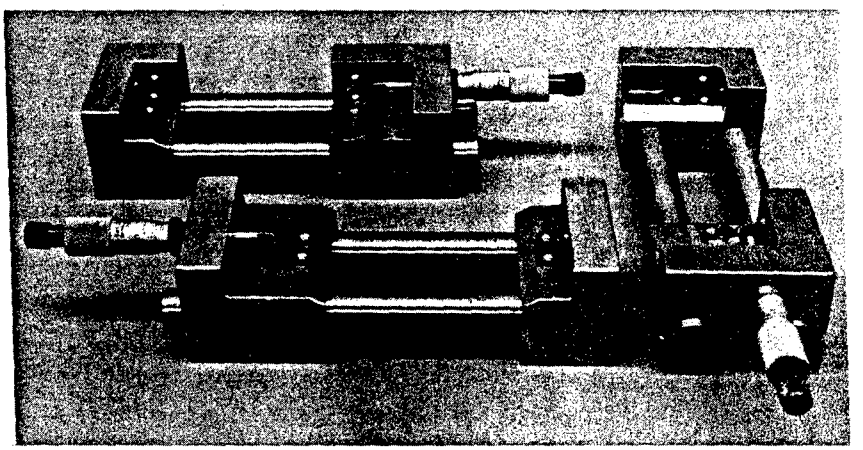


Figure 165. Tile Dimensional Inspection Gages

Information regarding details of the tile manufacturing procedures were not procured by Narmco; however, in general the process consisted of dry-pressing tile blanks from the prepared alumina powder, then firing and individually grinding them to the required dimensions. Surface finish, color, and freedom from specks was uniformly good. There was some slight variation in degree of whiteness with occasional areas which appeared a little off-white with a yellow or blue cast. These minor color variations were apparently associated with kiln atmosphere conditions during firing, and were found to have no adverse effects on mechanical or electrical properties. Any noticeable contamination and specks or spots were cause for rejection by Coors during the manufacture.

ALUMINA COMPONENTS (STRENGTH PROPERTIES)

It was originally specified that modulus of rupture (flexural) specimens be taken from actual fired tile segments and tested in accordance with ASTM standards. However, it became evident that test specimens could not be produced according to these standards because of insufficient tile thickness and curvature. Approval was therefore given to the supplier to utilize smaller microbar specimens for quality control strength testing of the mosaic radome alumina components. The flexural test specimens and test conditions were

Specimen Size:	2.54 cm x 0.254 cm x 0.254 cm nominal
Test Conditions:	Room temperature and 538°±2°C Three-point loading on 1.59-cm span Loading Rate: 13.6 Kg/minute

Ten specimens were prepared from tiles from each kiln firing and tested at room temperature. The average of these tests was used as representative of the MOR strength of that particular lot of tiles. Elevated temperature (1000°F) flexural tests were made in a similar manner from three of the kiln firings. Surface finish of specimens was diamond-ground in a manner similar to that for the tiles and nose cap components.

The results of the modulus of rupture testing are given in Table 34. The scatter exhibited by these test data (up to ±11% from the average for individual specimens, and ±8% from the average for the different heats) is considered normal for brittle materials of this type. On the basis of available information and experience, it was assumed that the tensile strength would be approximately one-half of the flexural strength or perhaps 22,000 psi as an average room temperature value for this alumina material, depending, of course, on the technique of specimen preparation and testing.

ALUMINA COMPONENTS (ELECTRICAL PROPERTIES)

Dielectric constant and loss tangent data on the AD-99 alumina was determined for Coors by Melpar, Incorporated, and certified by the Government Inspector that each lot of material met Narmco's specification requirements. Elevated temperature properties were not determined on a routine basis, since the relationship of elevated temperature to room temperature electromagnetic properties are well known for this commercial grade of alumina. The following data were furnished by Coors as being typical for this material:

Specimen No.	Dielectric Constant	Loss Tangent
1	8.86	0.00009
2	8.87	0.00013
3	8.85	0.00013
4	8.99	0.00015
5	8.87	0.00006

(Properties at room temperature and at a test frequency of 9.375 Gc)

FIRING TOOLING INSPECTION GAGE

Proper functioning of the differential expansion tooling concept was dependent on close dimensional control of the interior or working surfaces of the firing tools. As explained in Section V, these critical firing tool dimensions were constructed to the desired values by backcasting a thin Glasrock working surface layer over an accurately swept plaster mold. This final working surface was intentionally made a few thousandths of an inch oversize since this could be readily compensated for by layers of graphite and Fiberfrax cloth. However, in order to determine the exact amount of compensation required in each specific case, it was necessary that the tool diameters (or radii) at the various coordinates or stations be accurately measured. This required the design and fabrication of a special Firing Tool Inspection Gage as shown in Narmco Drawing NR 63-157 (see Appendix X). This inspection gage was fabricated by Arrowsmith Tool and Manufacturing Corporation and is shown

TABLE 34

MODULUS OF RUPTURE TEST RESULTS

Kiln Firing No.	Avg MOR Strength Values, psi	
	RT	1000°F
K9-323	46,864	39,717
K9-324	47,750	--
K9-325	41,788	--
K9-326	42,108	--
K9-331	41,223	--
K9-332	40,940	41,744
K9-339	47,850	38,158
Avg	44,433	39,873

Individual Specimen Data at 1000°F

Specimen No.	MOR Values, psi		
	Heat No. 323	Heat No. 333	Heat No. 339
1	40,399	43,485	40,173
2	40,010	37,683	38,574
3	39,591	41,082	38,525
4	36,904	39,581	35,195
5	41,796	40,237	39,523
6	43,411	44,631	38,459
7	37,968	46,629	38,794
8	34,780	39,916	37,998
9	40,244	40,588	36,818
10	42,062	43,607	37,518
Avg	39,717	41,744	38,158

in Figures 166 through 169. The gage, as initially fabricated and shown, was suitable for checking the truncated firing tools; however, minor modifications were possible to make it suitable for inspecting the full-scale firing tool as well as the interior dimensions and circularity of fabricated radomes.

Firing Tool Inspection Procedure

The following firing tool inspection procedures are incorporated herein as a matter of record as an an explanation of the tool and its use.

1. Calibrate the gage as follows:

   a. Measure the shaft diameter at a joint just above the arm supporting the dial indicators.

   b. Loosen the thumb screws on the bronze blocks used to support and guide the dial indicator rods. The rods should move freely in the blocks without evidence of sticking.

   c. Ensure that rod extensions and tips are not loose and that rods are fully extended.

   d. Push the dial indicator rods back until the revolution counters (the two small dials on the face of each indicator) are exactly on zero. Adjust the bezels of the indicators to zero and lock in place.

   e. Measure the distance between the shaft centerline and the tip of each indicator where the indicator reads exactly zero. This may be accomplished by measuring with an 18-in. vernier caliper and subtracting the shaft radius or using a height gage and adding the shaft radius.

   f. Record the values obtained on tags and attach the tags on the respective indicators. Calibration should be accomplished each time the gage is used.

2. Mount the gage on the firing tool with the leveling screws resting on steel pads.

3. Place steel pads between the firing tool wall and the centering screws.

4. Center the gage approximately by adjusting the centering screws until each screw indicates the same amount of adjustment and is just tight enough to prevent the steel pads from slipping.

5. Level the gage with respect to the horizontal surface of the shoulder inside the firing tool. This may be accomplished as follows:

   a. Mount a universal indicator (of the type that reads in the order of ±0.030-in. full scale with 0.0005-in. maximum increments) on a magnetic base and attach the unit to one end of the mounting arm that supports the primary dial indicators (identified as Nos. 1 and 2).

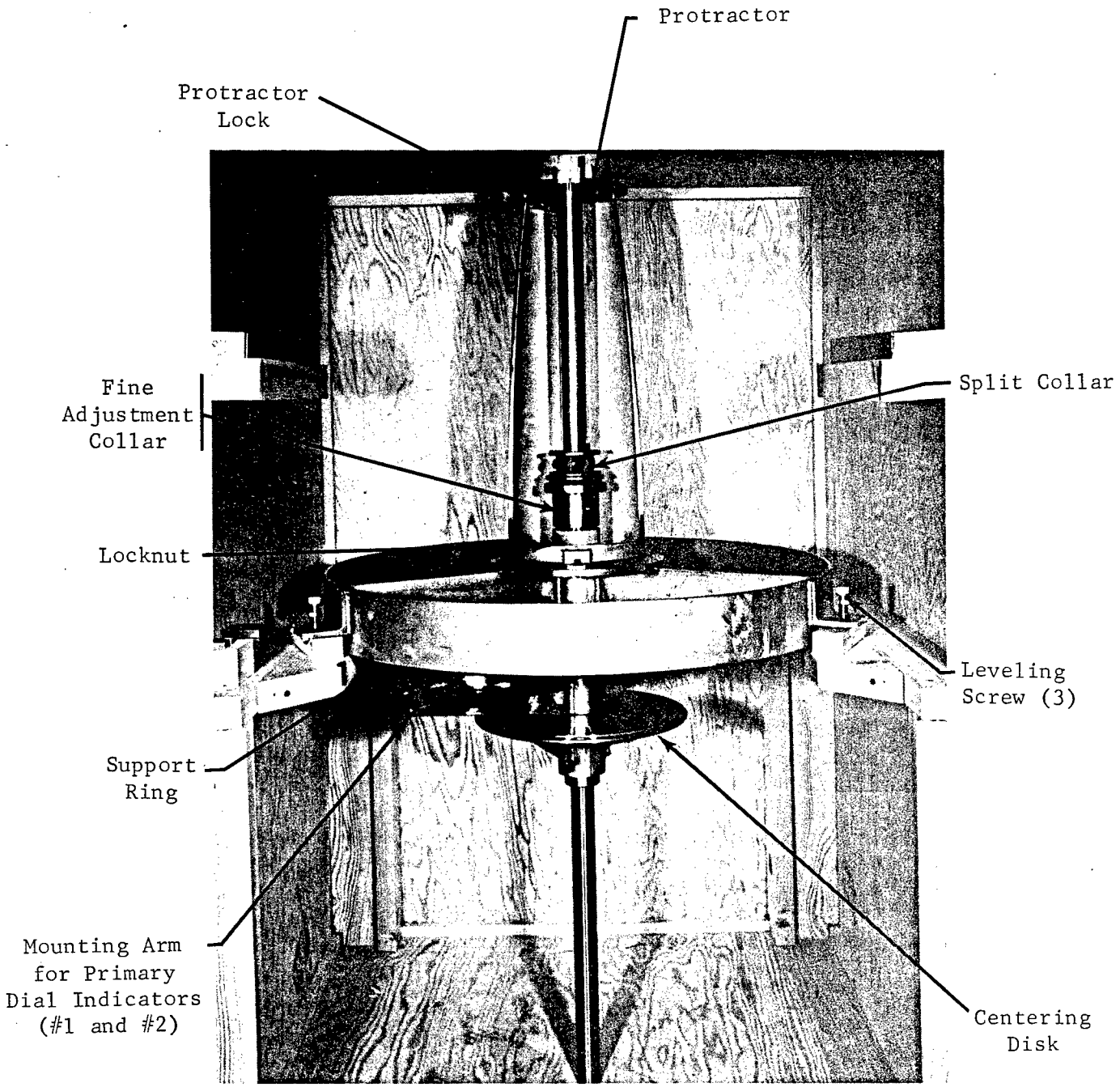


Figure 166. Check Gage, Truncated Mosaic Radome Firing Tool

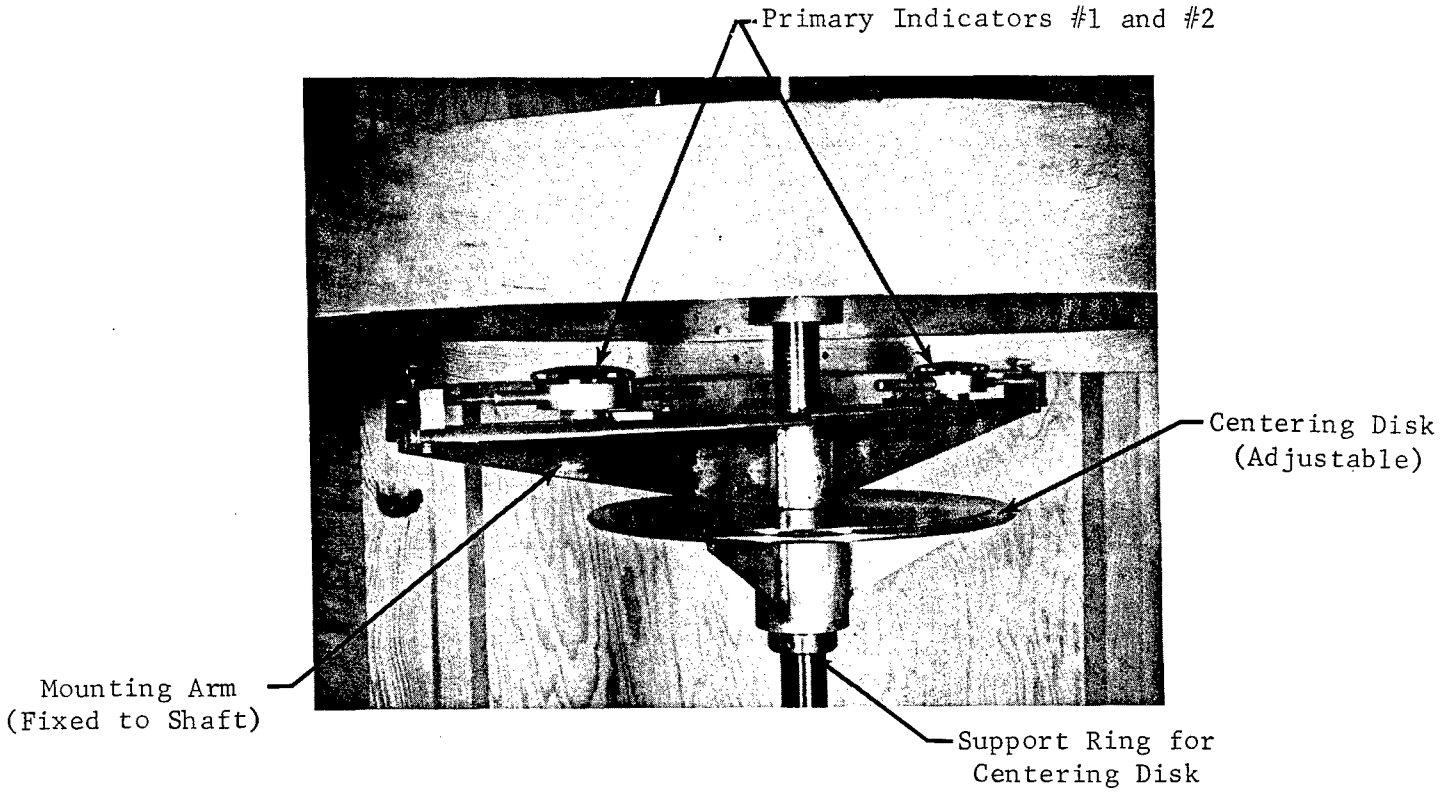


Figure 167. Check Gage, Mounting Ring and Movable Indicator Arm

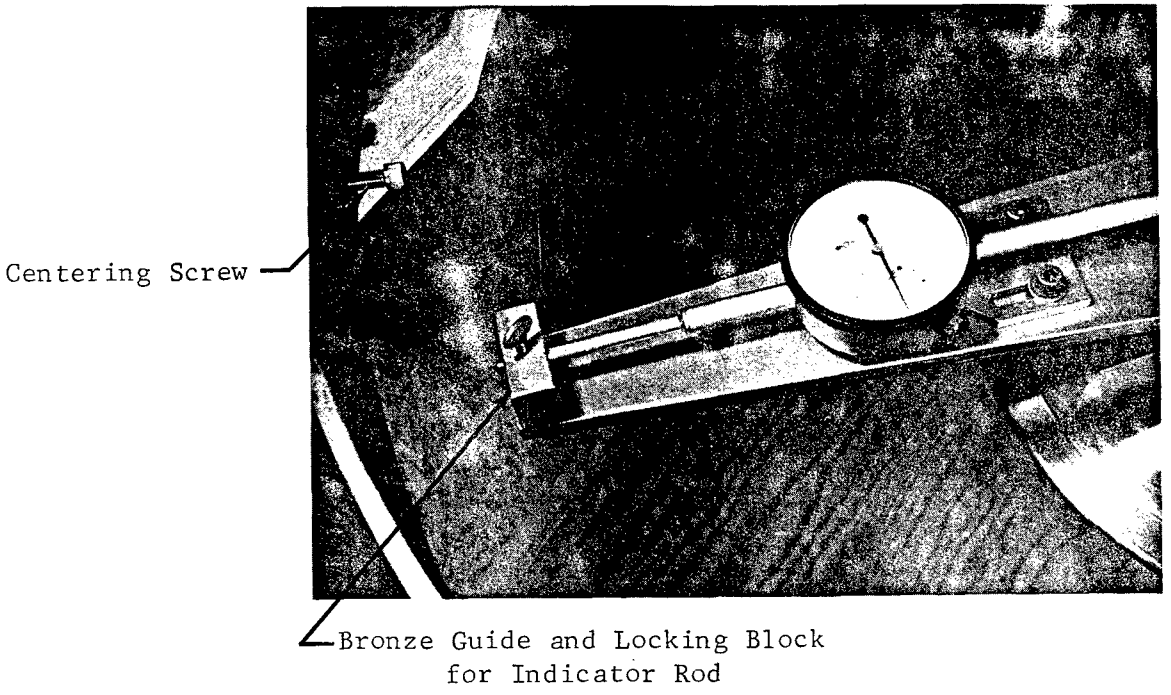


Figure 168. Detail Check Gage Indicator Arm

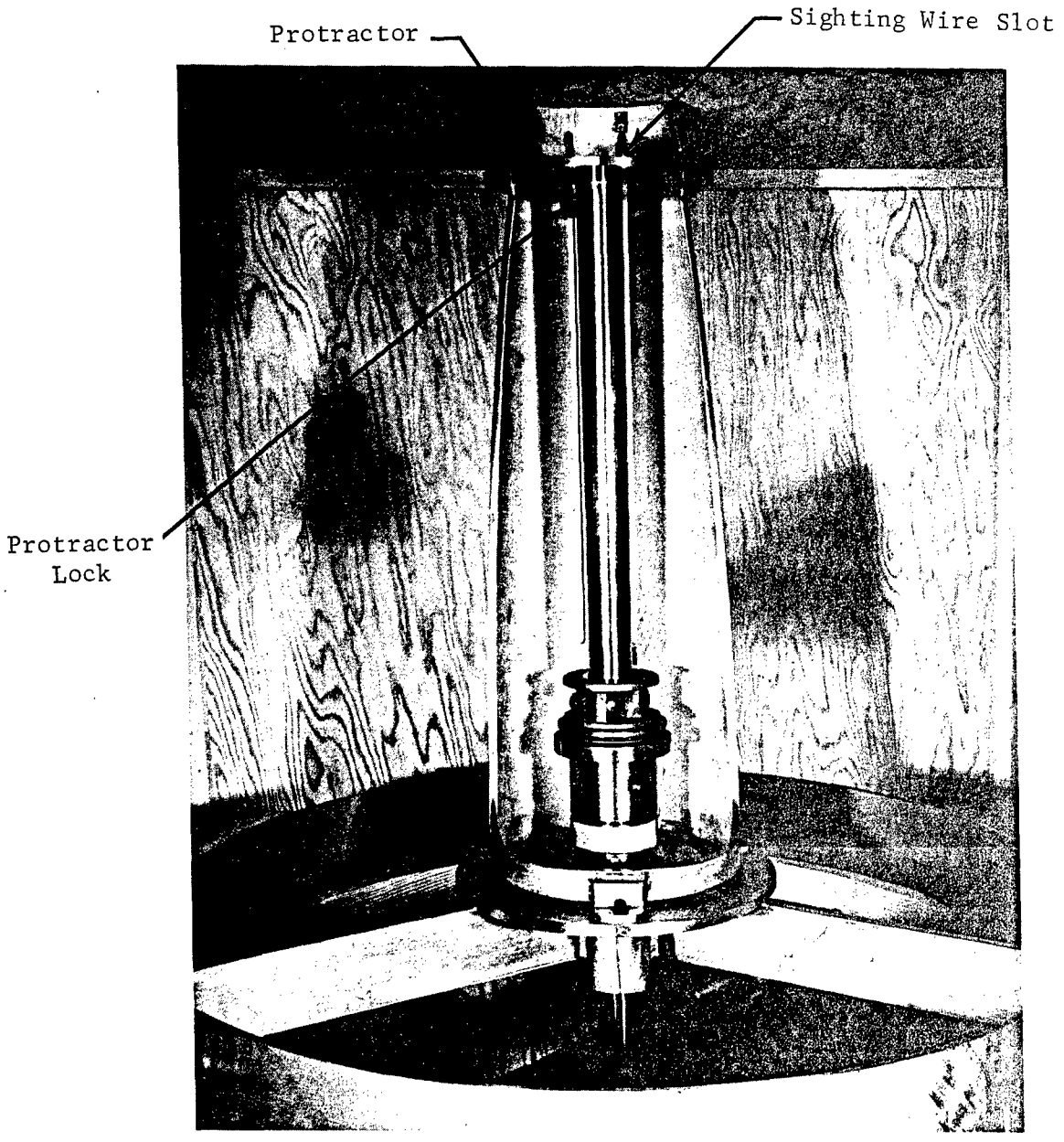


Figure 169. Check Gage, Calibrating Head

b. Place the ball tip of the universal indicator in contact with the horizontal face of the shoulder and adjust the indicator to zero.

c. Sweep the mounting arm 360 degrees while monitoring the universal indicator.

d. Adjust the leveling screws and rotate the mounting arm until the universal indicator shows no deviation.

6. Tighten the leveling screw locknuts and remove the universal indicator.

Note: Due to the porosity of the firing tool, it will be necessary to use shim stock between the wall and the tip of the dial indicator whenever taking measurements. Obtain 0.002-in. brass shim stock for this purpose.

7. Lower the centering disk on the shaft until it is wedged in position against the walls of the firing tool.

8. Check rotation of the dial indicator supporting arm. If it does not move freely as before, then the gage is not centered. Adjust centering screws until the arm swings freely (without binding or difficulty).

9. Make the final centering adjustment as follows:

a. Position the No. 1 dial indicator in line with one of the centering screws and take a reading.

b. Rotate the arm 180 degrees and take another reading with the No. 1 indicator. If it registers the same as before, then the gage is centered between the two measured points. If the readings are different, then adjust the centering screws until the indicator reads the same between the two points.

c. Repeat 9.a and 9.b with each of the centering screws until the indicator reads the same at all measured points.

Note: Elevation of indicators is done by loosening the two screws on the shaft split-collar, raising or lowering the shaft until the approximate required elevation is obtained, retightening the screws, then making the final adjustment with the fine-adjustment collar located just below the split-collar.

10. Adjust the shaft elevation until the dial indicator rod points are a known distance from the horizontal face of the reference shoulder as follows:

a. Place the Trans-Check height gage in a convenient location and zero it to 0.250 in. above the shoulder (use gage blocks positioned on shoulder).

b. Elevate the shaft until the top of the indicator rods are at the same level as the gage blocks (as indicated by getting a zero reading on the height gage when an indicator rod is positioned under the height gage transducer arm).

c. The point of each indicator rod is now known to be at an elevation above the reference shoulder that is equal to 0.250 in. minus the radius of the dial indicator rod.

11. With the gage adjusted to a known elevation with respect to the reference plane (shoulder), any other desired elevation can be obtained as follows:

    a. Place the Trans-Chek height gage in a position where the top of the shaft can be reached with the transducer arm.

    b. Select the combination of gage blocks that equal the required change in elevation.

    c. Zero the height gage to the top of the shaft.

    d. Lower the shaft until the selected gage blocks can be placed on top of the shaft without touching the height gage transducer arm. (The shaft position is slightly lower than the elevation desired.)

    e. Elevate the shaft with the fine adjustment collar until the height gage reads zero. This indicates that the desired elevation has been obtained.

12. Rotate the shaft until the 0-degree mark on the protractor is in line with the sighting wire and lock in position.

13. Make a reference mark on the firing tool in line with the centerline of No. 1 dial indicator.

14. Record measurements for every 60 degrees of rotation and a minimum of three elevations.

DIMENSIONAL ACCURACY OF FABRICATED RADOMES

Circularity measurements of fabricated mosaic radomes and truncated sections was originally contemplated by a modification of the techniques and firing tool inspection gage. Experience and cursory measurements of fabricated radome sections indicated, however, that achieving adequate circularity by the fabrication technique was not a problem. For this reason, the time and expense of modifying the inspection gage and accurately determining radome dimensions was not considered warrented. Circumference measurements (and radii) plus wall thicknesses and butt joint widths were determined by tape and caliper measurements and are included as appropriate in the discussion of results of fabricating the various radome sections and the full-scale radome. Rough circularity determinations made on truncated radome sections by profile tracing techniques indicated a general degree of circularity of at least ±0.03 in. On the basis of this information and the experience obtained, it appears that the original goals of maintaining contour and out-of-roundness within ±0.015 in. are feasible with this fabrication technique.

SECTION XIII

ENGINEERING TEST PROGRAM AND RESULTS

The purpose of the engineering test program was to evaluate the thermostructural capabilities of the composite mosaic radome structure under simulated conditions and to demonstrate the validity of the analytical techniques employed during the design and analysis phases of the program.

Initial plans under the program called for structural testing of truncated radome base sections, with and without base attachment fixtures, to provide preliminary experience and data for subsequent room temperature and elevated temperature structural testing of a full-scale radome. A more detailed analysis of the objectives and problems associated with testing of such ceramic structures resulted in some modification of these initial plans. It was recognized that thermal shock resistance of the alumina ceramic body could possibly prove to be a limiting factor in the utility of such a ceramic radome for high-temperature operation. Since analytical thermostructural investigations indicated that the thermal gradient across the radome wall thickness would be the critical parameter, it was decided that a thermal gradient test was desirable to determine the capability of the alumina mosaic structure in this regard. One of the truncated base sections was therefore utilized for such a thermal test.

It was also essential that the structural strength or integrity of the mosaic alumina structure be determined to indicate its ability to withstand the expected operational stresses and to experimentally check the analytical techniques and assumptions employed in the design. In view of the slight decrease in strength expected in the bonded alumina structure between room temperature and the design operational temperature of 1000°F, it was determined that elevated temperature structural testing was not essential for this initial test program. The test plan which was accomplished, therefore, included a room temperature cantilever beam test of a truncated section without base attachments and a similar test of a full-scale radome with base attachments. These two tests were to provide at least a first approximation of the load-carrying capability of the bonded mosaic alumina radome structure and an indication of the efficiency of the base attachment fixture design.

Statistically meaningful strength data should, of course, not be expected from a limited number of tests on such a brittle material which normally exhibits a wide scatter in mechanical property values.

THERMAL GRADIENT TESTS

Complete ground simulation of the aerodynamic heating condition for a large radome structure at supersonic speeds was not considered feasible. Even the simulation of analytically computed heat fluxes would require large-scale test facilities with highly sophisticated instrumentation and control capabilities. Such test simulation of aerodynamic heating conditions was beyond the scope of this program.

The results of the analytical thermostructural investigation indicated that the thermal gradient across the wall thickness was the only critical parameter causing significant thermal stresses. This observation made it possible to submit the radome structure to a simple, yet meaningful, thermal test. The test was designed to produce thermal gradients of varying magnitudes across the wall of a truncated radome base section by various degrees of thermal cooling.

The test structure shown in Figure 170 was installed on a wheel-mounted platform in front of a large over capable of approximately 500°F operation.

A 20-in. high truncated radome base section (No. 4) was instrumented with six pairs of differential thermocouples to measure wall gradient and three thermocouples to measure external surface temperatures. These thermocouples were located in groups of two differental readings and one direct reading approximately 120 degrees from each other around the circumference. One of these groups is visible in the photograph of Figure 170.

The top and bottom openings of the truncated section were covered by ½-in. thick asbestos boards to reduce the heat transfer from the internal surfaces.

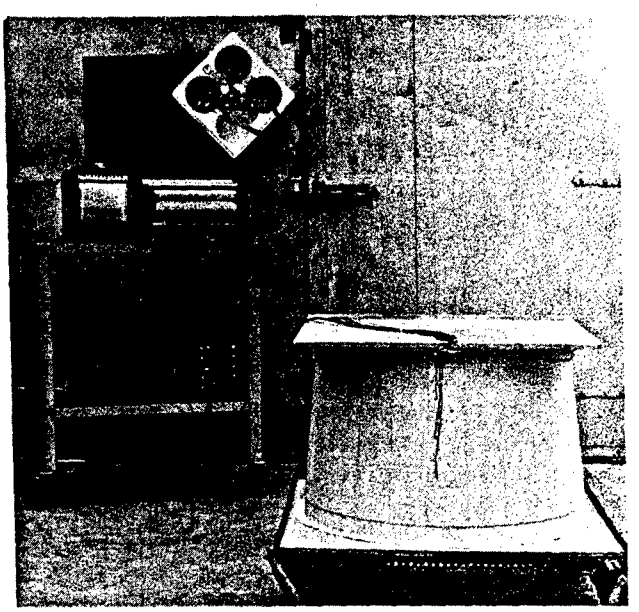


Figure 170. Thermal Shock Test Setup of Truncated Mosaic Radome Section

Test Procedure

The thermal shock tests up to approximately 500°F were conducted by rapidly inserting the test structure into the preheated oven at the desired temperature, holding it until the wall temperature readings became uniform and stabilized, then rapidly withdrawing it for cooling under atmospheric conditions. The higher temperature tests were conducted by heating the specimen slowly in the ceramic kiln to the desired temperature, then rapidly removing it from the kiln. All thermocouple readings were monitored for several minutes at the beginning of each heating and cooling cycle. Approximately 10 seconds were required for insertion or removal of the test item either into or from the hot chamber.

Test Conditions and Results

A summary of the six heating and cooling cycles is presented in Table 35. The first three heating cycles were performed in a circulating air oven and the second three tests in the large gas-fired kiln. In the case of Runs Nos. 4 through 6, the test structure was heated up slowly with the kiln as previously mentioned. This procedure was employed in these later cases to minimize thermal shock damage to the kiln refractories. No temperature gradient

TABLE 35

THERMAL SHOCK TEST CONDITIONS

Test No.	Max. Equilibrium Wall Temp, °F	Heating ΔT Max.	Cooling ΔT Max. @ Time t
1	250	5°F	10°F @ t = 20 sec
2	475	13°F	35°F @ t = 17 sec
3	510	13°F	49°F @ t = 45 sec
4	765	Not recorded	61°F @ t = 75 sec
5	1026	Not recorded	101°F @ t = 65 sec
6	1500	Not recorded	Est 130°F* @ t = 30 sec

* Failure occurred while partially removed from kiln ΔT had large amplitude oscillations at approximate time of failure.

recordings were made during heating. The cooling cycles were conducted, in all cases except No. 3, under free atmospheric conditions with only a slight natural breeze. Three large fans were used in Run No. 3 to provide increased air movement over the external surfaces and to produce a greater thermal gradient in the radome wall.

Several distinct pings were heard during the cooling cycle in Runs Nos. 4 and 5; however, no cracks or evidence of failure could be found. A die-check inspection of the total truncated section between Runs Nos. 4 and 5 did not reveal any external cracks. The pings may have been due to localized tensile failures in the adhesive butt joints between tiles.

Difficulties were encountered in removing the truncated section from the kiln in Run No. 6, due to fracture and warping of the asbestos board beneath the test structure. As a result, the section was quenched while it was partially inside the furnace, with one side being exposed to cooling air through the open door. A vertical crack occurred on the exposed side approximately 30 seconds after the door was opened.

The failed section is shown in Figure 171. The vertical crack in the front was apparently the primary failure, and there was a hairline secondary crack on the back side. The tiles remained mechanically interlocked at the secondary crack.

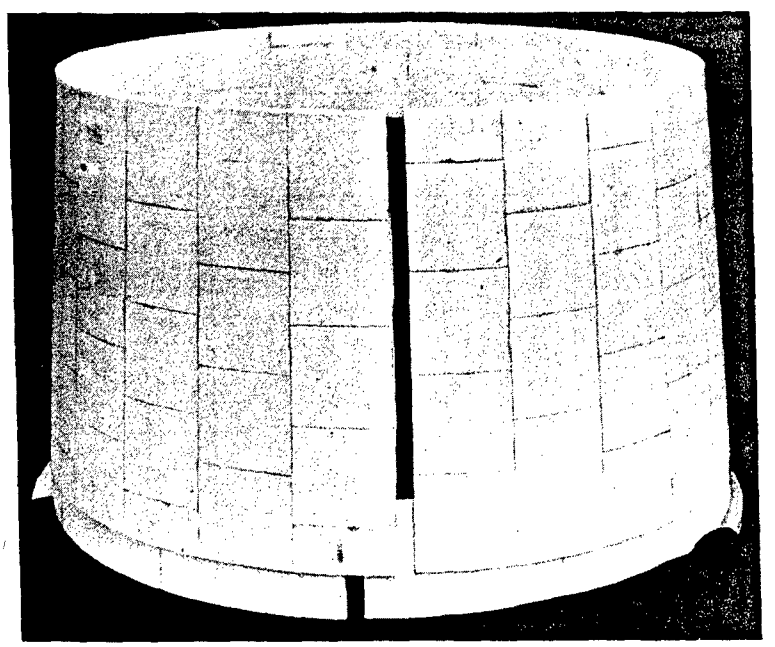


Figure 171. Thermoshocked Truncated Test Section

Conclusions

The combined results demonstrated that the composite mosaic radome structure can withstand a thermal gradient in excess of 100°F across its wall thickness when the average wall temperature is above 1000°F. This is over three times the maximum gradient of 30°F expected at any point in the tile array under the assumed Mach 5 flight trajectory profile. The actual thermal gradient at failure cannot be determined accurately due to oscillations in the differential thermocouple readings prior to failure and to the uncertainty of the exact failure time. However, a maximum gradient of 130°F was recorded during the first 30 seconds from the time the furnace door was opened for Test No. 6.

A close correlation can be drawn between the experimental results of the thermal shock test and the analytical predictions of the thermostructural analysis. Considering the estimated thermal gradient at failure to be 130°F and the ultimate tensile strength of the alumina tile to be at least 15,000 psi (at 1000°F temperature), the thermal stress per unit gradient can be computed:

$$\frac{\sigma_T}{\Delta T} = \frac{15,000}{130} = 115 \text{ psi/°F}$$

The computer analysis of the critical tile cross section resulted in a

$$\frac{\sigma_T}{\Delta T} = 166 \text{ psi/°F}$$

for a quadratic temperature gradient profile.

The comparison between the experimental and analytical results indicated that the computer analysis of a critical tile section was slightly conservative; i.e., according to the analytical study, the structure should have failed at a gradient of approximately 90°F (assuming the same material strength), rather than at the gradient of 100°F+ which was actually obtained. The major assumption used in the analytical computations was a completely adhesive-free butt joint between tiles, unable to transfer tensile or compressive loads. In actuality, however, there was at least partial end-to-end bonding between the tiles, and some load was certainly carried in tension and compression, in addition to the primary shear load transfer of the lap joints. This additional load transfer mode explains the redution in the predicted stress concentrations in the tiles. In general, however, the correlation with Narmco's analytical calculations and with normal thermal shock behavior of high-strength alumina ceramics is considered excellent.

STRUCTURAL TESTS AND EVALUATION

Structural analysis and design studies for the large mosaic ceramic radome (see Section IV and Appendixes VI and VII) indicated that the combined stresses due to external dynamic pressure, gust, and inertia effects plus acoustic loadings would be within the expected attainable strengths of the dense, high-strength alumina. The maximum radome wall stresses which could be expected are summarized in Table 36.

TABLE 36

MAXIMUM STRESSES AT STATION 0 (RADOME BASE), PSI

Stresses	Gust Loads	Dynamic Pressure	Acoustic Loads	Resultant
Longitudinal	±312	-1300	±155	-835 -1765
Circumferential	--	-600	--	-650
Shear	±128	--	±64	±192

These stresses would have to be added to the thermal stresses produced by aerodynamic heating and cooling, as discussed on page 271 . It should be noted, however, that the thermal stresses would be relatively minor at the radome base where the structural loads are at a maximum and the critical thermal and structural loads should not occur simultaneously during the flight profile. The total or algebraic sum of the structural loads produce the calculated maximum bending moment at the base (M_{max}) of 310,000 in.-lb, and the maximum shear load (V_{max}) of 5,770 lb to which the radome would likely be subjected under the assumed operational conditions. These values were therefore used as the design objectives in the program. More extensive combined thermal and structural testing under closely simulated operational conditions would, of course, be necessary to arrive at firm design factors for this type of a radome structure.

In summary, the purpose of the structural test program was to substantiate the structural integrity of the mosaic tile radome structure and to verify theoretical design approaches used under an overall bending and shear load. Since the complete load spectrum due to supersonic flight is difficult to duplicate in a static test, a constant shear and uniformly increasing bending moment was employed. These loads cause stresses at the base of the radome which are representative of the stresses caused by flight, inertia, and acoustic loads.

Truncated Section Test

Truncated radome base section No. 2 (reference Section X) was selected for structural testing. The main objectives of this test were to evaluate the integrity of the ceramic adhesive bonding and to verify the stress concentrations in the mosaic tile overlap areas as calculated in the computer analysis (see Appendix IX). The truncated section mounted on the test fixture prior to testing is shown in Figure 172. Details of the test fixture construction are shown in Narmco Drawings NR 63-060, NR 63-199, NR 63-120, NR 63-121 in Appendix X. The section was mounted on the test fixture support plate and loading tube by casting in epoxy resin between concentric 2-in. aluminum angle rings. The aluminum rings (top and bottom) were first bolted to the loading fixture components with intervening rubber gasket rings 0.5 in. thick and having a hardness of 65 Durameter reading. The section was then positioned in the rings and cast in place with an air-setting epoxy resin. This mounting procedure reduced the probability of undesired residual stresses and stress concentrations in the alumina section.

This truncated radome section was 20 in. high and had a uniform wall section without base attachment tiles. The geometry of the test setup was adjusted by using a steel loading tube of such a length as to produce the desired ratio between bending moment and shear load (310,000 in.-lb to 5,770 lb). The distance between the base plate surface and the point of load application was 53.8 in. which, after subtracting for the bottom rubber gasket thickness (0.5 in.), gave a true moment arm of 53.3 in.

The loading was accomplished in approximately 500-lb increments, with a few minutes pause between increments to permit optical observation and photographing of the photostress material (see page 279). Failure occurred at 5,700-lb load. The total elapsed time from initial load application to failure was about 1 hour due to the previously mentioned pauses in loading. As shown in Figures 173 and 174, the failure was in tension which apparently initiated approximately 2 in. above the mounting ring on the tension side of the section (right-hand side of the photograph in Figure 174). No evidence of bond failure was found. There was some tendency for the crack to follow tile joints, but this was not as pronounced as might have been expected.

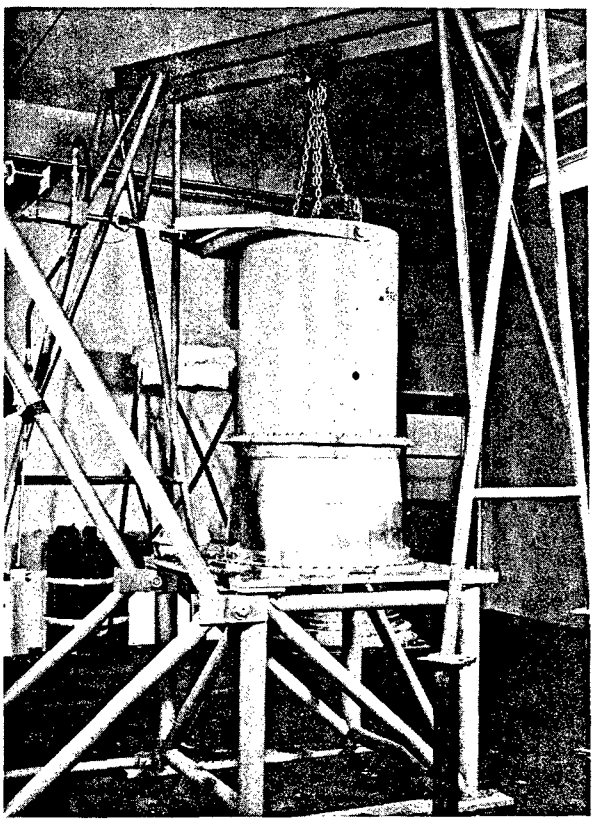


Figure 172. Truncated Section Test Setup

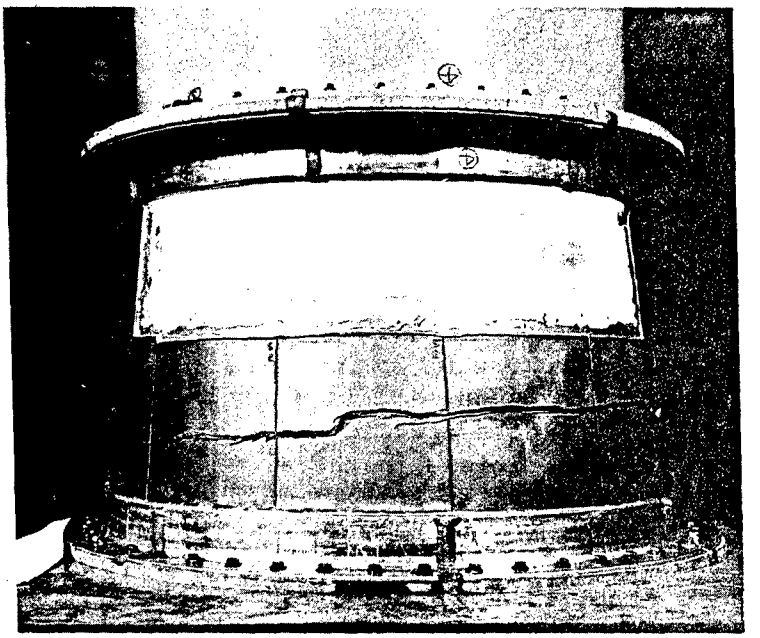


Figure 173. Failed Truncated Radome Section

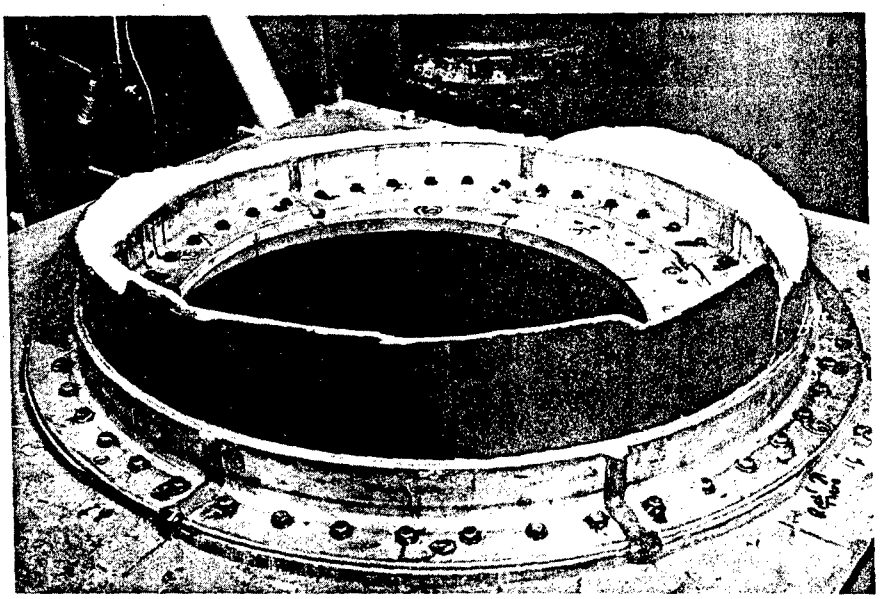


Figure 174. Failed Truncated Section

With a failure load of 5,700 lb, the corresponding shear load, bending moment, and maximum wall stresses in the section near the base, utilizing the design wall thickness of 0.221 in., were as follows:

1. Shear = V = 5700-lb Constant

2. $\text{Moment}_{\text{Base}} = M_B = 5700 \times (53.3) = 303{,}810$ in

3. Base Radius = R_B = 15.85 in

4. Base Thickness = t_B = 0.221 in (Constant)

5. Maximum Shear Stress at Base:

$$f_s = \frac{V}{\pi R_B t_B} = \frac{5700}{\pi (15.85)(0.221)}$$

$$f_s = \frac{5700}{11.00} = 518 \text{ psi}$$

6. Maximum Bending Stress at Base (Tension Side):

$$f_t = \frac{M R_b}{I_b} = \frac{303{,}810 \times 15.85}{\pi \times 15.85^3 \times 0.221}$$

$$f_t = \frac{4{,}815{,}390}{2{,}765} = 1{,}740 \text{ psi}$$

Assuming a stress concentration of 9 at the tile joints (reference Section IV):

$$f_t = 1740 \times 9.0 = 15{,}660 \text{ psi}$$

This exhibited strength is considered in good agreement with the tensile allowable for the alumina material from which the mosaic section was fabricated.

As was noted regarding the above calculations, the moment arm was taken from the load application to the base of the tiles. Consequently, the moment obtained is not truly representative of the moment at which the tensile failure initiated. An alternative would have been to take the moment arm to the point where the crack initiated; however, the exact point of failure initiation is not available from the test result. It is a valid and logical assumption that the mounting rings add to the stiffness of the base of the

truncated cone producing an end effect, which caused failure to occur a certain distance from the base. Due to these unknown parameters, it is believed that the use of the moment arm R_b to the base of the truncated section should be an acceptable assumption.

The results of the tests indicate that reliable predictions can be made for structural capability by utilizing the analytical techniques developed under this contract. The test results of 15,600-psi failure stress when compared with the design stress of 15,000 psi provides such close agreement that further analytical review of the test results would be redundant. Since the load level, location of failure, and mechanism of failure is as predicted, the validity of the design approach is well established.

Photostress Instrumentation and Analysis

Photostress is a photoelastic stress analysis method which makes it possible to determine the magnitude and direction of the stress distribution on the surface of a structure under load.

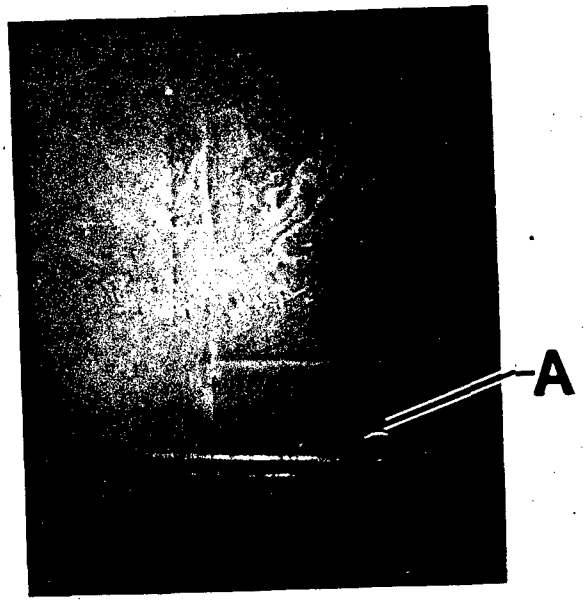
The truncated radome base section was instrumented by photostress coating which consists of thin plastic sheets bonded to the radome by a reflective adhesive. The photostress plastic becomes birefringent when strained and viewed through a polariscope. The colored patterns in the plastic can be interpreted, based on photoelastic principles, to provide the magnitude and direction of the strain at any point in the plastic which is equal to the strain on the surface of the structure being tested.

The results of the photostress analysis of the radome during structural testing were somewhat disappointing. The expected stress concentrations could not be detected from the color pattern because of the very low strain level in the high modulus alumina tiles. Only at loads very close to failure could a definite stress concentration area be identified in one of the tiles adjacent to the bonded attachment rings. This stress concentration area is visible in Figure 175, where the light yellow color represents higher stresses than the darker areas.

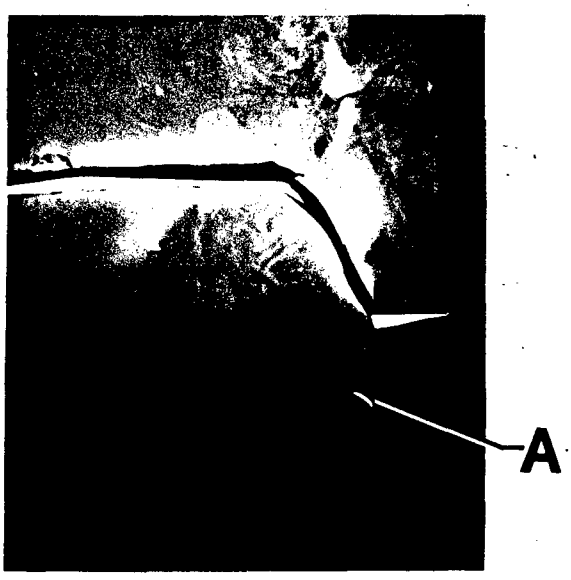
The vertical line of failure indicates that the shear stresses were high at the point A of Figure 175. It is speculated that the failure initiated at this point. The outline of the tile joints is visible in the photostress coating, indicating higher strain levels in the very narrow regions over the tile joints.

Full Scale Radome and Base Attachment

The objectives of the full-scale radome structural test was to obtain additional data on the load-carrying ability of the mosaic ceramic radome structure and in addition to verify the base attachment design. The full-scale radome used for this test was described in Section XI. The test fixture employed and the testing technique was similar to that used for the truncated section structural test. In this case, however, the loading tube was not required since the radome itself was of sufficient length to provide



(a)



(b)

Figure 175. Photoelastic Color Pattern on Stressed Radome

the desired relationship between the shear load and the induced bending moment. Also, the full-scale radome incorporated the special base attachment tiles and was fitted with the Kovar attachment fixtures; therefore, potting in the aluminum mounting rings was not required.

The full-scale radome test setup prior to testing is shown in Figure 176. Note that the load was applied through a 10-in. wide steel band contoured to the radome and bonded to it with approximately 1/8-in. thick epoxy resin. In order to prevent undue distortion and stressing of the radome at the loading point, a 1/8-in. thick steel cone approximately 15 in. long was bonded inside the radome opposite the loading band. This internal cone with appropriate cross members also served as a means of handling and support from the inside and below during mounting and adjustment of the attachment fixtures to the loading plate.

The Kovar base attachments as described in Section IV were affixed to the radome through the use of copper shims. The outer surface of the Kovar attachments opposite the base tiles was wound with three layers of 0.020-in. diameter Kovar wire under 2-lb tension as shown in Figure 77 on page 130. No problems were encountered in the winding operation.

The photostress material was not employed on the full-scale radome and loading was accomplished continuously at a rate of about 3000 lb/minute. Excellent test results were again obtained, with failure occurring at 4300-lb load. As shown in Figure 177, failure occurred in the mosaic tile structure near the base, but not in or adjacent to the base attachment fixtures. The test thus substantiated the base attachment structural analysis and design (see Appendix VI).

A detailed photograph of the failed section (see Figure 178 with the tension side in front) indicates that the failure mechanism was essentially identical to that which occurred at a significant distance from the attachment (approximately 5 in.).

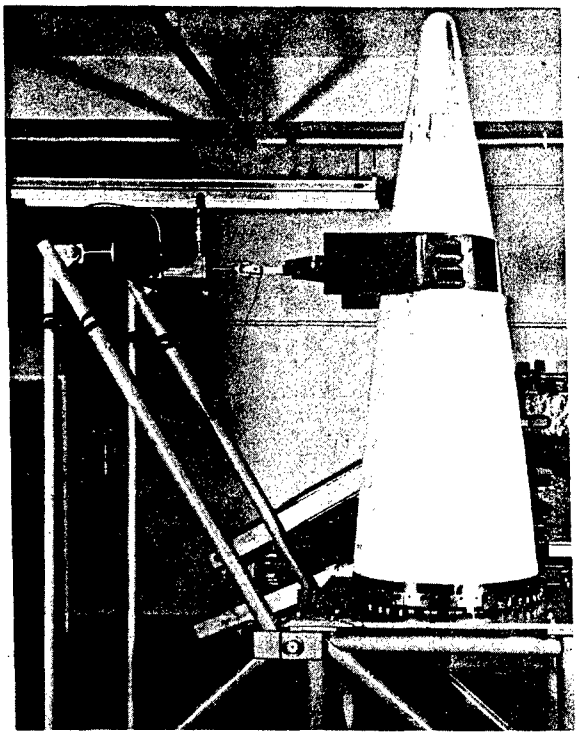


Figure 176. Full-Scale Radome Test Setup

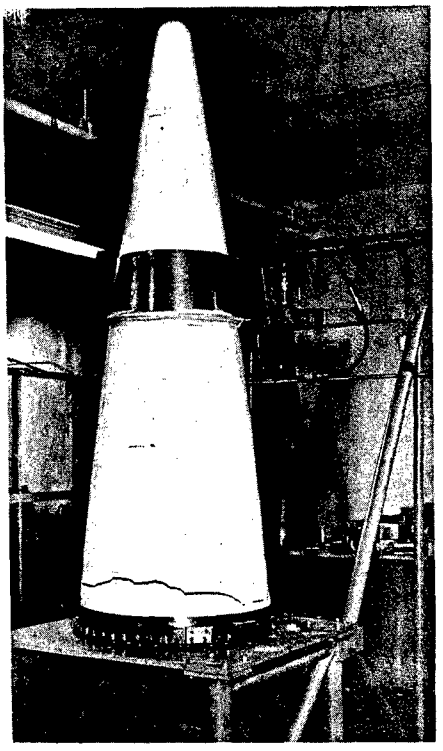


Figure 177. Full-Scale Radome after Test

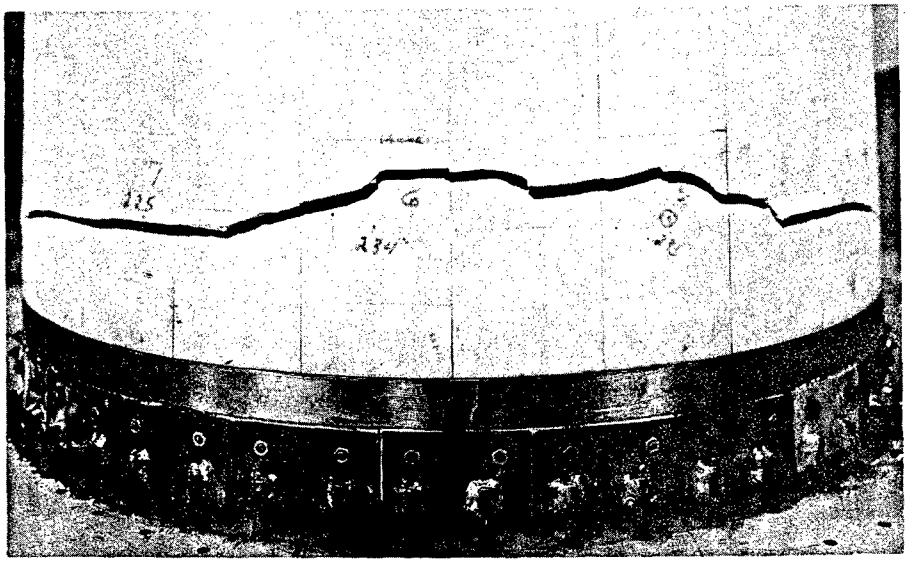


Figure 178. Full-Scale Radome – Failure Detail

The failure load of 4300 lb produces the following stress conditions in the tile section at the base with a design wall thickness of 0.221 in.

Moment at the base:

$$M_B = 4300\ (55.375 - 1.2)^*$$

$$= 4300\ (54.175)$$

$$= 232{,}950\ \text{in.-lb}$$

Tensile stress:

$$f_t = \frac{M_B R_b}{I_b} = \frac{232{,}950 \times 15.85}{2{,}765}$$

$$= \frac{3{,}692{,}260}{2{,}765}$$

$$= \underline{1{,}335\ \text{psi}}$$

Shear stress:

$$f_s = \frac{V}{\pi R_b t_b} = \frac{4300}{11.00}$$

$$= \underline{390\ \text{psi}}$$

The stress conditions at the base tile in the region between the wire wound Kovar attachment and the first outboard tile, where the ceramic wall thickness is only 0.108 in., are as follows:

$$I = \pi R^3 t = 3.1416 \times 15.85^3 \times 0.108$$

$$= 1351\ \text{in.}^4$$

Tension stress:

$$f_t = \frac{M_b R_b}{I_b} = \frac{303{,}810 \times 15.85}{1{,}351} = 3{,}560\ \text{psi}$$

---

* Moment arm in inches minus distance from end of base attachment to load plate.

Structural Test Conclusions

The failing stress for the truncated section utilizing the stress concentration factor of 9 at the tile joints was 15,660 psi. Calculating the full-scale radome failure stress with the same factor would indicate a tile stress of 12,015 psi. The tile was assumed to have a tensile strength of 15,000 psi. The difference in the magnitude of these stresses falls within the normal scatter of test results expected for brittle materials. Also, the joints on the truncated cone were much more uniform than those joints on the full-scale unit, where some slippage occurred between the outer tiles and the inner tiles. There was also more nonuniformity of the adhesive thickness in the full-scale radome. Under these circumstances, it is felt that good correlation was achieved between the analysis and the test results for both the truncated section and the full-scale radome.

The basic reason for testing the full-scale radome was to prove the validity of the attachment design. This, of course, was proven by the failure of the radome structure beyond the point of attachment. The attachment design was based on the philosophy that load must be transferred with a minimum of stress concentration. Since the apparent stress level (stress before applying concentration factor) for the attachment is approximately three times the magnitude of the stress in the failed conical section, it is apparent that a reduction in stress concentration was achieved at the attachment. The results of this test then indicate that the analytical and design approaches described in Section IV are not only valid but sufficiently accurate to be used with confidence.

SECTION XIV

SUMMARY AND CONCLUSIONS

The primary program objective – that of developing ceramic adhesive bonding techniques for fabricating large radomes from small ceramic segments or tiles – was accomplished essentially as desired. Extensive investigative, analytical, and design efforts culminated in the fabrication of four truncated radome base sections and one complete full-scale, ogive radome of approximately 31-in. diameter (at the base) and 8-ft length that weighed over 175 lb. The fabrication technique, which involved tile layup and firing to 2150°F in a fused-silica female firing tool employing differential thermal expansion concepts for dimensional control and bonding pressure, was characterized by a fairly steep learning curve. This is reflected by the fact that with the exception of the first truncated section, all the sections and the full-scale radome were of satisfactory quality for testing. Further quality improvements, primarily with respect to tile joint closure and dimensional control, could have been achieved with additional fabrication experience. However, since no firm Air Force requirement for such large ceramic radomes was currently apparent, and since general feasibility of the basic fabrication concept had been demonstrated, the decision was made not to utilize the remaining ceramic tiles for additional radome fabrication efforts. This decision also involved cancellation of full-scale radome electromagnetic test plans. Such testing, while desirable, was not mandatory at this time to the manufacturing technology objectives of the program.

The mosaic ceramic radome program constituted a radical departure from the conventional concepts of large ceramic component fabrication, and its accomplishment represents significant state-of-the-art advancements not only in respect to ceramic fabrication but also in several supporting technical areas. Significant technical areas which constituted the scope of the program are summarized below along with the pertinent conclusions reached.

MOSAIC CERAMIC RADOME FABRICATION

Coating of the alumina tiles with adhesive slip; layup of the coated tiles in a staggered, overlapping double array on the layup tool; mating into the female firing tool; removal of the layup tool; filling of the interior with bulk Fiberfrax and closure of the tool; instrumentation and firing to 2150°F; plus removal of the finished items, posed fewer problems and difficulties than were anticipated. Technique refinement progressed normally through the fabrication of four consecutive truncated sections, with the result that the first radome fabricated was satisfactory for structural testing.

The results demonstrated that large, high-strength ceramic structures can be made by fusing small segments together with a glassy ceramic adhesive. Such bonded ceramic structures obviously develop appreciable stress concentrations at the segment joints under load conditions; however, these concentrations may not affect the practical design strength of the structure significantly more than the normal defects inherent in brittle ceramic materials.

The thermal shock resistance of the mosaic alumina tile structure is apparently equal and perhaps superior to that of a similar monolithic structure. More comprehensive fundamental investigations would be desirable for a better understanding of the strength and thermal shock resistance of such bonded ceramic structures along with a comparison of these properties with those of similar monolithic structures.

Narmco's conclusion is that the high-temperature bonding together of ceramic segments, using a compatible glassy ceramic adhesive, offers great potential for fabricating large or complex ceramic structures such as radomes, which are difficult or impossible to make by conventional techniques.

FIRING TOOLING

The unique differential expansion tooling concept which was developed and employed during the program utilized the differential thermal expansion between the part and the firing fixture to close the tile joints and to provide bonding pressure at the adhesive firing temperature of 2150°F. The alumina tiles with faying surfaces coated with unfired adhesive were enclosed in the fused-silica (Glasrock) female firing fixture. The high expansion tiles "grew" with respect to the low expansion tool as the temperature was raised. By accurate design and control of both tile and tool dimensions, the differential expansion was used to generate pressure for closing the tile joints as the adhesive became viscous near the top firing temperature. On cooling, the adhesive developed strength rapidly and the formed radome structure contracted away from the tool surface. The inner cavity of the part was packed with a compressible ceramic fiber (Fiberfrax) to provide outward radial pressure during firing and still permit the part to contract without undue restraint on cooling.

Additional procedural developments which contributed to successful tooling construction and use were

1. A two-step tool construction procedure, whereby the tool body was first cast and fired to achieve the small amount of firing shrinkage, followed by backcasting a thin layer of Glasrock slurry on the inside to define a close tolerance working surface

2. The use of a Keltex-graphite parting agent on the plaster tool cores to permit separation of the cast and dried tool

3. The use of graphite cloth as a parting agent during firing to prevent adhesion of the radome adhesive to the tool surface (Prevention of oxidation of the graphite cloth also required use of a nitrogen atmosphere within the tool during firing.)

Two areas of tool performance which were not completely satisfactory included reuse capability of the fused-silica firing tool and the Fiberfrax pack system of developing internal radial pressure on the tiles during firing. These areas are discussed in the text to follow.

The characteristic transformation of fused silica to the cristobalite form occurred sufficiently at the adhesive firing temperature to increase the coefficient of thermal expansion of the tool by a measurable amount. This not only contributed to the tendency of the tool to crack, but also degraded the close dimensional control of the tool, which was required. While these problems were surmountable in this experimental program, the cristobalite formation would not be acceptable in production-type tooling where repeated use is essential. There are two possible approaches for eliminating this problem: (1) the selection of a lower melting adhesive so that the top firing temperature could be reduced below the cristobalite formation temperature of approximately 2000°F, and (2) the use of a different firing tool material such as graphite or one of the low expansion ceramic compositions such as lithium aluminosilicate which have recently been developed for such applications.

While the compressed Fiberfrax bulk fiber served reasonably well as the internal firing tool pressure generating medium, the adhesive bondline thickness between the inner and outer tile layers averaged several mils thicker than desired, and there were slight irregularities in radome surface smoothness from tile to tile. This indicated a need for still more radial outward pressure on the tiles at maximum firing temperature while the adhesive was fluid. It was concluded that this could probably be achieved by a denser packing of the Fiberfrax plus more extensive use of the internal metal pressure ring concept which was utilized near the top of the tool in the vicinity of the base attachment tiles.

CERAMIC ADHESIVE DEVELOPMENT

The magnesium aluminosilicate adhesive (Narmcad 110) selected for use in this program has a firing temperature of 2150°-2250°F. This high-melting adhesive was selected initially to provide a maximum operational temperature growth potential even though the program objective was only 1000°F operation over the tile array with a stagnation temperature at the radome nose of approximately 1500°F. Although this adhesive performed satisfactorily, it now appears that a composition with a lower softening temperature would have performed equally well and would have simplified the tooling and firing operations. It was concluded that development of slightly lower melting point ceramic adhesives, compatible with alumina and having the essential electromagnetic properties, is feasible. For nonradome applications (deep submersible structures, chemical and mechanical system components, etc.), considerably lower temperature adhesive glasses would be practical.

ALUMINA TILE MANUFACTURE

One of the outstanding advantages of the composite adhesive bonding approach to the fabrication of large ceramic structures results from the fact that the small segments can be manufactured, inspected, and selected for uniform properties and freedom from defects. This permits the use of existing ceramic manufacturing technology to produce building blocks for a quality and size of finished ceramic structure (in this case, a radome) not otherwise attainable. The supplier of the alumina radome components (Coors Porcelain

Company) demonstrated that radome quality tiles could be produced in quantity with the required close dimensional tolerances. It is considered that the techniques developed for producing the large number of alumina tiles required (i.e., forming, firing, and grinding), represents a significant advancement in this type of quality ceramic manufacturing technology.

MOSAIC RADOME ANALYSIS, DESIGN, AND TEST CONSIDERATIONS

A considerable portion of the mosaic ceramic radome program was devoted to an analytical study of the thermal and structural stress conditions expected in such a structure in actual operation; to the engineering design of the radome, the tooling, and related manufacturing and test equipment; and to the testing of the mosaic structures produced along with an interpretation of the test results. It is believed that the analytical and design work, which is documented in detail in this report, represents a unique contribution to the literature, and it should serve as a useful guide to any future efforts which may be conducted in this area.

MOSAIC RADOME MANUFACTURING FEASIBILITY AND COSTS

Manufacture of large ceramic radomes by adhesive-bonding mosaic techniques is definitely considered feasible. With further experience and procedural refinements, this manufacturing technology should be adaptable to quantity production of large ceramic radomes. The technique is also considered applicable to the manufacture of other types of ceramic structures where size, configuration, quality, or cost considerations rule out conventional ceramic manufacturing techniques. While any estimate as to probable costs of manufacturing a mosaic alumina ceramic radome of the type developed under this program is highly speculative, some rough approximations may be appropriate. Neglecting initial process development and design costs, assuming that finished radome grinding would not be necessary, and assuming that the firing tooling would be suitable for five reuse cycles, it can be estimated that large radomes could be manufactured in quantity for $30,000 to $35,000 each.

APPENDIX I

LITERATURE REVIEW

NARMCO REVIEW

References on Adhesives

"Adhesive for Extensometer Gages," Societé Francaise de Céramique, Fr. 1, 191, 664; CA, P2602h (1960)

An adhesive composition, resisting temperatures greater than 600°C, and having good electrical-insulation properties, is prepared by grinding to particles of less than 10 μ of at least one bi- or trivalent metal silicate, e.g., kaolin, asbestos, or wollastonite, and heating an equal volume of aqueous 35°Be. Na silicate at 250°C until dry. The product is ground and mixed with 35%-50% of an aqueous alkali silicate solution, e.g., 35°Be. Na silicates. The adhesive is hardened at room temperature, or by heating in an oven at 110°C for 1-2 hours.

"Approximating the Attractive Forces of Adhesion for Glass and Other Surfaces," ASTM Bull, No. 169, 62-6 (1950); CA, 419g (1951)

Contact angle measurements were used to predict polarity and adhesion. Compatibility and subsequent adhesion of materials can be obtained by using a heterogeneous adhesive containing both polar and nonpolar functional groups, which are compatible with dissimilar materials, or single-component materials having a poly-functional mol. with selective affinities. Compatibility between an adhesive and a surface was assumed if approximately the same angles were obtained for the adhesive-coated surface as for a clean surface.

Amberg, C. R., and S. F. Walton (to Exolon Co.), "Ceramic Coating," US Patent 2,544,060, pp 4421-b (1951)

Ceramic coatings are developed to be used as bonding agents or as glazes for refractory materials, such as fused Al_2O_3, graphite, and SiC. The ceramic coatings are frits of MnO_2, SiO_2, and Fe_2O_3 of a general batch composition covering an indicated area in a triaxial diagram and a preferred composition of MnO_2-45, Fe_2O_3-32.5, and SiO_2-22.5%. Mo is added as ferromolybdenum (Mo content 1.2-6% of batch weight) and helps to wet the particles.

Arkesi, K., "The Electron-Microscopic Investigation of Latently Hydraulic Binding Agents," Zement-Klak-Gips, 12 (Hungarian Academy of Science), 414-418 1959); CA, 8025g (1960)

Electron microscopic observations in conjunction with measurements of strength showed that the strength of hydraulic cements is closely associated with a needle-like structure of the crystals. Acicular crystals similar in shape to those found in natural binding agents were observed in the artificial system $Al(OH)_3 + Ca(OH)_2 + SiO_2 + H_2O$.

Buerger, M. J., and E. Wasken, "Cementing Bodies of Plastically Deformable Crystals," US Patent 2,548,344; CA, pp. 5898d (1951)

The bodies and cementing slurry are nonmetallic and inorganic, e.g., CaF_2 or BeO_2. They are heated at a temperature which promotes crystal growth but below the melting point.

Caldwell, O. G., "The Development of High Purity Alumina Laminates with Specific Dielectric Constants," Contract NOas 59-6222C, Gladding McBean and Company, 26 Jan 1961

The fabrication of the laminate was done by assembling the required sheets with a fired cement of nepheline syenite and talc. The mixture was sprayed on each sheet and the total assembly fired to 1250°C (2280°F) on flat alumina plates. During the firing, a weight was placed on each assembly to minimize horizontal shifting of the sheets. The fired adhesive provided a strong bond, as indicated by the success of edge machining without excessive loss.

Cement Binder "Italcementi," Fabbriche Riunite Cemento, Italian Patent 424,351, 28 Aug 1947; CA, P5560d (1950)

In the manufacture of a hydraulic cement binder with good mechanical properties, bentonite is calcined at temperatures of 100°F to 800°F and mixed with slaked lime. The proportions are 90-70 parts of bentonite to 10-30 parts of lime. Gypsum may also be added.

Cornely, Kurt W., "New Cements Prove Suitable for Applications Above 4000°F," Ceramic Age, Jan 1962, pp. 52-53

A cement, Astroceram, which is resistant to high temperatures and heat shock, has been developed. The cement offers a maximum service temperature of 4400°F and it does not react in contact with metals or ceramics. The cements have excellent cohesive properties including a Moh's hardness between 8 and 9. Chemically, the cements are insoluble in hydrochloric acid, nitric acid, phosphoric acid, and sulfuric acid at room temperature. There are two basically different cements available: one can be air-dried and the other must be fired to form a bond. Low porosity compounds of each type are intended for vacuum sealers.

Glass, quartz, zirconia, alumina, refractories, ceramics, and metals have been bonded. The cement may also be used for potting electronics components and for thermocouple protection sheaths. Its dielectric constant is between 7 and 9 at 10^6 cps.

Eastin, W. C., "Magnesium Oxychloride Cement Mix," US Patent 2,549,516; CA, p. 4907e (1951)

The tendency of seawater Mg-O to contract excessively during cure is avoided by the addition of a salt of phosphoric acid having a lower proportion of combined water than H_3PO_4.

"Eccoceram," Emerson & Cuming, Inc.

Eccoceram QC is a highly siliceous cement. It consists of two parts which set up at room temperature when mixed. The product maintains its physical strength and desirable electrical properties up to 2500°F. This cement has a cohesive tensile strength of 800 psi.

"Engelhard CA9R Cement," Charles Engelhard, Inc., East Newark, N.J., ca 1959

CA9R cement offers excellent adhesive characteristics in the temperature range of -420°F to 1000°F. Because of its electrical and thermally insulative attributes, the cement has many uses in the electromechanical field. The cement has a shear strength of 80 psi when used on metal surfaces. It has very good thermal shock properties.

Ershove, L. D., and R. M. Bosman, "The Cementing Properties of Calcium Phosphates Formed in the System $CaO-P_2O_5$," Ukrain. Khim Zhur, 21, 783-7 (1955); CA, 14199h (1956)

The binary system $CaO-P_2O_5$ was studied. At the following temperatures, 600°C, 800°C, 1000°C, and 1200°C, the corresponding compounds are formed: CaP_2O_6, $Ca_2P_2O_7$, $Ca_2(PO_4)_2$, and $Ca_4P_2O_9$. The best cements are the latter two.

Farran, J., "Mineralogical Study of the Adhesion Between Cement Pastes and Aggregate Materials in Concrete," Silicates Inds., 23, 528-34 (1958); CA, 6574b (1959)

Extensive experiments are described in which the reaction of cements on polished surfaces of aggregate mineral grains were examined by direct microscopic examination. The analogy of certain structural planes corresponds to Royer's principles of epitactic intergrowths. Aluminate and Portland cements received attention. For the aluminate cements, no epitaxis phenomenon was noted.

Gitzen, W. H., L. D. Hart, and G. MacZura, "Phosphate-Bonded Alumina Castables: Some Properties and Applications," Am. Cer. Soc. Bull., Vol. 35, No. 6, 15 June 1956

Phosphate bonding of sintered alumina grog using commercial grades of the phosphoric acid. The formation of aluminum phosphate giving a sintered bond was preferred to starting with this material. The result being in higher bond strength, 4000 psi vs 1200 psi for the modulus of rupture using ortho-phosphoric acid and aluminum phosphate, respectively. In admixing the concentrated acid and alumina, kneading or mulling type mixers have been found satisfactory for dispersing the viscous acid uniformly throughout the mixture. For a thickness of 1 inch or less, a curing temperature of 650°F for 4 hours is adequate to develop the permanent bond. Under-curing results in an unstable and hydroscopic bond due to incomplete conversion of pyrophosphoric acid (intermediate comp.) to aluminum phosphate.

Thermal expansion data were obtained on alumina phosphate mixtures as it goes through quartz, tridymite, and cristolite phases. No change in strength observed cycling 100, 200, 300 times through the α - β transition at 200°C to 226°C.

Greger, H. H., "Aluminum Phosphates - New Bonds for Refractories," Brick and Clay Record, 117, No. 2, 63-68 (1950); CA, 10284e (1950)

These phosphates containing approximately one mole Al_2O_3 : two moles P_2O_5 are good inorganic bonding materials at low, intermediate, and high temperatures. Above 1500°C, P_2O_5 volatilizes slowly. The phosphate can be employed in solid form or in aqueous solution. Grog, kyanite, mullite, Al_2O_3, SiC, and chromite can be bonded for use at cone 34 and above.

Jordan, T. G. (Project Manager), "Research on Binder Techniques for High Temperature Radome Structures," Contract No. AF 33(616)8176, General Electric Company, N.Y., ASTIA AD274732

Radomes for 1000°F use, made of silica fibers, glass microspheres, silica microspheres, asbestos fibers, and/or polygorskite paper with aluminum phosphate as the binder. Some promising laminates, very early in their development: October 1961 — January 1962.

Kingery, W. D., "Fundamental Study of Phosphate Bonding in Refractories: I-III," J. Amer. Chem. Soc., 33, No. 8, pp. 239-247, Aug 1950

Three major methods of utilizing phosphate bonding in refractories have been employed. Siliceous material forms a bond with phosphoric acid. For refractory applications, heat treatment is in general necessary for the development of any considerable strength. Certain oxides are reported to react with phosphoric acid, usually at slightly elevated temperatures, to form refractory bonds. Certain acid phosphates have been utilized as refractory bonds.

Except for dental cements, only vague references are made regarding the bonding reactions and bonding mechanisms in refractory phosphate bonds. Properties of phosphate bonds have not been systematically studied. The only data available are for the addition of metaphosphates to fire-clay mortars.

Cold-setting phosphate bonds may be formed from many cations by oxide-phosphoric acid reactions, by phosphate-phosphoric acid reactions, or by the direct use of liquid phosphate bonds. For oxide-phosphoric acid reactions to form bonding materials, a weakly basic or amphoteric cation is required since excess basicity causes violent reactions and acidic or inert materials show no reaction. In all cases, bond formation is due to the formation of acid phosphate. For optimum bond strength, a weakly basic cation having a moderately small ionic radius is required so that a nonordered structure can be formed. A lack of any weak zone on heating this bonding material is noted. This is probably due to the gradual loss of combined water and the gradual crystallization of the dehydration products which also act as bonds. Data on a large number of oxide-phosphoric acid reactions are reported.

In the case of phosphate bonds, the adsorption of phosphates by clay materials offers a new approach to reducing or eliminating bond migration. Bond migration causes variations in mortar and unfired refractory properties owing to variations in bond content throughout the structure.

Leatham, E., and F. E. Lathe, "Thermosetting Refractory Materials," Canadian Patent 592,482; CA, P 13597d (1960)

The basis of the invention is the discovery that low-melting silicates can be used for all types of granular refractories. The nonrefractory silicate must be readily fusible - formation of at least 50% liquid - at 1500°C.

"Melbond Ceramic Adhesive," Melpar, Incorporated, Falls Church, Va., Mar 1961

Melbond CA-100 is a ceramic adhesive with excellent bonding strength when used with refractory materials such as ceramics. Melbond adheres well to Melfoam, dense alumina, pyrophyllite, K-30 brick, Foamsil, and graphite at temperatures up to 2000°F; to dense zirconia up to 1500°F; and to Alumdum, cast MgO and cinder block to 1000°F. This cement has good electrical properties (dielectric constant below 2.5 and loss tangent below 0.04 at room temperature and 10^{10} cps), attains a high degree of mechanical strength and does not flake or disintegrate during use.

"Nucerite," Pfaudler-Permutit, Inc., Rochester, N.Y., 1960

The development of Nucerite holds promise for ceramic-metal applications and new production processes for which existing materials have proved inadequate. Controlled high temperature firings chemically and physically bond the Nucerite ceramic component to metal alloys. Good thermal shock, high impact strength and high temperature stability are the result of closely controlled nucleation and crystallization within a ceramic formulation.

"Phosphate Cement," Oxalloy Co., French Patent 943,944; CA, P3654f (1951)

A phosphoric or phosphorous acid is heated under pressure with a finely powdered oxide in the absence of free water to give a cement. The acid may be replaced by substances which give rise to such acids on heating.

Pitts, J. W., E. Buzzard, and D. G. Moore, "Resistance Measurement of Ceramic-Type Strain Gage Cement,: ASTM Publ. 230 (1957); CA, 5621h (1959)

Electrical resistance of commercial and experimental strain-gage cements were measured over the temperature range 80-1800°F. The specimens were also tested for breaking strength of the cement bond by a bend test at room temperature. Experimental cements of Al_2O_3, SiO_2, and Cr proved better at 1200-1800°F than did others tested.

Pland, H. T., "Development of Inorganic Binders," Contract NOas 58-850-c, General Electric Company, Final Report, 27 Oct 1960

Most of the inorganic bonds investigated could not be tested alone, but only in reinforced laminate specimens. From the inception to its conclusion, this project has almost exclusively used aluminum phosphate cement as bonding matrices for fiber reinforced laminates. Other bonding media were considered and briefly tested, but the results were invariably less promising than those produced by the aluminum phosphate bond. Iron phosphate cements, colloidal silica, magnesium silicate, arsenic-sulfur-tellurium low-melting glass, lead borate glass, and several higher temperature glasses were among those investigated as bonding media for silica fibers.

"Pyroceram Brand Cements,: Corning Glass Works, US Patent 2,889,952, Aug 1960

These cements are a new type of sealing glasses which when fired develop a partially crystalline structure analogous to Pyroceram 9606 and 9608 which results in a devitrified glass seal which is much stronger and harder than original glass. The strong seals are vacuum tight and they may be reheated to their firing temperature during their service. Pyroceram 45 has a maximum service temperature of 700°C (1292°F) and it is compatible with tungsten, molybdenum, several glasses and standard electrical ceramics (includes alumina). Pyroceram has a modulus of rupture at 25°C of 10,000 psi. Its dielectric constant is 6.1 at 1 kc and its loss tangent at 25°C and 1 kc is below 0.002.

Solacolu, S., and D. Serban, "Refractory Alumina Cements," Industria Constructillor si Material, Constructii, 8, 465-72 (1957); CA, 673b (1959)

Al_2O_3-base cements, which do not lose water upon heating, retain a compressive strength of about 100 kg/sq cm. Experimental work on the SiO_2-Al_2O_3-Fe_2O_3-CaO system shows that binders having good hydraulic and refractory properties may be prepared with Al_2O_3 and low SiO_2 and Fe_2O_3 content.

Shoichiro Nagai, J., "Hydraulic Refractory Cement III," Japan Ceram. Assoc., 50, (596), 399-404 (1942), Cer Abst. 1950, 3; in J. Am. Ceram. Soc, 33, No. 1; cf CA 32, 3109 (CA 5385d 1951)

Describes comparative study of Kast-O-Lite (US) and two Japanese samples.

"Solid Aluminum Hydrogen Phosphates," US Patent 2,538,867; CA, P 3133g (1951)

Methods are described for preparing Al-H phosphates having an Al_2O_3 to P_2O_5 ratio ranging from 1.5:3 to 1.85:3 in the form of an amorphous solid at 25°C, which are dispersable in water to produce clear viscous solutions with highly adhesive properties.

Stork, J., and V. Bysticky, "Electron-Microscope Study of the Structure of Hardened Cement," Rev. Materiaux Construct. et Trav. Publ., C, No. 526-527, 173-179 (1959); CA, 1822i (1960)

Photomicrographs of cement paste by the sandwich method of Bernard (Ibid., No. 507, 351-361, 1957) reveal amorphous material and irregular agglomerations of a fibrous crystal structure with numerous rods. The outlines of the hydration products show needles. Some preparations show spherical agglomerations of $Ca(OH)_2$ as a transitory phase.

Terasky, B., "Refractory Compositions," German Patent 1,043,911; CA, P 23247a (1960)

Mixtures of refractory clay and water-soluble aluminum phosphate, such as $Al(H_2PO_4)_3$ in a weight ratio of 1:5 to 4:1 are useful as binders for Al_2O_3-containing agents.

Williams, A. E., "Refractory Concrete and Cements," J. of Refractories, No. 25, pp. 390-400 (1949); CA, 5071i (1950)

The use of aluminous cement with refractory aggregates, preferably aluminous firebrick, produces a concrete of excellent resistance to high and prolonged temperatures. Aggregates of chrome, MgO, and fused Al_2O_3 enable the concrete to withstand temperatures around 1770°C.

Zimmerman, W. F., "Development of a Foamed Alumina Cement," Amer. Cer. Soc. Bull., 38, 97-98 (1959); CA 9604e (1959)

A lightweight, phosphate-bonded Al_2O_3 cement was formed by adding aluminum powder to a mixture of Al_2O_3, aqueous H_3PO_4 and starch. Modulus of rupture was found to be 700 lb/sq in. Refractory applications for temperatures up to 3100°F were suggested.

Recent References on Radomes

Atlas, L., and Nakarama, Research and Development Services Leading to the Control of Electrical Properties of Materials for High Temperature Radomes, WADC Technical Report 59-300, Part III, Armour Research Foundation, Aug 1961

Barnett, R. L., Utilization of Refractory Nonmetallic Materials in Future Aerospace Vehicles, FDL-TDR-64-123, Part I, IIT Research Institute, Sept 1964

Chase, V. A., and R. L. Copeland, Development of a 1200°F Radome, Summary Engineering Report No. 1, Contract AF 33(657)11469, Project 41461, Brunswick Corporation, Oct 1964

Eliason, L. K., and G. C. Zellner, A Survey of High Temperature Ceramic Materials for Radomes, Contract AF 33(657)10519, ML-TDR-296, Melpar, Incorporated, Sept 1964

Fleming, J. D., Fused Silica Manual, Final Report, Contract AF-40-1-2483, Project B-153, Georgia Institute of Technology, Engineering Experimental Station, Sept 1964

Frye, H., and S. Oken, Large Ceramic Radome Manufacture Attachment and Testing, ASD Technical Report 6217-632f, The Boeing Company, Apr 1962

Hallse, R. L., "Materials for Radome Applications," Materials Science and Technology for Advanced Applications, Vol II, Golden Gate Metals Conference, Feb 1964

Kufer, H. E., Jr., N. Bridez et al., Study of Attachments for Brittle Components, Final Report — Phase II, AD 428,202, IIT Research Institute, Nov 1963

Poulos, N. E., C. A. Murphy, and J. N. Harris, Design and Development of an Electromagnetic Window for Air Lift Reentry Vehicles, Technical Report AFAL TR-65-86, Georgia Institute of Technology, Engineering Experimental Station, May 1965

Smoke, E. J., et al., Development of Manufacturing Methods for the Production of Alumina Radomes, Contract NOas-58-872-c, Rutgers, the State University, School of Ceramics, June 1960

Spore, D., Development of Manufacturing Methods for the Production of Alumina Radomes — The Shenango Process for Manufacturing Alumina Radomes, Contract NOas 59-4148c, Shenango China, Incorporated, Aug 1961

Walton, J. D., and N. E. Poulos, Slip-Cast Fused Silica, Technical Documentary Report ML-TDR-64-195, Georgia Institute of Technology, Engineering Experimental Station, Oct 1964

BATTELLE LITERATURE REVIEW

References on Adhesives

Battelle Memorial Institute completed a literature search on ceramic adhesives and large ceramic shapes as requested by Narmco. The most pertinent references are included in the text that follows, along with Battelle's comments and suggestions for lines of future inquiry.

This search was confined to articles appearing during the past 10 years in Chemical Abstracts, British Ceramic Abstracts, and the Ceramic Abstracts section of the Journal of the American Ceramic Society. Refractory cements and mortars, such as calcium aluminate, aluminum phosphate, and sodium silicate compositions for laying up conventional refractories, were specifically excluded.

Abstracts on adhesives, per se, were relatively rare. However, the field of ceramic-to-metal and ceramic-to-glass seals proved fruitful. The reasoning used was that if a substance can be used to bond a metal or a glass and a ceramic together, it should also be useful for bonding two pieces of ceramic together. Ceramic-to-metal seals usually are one of four types, depending on the nature of the interfacial zone. The material in the interfacial zone may be predominately (1) metal, (2) glass, (3) glass containing metal powder, or (4) crystalline and nonmetallic. Battelle's attention was confined to the latter types. It was assumed that the function of metal powder dispersed in a glass is to provide electrical continuity across the seal, and would have little or no effect on the quality of the bonding.

A family of new high-temperature adhesives or cements designated "Astroceram" reportedly has been developed by American Thermocatalytic Corporation (Mineola, New York). According to a news release (Reference 1),* the cement has an extremely low coefficient of thermal expansion, and forms an excellent bond to ceramics, refractories, quartz, and metals. The composition of the cement was said to be proprietary, but based on oxides and silicates of the elements in Group IV of the Periodic Table. Properties reported for Astroceram showed tensile strengths from 10,000 to 15,000 psi, modulus of rupture close to 23,000 psi, and porosities of 0 to 0.2%. The dielectric constant was said to be approximately 9 at 60 cps.

A method for making vacuum-tight seals between Pyrex glass and refractory ceramic tubes (mullite, SiC, or alumina porcelain) has been described by P. J. Kent (Reference 2). The method consists essentially of applying a ring or coating of W-1 glass (G.E., Ltd.) on the surface of a ceramic tube while being heated to a high temperature in a glass sealing lathe. A Pyrex glass tube then could be sealed to the W-1 glass without difficulty. The seals made in this was reportedly could be used at temperatures up to 550°C.

Vacuum-tight ceramic-to-glass seals produced at the Anton Electronic Laboratory (Brooklyn, New York) were reported by N. Anton (Reference 3). In the method used, Corning No. 7570 glass is milled to 100/200 mesh powder and applied as a water-mixed paste to the parts to be sealed. The parts are assembled and heated to fuse in 7570 glass and form the seal.

---

* References are listed on pages 302-306.

A German patent (Reference 4) has disclosed a method of fusing (sealing) alumina blanks with glass. A glass having a thermal expansion coefficient greater than that of the Al_2O_3 and a "transformation point" greater than 540°C is needed. The Al_2O_3 blanks are covered with thin glass fibers before fusion to the glass.

A method reported for sealing glass to 0.5-in. diameter sapphire tubes involves the use of three different glasses (Reference 5). A thin zone of Corning 1826 powdered glass is fused onto the sapphire. This is followed by a band of Corning No. 7280 and a band of Corning 3320 Canary glass. The latter glass then may be sealed with ease to No. 7740 glass. Step-by-step operation for making the seal is outlined in the referenced article.

A method of joining insulator sections of glass or ceramic material by use of soft glass is disclosed in US Patent Application 204,514 (Reference 6). The glass is composed of PbO 70-92%, B_2O_3 6-15%, BaO and/or CaO and/or SrO 2-15%, and Al_2O_3 and/or TiO_2 and/or SiO_2 0-5% by weight. It becomes sufficiently plastic to flow and form a contact with the insulator sections at about 450°C. In another patent (Reference 7) by the same inventor, a method is disclosed to form a glass or ceramic insulator by joining two or more sections by use of a soft (soda-lime) glass.

A glass composed of PbO-70, B_2O_3-20, and SiO_2-10, for joining glass, metal, or porcelain was reported by Tadashi Oshida (Reference 8). Assemblies were formed by heating to 400°-500°C in an argon or nitrogen atmosphere.

An article in the German language (Reference 9) discusses the chemical composition of glasses for vacuum technology and includes a discussion of glass-to-ceramic seals. A composition table for 146 glasses is included. An older article by Knapp (Reference 10) also discusses properties of glasses suitable for sealing glass to ceramics. Important properties of the sealing glasses are their thermal-expansion characteristics and their transformation range. A tabulation of German and Russian glasses for ceramic-glass sealing is given.

A metal-to-ceramic seal formed by fusing a thin layer of porcelain enamel or glass in the area of contact between the two parts is described in US Patent 2,647,070 (Reference 11). The parts to be sealed are first machined to fit, then a thin layer of glass is applied, and the assembled parts are heated to a temperature sufficient to fuse the bonding glass.

Several of the references reviewed deal with methods of metallizing ceramic parts in preparation for joining to metals by soldering. Metallic coattings for this application may contain a fusible glass powder which serves to bond the metal layer to the ceramic.

In a method of bonding tungsten or molybdenum particles to a high-Al_2O_3 ceramic, disclosed in British Patent 656,724 (Reference 12), the preferred glass is Corning 7740, composed of SiO_2-80.5%, B_2O_3-12.9%, Na_2O_3-3.8%, Al_2O_3-2.2%, and K_2O-0.4% by weight. A metallizing mixture disclosed by US Patent 2,924,540 (Reference 13) contains a lead borosilicate glass frit obtained by smelting a batch consisting of PbO-50%, boric acid-35.4%, and SiO_2-14.6%. The glass is used to provide the bond for silver and palladium metal powders applied as a resistance coating on ceramic dielectrics. A method of forming

an electrically conductive joining between metallic and ceramic members is disclosed by US Patent 2,771,969 (Reference 14). The bonding layer consists essentially of glass containing dispersed finely divided particles of silver.

In another type of metal-to-ceramic seal, the bonding layer consists of primarily crystalline oxides. Several abstracts from articles describing this type of seal are cited in the following paragraphs.

A method for manufacturing a seal for vacuum-tube envelopes is disclosed in US Patent 3,023,492 (Reference 15). The seal comprises a pair of sections, at least one of which is a crystalline ceramic with an interface of a crystalline reaction product of a low-alkali borosilicate glass, with MnO_2 and a ceramic oxide (unidentified). The layer also contains metallic particles which form a surface that can be sealed to metal by hard soldering.

A coating to ensure vacuum tightness of Al_2O_3 is disclosed in USSR Patent 106,698 (Reference 16). According the the reference, Al_2O_3 articles after firing are coated with Al_2O_3 and BeO, mixed in a 1:1 molar ratio, then fired several minutes at 1850°C in vacuum or in an inert atmosphere.

A method of metallizing alumina ceramic bodies is disclosed in US Patent 2,820,727 (Reference 17). Coatings of platinum or iridium reportedly adhere well to high-alumina ceramic articles when a bonding layer of alumina mixed with Fe_2O_3 or Cr_2O_3 is applied. The bonding mixture is suspended in polyvinyl alcohol, nitrocellulose, or glycerol and painted on the alumina body. The coating is fired in air at 1200°C to 1600°C. Alumina may constitute 30% to 90% of the binding mixture. About 20% Fe_2O_3 or Cr_2O_3 gives good results when fired at 1500°C. With more Fe_2O_3, a lower firing temperature may be used.

An abstract of a German patent (Reference 18) states that the difficulty of vacuum sealing alumina, MgO, ar BeO to metals is overcome by coating the ceramic with another ceramic of lower melting point. A suggested material is talc, melting at 1300°C to 1500°C.

A high-melting-point seal is disclosed in US Patent 3,036,675 (Reference 19). A seal that maintains its tightness between a metal and ceramic part to 800°C is produced by applying a paste consisting of a double silicate of alumina and potash, mixed with a binder, to the parts to be sealed and heating the assembly under controlled pressure to fuse the paste.

Another reference (Reference 20) describes "high melting" seals that consist of a refractory metal such as tantalum, molybdenum, or Fe-Ni-Co alloy (Kovar) and an insulating ceramic such as sapphire, spinel, or sintered alumina. Seals are formed by application of a powdered mineral such as lepidolite or obsidian mixed with water or a suitable binder and heating in a neutral atmosphere to about 1250°C.

A method of joining sintered refractory bodies is disclosed in US Patent 2,717,225 (Reference 21). Presintered shaped bodies of refractory oxides are joined by holding them in contact with each other and applying a pressure of about 0.5 to 1 ton/sq in. while at a temperature of 1400°-2000°C. BeO, alumina, TiO_2, and MgO reportedly can be joined by this method. No bonding medium was indicated.

Some of the abstracts reviewed refer to methods of producing large ceramic shapes, either as monolithic structures or as sections joined together. Two British patents (References 22 and 23) cover the methods of manufacturing very large ceramic insulators by joining separately formed sections by use of organic adhesives. The techniques employed might be utilized for radome production with the substitution of inorganic adhesives.

An article by M. J. Kofoid (Reference 24) discusses the problem of producing large ceramic radomes in quantity. The author describes the problem of producing large shapes to precise thickness specification, and offers a solution by adding a thin layer of easily ground material to the inner wall, then grinding to the proper "electrical thickness."

A method of forming large, high-alumina ceramic radomes by isostatic processing was reported by R. A. Moultrop (Reference 25). It is postulated that radomes up to 36 in. x 144 in. could be made with proper equipment.

Battelle concluded that the most promising area for further investigation would be that of sealing ceramic members by use of glasses. Probably the simplest first approach would be to experiment with the lead-borosilicate glasses as referred to in References 9 and 14. These are relatively low-melting, and would not require high-temperature furnaces and highly refractory jigs and fixtures. Adhesives having more suitable electrical properties might be a Pyrex-type glass (Reference 13) or an alkaline earth aluminosilicate glass similar to those used as high-temperature glazes for alumina porcelain. Glazes of this type are discussed in an article by Eugene Fisher and Robert Twells (Reference 26).

Cited References (Battelle Review)

1. Anonymous, "Adhesive Takes High Heat and Shock," Missiles and Rockets, 24 Apr 1961, p. 40

2. P. J. C. Kent, "Glass-Refractory Seals," Jour. Sci. Inst. (London), 30, 1953, p. 485

3. N. Anton, "Fused Vacuum-Tight, Metal-to-Ceramic, Ceramic-to-Glass and Metal-to-Mica Sealing by Powdered Glass Techniques," Ceram. Age, 63, No. 6, 1954, p. 15

4. Karl Herald, "Duetsche Gold- und Silber-Scheideanstalt vorm. Roessler," German Patent 1,005,890, 4 Apr 1957

5. L. S. Nelson and G. P. Spindler, "Sealing Glass to Sapphire," Rev. Sci. Inst., 29, 1958, pp. 324-326

6. Eric H. Ball and John E. Stanworth, US Patent Application 204,514; Official Gazette, 658, 1952

7. E. H. Ball and J. E. Stanworth (to British Thomson-Houston Co., Ltd.), "Improvements Relating to the Manufacture of High Voltage Insulators," British Patent 678,811, 9 Oct 1952

8. Tadashi Oshida and Hirohide Miwa (to Kobe Industries Co.), Japan Patent 5328, 16 Oct 1953

9. O. Knapp, "The Chemical Composition of Glasses for Vacuum Technology," Silikattech, 6, 1955, p. 99

10. O. Knapp, "Properties and Classification of Glasses for Vacuum Tubes," Silikattech, 5, 1954, pp. 51-54

11. Charles V. Litton, "Metal-to-Ceramic Seals," US Patent 2,647,070, 28 July 1953

12. "Metallizing High-Alumina Ceramics;" British Patent 884,004 Application 17 Nov 1959, US 19 Nov 1958

13. James B. D'Andrea (to E. I. du Pont de Nemours & Co.), "Vitreous Enamel Resistor Compositions," US Patent 2,924,540, 9 Feb 1960

14. James M. Brownlow (to Gulton Industries, Inc.), "Method for Joining Metallic and Ceramic Members," US Patent 2,771,969, 27 Nov 1956

15. Robert H. Bristow (to General Electric Co.), "Metallized Ceramic Member and Composition and Method for Manufacturing It," US Patent 3,023,492, 6 Mar 1962

16. G. A. Metlin and L. A. Timoshen, "Vacuum Sealing of Alundûm Products," USSR Patent 106,698, 25 July 1957

17. Walter Grattridge (to General Electric Co.), "Metallizing Alumina Ceramic Bodies," US Patent 2,820,727, 21 Jan 1958

18. F. Reinhard, German Patent 930,738; Glas-Email-Keramo-Tech., 6, 1955, pp. 348, 432

19. Robert Benicho, "High Melting Point Seals," US Patent 3,036,675, 29 May 1962

20. Robert Benicho, "High Melting Seals for Metal Structures," French Patent 1,151,151, 21 Jan 1958

21. Albert E. Williams, "Joining Sintered Refractory Bodies," US Patent 2,717,225, 6 Sept 1955

22. "Improvements in or Relating to Electric Insulators," British Patent 716,987, 20 Oct 1954

23. "Improvements in or Relating to Process for Production of Ceramics," British Patent 728,753, 27 Apr 1955

24. M. J. Kofoid, "Ceramic Radome Wall Thickness Tolerance Requirements and Their Interpretation," Bull. Am. Cer. Soc., 37, No. 4, 1958

25. R. A. Moulthrop, "Forming and Manufacturing Ceramic Radomes," Ceram. Age, 68, No. 6, 1956, p. 23

26. Eugene Fisher and Robert Twells, "High Temperature Glazing of Alumina Bodies," J. Am. Cer. Soc., 40, No. 11, 1957, pp. 385-388

Uncited References (Battelle Review)

1. S. S. Cole and K. H. Styhr, "How to Make Beryllia Ceramic to Metal Seals," Ceram. Ind., 75, No. 4, 1960, p. 90

2. H. LaForge, "Ceramic Tube Structure Quality," Ceram. Age, 63, No. 2, 1945, p. 13

3. J. H. Koenig and E. J. Smoke, "Recent Technical Developments in Ceramics and Refractory Materials," Industr. Heat., 24, 1957, p. 1851

4. N. A. Iofis, "Joining Ceramic-to-Ceramic and Glass-to-Metal," USSR Patent 126,728, 1 Mar 1960

5. W. M. Sterry, "Ceramic Holds Key to Aircraft Development," Ceram. Ind., 68, No. 5, 1957, pp. 92-94, 113

6. W. F. Gibbons, "Ceramic Sealing Applied to Engineering Problems," Ceram., 9, No. 117, 1958, p. 8

7. D. Jenkins, "Ceramic-to-Metal Sealing," Electron. Eng., 27, 1955, p. 290

8. F. Moser, "Glass Adhesives," Ceram. Age, 60, No. 4, 1952, p. 31

9. R. J. Bondley and J. H. Westbrook, "Bibliography on Ceramic and Ceramic-Metal Seals," Ceram. Age, 64, No. 3, 1954, pp. 14, 15, 59 (123 references)

10. Jean Caln (to Compagnie Générale de Télégraphie san Fil), "Sealing Ceramic and Its Method of Production," US Patent 2,695,241, 23 Nov 1954

11. V. A. Bochkareva, "Ceramic Bases for Film Resistors," USSR Patent 112,795, 15 Aug 1958

12. Anonymous, "High Temperature Ceramic Seals," Engineers' Digest, 18, 1957, p. 482

13. A. P. Kreshov et al., "Electroinsulating Adhesive Material," Sbornik Ratsional, Predlozhenii Ministerstva Elektrotekh. Prom., USSR, 51, No. 31, 1955. Referat. Zhur. Electrotekh, No. 1990, 1956

14. Hans Neldel, "Sintered Process for the Manufacture of Electrically Insulating Coatings from Refractory Materials, German Patent 825,375, 17 Dec 1951

15. Nitschmann, "Sintered Olivine - A New Material," Technik, 9, No. 4, 1954 p. 232

16. Rolls-Royce, Ltd. and British Oxygen Co. Ltd., "Sealing Ceramics to Metal," British Patent 822,193, 21 Nov 1959 (from Patent Abstr. J)

17. M. Hillier and R. L. Bell, "Aluminosilicate and the High-Temperature Processing of Microwave Vacuum Tubes," British J. of Applied Phys., 9, 1958, pp. 94-97

18. D. W. Luks, "How to Finish Al_2O_3 Ceramics," Ceram. Ind., 67, No. 2, 1956, p. 97

19. D. W. Luks (to Frenchtown Porcelain Co.), "Method of Soft-Soldering to Nonmetallic Refractory Bodies," US Patent 2,848,802, 26 Aug 1958

20. Richard H. Thornton, "Bond Strength and Elastic Properties of Ceramic Adhesives," J. Am. Ceram. Soc., 45, No. 5, 1962, pp. 201-209

21. H. G. Lefort, "Ceramic Adhesives Score in High Temperature Uses: Outperform Organics," Ceram. Ind., 72, No. 4, 1959, p. 98

22. W. Bethge et al., "Durable Mechanical Bond," British Patent 846,570, 31 Aug 1960

23. Anonymous, "BeO at National," Ceram. Age, 76, No. 6, 1960, p. 25

24. H. Schubert, "Contribution to the Technology of Ceramic Bodies of Large Sizes," Sprechsaal, 91, 1958, pp. 533, 556

25. Anonymous, "What is New in Materials," Materials in Design Eng., Nov 1958, p. 141

26. George L. Vincent, "Gulton Pioneers Large-Size Ceramic Capacitors," Ceram. Ind., 78, No. 4, 1962, pp. 66-69

27. N. V. Konetskii et al., "A 1500-ton Hydraulic Press," Ogneupory, 26, 1961, pp. 62-69

28. Arthur Vickers and John Maloney (to Thermal Syndicate Ltd.), "Refractory Cements," US Patent 2,818,345, 31 Dec 1957

29. A. J. Metzger, "Lightweight Ceramics Seen as Ideal for Radomes," Ceram. Ind., 68, No. 6, 1957, p. 122

30. Norton Co., "Ceramic Shells," British Patent 847,449, 9 July 1960 (from Patent Abstr. J.)

31. N. V. Philip's Gloeilampenfabrieken (Arie Bol and Christiaan Klaasen, inventors, "Joining Ceramic Objects to Each Other or to Metal Objects," Dutch Patent 83,997, 15 Jan 1957)

32. M. A. Matveev and A. I. Rabukhin, "The Use of Aluminophosphate Compositions as Heat-Resistant Bonding Agents for the Cementing of Structural Materials," USSR Patent 128,992; Ogneupory, 26, pp. 281-285; CA, 55, 1090g; Greger, CA, 44, 10284e; Stone et al., CA, 50, 7560g; Sheets et al., CA, 52, 15865f, 1961

33. L. H. LaForge (to Eitel-McCullough, Inc.), "Metallized Ceramic Structure for Vacuum Tube Envelopes and Method of Making the Same," US Patent 2,798,577

34. E. J. Smoke and H. T. Smyth, "Work with Dense Ceramic Bodies," Ceram. Age, 69, No. 4, 1957, p. 32

35. H. F. Sterling (to Standard Telephones and Cables Ltd.), "Improvements in or Relating to Uniting Glass or Ceramic Materials to Metal," British Patent 796,398, 6 Nov 1958

36. D. B. McKenzie, "Electrical Materials and Components for Aircraft Power Equipment Operating at High Temperatures," Proc. Inst. Elect. Engrs., 106A, No. 28, 1959, p. 321

37. L. Ya. Mazelev, "The System B_2O_3-BeO-Li_2O in the Glasslike State," Vesti Akad. Navuk Belarus, USSR, No. 3, 1952, pp. 90-99

38. M. A. Matveev and V. V. Velya, "The Hydration of the Simple Lithium Glasses and Their Solubilities in the Hydrated Condition," Steklo i Keram, 17, No. 3, 1960, pp. 18-21

39. P. Best (to Bell Telephone Manufacturing Co.), "Sealing Methods," Belgian Patent 609,058, 12 Oct 1960; British Application 12 Apr 1962

40. W. A. Weyl, "Fundamentals of the Attack of Glasses on Refractory Oxides," Sprechsaal, 95, 1962, pp. 243-250

41. Charles Haber, "Development of Thermally Stable Polymeric Materials," US Atomic Energy Commision NOLC-368, 1957

42. Societe Francaise Radio-Electrique, "Insulating Surfaces," French Patent 991,230, 3 Oct 1951

43. H. Menzel and J. Adam, "Investigations of Borate Glass Systems," Silika-Tech., 2, No. 5, 1951 p. 137; Ceram. Abstr., 1952, p. 200 (in J. Am. Ceram. Soc., 35, No. 11); cf. CA, 46, 6344d and 44, 9645i

44. Kenneth C. Nicholson (toCarborundum Co.), "Silicon Nitride-Bonded Refractory Oxides," US Patent 2,636,828

45. John S. Thompson (to Parker Rust Proof Co.), "Bonding Materials," US Patent 2,702,425, 22 Feb 1955

46. Francesco de Andreis, "Apparatus for High-Frequency Soldering of Dielectrics and Plastics," Italian Patent 474,877, 3 Oct 1952

47. Douglas Peter Dodgson (to Monsanto Chemicals),"Ethyl Silicate," British Patent 722,425, 26 Jan 1955

48. Chihiro Kawashima and Takashi Nakamura, "Heat-Resistant Adhesive from Carborundum," Japanese Patent 1291, 11 Mar 1954

APPENDIX II

STRESSES IN ADHESIVE JOINTS

STRESSES IN ADHESIVE JOINTS

Adhesive joints may be classified into butt, scarf, lap, and double lap joints. The theories on stresses of these joints have been partially developed and are applied in the following analysis.

Theories on lap joints have been given by Galand and Reissner (Reference 1), Carnell (Reference 2), and Sherrer (Reference 3) independently. The theory from Reference 1 should give a reliable result and is applied herein. By neglecting the free-edge disturbances and boundary curvature effects, Lubkin (Reference 4) has established the conditions for a state of uniform stress in scarf joints. The stresses in butt joints may be treated as a special case of scarf joints. An approximate solution for the stresses in double lap joints can be found in Reference 5.

A brief review of the literature shows that no theories can determine the concentrated stresses in scarf joints, which are of the most interest in the present study. Therefore, a method for the determination of such stresses is developed. Supplements to Reference 1, for the stresses produced by concentrated forces to eliminate the surface stresses due to the suggested stress function, are also made such that comparison may be drawn for the optimum joint.

STRESSES IN SCARF JOINTS

If the adherends have identical elastic properties and if the free-edge stress disturbances and boundary curvature effects are neglected, a state of uniform stresses exists along the length of the joint. As shown in Reference 4, the adhesive stresses $\sigma_{n,1}$, $\sigma_{s,1}$, $\sigma_{z,1}$, and τ_1 are respectively given by

$$\left.\begin{aligned}
\sigma_{n,1} &= \frac{F}{t}\sin^2\theta \\
\sigma_{s,1} &= \frac{F}{t}\left[\mu + \left(\frac{\nu_a}{1-\nu_a} - \frac{\mu}{1-\nu}\right)\sin^2\theta\right] \\
\tau_1 &= \frac{F}{t}\sin\theta\cos\theta \\
\sigma_{z,1} &= \nu_a\frac{F}{t}\left[\mu + \left(1 + \frac{\nu_a}{1-\nu_a} - \frac{\mu}{1-\nu}\right)\sin^2\theta\right]
\end{aligned}\right\} \qquad (1)$$

where F , t , and θ are applied tension per unit width, thickness of adherends, and scarf angle respectively (see Figure 1), and where

$$\mu = \frac{E_a \left(1-\nu^2\right)}{E \left(1-\nu_a^2\right)} \tag{2}$$

with E_a , ν_a , E , and ν being Young's moduli, Poisson's ratio of adhesive and adherends, respectively. It is understood that equations (1) and (2) are valid for plane strain problems under the assumptions of negligible free-edge stress disturbances and boundary curvature effects. These effects, however, may be more significant than uniform stresses. Therefore, the stresses that are produced by free-edge stress disturbances and by change of boundary curvature are approximately determined below:

Consider the stresses due to free-edge disturbance. The strains of adherends and adhesive along the S-direction are approximately given by

$$\epsilon = -\frac{\nu F}{E t} \sin^2 \theta, \qquad \epsilon_a = -\frac{\nu_a F}{E_a t} \sin^2 \theta \tag{3}$$

and the total displacements by

$$U = t \epsilon \qquad \text{and} \qquad U_a = t \epsilon_a$$

Then the difference of displacement between adherends and adhesive at three-phase points is in the S-direction

$$\Delta U = U - U_a = \left(\frac{\nu_a}{E_a} - \frac{\nu}{E}\right) F \sin^2 \theta \tag{4}$$

Since no discontinuity in displacement can occur at any point of the joint, concentrated forces and moments have to be produced at three phase points, such that there is a continuity in displacement. Assume now that the displacement difference ΔU is eliminated by uniform forces P per unit length according to the ratio of Young's moduli. Then the stresses of adhesive due to P are

$$\sigma_s = \frac{F E_a^2}{t(E+E_a)} \left(\frac{\nu_a}{E_a} - \frac{\nu}{E}\right) \sin^3 \theta \tag{5}$$

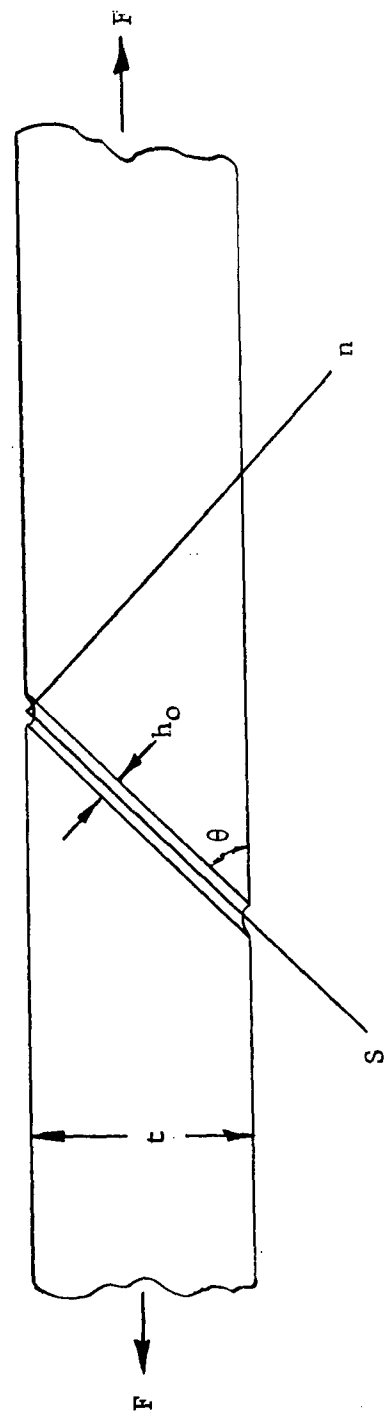


Figure 1. Scarf Joint

Superposing the stress σ_s on $\sigma_{s,1}$ yields

$$\sigma'_{s,1} = \sigma_{s,1} + \sigma_s \tag{6}$$

Assume that the adherents are rigid on the determination of change of the boundary curvature for the adhesive, and that the boundary curve during the deformation is a semi-ellipse, with the center at the midpoint of the free edge before deformation. If the major axis (or the x_1 axis) as shown in Figure 2 is an angle β with the n-direction, and if the semi-axes are denoted by a and b respectively, the equation for the ellipse is given by

$$\frac{x_1^2}{a^2} + \frac{y_1^2}{b^2} = 1 \tag{7}$$

and the coordinates of the three-phase point A by

$$x_A = \frac{h}{2} \cos \varphi , \qquad y_A = \frac{h}{2} \sin \varphi \tag{8}$$

where $$\varphi = \beta + \theta - \frac{\pi}{2} \tag{9}$$

The substitution of equations (8) in (7) yields

$$a^2 \sin^2\varphi + b^2 \cos^2\varphi = \frac{4}{h^2} a^2 b^2 \tag{10}$$

where the values of a, b, and φ (or β) are to be determined. The interfacial line which passes through the point A is represented by

$$y_1 + x_1 \cot \beta - f(\varphi) = 0 \tag{11}$$

where

$$f(\varphi) = \frac{h}{2} \left| \sin \varphi - \cos \varphi \cot \beta \right| \tag{12}$$

By geometrical restriction, the line does not intersect the ellipse below the line AB (or the free edge of the joint). The assumption that the line is tangential to the ellipse requires equations (7) and (11) to be solved simultaneously:

$$a^2 \cot^2\beta + b^2 - [f(\varphi)]^2 = 0 \tag{13}$$

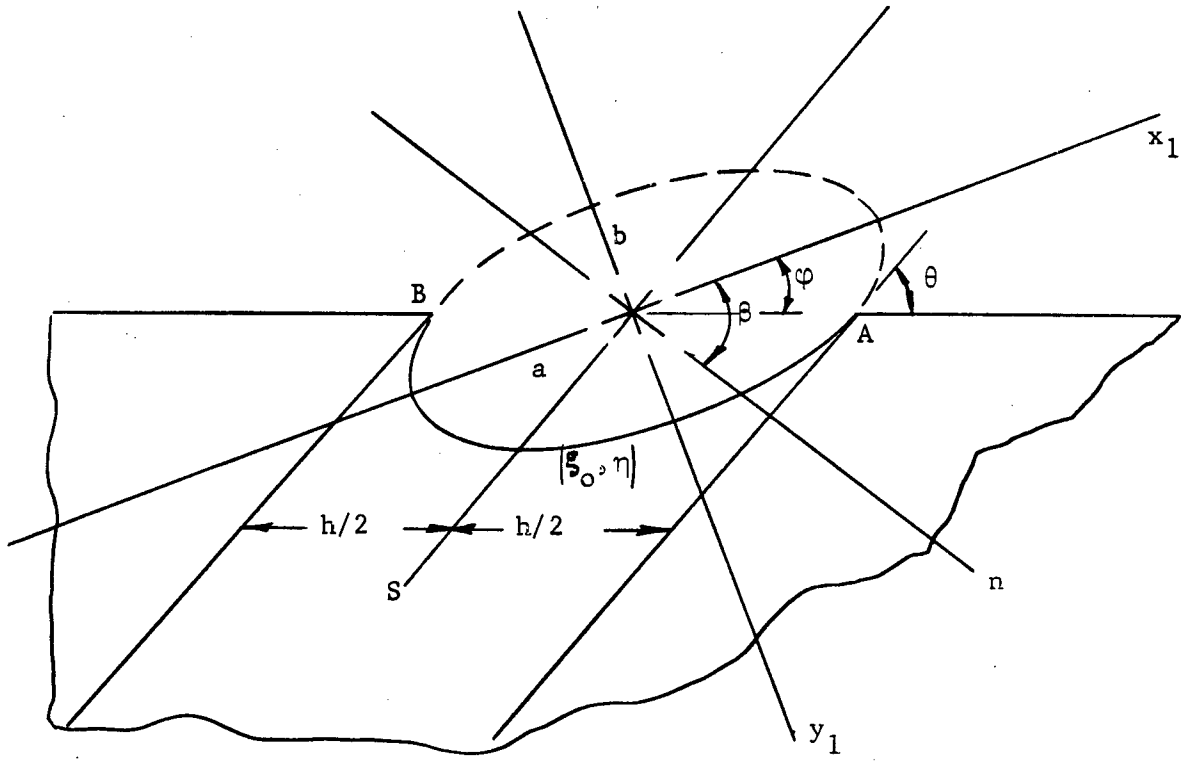


Figure 2. Boundary Curvature of a Scarf Joint

Note that equation (13) can also be obtained by the condition of another interfacial line tangential to the ellipse.

Assuming that the ratio of minor axis to major axis may be expressed in the form

$$\frac{a}{b} = \alpha \cdot g(\theta) \tag{14}$$

where α is a function of material properties, thickness of adhesives and applied tension, and $g(\theta)$ is a function of θ only to be determined experimentally. Impose the condition that $g(\theta) = 1$ at $\theta = 90$ degrees, and it can be seen from Figure 1 that the joint becomes butt at $\theta = \frac{\pi}{2}$. Then the value of α is, by following a similar calculation in Reference 5 (page 146),

$$\alpha = \frac{2 \nu_a F}{E_a h} \tag{15}$$

Using equations (10) and (15), the following is obtained:

$$\left.\begin{aligned} a &= \frac{h}{2}\left[\alpha^2 g^2(\theta) \sin^2\varphi + \cos^2\varphi\right]^{1/2} \\ b &= \frac{h}{2\alpha\, g(\theta)}\left[\alpha^2 g^2(\theta) \sin^2\varphi + \cos^2\varphi\right]^{1/2} \end{aligned}\right\} \tag{16}$$

Substituting equations (14) and (16) in equation (13), and using equation (9) yields

$$\beta = \tan^{-1}\left[-\frac{1}{2}\left(1+\alpha^2 g^2\right)\tan\theta \pm \frac{1}{2}\sqrt{\left(1+\alpha^2 g^2\right)^2 \tan^2\theta + 4\alpha^2 g^2}\right] \tag{17}$$

Equation (17) indicates that two solutions for β may occur. However, the values of α must satisfy the geometrical constraint.

After the semi-axes of the ellipse are determined, the stresses due to the change of boundary curvature may be found as follows:

Let ξ and η be elliptic coordinates defined by

$$z = c \cosh \zeta \tag{18}$$

where c is a constant, and where

$$\left.\begin{aligned} z &= x_1 + i\, y_1 \\ \zeta &= \xi + i\, \eta \end{aligned}\right\} \tag{19}$$

Equation (14) can be written in the form

$$\left.\begin{aligned} x_1 &= c \cosh \xi \cos \eta \\ y_1 &= c \sinh \xi \sin \eta \end{aligned}\right\} \tag{20}$$

For constant ξ, assume that ξ_o, the solution curve for equation (18) or (20), is an ellipse with semi-axes $c \cosh \xi_o$ and $c \sinh \xi_o$. Then the constant c and ξ_o are given by

$$\left.\begin{aligned} c^2 &= a^2 - b^2 \\ \xi_o &= \coth^{-1} \frac{a}{b} \end{aligned}\right\} \tag{21}$$

The coordinate η in the present case is called the eccentric angle of a point on the ellipse, and varies through a range 2π.

Assume that the stresses produced by the presence of a semi-ellipse at the free boundary of the adhesive may be approximated by those of an infinite plate with an elliptic hole under biaxial tension and pure shear. The stresses at the semi-ellipse produced by uniform tensile stress, $\sigma_{n,1}$, in a direction at an angle β with the major axis has been given in equation (6) with the result

$$\left(\sigma_{\eta,1}\right)_{\xi=\xi_o} = \sigma_{n,1} \frac{\sinh 2\xi_o + \cos 2\beta - e^{2\xi_o} \cos 2(\beta-\eta)}{\cosh 2\xi_o - \cos 2\eta} \tag{22}$$

Similarly, the stresses at the semi-ellipse due to the stress $\sigma'_{s,1}$ are

$$\left(\sigma_{\eta,2}\right)_{\xi=\xi_o} = \sigma'_{s,1} \frac{\sinh 2\xi_o - \cos 2\beta + e^{2\xi_o} \cos 2(\beta-\eta)}{\cos 2\xi_o - \cos 2\eta} \tag{23}$$

The effect of the semi-elliptic hole on a state of pure shear τ, can be found by superposing the case of tension τ, at an angle $\left(\beta+\frac{\pi}{4}\right)$ with the major axis on that of compression $(-\tau_1)$ at an angle $\left(\beta+\frac{3\pi}{4}\right)$. Then one obtains

$$\left(\sigma_{\eta,3}\right)_{\xi=\xi_o} = 2\tau \frac{e^{2\xi_o} \sin 2(\beta-\eta) - \sin 2\beta}{\cosh 2\xi_o - \cos 2\eta} \tag{24}$$

The stress component $\left(\sigma_\xi\right)_{\xi=\xi_o}$ at the semi-ellipse is zero. It can be seen that equation (24) is identical with the expression given in Reference 6, p. 203, by setting $\beta = 0$ in the equation. The total stress is given by

$$\left(\sigma_\eta\right)_{\xi=\xi_o} = \left(\sigma_{\eta,1}\right)_{\xi=\xi_o} + \left(\sigma_{\eta,2}\right)_{\xi=\xi_o} + \left(\sigma_{\eta,3}\right)_{\xi=\xi_o} \tag{25}$$

The angle γ formed by the major axis and the tangent to the ellipse at an arbitrary point (ξ_o, η) is

$$\gamma = \frac{\pi}{2} + \tan^{-1}\left(\coth \xi_o \tan \eta\right) \tag{26}$$

The components of the stress $\left(\sigma_\eta\right)_{\xi=\xi_o}$ in the n- and s-directions are

$$\left.\begin{aligned} \left(\sigma_{n,2}\right)_{\xi=\xi_o} &= \left(\sigma_\eta\right)_{\xi=\xi_o} \sin^2(\beta-\gamma) \\ \left(\sigma_{s,2}\right)_{\xi=\xi_o} &= \left(\sigma_\eta\right)_{\xi=\xi_o} \cos^2(\beta-\gamma) \\ \left(\tau_2\right)_{\xi=\xi_o} &= \left(\sigma_\eta\right)_{\xi=\xi_o} \sin(\beta-\gamma)\cos(\beta-\gamma) \end{aligned}\right\} \tag{27}$$

For plane strain the stress $\sigma_{z,2}$ in the direction perpendicular to the n-s plane is

$$\left(\sigma_{z,2}\right)_{\xi=\xi_o} = \nu_a \left(\sigma_\eta\right)_{\xi=\xi_o} \tag{28}$$

Equations (27) and (28) are the adhesive stresses produced by the change of boundary curvature. The superposition of these stresses on the stresses given by equations (1a), (1c), (1d), and (6) yields

$$\left.\begin{aligned} \sigma_n &= \sigma_{n,1} + (\sigma_{n,2})_{\xi=\xi_o} \\ \sigma_s &= \sigma_{s,1} + (\sigma_{s,2})_{\xi=\xi_o} \\ \sigma_z &= \sigma_{z,1} + (\sigma_{z,2})_{\xi=\xi_o} \\ \tau &= \tau_1 + (\tau_z)_{\xi=\xi_o} \end{aligned}\right\} \qquad (29)$$

which are the total adhesive stresses at the semi-ellipse. Since the maximum stress occurs at the curved boundary, the stress expression at an arbitrary point is not included.

As mentioned above, butt joints can be trested as a special case of scarf joints; i.e., the stresses in butt joints are obtained by setting $\varrho = \frac{-}{2}$ in the equations of this section.

STRESSES IN LAP JOINTS FOR RELATIVELY INFLEXIBLE ADHESIVE LAYERS

To determine the stresses in lap joints, the theory by Goland and Reissner (Reference 1) is applied for the relative thinness of the adhesive layer and the smallness of its elastic moduli as compared with the elastic moduli of the adherents. If applied tensile forces per unit width, applied tensile stress in the adherents, and the length of the lap joint (see Figure 3) are denoted by F, p, and $2c$ respectively, then the moment factor K is defined by

$$K = \frac{\cosh U_2 C}{\cosh U_2 C + 2\sqrt{2} \sinh U_2 C} \qquad (30)$$

where $U_2 C = \sqrt{\frac{3(1-U^2)}{2}} \frac{C}{t} \sqrt{\frac{p}{E}}$

If the length of the joint is large compared with its thickness, the stresses in the joint regions near the edges are given by

$$\sigma_{x,1} = \sum_{n=1}^{\infty} \left(A_n + B_n\right) \left[\frac{1}{2} e^y (y+1)\right] \cos \frac{n\pi x_2}{2t} \qquad (31)$$

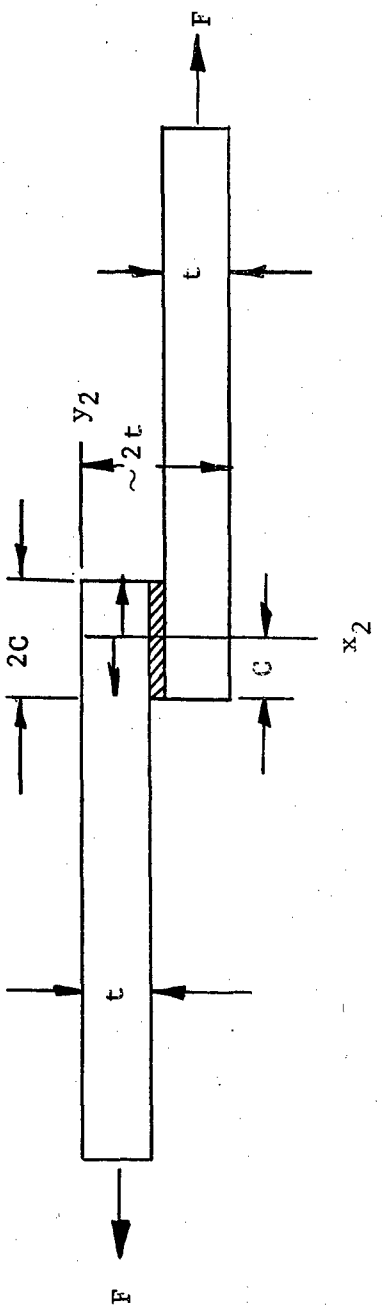


Figure 3. Lap Joint

$$\sigma_{y,1} = \frac{p}{2} + \sum_{n=1}^{\infty} \left(A_n + B_n\right)\left[\frac{1}{2}\, e^{y}(y+1)\right] \cos \frac{n\pi x_2}{2t} \tag{32}$$

$$\tau_{xy,1} = \sum_{n=1}^{\infty} \left(A_n + B_n\right)\left[\frac{1}{2}\, e^{y} y\right] \sin \frac{n\pi x_2}{2t} \tag{33}$$

where $$A_n + B_n = \frac{4p}{n\pi}\left[\frac{12K}{n\pi}\left(\cos\frac{n\pi}{2} - \cos n\pi\right) - (3K+1)\sin\frac{n\pi}{2}\right]$$

and $$y = \frac{n\pi}{2t}\left(y_2 - e\right)^{-(3K+1)\sin\frac{n\pi}{2}}$$

Supplements to Reference 1 for the stresses in the shear plane due to six concentrated forces which are used to eliminate the surface stresses produced by the stress function σ, are

$$\sigma_{x,2} = -\frac{4t^2}{\pi}\left[\frac{18d\left(P_1+P_3\right) + 27tQ_1}{\left(4d^2 + 9t^2\right)^2} + \frac{2d\left(P_2+P_4\right) - 4tQ_4}{\left(d^2 + 4t^2\right)^2}\right] \tag{34}$$

$$\sigma_{y,2} = -\frac{2d^2}{\pi}\left[\frac{16d\left(P_1+P_3\right) + 24tQ_1}{\left(4d^2 + 9t^2\right)^2} + \frac{d\left(P_2+P_4\right) - 2tQ_4}{\left(d^2 + 4t^2\right)^2}\right] \tag{35}$$

$$\tau_{xy,2} = -\frac{4dt}{\pi}\left[\frac{12d\left(P_1-P_3\right) - 18tQ_1}{\left(4d^2 + 9t^2\right)^2} + \frac{d\left(P_2-P_4\right) - 2tQ_4}{\left(d^2 + 4t^2\right)^2}\right] \tag{36}$$

where d is the distance from the joint edge and where

$$P_1 = (-0.07 + 0.77K)\pi tp$$

$$P_2 = -0.30K\,\pi tp$$

$$P_3 = (0.14 - 0.30K)\pi tp$$

$$P_4 = 0.16\,\pi tp$$

$$Q_1 = (0.13 - 0.75K)\pi tp$$

$$Q_4 = (0.25 - 0.25K)\pi tp$$

Then the total stresses in the joint regions near the edges are, by the method of superposition,

$$\sigma_x = \sigma_{x,1} + \sigma_{x,2} \tag{37}$$

$$\sigma_y = \sigma_{y,1} + \sigma_{y,2} \tag{38}$$

$$\tau_{xy} = \tau_{xy,1} + \tau_{xy,2} \tag{39}$$

Again, the expressions given in this section are useful only when the elastic modulus of the adhesive is small compared to that of adherends. If the moduli of adherends and adhesive have the same order of magnitude, an experimentally determined correction factor should be applied. No attempt is made to rederive the expression in the present analysis for equal moduli.

STRESSES IN DOUBLE LAP JOINTS

An approximate method has been developed by Bikerman (Reference 5, p. 161) on the determination of stresses in double lap joints (see Figure 4). If shear modulus and thickness of the adhesive layer are denoted by G_a and h_o respectively, the tensile stresses σ_y in the middle adherend are given by

$$\sigma_y = \frac{F \cosh \lambda y_3}{t \cosh \lambda \ell} \tag{40}$$

where $\lambda = \dfrac{2 G_a}{E t h_o}$

The maximum shear stress which occurs at the points C and D is

$$\tau_{max} = \frac{F}{t}\left(\frac{G_a t}{2Eh_o}\right)^{1/2} \tag{41}$$

The author pointed out that equation (40) does not satisfy the condition at $y_3 = 0$. There is another contradiction that it may not satisfy the stress distribution for the region at $y > \ell$, especially at $y_3 = L$. These contradictions mainly arise from the simplified assumptions. However, equations (40) and (41) are used to calculate the stresses in double lap joints for purposes of this analysis.

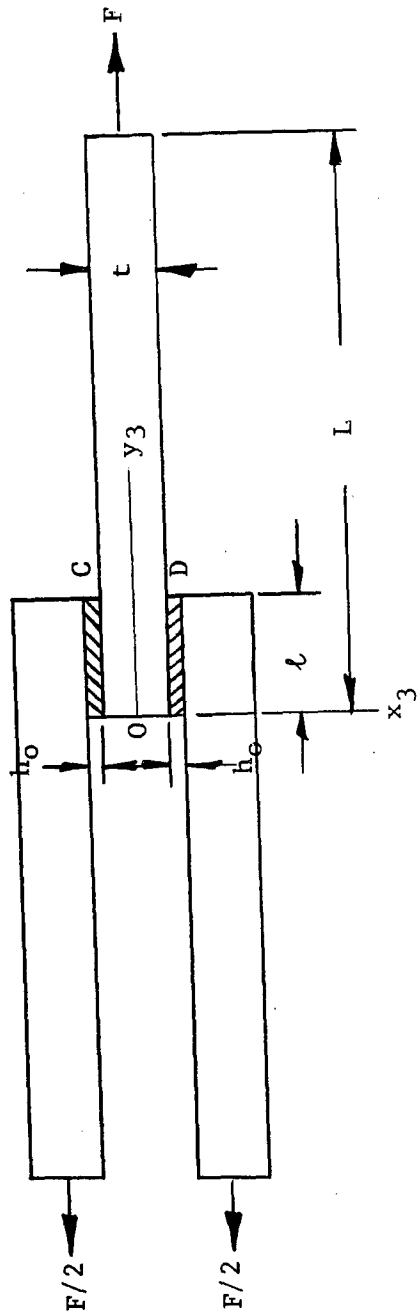


Figure 4. Double Lap Joint

DISCUSSION

The approximate formulas for stresses in butt, scarf, lap, and double lap joints as given above are simply applied to thin rectangular adherends in the elastic range. The other configurations of adherends which are expected to have high stress concentration at certain points are not considered herein. By using these formulas, the optimum joint can be analytically determined. For example, from equations (29), the curve for maximum stress vs scarf angle can be plotted so that the angle corresponding to the small concentrated stress may be found. Then an optimum joint can be determined by comparing the maximum stresses in these different joints.

NUMERICAL RESULTS

Uniform Adhesive Stress Variation with Scarf Joints

Let the applied tensile stress $\frac{F}{t}$ in a scarf joint be denoted by σ. By using equations (1) and (2), the values of $\frac{\sigma_{n,1}}{\sigma}$, $\frac{\sigma_{s,1}}{\sigma}$, $\frac{\sigma_{z,1}}{\sigma}$, and $\frac{\tau_1}{\sigma}$ are calculated for various scarf angles with the following assumed material properties:

$$\frac{E_a}{E} = 5 \qquad \text{and} \qquad \nu = \nu_a = 0.32$$

The numerical results are given below:

θ	$\sigma_{n,1}/\sigma$	$\sigma_{s,1}/\sigma$	$\sigma_{z,1}/\sigma$	τ_1/σ
5°	0.0076	0.2013	0.0669	0.0869
10°	0.0301	0.2053	0.0754	0.1710
20°	0.1170	0.2206	0.1080	0.3214
30°	0.2500	0.2441	0.1581	0.4330
45°	0.5000	0.2883	0.2523	0.5000
60°	0.7500	0.3324	0.3464	0.4330
80°	0.9698	0.3712	0.4291	0.1710
90°	1.0000	0.3765	0.4405	0

Figure 5 also shows the results for the uniform adhesive stress variation with the scarf angle. This figure indicates that the normal stresses increase with increasing θ and that the shearing stress increases with increasing θ until a maximum value is reached at $\theta = 90$ degrees, or in butt joints.

REFERENCES

1. M. Galand and E. Reissner, "The Stresses in Cemented Joints," J. Appl. Mech., Vol. 11, No. 1, Mar 1944

2. R. W. Corness, "Determination of Stresses in Cemented Lap Joints," J. Appl. Mech., Vol. 20, No. 3, Sept 1953

3. R. E. Sherrer, Stresses in a Lap Joint with Elastic Adhesives, Forest Products Laboratory Report No. FPL 1864, Sept 1957

4. J. L. Lubkin, "A Theory of Adhesive Scarf Joints," J. Appl. Mech., Vol. 24, No. 2, June 1957

5. J. J. Bikerman, The Science of Adhesive Joints, Academic Press Inc., New York, 1961

6. S. Timoshenko and J. N. Goodier, Theory of Elasticity, Second Edition, McGraw-Hill, New York, 1954, p. 203

7. R. T. Shield,"The Application of Limit Analysis to the Determination of the Strength of Butt Joints," Quart. Appl. Math., Vol. 15, No. 2, 1957, pp. 139-147

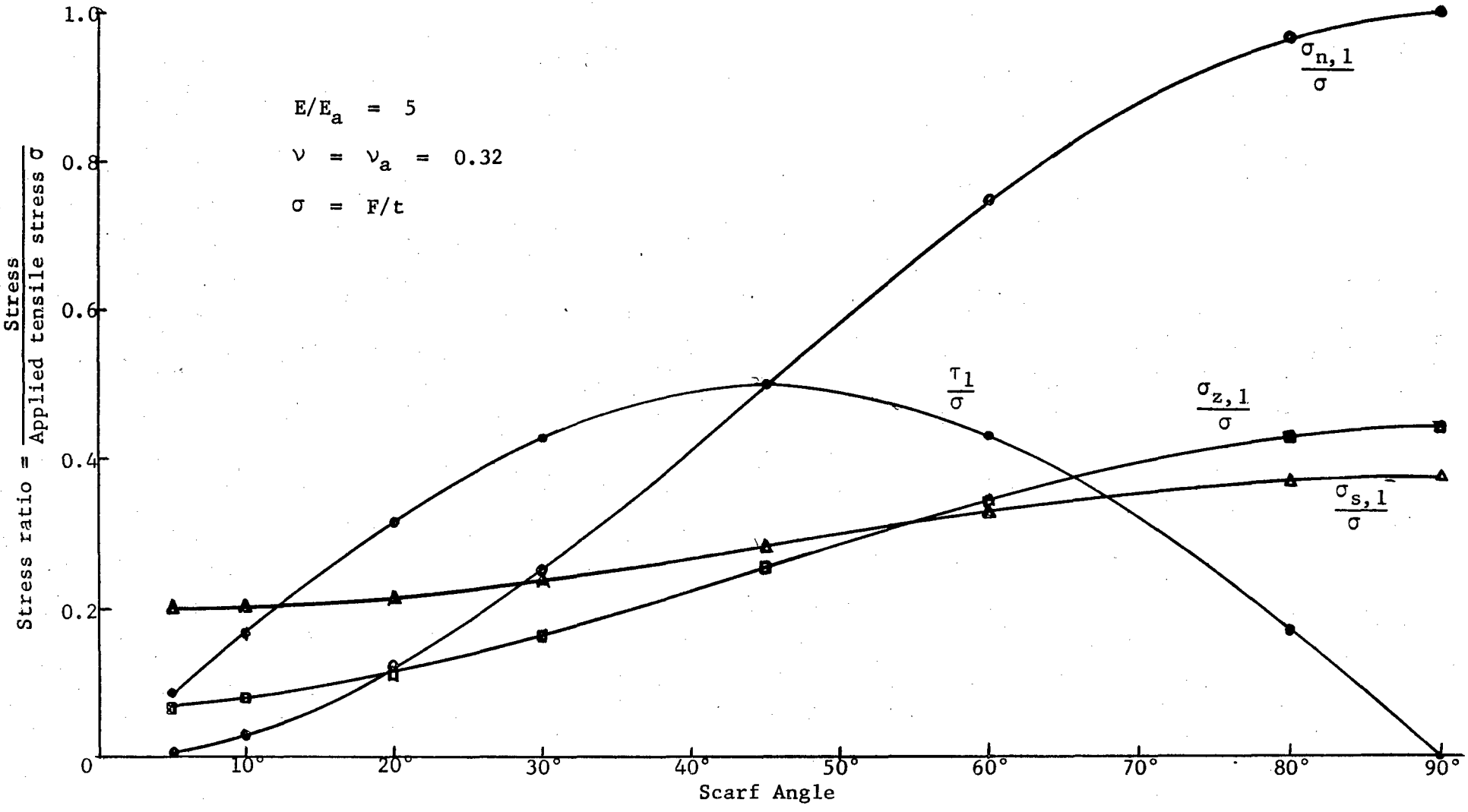


Figure 5. Uniform Adhesive Stress Variation with Scarf Angle

APPENDIX III

DETERMINATION OF RHOMBIC SEGMENT GEOMETRY

DETERMINATION OF RHOMBIC SEGMENT GEOMETRY

The rhombic shape was assumed to be oriented in the longitudinal direction. The total projected area for the rhombic segment was found to be:

$$A_{Tot} = \frac{b^2}{2} \tan \frac{\alpha}{2} \qquad (1)$$

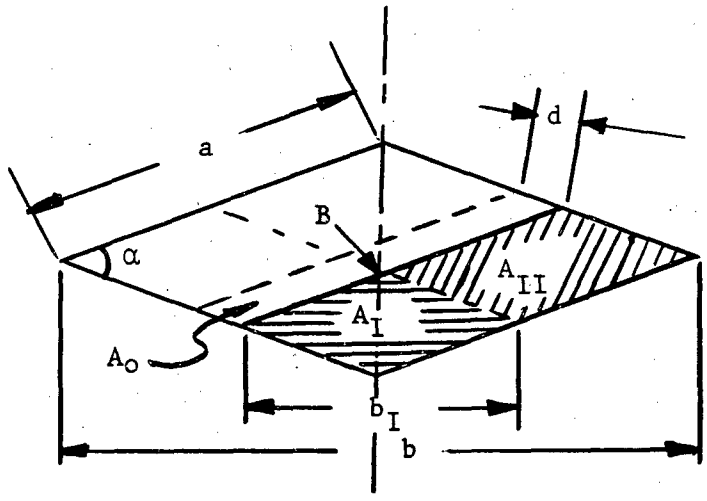
where b = length of the segment

α = rhombic angle

A_{Tot} = total area

The total area for various lengths versus angles is plotted in Figure 1. This figure shows that a small angle rhombus has little surface area for a given length. This would require either a very large number of tiles or tiles of extreme length.

The next area of study for the rhombic segment shape was to determine the effect of required area for attaching to adjacent tiles. The following sketch defines the nomenclature used in the analysis.



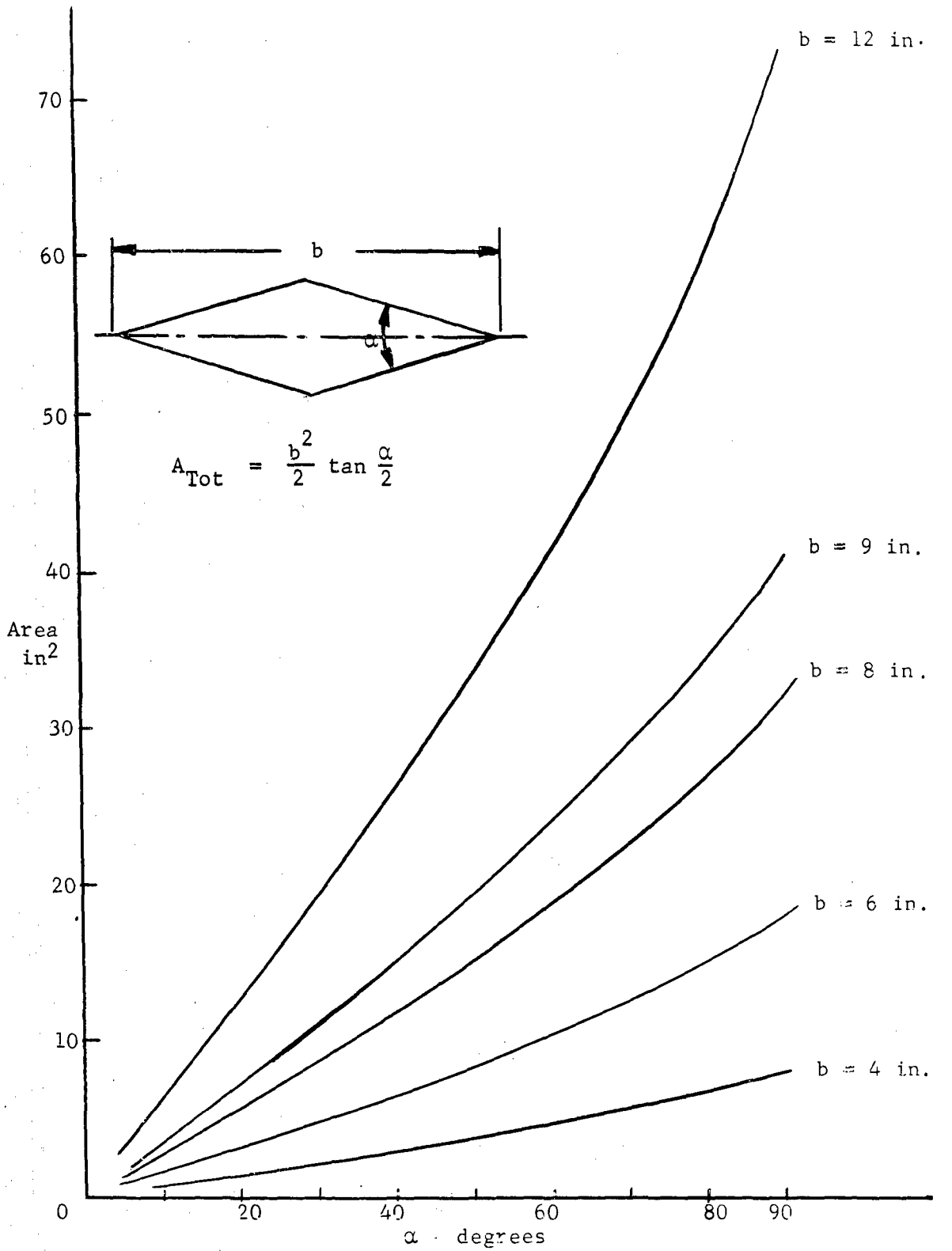


Figure 1. Rhombic Projected Area vs Rhombic Angle

where A_o = Area of no shear to adjacent segments

A_I = Shear area to adjacent circumferential segment

A_{II} = Shear area to adjacent longitudinal segment

a = Length of segment side

b = Total segment length

b_I = Length of circumferential shear area A_I

d = Length of the side cf no shear area A_o

α = Rhombic angle

The areas A_I and A_{II} will change disproportionately as the area of no shear is changed. It was assumed that the point "B" remains along the tile line of symmetry. This condition resulted in the boundary conditions:

1) If $A_o = 0$ then $A_I = A_{II} = \frac{A_{Tot}}{4}$

2) If $A_o = A_{Tot}$ then $d = a$ and $A_I = A_{II} = 0$

The total area of the rhombus is equal to

$$A_{Tot} = A_o + 2A_I = 2A_{II} \tag{2}$$

By rearranging equation (2),

$$\left(1 - \frac{A_o}{A_{Tot}}\right) \frac{A_{Tot}}{2A_I} = \frac{A_{II}}{A_I} + 1 \tag{3}$$

From equation (1),

$$A_{Tot} = \frac{b^2}{2} \tan \frac{\alpha}{2}$$

And similarly

$$A_I = \frac{b_I^2}{2} \tan \frac{\alpha}{2}$$

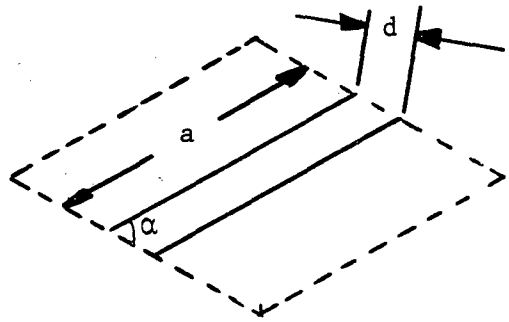
Substituting into equation (3) results in

$$\left(1 - \frac{A_o}{A_{Tot}}\right) \frac{\frac{b^2}{2} \tan\frac{\alpha}{2}}{\frac{b_I^2}{2} \tan\frac{\alpha}{2}} = \frac{A_{II}}{A_I} + 1$$

or

$$\left(1 - \frac{A_o}{A_{Tot}}\right)\left(\frac{b^2}{2b_I^2}\right) - 1 = \frac{A_{II}}{A_I} \qquad (4)$$

The area relation of A_o is found geometrically



where $A_o = ad \sin\alpha$ (5)

By geometry: $a = \frac{b}{2\cos\frac{\alpha}{2}}$

and $d = a - 2\left(\frac{b_I}{2\cos\frac{\alpha}{2}}\right)$

$$d = \frac{b}{2\cos\frac{\alpha}{2}} - \frac{b_I}{2\cos\frac{\alpha}{2}}$$

Substitution into equation (5) gives:

$$A_o = \frac{b}{2\cos\frac{\alpha}{2}}\left(\frac{b - b_I}{2\cos\frac{\alpha}{2}}\right)\sin\alpha$$

$$= \frac{b^2 \sin\alpha}{4\cos^2\frac{\alpha}{2}}\left(1 - \frac{2b_I}{b}\right) \qquad (6)$$

With the trigonometric identity

$$\sin \alpha = 2 \sin \frac{\alpha}{2} \cos \frac{\alpha}{2}$$

Equation (6) can be rewritten as

$$A_o = \frac{b^2 \left(2 \sin \frac{\alpha}{2} \cos \frac{\alpha}{2} \right)}{4 \cos^2 \frac{\alpha}{2}} \left(1 - \frac{2 b_I}{b} \right)$$

or

$$A_o = \frac{b^2 \tan \frac{\alpha}{2}}{2} \left(1 - \frac{2 b_I}{b} \right) \tag{7}$$

Hence substituting into equation (4) gives the shear area ratio as:

$$\left\{ 1 - \frac{\frac{b^2}{2} \tan \frac{\alpha}{2} \left(1 - \frac{2b_I}{b} \right)}{\frac{b^2}{2} \tan \frac{\alpha}{2}} \right\} \frac{b^2}{2b_I^2} - 1 = \frac{A_{II}}{A_I}$$

or

$$\frac{b}{b_I} - 1 = \frac{A_{II}}{A_I} \tag{8}$$

This simplified equation is plotted in Figure 2 which shows the shear area ratio for the rhombus versus the length ratio.

In order to more fully describe the geometry of the rhombic shape, Figure 3 was developed to find the shear area ratio $\frac{A_{II}}{A_I}$ as a function of the ratio of $\frac{A_{Tot}}{A_I}$. The relation is found to be

$$\frac{A_{II}}{A_I} = \left(\frac{A_{Tot}}{A_I} \right)^{1/2} - 1$$

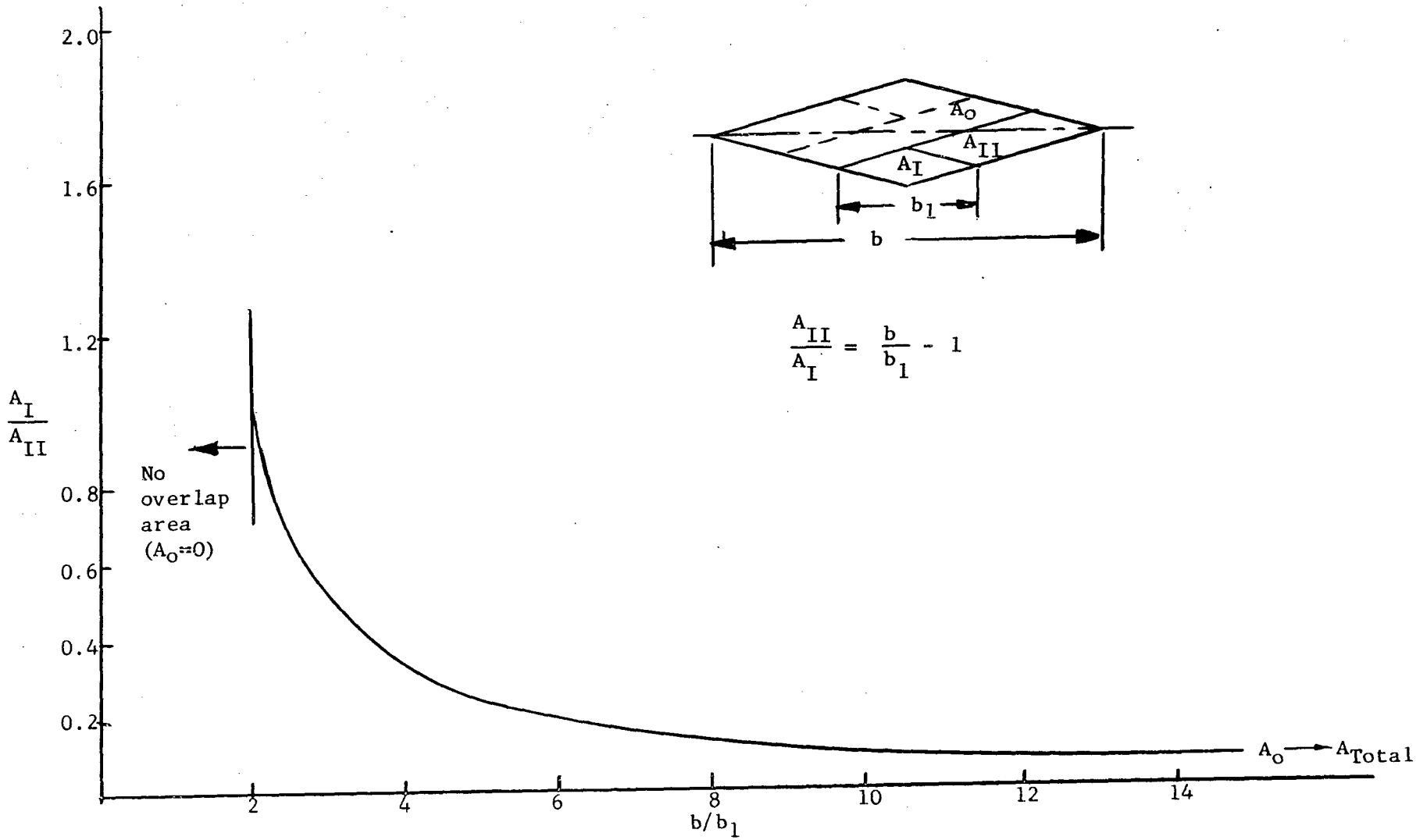


Figure 2. Shear Area Ratio vs Length Ratio Rhombic Tile Shape

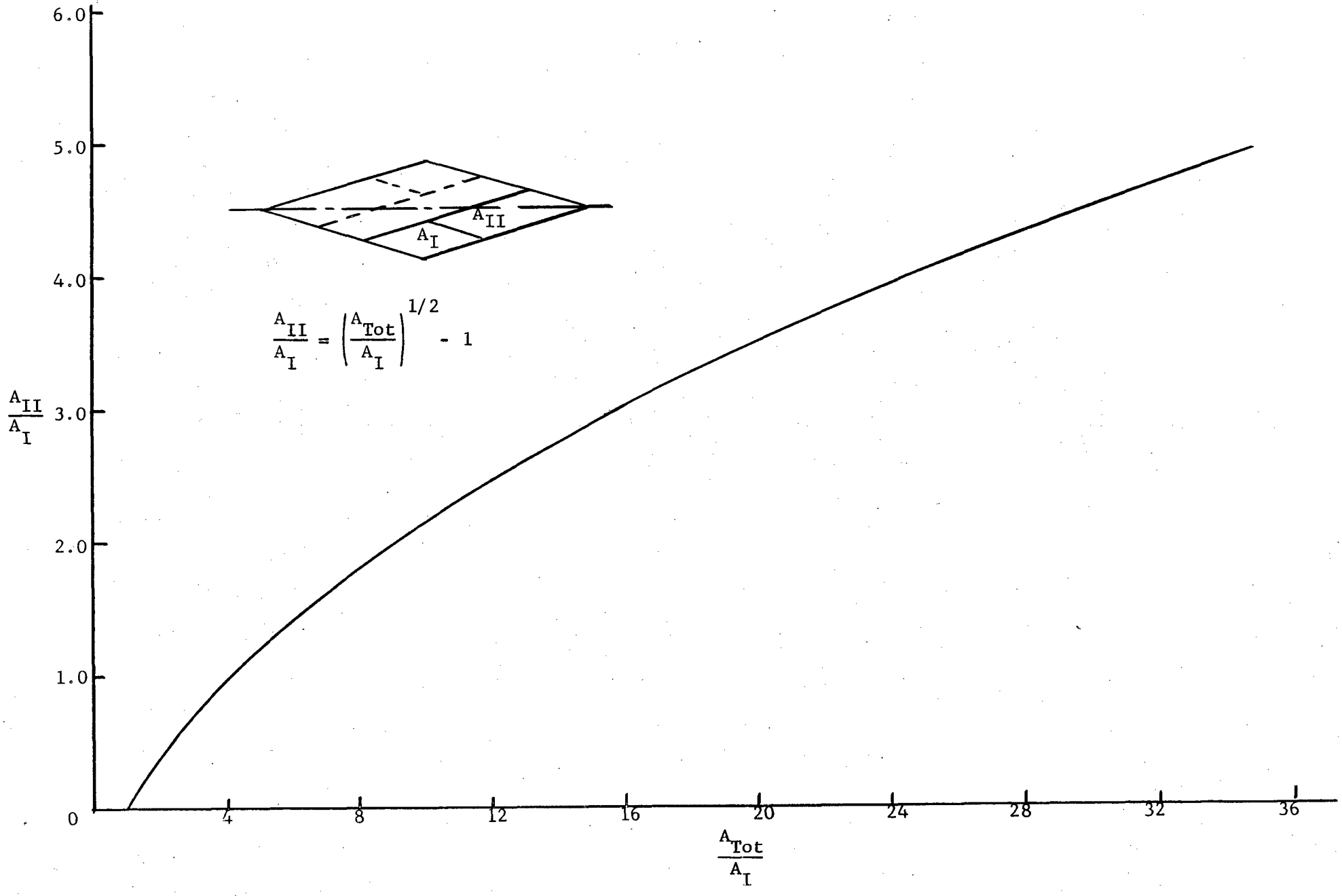


Figure 3. Shear Area Ratio $\frac{A_{II}}{A_I}$ vs Rhombic Area Ratio $\frac{A_{Tot}}{A_I}$

The use of the curves can be demonstrated starting with the following assumptions:

1. The bond area, A_{II}, transfers longitudinal load only from the adjacent force or tile.
2. The bond area A_I transfers circumferential load only from the adjacent side tile.

The rhombus configuration can now be determined by further assuming that a longitudinal-to-circumferential stress equals the bond area ratio. The length of the tile is also assumed. For a known stress ratio,

$$\frac{A_{II}}{A_I} = \frac{\sigma_{long.}}{\sigma_{circ.}}$$

From Figure 3 the ratio of $\frac{A_{Tot}}{A_I}$ is determined. Then, using this value, the length ratio $\frac{b}{b_I}$ is found from Figure 2.

When the tile length is selected, the length of the shear area A_I can be found.

The area A_I is dependent upon the magnitude of the circumferential stresses and the shear strength of the adhesive. At this point the material properties of the adherend and adhesive must be known. From the adhesive shear values, the circumferential load and the shear area A_I can be found. Since $A_I = \frac{b_I^2}{2} \tan \frac{\alpha}{2}$, the rhombic angle α can be found, and from Figure 1. the total segment area can be found.

APPENDIX IV

GEOMETRY AND SIZE OF RADOME TILES

GEOMETRY AND SIZE OF RADOME TILES

Symbols:

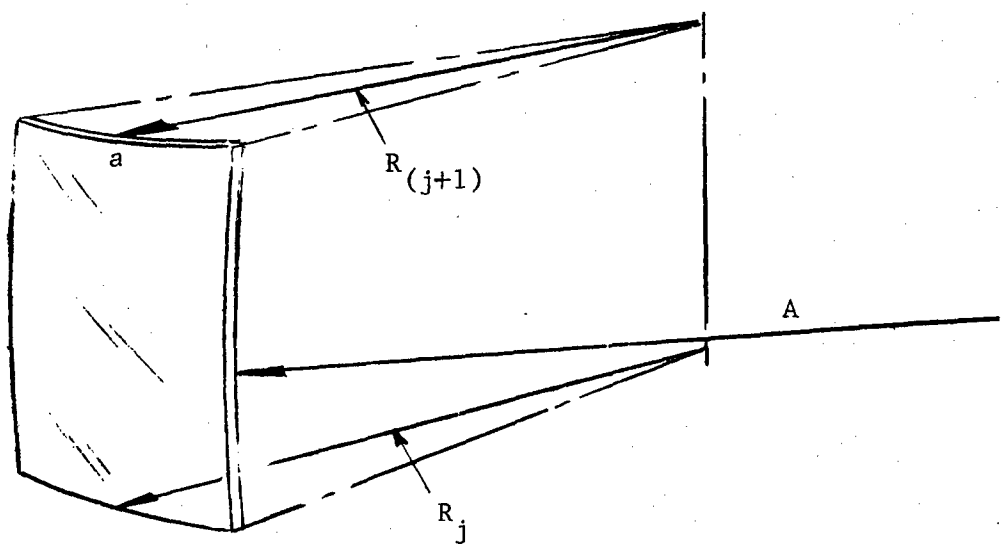
- a - Chord length
- a_j - Length of the contour measured along the tile horizontally
- A - Constant radius of ogive
- D - Diameter of the radome or cone
- D_o - Diameter of the radome or cone at $h = 0$
- D_r - Reference diameter radome or cone
- D_j - Diameter of radome or cone at h_j
- d - Wall thickness of radome or cone
- h - Height of an individual tile measured parallel to ogive axis
- h_j - Distance of the observed contour from D_r
- H - Total height of truncated cone
- n - Number of tiles in one layer row
- R - Radius
- R_o - Radius at $h = 0$
- R_r - Reference radius
- R_H - Radius of truncated cone at $h_j = H$
- W - Width of tiles
- t - Tile thickness
- t_a - Adhesive thickness
- φ - Angle defined on page

Subscripts:* o - outside
i - inside
j - station

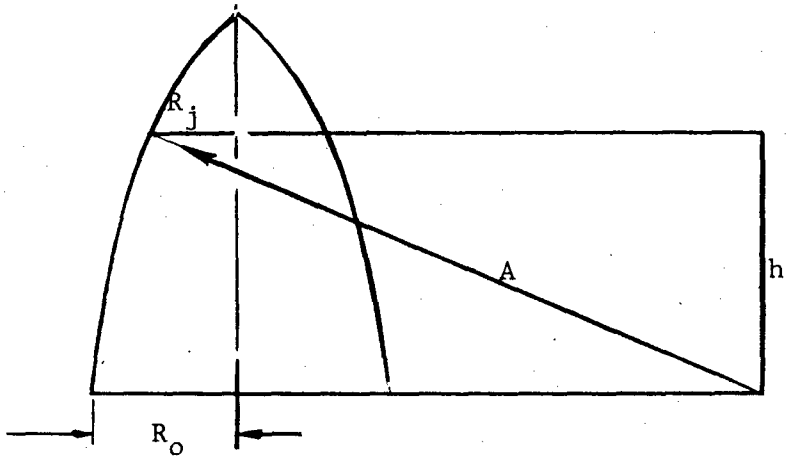
* Sample usage: $W_{(oij)}$ = outside width of inner tile at station j;
$D_{(ioj)}$ = inside diameter of outer tile at station j; etc.

A series of 50 systematical tensile shear tests of trapezoidal and rhombic overlapped tiles indicated that the trapezoidal shape did not offer any advantages over that of the rhombic shape. It appears reasonable to assume that this phenomenon is due to the brittleness of the material.

The trapezoidal shape geometry selected to form an ogive is a two-dimensional curved plate.



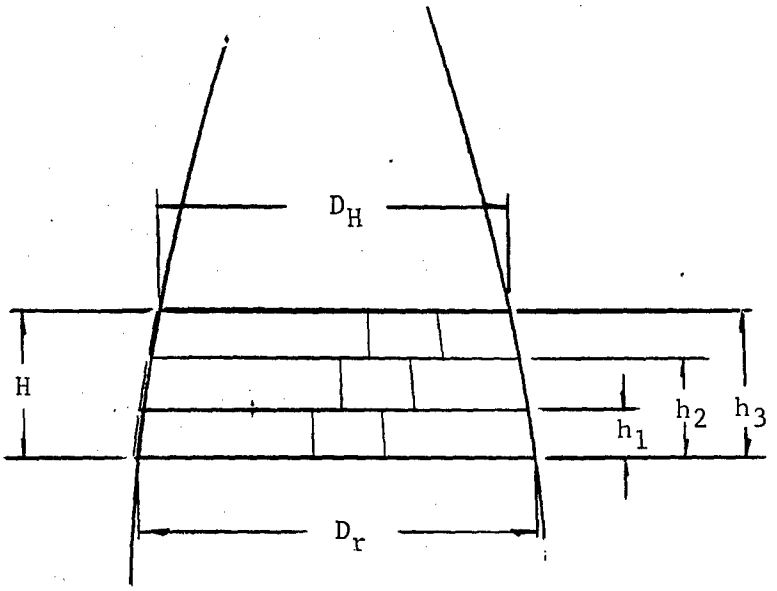
Each tile has three contour radii with which the curvature can be approximately determined. The radius A is constant for all tiles in one layer, while R_j depends on the vertical location of the contour. The exact length of the radius R_j can be obtained from the following sketch:



$$R_j = \sqrt{A^2 - h_j^2} + R_o - A \qquad (2.1)$$

$$R_r = \sqrt{A^2 - h_r^2} + R_o - A \qquad (2.2)$$

For a truncated cone, as an increment of the ogive, one obtains



$$D_j = D_r - D_j \frac{D_r - D_H}{H} \qquad (3.1)$$

The length of the contour measured along the curvature is

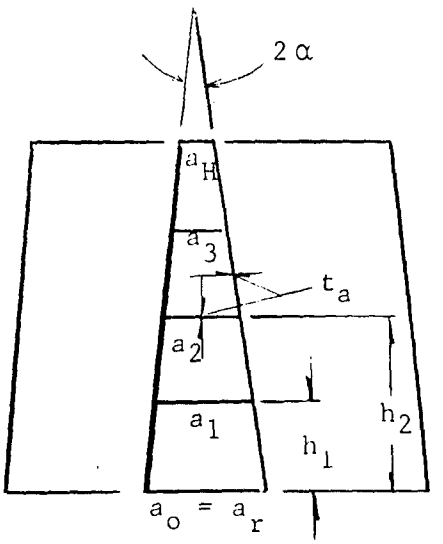
$$a_1 = a_H + 2(H - h_1) \tan \alpha$$

$$= a_H + \left(1 - \frac{h_1}{H}\right)\left(a_r - a_H\right)$$

$$= a_r - \frac{h_1}{H}\left(a_r - a_H\right)$$

$$= \frac{\pi D_r}{n} - t_a - \frac{h_1}{H}\left[\frac{\pi D_r}{n} - t_a - \left(\frac{\pi D_H}{n} - t_a\right)\right]$$

$$= \frac{\pi D_r}{n} - t_a - \frac{h_1}{H}\,\frac{\pi}{n}\left(D_r - D_H\right) \qquad (3.2)$$



The straight width or chord of the tile at h_j is then

$$W_j = D_j \sin \frac{\varphi}{2} \tag{4.1}$$

while

$$\varphi = \frac{360}{n} \left(1 - \frac{2\, t_a\, n}{D_{oj} + D_{ij}\, \pi} \right) \tag{4.2}$$

The equation (4.2) expresses that φ, the angle defined in Figure 1 decreases slightly in the upper part of the ogive. For instance, if at $h = 0$, $D_{oj} = D_o$ twice as large as at $h_{100} = 100$, then

$$\varphi_0 - \varphi_{100} = \frac{360}{n} \left(1 - \frac{2\, t_a\, n}{2\, D_o\, \pi} \right) - \frac{360}{n} \left(1 - \frac{2\, t_a\, n}{D_o\, \pi} \right)$$

$$= \frac{360\, t_a}{D_o\, \pi} - 1 + 2 = \frac{360\, t_a}{D_o\, \pi}$$

and, for this case, would be

$$\varphi_0 - \varphi_{100} = \frac{360 \times 0.005}{32 \times \pi} = 0.018 \text{ degrees}$$

For 28 tiles and at a diameter of 16 in., the circumferential length would increase by $\Delta \ell = 28 \times \Delta\varphi \times R$

$$28 \times \frac{2\pi}{360} \times 0.018 \times \frac{16}{2} = 0.0704 \text{ in.}$$

The diameter would increase from 16 in. to

$$16 + \frac{0.0704}{\pi} = 16.0258 \text{ in.}$$

Since the tolerance of the wall thickness is ±0.002, the length of the tiles must be calculated in an exact manner. The individual length does not require a tolerance of $\pm\frac{1}{28} \frac{0.002}{\pi}$, but the sum of all 28 tiles plus adhesive must have the exact length of $\pi \cdot 16 \pm 0.002$. It will be easier to maintain the circumferential length than the individual length of the tiles.

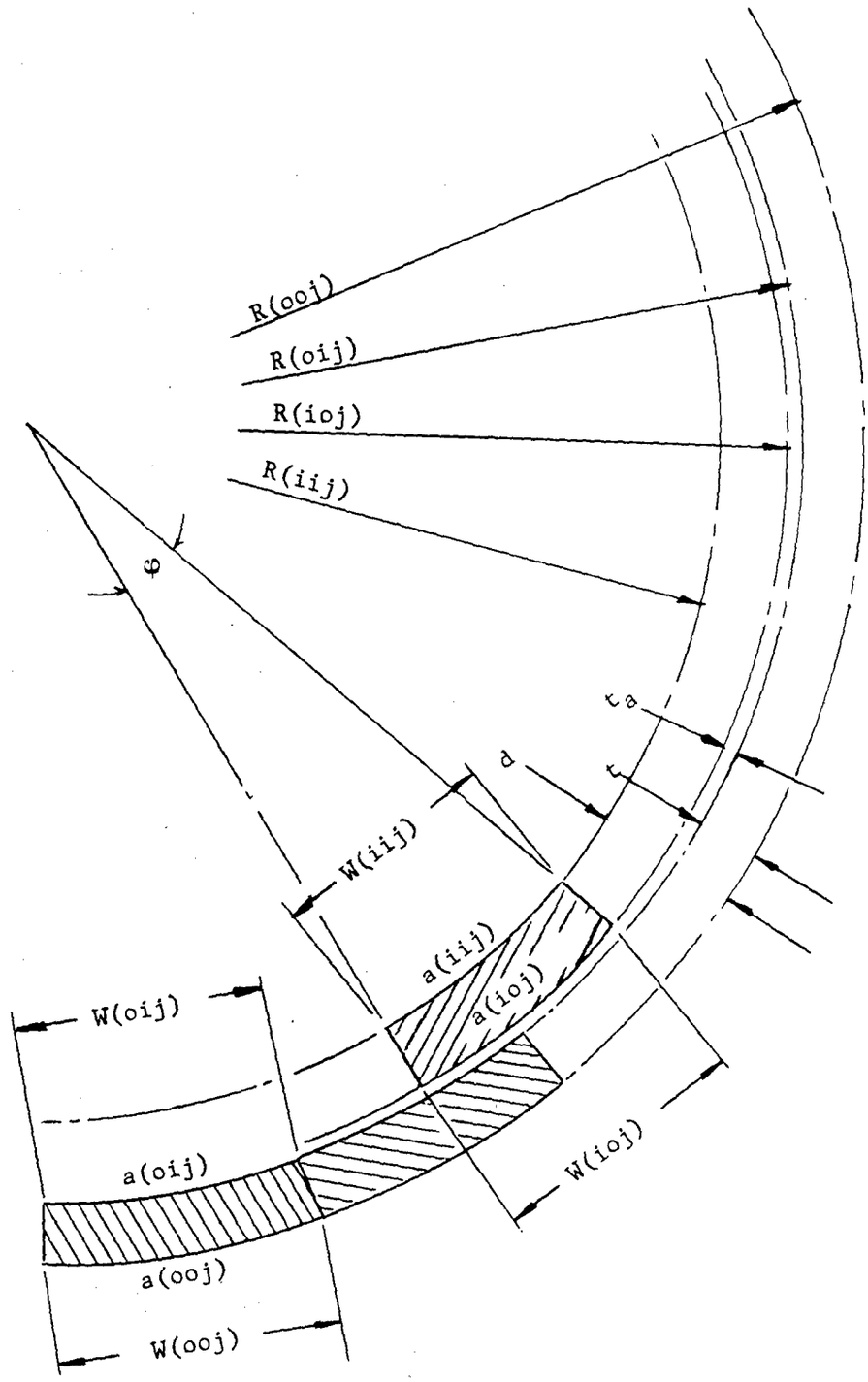


Figure 1. Angular Definition of Tile Length

There are two layers, each having n tiles in one row. Each tile has inner and outer dimensions. The inner dimensions of the outer tiles differ very little from the outer dimensions of the inner tiles. The difference is given by the bond thickness t_a. Taking all these possible areas of confusion into account, the dimensions must be defined.

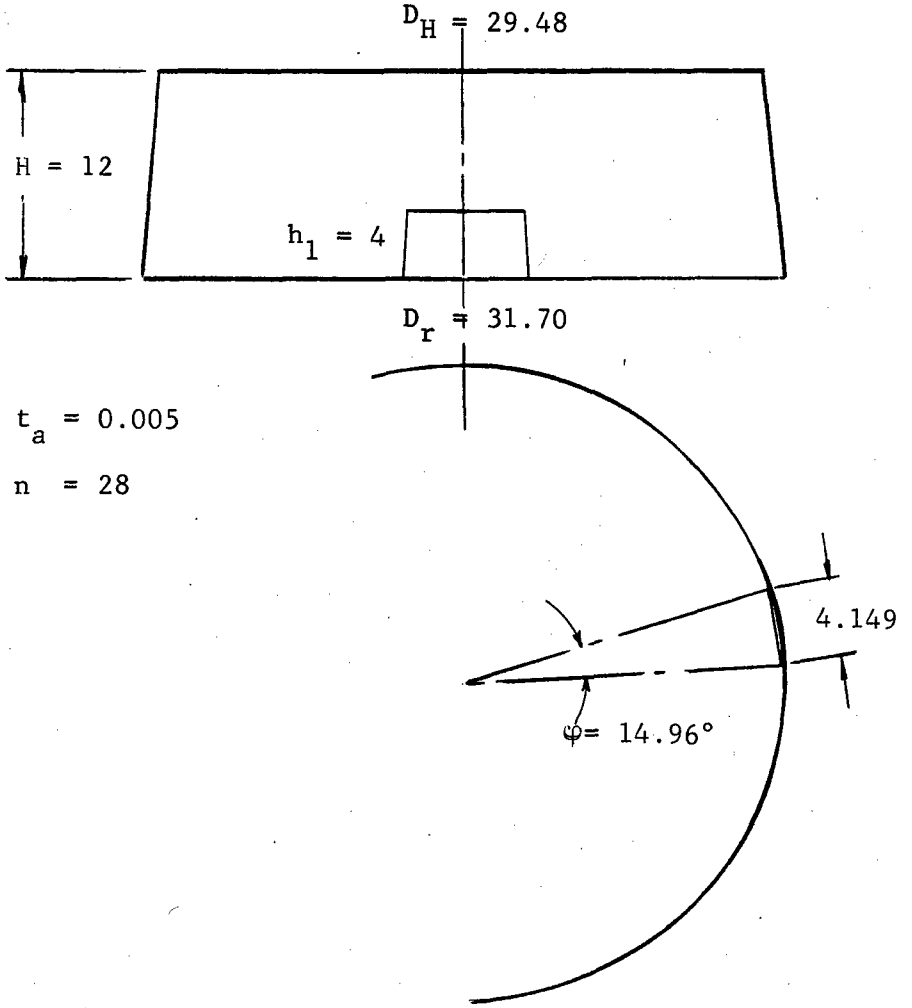
a(oij) = "a" of the outer tile measured inside at station j

a(ooj) = "a" of the outer tile measured outside at station j

Dimensions a(ioj), a(iij), R(ooj), R(oij), R(ioj), R(iij), W(ooj), W(oij), and W(iij) are similarly defined.

Numerical example:

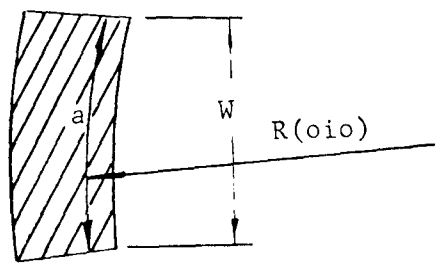
Truncated cone for test purposes



The following is obtained from equation (3.2)·

$$a(ioj) = 3.5267 - h_j\ 0\ 020750$$

$$a(oij) = 3\ 5275 - h_j\ 0.020756$$



Outer Tiles (n = 28)

Inner Dimensions:

$$D_j = D_r \cdot h_j\ 0.185$$

$$a(oij) = 3.5275 - h_j\ 0.020756$$

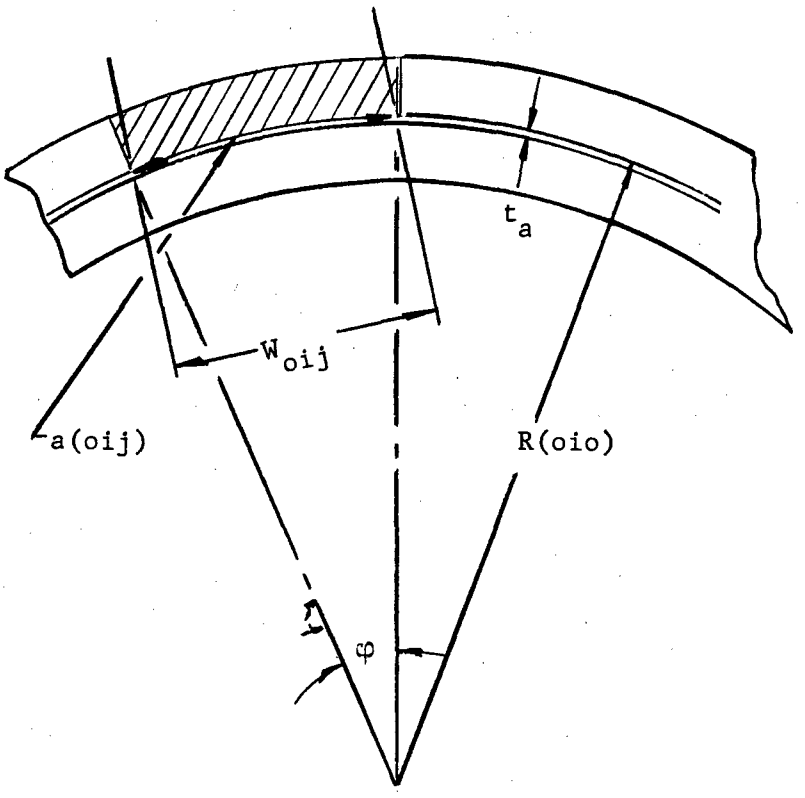
D(oio) = 31.484

①	②	a(oij)	④	D_j =	
h_j	h_j x 0 020756	3.52749 - ②	h_j x 0.185	31.484 - ④	R(oio)
0	0	3.5275	0	31.484	15.742
2 99625	0.062190	3.4653	0.55486	30.92914	15.4645
5.9975	0.124484	3.4030	1 110647	30.3693	15.18465
8 99875	0.186778	3.3407	1.66643	29.81757	14.9087
12	0.249072	3.2784	2.22222	29.2618	14.63089

$$W = D \sin\frac{\Phi}{2} \qquad \Phi = \frac{360}{n}\left(1 - \frac{2\ t_a\ n}{D_o + D_i\pi}\right) =$$

$$= D \qquad \sin\frac{\Phi}{2} = 0.1118$$

h_j	W(oij)
0	3.5199
2.99625	3.4578
5.9975	3.3953
8.9987	3.3360
12	3.2714



APPENDIX V

CALCULATIVE APPROACH TO RADOME DESIGN DIMENSIONS

CALCULATIVE APPROACH TO RADOME DESIGN DIMENSIONS

PRELIMINARY NOTES

General Layout

Figure 1 shows the meridional outer profile curve of the mosaic radome, which is basically an ogive. The following nomenclature is used within the figure:

C = Center of the circular radome profile of radius R_o

T = Tangent point

S = The point designating the base of the radome

ox = Axis of revolution and the radome's center line

o = The point where the profile meets ox

G = The point where the profile becomes tangential to the circular arc (of radius 3 in.) describing the nose of the radome which has its center of curvature (c_1) on OX

O = Origin of the x-y Cartesian coordinate system

OX = x-axis

OY = y-axis

For any arbitrary point "p" on the meridional plane, TCP $\triangleq \theta_p$.*
In addition, if P be on the radome, it is obvious that:

$$\text{Radius of revolution at P } (\triangleq r_p) = y_p$$

Initial Data

R_0 = 890.59000 in.

r_T = 19.12000 in.

r_S = 15.85000 in.

---

* The symbol $\triangleq$ "is defined as"

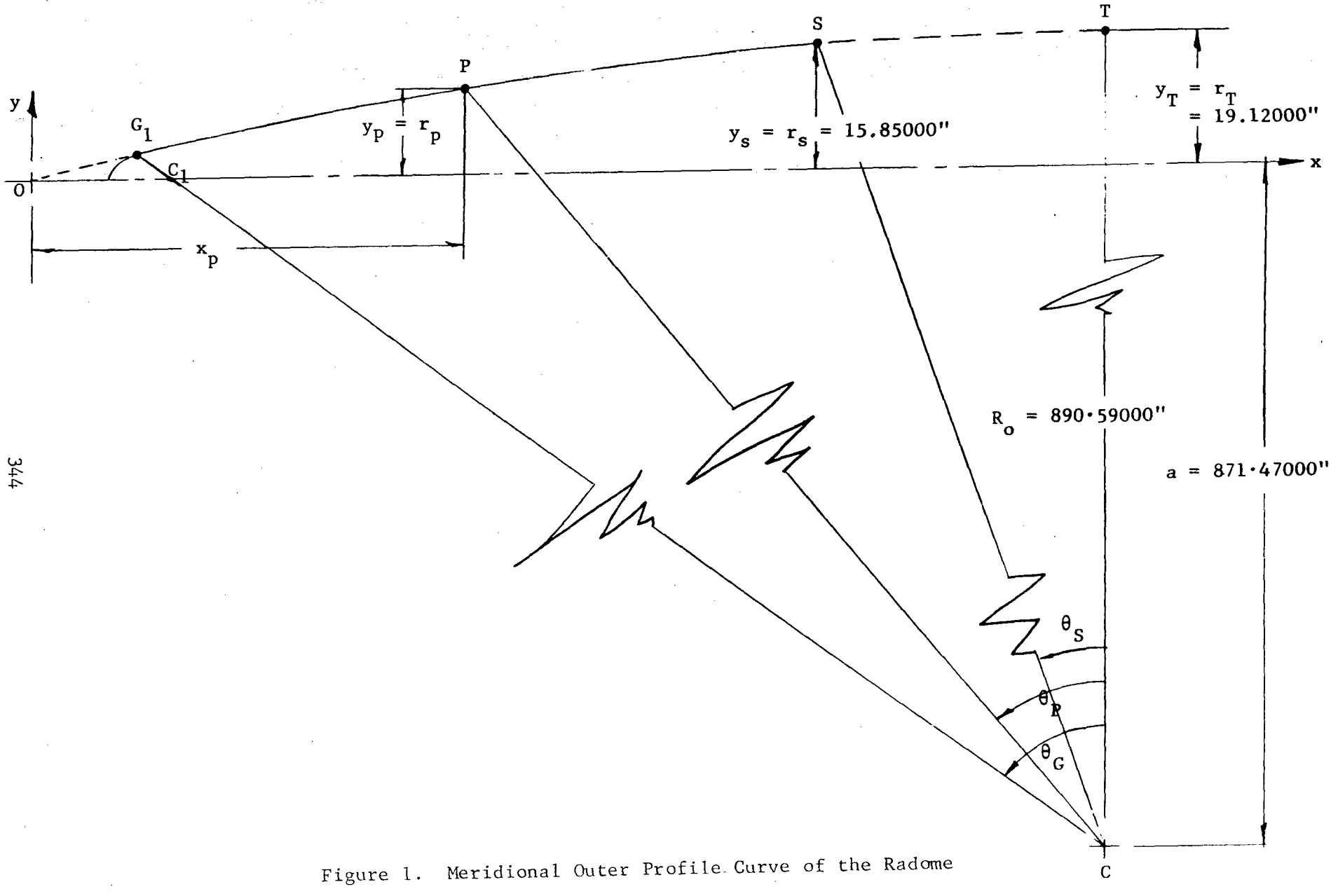


Figure 1. Meridional Outer Profile Curve of the Radome

Preliminary Computations

$$a \triangleq R_o - r_T = 871.47000 \text{ in.}$$

$$x_T = \sqrt{R_o^2 - a^2} = 183.54991 \text{ in.}$$

$$\theta_S = \cos^{-1} \frac{a + r_S}{R} = 4°54'41.055"$$

$$\theta_G = \cos^{-1} \frac{a}{R_o - 3"} = 10°56'10.95"$$

$$x_{c_1} = x_T - a \tan \theta_G = 15.15742 \text{ in.}$$

Nomenclature

All the tiles in the outer layer are arranged so that they overlap the tiles in the inner layer in both the circumferential and longitudinal directions. In each layer, there are staggered rows of tiles beginning at point S. The radome is composed of 87 distinct types of tiles with a total of 870 tiles. Outer layer tiles are identified with one- and two-digit dash numbers (e.g. -7, -9, -11,....,-91, -93) while inner tiles are identified with three-digit dash numbers (e.g. -107, -109,...-189, -191). A single-piece nose cap completes the radome at its forward end,* as shown in Drawings NR 63-044 and NR 63-046.**

Subscripts L and u, when referring to an identified tile, denote the tile-ends near and away from the base, respectively. Thus, a point $P_{19\ u}$ would denote the end face, away from the base S, of a tile identified by the number 19. Chord length along the radome profile is called c_f. Notations C_p, ϕ_p, and n are defined in Figure 2.

---

* The symbol $\triangleq$ = "is defined as"

** See Appendix X.

Assumptions

Tiles have no curvature in the longitudinal direction.

Tiles have a constant thickness of 0.108 in. in the direction normal to the radome profile.

End cut-offs, both in longitudinal and circumferential directions, are normal to the surface of the tile (see Figures 2 and 3).

Typical overlap and relative spacing between inner and outer tiles are as shown in Figure 3.

Joint adhesive thickness, in both profile and circumferential directions, is 0.006 in.

Tiles are arranged along the radome profile so that their ends, in longitudinal direction, make contact with the prescribed ogival profile.

The tile and ceramic adhesive materials are assumed to be electrically equivalent, so that the total electrical wall thickness (given in terms of the tile material) is the same as overall physical wall thickness.

Computation of Radius of Outer Profile for the Inner Tile Layer

Referring to Figure 3, profile radius at point A' is to be computed. From the sketch on page 349, noting that $\delta\theta$ is very small,

$$A = \frac{BC}{BC + AB}\delta\theta = \frac{3}{4}\delta\theta = 11'35.86''$$

$$BD = AB \sin A \triangleq 0.00337 \text{ in.}$$

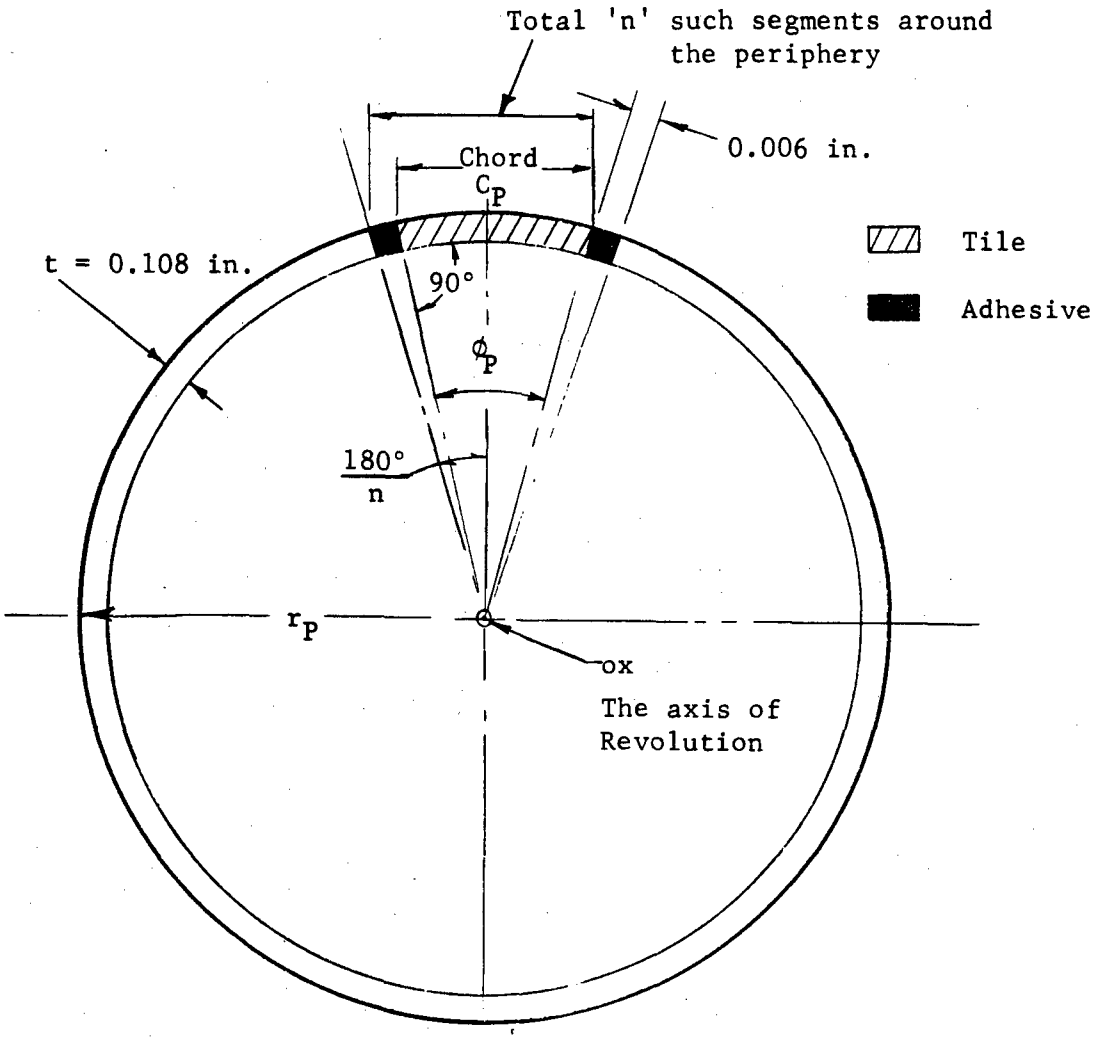
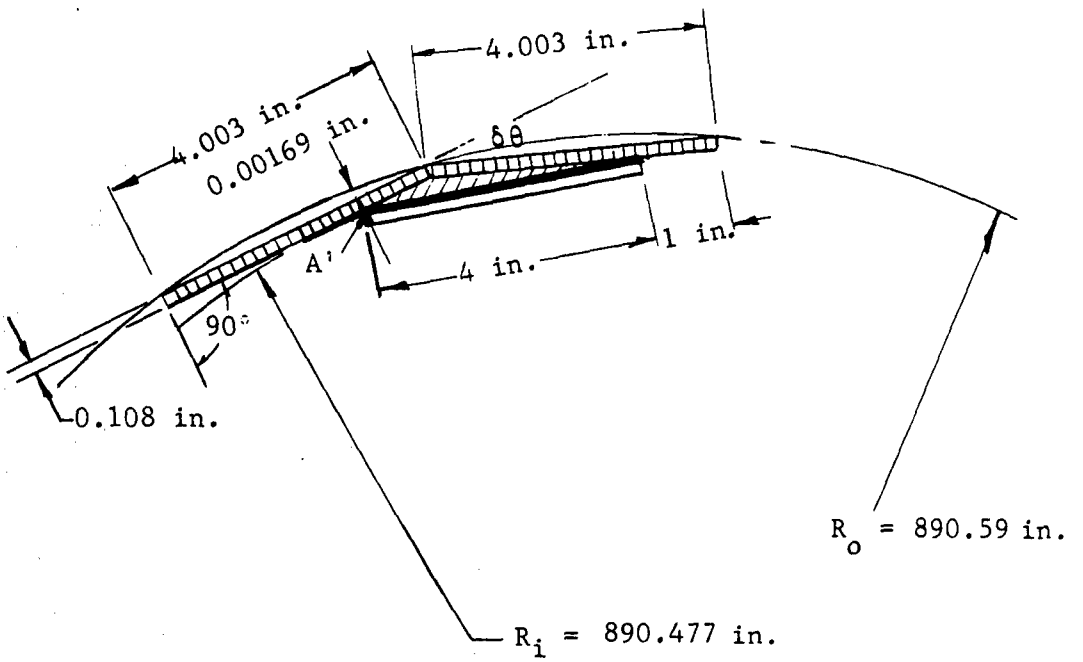


Figure 2. Representative Section of the Radome Showing a Layer of Tiles Through a Point P on the Profile and Perpendicular to the Axis of Revolution ox



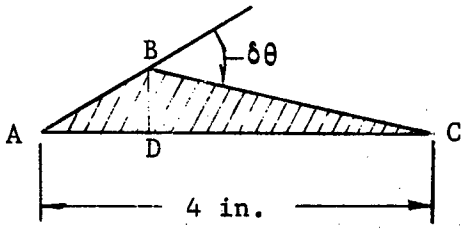
Inner tiles

Outer tiles

Constant thickness adhesive (t in.)

Variable thickness of adhesive, imposed due to the geometry

Figure 3 . Typical Overlap and Relative Spacing between the Inner and Outer Tiles



From geometry

$$\frac{AB}{BC} \approx \frac{1}{3}$$

$\delta\theta$ = 15'27.81"
= angle subtended by chord of 4 in. length at the profile center C

Letting t represent the minimum adhesive thickness at point A' in Figure 3 and h the aggregate wall thickness in the direction normal to the profile,

$$h_{min} = 0.108 + t + 0.108 \text{ in.}$$

$$h_{max} = 0.108 + 0.00337 + t + 0.108 \text{ in.}$$

$$h_{prescribed} = 0.221 \pm 0.002 \text{ in.}$$

Theoretically, optimum t would be given by

$$h_{\text{prescribed max}} - h_{max} = h_{min} - h_{\text{prescribed min}}$$

This gives t = 0.00331 in. Then, from Figure 3,

$$R_i = R_o - (0.00169 + 0.108 + 0.00331) \text{ in.}$$

$$= 890.47700 \text{ in.}$$

Formulas

Let P be a point on the radome profile and P' a point preceding P. Then C_f, the chord length along profile = PP'. Now the following formulas follow from the geometry.

$$\delta\theta = 2 \sin^{-1} \frac{C_f}{2R}$$

$$\approx \frac{C_f}{R} \text{ radians (exact to eight decimal places for required } C_f/R \text{ range)} \quad (1)$$

$$\theta_P = \theta_{P'} + \delta\theta \quad (1a)$$

$$x_P = x_T - R \sin \theta_P = 183.54996 - R \sin \theta_P \quad (2)$$

$$y_P = R \cos \theta_P - a = R \cos \theta_P - 871.47000 \text{ in.} \quad (3)$$

$$\frac{\phi_P}{2} = \left(\frac{180}{n} - \frac{0.006}{2\, r_P} \times 57.295780 \right) \text{ degrees} \quad (4)$$

$$= \frac{180^\circ}{n} - \frac{618.79442''}{r_P} \quad (4a)$$

$$C_P = 2\, r_p \sin \frac{\phi_P}{2}$$

Notes: 1) Use R_o for R if P is a point on the outer tile profile.
Use R_i for R if P is a point on the inner tile profile.

2) "n" is defined in Figure 2.
n = 24 or 12, depending on the point "P" under consideration.

Computation Procedure

Each row starts at the radome base denoted by the point S. From section 1.3, $\theta_S = 4°54'41.055''$. From the design drawing,* one obtains the sequence of tiles. Knowing the tile lengths and intervening adhesive gaps (of 0.006 in.), a set of C_f's (i.e., chords along the profile) can be obtained. Cyclic use of the formulas in section 2.4 for a row would give the outer radius r_P and chord C_P (Figure 2) for ends of all the tiles in the specific row. Calculation tables** were prepared for systematic computations.

* Narmco Engineering Drawing NR 63-044, Appendix X

** Not published

Length C_f , radius r_p , and chord C_p for the two ends of a tile, together with the assumptions on page , define the tile geometry. The dimension table* tabulates the adequate dimensions for all the distinct tiles.

Tolerance (δr) for Tile Radius (r)

Referring to Figure 4, the tolerance δS is given as 0.001 in. By coordinate geometry, δr and δS can be related by the following formulas:

$$\delta r = \frac{\delta S\left(r - \frac{\delta S}{2}\right)}{r - (r - \delta S)\cos\frac{\phi}{2}} \tag{5}$$

$$\underline{\Omega}\ \frac{\delta S}{1 - \cos\frac{\phi}{2}} \tag{6}$$

Sample results are listed in Table 1.

TABLE 1

SAMPLE RESULTS FOR THE TOLERANCE (δr)

Point	r, in.	$\phi/2$			δr from Formula, in.	
		°	'	"	(5)	(6)
S	15-85000	7	29	20.96	0.1163693	0.1172271
P_{49u}	5-41149	14	58	5.65	0.029315	0.029472
P_{183u}	8-11466	7	28	43.74	0.11587948	---

* Narmco Engineering Drawing NR 63-045, Appendix X

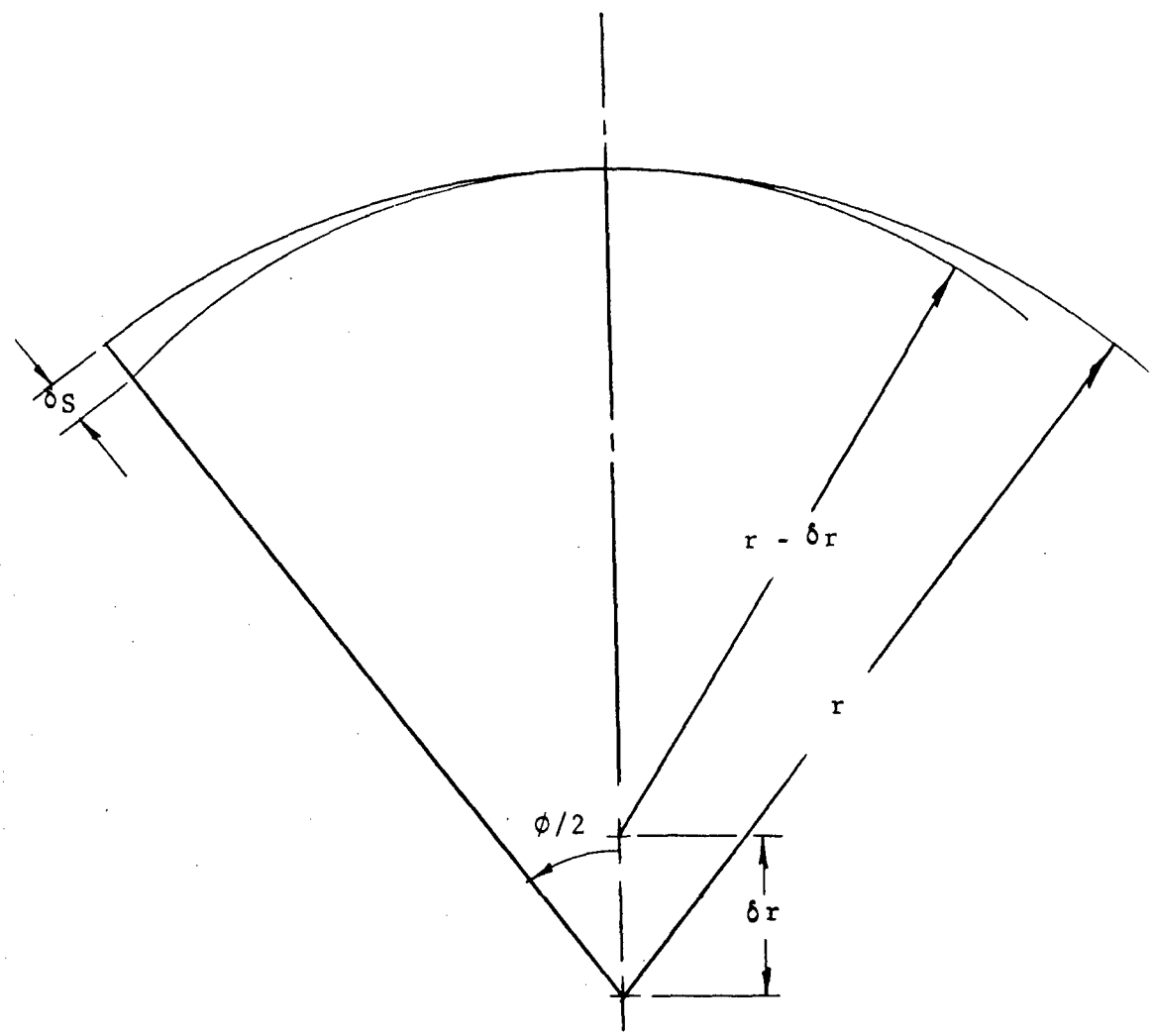


Figure 4. Geometrical Interrelation Between Tolerances δS and δr

CAP DIMENSIONS

The cap is to be joined to tile structure. The dimensions of the cap at this junction will follow those of the end tiles. Figure 5 shows the junction end of the cap. From the assembly configuration,* points C and B correspond to points P_{49u} and P_{191u} respectively, with intervening 0.006-in. thick gluelines.

Dimension Computations

$$P_{49u} = 10°15'32.05"$$

$$P_{191u} = 10°11'43.54"$$

$$\delta\theta_g \text{ for glueline} = 1.39"$$

$$\theta_c = \theta_{P49u} + \delta\theta_g \tag{7}$$

$$\theta_B = \theta_{P191u} + \delta\theta_g \tag{8}$$

Remembering that c lies on the outer tile profile while B is on the inner tile profile, using formula (3), r_c and r_B can be obtained.

Referring to Figure 5,

$$r_A = r_B - 0.108 \cos B \text{ in.} \tag{9}$$

$$r_D = r_A + \frac{0.221}{\cos B} \text{ in.} \tag{10}$$

Knowing $y(\overset{\Delta}{=} r)$, from formula (3), θ for points A and D can be calculated. Also, θ_G is computed on page 345. Knowing θ, one can calculate x from formula (2). Table 2 lists the related results mentioned in this section.

*Narmco Engineering Drawings NR 63-044 and NR 63-046, Appendix X

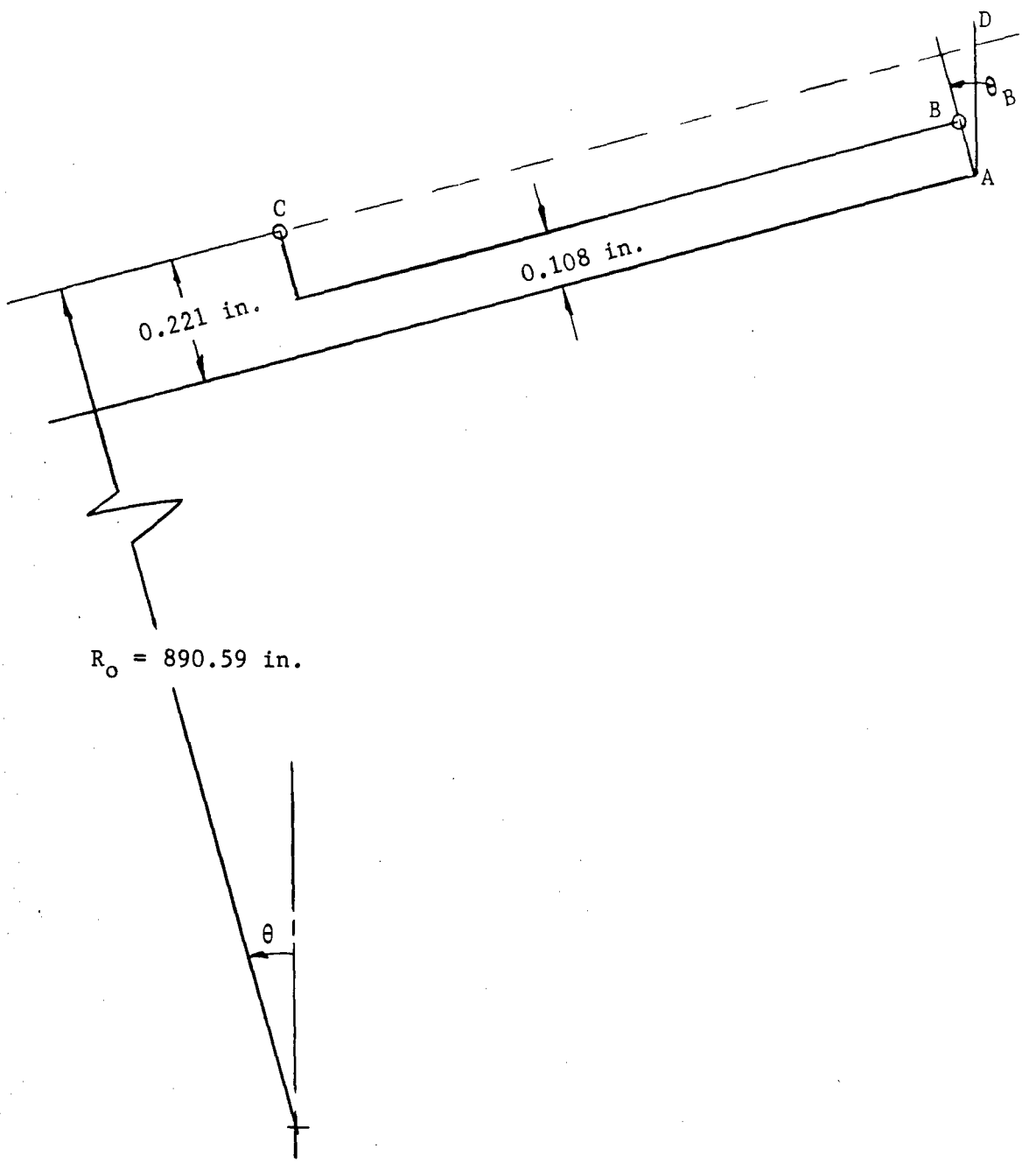


Figure 5. Portion of the Cap at Junction With the Tile Structure

TABLE 2

SOME RESULTS PERTINENT TO THE CAP DIMENSIONS

Point p	θ_p			$r_p \triangleq y_p$, in.	x_p, in.
	°	'	"		
C	10	15	33.44	4.88111	24.93314
B	10	11	43.54	4.94614	---
A	10	11	43.54	4.83985	25.94923
D	10	11	34.31	5.06440	25.94923
G	10	56	10.95	2.94551	14.58829

In the above table, $\theta_B = \theta_A$ and $x_D = x_A$

Computed Tolerances for Cap Dimensions

Profile tolerance (δR_o) – Referring to Figure 6, δS is given as 0.001 in. R and chord AB are known. Let AB = a . Then

$$\sin \frac{\phi}{2} = \frac{a}{2R} \quad \text{and} \quad \sin \frac{\phi'}{2} = \frac{a}{2(R + \delta R)} \tag{11}$$

It can be shown by the geometry that

$$DD' = \delta S = R\left(\cos \frac{\phi'}{2} - \cos \frac{\phi}{2}\right) - \delta R\left(1 - \cos \frac{\phi'}{2}\right) \tag{12}$$

Given: $R = R_o = 890.59$ in.

$a \leq 13$ in.

Assuming δR, angles ϕ and ϕ' can be found from formula (11). Substitution for R, δR, ϕ', and ϕ in equation (12) gives δS. This process is repeated until $\delta S \leq 0.001$ in., the prescribed value. This gives 30 in. $< \delta R_o$ < 40 in.

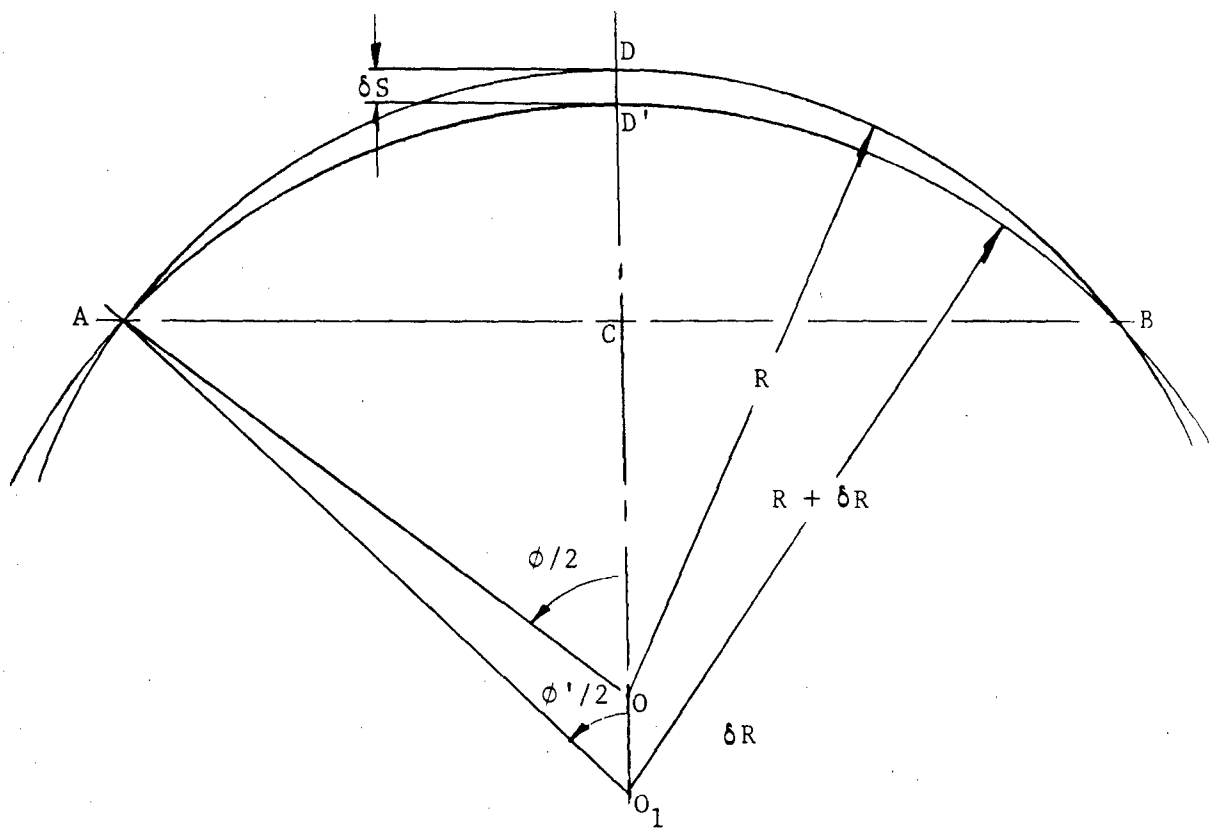


Figure 6. Geometrical Interrelation for Cap Profile Tolerances δS and δr

Location of point G: A tolerance of 0.0005 in. is given in r_G (i.e., in y_G). Finding the tolerance in x_G is required.

Differentiating formulas (2) and (3), and dividing the results, one obtains

$$\frac{dx_p}{dy_p} = \frac{-R \cos \theta_P}{R(-\sin \theta_P)} = \cot \theta_P$$

$$\therefore \quad dx_G = dy_G \cos \theta_G = (0.0005) \text{ in. cot } 10°56'10.95''$$

$$= 0.0025876 \text{ in.}$$

APPENDIX VI

STRUCTURAL ANALYSIS OF RADOME BASE ATTACHMENT

STRUCTURAL ANALYSIS OF RADOME BASE ATTACHMENT

The method outlined in WADD-TR 59-22, Aerodynamic and Structural Analysis of Radome Shells, Volume I, was used to obtain the external dynamic pressure. The external pressure along the radome obtained by this procedure is shown on page 360. The dynamic pressure was established by assuming an attached shock at the nose of the radome. The station pressure was then found by the shock expansion method.

The resulting shear and bending moment for this radome is given on page 361. reflecting the same wall stress as the combined loads of external pressures, weight, and inertia effects. The wall stress was calculated as 1765 psi; this would result in a bending moment of 310,000 in./lb at the radome attach point.

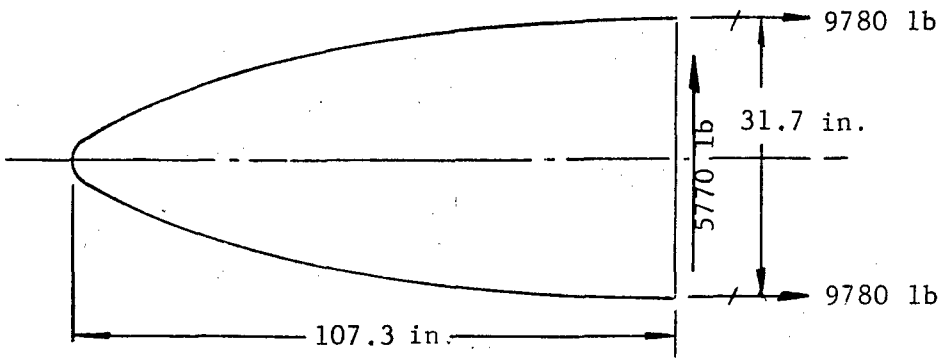
The temperature profiles and the shear and bending moment curves give the recommended loading information for the test program.

Attachment – Radome Base

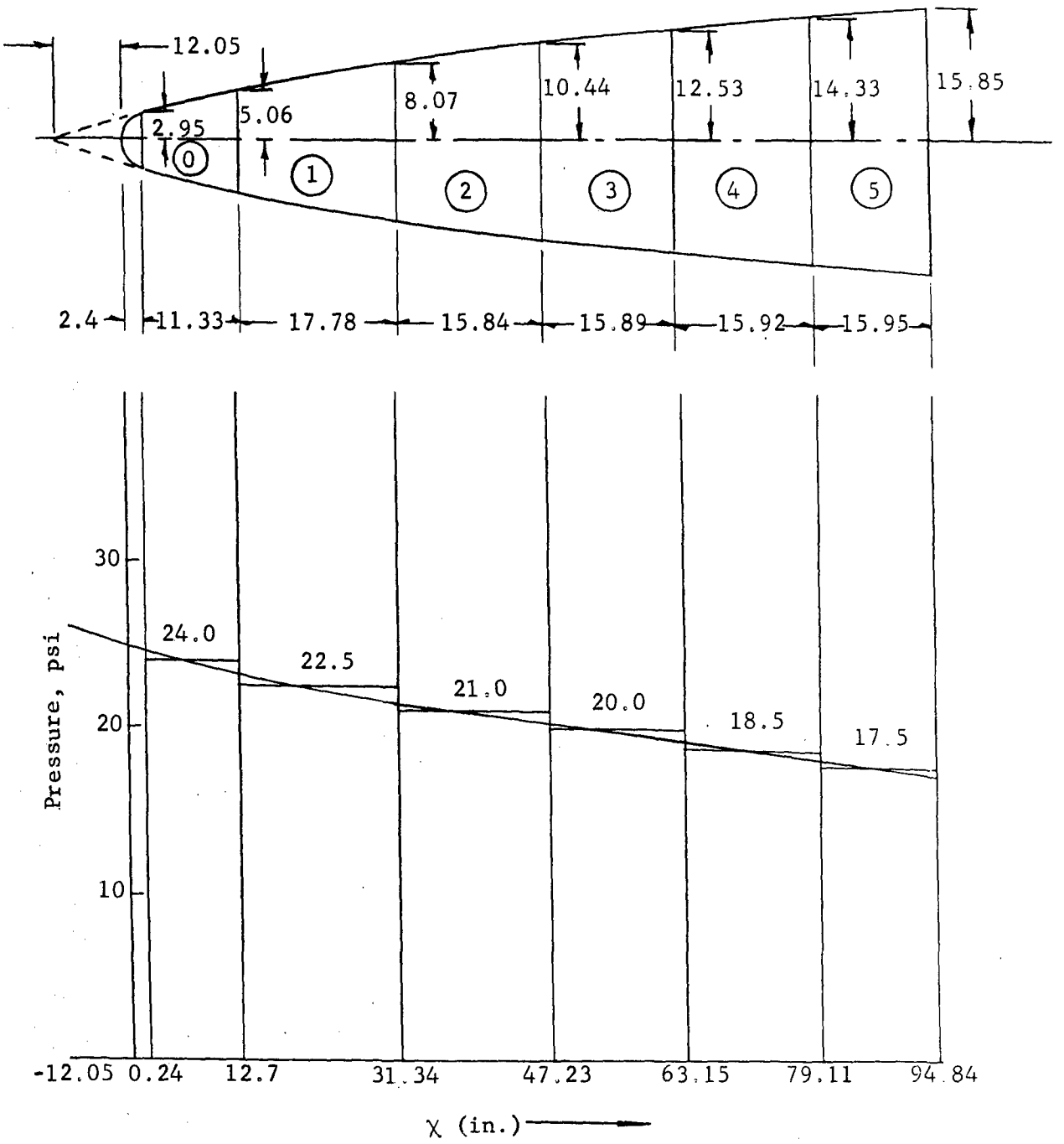
Loads: $M_{max} = 310{,}000$ in.-lb

$V_{max} = 5{,}770$ lb

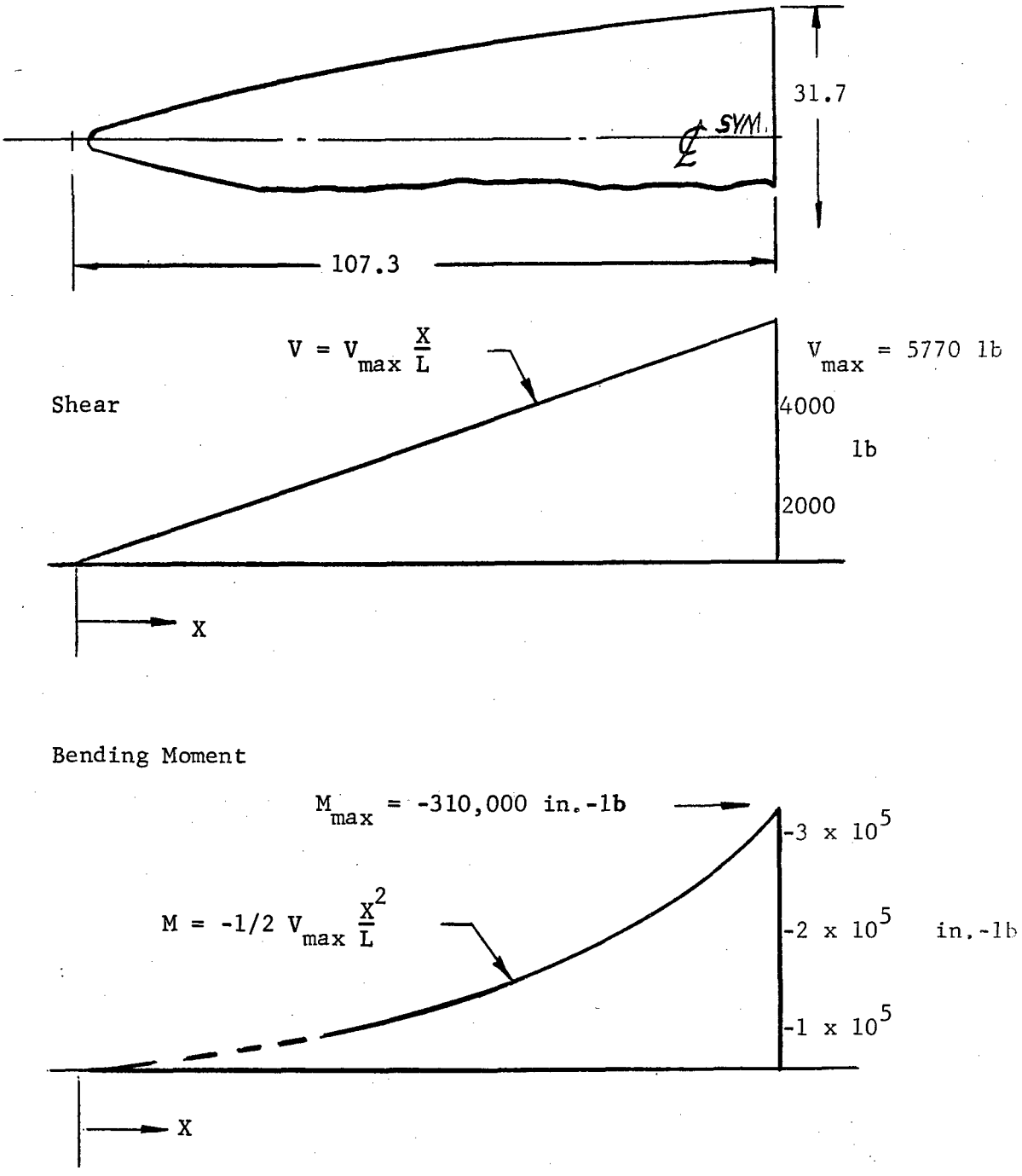
Bending Loads:



$$P = \frac{310{,}000}{31.7} = 9780 \text{ lb}$$

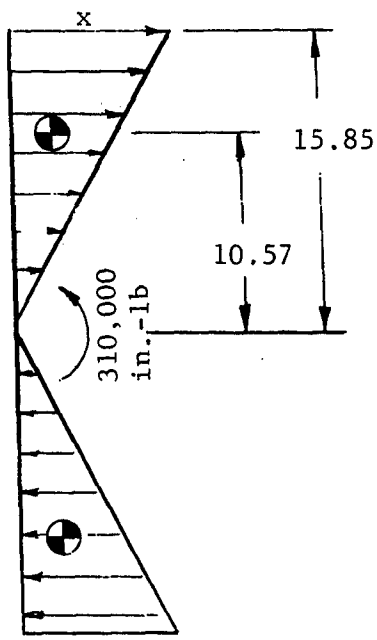


Dynamic Pressure Distribution



Static Shear and Bending Moment

Assume a triangular load distribution.

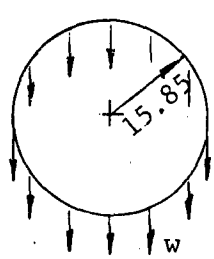


$$\frac{310{,}000}{2(10.57)} = 14{,}664 \text{ lb}$$

$$\frac{x \cdot 15.85}{2} = 14.664$$

$$x = 1850 \text{ lb/in. max}$$

Shear Loads:



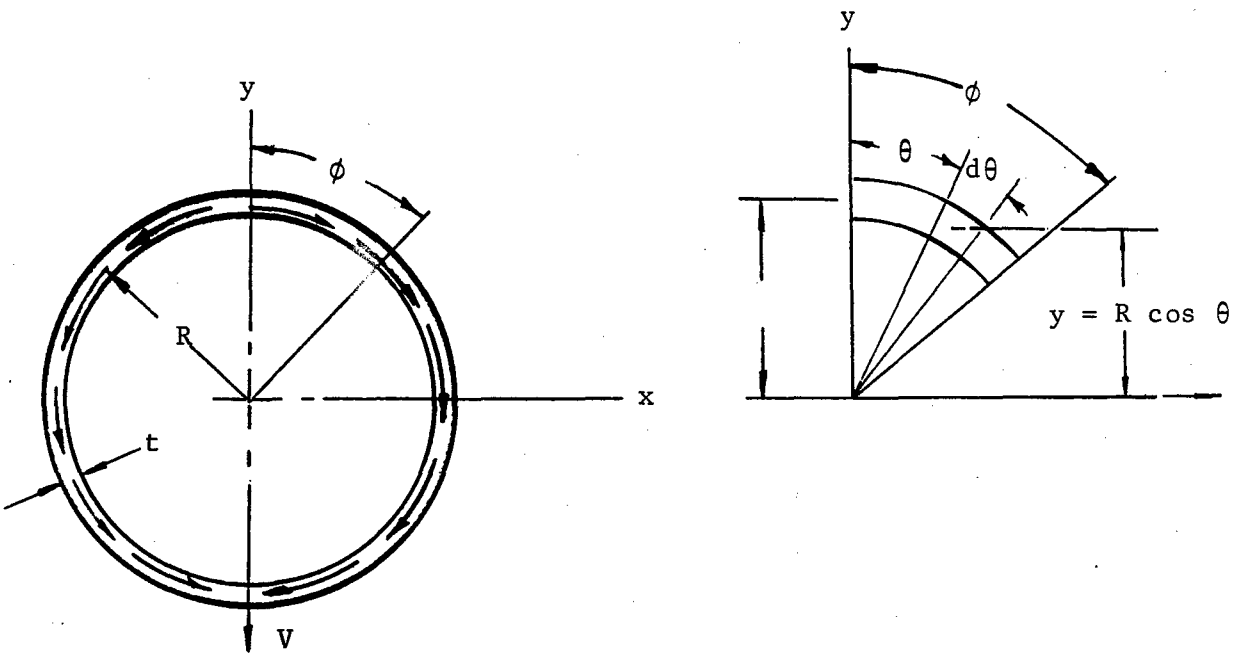
$V = 5770$ lb

$C = 2\pi R = 2(3.1416)(15.85)$

$C = 99.59$ in.

$$W = \frac{5770}{99.59} = 58 \text{ lb/in.}$$

Shear Flow:



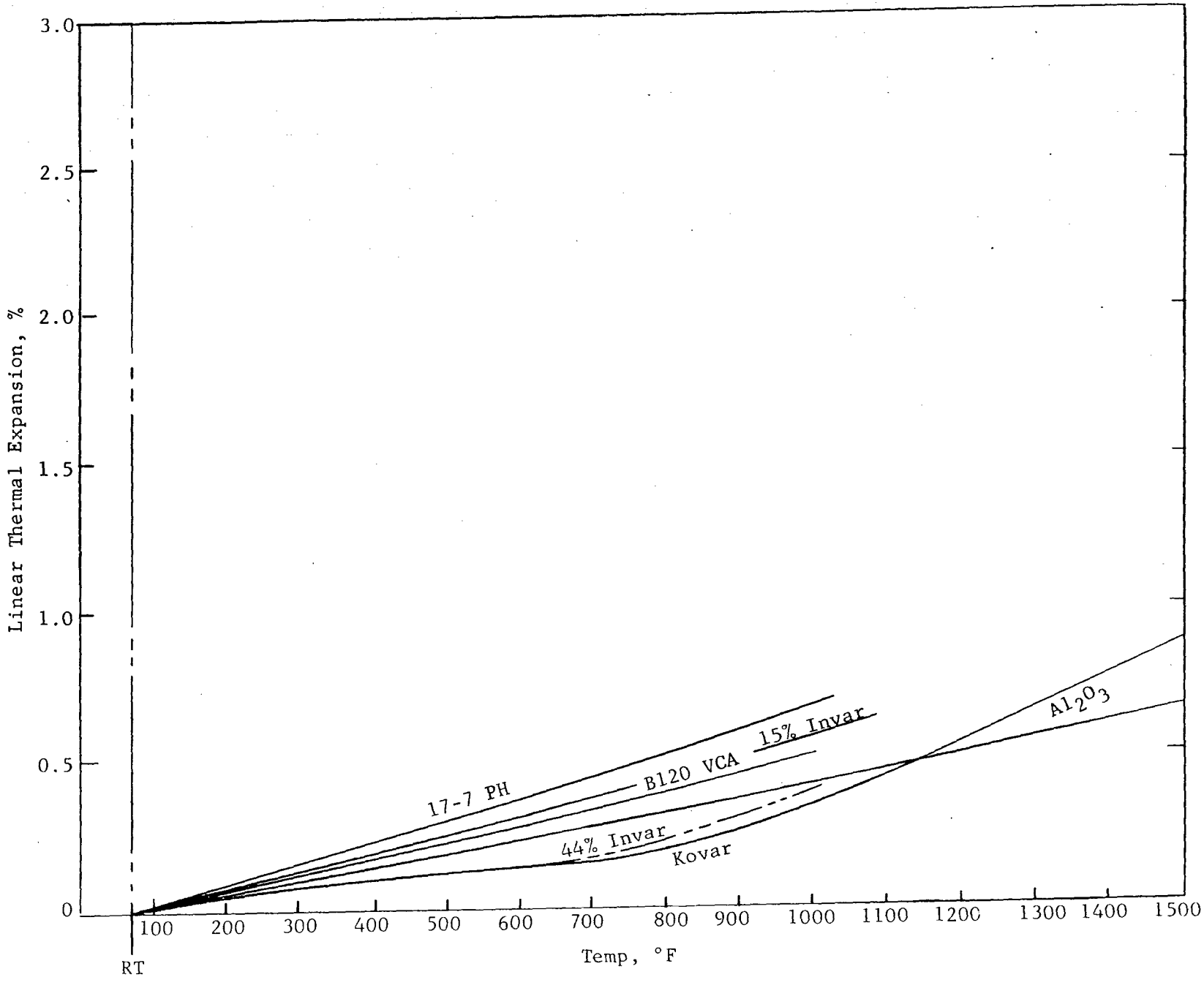
$$q = f_s b = \frac{V}{I}\int y\, d\, A\ ; \qquad \int y\, d\, A = \int_o^{\phi} R^2 t \cos\theta\, d\theta = R^2 t \sin\Phi$$

where $dA = R\, t\, d\theta$ and $y = R \cos\theta$

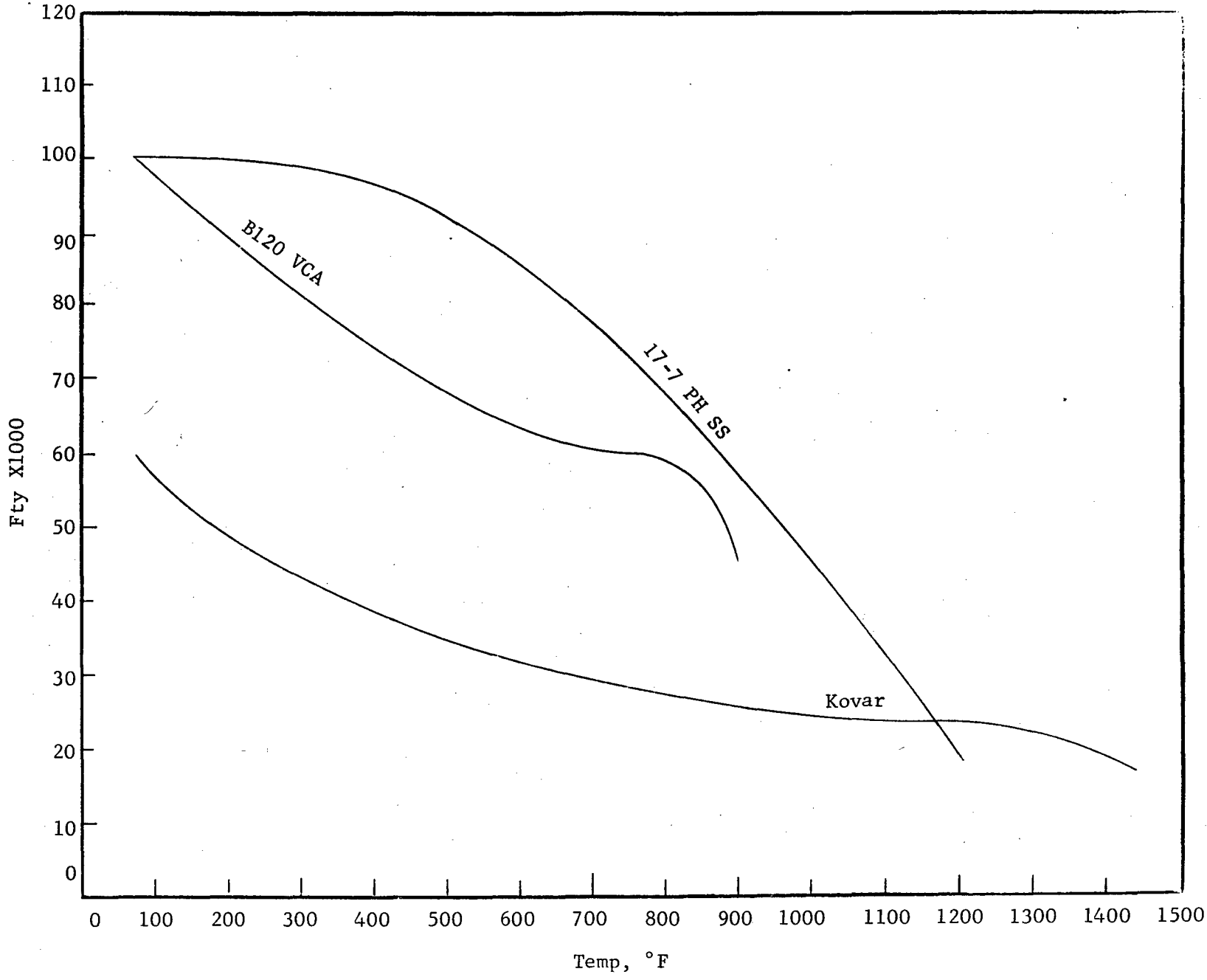
Therefore:

$$q = \frac{V}{I}\int y\, d\, A = \frac{V}{\pi R^3 t} R^2\, t \sin\phi$$

$$\boxed{q = \frac{V}{\pi R} \sin\phi}$$



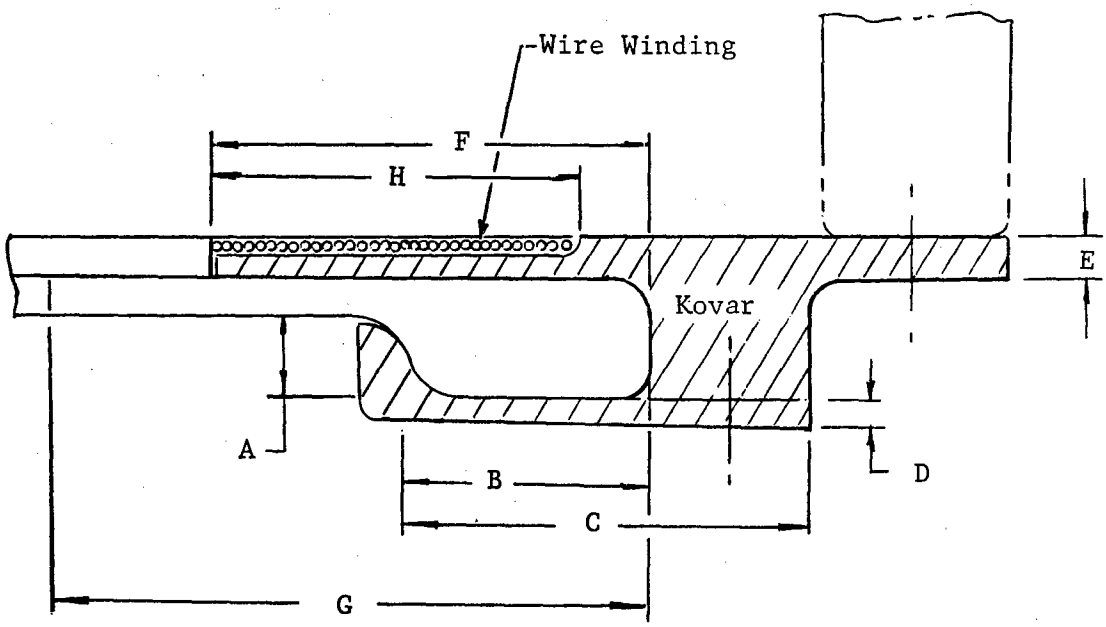
Thermal Expansion of Candidate Design Materials



Tensile Yield Strength of Candidate Design Materials

$$q = \frac{V}{\pi R} \sin \Phi \qquad \text{where} \quad V = 5770 \text{ lb}, \quad R = 15.85 \text{ in.}$$

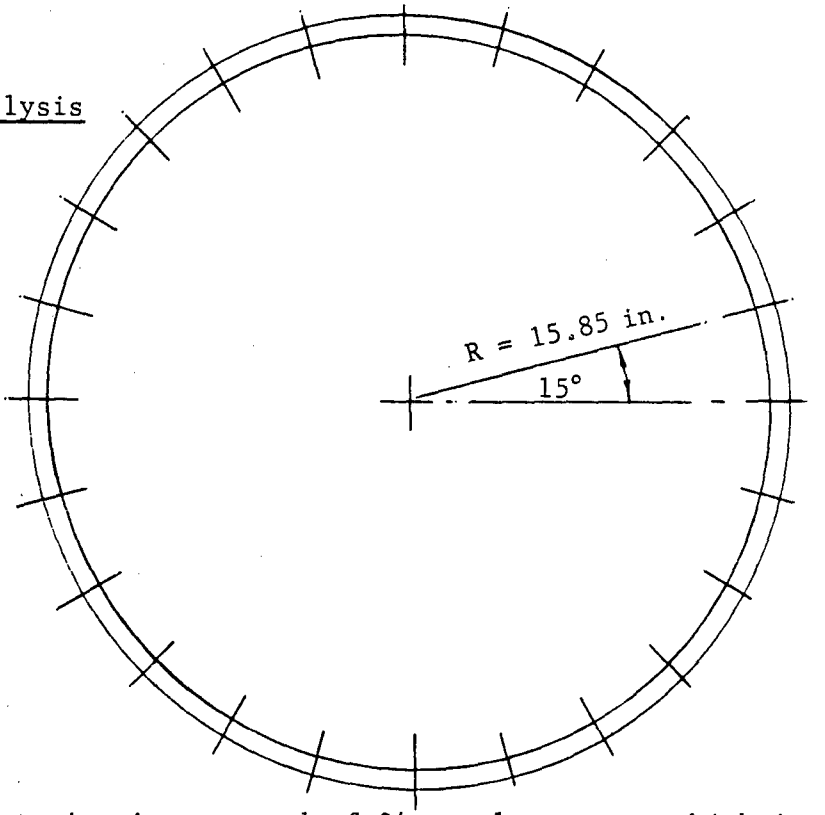
ϕ	$\sin \Phi$	$\frac{V}{\pi R}$	q
0°	0	115.89	0
30°	0.500		57.94
45°	0.707		81.93
60°	0.866		100.36
75°	0.966		111.95
90°	1.000		115.89



Letter	Dimension, in.
A	0.38
B	1.20
C	1.80
D	0.10
E	0.20
F	1.997
G	3.000 and 5.00
H	1.70

Edge Attachment Compression Design

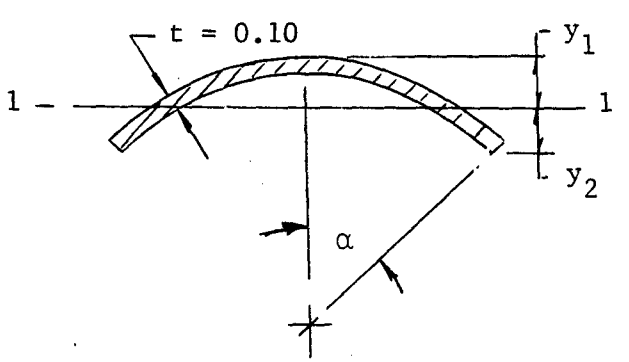
Stress Analysis



The support ring is composed of 24 equal segments which in turn are bolted to the base ring.

Circumference = $2\pi R$ = 2(3.1416)(15.85) = 99.5 in.

24 segments of 99.5/24 = 4.15 in. each.



$$I_{1\text{-}1} = R^3 t \left(\alpha + \sin\alpha \cos\alpha - \frac{2\sin^2\alpha}{\alpha}\right)$$

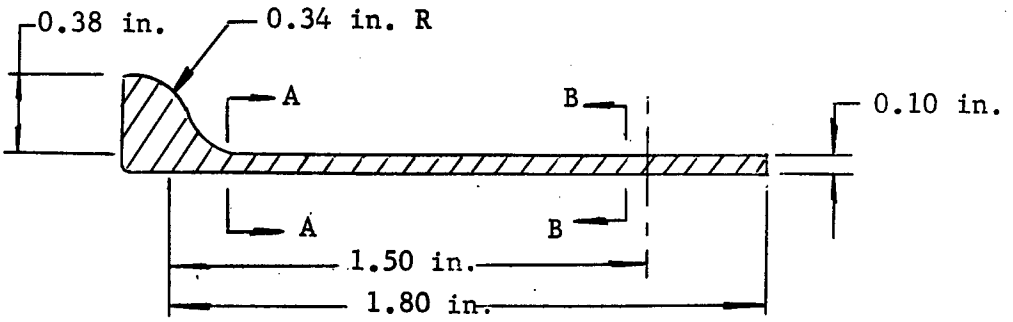
$$y_1 = R\left(1 - \frac{\sin\alpha}{\alpha}\right)$$

$$y_2 = R\left(\frac{\sin\alpha}{\alpha} - \cos\alpha\right)$$

$$\alpha = 15°/2 = 7.5°$$

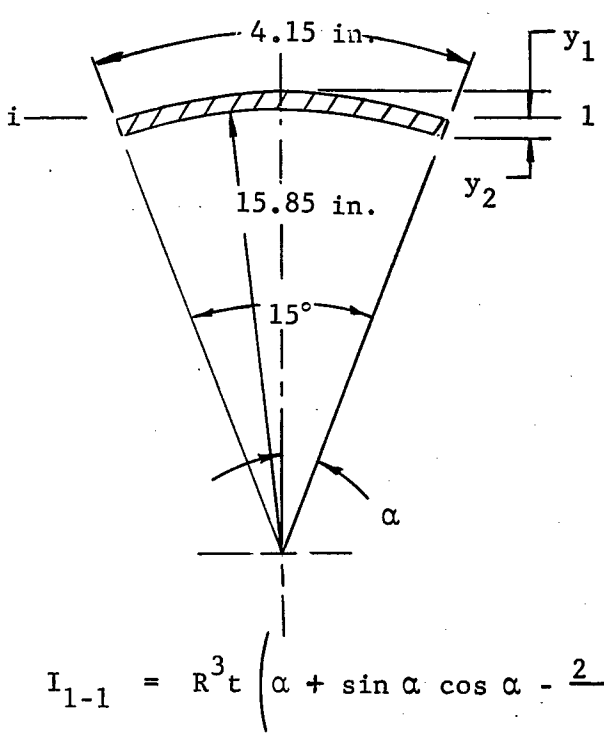
$$\alpha = 0.13089 \text{ radians}$$

Tension Lip



There are 24 tension lips on the inside periphery of the radome. The only load applied on these lips is the tension produced by the bending of the radome.

Max. tension load = 1850 lb/in.



Circumference of radome = 2 π R

= 2(3.1416)(15.85) = 99.5 in.

24 segments of 99.5/24 = 4.15 in. each

$2\alpha = 15°$

$\alpha = 7.5° = 0.13098$ radians

$\sin\alpha = \sin 7.5° = 0.13053$

$\cos\alpha = \cos 7.5° = 0.99144$

$$I_{1\text{-}1} = R^3 t \left(\alpha + \sin\alpha \cos\alpha - \frac{2\sin^2\alpha}{\alpha} \right)$$

Tension Lip – Stress Analysis

$$I_{1\text{-}1} = (15.85^3)(0.10)\left[0.131 + (0.13053)(0.99144) - \frac{2(0.13053^2)}{0.131}\right]$$

$$I_{1\text{-}1} = 0.11547 \text{ in.}^4$$

$$y_1 = R\left(1 - \frac{\sin\alpha}{\alpha}\right) = 15.85\left(1 - \frac{0.13053}{0.13089}\right)$$

$$y_1 = 0.0437 \text{ in.}$$

$$y_2 = R\left(\frac{\sin\alpha}{\alpha} - \cos\alpha\right) = 15.85\left(\frac{0.13053}{0.13089} - 0.99144\right)$$

$$y_2 = 0.0919 \text{ in.}$$

Max. moment due to tension load on protrusion:

$$M = 1850 \times 0.24 = 444 \text{ in.-lb}$$

Maximum deflection:

$$\delta = \frac{1}{2}\frac{M\ell^2}{EI} = \frac{1}{2}\frac{444(1.5^2)}{0.11547 \times 21.46 \times 10^6}$$

For 17-7 PH:

$E = 29 \times 10^6$ at room temperature

For 1000°F take 74%

$E = 21.46 \times 10^6$ at 1000°F

} MIL-HDBK-5, Aug 1962

$$\therefore \delta = \frac{999}{4.956 \times 10^6}$$

$$\delta = 0.000201 \text{ in.}$$

Tension Side:

$$f_t = \frac{M\,c}{I} + \frac{P}{A}$$

$$f_t = \frac{444 \times 0.0437}{0.11547} + \frac{1850}{4.15 \times 0.10}$$

$$f_t = 4628 \text{ psi}$$

APPENDIX VII

RADOME STRUCTURAL ANALYSIS

RADOME STRUCTURAL ANALYSIS

Radome Structure

The radome has an ogive shape, and cannot be analyzed as a single truncated cone. The shell structure can be approximated by a series of separate, truncated, conical shells, and a spherical cap.

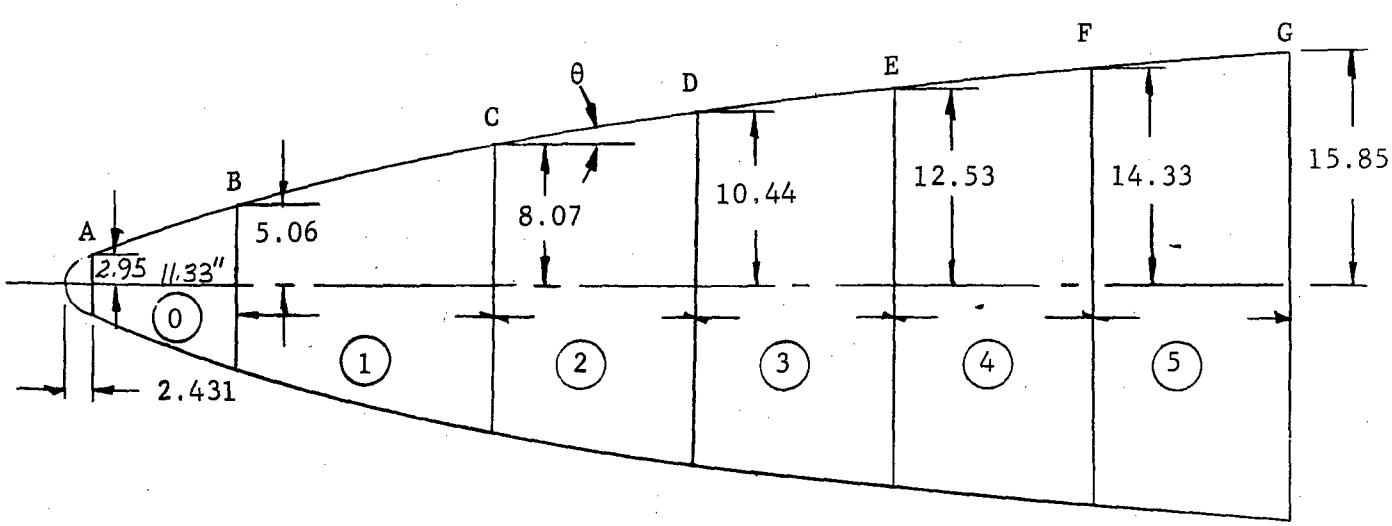
Due to the geometry of the radome, it was decided to perform a membrane stress analysis for the pressure loading. The cross-sectional diameter of the radome is considerably larger than the wall thickness, which justifies the approach.

The structural analysis is a pure membrane analysis, with a modification required to obtain the hoop and longitudinal bending moments at the boundaries of the truncated cones.

The stress analysis is performed for an axisymmetric radial pressure, varying from the tip of the radome to the base. The radome is divided into six arbitrary, truncated cones, and a uniform pressure is applied to each cone. The membrane loads are obtained for each cone and the longitudinal and tangential stresses are subsequently obtained.

As a conclusion to this stress analysis, a summary is presented showing the hoop and longitudinal loads, moments, and the stresses generated by these loads for each truncated cone.

Radome Geometry



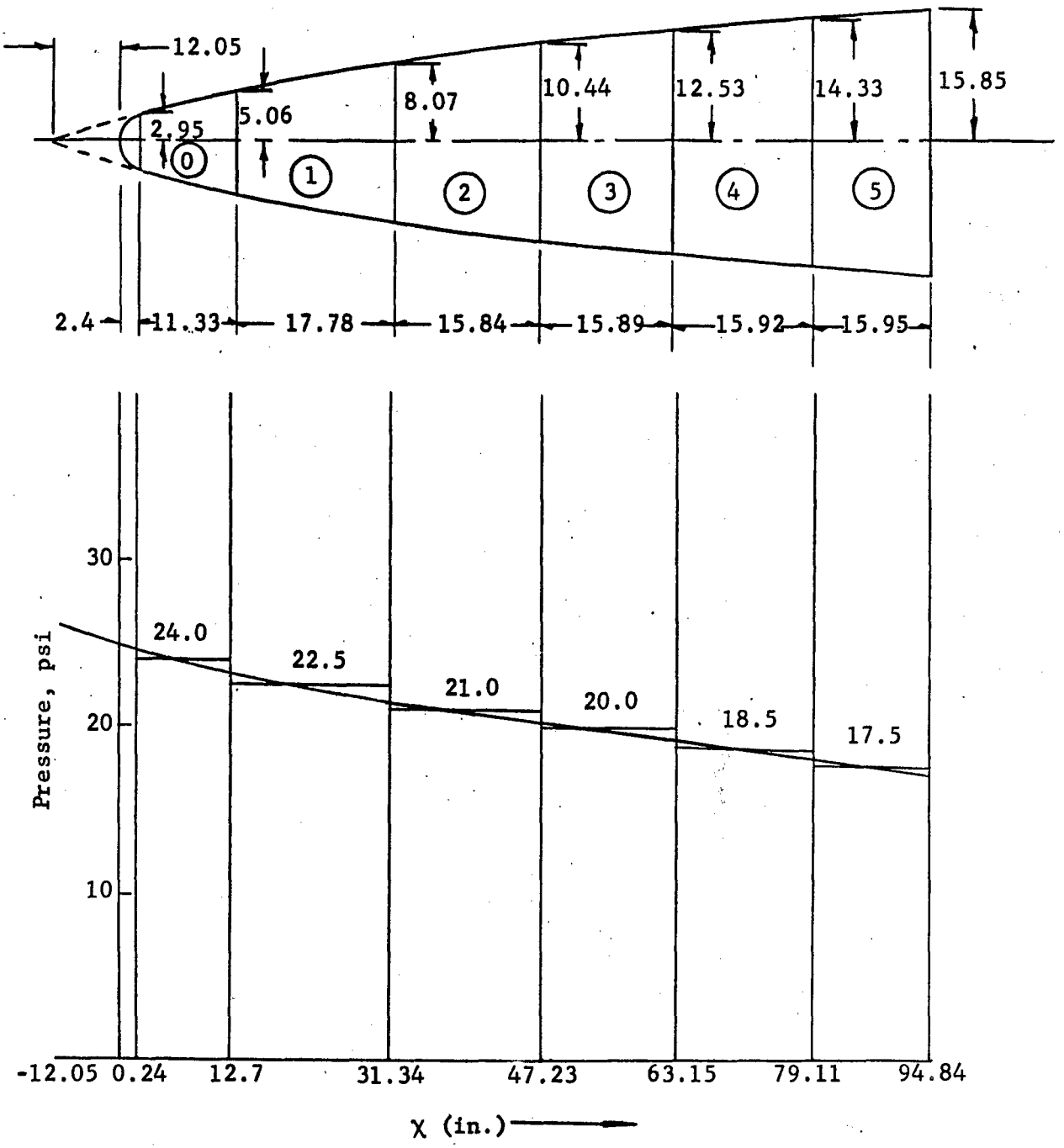
The radome has an ogive shape and it cannot be analyzed as a single truncated cone. The shell structure can be approximated by a series of separate, truncated, conical shells

Ogive Radius = 890.50 in. = R

The following is a pure membrane analysis, plus a modification, in order to get the hoop and longitudinal bending moments at the boundaries of the truncated cones:

	θ	Sin θ	Diff.	Axial Distance
	①	②	Δ ② = ③	R x ③ = ④
B	10° 11' 40.44"	0.17699		11.33489
			0.01996	
C	9° 2' 4.60"	0.15703		17.776568
			0.01779	
D	8° 0' 14.76"	0.13924		15.8409
			0.01784	
E	6° 58' 23.54"	0.12140		15.8871
			0.01788	
F	5° 56' 32.30"	0.10353		15.922
			0.01791	
G	4° 54' 41.06"	0.08561		15.952

DYNAMIC PRESSURE DISTRIBUTION

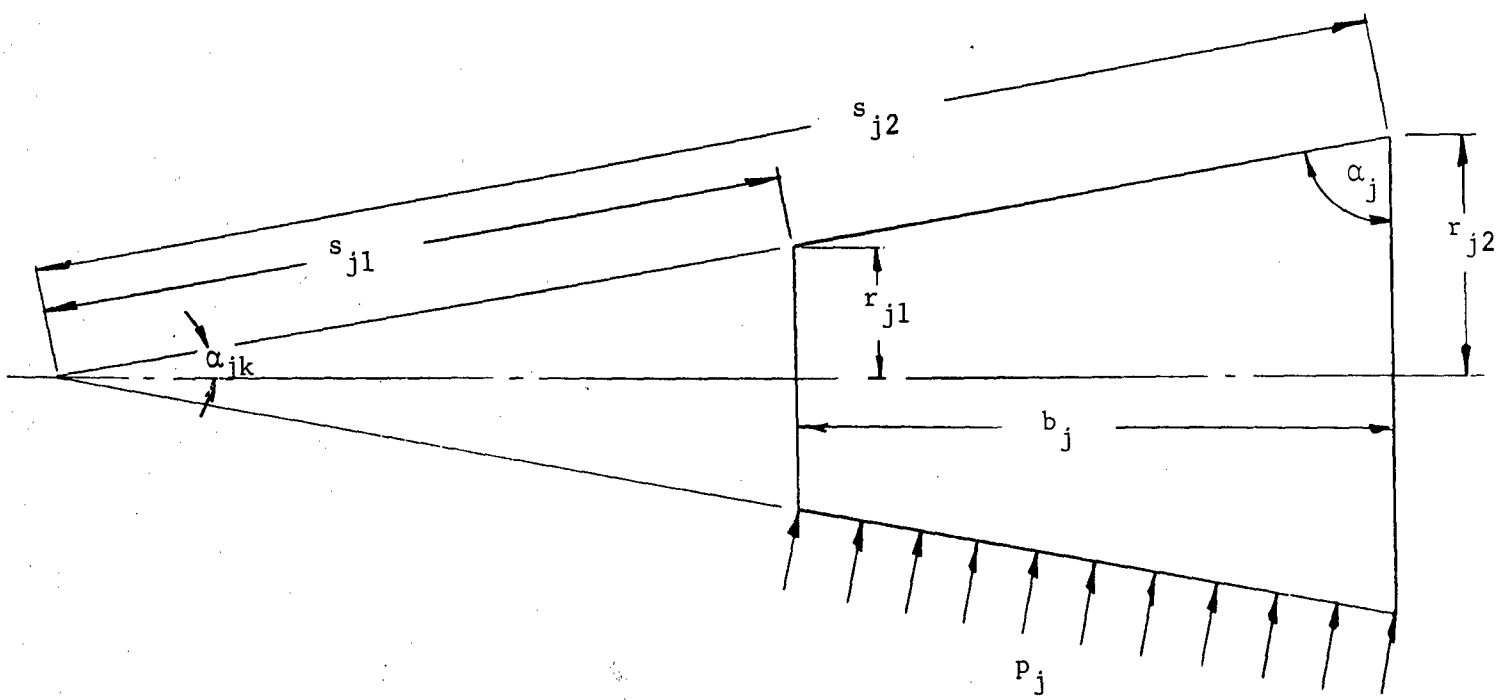


Membrane Analysis

The stress analysis is performed for an axisymmetric radial pressure, varying from the tip of the radome to the base.

The radome is divided into six arbitrary truncated cones, and a uniform pressure is applied to each cone. The membrane loads will be obtained for each cone and the longitudinal and tangential stresses will be subsequently obtained.

The nomenclature for each cone is as follows:



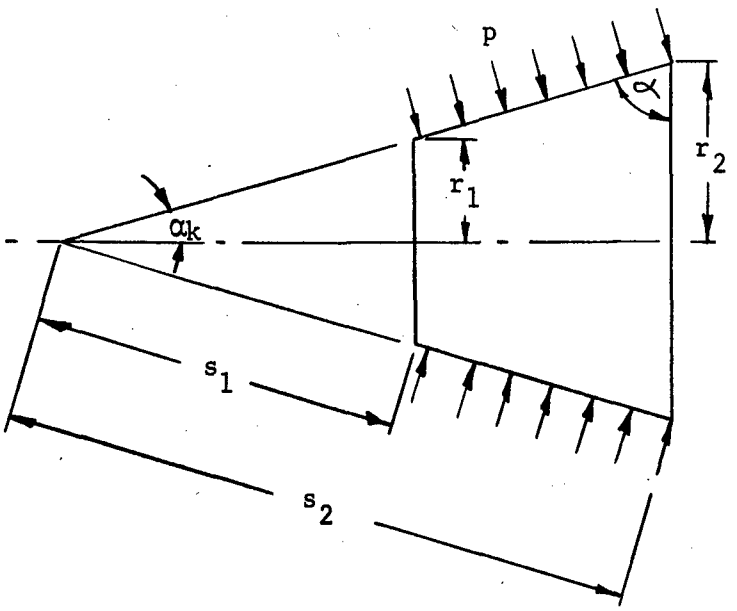
The above sketch shows the jth truncated cone when the quantities r_{j1}, r_{j2}, and b_j are known. Then:

$$\cot \alpha_j = \frac{r_{j2} - r_{j1}}{b_j} \tag{1}$$

$$s_{j1} = \frac{r_{j1}}{\cos \alpha_j} \tag{2}$$

$$s_{j2} = \frac{r_{j2}}{\cos \alpha_j} \tag{3}$$

The following approach is used to find the longitudinal and hoop loads (Reference 1):



where

$$\phi = \alpha$$

$$\alpha_k + \alpha = 90°$$

$$r = s \cos \alpha$$

$$s = \frac{r}{\cos \alpha}$$

$$r_2 = \frac{r}{\sin \alpha} = s \cot \alpha$$

From Reference 1,

$$\frac{d}{ds}(N_s s) - N_\theta = - p_s s$$

$$\underline{\underline{N_\theta = p_r s \cot \alpha}} \qquad (4)$$

(1) W. Flügge, Stresses in Shells, 1960, p. 37.

By simple addition of the above two equations, a first-order differential equation is obtained for N_s:

$$\frac{d}{ds}(N_s s) = -(p_s - p_r \cot \alpha)s$$

By simple integration, the meridional force is found from the previous equation:

$$N_s = -\frac{1}{s}\int (p_s - p_r \cot \alpha)s \, ds$$

where p_r = Pressure normal to surface = p

p_s = Pressure parallel to surface = 0

Therefore:

$$N_s = -\frac{1}{s}\int (-p \cot \alpha)s \, ds$$

$$N_s = \frac{p \cot \alpha}{2s}\left[\frac{s_2^2}{2}\right]_{s_1}^{s}$$

$$\underline{\underline{N_s = \frac{p \cot \alpha}{2s}\left[s_2^2 - s_1^2\right]}} \qquad (5)$$

Summarizing, the following expressions for the membrane loads are

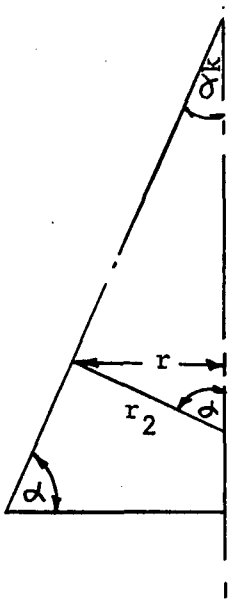
$$N_\theta = p\, s \cot \alpha$$

$$N_s = \frac{p \cot \alpha}{2s}\left(s_2^2 - s_1^2\right)$$

$$N_s = \frac{N_\theta}{2}\left(1 - \frac{s_1^2}{s_2^2}\right)$$

Deflections (Reference 2)

For the dynamic pressure analysis, the radome is a symmetrically loaded shell having the form of a surface of revolution. In the case of symmetrical deformation of a shell, a small displacement of a point can be resolved into two components: v in the direction of the tangent to the meridian, and w in the direction of the normal to the middle surface.



The strain of the shell in the meridional direction is

$$\epsilon_s = \frac{dv}{ds} \qquad (6)$$

The radius r of the circle increases by the amount

$$v \cos \alpha - w \sin \alpha$$

The circumference of the parallel circle increases in the same proportion as its radius

$$\epsilon_\theta = \frac{1}{r} (v \cos \alpha - w \sin \alpha) \qquad (7)$$

But: $r = s \cos \alpha$

Therefore: $\epsilon_\theta = \frac{1}{s \cos \alpha} (v \cos \alpha - w \sin \alpha)$

$$= \frac{1}{s} (v - w \tan \alpha)$$

The following is obtained from the previous equation:

$$w = (v - \epsilon_\theta s) \cot \alpha$$

And:

$$\frac{dw}{ds} = \cot \alpha \left(\frac{dv}{ds} - \frac{d}{ds} \epsilon_\theta s \right) \qquad (8)$$

(2) S. Timoshenko, Theory of Plates and Shells, p. 446.

The strain components can be expressed as follows:

$$\epsilon_s = \frac{dv}{ds} = \frac{1}{Eh} (N_s - \mu N_\theta) \text{ (Reference 2)}$$

Substituting values of N_s and N_θ:

$$\epsilon_s = \frac{p \cot \alpha}{Eh} \left\{ \frac{s^2}{2s} - \frac{s_1^2}{2s} - \mu s \right\}$$

Let:

$$A = \frac{p \cot \alpha}{Eh}$$

$$\epsilon_s = A \left\{ s \left(\frac{1}{2} - \mu \right) - \frac{s_1^2}{2s} \right\} \tag{9}$$

Similarly:

$$\epsilon_\theta = \frac{1}{Eh} (N_\theta - \mu N_s) \text{ (Reference 2)}$$

$$\epsilon_\theta = \frac{p \cot \alpha}{Eh} \left\{ s - \mu \left(\frac{s}{2} - \frac{s_1}{2s} \right) \right\}$$

$$\epsilon_\theta = A \left\{ s \left(1 - \frac{\mu}{2} \right) + \frac{\mu s_1^2}{2s} \right\} \tag{10}$$

Multiplying the previous equation by s and differentiating with respect to s:

$$\frac{d}{ds} (\epsilon_\theta s) = \frac{d}{ds} \left\{ A \left[s^2 \left(1 - \frac{\mu}{2} \right) + \frac{\mu s_1^2}{2} \right] \right\}$$

$$= A \cdot 2s \cdot \left(1 - \frac{\mu}{2} \right) \tag{11}$$

By substituting equation (11) back into equation (8), one obtains:

$$\frac{dv}{ds} = A\left\{s\left(\frac{1}{2} - \mu\right) - \frac{s_1^2}{2s}\right\}$$

and

$$\frac{d}{ds}(\epsilon_\theta s) = A \cdot 2s \cdot \left(1 - \frac{\mu}{2}\right)$$

This into equation (8):

$$\frac{dw}{ds} = \cot\alpha\left\{As\left(\frac{1}{2} - \mu\right) - \frac{A s_1^2}{2s} - 2As\left(1 - \frac{\mu}{2}\right)\right\}$$

$$\frac{dw}{ds} = \cot\alpha\left\{As\left(\frac{1}{2} - \mu - 2 + \mu\right) - \frac{A s_1^2}{2s}\right\}$$

$$\frac{dw}{ds} = \cot\alpha\left\{-1.5\,As - \frac{A s_1^2}{2s}\right\}$$

$$\frac{dw}{ds} = A\cot\alpha\left\{-1.5\,s - \frac{s_1^2}{2s}\right\} \qquad (12)$$

Differentiating:

$$\frac{d^2w}{ds^2} = A\cot\alpha\left(-1.5 + \frac{s_1^2}{2}\quad\frac{1}{s^2}\right) \qquad (13)$$

Change of Curvature

From Reference 2, the change of curvature of the meridian is

$$\chi_s = \frac{d^2w}{ds^2} \qquad (14)$$

The change of curvature in the plane perpendicular to the meridian is

$$\chi_\theta = \frac{\cot\alpha}{s\cot\alpha}\frac{dw}{ds} = \frac{1}{s}\frac{dw}{ds} \qquad (15)$$

Also, from equation (12):

$$\frac{dw}{ds} = A \cot \alpha \left(- 1.5 \, s - \frac{s_1^2}{2s} \right)$$

Therefore:

$$\chi_\theta = A \cot \alpha \left(- 1.5 - \frac{s_1^2}{2s^2} \right) \tag{16}$$

From equation (13):

$$\frac{d^2w}{ds^2} = A \cot \alpha \left(- 1.5 + \frac{s_1^2}{2s^2} \right)$$

and:

$$\chi_s = \frac{d^2w}{ds^2} = A \cot \alpha \left(\frac{s_1^2}{2s^2} - 1.5 \right) \tag{17}$$

Using equations (14) and (15):

$$M_s = - D \left\{ \frac{d^2w}{ds^2} + \mu \frac{1}{s} \frac{dw}{ds} \right\}$$

$$M_s = - D \left\{ \chi_s + \mu \chi_\theta \right\}$$

Substituting for χ_s and χ_θ:

$$M_s = - D \cot \alpha \, A \left[\frac{s_1^2}{2s^2} - 1.5 + \mu \left(- 1.5 - \frac{s_1^2}{2s^2} \right) \right]$$

$$M_s = - DA \cot \alpha \left[\frac{s_1^2}{2s^2} (1 - \mu) - 1.5 (1 + \mu) \right]$$

$$M_s = DA \cot \alpha \left[1.5 (1 + \mu) - \frac{s_1^2}{2s^2} (1 - \mu) \right] \tag{18}$$

Similarly, for M_θ:

$$M_\theta = - D \left[\frac{1}{s} \frac{dw}{ds} + \mu \frac{d^2 w}{ds^2} \right] = - D \left[\chi_\theta + \mu \chi_s \right]$$

$$M_\theta = - DA \cot \alpha \left[- 1.5 - \frac{s_1^2}{2s^2} + \mu \frac{s_1^2}{2s^2} - 1.5 \mu \right]$$

$$M_\theta = DA \cot \alpha \left[1.5 (1 + \mu) + \frac{s_1^2}{2s^2} (1 - \mu) \right] \qquad (19)$$

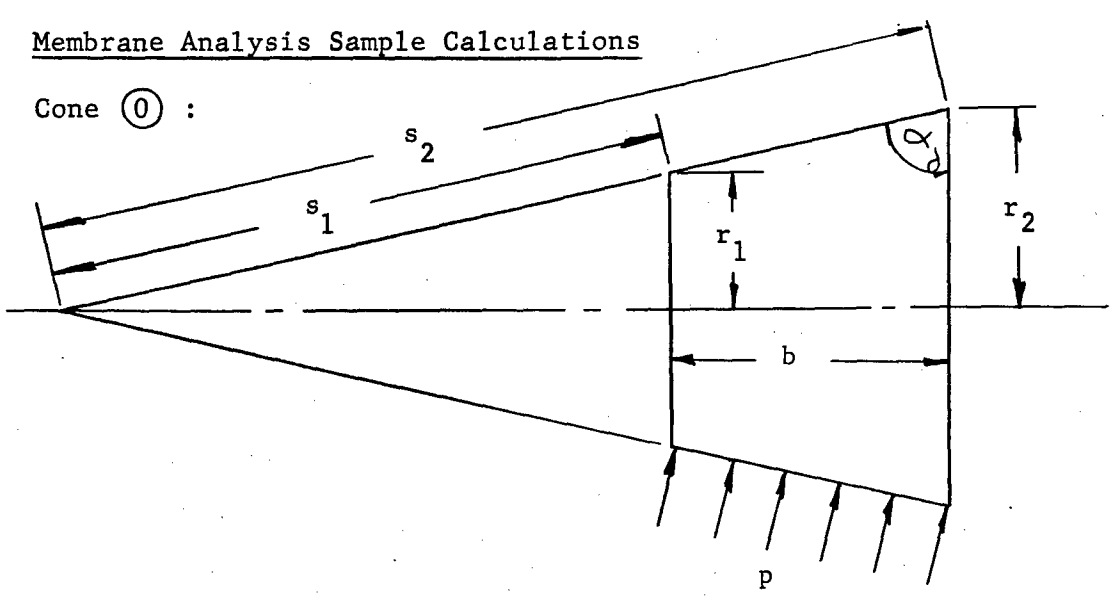
Summarizing:

$$M_s = DA \cot \alpha \left[1.5 (1 + \mu) - \frac{s_1^2}{2s^2} (1 - \mu) \right]$$

$$M_\theta = DA \cot \alpha \left[1.5 (1 + \mu) + \frac{s_1^2}{2s^2} (1 - \mu) \right]$$

Membrane Analysis Sample Calculations

Cone ⓪ :



r_1	r_2	b	p	α	s_1	s_2
2.95	5.06	11.33	-24.0 psi	79° 27'	16.11229	27.63668

From equations (4) and (5):

$$N_\theta = p\, s_2 \cot \alpha = 24.0 \times 27.63668 \times 0.18623$$

$$\underline{N_\theta = -123.524 \text{ lb/in.}}$$

$$N_s = \frac{-123.524}{2}\left(1 - \frac{s_1^2}{s_2^2}\right) = \frac{-123.524}{2}\left(1 - \frac{16.11229^2}{27.63668^2}\right)$$

$$N_s = -61.762\left(1 - \frac{259.606}{763.786}\right) = -61.762\ (1 - 0.340) = -61.762\ (0.66)$$

$$\underline{N_s = -40.769 \text{ lb/in.}}$$

From equations (18) and (19):

$$M_s = DA \cot \alpha \left[1.5\ (1 + \mu) - \frac{s_1^2}{2\, s_2^2}\ (1 - \mu)\right]$$

Where:

$$D = \frac{Eh^3}{12\ (1 - \mu^2)}$$

$$A = \frac{p \cot \alpha}{Eh}$$

Assuming:

$$\mu_{@\ 1000°F} = 0.19 \qquad \text{and} \qquad h = 0.221 \text{ in.}$$

$$M_s = \frac{Eh^3}{12\ (1 - \mu^2)} \cdot \frac{p \cot^2 \alpha}{Eh}\left[1.785 - 0.405\ \frac{s_1^2}{s_2^2}\right]$$

$$M_s = \frac{h^2 \, p \cot^2 \alpha}{11.57} \left[1.785 - 0.405 \frac{s_1^2}{s_2^2} \right]$$

$$\underline{M_s = p \cot^2 \alpha \left[0.00753 - 0.0017 \frac{s_1^2}{s_2^2} \right]}$$

Similarly, fron equation (19):

$$\underline{M_\theta = p \cot^2 \alpha \left[0.00753 + 0.0017 \frac{s_1^2}{s_2^2} \right]}$$

Therefore:

$$M_s = -24.0 \times 0.18623^2 \left[0.00753 - 0.0017 \times \frac{16.11229^2}{27.63668^2} \right]$$

$$M_s = -0.832 \left[0.00753 - 0.00058 \right] = -0.832 \left[0.00695 \right]$$

$$\underline{M_s = -0.00578 \frac{\text{lb-in.}}{\text{in.}}}$$

$$M_\theta = -0.832 \left[0.00753 + 0.00058 \right] = -0.832 \left[0.00811 \right]$$

$$\underline{M_\theta = -0.00675 \frac{\text{lb-in.}}{\text{in.}}}$$

$$\sigma_s = \frac{N_s}{h} + \frac{6 \, M_s}{h^2} = \frac{-46.769}{0.221} - \frac{6 \times 0.00578}{0.2212} = -211.62 - 0.711$$

$$\underline{\sigma_s = -212.33 \text{ psi}}$$

$$\sigma_\theta = \frac{N_\theta}{h} + \frac{6 \, M_\theta}{h^2} = \frac{-123.524}{0.221} - \frac{6 \times 0.00675}{0.0488} = -558.932 - 0.83$$

$$\underline{\sigma_\theta = -559.76 \text{ psi}}$$

SUMMARY

RADOME STRESS ANALYSIS

Cone No.	r_1, in.	r_2, in.	b, in.	p, psi	α, °	cot α	cos α	s_1, in.	s_2, in.	$\frac{s_1^2}{s_2^2}$	N_θ, lb/in.	N_s, lb/in.	M_θ, $\frac{\text{lb-in.}}{\text{in.}}$	M_s, $\frac{\text{lb-in.}}{\text{in.}}$	σ_s, psi	σ_θ, psi
0	2.95	5.06	11.33	-24.0	79° 27'	0.18623	0.18309	16.11229	27.63668	0.3399	-123.524	-40.769	-0.00675	-0.00578	-212.33	-559.76
1	5.06	8.07	17.78	-22.5	80° 23'	0.16929	0.16690	30.318	48.352	0.3931	-184.174	-55.888	-0.00535	-0.00449	-253.44	-836.59
2	8.07	10.44	15.84	-21.0	81° 29'	0.14962	0.14840	54.380	70.350	0.5975	-221.041	-44.485	-0.00406	-0.00312	-201.67	-1000.68
3	10.44	12.53	15.89	-20.0	82° 30'	0.13152	0.13040	80.061	96.089	0.6942	-252.753	-38.646	-0.00305	-0.00223	-175.144	-1144.05
4	12.53	14.33	15.92	-18.5	83° 33'	0.11306	0.11234	111.536	127.559	0.7645	-266.804	-31.416	-0.00211	-0.00150	-142.33	-1207.52
5	14.33	15.85	15.95	-17.5	84° 33'	0.09529	0.09485	151.081	167.106	0.8174	-278.660	-25.442	-0.00142	-0.00078	-115.24	-1261.07

Material properties used:

Property	Alumina Tile	Adhesive
Tensile, psi	15,000	10,400 (RT)
Compressive	215,000	49,000 (RT)
Flexural	25,000	21,500 (RT)
E	45×10^6	9.5×10^6
G	21×10^6	
μ	0.19	0.25
Density lb/in.^{3}	0.135	
Thermal Expansion	3.9×10^{-6} in./in./°F	4.3×10^{-6} in./in./°F
Lap Shear		10,000 psi

The above properties are at 1000°F except where noted.

APPENDIX VIII

RADOME AERODYNAMIC HEATING ANALYSIS

RADOME AERODYNAMIC HEATING ANALYSIS

FLIGHT TRAJECTORY

The basic design specification of the mosaic radome states that the structure shall withstand 1000°F temperature at the first joint between the tile structure and the alumina nose cone of the radome. The flight trajectory chosen for purposes of determining the aerodynamic heating of the radome must satisfy this basic requirement. For this reason, level flight condition at 100,000-ft altitude and Mach 5.0 speed was selected, representing a feasible cruising altitude and speed for future advanced aircraft. In order to satisfy the thermal shock requirement specified, however, the flight trajectory includes: a period of acceleration, with climb to altitude; and slowdown, with descent to sea level. Flight trajectory profile is shown in Figure 1.

AERODYNAMIC HEATING AND HEAT FLOW ACROSS RADOME WALL

The rate of heat flux on a flying body at supersonic speeds is a function of the velocity and altitude. In the following analysis, the aerodynamic heat flux over the radome is determined at the various altitudes and flight speeds given by the flight trajectory profile. However, the rate of cooling over the internal wall surfaces by the enclosed air mass is determined for sea level pressure and density, realizing that this normally is not the case in actual flight unless the radome is pressurized. The reason for choosing sea level conditions for the internal cooling is the consideration that the results of this analysis will provide the input data for thermal testing the radome prototypes, and simulated high altitude would cause unnecessary complications.

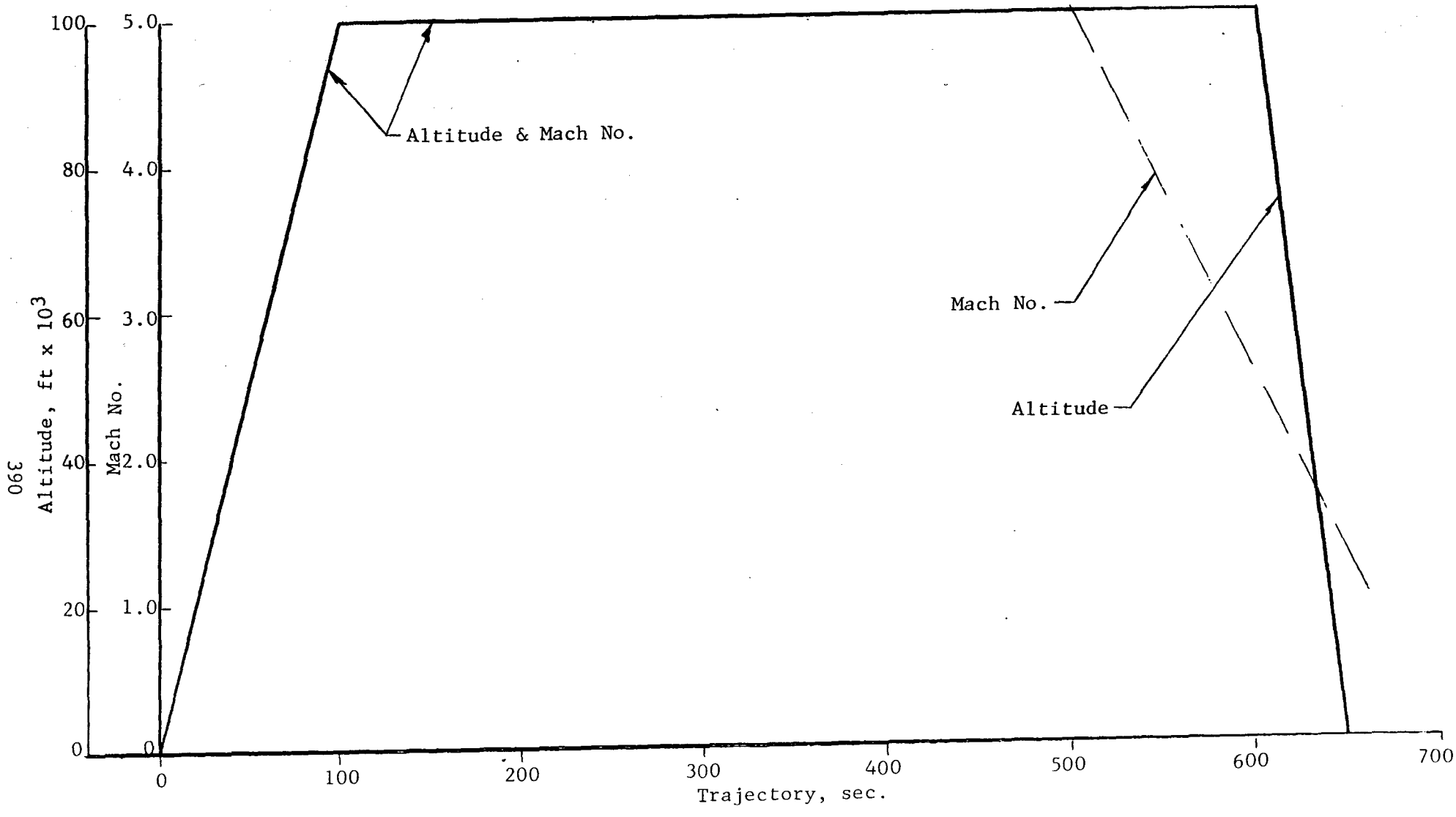
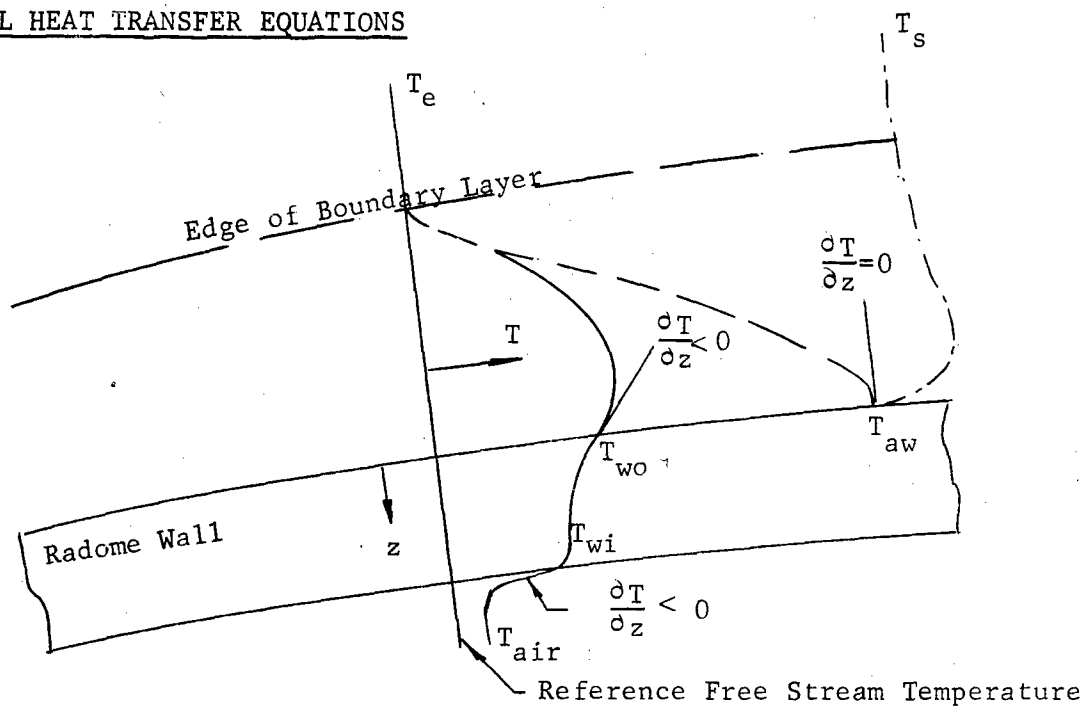


Figure 1. Flight Trajectory

GENERAL HEAT TRANSFER EQUATIONS



Boundary Layer Temperature Profile

Heat flow at the outside wall surface is given by equation (1) per unit area:

$$q_{external} = h_{ext}(T_{aw} - T_{wo}) - \sigma\epsilon T_{wo}^{4}$$ (Reference 1)

$$q_{internal} = h_{int}(T_{wi} - T_{air})$$

h : convective heat transfer coefficient

T_{aw} : adiabatic wall temperature

T_{wo} : outside wall surface temperature

σ : Stefan-Boltzmann radiation constant

ϵ : emissivity of wall surface

---

(1) General Applied Science Laboratory, Inc., Charts and Equations for the Determination of Aerodynamic Heat Transfer to Radome-Shaped Bodies, by H. S. Pergament and M. Epstein, WADD Technical Report 59-22, Vol. I, Feb 1961

To determine the rate of convective heat transfer, the flow around the radome is divided into three areas: stagnation point, sonic point, and points along ogive.

Stagnation Point

The equation used to determine the convective heat transfer coefficient at the stagnation point of a blunt nose body (with detached normal shock) is given in Reference 1:

$$h = \frac{0.707\ c_p}{\bar{P}r^{2/3}} \left(\frac{\rho_{st}\ \mu_{st}\ V_\infty}{R} \right)^{\frac{1}{2}} \left(\frac{\bar{\gamma}-1}{\gamma} \right)^{\frac{1}{4}} \left(1 + \frac{2}{(\gamma_\infty - 1)\ M^2} \right)^{\frac{3}{4}} \left(1 - \frac{1}{\gamma_\infty\ M_\infty^{\ 2}} \right)^{\frac{3}{4}}$$

where

c_p = specific heat of air at $T_{av} = \frac{T_\infty + T_o}{2}$

$\bar{\gamma}$ = ratio of specific heats at T_{av}

$\bar{P}r$ = Prandtl number at T_{av}

γ_∞ = ratio of specific heats at T

ρ_{st} = density behind the normal shock

μ_{st} = viscosity behind the normal shock

V_∞ = free stream velocity

M_∞ = free stream Mach number

R = nose radius

T_∞ = free stream temperature

T_o = stagnation temperature

For the flight conditions under consideration, assume the following properties of air to be constant:

c_p = 0.240 Btu/lb °F $\qquad \bar{P}r = 0.71$

$\bar{\gamma}$ = 1.40

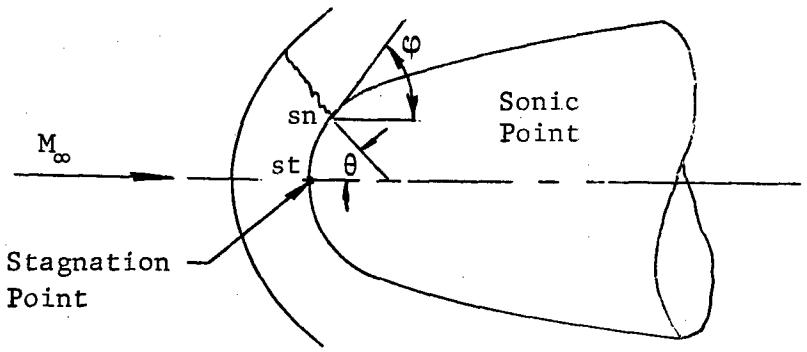
γ_∞ = 1.40

$$\therefore h = 0.156 \left(\frac{\rho_{st}\ \mu_{st}\ V_\infty}{R} \right)^{\frac{1}{2}} \left(1 + \frac{5}{M_\infty^{\ 2}} \right)^{\frac{3}{4}} \left(1 - \frac{716}{M_\infty^{\ 2}} \right)^{\frac{1}{4}}$$

Sonic Point

For gradually curved bodies the sonic point on the body is approximately at the point where the contour is inclined at the maximum cone angle for a shock at the given free stream Mach number (Reference 2).

The location of the sonic point is calculated for the given flight trajectory by use of compressive fluid flow tables (Reference 3).



Sonic Point Behind Normal Shock

A generally accepted equation to be used for the laminar heat transfer distribution around a blunt body is given in Reference 1:

$$\boxed{\frac{q_{sn}}{q_{st}} = f(\theta)} \qquad \therefore h_{sn} = \left(\frac{q_{sn}}{q_{st}}\right) h_{st}$$

$f(\theta)$ is given in Reference 1, where $\frac{q_{sn}}{q_{st}}\sqrt{\frac{S}{R_o}}$ v_s θ is plotted for various nose shapes.

where S- surface length from stagnation point to sonic point

$$S = \frac{\theta}{57.3} \times R_o$$

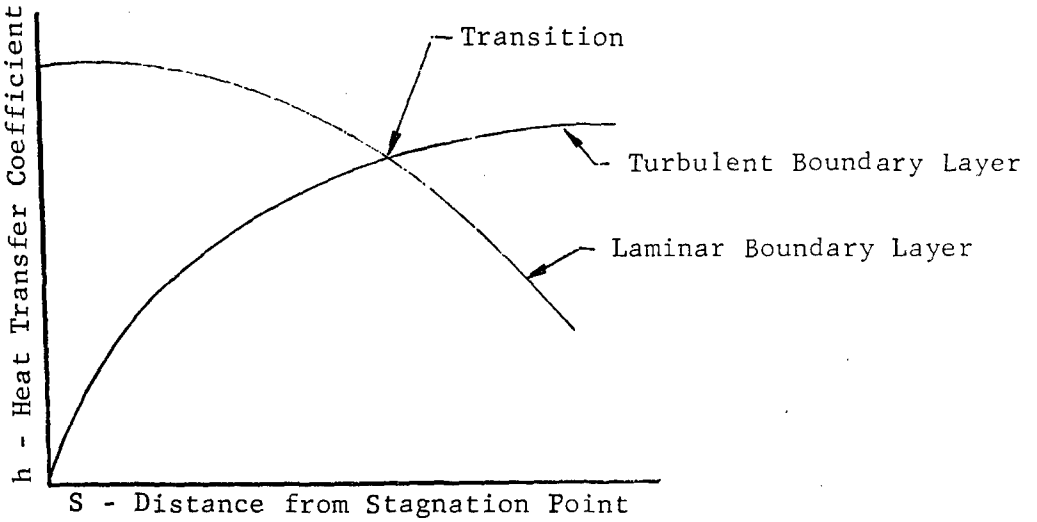
$$h_{sn} = \left[\frac{q_{sn}}{q_{st}}\sqrt{\frac{S}{R_o}}\right] \times \left(\frac{57.3}{\theta}\right)^{\frac{1}{2}} h_{st}$$

(2) A.H. Shapiro, The Dynamics and Thermodynamics of Compressible Fluid Flow, Vol. II, The Ronald Press Co., N.Y.

(3) NACA Report No. 1135, Equations, Tables, and Charts for Compressible Flow, 1953

Points Along Ogive

For the flight trajectory under consideration, the flow will be laminar near the nose of the radome. However, the local Reynold's number increases with the distance from the stagnation point. Therefore, the flow could be turbulent over the major portion of the ogive despite the high flight altitudes. There is no reliable method for determining the transition point from laminar to turbulent boundary layer flow. A good conservative estimate of transition point from the aerodynamic heating viewpoint can be obtained by calculating both the laminar and turbulent heat transfer rates and plotting a curve as shown below:



Laminar and Turbulent Heat Transfer Rates
Along an Ogive Shape

For points forward of the intersection of the two curves use laminar flow, and for points aft of the intersection use turbulent flow heat transfer rates.

Laminar Flow

The equation used for determining the heat transfer coefficient for laminar flow along the ogive is given in Reference 1

$$h_L = \frac{0.0796}{(Pr)^{2/3}} A \left(\frac{\rho e \, \mu r \, Ve}{S} \right)^{\frac{1}{2}}$$

where $A = 0.714 \frac{\alpha}{90^\circ} + 1$ α - local tangent angle

Pr = Prandtl number Let Pr = 0.71

ρe = density at edge of boundary layer

Ve = local velocity at edge of boundary layer

S = distance from stagnation point

μ_r = viscosity at reference temperature T_r

$$T_r = 0.50\ T_w + 0.22\ T_o + 0.28\ T_e$$

T_w = local wall temperature

T_o = local stagnation temperature

T_e = local static temperature at edge of boundary layer

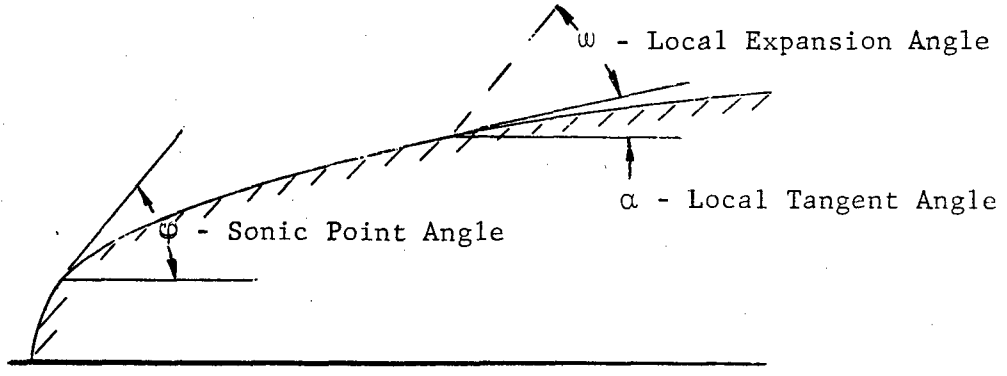
Turbulent Flow

The equation used for determining the heat transfer coefficient for turbulent flow along the ogive is given in Reference 1:

$$h_T = \frac{0.00828}{(Pr)^{2/3}} \frac{(Ve\ \rho e)^{0.8}}{S^{0.2}} \mu_r^{0.2}$$

Flow Properties Downstream from Sonic Point

Flow properties at points along the ogive downstream from the sonic point are determined by the shock expansion method.



Downstream Flow Angles

Knowing the flow properties at the sonic point the flow properties can be determined from tables (Reference 4) for a given local tangent and expansion angle.

Flow properties to be calculated:

M - local Mach number
Ve - local velocity at edge of boundary layer
ρe - local density at edge of boundary layer
T_e - local static temperature at edge of boundary layer
P_e - local static pressure at edge of boundary layer

$$T_{qw} = Pr\ T_o + (1-Pr)T_e = 0.843\ T_o + 0.157\ T_e$$

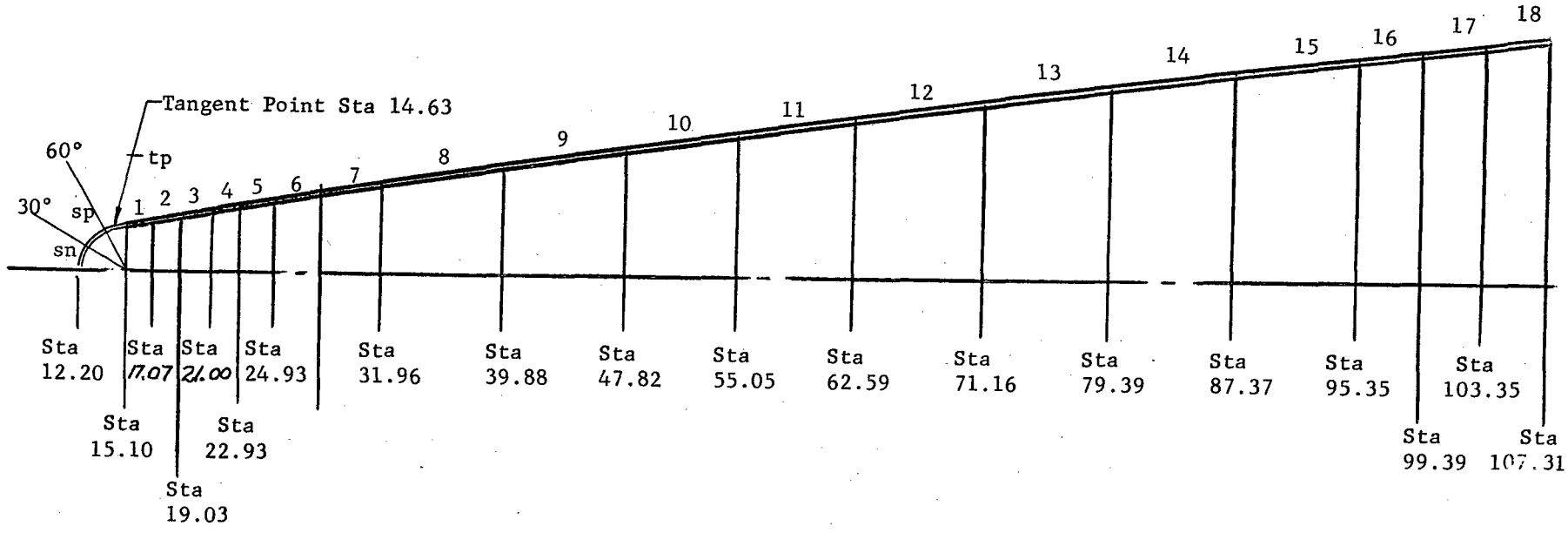
The ogive shape is subdivided into a number of rings along its length as shown in Figure 2. The flow properties are calculated at each one of these sections.

Figure 3 is a plot of the adiabatic wall temperature as a function of time along the length of the ogive. Similarly, Figure 4 graphs the heat transfer coefficient as a function of time along the ogive length. These data are necessary for preparation of the computer input to obtain the temperature gradients along and through the radome.

Internal Cooling

The internal surface of the radome wall is cooled by free convection of air and radiation. The net radiation heat flow is assumed to be zero due to the enclosed shape of the internal surfaces.

(4) Keenan and Kay, Gas Tables, John Wiley & Sons, Inc., N.Y.



Section	1	2	3	4	5	6	7	8	9	10	11	12	13	14	15	16	17	18	End
α	10°54'	10°46'	10°39'	10°31'	10°23'	10°16'	10°03'	9°48'	9°17'	8°46'	8°16'	7°45'	7°15'	6°43'	6°12'	5°41'	5°25'	5°10'	
S (in.)	4.71	6.71	8.71	10.71	12.71	14.71	17.71	21.71	29.72	37.73	45.74	53.75	61.76	69.77	77.78	85.80	89.80	93.80	97.80
S (ft)	0.39	0.56	0.73	0.89	1.06	1.23	1.48	1.81	2.48	3.14	3.81	4.48	5.15	5.81	6.48	7.15	7.43	7.82	8.15

Figure 2. Radome Sections

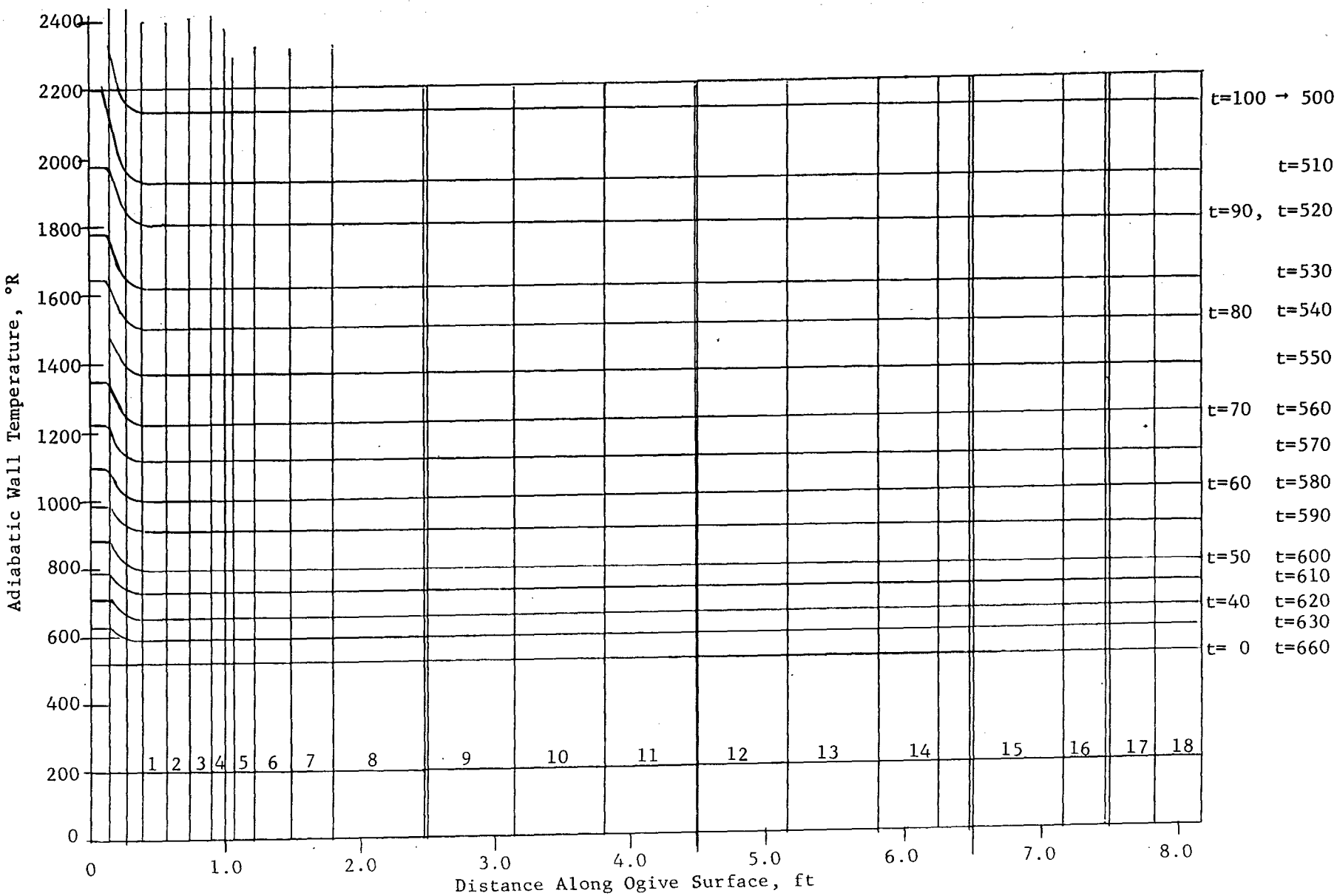


Figure 3. Adiabatic Wall Temperature vs Distance along Ogive

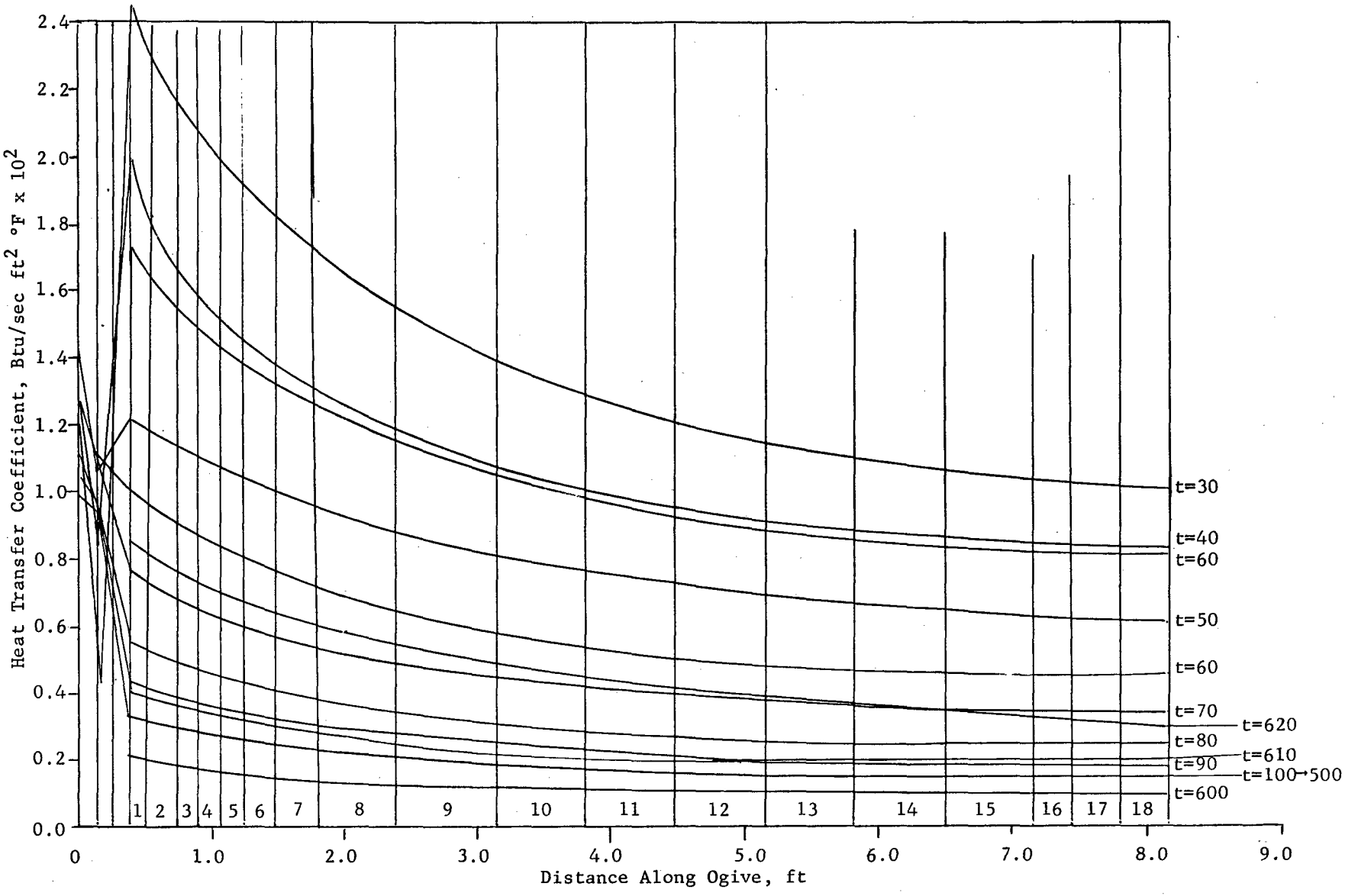


Figure 4. Heat Transfer Coefficient vs Distance along Ogive

The free convection heat transfer coefficient is calculated from curves given in Reference 4.

Find $\text{Log}_{10}\left(\frac{c_p \rho^2 g \beta \Delta T D_o^3}{\mu k}\right)$ for air assume $T_{air_{av}} = 500°F$

Specific heat	c_p	= 0.247 Btu/lb°F
Density	ρ	= 0.0412 lb/ft^3
Viscosity	μ	= 1.89 x 10^{-6} lb/ft sec
Conductivity	k	= 0.0231 Btu/hr ft°F = 0.64 x 10^{-5} Btu/sec ft°F
Bulk modulus	β	= 1.04 x 10^{-3} °F^{-1}
Gravity	g	= 32.2 ft/sec^2
Diameter	D_o	= 1.0 ft - average
Average Temperature Differential	ΔT	= 150°F

$$\text{Log}_{10}\frac{c_p \rho^2 g \beta \Delta T D^3}{\mu k} = \text{Log}_{10}\left(\frac{.247 \times 4.12^2 \times 10^{-4} \times 32.2 \times 1.04 \times .50 \times 1}{1.89 \times 10^{-5} \times .64 \times 10^{-5}}\right) = 9.764$$

From Figure 7-3 of Reference 4

$$\text{Log}_{10}\left(\frac{hD}{k}\right) = 2.00 \qquad \therefore h = \frac{k}{D} 100 = 100 \times 0.64 \times 10^{-5}$$

$$h_i = 0.00064 \text{ Btu/sec ft}^{2o}\text{F}$$

Aerodynamic Heating Analysis and Computer Program

A computer program developed by the Lockheed-California Company* was selected to carry out the numerical computations of the transient heat transfer analysis. The Lockheed Thermal Analyzer program is well known and widely used throughout the industry. The solution of the heat transfer problem was done by setting up an electrical analog for the physical systems and solving the electrical RC circuit problem with small, incremental time steps made possible by the use of large IBM 7094 computer facilities.

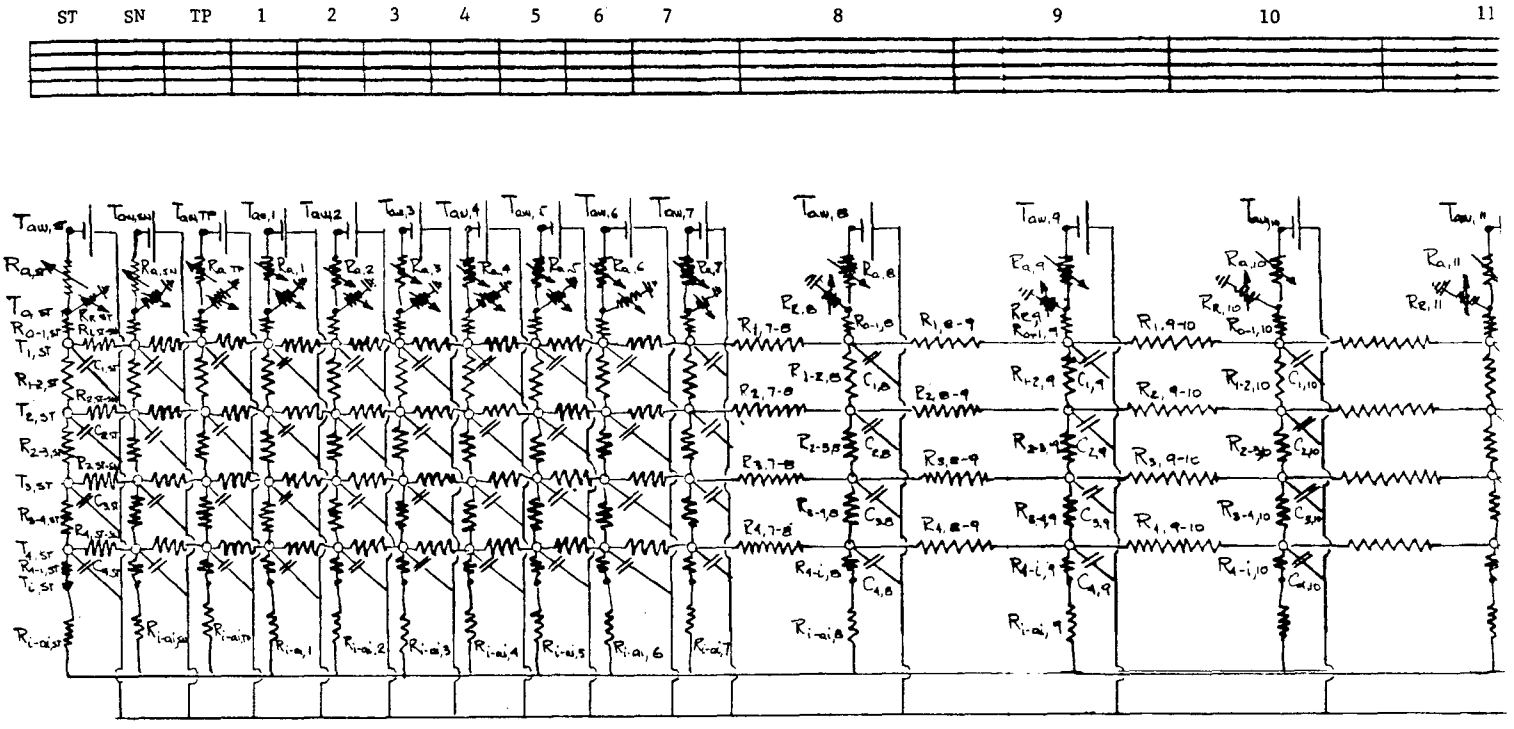
The mosaic radome was divided into incremental rings along its length and four layers through the wall thickness. Each of the incremental sections of the radome shell has a value of thermal capacitance analogous to an electrical capacitance, and between the individual sections of the radome wall, the heat flow path has a value of thermal resistance analogous to electrical resistances in the analog circuit.

Figure 5 shows the subdivisions of the physical radome wall and the analogous electrical circuit representing the thermal characteristics of the radome. The aerodynamic heating coefficients are represented by variable electrical resistance between the outside surface of the wall and an imaginary temperature node analogous to the adiabatic wall temperature of the boundary layer. Surface-emitted radiation is also included in the analog circuit in the form of a variable resistance function of the third power of the external wall surface temperature. The internal wall surface of each section of the subdivided radome is connected to the internal air mass by a resistance representing the internal cooling convective heat transfer coefficient.

At the aft end of the radome, a large external mass acting as a heat sink is simulated by a large thermal capacitance representing the structure to which the radome is attached.

Temperature – Time History. The primary purpose of the analysis was to determine the temperature – time history of the radome shell under aerodynamic heating. Figures 6 and 7 show the results of the temperature computations. Figure 6 demonstrates the temperature distribution along the length of the radome at various times during the supersonic flight trajectory, indicating

* Lockheed-California Company, "Thermal Analyzer," Mathematical Analysis Department, Job No. 1318.

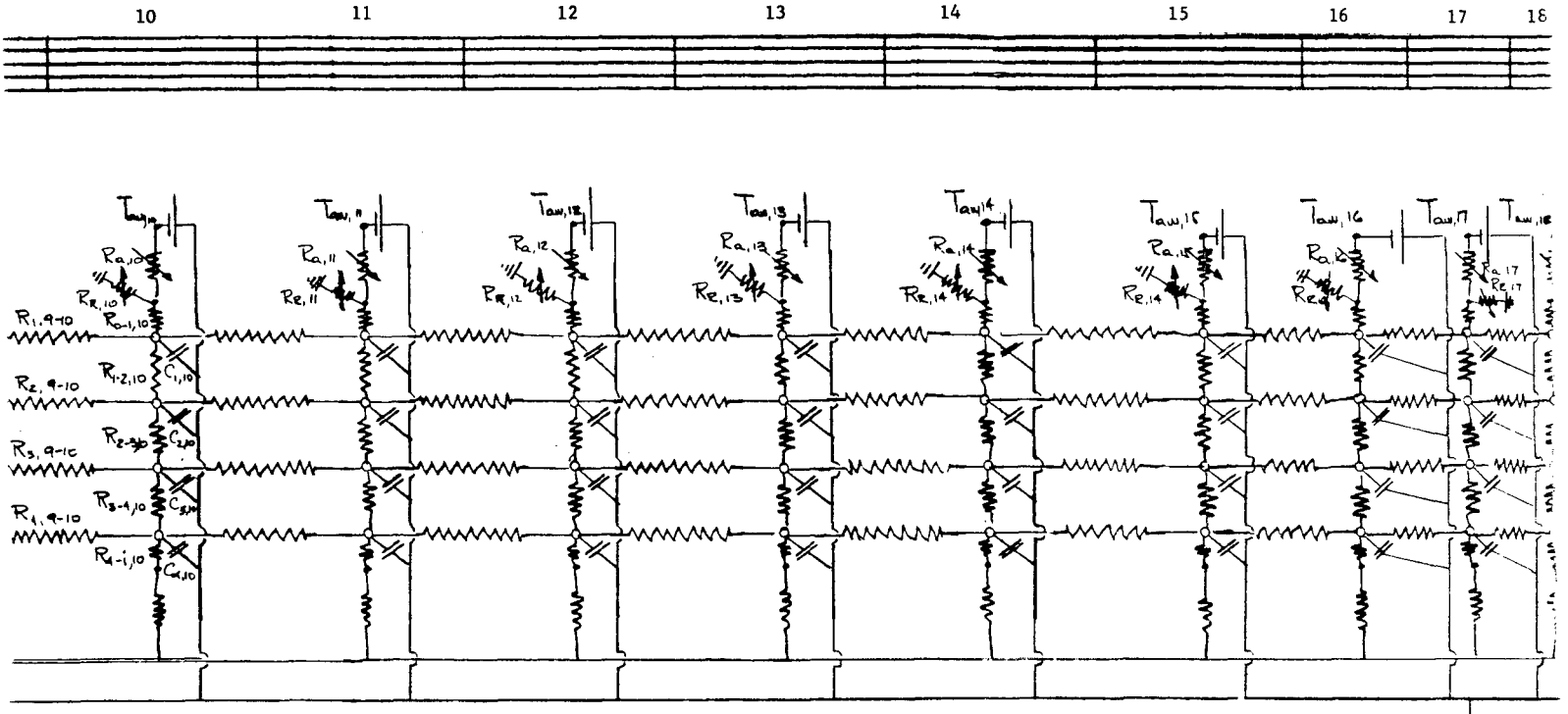


(Circuit component callout examples are shown on diagram)

- T_{aw} - Adiabatic wall tamp
- T_o - External wall surface temp
- T_1, T_2, T_3, T_4 - Internal wall temp
- T_i - Inner wall surface temp
- T_{ai} - Internal air temp

- R_{o-1}, R_{1-2}, R_{2-3}, R_{3-4}, R_{4-i} - Internal wall conductive resistances
- R_{i-ai} - Internal surface cooling resistance

Figure 5. Analogous Circuit



1 conductive resistances

face cooling resistance

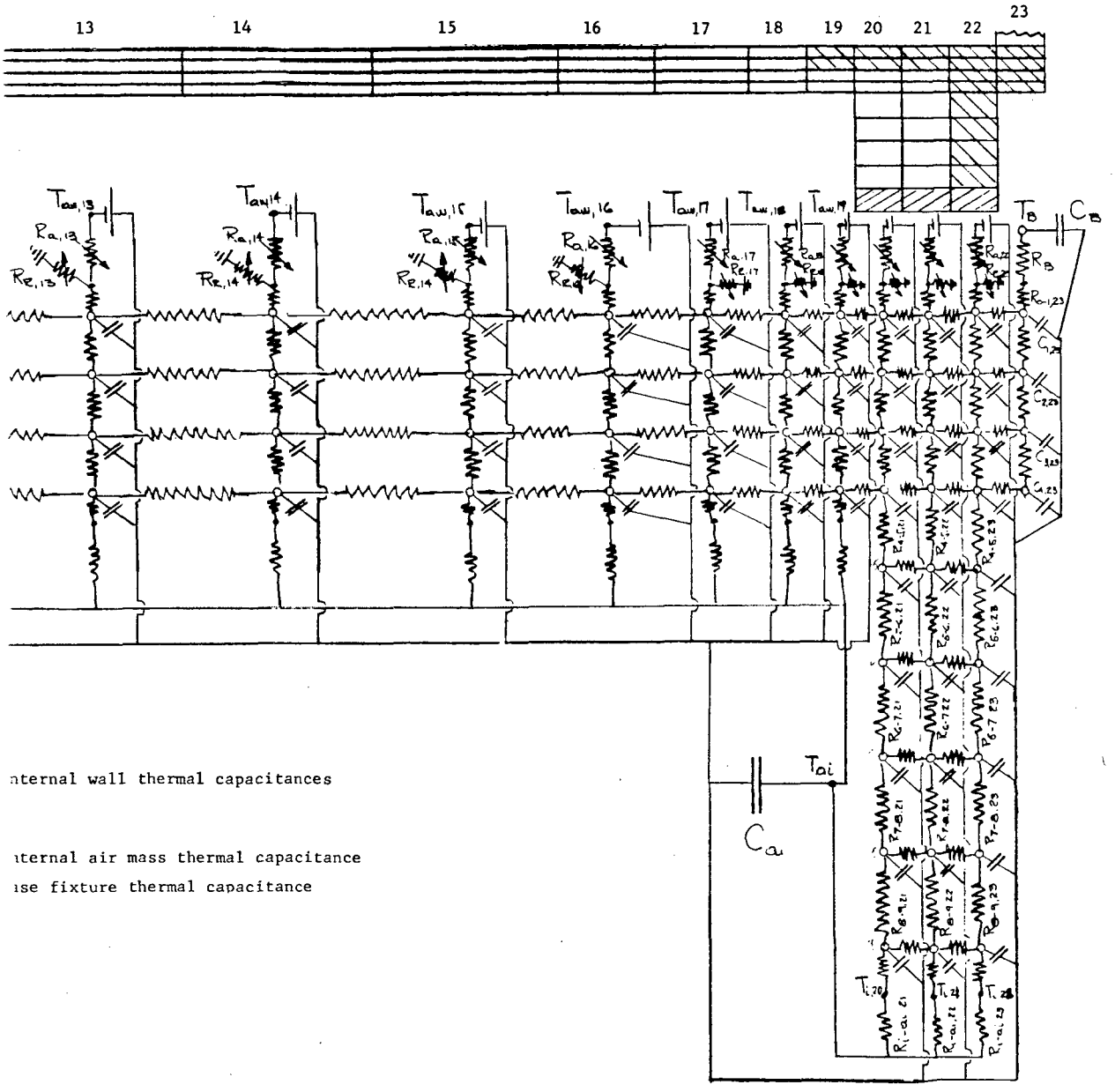
C_1
C_2
C_3
C_4 — Internal wall thermal capacitances

C_{ai} - Internal air mass thermal capacitance

C_b - Base fixture thermal capacitance

C_a

5. Analogous Circuit for Wall Heat Transfer Analysis



nternal wall thermal capacitances

ıternal air mass thermal capacitance

ıse fixture thermal capacitance

ɜr Analysis

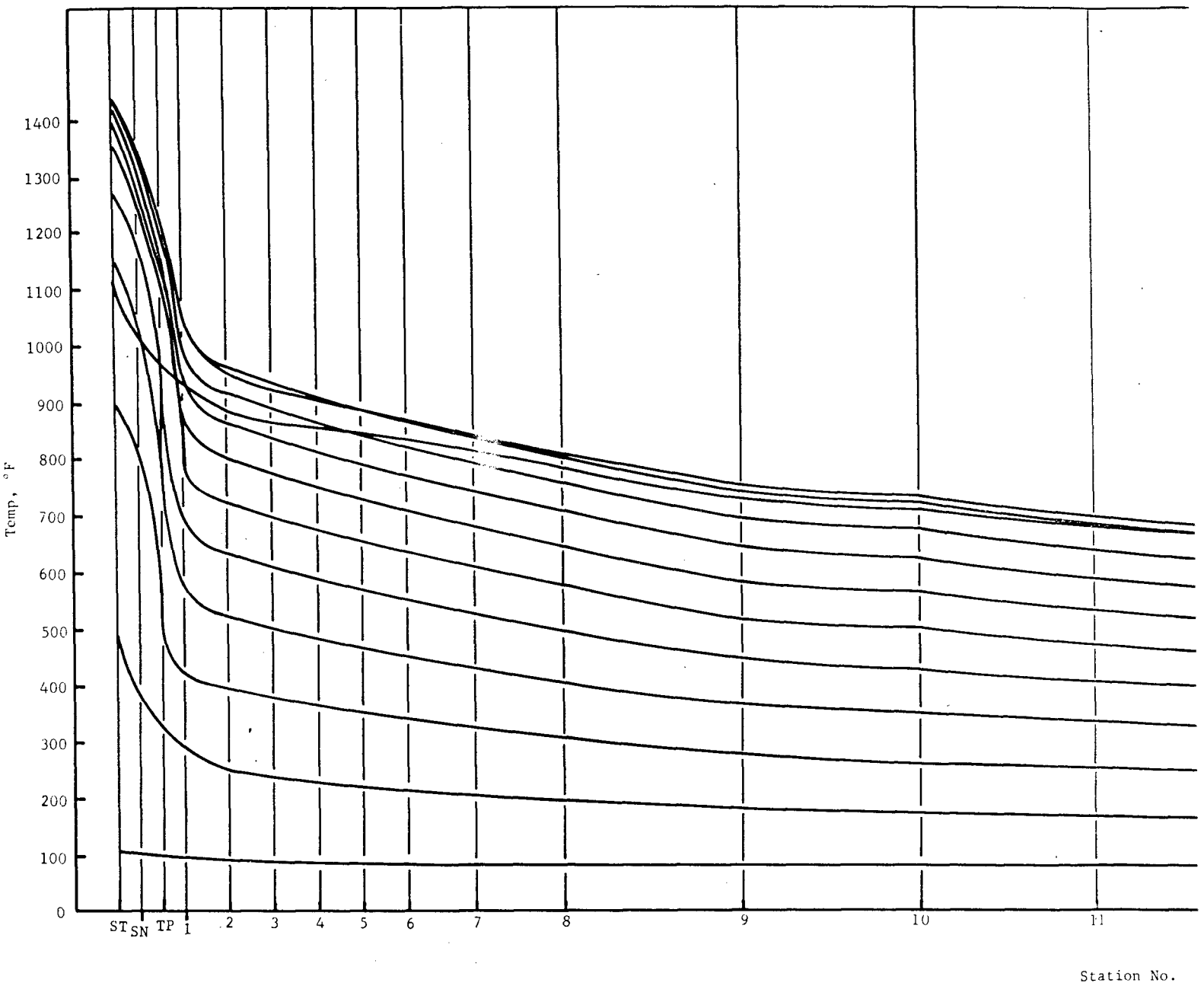
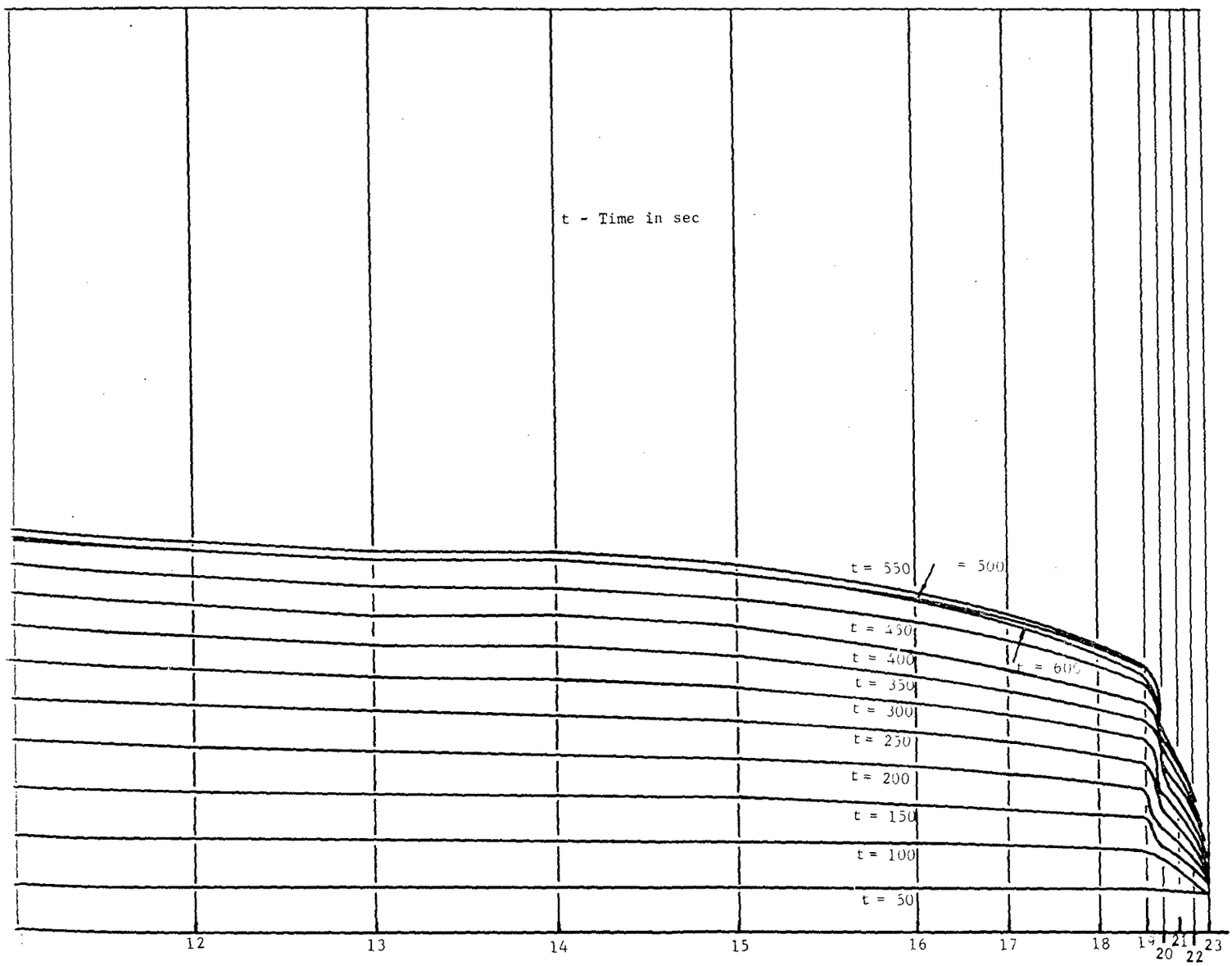


Figure 6. Outside Surface Temper



ıtion No.

ːe Temperature Along Radome

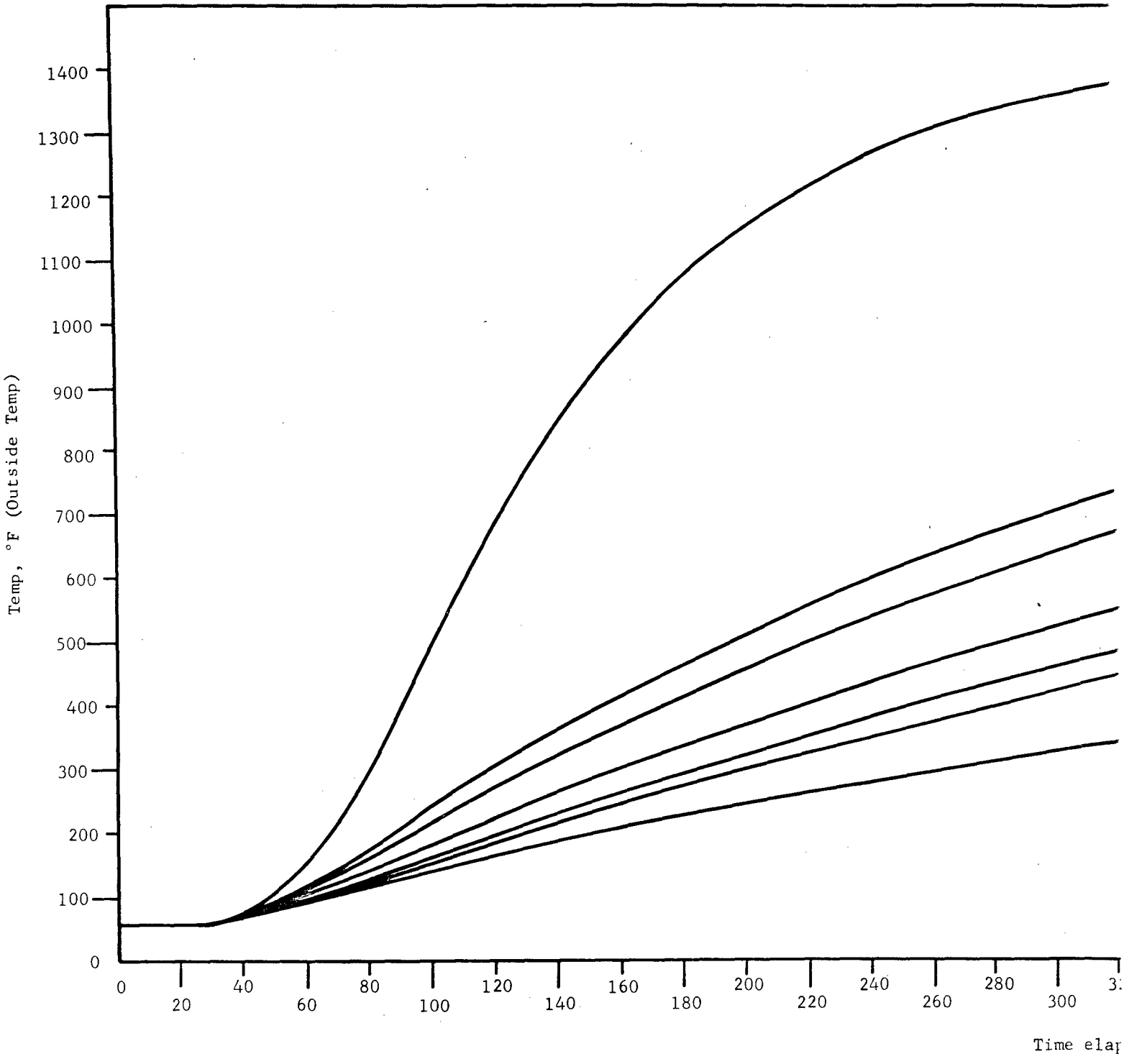
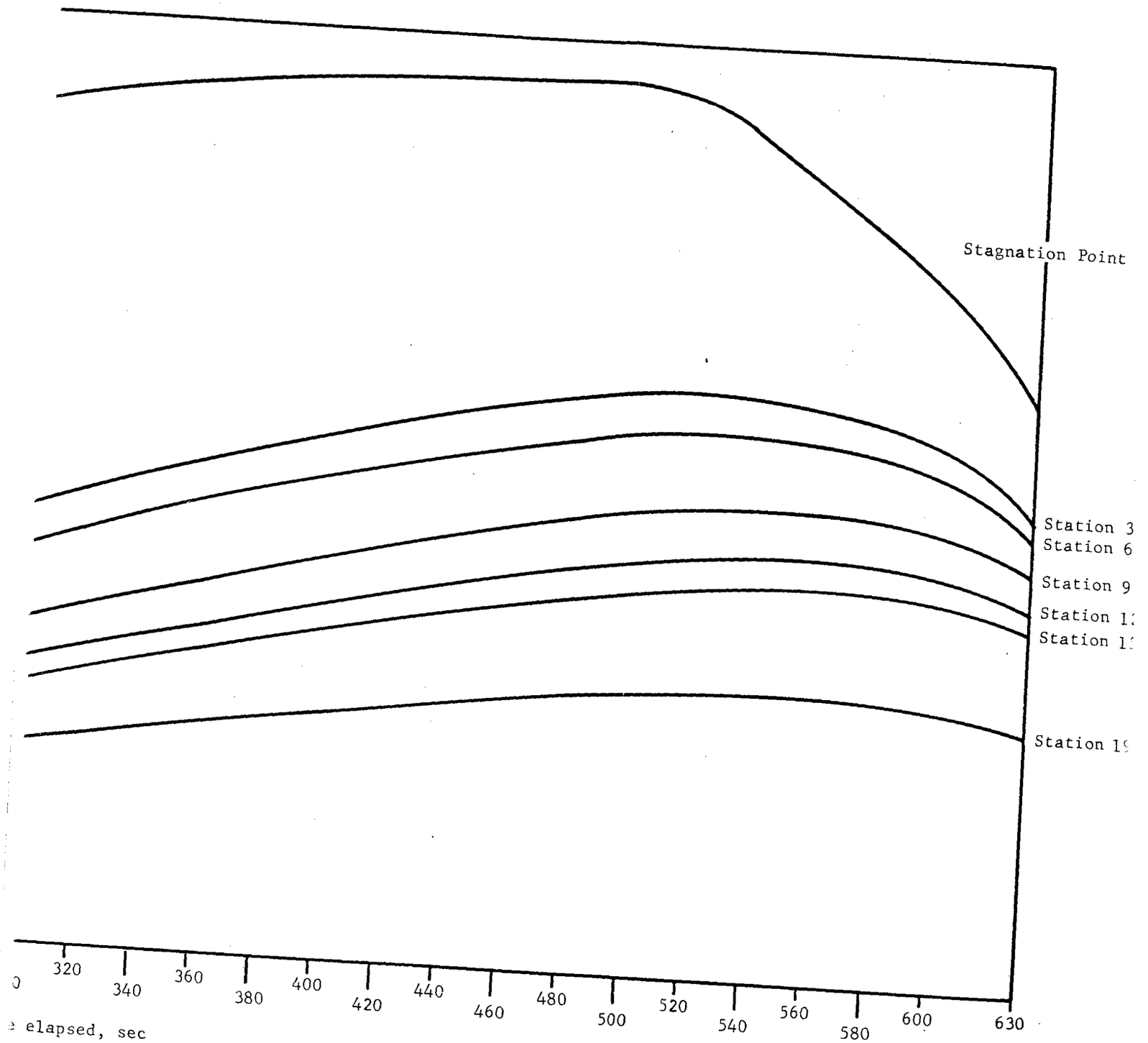


Figure 7. Outside Surface



rface Temperature vs. Time

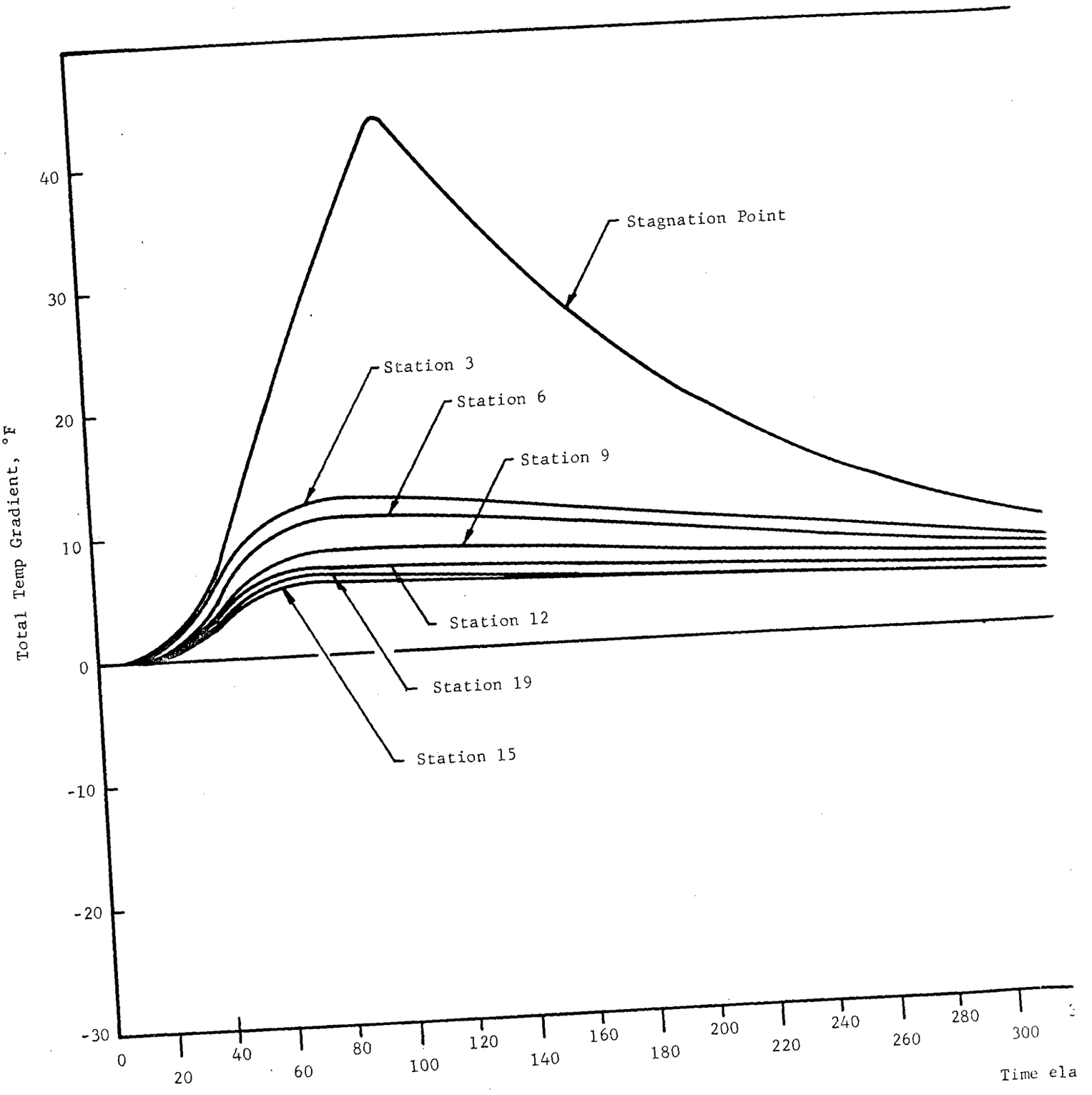
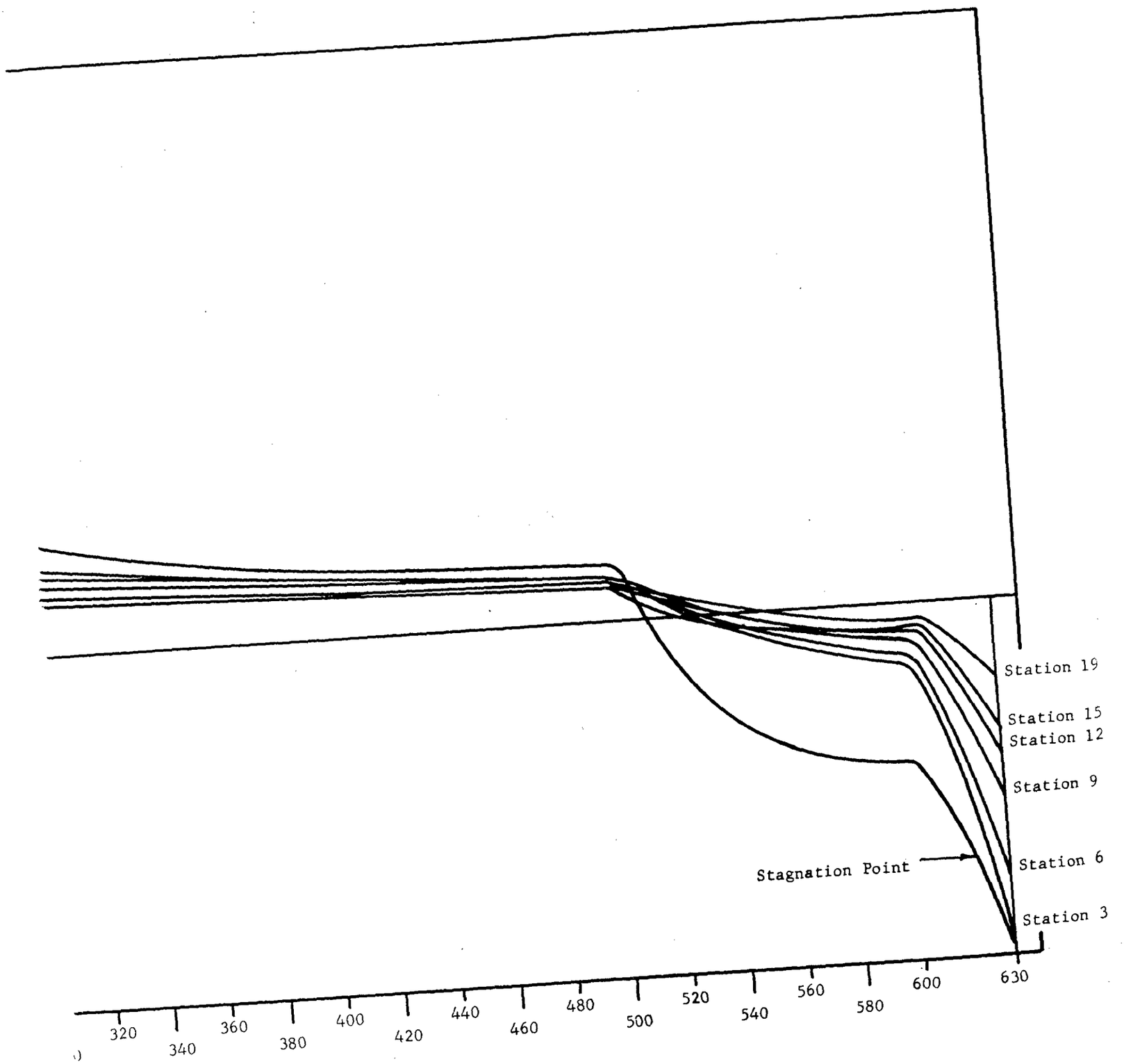


Figure 8. Temperature Gradien



elapsed, sec

lient Across Radome Wall vs. Time

APPENDIX IX

MOSAIC RADOME TILE STRESS ANALYSIS

(By The MacNeal-Schwendler Corporation)

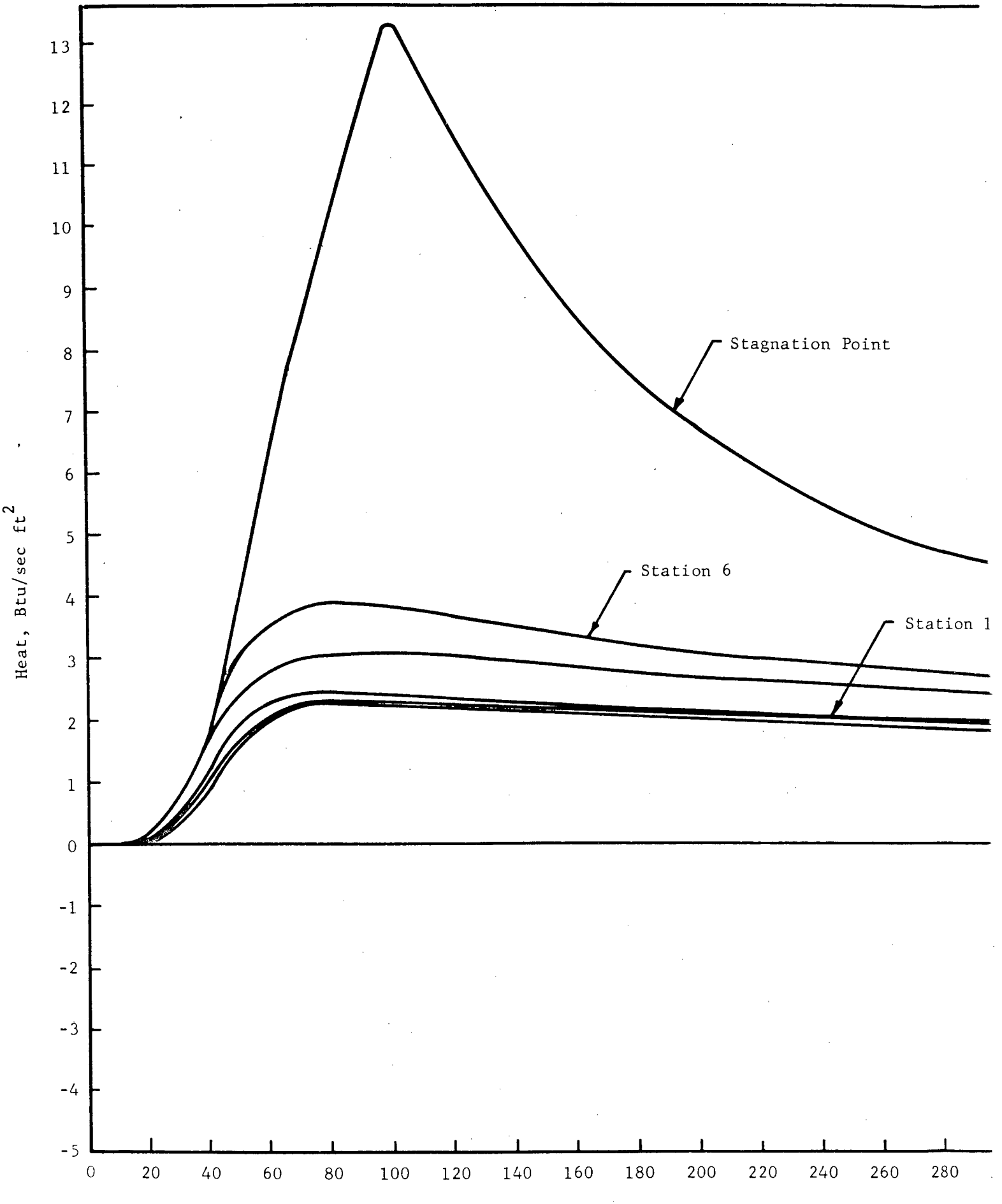
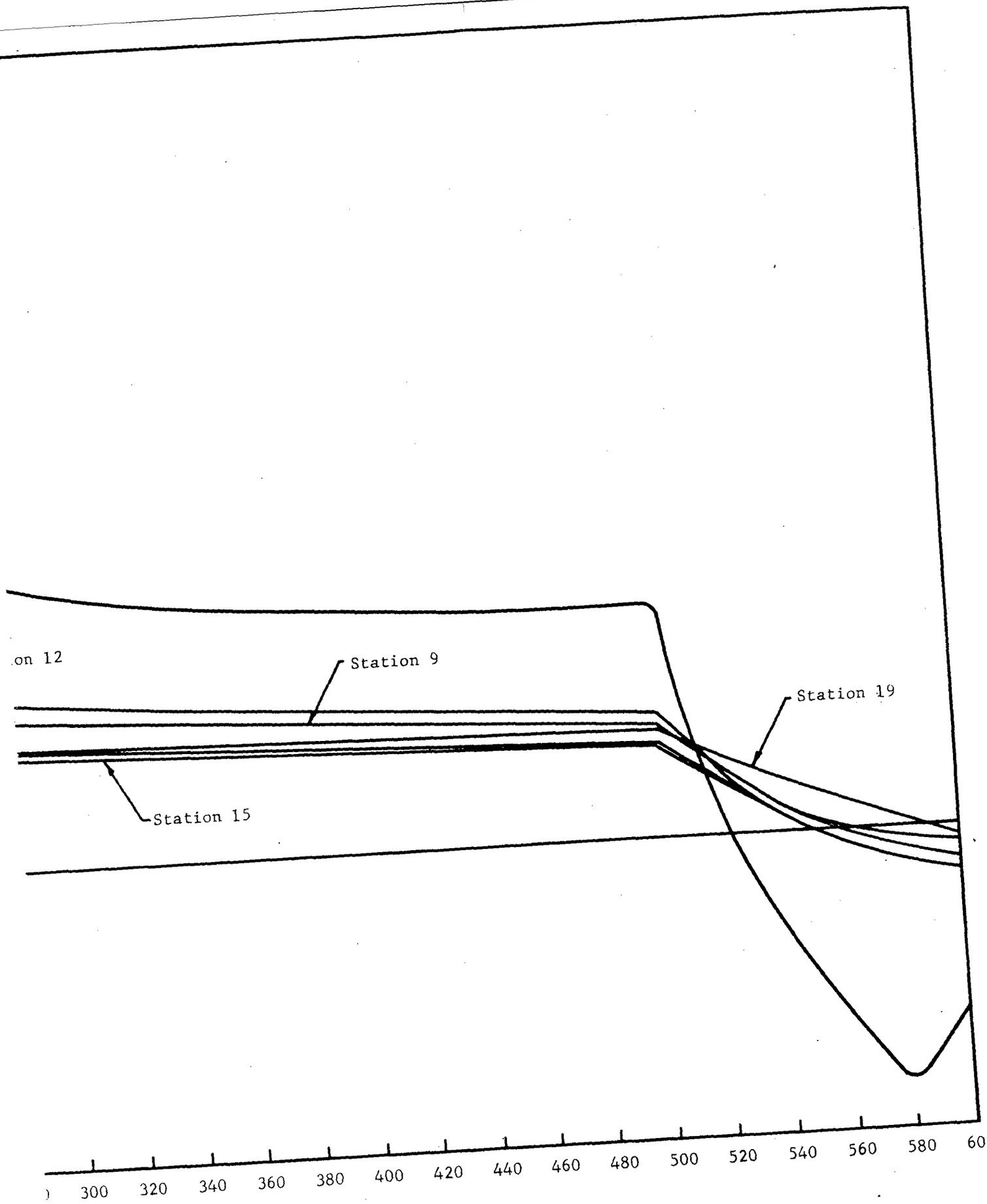


Figure 9. Aerodynamic



amic Heating Rate vs. Time

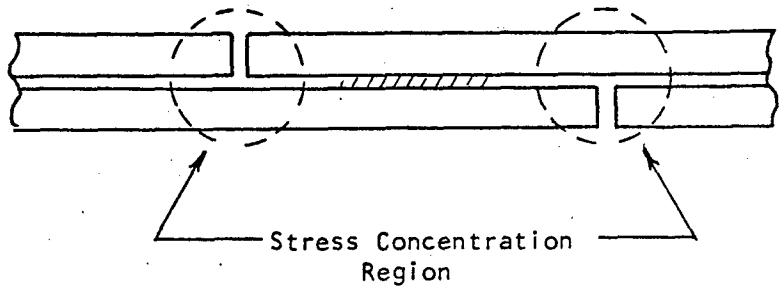
M O S A I C R A D O M E T I L E S T R E S S A N A L Y S I S

SECTION A

INTRODUCTION

The analysis described herein was made in order to establish in some detail the distribution of stresses within the individual tile used in the construction of the Narmco Mosaic Radome. The general configuration of the radome and the basic technique used in its construction are shown schematically in Figure 1. It is constructed by the bonding together of a number of small, approximately 4 in. by 4 in. by 0.108 in., alumina tile.

The objectives of the analysis were twofold. First, the quest of information regarding stress concentration effects near the tile junctures (see sketch) and second to establish the distribution of loads across the bond holding the tile together.



Two types of loading were considered in the analysis, one being analogous to a pressure loading of the radome and the other a thermal gradient across the thickness of the tile.

In formulating the analysis, the following basic assumptions were made.

1. It was assumed that the radius of curvature of the tile was large enough in comparison to the tile thickness that it could be safely ignored.

2. It was assumed that a certain amount of symmetry was involved in the tile pattern.

3. It was assumed that reasonable results could be obtained from a quasi-two-dimensional analysis.

Regarding the first assumption, it is quite obvious that the radius of curvature of the tile (radome radius) governs explicitly the gross stress at any particular location throughout the radome, but, it is inconceivable that it can play any significant role in the distribution of stresses across any given section and therefore have any control over the magnitude of any stress concentration. This is in effect a statement that the local distribution of stresses will be the same for an assumed flat plate geometry as for the curved geometry of the radome with the same gross load on the cross section.

The second and third assumptions were required in order to simplify the analysis to a point whereby a reasonable amount of analysis effort would yield useful information regarding the distribution of stresses.

Figure 2 shows the structural model selected as representative of the actual configuration, a flat-plate approximation. In the model, there is assumed no variation of any type in the z-direction. Stresses

along the z-coordinate are allowed, but, strains and displacements in the z-direction are assumed to be everywhere the same.

A review of the design of the radome concluded with the selection of a dimension, L, (see Figure 2)of 1.0 inch as an approximate minimum distance between upper and lower tile boundaries. This minimum dimension was used in the analysis since the smaller the dimension, the more rapidly the loads are forced to traverse the bond between the tile and should, therefore, result in the highest stress concentrations. Also, from the results of this analysis, it is easily seen that a greater tile length would result in the same stress distribution because in all conditions studied the direct stresses were virtually uniform and the shear stresses zero over the middle half of the specimen.

METHOD OF ANALYSIS

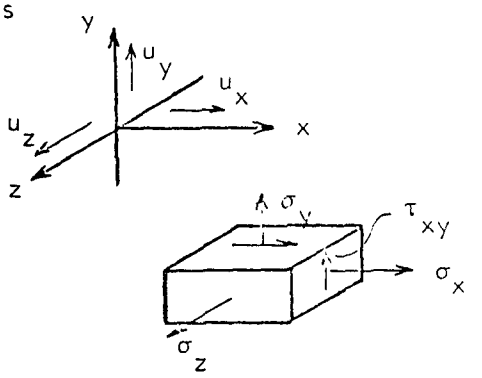
The stress analysis was carried out by forming a lumped element representation of the selected structural model. The lumped elements were represented by a set of electric analog circuits which were analyzed with the aid of a digital computer program known as SADSAM (Structural Analysis by Digital Simulation of Analog Methods). In the analog method employed, the following analogies were used

Mechanical System	Electric Analog
Force (F)	Current (I)
Displacement (u)	Voltage (E)
Flexibility (1/K)	Resistance
Strain Energy (U)	1/2 Power Dissipation (1/2 P)

The analog circuits used in the analysis are developed in the following section.

DEVELOPMENT OF THE IDEALIZED MODEL

Consider an x, y, z coordinate system as shown. In this coordinate system unit strains may be defined as



$$\epsilon_x = \frac{\partial u_x}{\partial x} \tag{1}$$

$$\epsilon_y = \frac{\partial u_y}{\partial y} \tag{2}$$

$$\epsilon_z = \frac{\partial u_z}{\partial z} \text{ (assumed equal to a constant)} \tag{3}$$

$$\gamma_{xy} = \frac{1}{2}\left\{\frac{\partial u_x}{\partial y} + \frac{\partial u_y}{\partial x}\right\} \tag{4}$$

$$\gamma_{xz} = \gamma_{yz} = 0 \text{ (For the system being investigated)} \tag{5}$$

The stress-strain relation may be expressed as

$$\begin{bmatrix} \sigma_x \\ \sigma_y \\ \sigma_z \\ \tau_{xy} \end{bmatrix} = \begin{bmatrix} (2G + \lambda) & \lambda & \lambda & 0 \\ \lambda & (2G + \lambda) & \lambda & 0 \\ \lambda & \lambda & (2G + \lambda) & 0 \\ 0 & 0 & 0 & 2G \end{bmatrix} \begin{bmatrix} \epsilon_x - \alpha T \\ \epsilon_y - \alpha T \\ \epsilon_z - \alpha T \\ \gamma_{xy} \end{bmatrix} \tag{6}$$

where

G = Shear modulus

λ = Lame's constant

α = Coefficient of thermal expansion

T = Temperature change

The strain energy per unit volume may be expressed as

$$2dU = \sigma_x \epsilon_x + \sigma_y \epsilon_y + \sigma_z \epsilon_z + 2\tau_{xy}\gamma_{xy} \tag{7}$$

$$= \begin{bmatrix} \sigma_x \\ \sigma_y \\ \sigma_z \\ \tau_{xy} \end{bmatrix}^T \begin{bmatrix} \epsilon_x \\ \epsilon_y \\ \epsilon_z \\ 2\gamma_{xy} \end{bmatrix} \tag{8}$$

Substituting for the stress vector from Equation (6) yields

$$2dU = \begin{bmatrix} \epsilon_x - \alpha T \\ \epsilon_y - \alpha T \\ \epsilon_z - \alpha T \\ \gamma_{xy} \end{bmatrix}^T \begin{bmatrix} (2G + \lambda) & \lambda & \lambda & 0 \\ \lambda & (2G + \lambda) & \lambda & 0 \\ \lambda & \lambda & (2G + \lambda) & 0 \\ \lambda & \lambda & \lambda & 2G \end{bmatrix} \begin{bmatrix} \epsilon_x \\ \epsilon_y \\ \epsilon_z \\ 2\gamma_{xy} \end{bmatrix} \tag{9}$$

Expanding Equation (9) yields

$$2dU = 2G\epsilon_x^2 + 2G\epsilon_y^2 + 2G\epsilon_z^2 + \lambda e^2 - (2G + 3\lambda)(\alpha T)e + 4G\gamma_{xy}^2 \qquad (10)$$

where

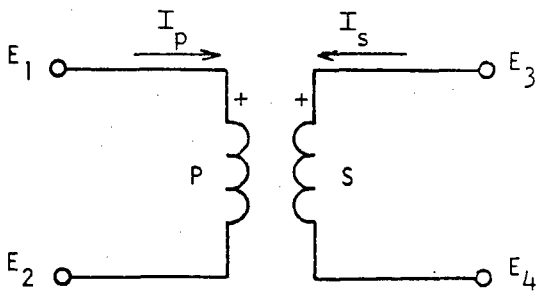
$$e = \text{the volumetric strain} = \epsilon_x + \epsilon_y + \epsilon_z \qquad (11)$$

For the finite volume of dimensions Δx, Δy, Δz, the total strain energy is approximated by

$$\begin{aligned} 2\Delta U &= 2dU(\Delta x \Delta y \Delta z) \\ &= 2G\Delta x\Delta y\Delta z(\epsilon_x^2 + \epsilon_y^2 + \epsilon_z^2) + \lambda\Delta x\Delta y\Delta z(e^2) \\ &\quad + 4G\Delta x\Delta y\Delta z(\gamma_{xy}^2) - (2G + 3\lambda)(\alpha T)(\Delta x\Delta y\Delta z)e \end{aligned} \qquad (12)$$

There exist a number of methods that can be used to synthesize a set of electric analog circuits with which a given set of equations or a particular system can be represented. One of the most convenient methods is carried out by working with the strain energy and the strain-displacement relations. For the static stress problem, only two types of electrical elements are required, the electrical transformer and the resistor. The transformer is used to incorporate various coupling mechanisms and specify general constraint relations. The transformer relations of importance are as follows. Let P denote the number of turns on the primary winding and S denote the number of turns on the secondary. The transformer voltage relation is given by

$$\frac{E_1 - E_2}{P} = \frac{E_3 - E_4}{S} \qquad (13)$$



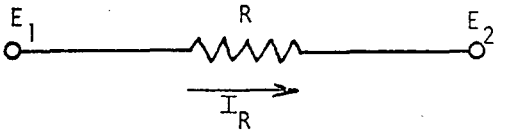
and the current relation given by

$$I_p P + I_s S = 0 \qquad (14)$$

Note that it is important to keep the relative polarity of the transformer in mind when writing the transformer relations.

The resistor relations of importance are as follows. Denote the resistance value by R, then the current voltage relation is given by

$$I_R = \frac{E_1 - E_2}{R} \qquad (15)$$



The power dissipated in the resistor may be expressed as

$$P = \frac{1}{R}(E_1 - E_2)^2 = (E_1 - E_2)I \qquad (16)$$

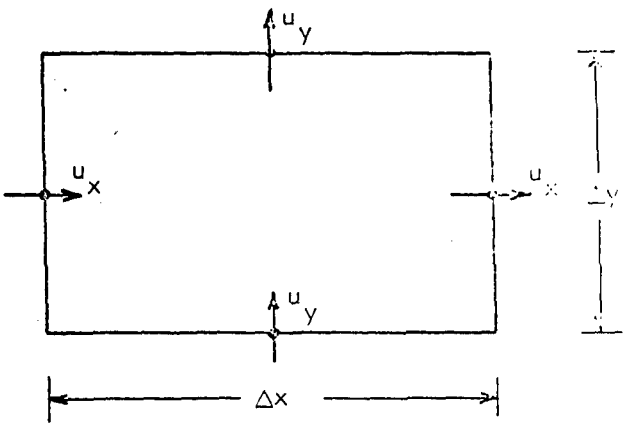
In developing the analog circuits with which to simulate the system, consider first the strain displacement relations. In finite difference form these may be expressed as

$$\epsilon_x = \frac{\Delta_x(u_x)}{\Delta x} = \frac{1}{\Delta x}(u_x^+ - u_x^-) \qquad (17)$$

$$\epsilon_y = \frac{\Delta_y(u_y)}{\Delta y} = \frac{1}{\Delta y}(u_y^+ - u_y^-) \qquad (18)$$

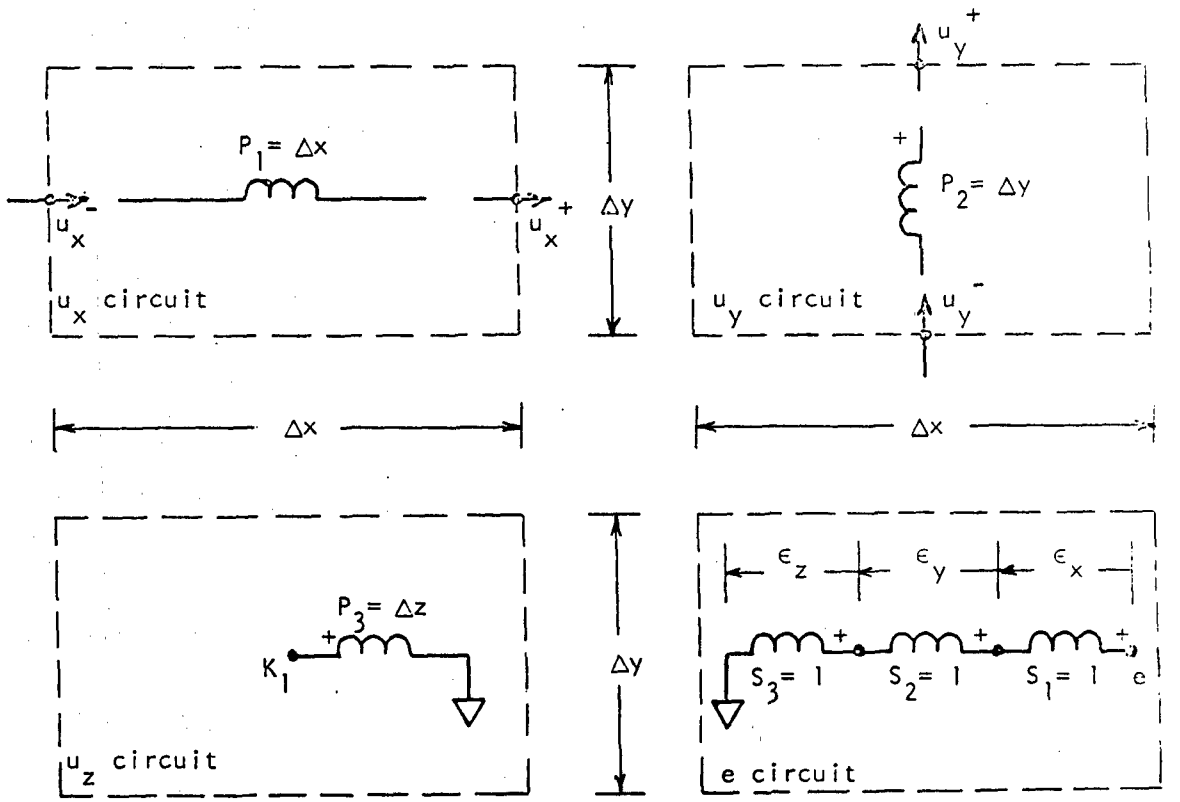
$$\epsilon_z = \frac{\text{constant}}{\Delta z} = \frac{K_1}{\Delta z} \qquad (19)$$

It is convenient to consider a finite element of dimensions Δx, Δy, Δz as shown below. Define the displacements u_x and u_y as shown. Then, Equations (17), (18) and (19), and the strain constraint equation,



$$e = \epsilon_x + \epsilon_y + \epsilon_z$$

are all satisfied by the transformer network shown below.



The transformer network shown on the preceding page accomplishes the task of defining each of the direct-strains and the volumetric strain in terms of the included displacement coordinates. Note that there are four separate circuits involved and that they are coupled through the magnetic coupling of the transformers involved. In the u_x circuit, the node voltages correspond to the u_x displacements. Similarly in the u_y and u_z circuits. In the e-circuit, the voltage drops are the direct strains and their sum the volumetric strain.

Insofar as the direct stress representation is concerned, it is left only to account for the strain energy involved. The direct-strain portion of Equation (12) can be written in electrical terms as

$$2\Delta U = \frac{1}{R_x}\epsilon_x^2 + \frac{1}{R_y}\epsilon_y^2 + \frac{1}{R_z}\epsilon_z^2 + \frac{1}{R_\lambda}e^2 - I_T e \qquad (20)$$

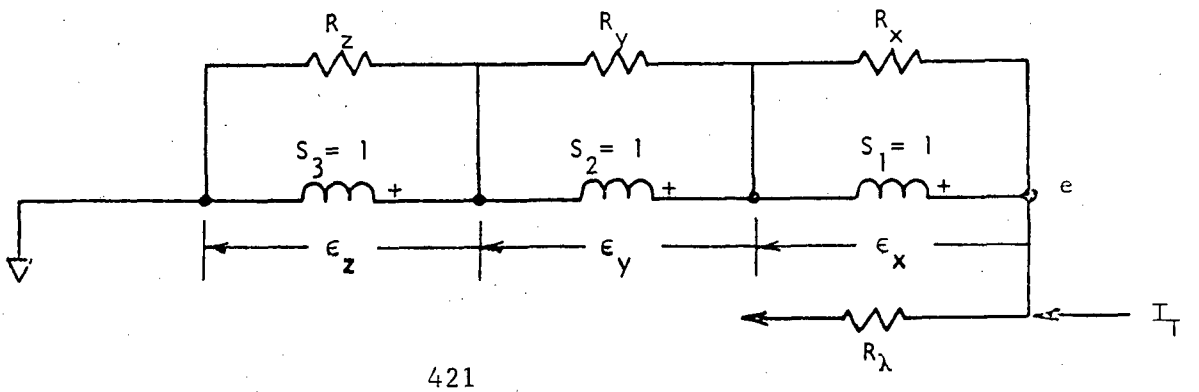
where

$$R_x = R_y = R_z = (2G\Delta x\Delta y\Delta z)^{-1} \quad , \quad \text{resistance}$$

$$R_\lambda = (\lambda\Delta x\Delta y\Delta z)^{-1} \quad , \quad \text{resistance}$$

$$I_T = (2G + 3\lambda)(\alpha T)(\Delta x\Delta y\Delta z) \quad , \quad \text{current}$$

Equation (20) is simulated in the electrical analog simply by placing the above resistances across the indicated strains and introducing a "thermal loading" current at the volumetric strain node as shown below.



It should be noted that I_T, the thermal loading current, flowing into the circuit corresponds to a condition of heating and I_T flowing out of the circuit corresponds to a condition of cooling. This is seen quite simply since an inflow of current will cause the volumetric strain, e, to be positive and, therefore, cause the element to expand.

It is also of interest to examine the currents flowing in the e-circuit and their relation to the stress components. From Equation (3) the direct stress components may be written as

$$\sigma_i = 2G\epsilon_i + \lambda e - (2G + 3\lambda)\alpha T , \quad (i = x, y, z) \tag{21}$$

If we multiply both sides of Equation (21) by the volume of the finite element we obtain

$$\begin{aligned}(\Delta x\Delta y\Delta z)\sigma_i &= (2G\Delta x\Delta y\Delta z)\epsilon_i + (\lambda\Delta x\Delta y\Delta z)e - \\ &\quad - (2G + 3\lambda)(\alpha T)(\Delta x\Delta y\Delta z) \\ &= \frac{1}{R_i}\epsilon_i + \frac{1}{R_\lambda}e - I_T\end{aligned} \tag{22}$$

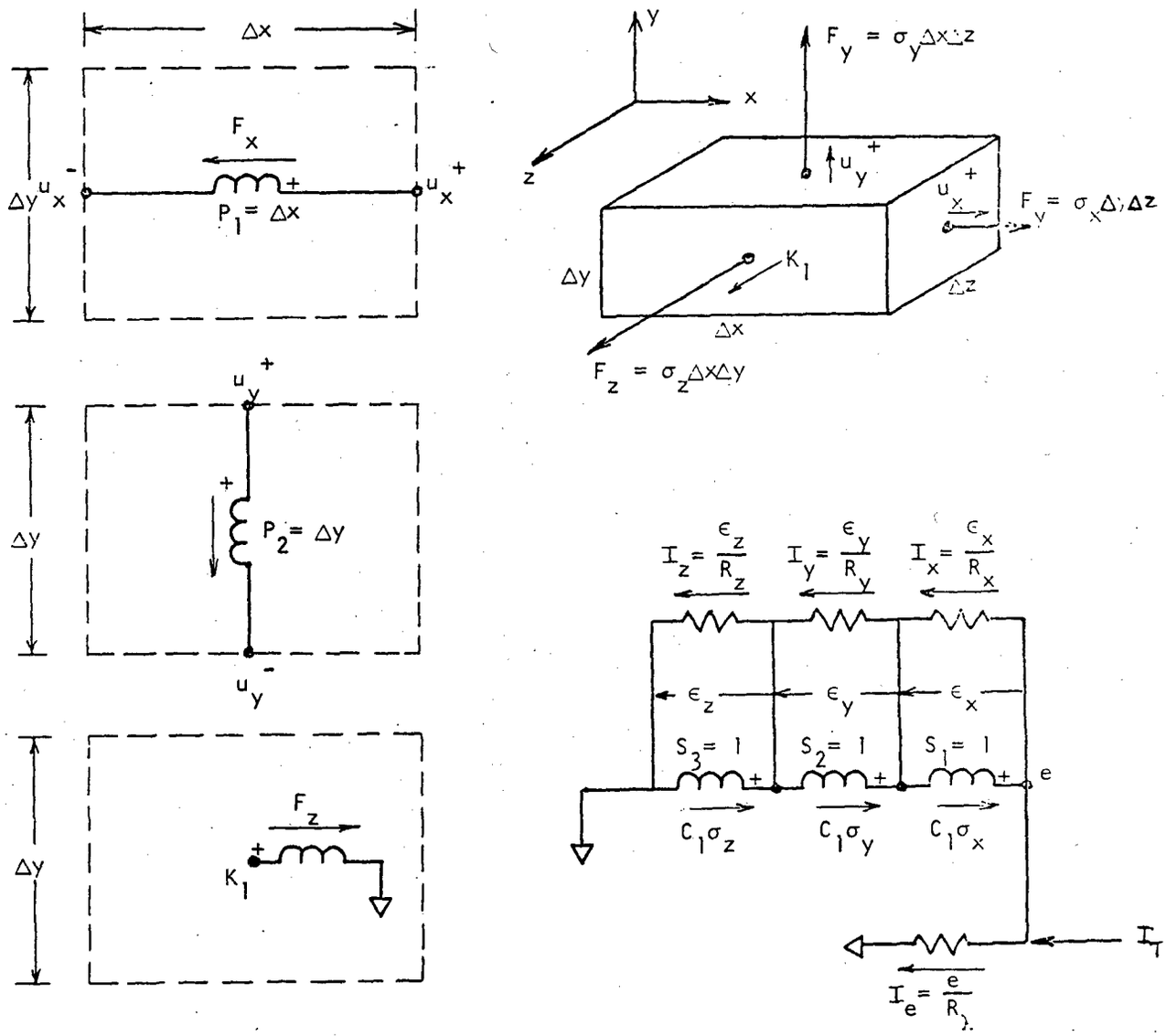
or

$$C_1\sigma_i = I_i + I_e - I_T , \quad i = x, y, z \tag{23}$$

where

$$\left.\begin{aligned} C_1 &= \Delta x\Delta y\Delta z \\ I_i &= \frac{\epsilon_i}{R_i} , \quad i = x, y, z \\ I_e &= \frac{e}{R_\lambda} \\ I_T &= (2G + 3\lambda)(\Delta x\Delta y\Delta z)(\alpha T) \end{aligned}\right\} \tag{24}$$

Examination of the currents flowing in the e-circuit in light of the above. shows the currents flowing in the transformer secondaries to be exactly the stress components multiplied by the volume of the element, as indicated below. Reflecting these currents into the transformer primaries shows that the primary currents are exactly the stress components multiplied by the area over which the stress components act, or in other words, the forces acting on the respective faces of the finite element as shown below.



Direct Stress Circuit Representation

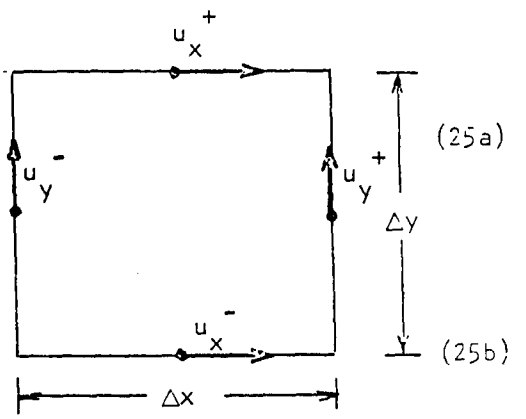
Concerning the shear strain displacement relation and strain energy we have the following. Consider first a finite element with displacement coordinates defined as shown.

In finite difference form the strain displacement relation can be written as

$$2\Delta y\, \gamma_{xy} = \Delta_y(u_x) + \frac{\Delta y}{\Delta x}\Delta_x(u_y) \qquad (25a)$$

or as

$$\Delta_y(u_x) = 2\Delta y\, \gamma_{xy} - \frac{\Delta y}{\Delta x}\Delta_x(u_y) \qquad (25b)$$

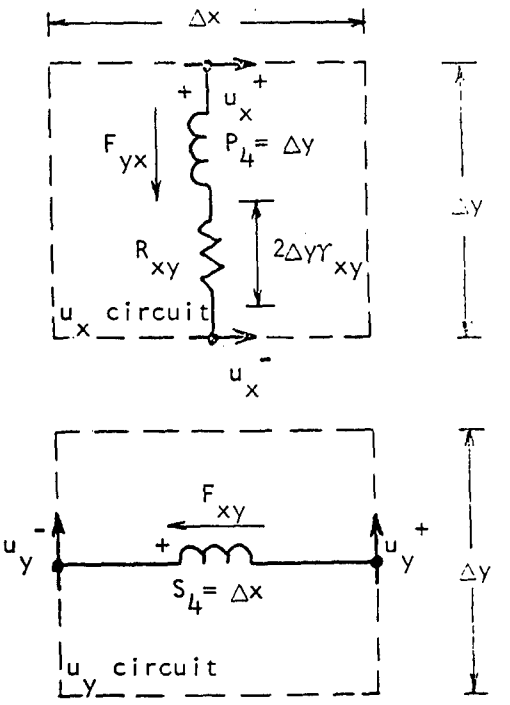


Equations (25) and (26) are satisfied by the subcircuits shown below where

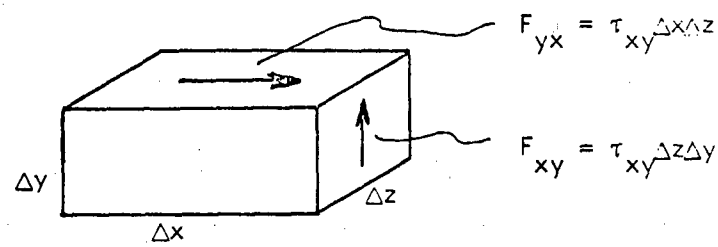
$$R_{xy} = (G\Delta x\Delta z/\Delta y)^{-1}$$

The currents flowing in the shear circuit can be established simply by examining the shear stress-strain relation. From Equation (6)

$$\tau_{xy} = 2G\gamma_{xy}$$



such that



$$F_{yx} = \Delta x\Delta z\tau_{xy}$$

$$= \frac{G\Delta x\Delta z}{\Delta y}(2\Delta y\gamma_{xy}) = \frac{1}{R_{xy}}(2\Delta y\gamma_{xy}) \qquad (27)$$

Hence, the current flowing in the u_x-circuit is exactly the shear force ($\tau_{xy}\Delta x\Delta z$) acting on the y-face of the element in the x-direction. From the transformer relations it is seen that the current flowing in the u_y-circuit is the shear force acting on the x-face of the element in the y-direction. Note that the transformer current relation requiring

$$\frac{F_{yx}}{\Delta y} = \frac{F_{xy}}{\Delta x} \qquad (28)$$

is an exact statement of the shear force relations required by equilibrium of the element in rotation about the z-axis.

In order to construct the set of circuits with which to conduct an analysis, the body under consideration is first assigned a rectangular grid system and displacement coordinates assigned as shown in Figure 3(a). Once the grid system is formed, the construction of the analog circuit representation is accomplished simply by the straight forward interconnection of the set of subcircuits discussed above. Such an array of circuits is shown in Figure 3(b). The value of each element within the circuit is evaluated according to its location. Once the complete circuit has been established and element values computed, the digital computer program SADSAM is used to solve for all of the unknowns.

LUMPED ELEMENT TILE MODEL

Figure 4 shows the lumped element model representation used in the analysis of the tile. In all, a total of 48 direct stress cells were included, plus a representation of the elastic properties of the bond joining the inner and outer tile. The size of the cells was varied along the length of the tile in an attempt to cut down the cell size in the region where the most rapid variation of stresses was expected. Due to the assumed symmetry, the model was terminated midway between the tile boundaries (Station 60 in Figure 4)with a skew-symmetric boundary. This still allowed all conditions of interest to be investigated and made possible a much finer grid work of elements for the analysis. The material properties used in the analysis are summarized in Table1 .

CONDITIONS INVESTIGATED AND OBSERVED RESULTS

In all a total of six loading conditions were investigated. These are summarized in Table 2. The first condition is related to the loading of the tile by a pressure loading of the radome. In the analysis, an axial load (applied along the x-coordinate) equivalent to an average stress of one psi compression was applied. In loading conditions A and B, thermal gradients resulting from a previous thermal analysis of the radome (Reference *) were applied to the cross section. Loading conditions C, D and E were applied simply to generate stress influence coefficients for linear, quadratic and quartic thermal distributions across the section with the idea that these distributions might be superimposed in various proportions in order to gain insight into other thermal loadings.

---

* Thermal Analysis of the Narmco Mosaic Radome using the Lockheed "Thermal Analyzer Program" see Appendix VIII

The results of the analysis are presented in field form in Section B. Using the σ_x (1 psi average) as a basis for interpreting the results, it is seen that significant stress concentrations do exist. For the axial stresses (σ_x) a magnification of approximately 10 is shown in the region of the tile boundary. The transverse stress (σ_y) is shown to be about 1.5 times the average axial stress across the bond and the shear stress in the bond is shown to be approximately 1.5 times the average axial stress.

It is of interest to note that the stress concentrations decay very rapidly as one moves away from the tile boundary. This helps to justify the assumptions of symmetry made in formulating the analysis and points out that as long as the tile boundaries are reasonably remote (at least an inch) that they will have relatively little effect on each other.

The fact that the effect of stress concentrations is limited to a very small region around the tile discontinuaties also helps to justify the omission of curvature effects in the analysis. The effects of curvature are incorporated in the determination of the gross-average stress in the membrane analysis of the radome. This analysis shows that a large percentage of the mosaic radome will have these "membrane" stresses and the changes in the direction of the structure in the vicinity of the stress concentration are very small and can undoubtedly be ignored.

At the onset of the analysis it was questionable as to whether or not the small temperature drop across the tile thickness (see Figures 5

and 6) would produce significant stresses. The analysis indicates that axial stresses near the joints in the order of 4000 psi (Condition A) will exist and that thermal effects from even small temperature drops across the tile, play a quite significant role in the total stress picture. Figure 7 shows temperature distributions for Conditions C, D, and E.

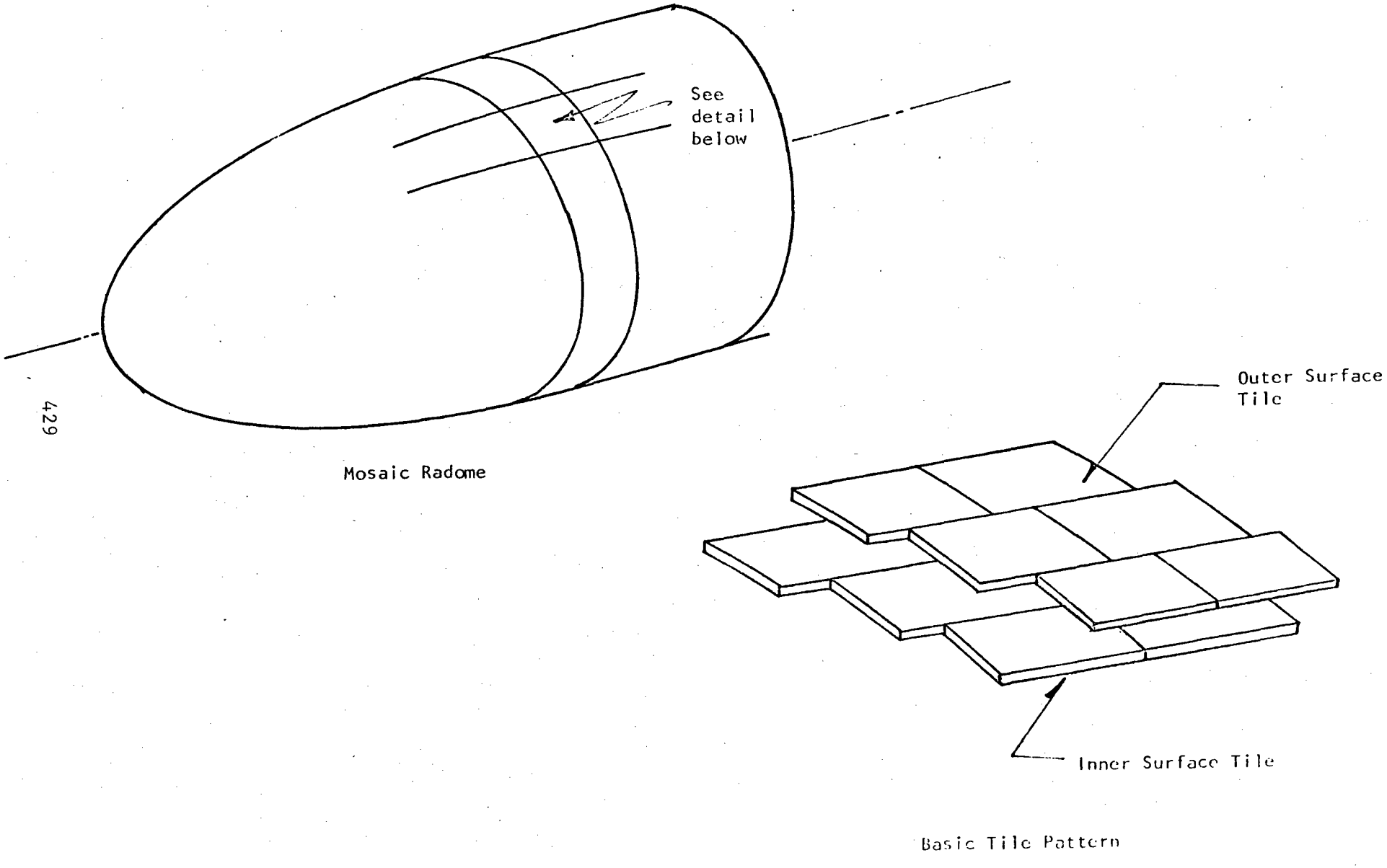


FIGURE 1 . Basic Geometric Configuration

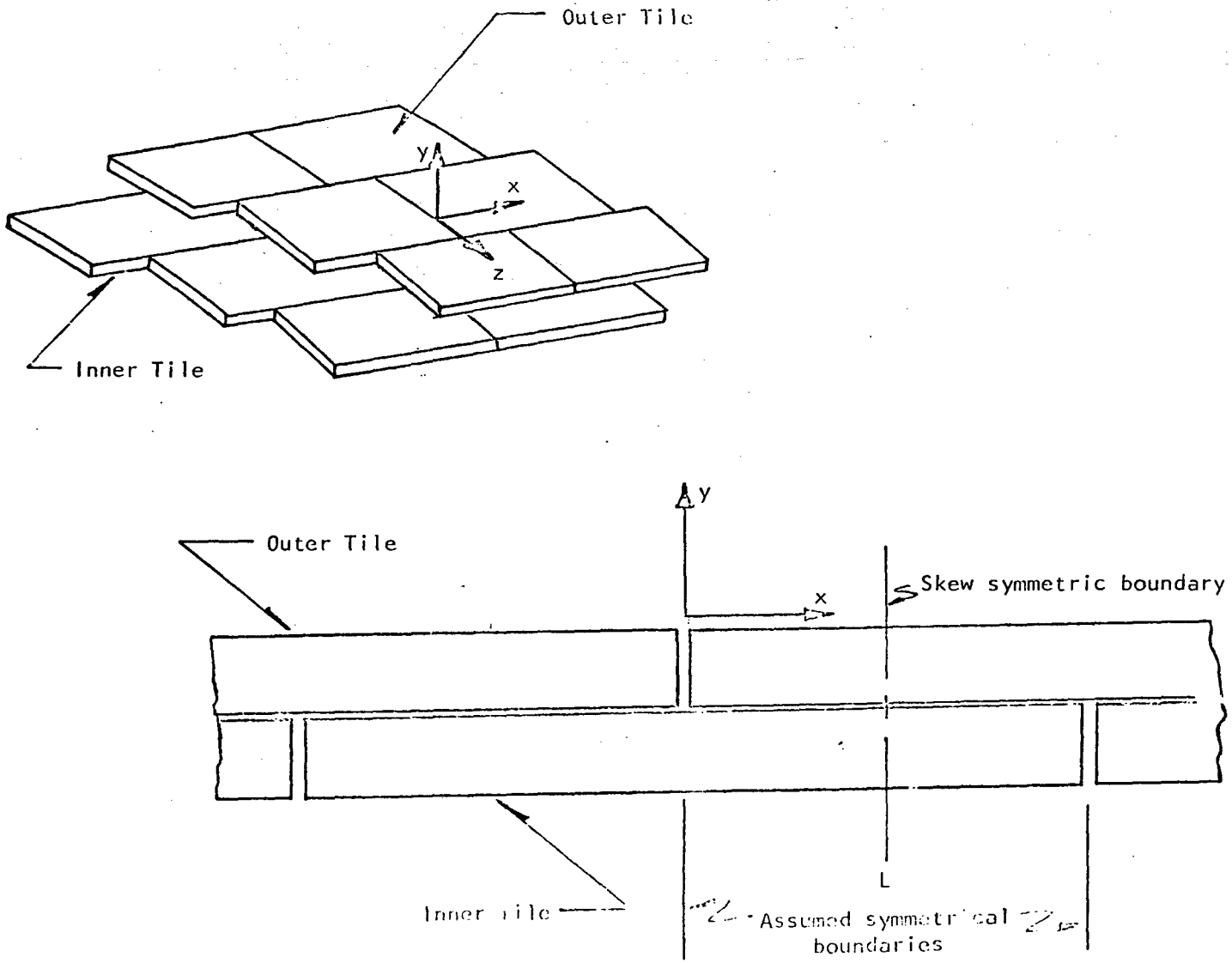
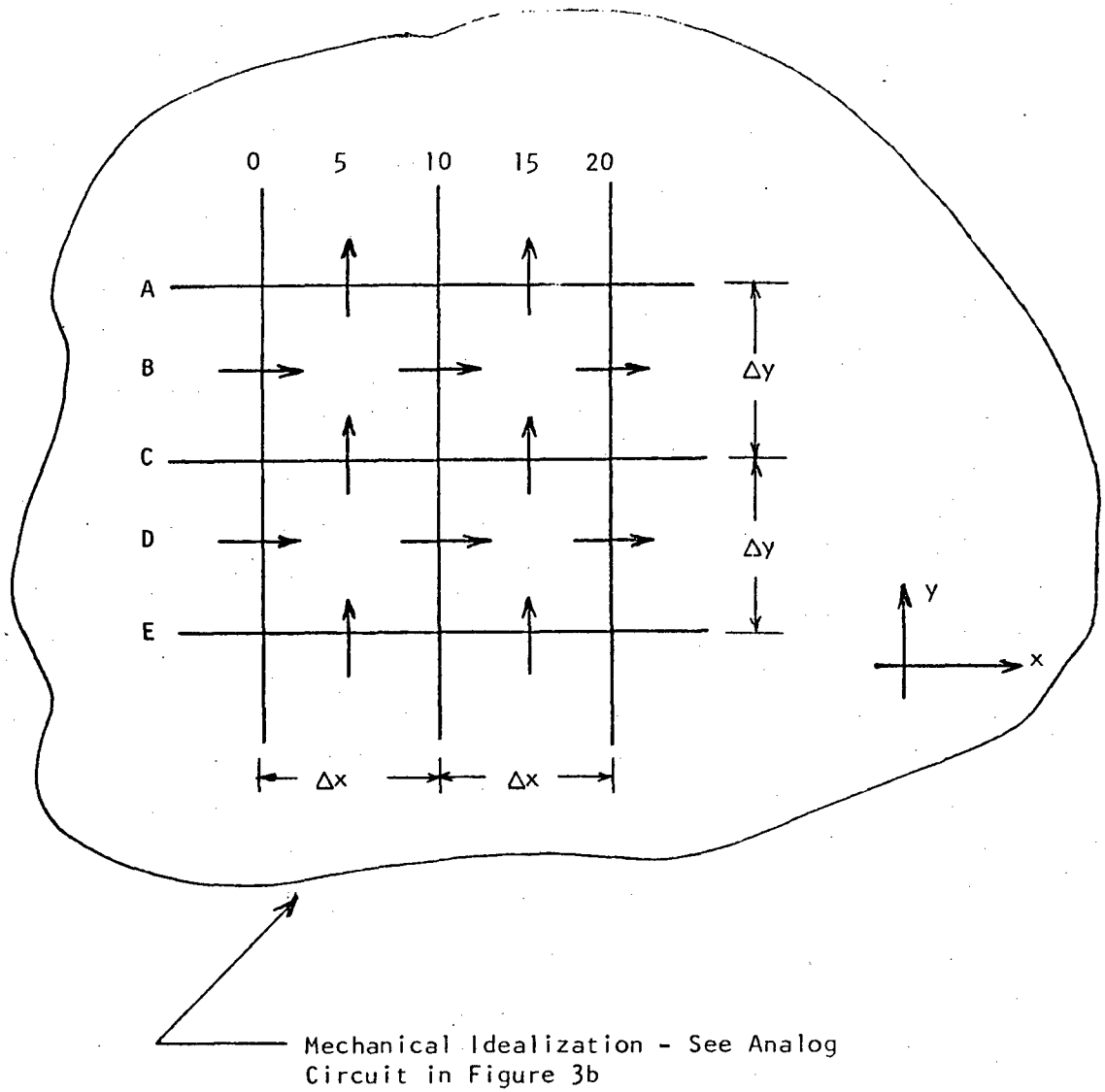


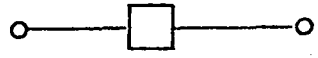
FIGURE 2 . Idealized Structural Model



Mechanical Idealization - See Analog Circuit in Figure 3b



(Transformer Winding)



(Resistor)

$$\frac{P_1}{S_1} = \Delta x$$

$$\frac{P_2}{S_2} = \Delta y$$

$$\frac{P_3}{S_3} = \Delta z$$

$$\frac{P_4}{S_4} = \Delta y/\Delta x$$

$$R_x = R_y = R_z = (2G\Delta x\Delta y\Delta z)^{-1}$$

$$R_\lambda = (\lambda\Delta x\Delta y\Delta z)^{-1}$$

See Analog Circuit in Figure 3b

FIGURE 3 a. Basic Lumped Element Model

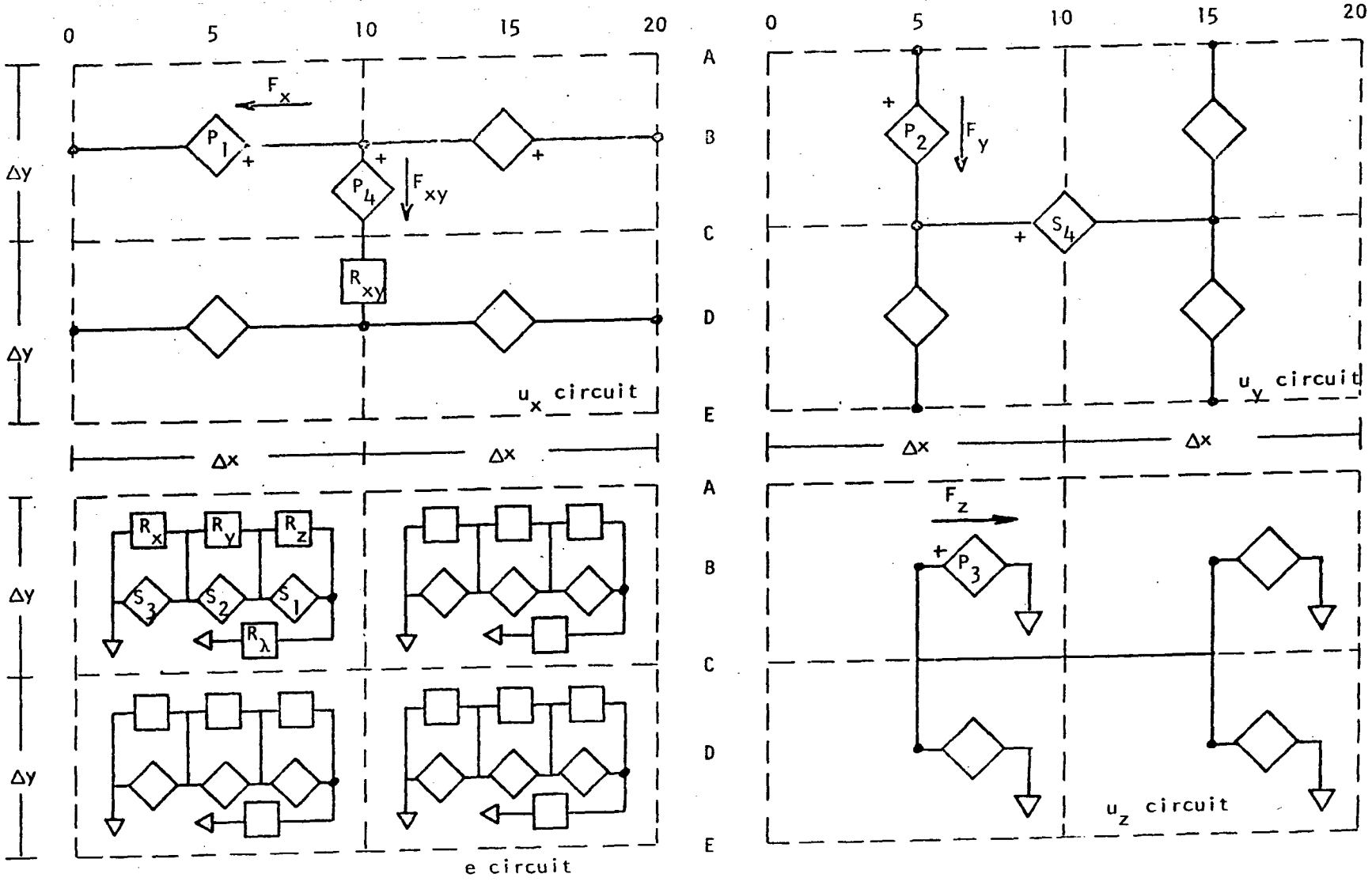
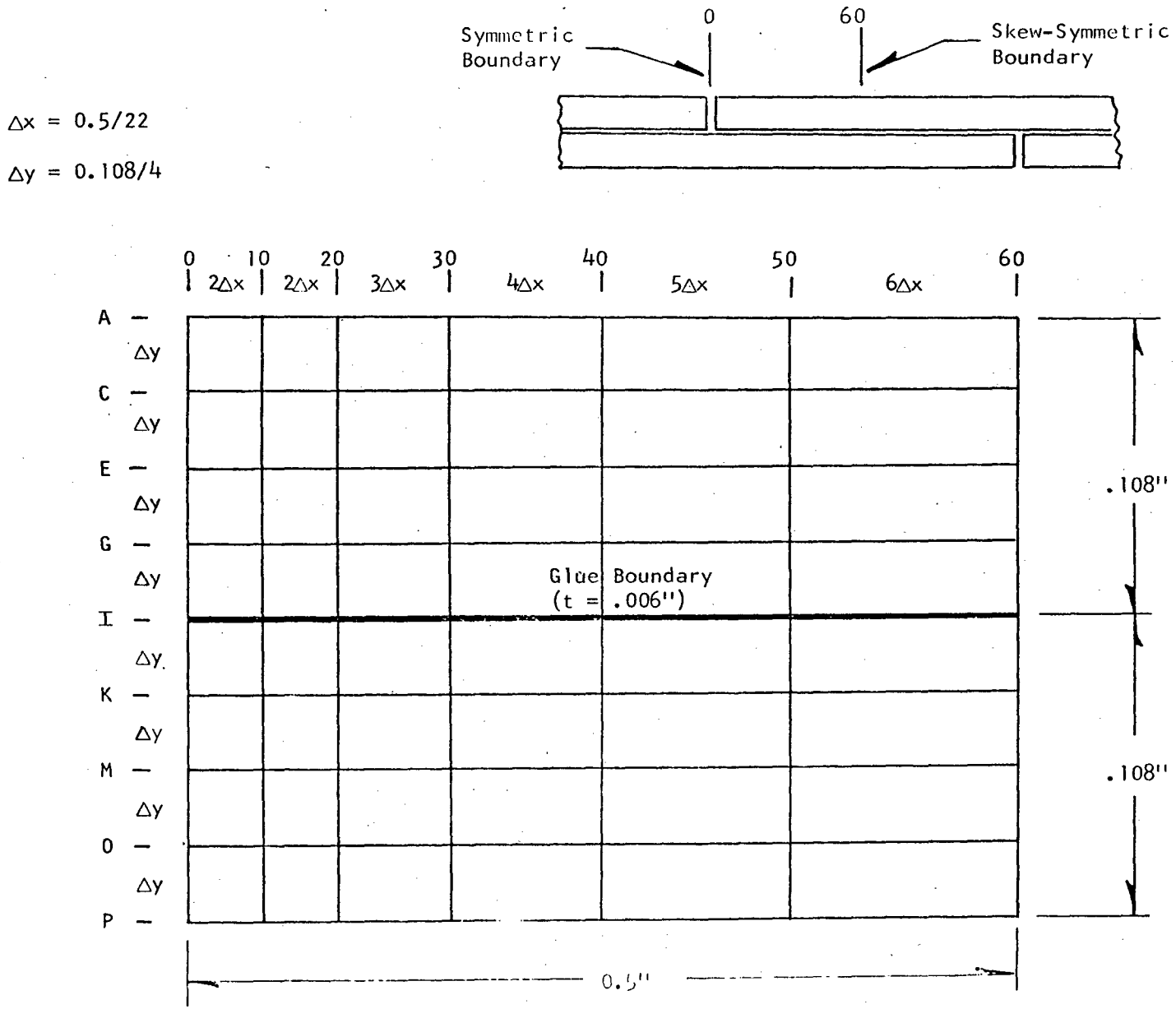


FIGURE 3 b. Basic Analog Circuit Representation



Structural Idealization - Alumina Tile Stress Analysis

FIGURE 4

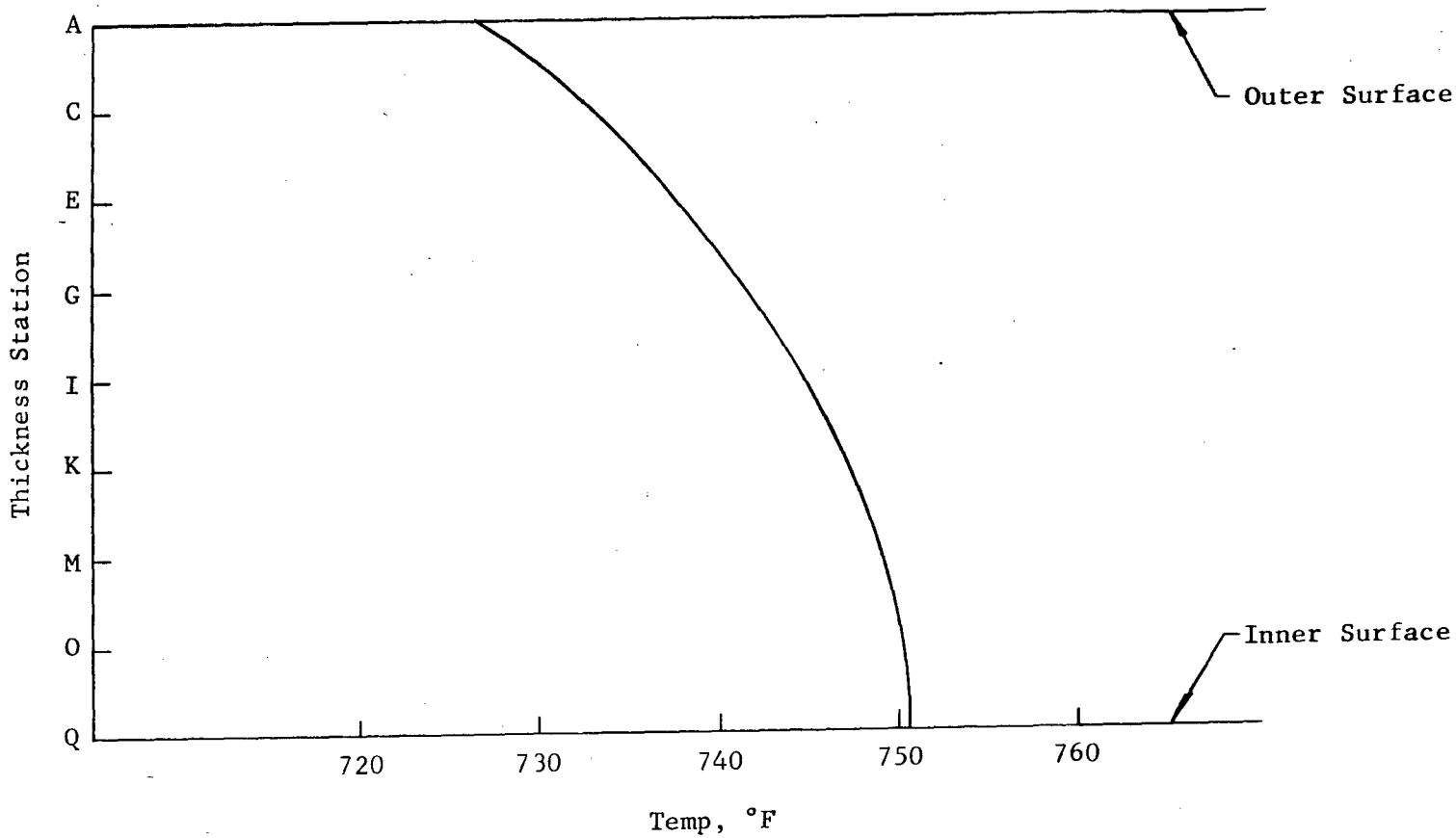


Figure 5 . Temperature Distribution A
(Maximum Thermal Gradient - t = 600 sec)

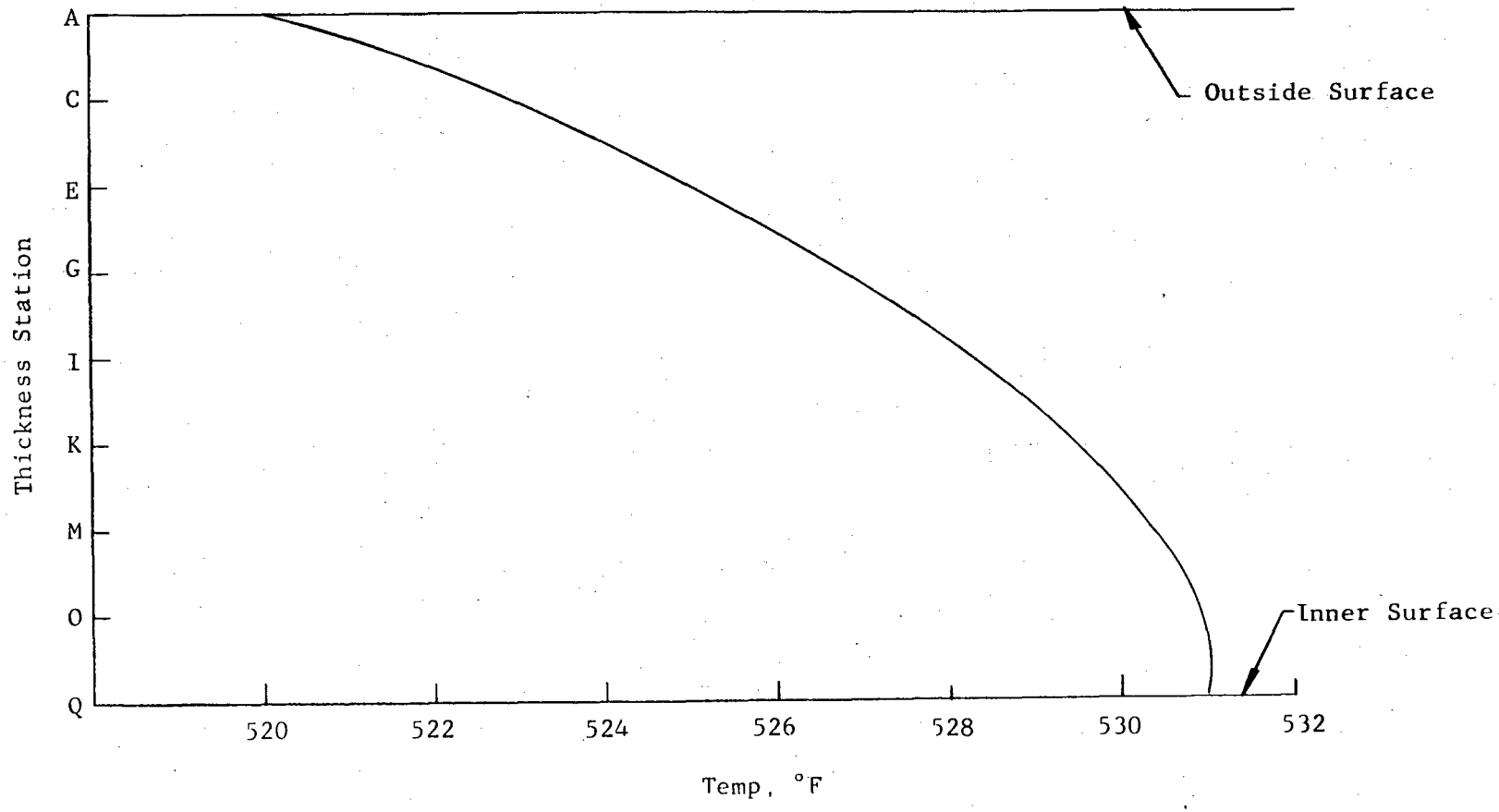
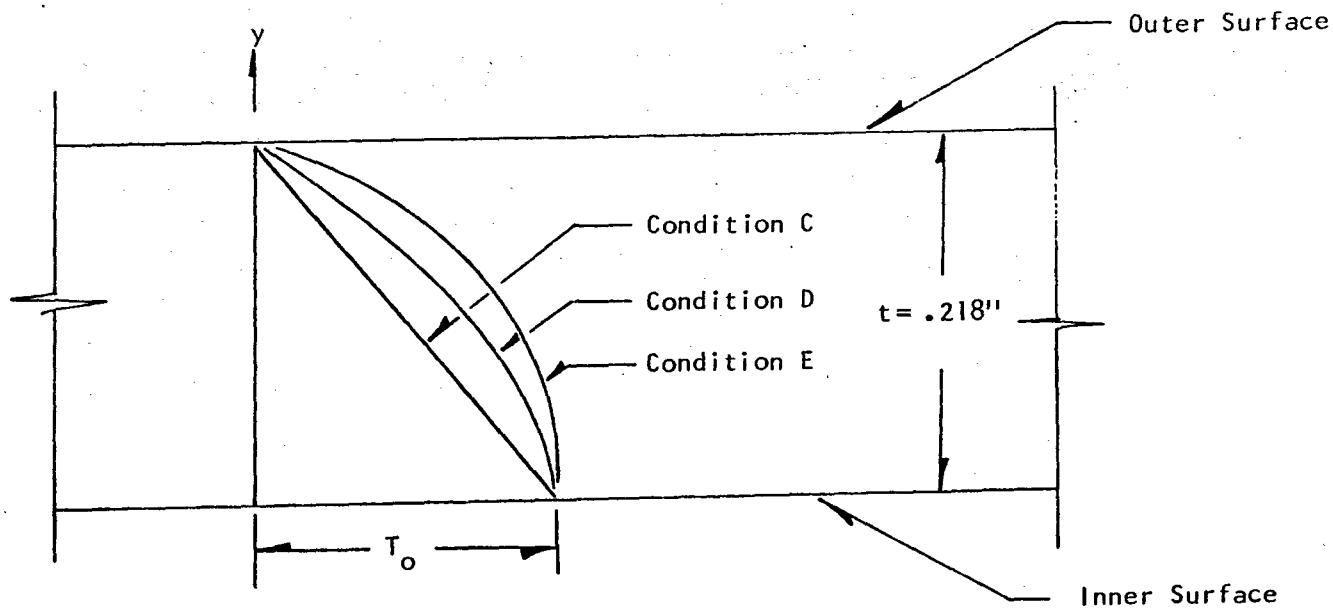


Figure 6 Temperature Distribution B



Condition	Thermal Distribution
C	$T = T_o[1 - (y/t)]$
D	$T = T_o[1 - (y/t)^2]$
E	$T = T_o[1 - (y/t)^4]$

Temperature Distributions for Conditions C, D and E

FIGURE 7

TABLE 1. Material Properties

Alumina

$E = 45 \times 10^6$ psi (Young's Modulus)

$G = 21 \times 10^6$ psi (Shear Modulus)

$\alpha = 3.9 \times 10^{-6}$ in/in/°F (Coefficient of Thermal Expansion)

Bond Material

$E = 9.5 \times 10^6$ psi (Young's Modulus)

$\nu = .25$ (Poisson's Ratio)

TABLE 2. Conditions Investigated

Condition	Loading	Remarks
σ_x	σ_x (1 psi)	Axial loading of the tile of 1 psi compression
A	Thermal	Thermal gradient as shown in Figure 5
B	Thermal	Thermal gradient as shown in Figure 6
C	Thermal	Linear thermal gradient (see Figure 7)
D	Thermal	Quadratic thermal gradient (see Figure 7)
E	Thermal	Quartic thermal gradient (see Figure 7)

SECTION B

RESULTS

0	10	20	30	40	50	60	50	40	30	20	10	0
0	-.134	-.589	-.933	-1.01	-1.00	-1.00	-1.00	-.887	-.259	1.13	2.59	
0	-.365	-.759	-.951	-.998	-1.00	-1.00	-.998	-.965	-.851	-.661	-.302	
0	-.679	-1.00	-1.01	-.996	-.999	-1.00	-1.00	-1.07	-1.46	-2.39	-3.17	
0	-1.34	-1.31	-1.06	-.997	-.997	-.998	-1.00	-1.12	-1.78	-3.57	-7.12	
-7.12	-3.57	-1.78	-1.12	-1.00	-.998	-.997	-.997	-1.06	-1.31	-1.34	0	
-3.17	-2.39	-1.46	-1.07	-1.00	-1.00	-.999	-.996	-1.01	-1.00	-.679	0	
-.302	-.661	-.851	-.965	-.998	-1.00	-1.00	-.998	-.954	-.759	-.365	0	
2.59	1.13	-.259	-.887	-1.00	-1.00	-1.00	-1.01	-.933	-.389	-.134	0	

Slot

Slot

A

B

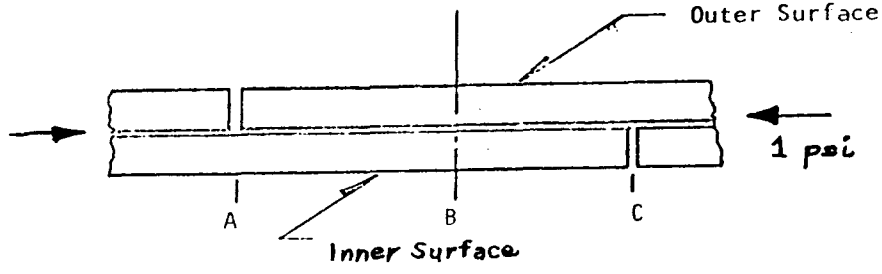
C

y

x

LOADING CONDITION σ_x

STRESS COMPONENT σ_x psi/psi

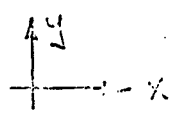


0	10	20	30	40	50	60	50	40	30	20	10	0
0	0	0	0	0	0	0	0	0	0	0	0	0
-.047	-.031	.023	.009	.001	0	0	.003	.013	.177	.125	-.017	
-.223	-.145	.127	.072	.013	0	0	.018	.115	.274	.060	-1.16	
-.680	-.060	.274	.118	.021	0	0	.024	.144	.440	.006	-1.53	
-1.53	.506	.440	.144	.024	0	0	.021	.118	.274	-.060	-.680	
-1.16	.323	.274	.115	.018	0	0	.013	.072	.127	-.145	-.223	
-.517	.125	.177	.053	.006	0	0	.005	.023	.013	-.031	-.047	
0	0	0	0	0	0	0	0	0	0	0		

Slot

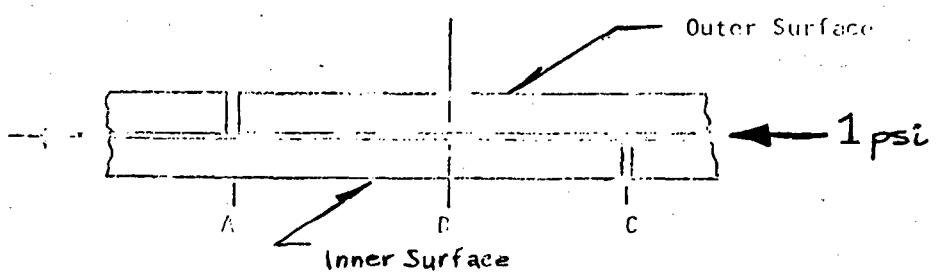
Slot

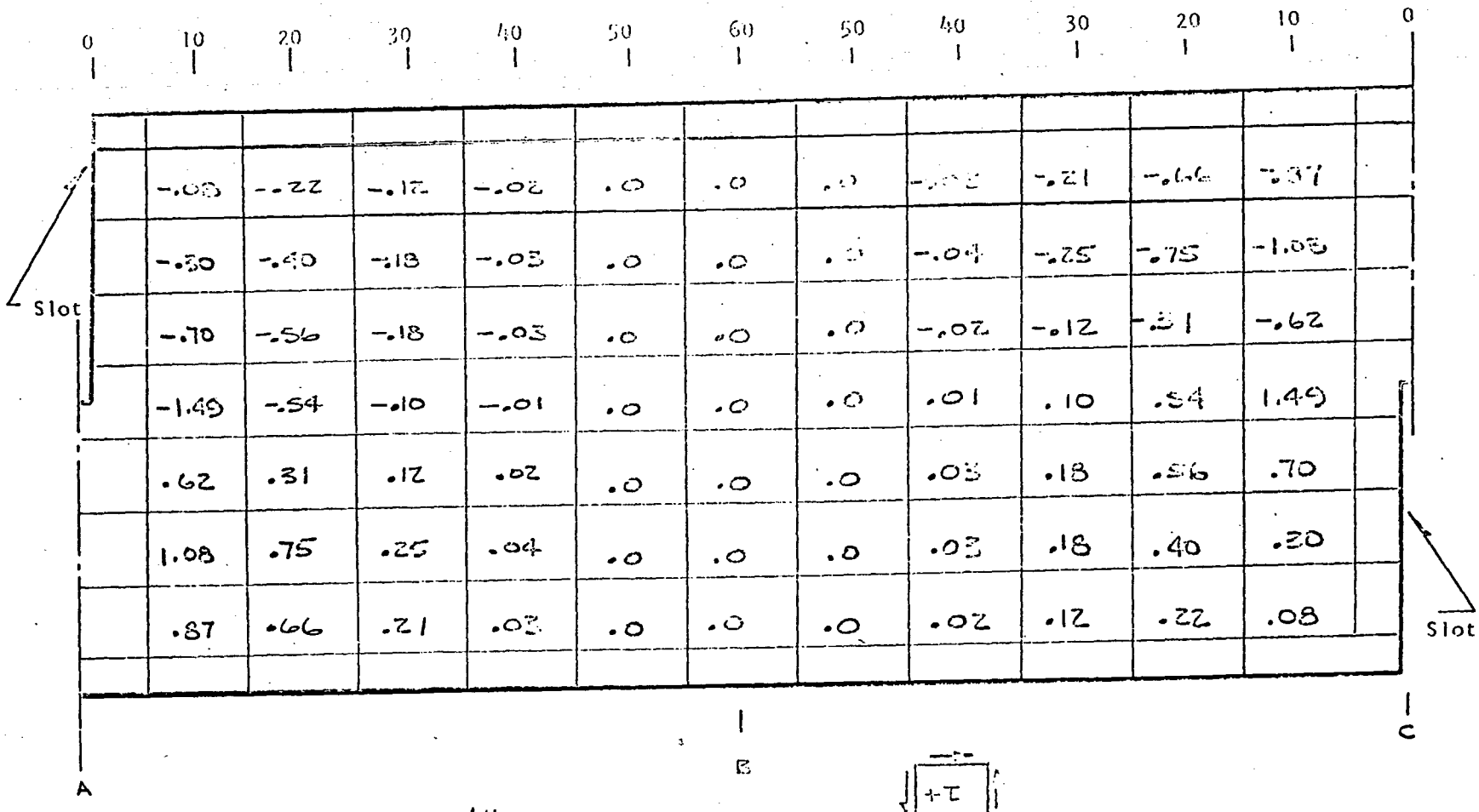
A B C

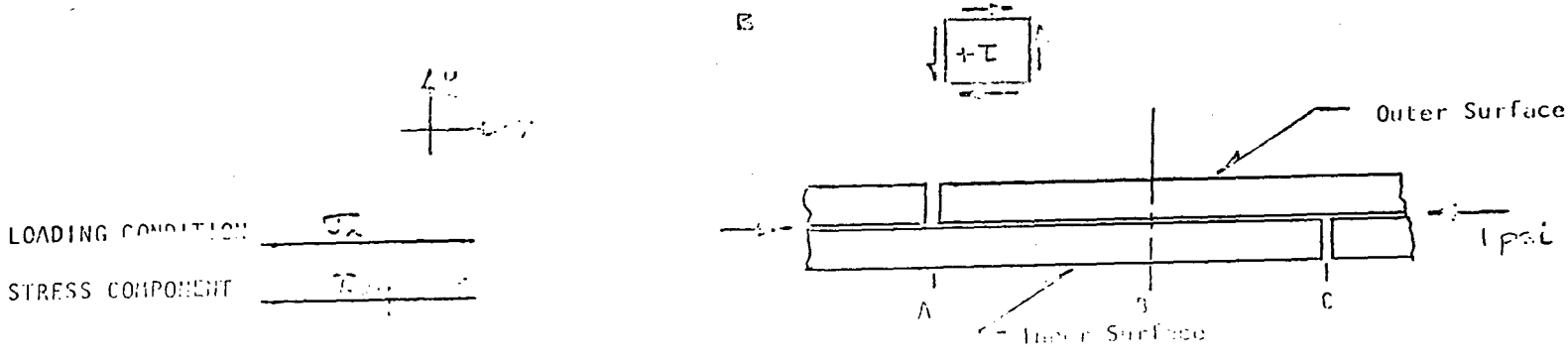


LOADING CONDITION σ_x

STRESS COMPONENT σ_y psi/psi







LOADING CONDITION σ_x

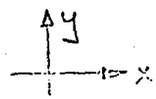
STRESS COMPONENT σ_{xx}

0	10	20	30	40	50	60	50	40	30	20	10	0
0	[illegible]	1062.	1432.	1494.	1482.	1477.	1470.	1564.	1593.	2081.	2475.	
0	216.4	402.0	645.1	670.5	680.4	684.7	684.9	703.0	766.9	874.8	1072.	
0	238.0	268.2	201.7	179.5	180.3	184.5	180.9	146.2	-71.0	-576.0	-1004.	
0	477.0	177.1	-110.6	-171.3	-173.2	-170.5	-171.4	-244.3	-601.7	-1503.	-3328.	
3763.	1466.	176.5	-381.7	-428.4	-438.1	-428.4	-428.5	-466.6	-593.7	-640.2	0.	
770.8	300.2	-317.0	-590.6	-648.3	-642.9	-641.5	-641.7	-644.5	-642.0	-488.2	0.	
-1320.	-1014.	-818.3	-705.2	-676.8	-671.6	-672.2	-672.6	-646.5	-524.6	-287.8	0.	
-3218.	-2126.	-1040.	-589.4	-456.5	-442.3	-442.6	-440.9	-400.4	-215.2	2.1	0.	

Slot

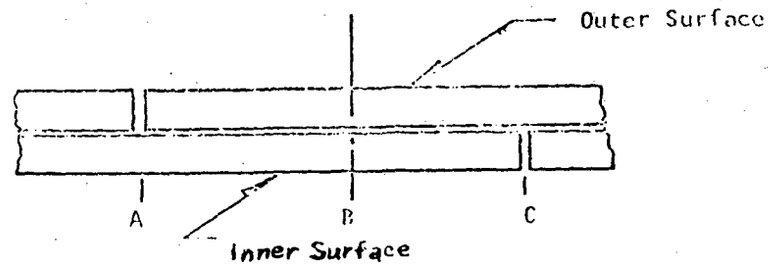
Slot

A B C



LOADING CONDITION A (See Figure 5)

STRESS COMPONENT σ_x psi



0	10	20	30	40	50	60	50	40	30	20	10	0
0	0	0	0	0	0	0	0	0	0	0	0	0
150.4	12.8	-66.8	-30.1	-5.8	-.1	.3	4.3	29.2	95.7	60.6	-282.8	
395.1	27.1	-162.0	-72.6	-12.7	-.1	.6	10.1	65.1	208.2	173.4	-685.2	
783.8	-34.1	-276.2	-110.3	-18.4	-.4	.6	13.6	78.1	244.8	279.0	-857.1	
1203.	-348.2	-370.6	-124.2	-19.0	-.5	.5	12.1	68.6	148.8	-25.3	-378.6	
876.7	-253.2	-292.8	-95.2	-15.2	-.2	.4	7.5	39.1	63.4	-92.5	-100.1	
384.4	-78.4	-135.5	-48.1	-6.7	-.0	.2	2.8	15.1	16.0	-62.1	.73	
0	0	0	0	0	0	0	0	0	0	0	0	

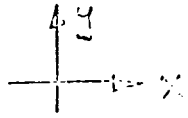
Slot

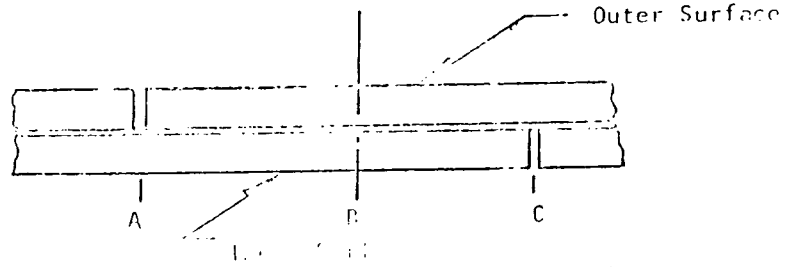
Slot

A

B

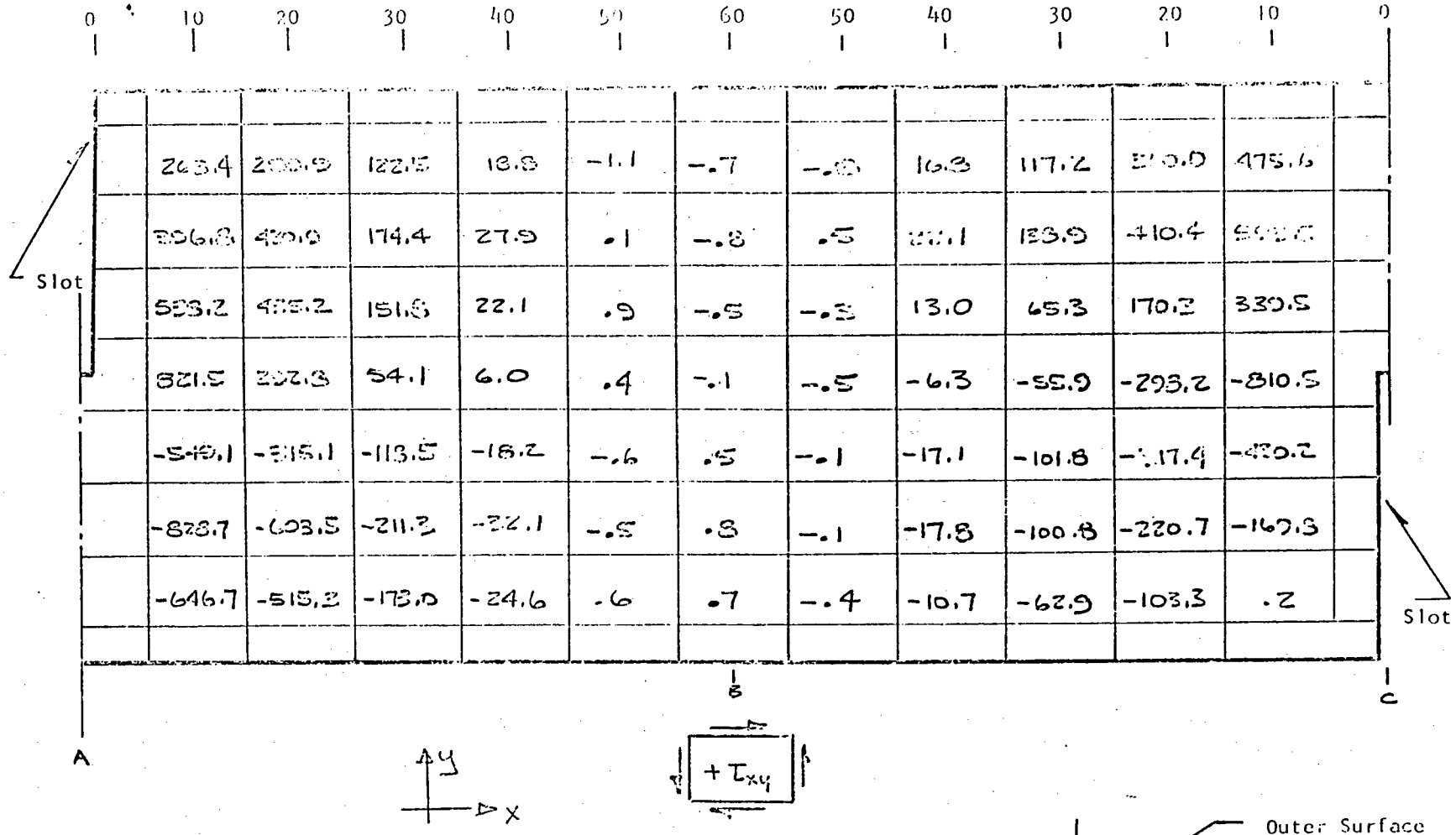
C





LOADING CONDITION

STRESS COMPONENT



LOADING CONDITION A (See Figure 5)

STRESS COMPONENT τ_{xy}

0	10	20	30	40	50	60	50	40	30	20	10	0
0	212.1	498.4	696.0	698.6	682.0	674.8	688.6	713.9	866.8	1196.	1577.	
0	91.4	213.8	285.9	301.5	303.2	303.0	306.8	311.6	336.1	392.9	469.8	
0	100.2	176.1	71.8	64.1	66.0	66.6	64.6	47.1	-46.6	-263.4	-451.1	
0	201.1	66.8	-65.1	-98.8	-98.4	-94.2	-95.4	-124.6	-289.0	-713.7	-1565.	
1655.	630.7	62.4	-166.1	-210.0	-206.4	-210.2	-210.1	-225.4	-288.4	-290.0	0	
360.5	161.2	-117.6	-241.1	-262.4	-261.8	-261.2	-261.7	-265.2	-191.9	-174.9	0	
-573.4	-435.9	-346.7	-291.6	-276.0	-277.4	-277.7	-274.5	-265.4	-220.8	-116.6	0	
-1451.	-964.2	-475.0	-248.5	-208.8	-207.5	-209.0	-210.5	-190.8	-107.6	-10.1	0	

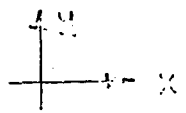
Slot

Slot

A

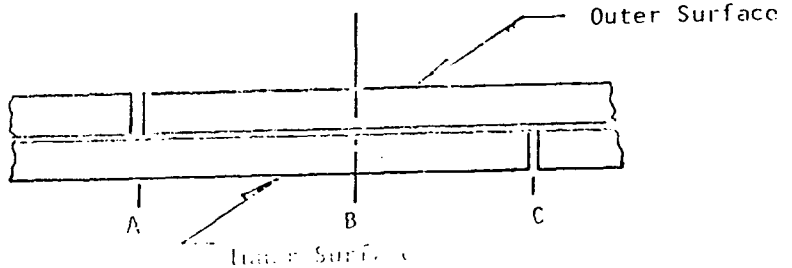
B

C



LOADING CONDITION E (Cross Section) 6

STRESS COMPONENT σ_{xx}



0	10	20	30	40	50	60	50	40	30	20	10	0
0	0	0	0	0	0	0	0	0	0	0	0	
74.8	4.6	-31.1	-13.5	-2.1	-.1	.0	2.2	12.7	41.4	31.1	-121.0	
181.9	11.4	-75.5	-33.1	-5.5	-.1	.2	4.6	27.3	88.4	79.5	-278.4	
324.4	-16.0	-125.1	-49.9	-8.2	-.2	.3	5.9	34.1	107.1	122.9	-376.7	
538.9	-154.2	-166.6	-56.0	-9.0	-.2	.2	5.5	27.8	65.1	-11.6	-194.8	
392.2	-91.6	-121.8	-43.0	-6.6	-.2	.1	3.5	17.0	27.9	-36.1	-48.3	
171.8	-34.1	-61.2	-19.4	-2.7	-.1	.0	1.5	6.6	7.2	-23.9	-3.6	
0	0	0	0	0	0	0	0	0	0	0	0	

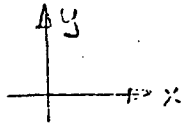
Slot

Slot

A

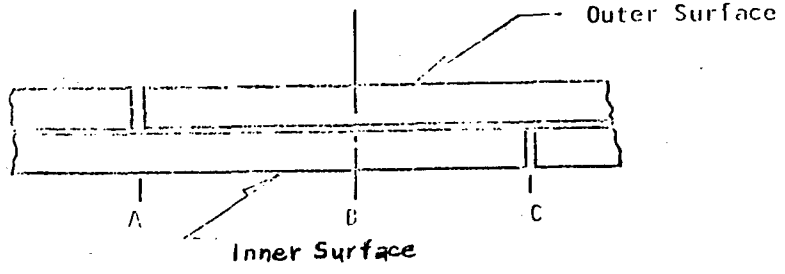
B

C

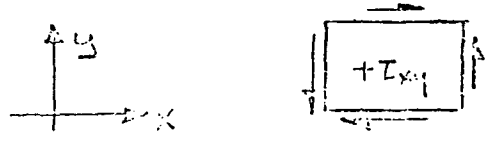


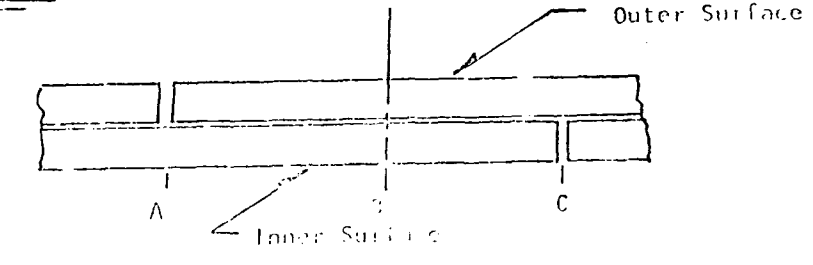
LOADING CONDITION B (See Figure 6.)

STRESS COMPONENT σ_y



0	10	20	30	40	50	60	50	40	30	20	10	0
Slot												
	126.0	[illegible]	55.2	7.8	.0	-.2	-.2	2.0	31.7	[illegible]	[illegible]	
	180.2	191.8	70.6	12.7	-.2	-.1	.9	9.6	60.1	170.6	260.1	
	289.8	198.7	60.4	10.7	.2	-.2	.0	4.9	28.3	75.6	143.6	
	361.1	120.5	25.7	2.7	.2	-.0	-.2	-2.8	-24.4	-130.5	-256.0	
	-247.2	-141.6	-58.0	-8.9	-.1	.2	-.2	-6.8	-44.1	-137.9	-179.1	
	-270.9	-274.2	-95.8	-14.6	.0	.3	-.3	-7.7	-45.6	-95.8	-75.3	
	-289.3	-251.8	-77.2	-10.5	-.3	.5	.4	-5.3	-28.3	-46.3	-6.0	
												Slot





LOADING CONDITION B (See Figure 6)

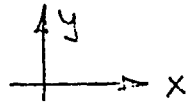
STRESS COMPONENT T_{x-y}

0	10	20	30	40	50	60	50	40	30	20	10	0
0	5.24	26.4	37.8	40.2	40.1	40.0	40.0	43.2	61.1	99.5	139.0	
0	10.7	21.7	27.2	28.5	28.6	28.6	28.6	29.7	33.4	39.7	50.2	
0	14.0	18.9	17.6	17.1	17.1	17.2	17.2	15.3	5.02	-18.4	-37.3	
0	23.6	16.6	7.78	5.66	5.66	5.77	5.65	2.21	15.9	-63.2	-152.0	
152.0	63.2	15.9	-2.21	-5.65	-5.77	-5.66	-5.66	-7.78	-16.6	-23.6	0	
37.3	18.4	-5.02	-15.2	-17.2	-17.2	-17.1	-17.1	-17.6	-18.9	-14.0	0	
-50.2	-30.7	-33.4	-29.7	-28.6	-28.6	-28.6	-28.5	-27.2	-21.7	-10.7	0	
-139.0	-99.5	-61.1	-43.2	-40.0	-40.0	-40.1	-40.2	-37.8	-26.4	-9.24	0	

Slot

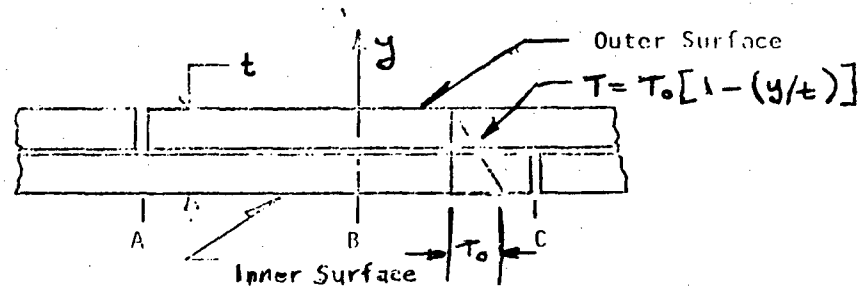
Slot

A B C



LOADING CONDITION C

STRESS COMPONENT σ_x / T_o (psi/°F)



0	10	20	30	40	50	60	50	40	30	20	10	0
0	0	0	0	0	0	0	0	0	0	0	0	0
3.26	1.60	-1.71	-.94	-.17	-.00	.00	.23	1.51	4.83	3.09	-13.9	
10.3	2.50	-4.73	-2.33	-.42	-.01	.02	.53	3.31	10.4	8.11	-31.6	
22.3	-.15	-8.86	-3.63	-.64	-.02	.02	.70	4.23	12.9	13.1	-42.6	
42.6	-13.1	-12.9	-4.23	-.70	-.02	.02	.64	3.63	8.86	.15	-22.3	
31.6	-8.11	-10.4	-3.31	-.53	-.02	.01	.42	2.33	4.73	-2.50	-10.3	
13.9	-3.09	-4.83	-1.51	-.23	-.00	.00	.17	.94	1.71	-1.60	-3.26	
0	0	0	0	0	0	0	0	0	0	0	0	0

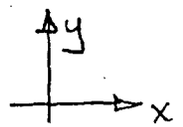
Slot

Slot

A

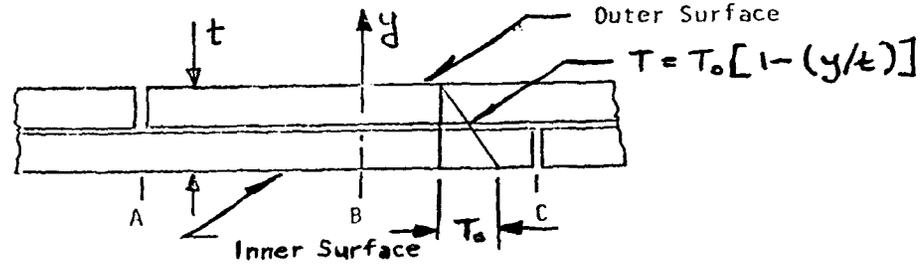
B

C



LOADING CONDITION C

STRESS COMPONENT σ_y/T_o psi/°F



0	10	20	30	40	50	60	50	40	30	20	10	0
	5.5	8.2	3.9	.6	.0	.0	.0	.9	6.1	18.3	23.5	
	11.9	13.4	5.7	1.0	.0	.0	.0	1.1	7.3	21.3	29.7	
	20.2	15.7	5.3	.8	.0	.0	.0	.6	3.8	10.1	18.6	
	34.2	12.4	2.3	.3	.0	.0	.0	-.3	-2.3	-12.4	-34.2	
	-18.6	-10.1	-3.8	-.6	.0	.0	.0	-.8	-5.3	-15.7	-20.2	
	-29.7	-21.3	-7.3	-1.1	.0	.0	.0	-1.0	-5.7	-13.4	-11.9	
	-23.5	-18.3	-6.1	-.9	.0	.0	.0	-.6	-3.9	-8.2	-5.5	

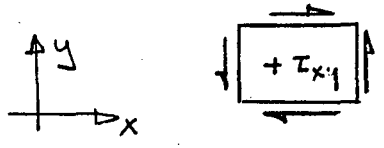
Slot

Slot

A

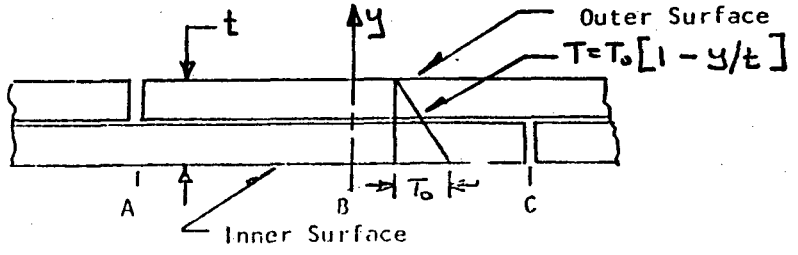
B

C



LOADING CONDITION C

STRESS COMPONENT τ_{xy} / T_o psi/°F



0	10	20	30	40	50	60	50	40	30	20	10	0
0	18.3	44.0	59.4	62.4	62.4	62.2	62.3	64.8	78.8	110.0	142.5	
0	11.1	23.5	30.1	31.6	31.8	31.8	31.8	32.5	35.0	39.1	46.9	
0	10.0	11.4	8.28	7.60	7.57	7.63	7.56	6.03	-2.71	-23.7	-41.5	
0	18.4	4.97	-7.38	-10.3	-10.3	-10.2	-10.3	-17.4	-27.5	-67.9	-149.0	
155.9	58.5	4.20	-13.0	-21.6	-21.7	-21.6	-21.6	-23.0	-28.2	-28.3	0	
33.0	13.2	-12.8	-24.5	-26.7	-26.7	-26.7	-26.5	-26.8	-26.4	-17.9	0	
-53.3	-40.3	-31.7	-32.5	-25.5	-25.4	-25.4	-25.4	-24.4	-20.0	-10.4	0	
-135.5	-88.3	-43.4	-21.7	-17.7	-17.7	-17.8	-17.9	-16.3	-8.97	-.20	0	

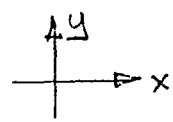
Slot

Slot

A

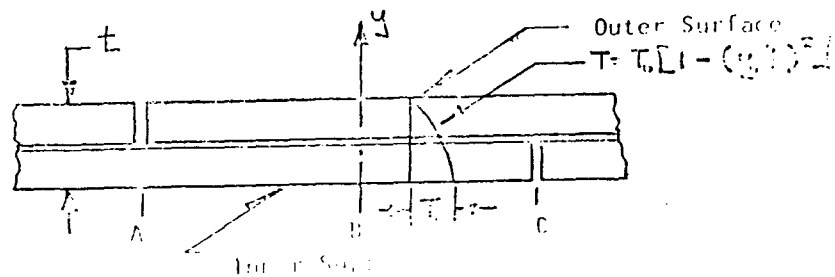
B

C



LOADING CONDITION D

STRESS COMPONENT σ_x/T_o psi/°F



0	10	20	30	40	50	60	50	40	30	20	10	0
0	0	0	0	0	0	0	0	0	0	0	0	0
6.46	.75	-2.7	-1.3	-.2	.0	.0	.2	1.2	3.6	2.8	-11.6	
16.8	1.13	-6.9	-3.1	-.5	.0	.0	.4	2.6	8.3	7.3	-26.0	
30.7	-1.68	-11.8	-4.7	-.8	.0	.0	.5	3.2	10.0	11.4	-34.1	
51.2	-14.8	-15.7	-5.3	-.9	.0	.0	.5	2.6	6.0	-1.4	-13.8	
37.2	-8.9	-12.3	-4.1	-.7	.0	.0	.3	1.6	2.5	-3.9	-3.7	
16.3	-3.4	-5.7	-1.8	-.3	.0	.0	.1	.6	.7	-2.4	-.1	
0	0	0	0	0	0	0	0	0	0	0	0	

Slot

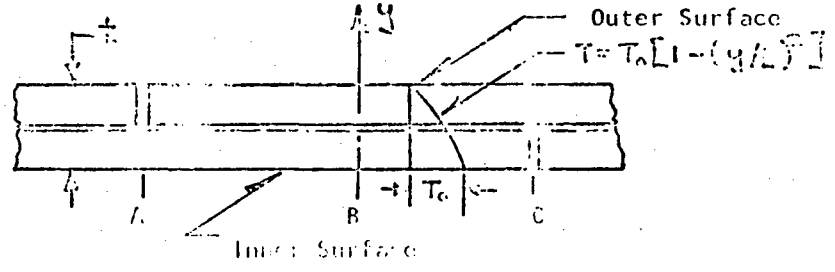
Slot

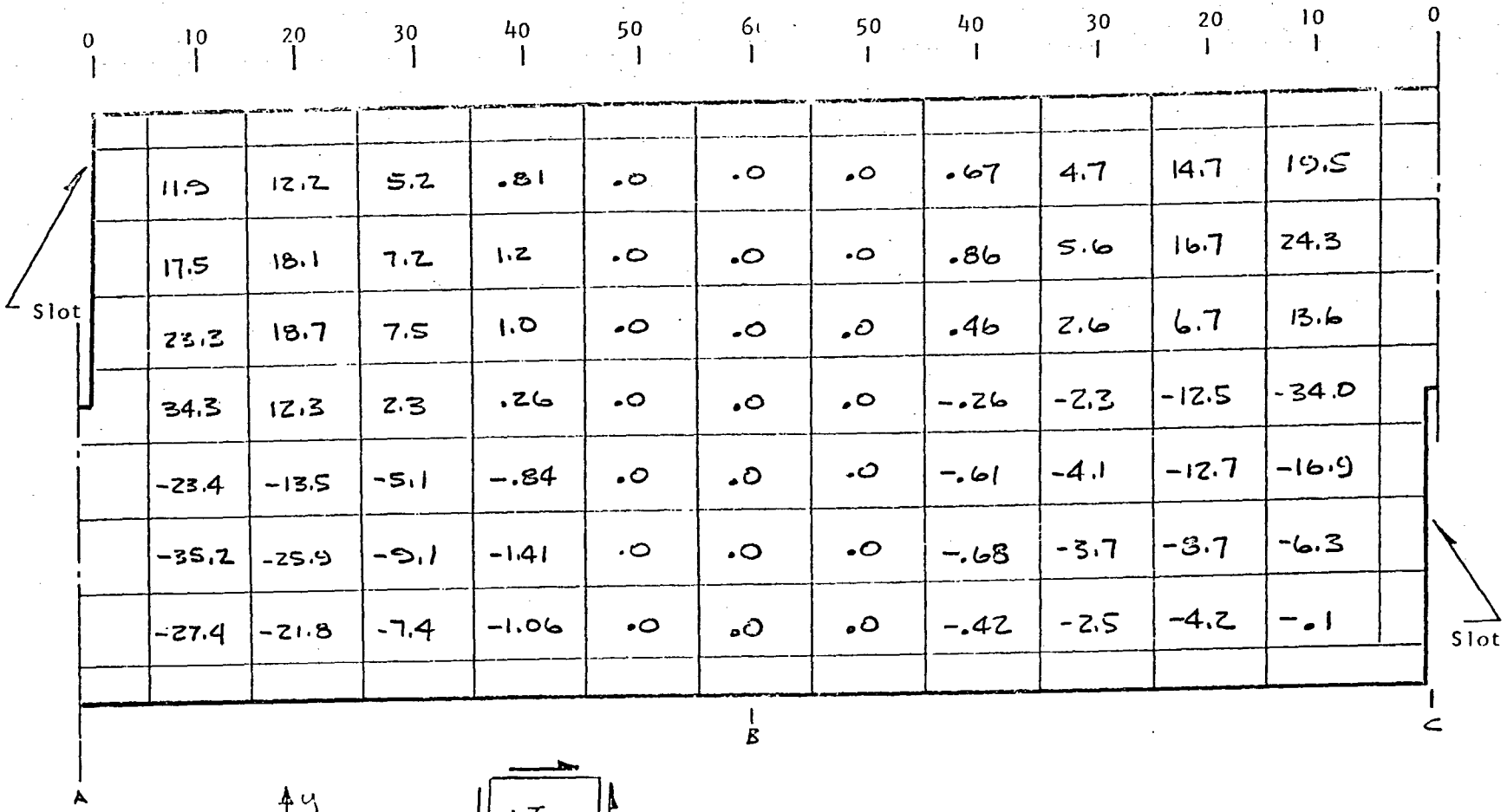
A B C

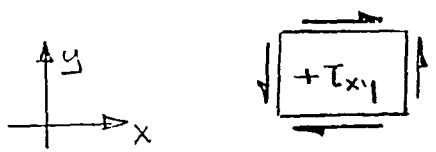


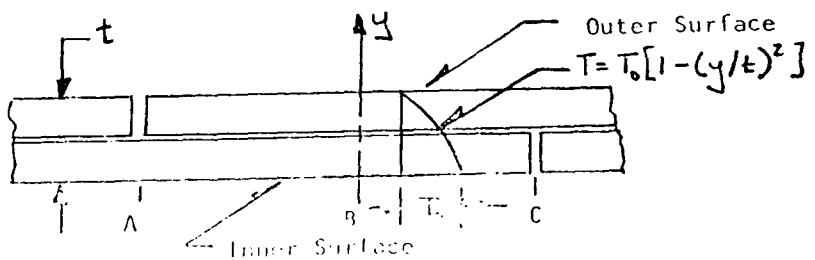
CONDITION D

COMPONENT σ_y/T_o psi/°F









LOADING CONDITION D

STRESS COMPONENT τ_{xy}/T_0 psi/in

0	10	20	30	40	50	60	50	40	30	20	10	0
0	28.6	59.3	76.1	79.4	79.3	79.2	79.2	80.6	88.1	105.6	124.8	
0	4.3	12.8	19.9	21.4	21.5	21.3	21.5	21.8	22.9	24.5	28.6	
0	-.4	-5.3	-9.9	-11.0	-11.0	-10.9	-10.9	-11.8	-17.1	-30.4	-42.5	
0	9.0	-8.6	-22.2	-25.2	-25.3	-25.2	-25.2	-26.7	-34.1	-59.2	-110.9	
125.3	44.7	-3.3	-23.3	-27.2	-27.4	-27.3	-27.3	-27.8	-29.4	-25.5	0	
27.3	12.0	-9.7	-20.1	-22.0	-22.1	-22.0	-22.0	-21.9	-20.7	-13.3	0	
-41.3	-28.6	-19.5	-14.4	-13.0	-12.9	-12.9	-12.9	-12.4	-10.0	-4.81	0	
-111.3	-69.5	-26.8	-6.1	-2.3	-2.3	-2.4	-2.4	-1.7	1.2	3.2	0	

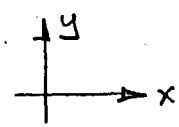
Slot

Slot

A

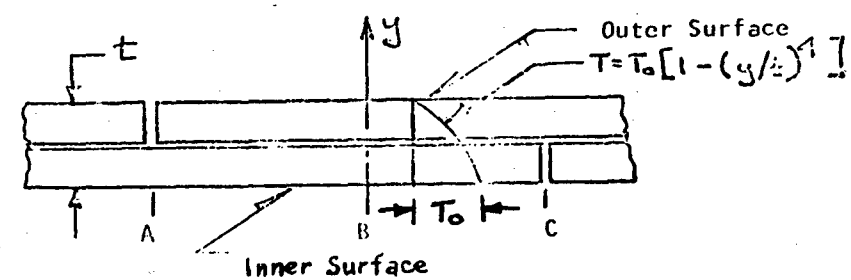
B

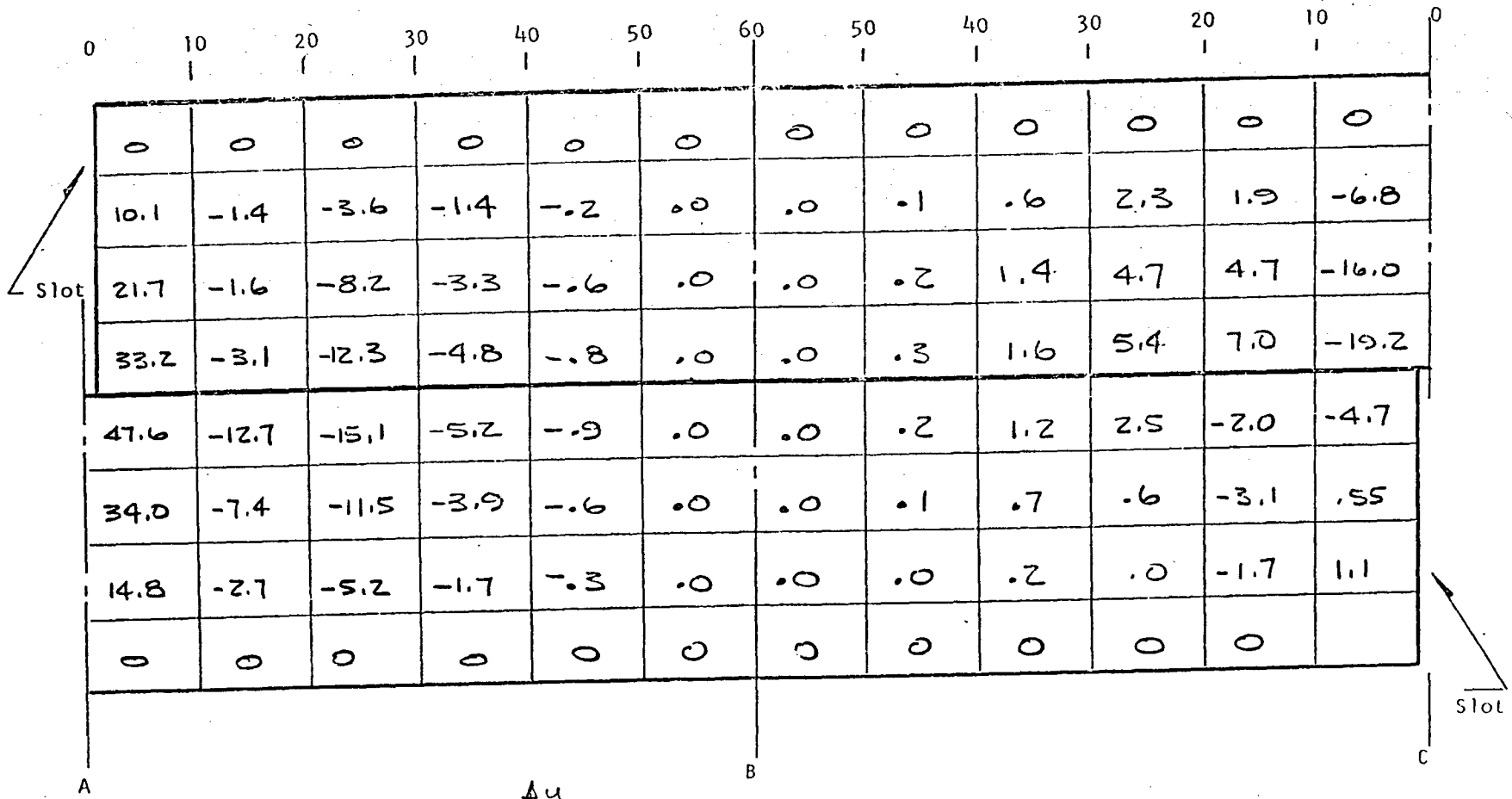
C



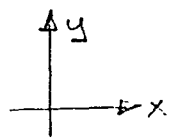
LOADING CONDITION E

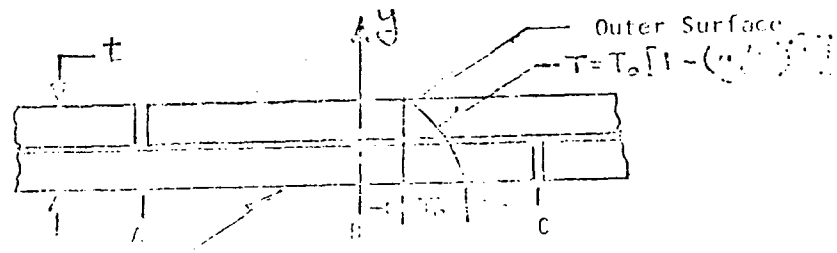
STRESS COMPONENT σ_x/T_o psi/°F





0	0	0	0	0	0	0	0	0	0	0	0
10.1	-1.4	-3.6	-1.4	-.2	.0	.0	.1	.6	2.3	1.9	-6.8
21.7	-1.6	-8.2	-3.3	-.6	.0	.0	.2	1.4	4.7	4.7	-16.0
33.2	-3.1	-12.3	-4.8	-.8	.0	.0	.3	1.6	5.4	7.0	-19.2
47.6	-12.7	-15.1	-5.2	-.9	.0	.0	.2	1.2	2.5	-2.0	-4.7
34.0	-7.4	-11.5	-3.9	-.6	.0	.0	.1	.7	.6	-3.1	.55
14.8	-2.7	-5.2	-1.7	-.3	.0	.0	.0	.2	.0	-1.7	1.1
0	0	0	0	0	0	0	0	0	0	0	





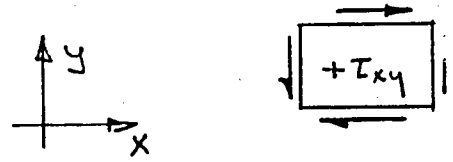
LOADING CONDITION E

STRESS COMPONENT σ_y / T_o psi/in

0	10	20	30	40	50	60	50	40	30	20	10	0
	17.0	14.6	5.7	.89	.0	.0	.0	.36	2.6	8.3	11.3	
	19.6	19.2	7.7	1.26	.0	.0	.0	.44	2.9	9.1	13.9	
	19.3	16.9	6.1	.98	.0	.0	.0	.20	1.1	2.8	6.7	
	24.7	8.5	1.5	.17	.0	.0	.0	-.19	-1.6	-8.8	-24.0	
	-23.3	-14.3	-5.3	-.87	.0	.0	.0	-.33	-2.2	-6.9	-8.9	
	-32.4	-24.6	-8.8	-1.38	.0	.0	.0	-.31	-1.8	-3.4	-.97	
	-24.8	-20.3	-7.0	-1.02	.0	.0	.0	-.21	-.98	-.96	1.89	

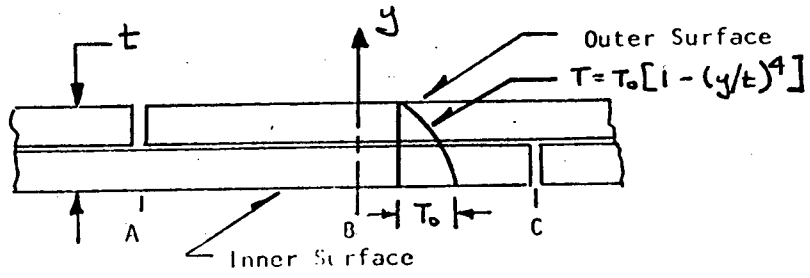
Slot

Slot



LOADING CONDITION E

STRESS COMPONENT τ_{xy}/T_o psi/°F



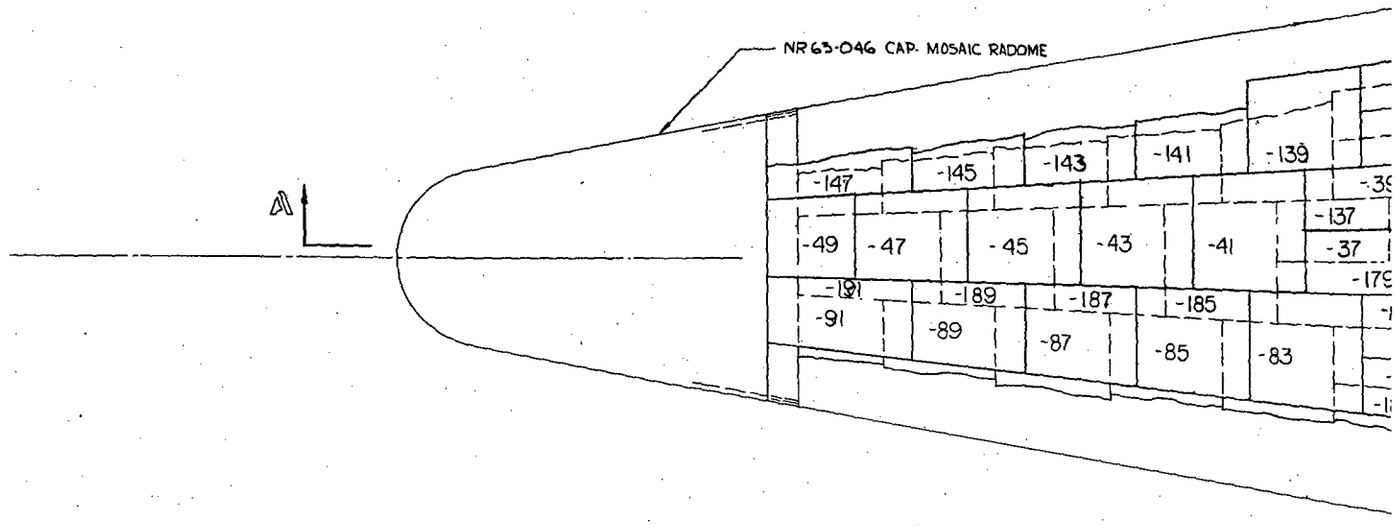
APPENDIX X

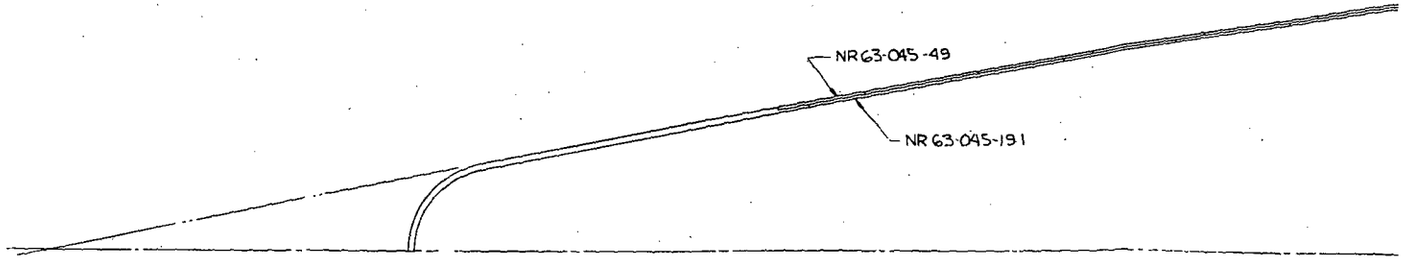
MOSAIC RADOME AND AFFILIATED DRAWINGS

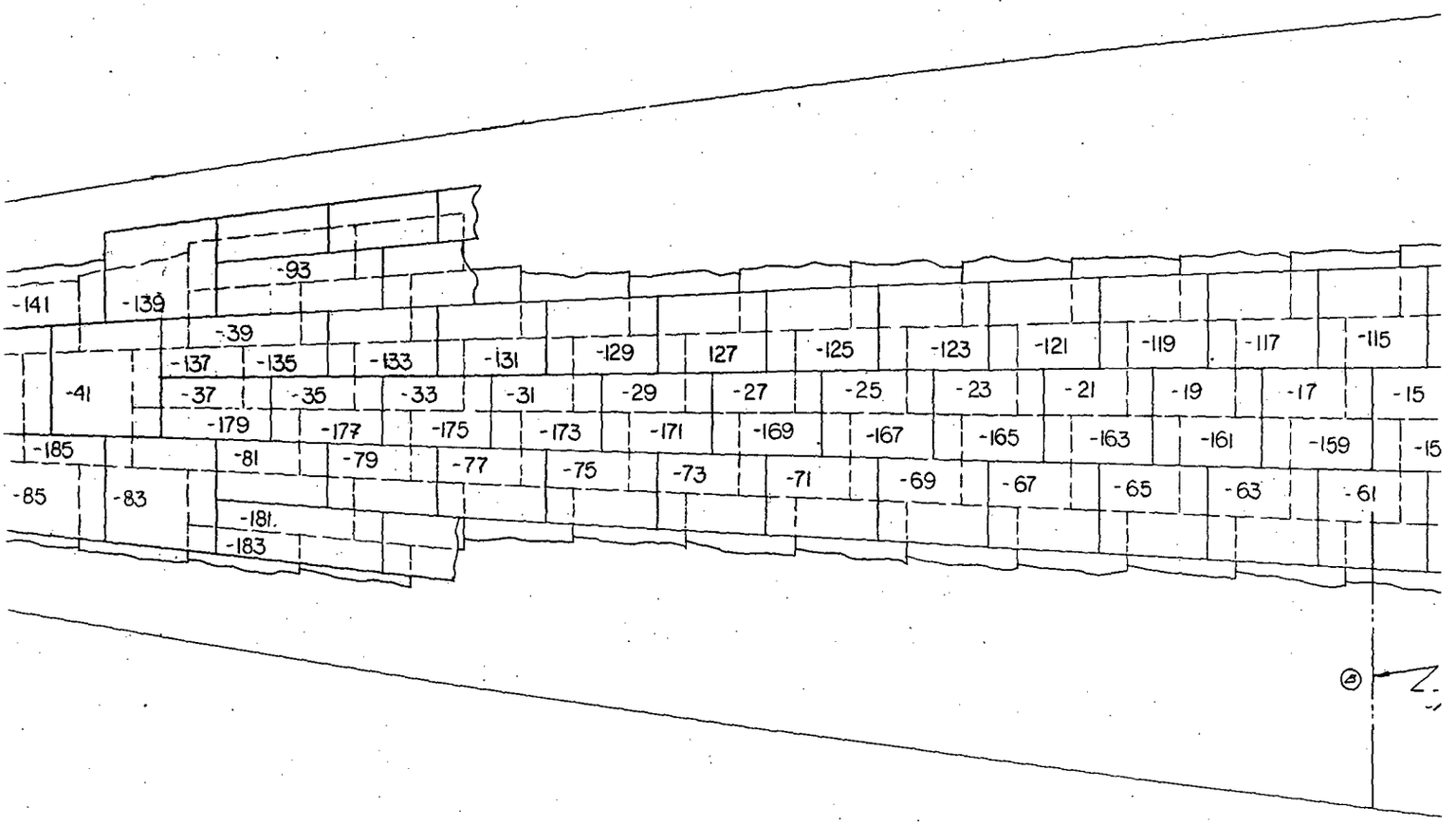
MOSAIC RADOME AND AFFILIATED DRAWINGS

The drawings listed below are included on the subsequent pages of this appendix.

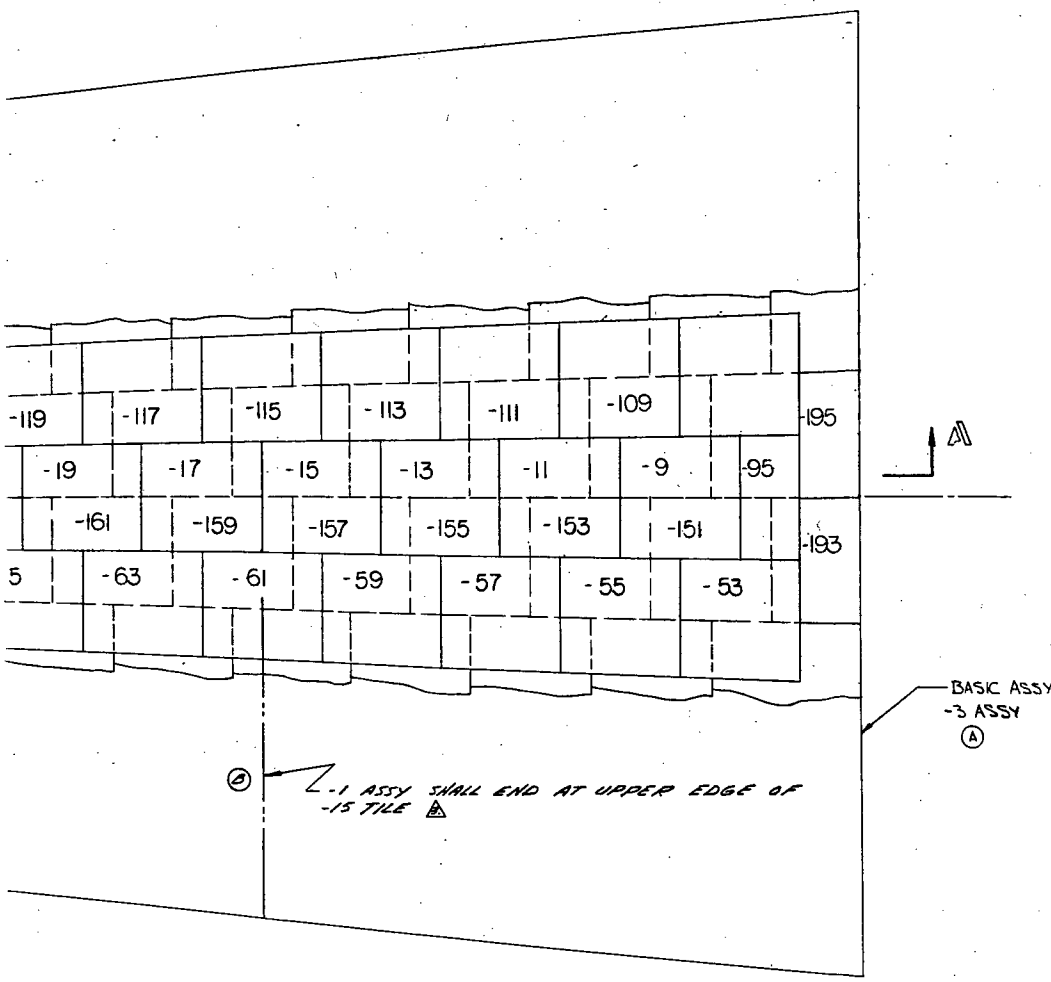
NR 63-044	Mosaic Radome Assembly
NR 63-045	Mosaic Detail
NR 63-046	Cap – Mosaic Radome
NR 63-114	Firing Fixture Assembly – Full Mosaic Radome
NR 63-079	Template – Layup Tool – Truncated Mosaic Radome
NR 63-080	Template – Firing Tool – Truncated Mosaic Radome
NR 63-092	Template – Layup Tool – Full Mosaic Radome
NR 63-093	Template – Firing Tool – Full Mosaic Radome
NR 63-104	Master Layup Tool – Full Mosaic Radome
NR 63-105	Firing Tool Glasrock – Full Mosaic Radome
NR 63-152	Support Structure – Radome Template
NR 63-153	Handling Device – Radome Assembly
NR 63-157	Check Gage – Firing Tool – Mosaic Radome
NR 63-060	Test Fixture – Mosaic Radome
NR 63-199	Loading Tube – Radome
NR 63-120	Loading Fixture – Mosaic Radome
NR 63-121	Support Plate – Radome Loading Fixture
NR 63-061	Radome Base Attachment

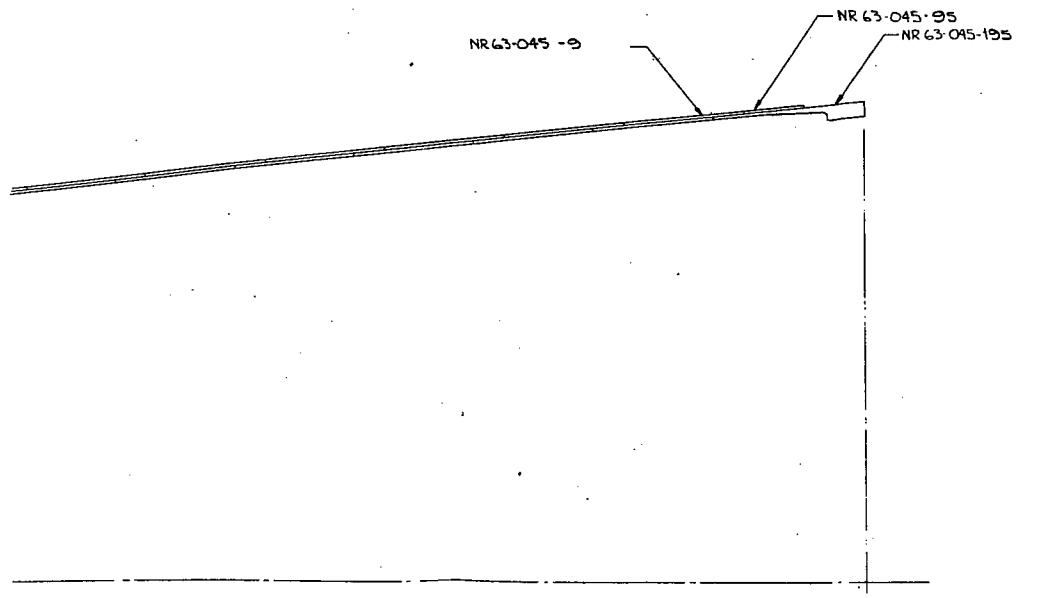

NR63-046 CAP- MOSAIC RADOME
-147
-145
-143
-141
-139
-49
-47
-45
-43
-41
-137
-37
-91
-89
-87
-85
-83

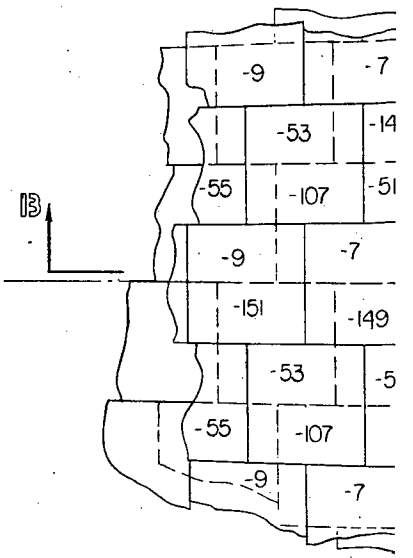

NR63-045-49
NR63-045-191

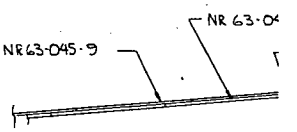

-93
-141
-139
-39
-137
-135
-133
-131
-129
127
-125
-123
-121
-119
-117
-115
-41
-37
-35
-33
-31
-29
-27
-25
-23
-21
-19
-17
-15
-179
-177
-175
-173
-171
-169
-167
-165
-163
-161
-159
-185
-81
-79
-77
-75
-73
-71
-69
-67
-65
-63
-61
-85
-83
-181
-183
A

SECTION A - A







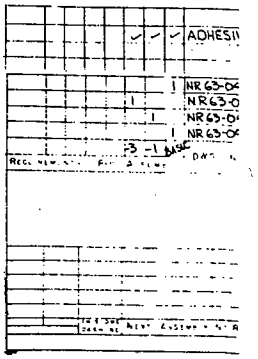


SECTION B = B (A)

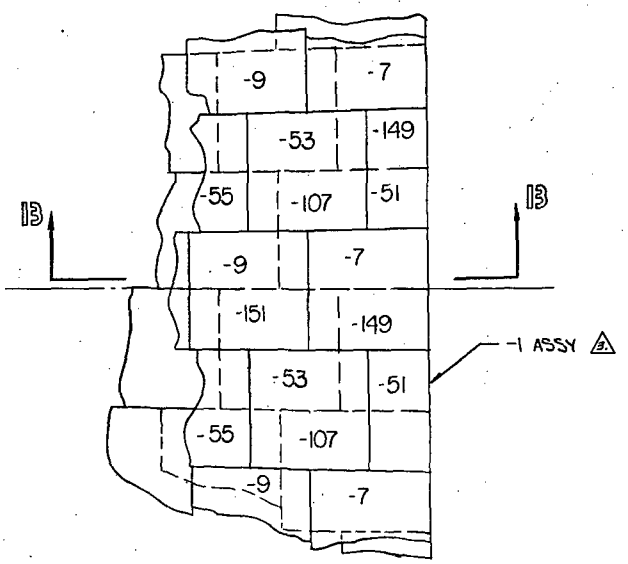
(A) 2 IN -1 ASSY, TILES -61, -115 & -159 ARE TO OF -15 TILE AS NOTED IN F/D. THE SHO -61A, -115A & -159A.

(A) 2. TWO DIGIT DASH NOS (NR 63-045 -7 THRU-95) INDICATI THREE DIGIT DASH NOS (NR 63-045-107 THRU-195) INDICA
1. NUMBERS SHOWN ON TILES ON F/D ARE DASH

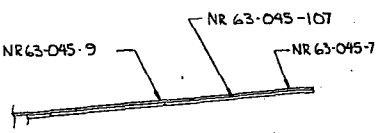
NOTES:



CHG	REVISION	BY	
A	ADDED VIEW SHOWING -1 ASSY.		
	CHANGED MAIN VIEW TO SHOW		
	NEW BASE TILES (NR 63-045		
	-193, -193 (-195) CHG NOTE 2	JLR	5-12-64
B	ADDED NOTE 5 & 6	JLR	6-4-64
	NOTE IN F/D	GUARINO	



BASIC ASSY
3 ASSY
(A)



SECTION B = B (4)

(6) 2 IN -1 ASSY, TILES -61, -115 & -159 ARE TO BE CUT TO MATCH THE UPPER EDGE OF -15 TILE AS NOTED IN F/D. THE SHORTENED TILES SHALL BE IDENTIFIED AS -61A, -115A & -159A.

(4) 2. TWO DIGIT DASH NOS (NR 63-045 -7 THRU-95) INDICATE TILES IN OUTER LAYER (BOUNDED BY SOLID LINES)
THREE DIGIT DASH NOS (NR 63-045-107 THRU-195) INDICATE TILES IN INNER LAYER (BOUNDED BY DASHED LINES)
1. NUMBERS SHOWN ON TILES ON F/D ARE DASH NOS FROM NR 63-045 MOSAIC DETAIL

5
045-195

NOTES:

		✓ ✓ ✓	ADHESIVE	NARMCAD	110
		1	NR 63-046 BASIC		
	1		NR 63-048-3		
		1	NR 63-045-1		
		1	NR 63-045 BASIC		
	3-1 BASIC				

REQUIREMENTS PER ASSEMBLY | DWG NO | OPTION | PART NAME

REVISION 2-17-64

T. B. Walker
Engineering
Approved

NARMCO
RESEARCH & DEVELOPMENT

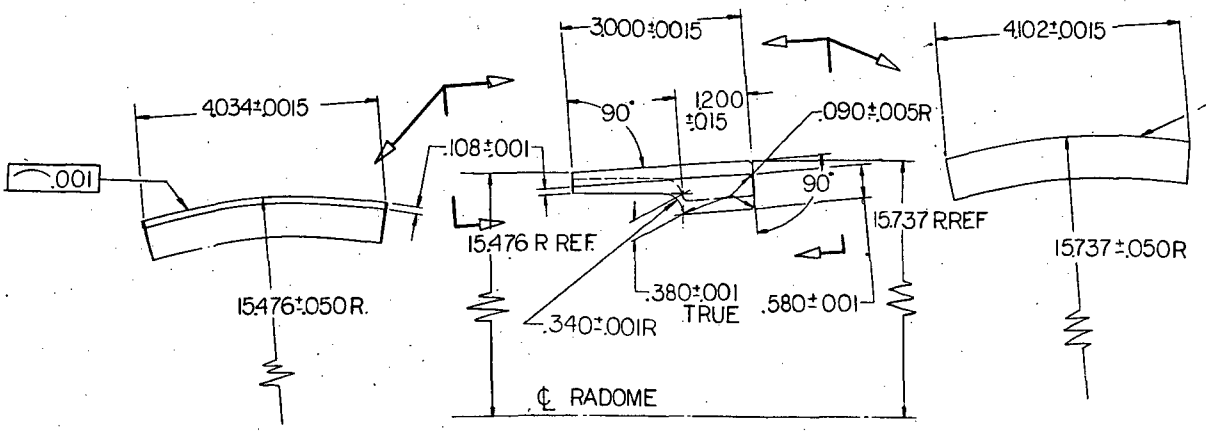
MOSAIC RADOME ASSY

HALF 338-103

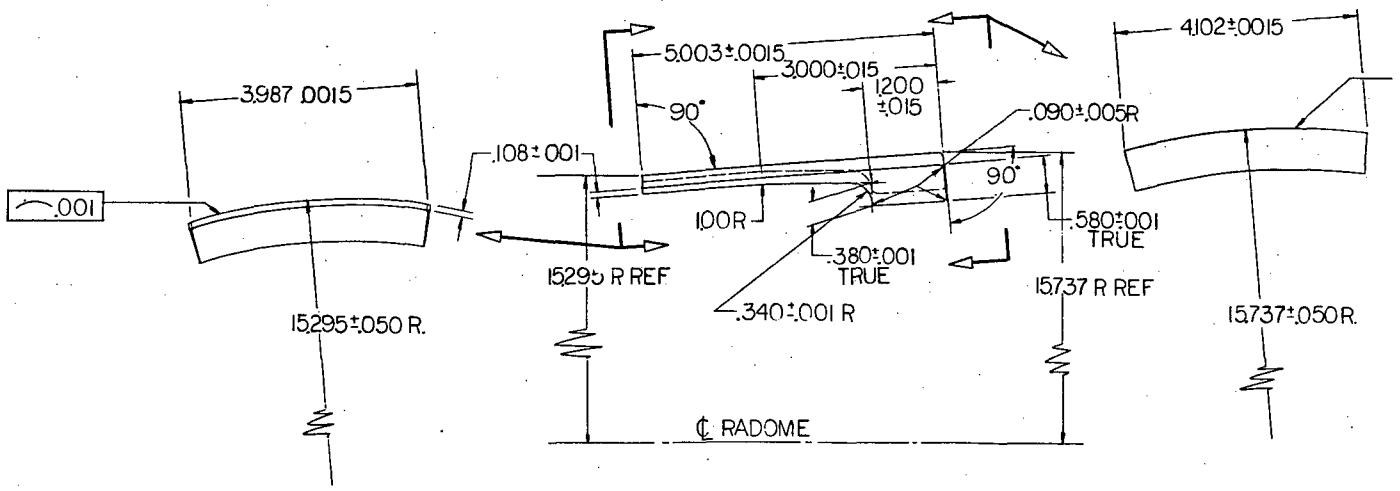
R | NR 63-044 | B

DWG SIZE | SHEET 1 OF 1 | CHANGE LETTER

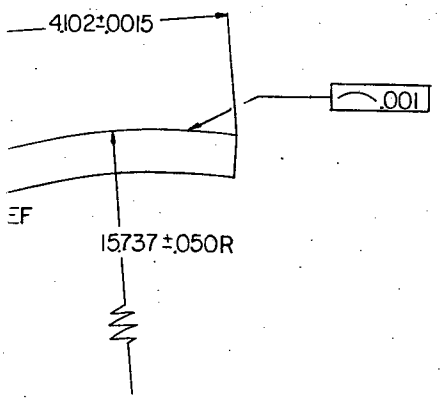
NEXT ASSEMBLY NO REQD

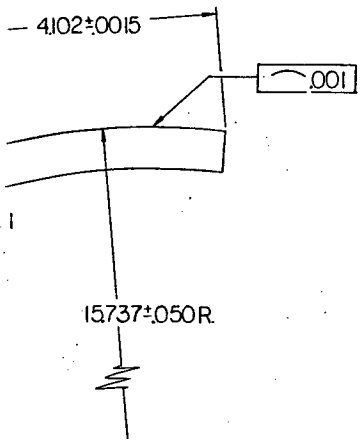


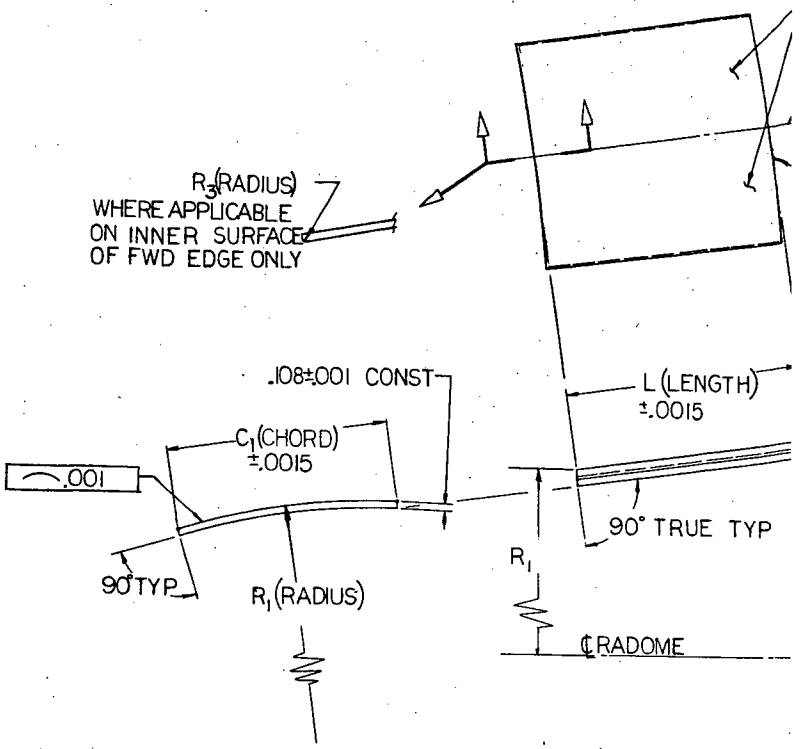
DETAIL - 193 Ⓑ



DETAIL - 195 Ⓑ







(2) ⚠ FOR -1 ASSY ONLY TILES -61, -115 & -159 ARE TO BE CUT TO SHORTER LENGTHS AND IDENTIFIED AS -61A, -115A & -159A. THE NEW LENGTHS SHALL BE MEASURED FROM THE BASE OF THE TILES AND SHALL BE AS FOLLOWS: -61A TO BE 1.997, -115A TO BE 2.997 & -159A TO BE .994

(A) 13. ALL VISIBLE DEFECTS, SUCH AS PITS, POCKS, CHIPS, AND BLISTERS, SHALL BE CONTAINABLE WITHIN A CUBE MEASURING .020 PER SIDE (MAX.). THE RATIO OF ANY SURFACE AREA DIVIDED BY THE NUMBER OF DEFECTS SHALL NOT BE LESS THAN TWO, (A/D ≥ 2). THE MINIMUM DISTANCE BETWEEN DEFECTS SHALL BE .75 INCH INCLUDING BOTH SURFACES.

(B) EDGE DEFECTS SHALL NOT EXCEED .005. EDGES MAY BE RADIUSED .010 MAX. NO CRACKS WILL BE PERMITTED.

12. THE DIELECTRIC CONSTANT AT ROOM TEMPERATURE AND AT 9.375 KMC SHALL NOT VARY MORE THAN .2 FROM NOMINAL. THE RANGE OF ACCEPTABLE ROOM TEMPERATURE DIELECTRIC CONSTANTS MAY VARY FROM 8.2(MIN) TO 9.4(MAX)

11. TOLERANCES ON RADII R_1 & R_2 SHALL BE .020 FOR DASH NOS -41 THRU-49, -83 THRU-91, -139 THRU-147, AND -185 THRU-191. ALL OTHER DASH NOS TO HAVE ±.050

10 ALL PARTS SHALL BE HANDLED INSPECTED AND PACKED SO AS TO AVOID CONTAMINATION AND TO PREVENT CONTACT WITH DIFFICULT-TO-REMOVE CONTAMINANTS, PARTICULARLY METALS.

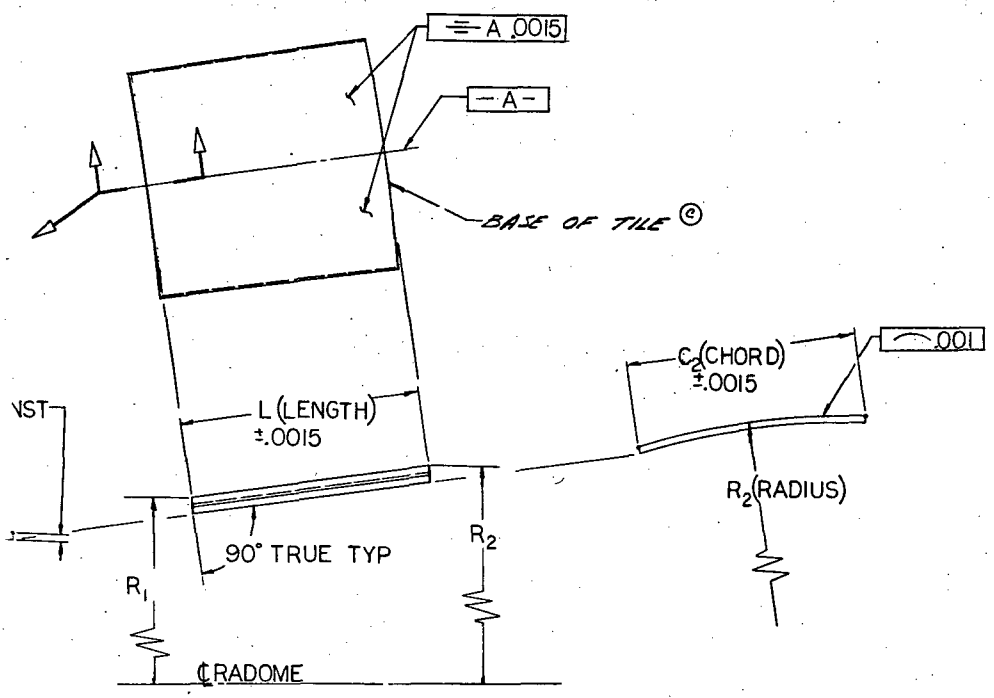
(A) 9.

8. ALL TILES SHALL BE UNIFORM IN COLOR AND TEXTURE.
7. ALL TILES SHALL BE IMPERVIOUS TO DYE PENETRATION TO 10 MIL THICKNESS PER ASTM D116-61
6 ROOM TEMPERATURE LOSS TANGENT AT 9375 KMC SHALL BE .0007 MAXIMUM
5. FLEXURAL STRENGTH AT ROOM TEMPERATURE — 40,000 PSI (MINIMUM) PER ASTM D116-61 AND ASTM D667-44.

(B) OPTIONAL FLEXURAL TEST SPECIMEN MAY BE USED WITH NARMCO APPROVAL.

4. DENSITY — 3.75 GRAMS/CC (MINIMUM)
3. MATERIAL — 97.6% (MINIMUM) ALUMINA, CERAMIC RADOME GRADE
2. ALL PARTS TO BE STAMPED WITH APPROPRIATE DASH NO. WITH INDELIBLE INK
1. TWO DIGIT DASH NOS (-7 THRU -95) INDICATE TILES IN THE OUTER LAYER
THREE DIGIT DASH NOS (-107 THRU -195) INDICATE TILES IN THE INNER LAYER

NOTES: (B)



TILE DASH NO	C_1 CHORD	C_2 CHORD	R_1 RADIUS	R_2 RADIUS	L LENGTH	R_3 RADIUS
-7	4.040	4.132	15.499	15.850	4.000	
-9	3.943	4.040	15.129	15.498	4.000	
-11	3.842	3.943	14.741	15.128	4.000	
-13	3.736	3.842	14.335	14.740	4.000	
-15	3.626	3.736	13.912	14.335	4.000	
-17	3.510	3.626	13.470	13.911	4.000	
-19	3.390	3.510	13.010	13.469	4.000	
-21	3.266	3.390	12.533	13.010	4.000	
-23	3.137	3.266	12.038	12.532	4.000	
-25	3.003	3.136	11.525	12.037	4.000	
-27	2.864	3.002	10.994	11.524	4.000	
-29	2.721	2.864	10.445	10.993	4.000	
-31	2.573	2.720	9.878	10.444	4.000	
-33	2.420	2.573	9.294	9.877	4.000	
-35	2.263	2.420	8.691	9.293	4.000	
-37	2.101	2.263	8.071	8.690	4.000	
-39	2.101	2.342	8.071	8.994	6.003	
-41	3.842	4.172	7.433	8.070	4.000	
-43	3.502	3.841	6.778	7.432	4.000	
-45	3.154	3.502	6.104	6.776	4.000	
-47	2.796	3.153	5.413	6.103	4.000	
-49	2.521	2.795	4.882	5.411	3.000	.060
-51	4.087	4.132	15.677	15.850	1.997	
-53	3.992	4.086	15.316	15.676	4.000	
-55	3.893	3.992	14.937	15.315	4.000	
-57	3.790	3.893	14.540	14.936	4.000	
-59	3.682	3.790	14.126	14.540	4.000	
-61	3.569	3.681	13.693	14.125	4.000	
-63	3.451	3.568	13.242	13.692	4.000	
-65	3.329	3.451	12.774	13.242	4.000	
-67	3.202	3.329	12.288	12.773	4.000	
-69	3.070	3.202	11.783	12.287	4.000	
-71	2.934	3.070	11.261	11.783	4.000	
-73	2.793	2.934	10.721	11.261	4.000	
-75	2.647	2.793	10.164	10.721	4.000	

TILE DASH NO	C_1 CHORD	C_2 CHORD	R_1 RADIUS	R_2 RADIUS	L LENGTH	R_3 RADIUS
-77	2.497	2.647	9.588	10.163	4.000	
-79	2.342	2.497	8.995	9.587	4.000	
-81	2.183	2.342	8.383	8.994	4.000	
-83	4.008	4.333	7.754	8.382	4.000	
-85	3.673	4.008	7.107	7.753	4.000	
-87	3.329	3.673	6.443	7.106	4.000	
-89	2.976	3.329	5.760	6.442	4.000	
-91	2.521	2.975	4.882	5.759	5.003	.060
-93	2.183	2.420	8.383	9.293	6.003	
Ⓑ -95	4.040	4.087	15.499	15.677	1.997	
-107	3.987	4.102	15.295	15.737	5.003	
-109	3.889	3.987	14.921	15.295	4.000	
-111	3.787	3.889	14.528	14.920	4.000	
-113	3.680	3.787	14.118	14.528	4.000	
-115	3.568	3.679	13.690	14.118	4.000	
-117	3.451	3.568	13.244	13.689	4.000	
-119	3.330	3.451	12.780	13.243	4.000	
-121	3.204	3.330	12.298	12.779	4.000	
-123	3.074	3.204	11.798	12.297	4.000	
-125	2.939	3.074	11.281	11.798	4.000	
-127	2.799	2.939	10.745	11.280	4.000	
-129	2.655	2.799	10.192	10.744	4.000	
-131	2.506	2.654	9.621	10.191	4.000	
-133	2.352	2.505	9.032	9.620	4.000	
-135	2.193	2.352	8.425	9.031	4.000	
-137	2.030	2.193	7.800	8.424	4.000	
-139	3.867	4.194	7.481	8.114	4.000	
-141	3.530	3.866	6.830	7.480	4.000	
-143	3.183	3.529	6.161	6.829	4.000	
-145	2.828	3.183	5.474	6.160	4.000	
-147	2.555	2.827	4.947	5.473	2.997	
-149	4.034	4.102	15.476	15.737	3.000	
-151	3.939	4.034	15.110	15.475	4.000	
-153	3.839	3.938	14.727	15.110	4.000	
-155	3.734	3.838	14.326	14.726	4.000	
-157	3.624	3.734	13.906	14.325	4.000	
-159	3.510	3.624	13.469	13.906	4.000	
-161	3.391	3.510	13.014	13.469	4.000	
-163	3.268	3.391	12.541	13.014	4.000	
-165	3.140	3.268	12.050	12.541	4.000	
-167	3.007	3.140	11.542	12.050	4.000	
-169	2.870	3.007	11.015	11.541	4.000	
-171	2.727	2.869	10.471	11.014	4.000	
-173	2.581	2.727	9.908	10.470	4.000	
-175	2.429	2.580	9.328	9.908	4.000	
-177	2.273	2.429	8.730	9.327	4.000	
-179	2.030	2.273	7.800	8.730	6.003	
-181	2.112	2.352	8.115	9.031	6.003	
-183	2.112	2.273	8.115	8.730	4.000	
-185	3.699	4.031	7.158	7.799	4.000	
-187	3.358	3.699	6.497	7.157	4.000	
-189	3.007	3.357	5.819	6.496	4.000	
-191	2.555	3.006	4.947	5.818	5.000	
Ⓑ -193	SEE	F/D				
Ⓑ -195	SEE	F/D				

D SHORTER LENGTHS AND IDENTIFIED FROM THE BASE OF THE TILES -99.7 & -159.A TO BE .99.A

S, SHALL BE CONTAINABLE WITHIN A
BY THE NUMBER OF DEFECTS SHALL NOT-
L BE .75 INCH INCLUDING BOTH SURFACES.
NO CRACKS WILL BE PERMITTED.
HALL NOT VARY
EMPERATURE

HRU-49, -83 THRU-91, -139 THRU-147,

ONTAMINATION AND TO
IETALS.

ASTM D116-61

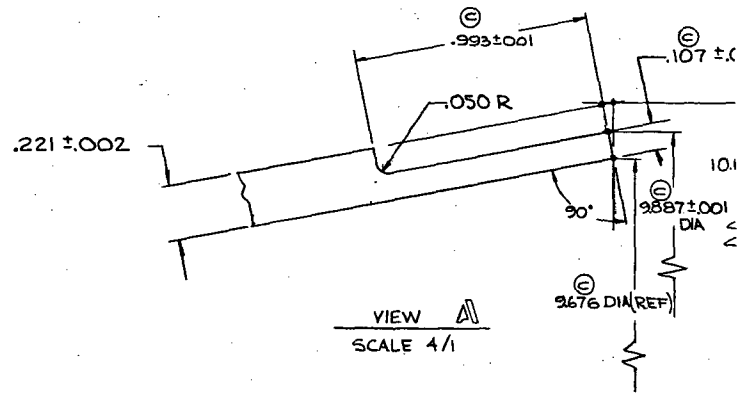
D116-61 AND ASTM D667-44.

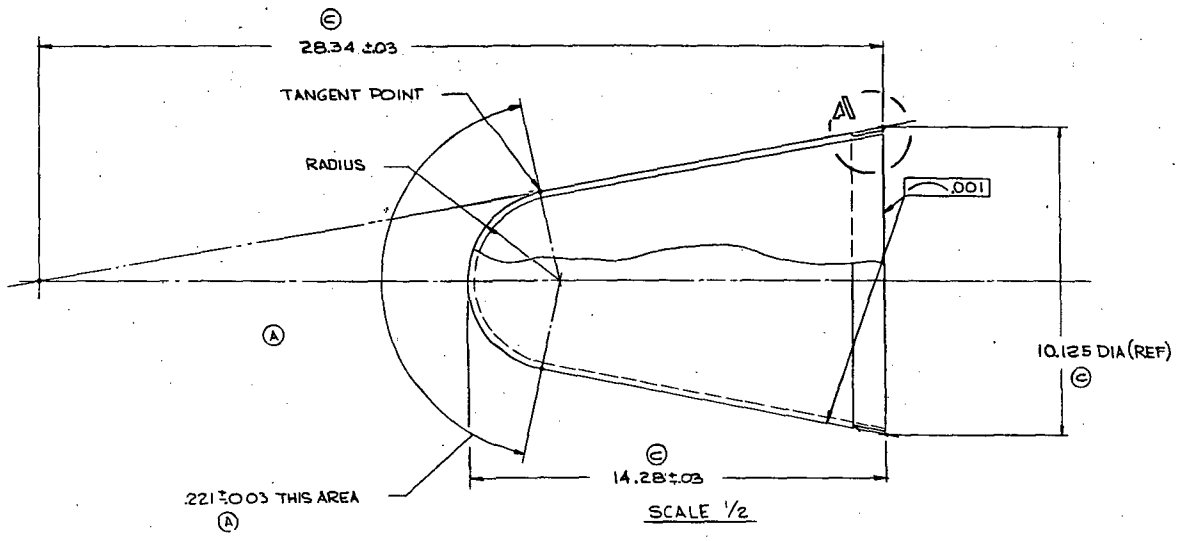
K

2

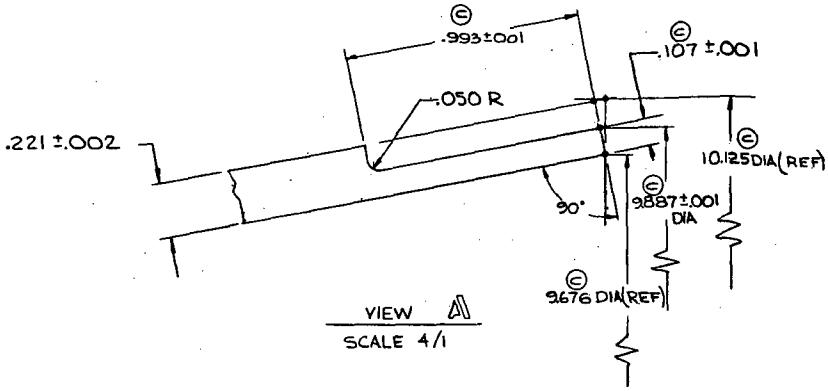
CHG	REVISION	BY
A	NOTE 9 REMOVED. ADDED NOTE 13.	JLR 5/64
B	CHANGED "EDGE DEFECT" PART OF NOTE 15. CHANGED NOTE 5. ADDED DETAILS -193, -195 & -99 TO F/D. & D/M, ADD -53 & -151 TO BASIC -3. CHG NOTE 1	JLR 5/64
C	ADDED NOTE 14 & CALLOUT ON F/D ADDED DETAILS IN 4 PLS	JLR 6/64

LENGTH	R_3 RADIUS
4.000	
4.000	
4.000	
4.000	
4.000	
4.000	
4.000	
5.003"	.060
6.003"	
1.997"	
5.003"	
4.000	
4.000	
4.000	
4.000	
4.000	
4.000	
4.000	
4.000	
4.000	
4.000	
4.000	
4.000	
4.000	
4.000	
4.000	
4.000	
4.000	
4.000	
2.997"	
3.000"	
4.000	
4.000	
4.000	
4.000	
4.000	
4.000	
4.000	
4.000	
4.000	
4.000	
4.000	
4.000	
4.000	
4.000	
4.000	
4.000	
4.000	
4.000

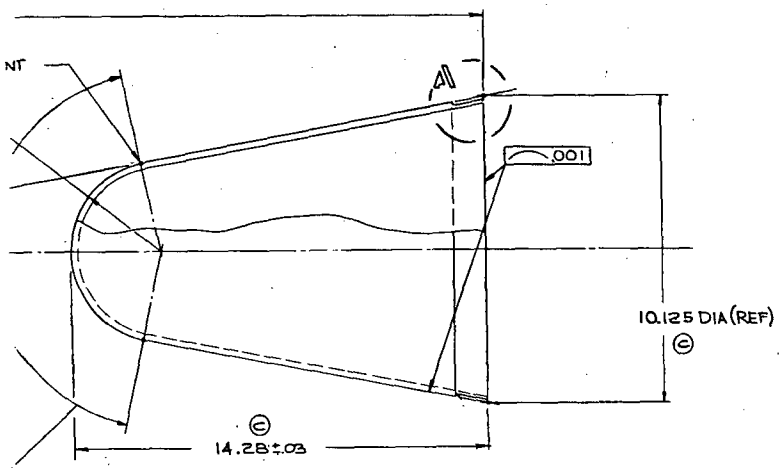

.993±001
.107 ±.
.050 R
.221 ±.002
90°
9887±001
DIA
9676 DIA (REF)
VIEW A
SCALE 4/1


28.34 ±.03
TANGENT POINT
RADIUS
.001
10.125 DIA (REF)
14.28±.03
.221±.003 THIS AREA
A
SCALE 1/2

CHG	REVISION	BY		
A	REMOVE NOTE 7, ADD NOTE 11, REMOVE 11.361±.0025, 5891±.001 DIA #89059, ±.500 DIMS. ADD 14.24, 5.03, #2.816 ±.05 DIMS, ADD NOTE .221±.003 THIS AREA EXTENDED .001 TO WALLS.			
B	CHANGED "EDGE DEFECT" IN OF NOTE 11. CHANGED NOTE 3 28.38 WAS 28.16, REMOVED 1.016±.001, ADDED 1.006±.001 10.141 DIA REF WAS 10.125 DIA REF; 14.323±.03 WAS 14.25±.03			
C	REMOVED .108±.001, 28.38±.03, 14.32±.03, 10.141 DIA (REF), 9.881 ±.001 DIA, 9.680 DIA (REF) 1.006±.001; ADDED: 1.107±.001, 28.34±.03 14.28±.03, 10.125 DIA (REF), 9.887±.001 DIA 9.676 DIA (REF), .993 ±.001.			



VIEW A
SCALE 4/1



SCALE 1/2

(B) 11. ALL VISIBLE DEFECTS SUCH AS PITS, POCKS CHIPS AND BLISTERS SHALL BE CONTAINABLE WITHIN A CUBE MEASURING .020 PER SIDE (MAX). THE RATIO OF ANY SURFACE AREA DIVIDED BY THE NUMBER OF DEFECTS SHALL NOT BE LESS THAN TWO. (A/D ≥ 2) THE MINIMUM DISTANCE BETWEEN DEFECTS SHALL BE .75 IN. INCLUDING BOTH SURFACES. EDGE DEFECTS SHALL NOT EXCEED .005", EDGES MAY BE RADIUSED .010 (MAX) NO CRACKS WILL BE PERMITTED.

10. THE DIELECTRIC CONSTANT AT ROOM TEMPERATURE AND AT 9.375 KMC SHALL NOT VARY MORE THAN .2 FROM NOMINAL. THE RANGE OF ACCEPTABLE R.T. DIELECTRIC CONSTANTS MAY VARY FROM 8.2 (MIN) TO 9.4 (MAX)

9. PART TO BE STAMPED WITH DWG NO & DASH NO WITH INDELIBLE INK.

8. ALL PARTS SHALL BE HANDLED AND PACKED SO AS TO AVOID CONTAMINATION AND TO PREVENT CONTACT WITH DIFFICULT-TO-REMOVE CONTAMINANTS, PARTICULARLY METALS.

(A) 3.

6. THE CAP SHALL BE UNIFORM IN COLOR AND TEXTURE.

5 THE CAP SHALL BE IMPERVIOUS TO DYE PENETRATION TO 10 MIL THICKNESS PER ASTM D 116-61.

4 ROOM TEMPERATURE LOSS TANGENT AT 9375 KMC — .0007 MAXIMUM.

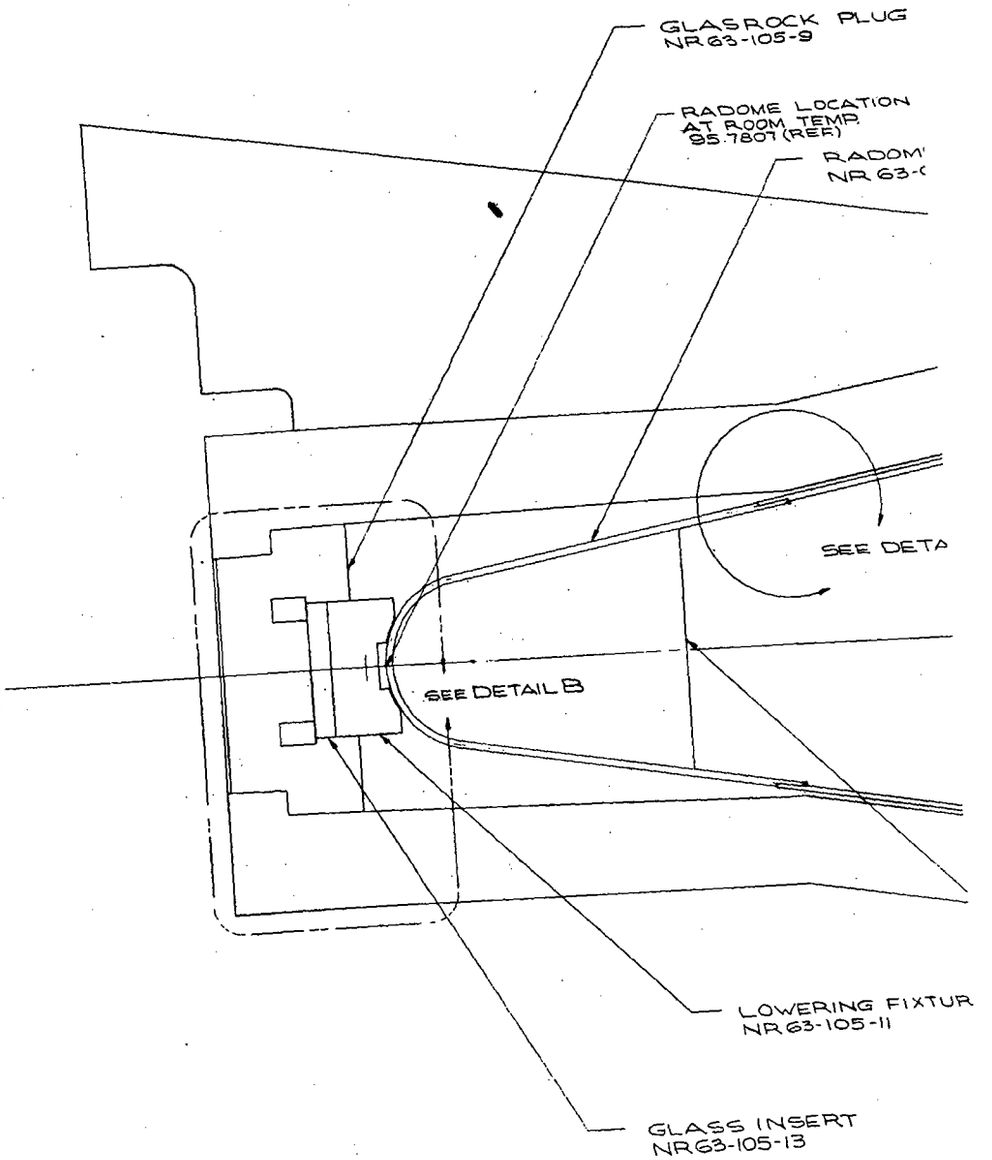
(B) 3. FLEXURAL STRENGTH AT ROOM TEMP — 40,000 PSI (MINIMUM) PER ASTM D 116-61 AND ASTM D 667-44. OPTIONAL FLEXURAL TEST SPECIMEN MAY BE USED WITH NARMCO APPROVAL

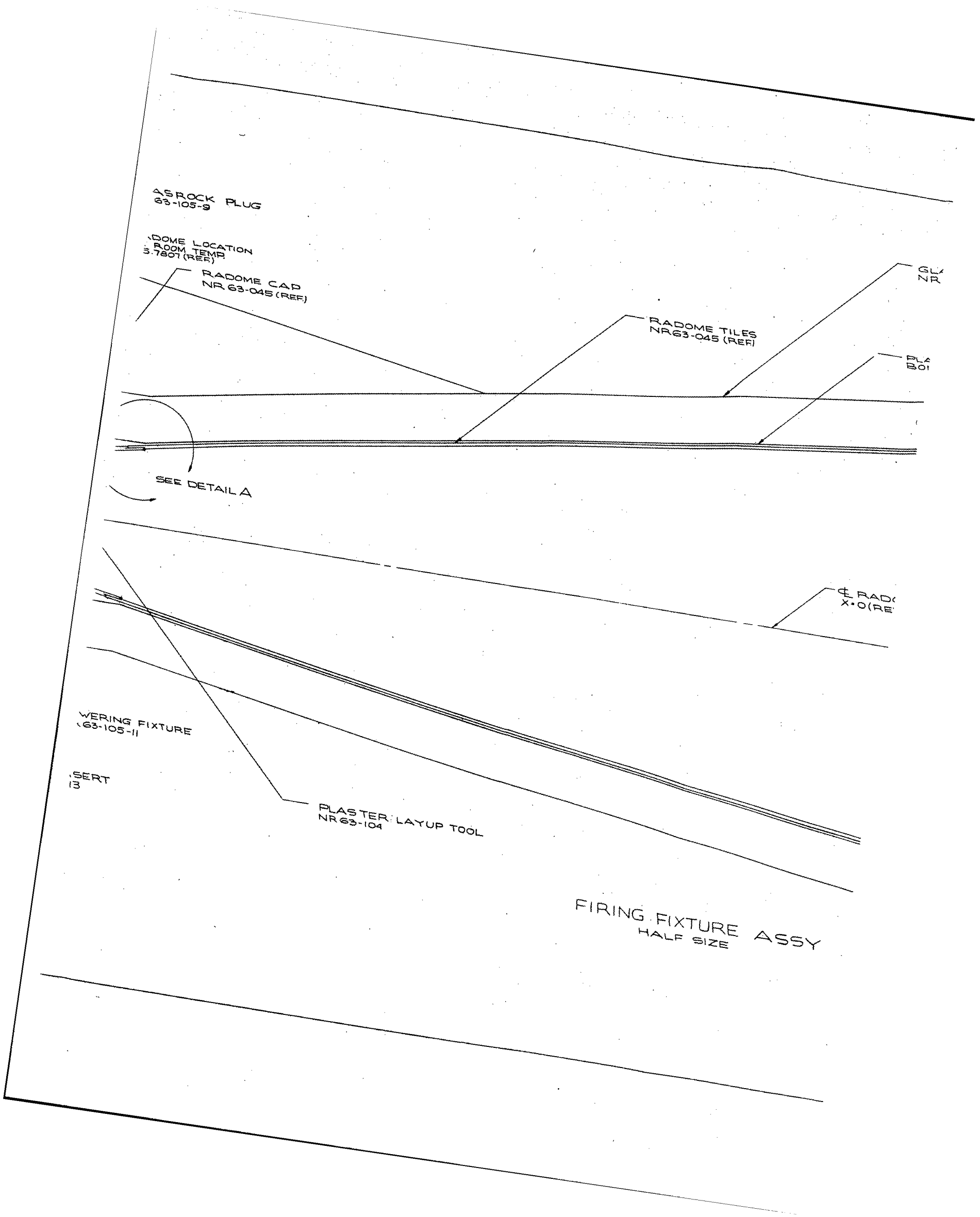
2. DENSITY — 3.75 GRAMS/CC (MINIMUM)

1. MATERIAL — 97.6 % (MINIMUM) ALUMINA, CERAMIC RADOME GRADE

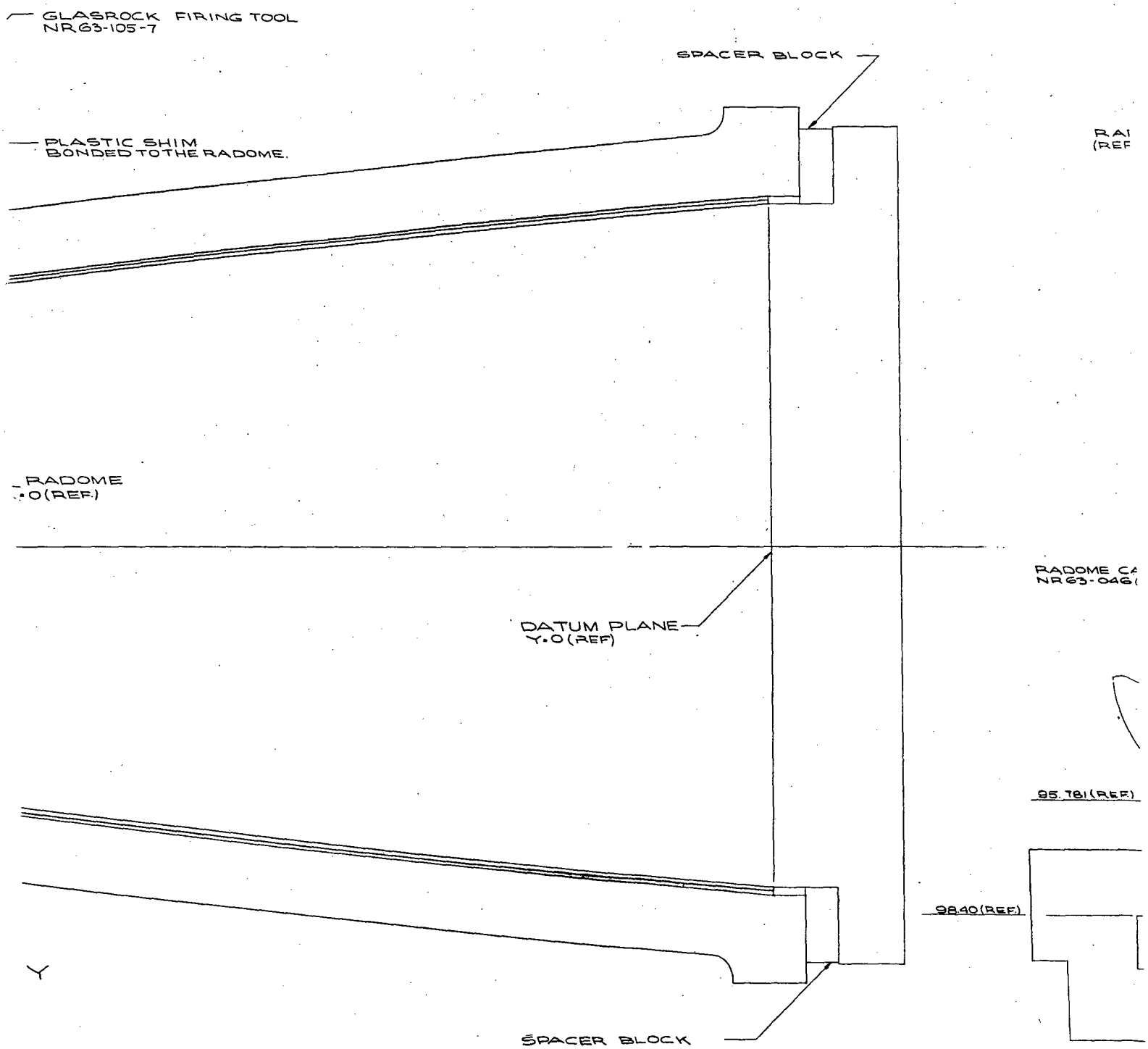
NOTES:

REQUIREMENTS PER ASSEMBLY	DWG NO.	OPP SHN DASH NO.	PART NAME	BASIC CAP	97.6% (MIN) RADOME GRADE Al_2O_3 SEE NOTES 1-8
				DESIGN Rawlson 2-2-64	NARMCO RESEARCH & DEVELOPMENT 5340 ALEC COURT SAN DIEGO 23 CALIFORNIA
				CHECK D. M. Mark	
				MFG APPROVAL	
				QUALITY APPROVAL	
				PROJECT ENGR	
				TITLE CAP-MOSAIC RADOME	SCALE NOTED DWG NO 338-105
BASIC PART DASH NO NR 63-044				NEXT ASSEMBLY No Req'd	R DWG SIZE NR63-046 SHEET OF

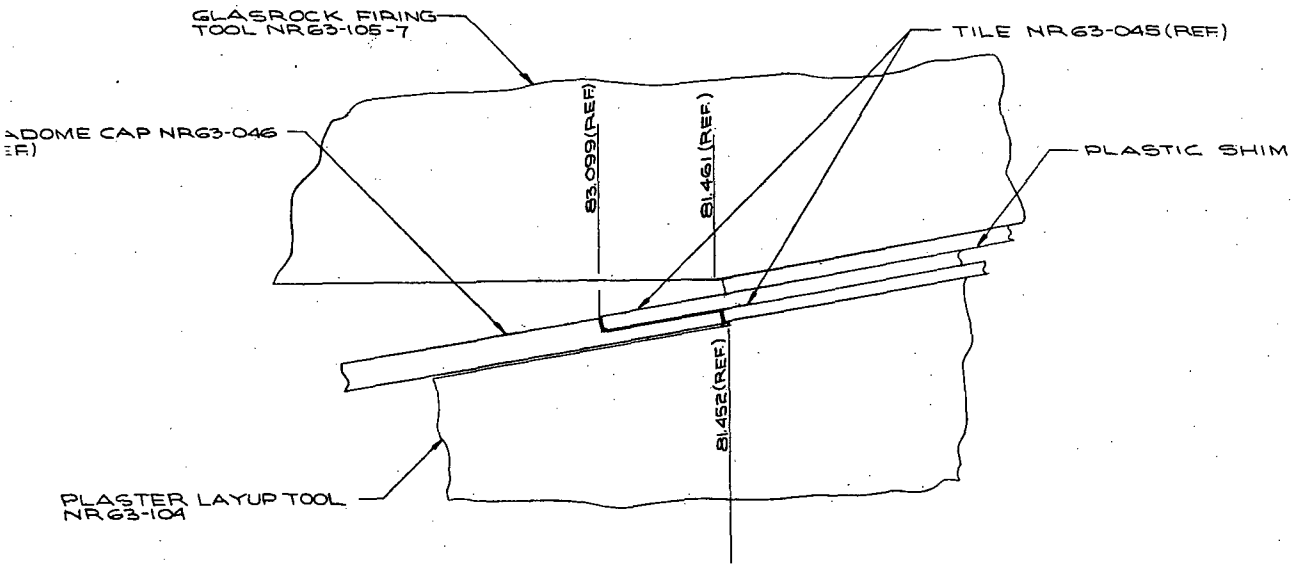

GLASROCK PLUG
NR 63-105-9
RADOME LOCATION
AT ROOM TEMP
95.7807 (REF)
RADOM
NR 63-
SEE DETA
SEE DETAIL B
LOWERING FIXTUR
NR 63-105-11
GLASS INSERT
NR 63-105-13



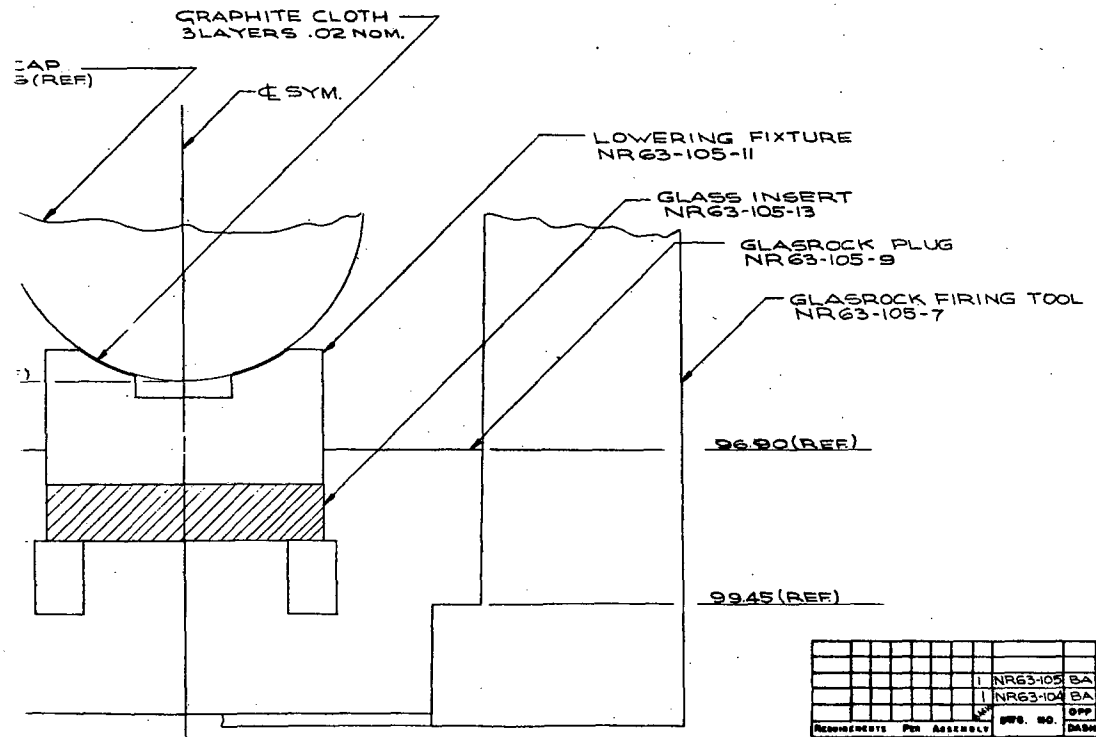
FIRING FIXTURE ASSY
HALF SIZE


GLASROCK FIRING TOOL
NR63-105-7
SPACER BLOCK
PLASTIC SHIM
BONDED TO THE RADOME.
RADOME
.0 (REF.)
DATUM PLANE
Y.0 (REF)
95.781 (REF.)
98.40 (REF.)
Y
SPACER BLOCK

CHG	REVISION	BY



DETAIL A
TWICE SIZE



DETAIL B
FULL SIZE

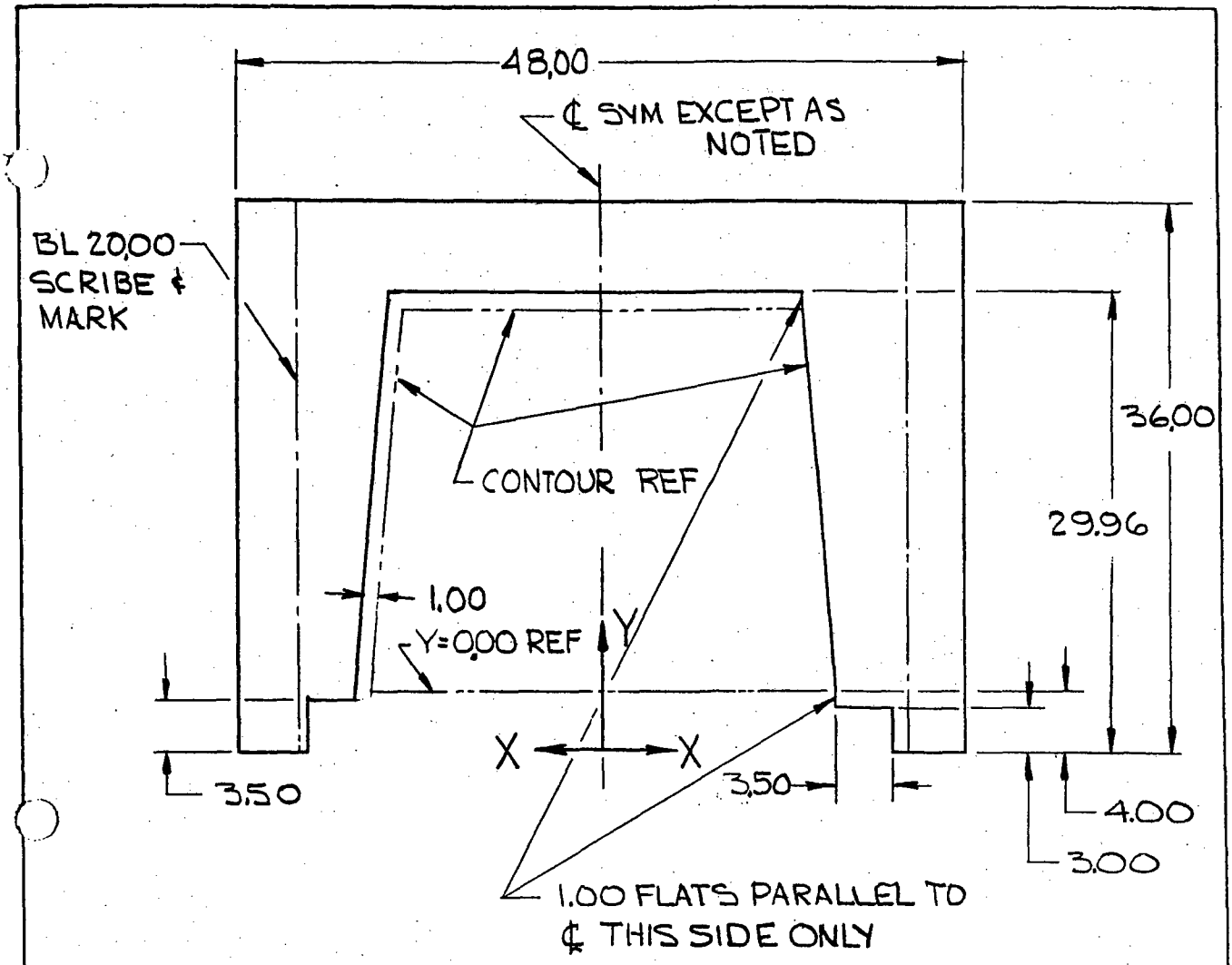
QTY. REQUIREMENTS PER ASSEMBLY	DWG. NO.	PART NAME
1	NR63-105	BASIC
1	NR63-104	BASIC

Next Assembly

Title: FIRING FIXTURE ASSY FULL MOSAIC RADOME

Size: NOTED | DWG NO. NR63-114 | Sheet 1 of 1

Rockwell International
Rocketdyne & Development Division
6633 Canoga Avenue
Canoga Park, California 91304



SEE SHT 2 FOR CONTOUR COORDINATES

MATL - .064 SHEET STEEL

MANUFACTURING TOLERANCES ARE UNLESS OTHERWISE NOTED FRACTIONS ± 031 DECIMALS .XX ± .020 .XXX ± .005 ANGLES ± 1/2 DEG √ ALL MACHINED SURFACES & AS NOTED REF NAS 30	DESIGN Robinson July 20-64 STRESS PROCESS TOOLING CHECK WEIGHT APPROVED
HEAT TREAT	
FINISH	

Marco

RESEARCH & DEVELOPMENT

A DIVISION OF TELECOMPUTING CORPORATION

3540 AERO COURT

SAN DIEGO 23, CALIFORNIA

TITLE

TEMPLATE - LAYUP TOOL MOSAIC RADOME

SCALE 1/10 | PART NO. 338-108

DWG SIZE	DWG NO.	CHANGE LETTER
A	NR 63-079	N/C
	SHEET 1 OF 2	

LAYUP TOOL COORDINATES			
POINT	TILE NO	X	Y
A	107 & -149	15655	0.00
B	-151	15.393	3.001
C	-109	15.213	4.990
D	-153	15.028	6.998
E	-111	14.839	8.988
F	-155	14.644	10.993
G	-113	14.446	12.986
H	-157	14.243	14.986
I	-115	14.036	16.978
J	-159	13.824	18.977
K	-117	13.607	20.968
L	-161	13.387	22.968
M	-119	13.161	24.957

LAYOUT TOLERANCE ON COORDINATE DIMS ±.0005

CUTTING TOLERANCE ON COORDINATE DIMS ±.0015

MANUFACTURING TOLERANCES ARE UNLESS OTHERWISE NOTED:
FRACTIONS ± .031
DECIMALS .XX ± 020
XXX ± .005
ANGLES ± 1/2 DEG
√ ALL MACHINED SURFACES & AS NOTED REF NAS 30

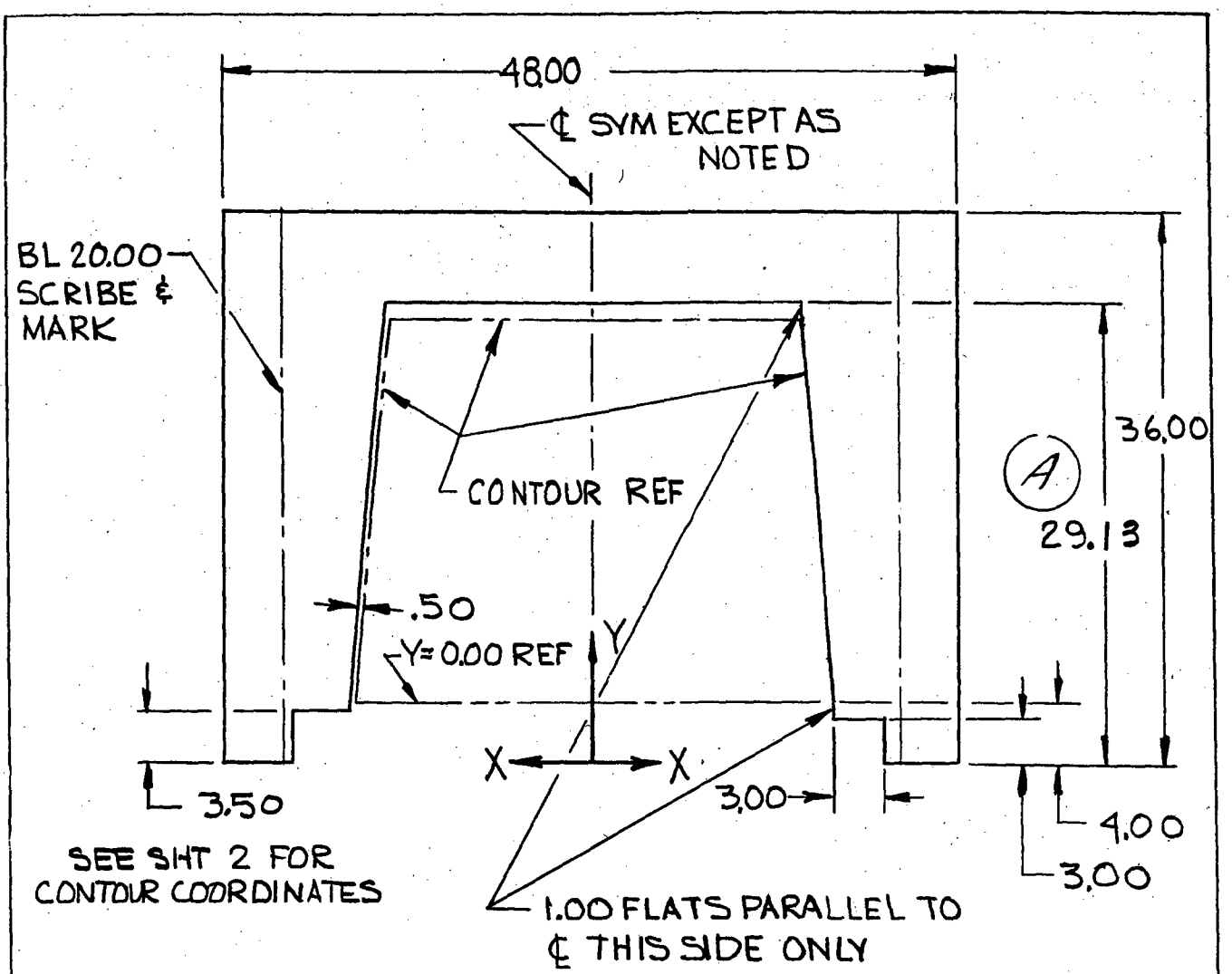
DESIGN ROBINSON July 20-64
STRESS
PROCESS
TOOLING
CHECK
WEIGHT
APPROVED

HEAT TREAT
FINISH

NARMCO
RESEARCH & DEVELOPMENT
A DIVISION OF TELECOMPUTING CORPORATION
3540 AERO COURT
SAN DIEGO 23, CALIFORNIA

TITLE
TEMPLATE - LAYUP TOOL
MOSAIC RADOME

SCALE NONE
WO 338-108
DWG NO. NR 63-079
A DWG SIZE
SHEET 2 OF 2
N/C CHANGE LETTER



MATL-.064 SHEET STEEL

REV		
A	29.13 WAS 29.96	GLM 8-10-64

MANUFACTURING TOLERANCES ARE UNLESS OTHERWISE NOTED
FRACTIONS ± .031
DECIMALS .XX ± .020
.XXX ± .005
ANGLES ± 1/2 DEG.
√ ALL MACHINED SURFACES & AS NOTED REF NAS 30

DESIGN	ROBINSON JULY 21-64
STRESS	
PROCESS	
TOOLING	
CHECK	
WEIGHT	
APPROVED	

HEAT TREAT
FINISH

NARMCO
RESEARCH & DEVELOPMENT
A DIVISION OF TELECOMPUTING CORPORATION
3540 AERO COURT
SAN DIEGO 23 CALIFORNIA

TITLE
TEMPLATE - FIRING TOOL MOSAIC RADOME

SCALE 1/10 | W.O. 338-108

DWG SIZE	DWG NO	CHANGE LETTER
A	NR 63-080	A
	SHEET 1 OF 2	

LAYUP TOOL COORDINATES			
POINT	TILE NO	X	Y
AA	-7 & -51	16.001	0.00
BB	-53	15.825	2.012
CC	-9	15.646	4.027
DD	-55	15.461	6.038
EE	-11	15.272	8.051
FF	-57	15.079	10.063
GG	-13	14.881	12.074
HH	-59	14.679	14.085
II	-15	14.472	16.095
JJ	-61	14.260	18.105
KK	-17	14.044	20.115
LL	-63	13.824	22.125
MM	-19	13.598	24.132

LAYOUT TOLERANCE ON COORDINATE DIMS ±.0005
CUTTING TOLERANCE ON COORDINATE DIMS ±.0015

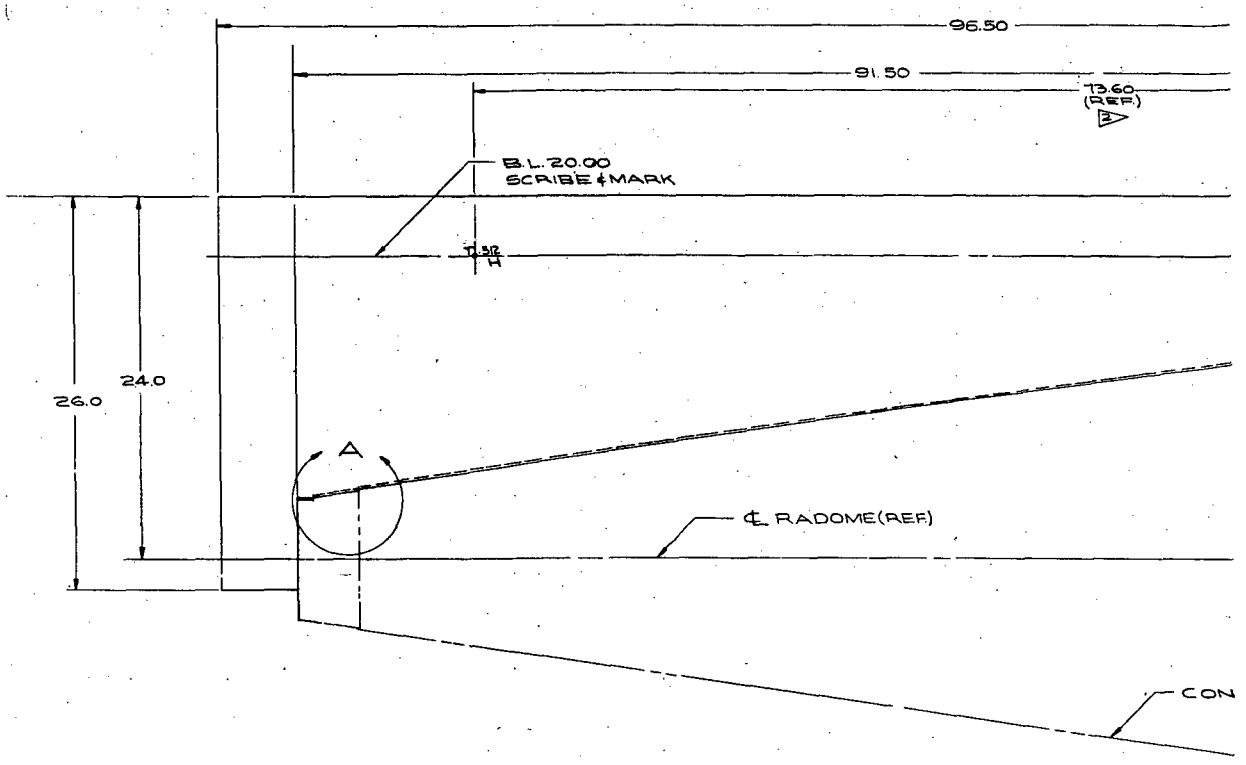
MANUFACTURING TOLERANCES ARE UNLESS OTHERWISE NOTED:
FRACTIONS ± .031
DECIMALS .XX ± 020
XXX ± .005
ANGLES ± 1/2 DEG.
√ ALL MACHINED SURFACES & AS NOTED REF NAS 30
HEAT TREAT
FINISH

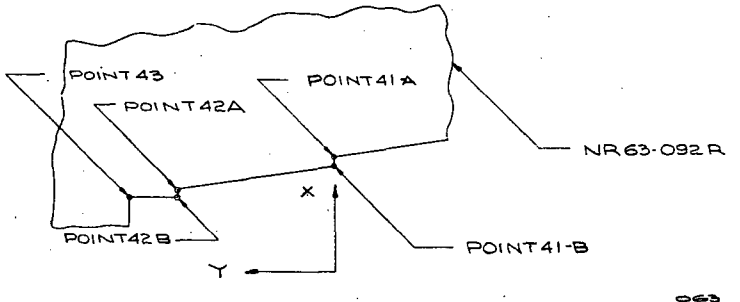
DESIGN Robinson July 21-64
STRESS
PROCESS
TOOLING
CHECK
WEIGHT
APPROVED

NARMCO
RESEARCH & DEVELOPMENT
A DIVISION OF TELECOMPUTING CORPORATION
3540 AERO COURT
SAN DIEGO 23, CALIFORNIA

TITLE
TEMPLATE - FIRING TOOL
MOSAIC RADOME

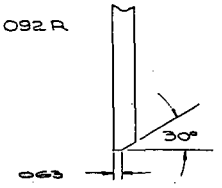
SCALE NONE
WO 338-108
DWG NO NR63-080
DWG SIZE
SHEET 2 OF 2
N/C CHANGE LETTER





DETAIL A

NO SCALE

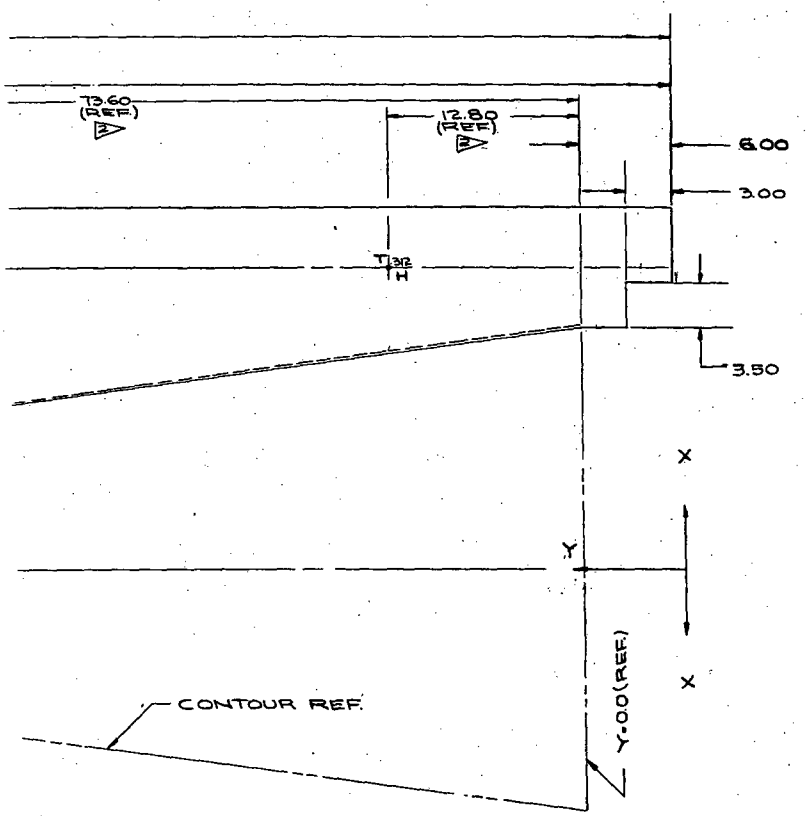


TYPICAL CHAMFER

FROM POINT 1 TO POINT 43

SCALE 2/1

LAYUP TOOL



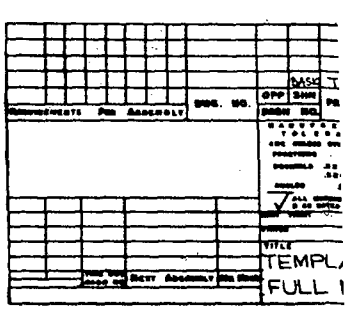
POINT	TILE	X	Y
1	193,195	15.6550	0.00
2	151	15.3934	3.001
3	109	15.2134	4.9962
4	153	15.0285	6.9973
5	111	14.8385	8.9917
6	155	14.6445	10.9919
7	113	14.4466	12.9855
8	157	14.2436	14.9848
9	115	14.0366	16.9775
10	159	13.8246	18.9760
11	117	13.6077	20.9675
12	161	13.3877	22.9654
13	119	13.1617	24.9557
14	163	12.9327	26.9526
15	121	12.6978	28.9417
16	165	12.4598	30.9316
17	123	12.2158	32.9255
18	167	11.9688	34.9205
19	125	11.7168	36.9074
20	169	11.4599	38.9011
21	127	11.1989	40.8868
22	171	10.9329	42.8794
23	129	10.6629	44.8639
24	173	10.3890	46.8553
25	131	10.1100	48.8386
26	175	9.8271	50.8287
27	133	9.5392	52.8108
28	177	9.2462	54.7994
29	135,181	8.9503	56.7803
30	179,183	8.6493	58.7677
31	137	8.3433	60.7469
32	139	8.0313	62.7255
33	185	7.7184	64.7094
34	141	7.3864	66.6880
35	187	7.0634	68.6707
36	143	6.7354	70.6470
37	189	6.4025	72.6296
38	145	6.0655	74.6046
39	191	5.7246	76.5849
40	147	5.3796	78.5584
41A		4.8597	81.4522
41 B		4.8231	81.4522
42A		4.2817	84.5022
42 B		4.1030	84.5022
43		4.1030	85.5022

AYUP TOOL TEMPLATE ▷

▷ LOCATE T
ALIGNME
& LAYUP T

▷ SEE TABL

CUTTING TOLE



ZONE	REVISION	BY	

T	TILE	X	Y
	193,195	15.6550	0.00
	151	15.3934	3.001
	109	15.2134	4.9962
	153	15.0285	6.9973
	111	14.8385	8.9917
	155	14.6445	10.9919
	113	14.4466	12.9855
	157	14.2436	14.9848
	115	14.0366	16.9775
	159	13.8246	18.9760
	117	13.6077	20.9675
	161	13.3877	22.9654
	119	13.1617	24.9557
	163	12.9327	26.9526
	121	12.6978	28.9417
	165	12.4598	30.9316
	123	12.2158	32.9255
	167	11.9688	34.9205
	125	11.7168	36.9074
	169	11.4599	38.9011
	127	11.1989	40.8868
	171	10.9329	42.8794
	129	10.6629	44.8639
	173	10.3890	46.8553
	131	10.1100	48.8386
	175	9.8271	50.8287
	133	9.5392	52.8108
	177	9.2462	54.7994
	135,181	8.9503	56.7803
	179,183	8.6493	58.7677
	137	8.3433	60.7459
2	139	8.0313	62.7255
3	185	7.7184	64.7094
4	141	7.3864	66.6880
5	187	7.0634	68.6707
5	143	6.7354	70.6470
7	189	6.4025	72.6296
3	145	6.0655	74.6046
9	191	5.7246	76.5849
0	147	5.3796	78.5584
A		4.8597	81.4522
B		4.8231	81.4522
2A		4.2817	84.5022
B		4.1030	84.5022
		4.1030	85.5022

2 LOCATE TOOLING HOLES TO ASSURE ALIGNMENT OF THE CORRESPONDING FIRING & LAYUP TOOL COORDINATE POINTS.

1 SEE TABLE FOR COORDINATES.

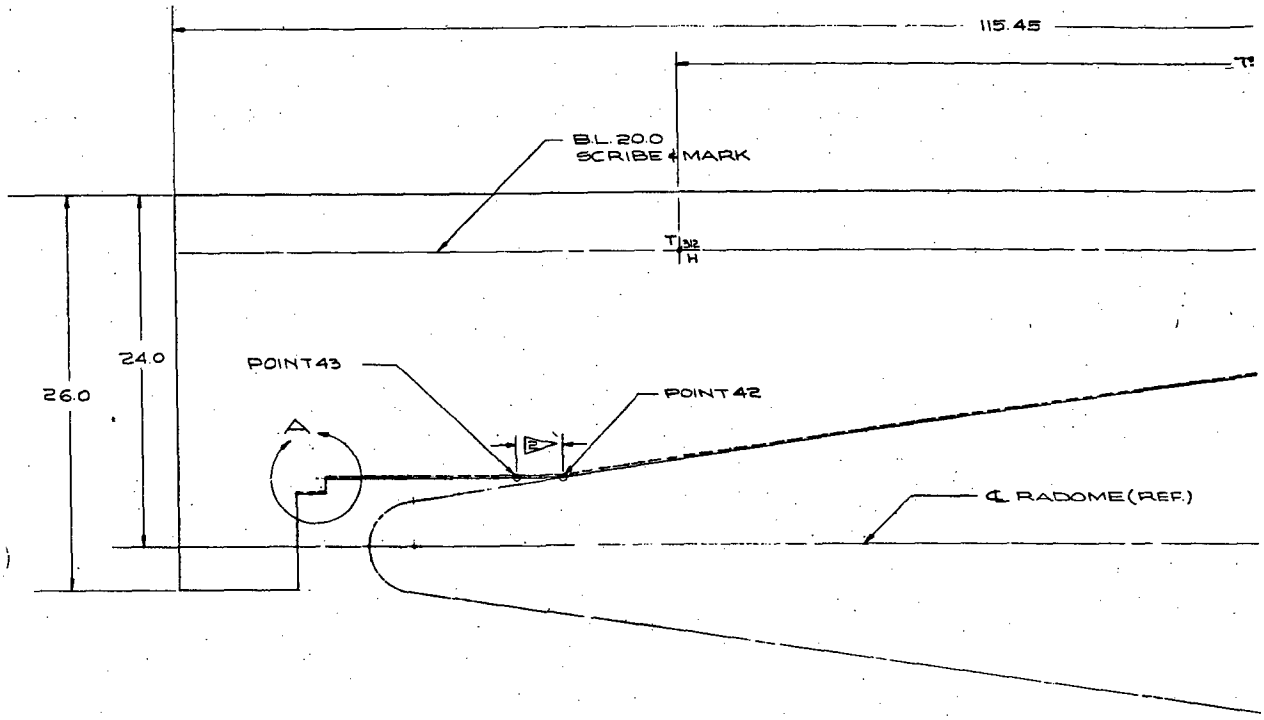
CUTTING TOLERANCE ON COORDINATE DIMS ± .0015

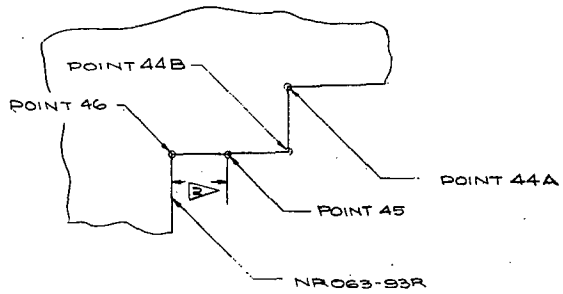
DASH TEMPLATE, .179 STEEL PLATE

Westinghouse

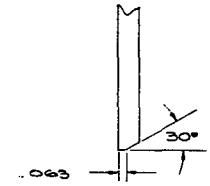
TITLE
TEMPLATE-LAYUP TOOL
FULL MOSAIC RADOME

NF463092F



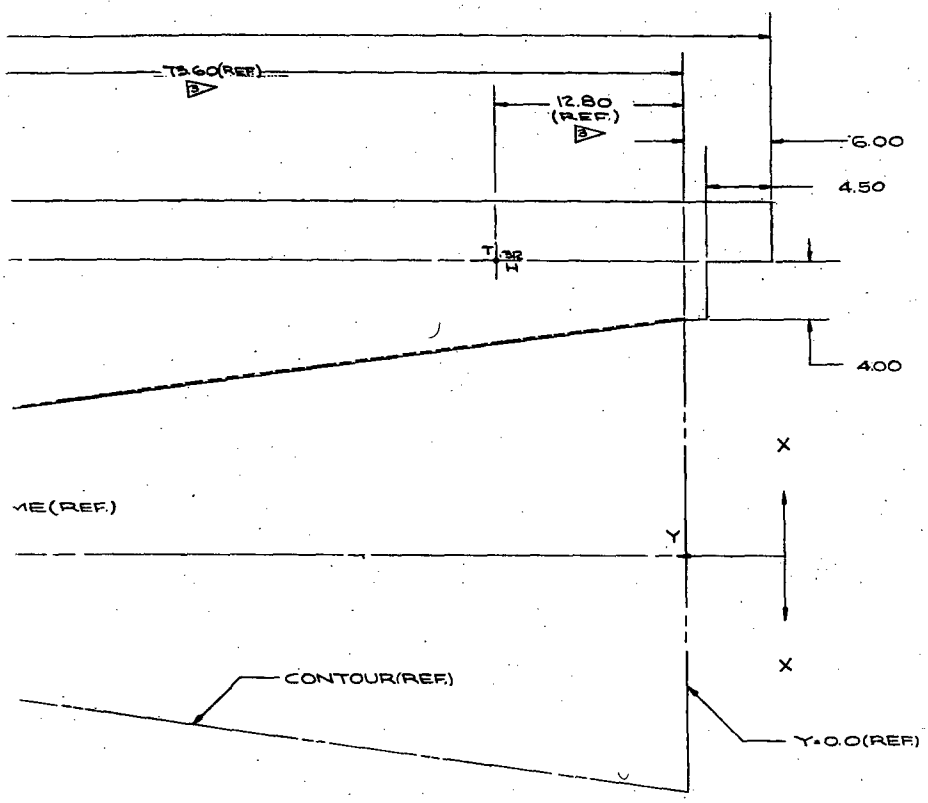


DETAIL A
NO SCALE



TYPICAL CHAMFER
FROM POINT 1 TO POINT 46
SCALE 2/1

FIR



POINT	TILE (REF.)	X	Y
1		16.0010	0.000
2	9553	15.8252	2.0123
3	9	15.6456	4.0246
4	55	15.4610	6.0376
5	11	15.2723	8.0489
6	57	15.0786	10.0611
7	13	14.8809	12.0715
8	59	14.6791	14.0829
9	15	14.4723	16.0924
10	61	14.2604	18.1027
11	17	14.0445	20.1112
12	63	13.8236	22.1206
13	19	13.5986	24.1280
14	65	13.3696	26.1366
15	21	13.1355	28.1430
16	67	12.8964	30.1504
17	23	12.6533	32.1557
18	69	12.4061	34.1621
19	25	12.1539	36.1663
20	71	11.8976	38.1715
21	27	11.6363	40.1746
22	73	11.3710	42.1785
23	29	11.1006	44.1805
24	75	10.8262	46.1832
25	31	10.5467	48.1840
26	77	10.2632	50.1854
27	33	9.9747	52.1849
28	79	9.6821	54.1850
29	35	9.3855	56.1833
30	81,39	9.0838	58.1821
31	37	8.7772	60.1788
32	83	8.4664	62.1759
33	41	8.1516	64.1716
34	85	7.8318	66.1674
35	43	7.5080	68.1616
36	87	7.1791	70.1559
37	45	6.8462	72.1486
38	89	6.5092	74.1415
39	47	6.1672	76.1328
40	91	5.8201	78.1239
41	49	5.4690	80.1138
42		5.2208	81.4950
43		5.2203	82.5820
44A		4.9256	99.4500
44B		4.1256	99.4500
45		4.1055	100.4500
46		4.1055	101.4500

FIRING TOOL TEMPLATE ▷

▷ P.O.
P.O.
▷ N.
▷ SE

REQUIRED

Ltr.	REVISION	BY

[3] LOCATE TOOLING HOLES TO ASSURE ALIGNMENT OF THE CORRESPONDING FIRING & LAYUP TOOL COORDINATE POINTS.

[6] NO TAPER BETWEEN THESE POINTS
[7] SEE TABLE FOR COORDINATES.

CUTTING TOLERANCE ON COORDINATE DIMS ± .0015

REQUIREMENTS PER ASSEMBLY	DWG. NO	OPP SHN DASH NO.	PART NAME
		1	TEMPLATE, .179 STEEL PLATE

MANUFACTURING TOLERANCES ARE UNLESS OTHERWISE NOTED
FRACTIONS ± .031
DECIMALS .XX ± .010
.XXX ± .005
ANGLES ± 1/2 DEG.
√ ALL MACHINED SURFACES TO BE 63 MICRO INCH OR BETTER

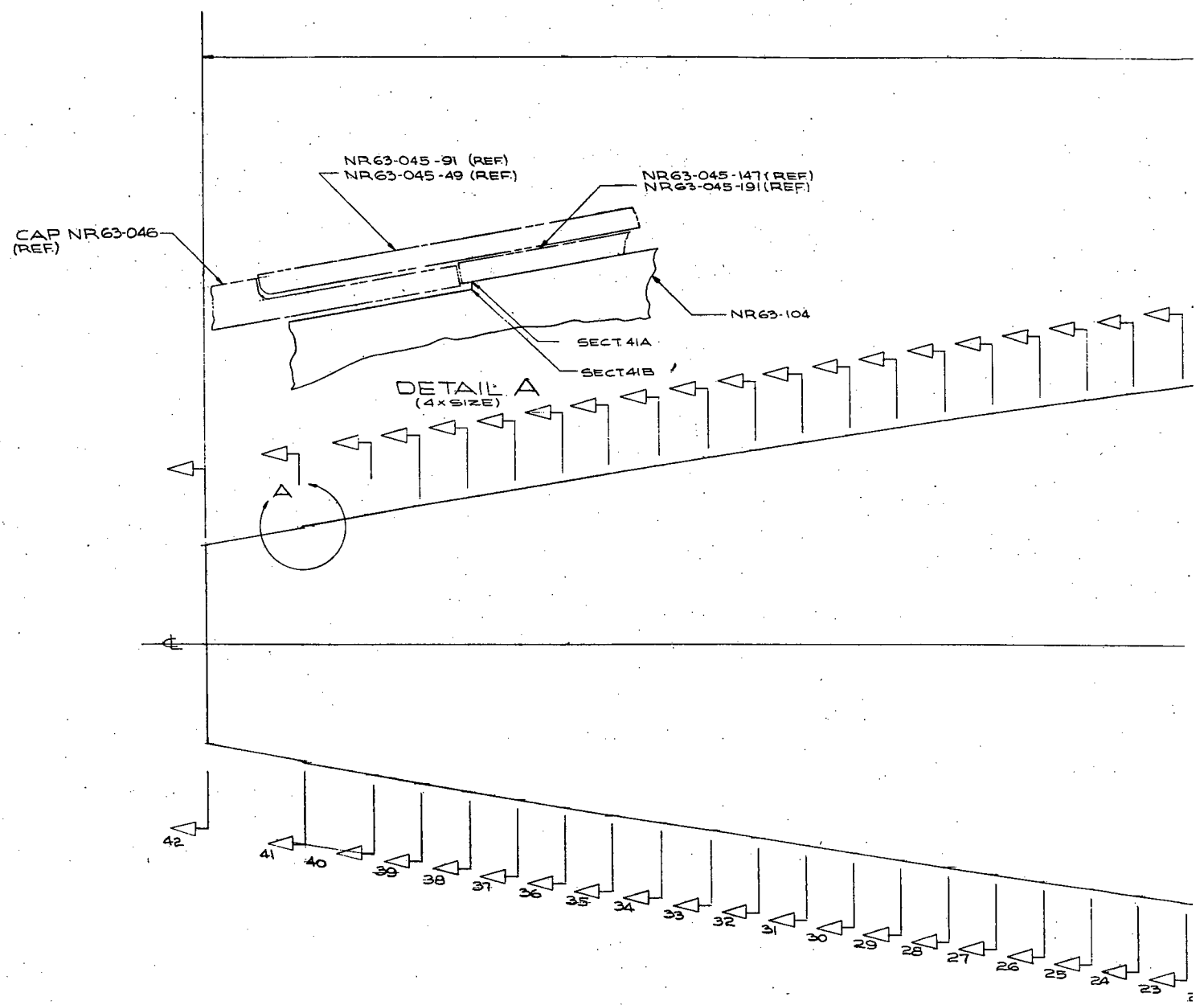
DRAWN K. Fisher 10/8/64
STRESS
PROCESS
TOOLING J. W. Fox 11-23-64
CODE
WEIGHT
ENGINEER 10-28-64
NEXT SHEET
FINISH

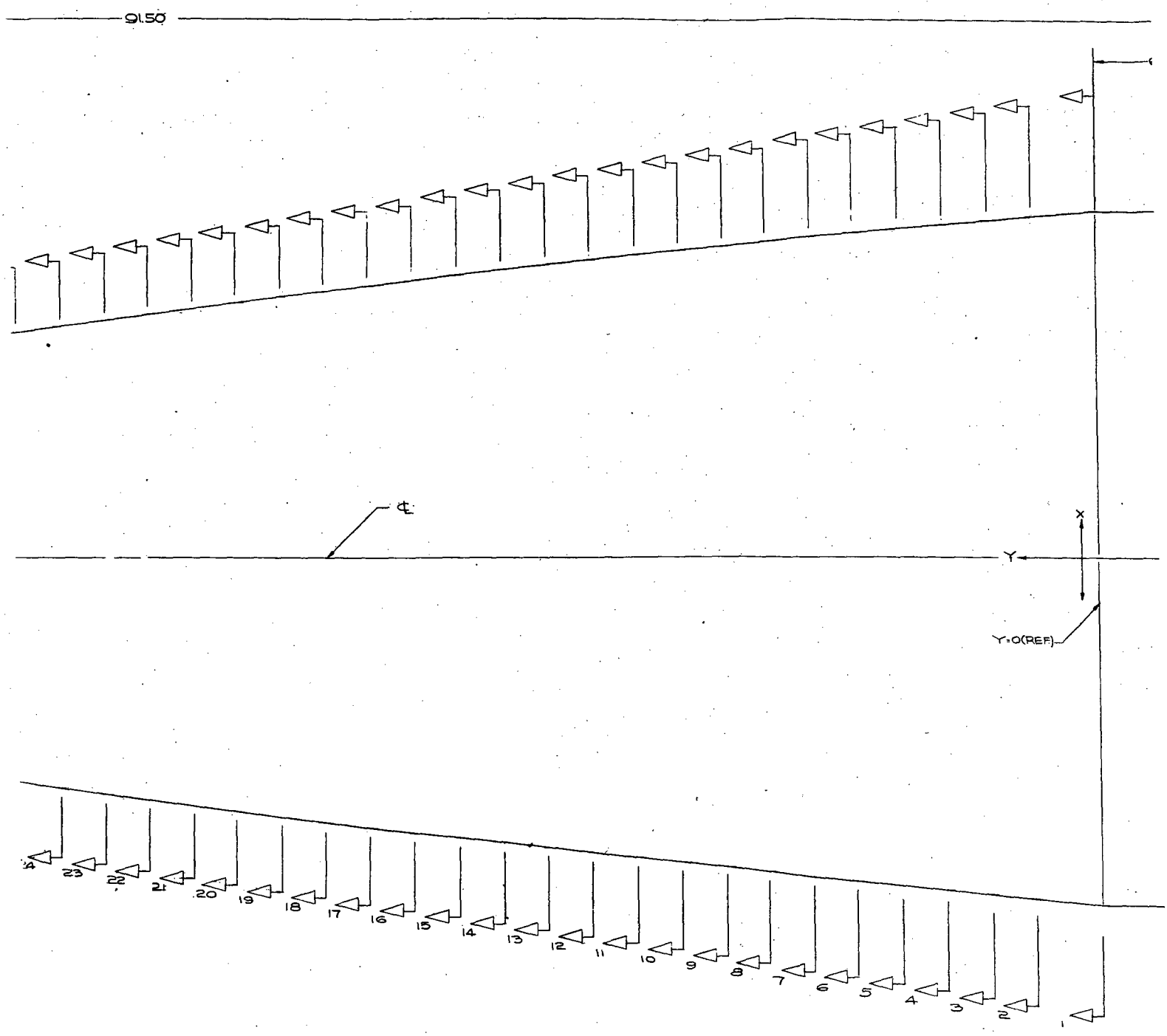
Whittaker Corporation
NARMCO
RESEARCH & DEVELOPMENT DIVISION
•
8540 Aero Court
San Diego, California 92123

TITLE
TEMPLATE-FIRING TOOL
FULL MOSAIC RADOME

NEXT ASSEMBLY

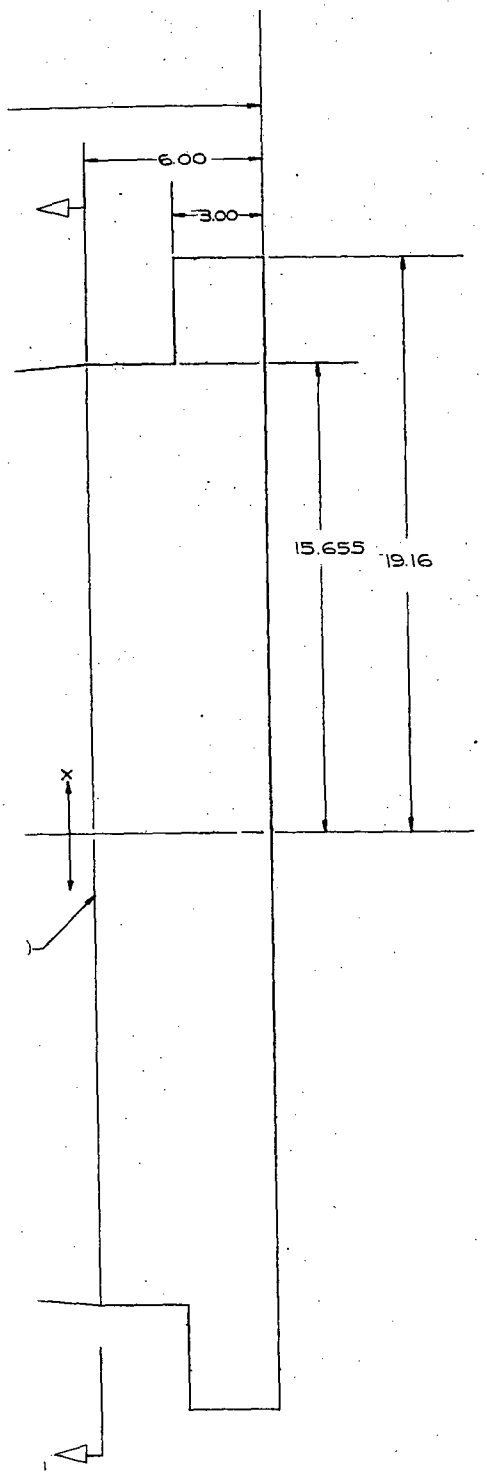
SIZE NR63-093R
DWG SIZE


NR63-045-91 (REF.)
NR63-045-49 (REF.)
NR63-045-147 (REF.)
NR63-045-191 (REF.)
CAP NR63-046 (REF.)
NR63-104
SECT 41A
SECT41B
DETAIL A
(4 x SIZE)
A
42
41
40
39
38
37
36
35
34
33
32
31
30
29
28
27
26
25
24
23



LAY UP TOOL ▷

1/2 SIZE



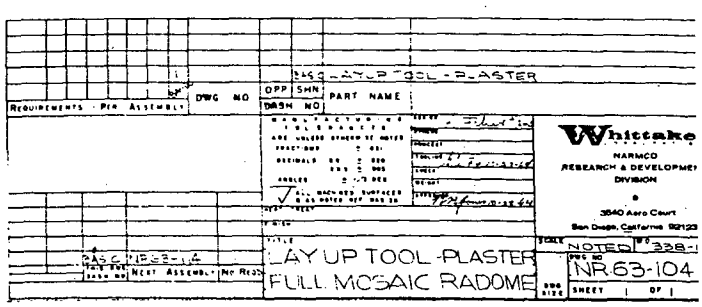
SECT NO.	TILE NO (REF)	RADIUS (REF)	X	Y	SECT NO.	TILE NO (REF)
1	193,195	15.737	15.6550	0.00	22	171
2	151	15.475	15.3934	3.001	23	129
3	109	15.295	15.2134	4.9962	24	173
4	153	15.110	15.0285	6.9973	25	131
5	111	14.920	14.8385	8.9917	26	175
6	155	14.726	14.6445	10.9919	27	133
7	113	14.528	14.4466	12.9855	28	177
8	157	14.325	14.2436	14.9848	29	135, 181
9	115	14.118	14.0366	16.9775	30	179, 183
10	159	13.906	13.8246	18.9760	31	137
11	117	13.689	13.6077	20.9675	32	139
12	161	13.469	13.3877	22.9654	33	185
13	119	13.243	13.1617	24.9557	34	141
14	163	13.014	12.9327	26.9526	35	187
15	121	12.779	12.6978	28.9417	36	143
16	165	12.541	12.4598	30.9316	37	189
17	123	12.297	12.2158	32.9255	38	145
18	167	12.050	11.9688	34.9205	39	191
19	125	11.798	11.7168	36.9074	40	147
20	169	11.541	11.4599	38.9011	41A	
21	127	11.280	11.1989	40.8868	41B	
					42A	
					42B	
					43	

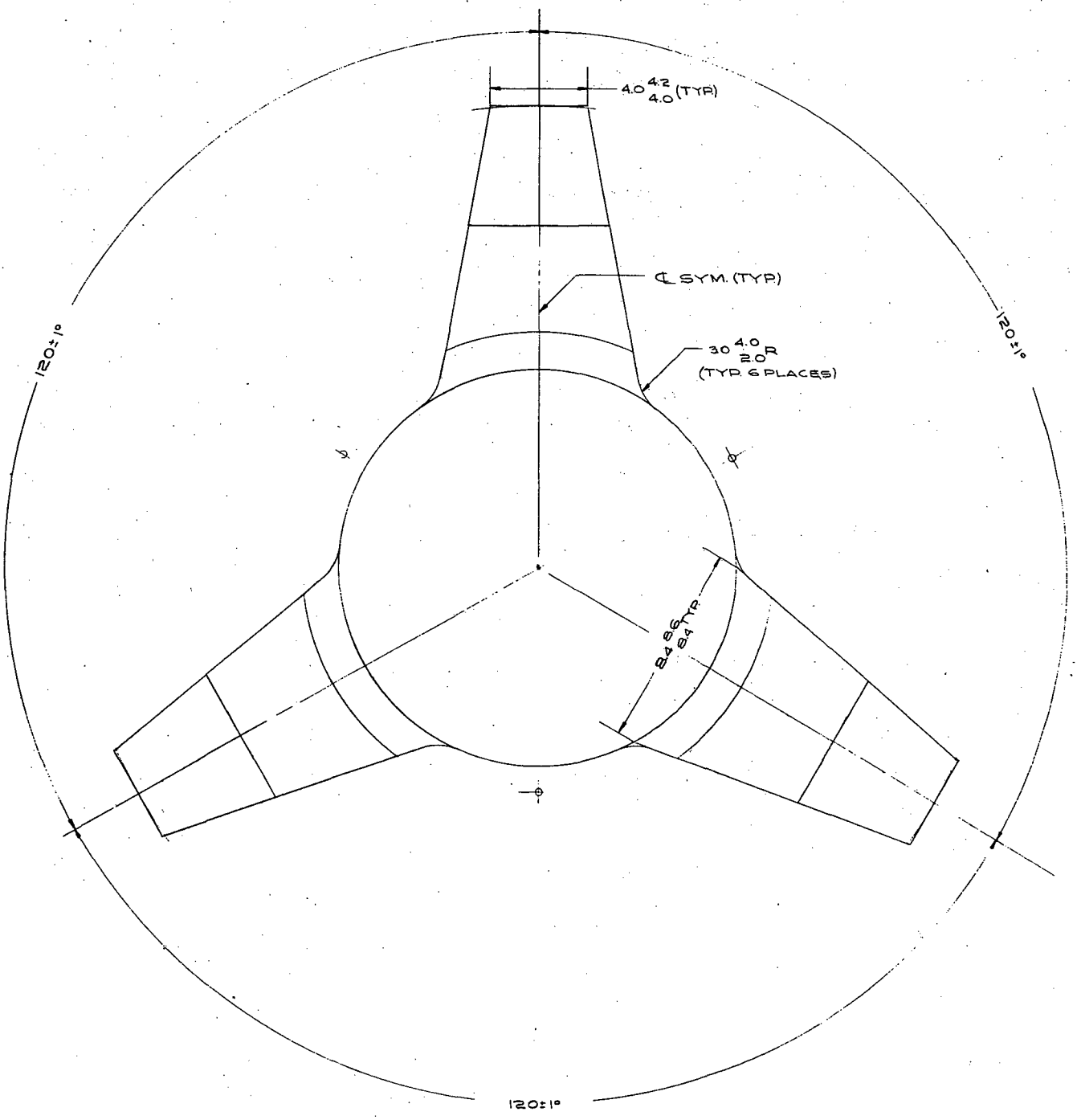
MATL: PLASTER. WALL THICKNESS 1.50 M

▷ SEE TABLE FOR COORDINATES.

CT O.	TILE NO (REF)	RADIUS (REF)	X	Y	SECT NO.	TILE NO (REF)	RADIUS (REF)	X	Y
	193,195	15.737	15.6550	0.00	22	171	11.014	10.9329	42.8794
	151	15.475	15.3934	3.001	23	129	10.744	10.6629	44.8639
	109	15.295	15.2134	4.9962	24	173	10.470	10.3890	46.8553
	153	15.110	15.0285	6.9973	25	131	10.191	10.1100	48.8386
5	111	14.920	14.8385	8.9917	26	175	9.908	9.8271	50.8287
	155	14.726	14.6445	10.9919	27	133	9.620	9.5392	52.8108
	113	14.528	14.4466	12.9855	28	177	9.327	9.2462	54.7994
3	157	14.325	14.2436	14.9848	29	135, 181	9.031	8.9503	56.7803
	115	14.118	14.0366	16.9775	30	179, 183	8.730	8.6493	58.7617
	159	13.906	13.8246	18.9760	31	137	8.424	8.3433	60.7469
	117	13.689	13.6077	20.9675	32	139	8.114	8.0313	62.7255
	161	13.469	13.3877	22.9654	33	185	7.799	7.7184	64.7094
	119	13.243	13.1617	24.9557	34	141	7.480	7.3864	66.6880
	163	13.014	12.9327	26.9526	35	187	7.157	7.0634	68.6707
	121	12.779	12.6978	28.9417	36	143	6.829	6.7354	70.6470
	165	12.541	12.4598	30.9316	37	189	6.496	6.4025	72.6296
	123	12.297	12.2158	32.9255	38	145	6.160	6.0655	74.6046
	167	12.050	11.9688	34.9205	39	191	5.818	5.7246	76.5849
:	125	11.798	11.7168	36.9074	40	147	5.473	5.3796	78.5584
:	169	11.541	11.4599	38.9011	41A			4.8597	81.4522
	127	11.280	11.1989	40.8868	41B			4.8231	81.4522
					42A			4.2817	85.5022
					42B			4.1030	84.5022
					43			4.1030	86.5022

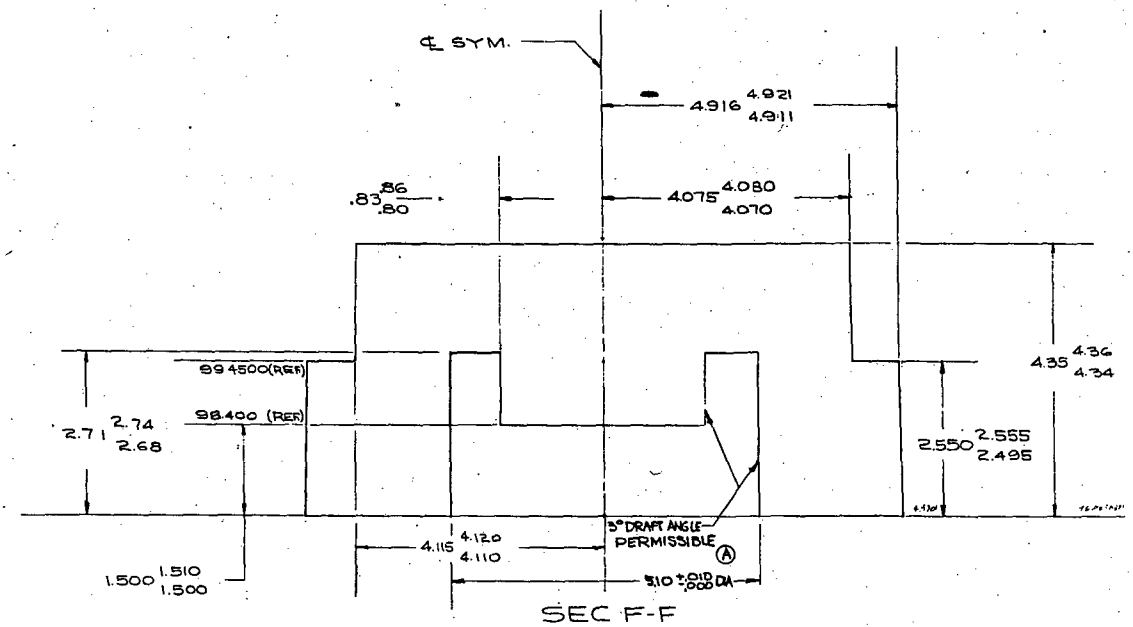
L: PLASTER. WALL THICKNESS 1.50 MAX. 1.00 MIN.
: TABLE FOR COORDINATES.



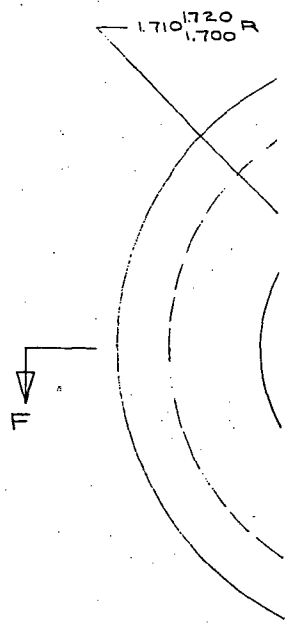


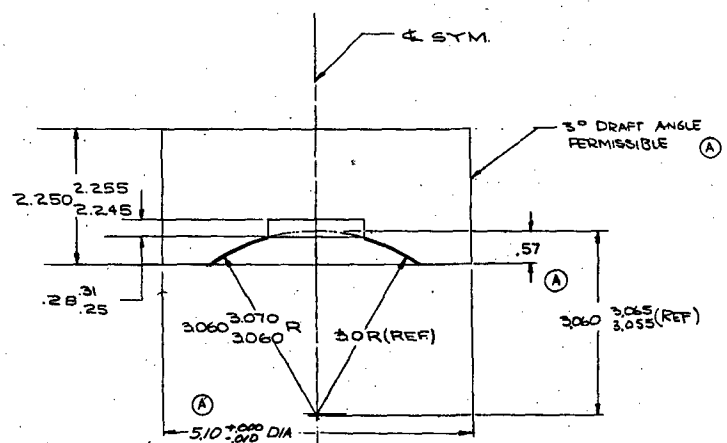
VIEW A-A

1/2 SIZE

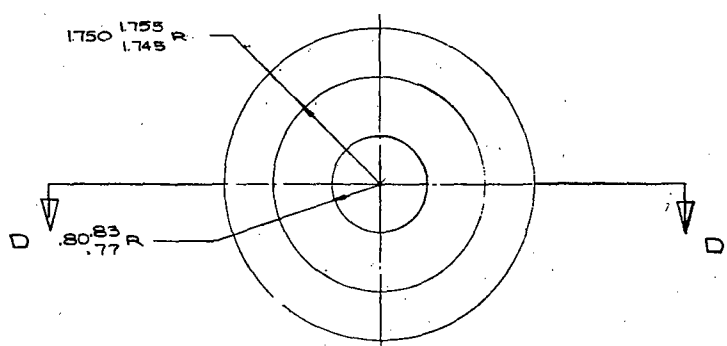


SEC F-F





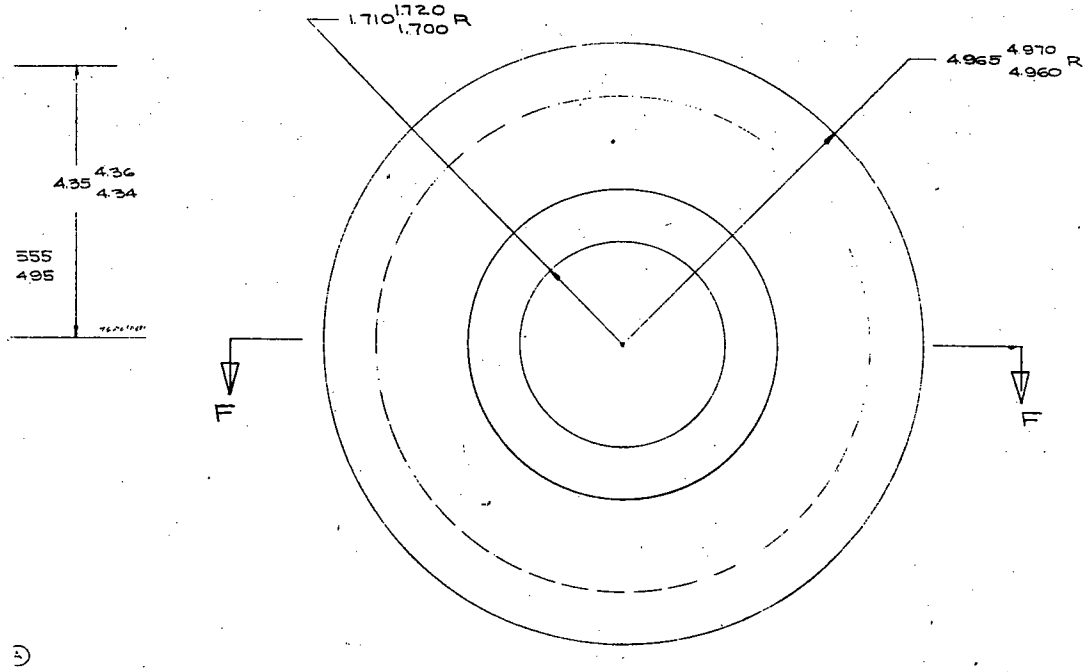
SEC D-D



DETAIL-11

FULL SIZE

CHG	REVISION	BY	
A	5.10±.010 DIA WAS 2.35/2.300		
	B 5.10±.005 DIA WAS 2.35/2.300		
	C ADD DRAFT ANGLE NOTES.		
	R.00.3% DIM. 3060 WAS 3030	JLR	8-66



DETAIL -9
FULL SIZE

DASH NO.	PART NAME
-13	INSERT - GLASS
-11	LOWERING PLATE
-9	PLUG - REMOVABLE
-7	FIRING TOOL

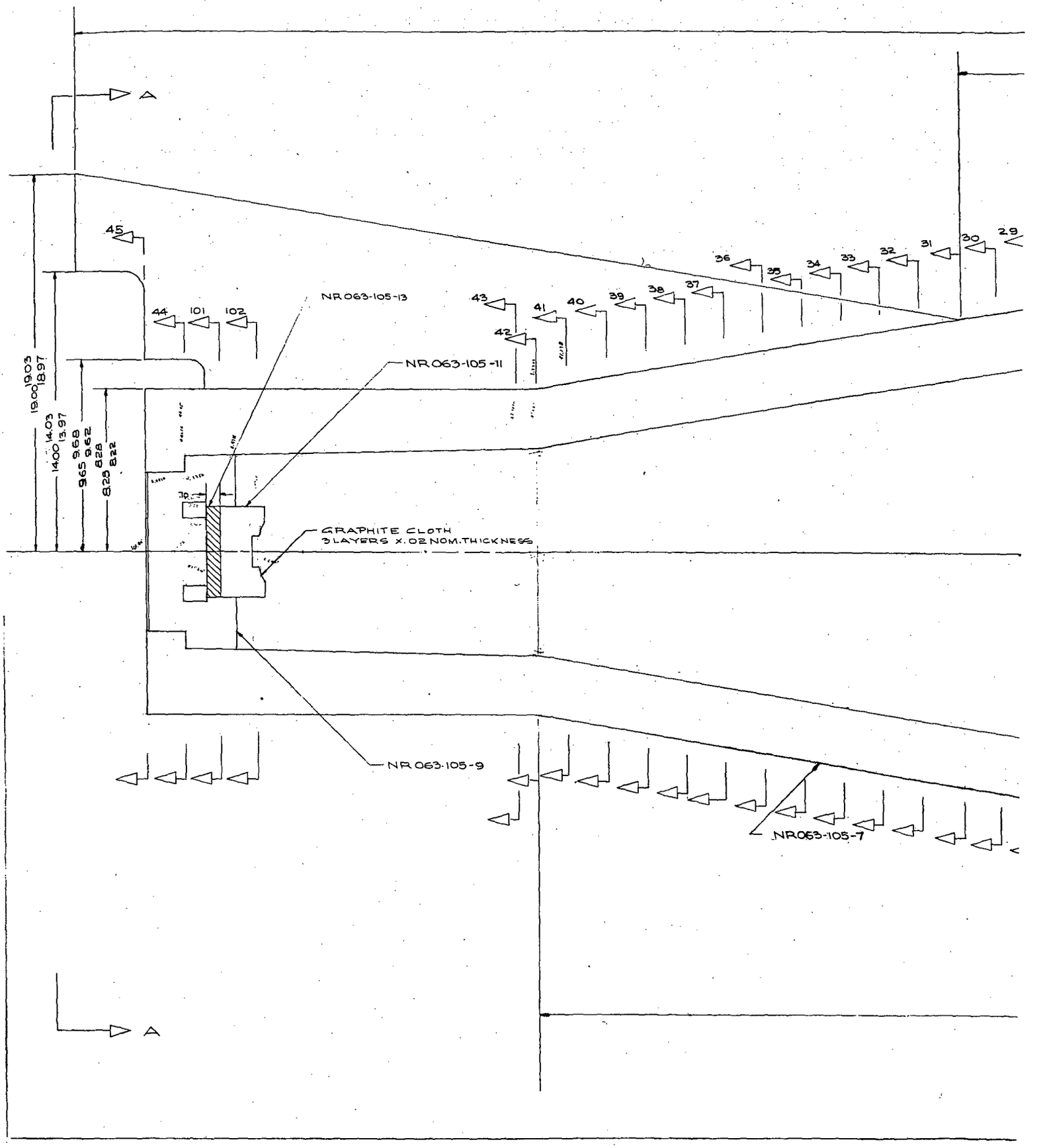
DWG. NO. NR063-114 1

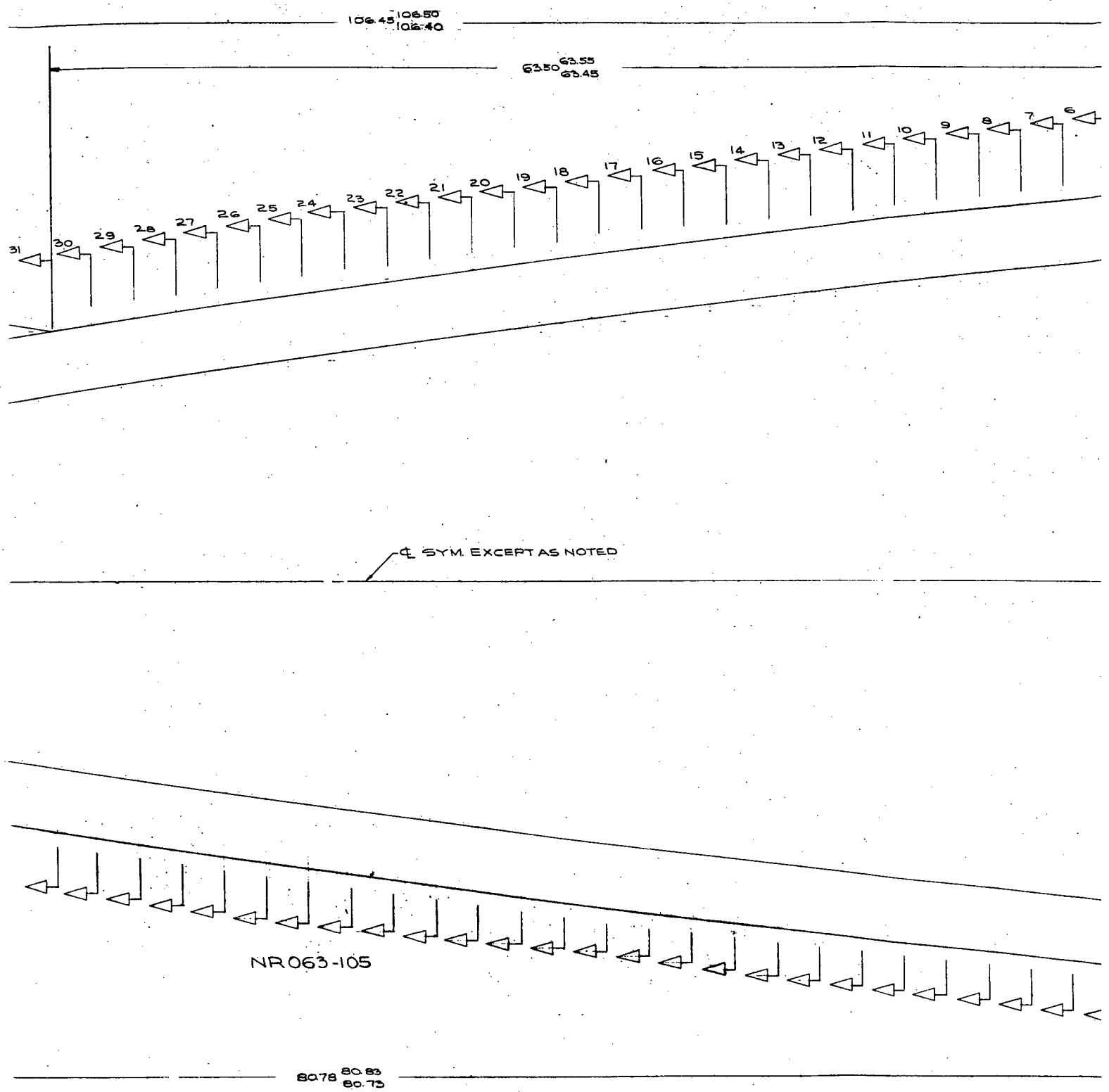
TITLE
FIRING TOOL-GLASROCK
FULL MOSAIC RADOME

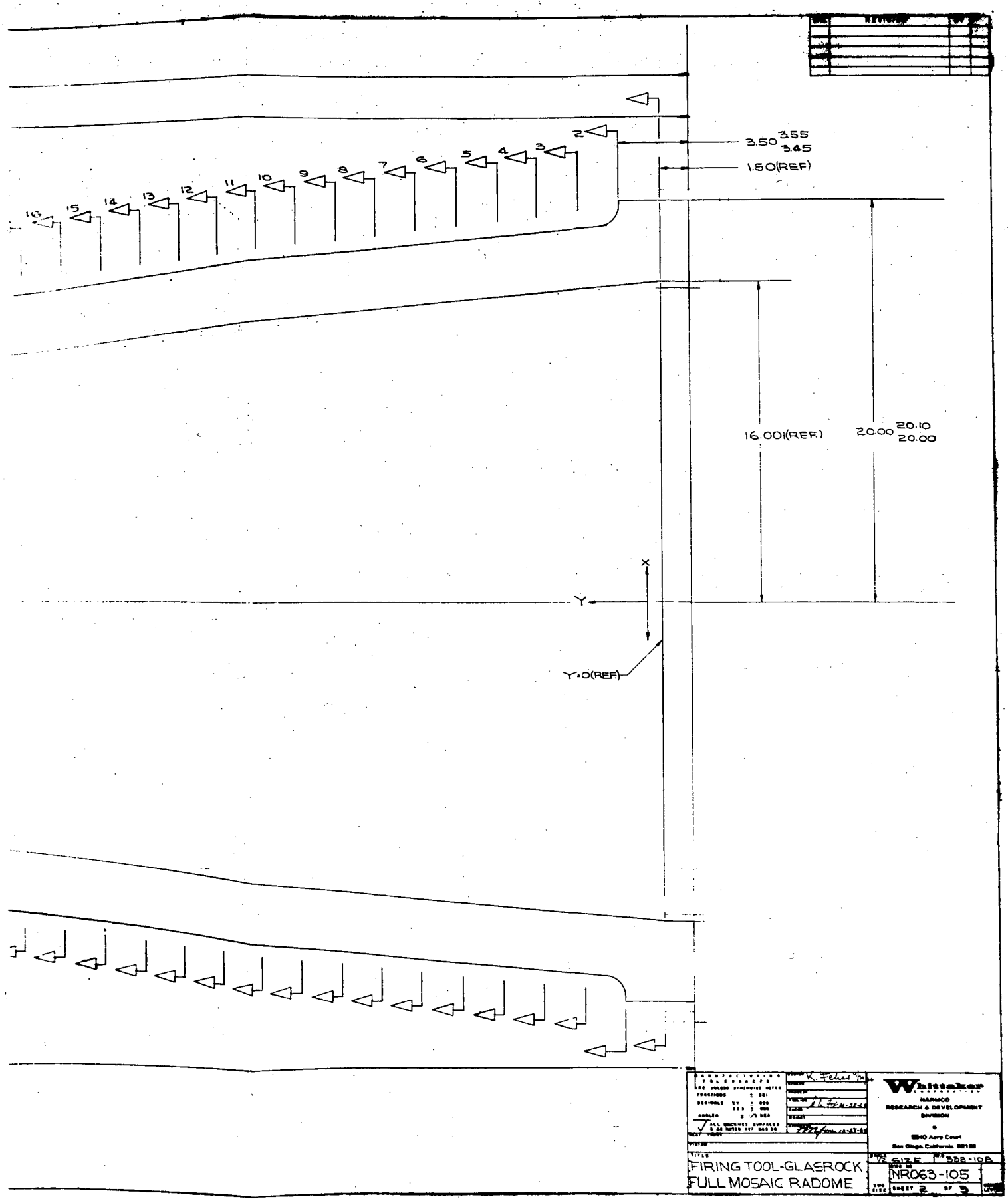
NOTED 338-108

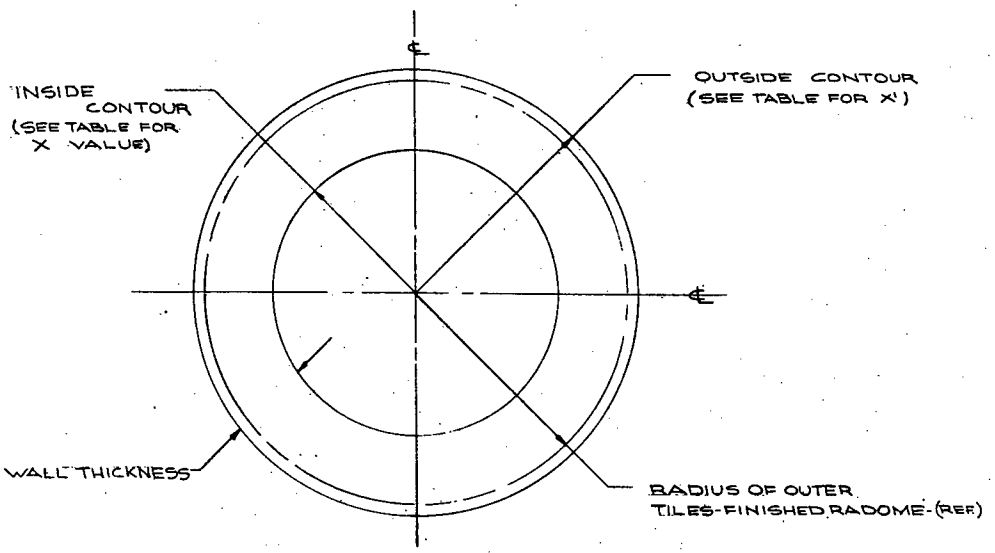
NR063-105

SHEET 1 OF 3


A
45
44
101
102
43
42
41
40
39
38
37
36
35
34
33
32
31
30
29
NR063-105-13
NR063-105-11
19.00
19.03
18.97
14.00
14.03
13.97
9.65
9.68
9.62
8.25
8.28
8.22
GRAPHITE CLOTH
3 LAYERS x .02 NOM. THICKNESS
NR063-105-9
NR063-105-7
A


106.45 106.50 106.40
63.50 63.55 63.45
31
30
29
28
27
26
25
24
23
22
21
20
19
18
17
16
15
14
13
12
11
10
9
8
7
6
℄ SYM. EXCEPT AS NOTED
NR063-105
80.78 80.83 80.73


REVISIONS
1
2
3
4
5
6
7
8
9
10
11
12
13
14
15
16
3.50 3.55 3.45
1.50(REF)
16.001(REF.)
20.00 20.10 20.00
X
Y
Y=0(REF)
DRAWN K. Fehr
TRACED
CHECKED
ENGR
PROJ ENGR
DEPT
Whittaker
NARMCO
RESEARCH & DEVELOPMENT
DIVISION
1040 Aero Court
San Diego, California 92123
TITLE
FIRING TOOL-GLASROCK
FULL MOSAIC RADOME
SIZE E
338-108
DWG NO NR063-105
SHEET 2 OF 3

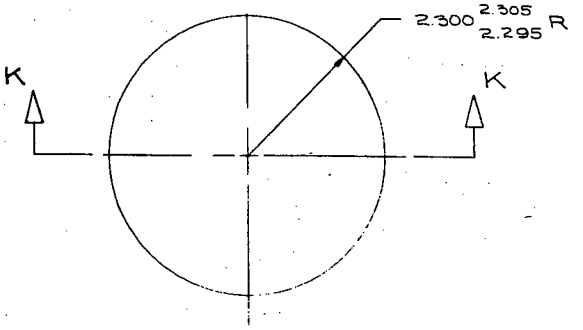


TYPICAL SECT

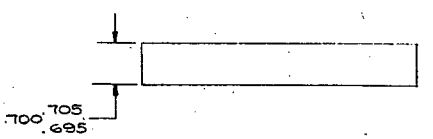
NO SCALE

SECT NO.	TILE NO (REF.)	X	Y	RADIUS (REF.)	X'
1		16.0010	0.000	15.850	
2	95,53	15.8252	2.0123	15.676	
3	9	15.6456	4.0246	15.498	18.65
4	55	15.4610	6.0376	15.315	
5	11	15.2725	8.0489	15.128	
6	57	15.0786	10.0611	14.936	
7	13	14.8809	12.0715	14.740	
8	59	14.6791	14.0829	14.540	
9	15	14.4723	16.0924	14.335	
10	61	14.2604	18.1027	14.126	
11	17	14.0445	20.1112	13.911	
12	63	13.8236	22.1206	13.692	16.83
13	19	13.5986	24.1280	13.469	
14	65	13.3696	26.1366	13.242	
15	21	13.1355	28.1430	13.010	
16	67	12.8964	30.1504	12.773	
17	23	12.6533	32.1557	12.532	
18	69	12.4061	34.1621	12.287	
19	25	12.1539	36.1663	12.037	
20	71	11.8976	38.1715	11.783	
21	27	11.6363	40.1746	11.524	14.64
22	73	11.3710	42.1785	11.261	
23	29	11.1006	44.1805	10.993	
101			98.400	(REF)	
102			95.7807	(REF.)	

Y	RADIUS (REF.)	X'	SECT. NO.	TILE NO. (REF.)	X	Y	RADIUS (REF.)	X'
.00	15.850		24	75	10.8262	46.1832	10.721	
0123	15.676		25	31	10.5467	48.1840	10.444	
0246	15.498	18.65	26	77	10.2632	50.1854	10.163	
0376	15.315		27	33	9.9747	52.1849	9.877	
0489	15.128		28	79	9.6821	54.1850	9.587	
0611	14.936		29	35	9.3855	56.1833	9.293	12.40
0715	14.740		30	81,39	9.0838	58.1821	8.994	
0829	14.540		31	37	8.7772	60.1788	8.690	
0924	14.335		32	83	8.4664	62.1759	8.382	
1027	14.125		33	41	8.1516	64.1716	8.070	
1112	13.911		34	85	7.8317	66.1674	7.753	
1206	13.692	16.83	35	43	7.5080	68.1616	7.432	
1280	13.469		36	87	7.1791	70.1559	7.106	10.20
1366	13.242		37	45	6.8462	72.1486	6.776	
1430	13.010		38	89	6.5092	74.1415	6.442	
1504	12.773		39	47	6.1672	76.1328	6.103	
1557	12.532		40	91	5.8201	78.1239	5.759	
1621	12.287		41	49	5.4690	80.1138	5.411	
1663	12.037		42		5.2203	81.4950		8.25
1715	11.783		43		5.2203	82.5820		
1746	11.524	14.64	44A		4.9256	99.4500		
1785	11.261		44B		4.12.56	99.4500		
1805	10.993		45		4.0854	101.4500		
3400	(REF.)		46		4.1055	101.4500		8.25
7807	(REF.)							



DETAIL-13
FULL SIZE



SEC K-K

REQUIREMENTS PER ASSEMBLY

DWG. NO.

DASH NO.

PART NAME

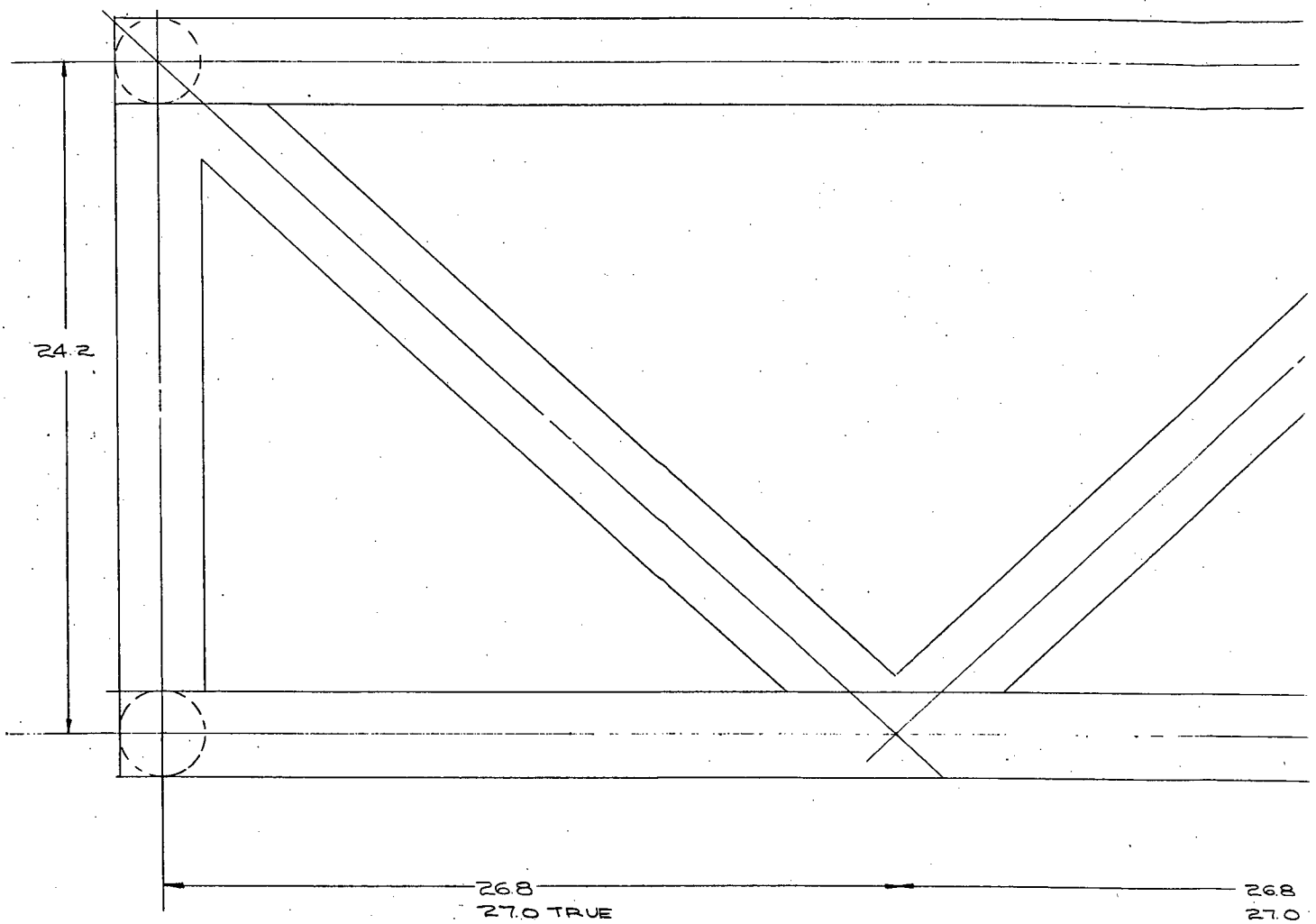
TOLERANCES

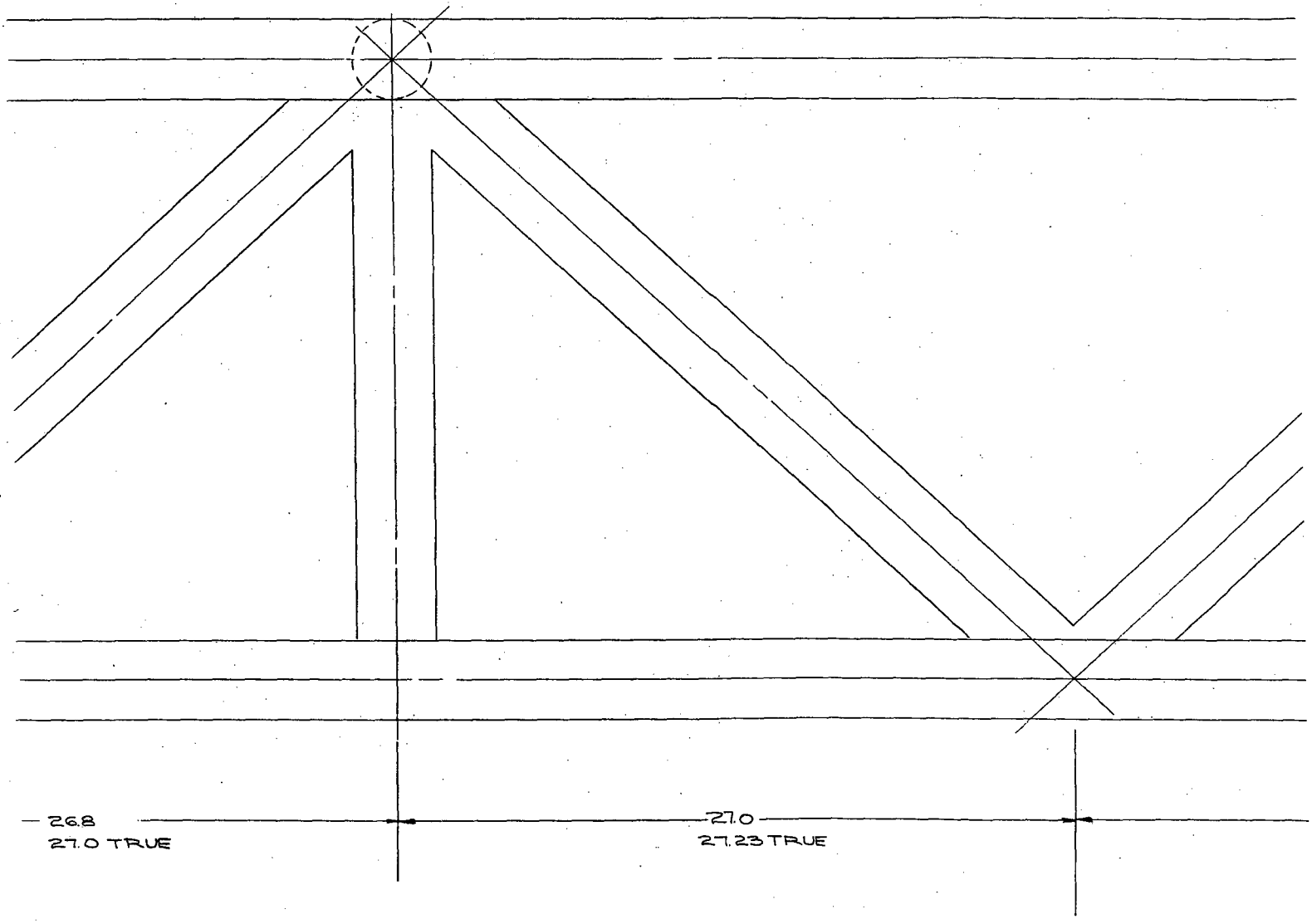
TITLE
FIRING TOOL-GLASROCK
FULL MOSAIC RADOME

NEXT ASSEMBLY

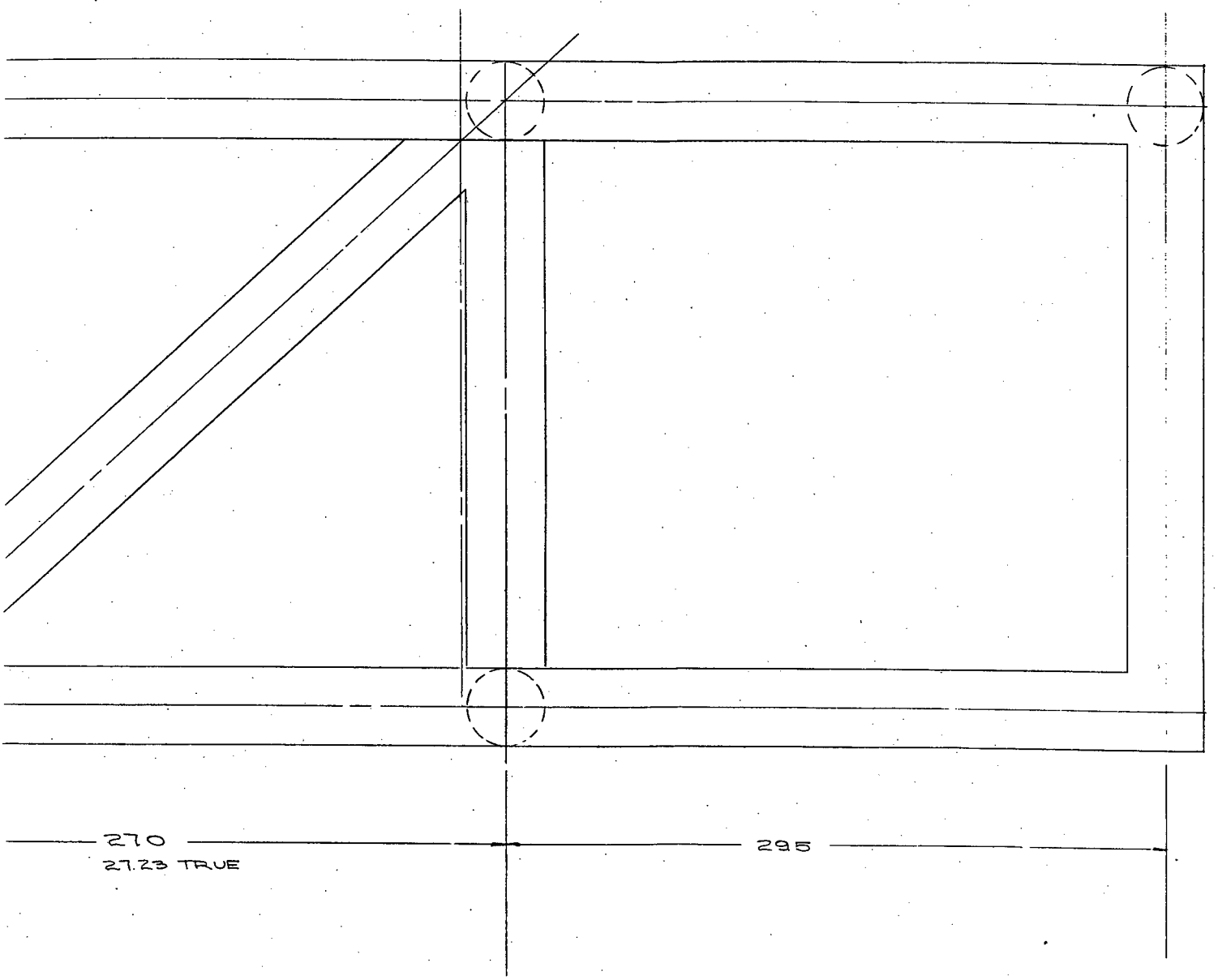
NR063

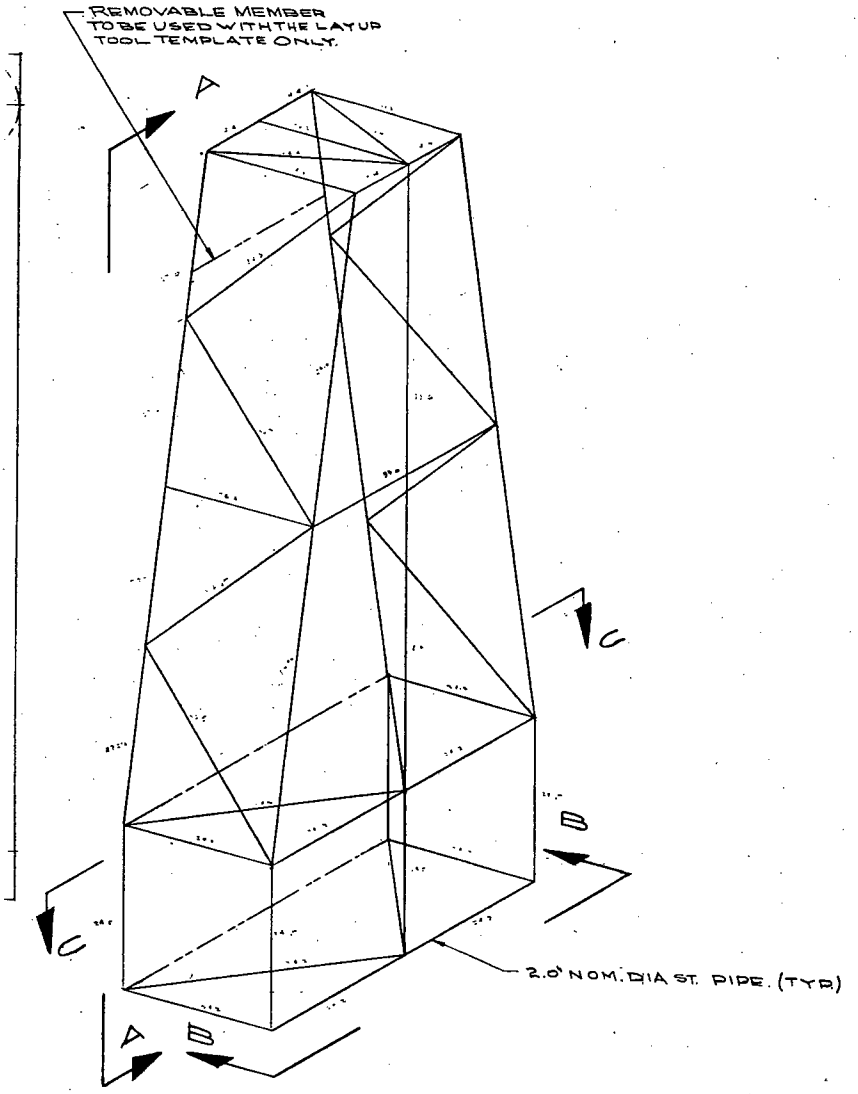
SHEET 3


24.2
26.8
27.0 TRUE
26.8
27.0



VIEW A-A 1/2 SCALE


270
27.23 TRUE
295



REQUIREMENTS PER ASSEMBLY	DWG. NO.	OPP	SHN	-9	STANDARD STEEL PIPE 2.0 NOM DIA. X 154.0 LG
		DASH NO.		PART NAME	

MANUFACTURING TOLERANCES ARE UNLESS OTHERWISE NOTED
FRACTIONS ± .031
DECIMALS .XX ± .030
.XXX ± .005
ANGLES ± 1/2 DEG
√ ALL MACHINED SURFACES 63 AS NOTED REF MIL STD 10

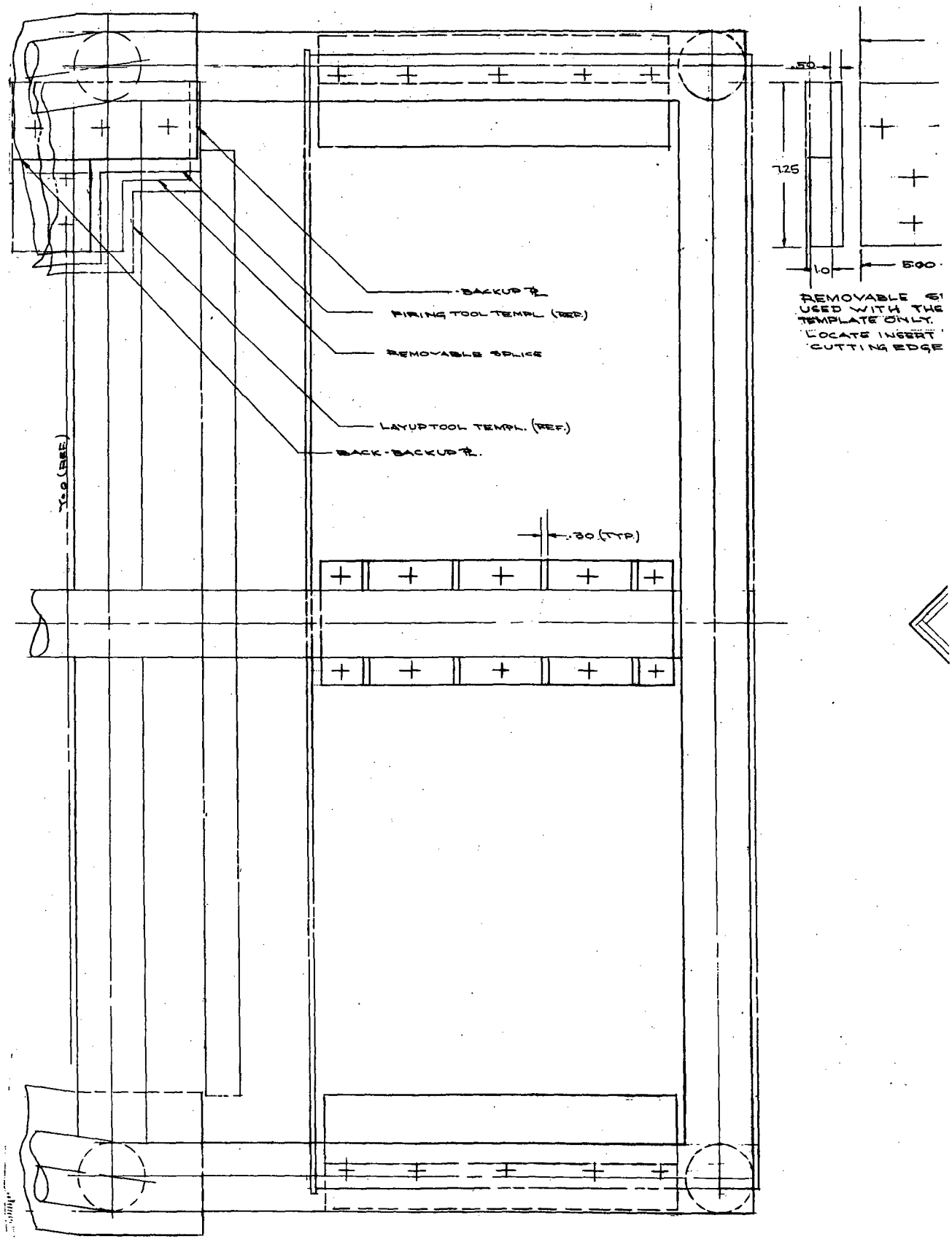
HEAT TREAT
FINISH
TITLE: SUPPT. STRUCT. - RADOME TEMPL.

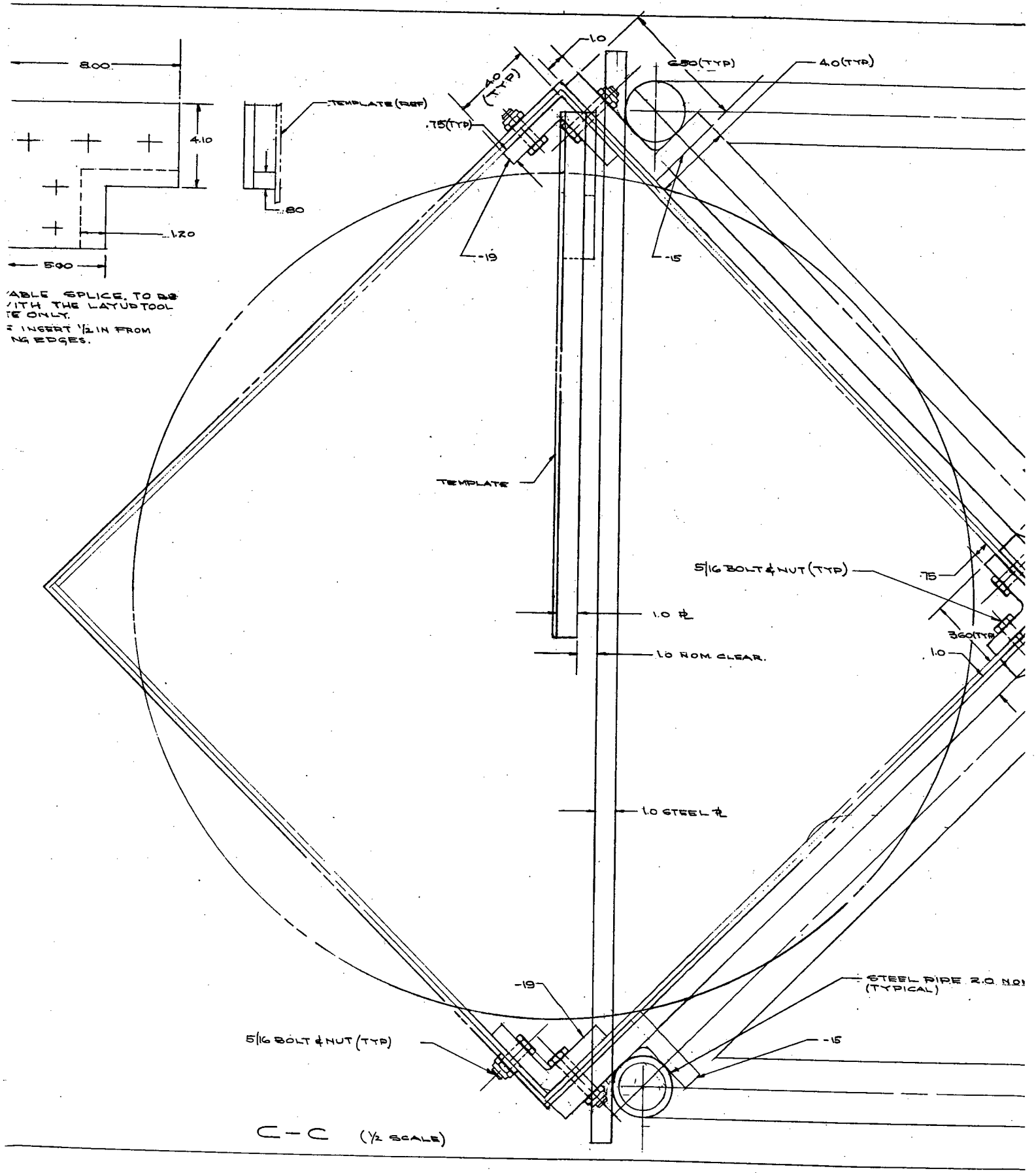
STRESS Holwell 11/16/64
PROCESS
TOOLING R.J. 1-4-65 I.V. 1-6-65
CHECK LR 1-6-65
METHOD
ENGINEER [illegible] 1-6-65
[illegible] 1-6-65

THIS DWG. DASH NO. | NEXT ASSEMBLY | No Reqd

Whittaker CORPORATION
NARMCO RESEARCH & DEVELOPMENT DIVISION
3540 Aero Court
San Diego, California 92123

SCALE HALF | DO 339-109
DWG NO NRG3-152 | N/C
SIZE D | SHEET 1 OF 3 | CHANGE LETTER

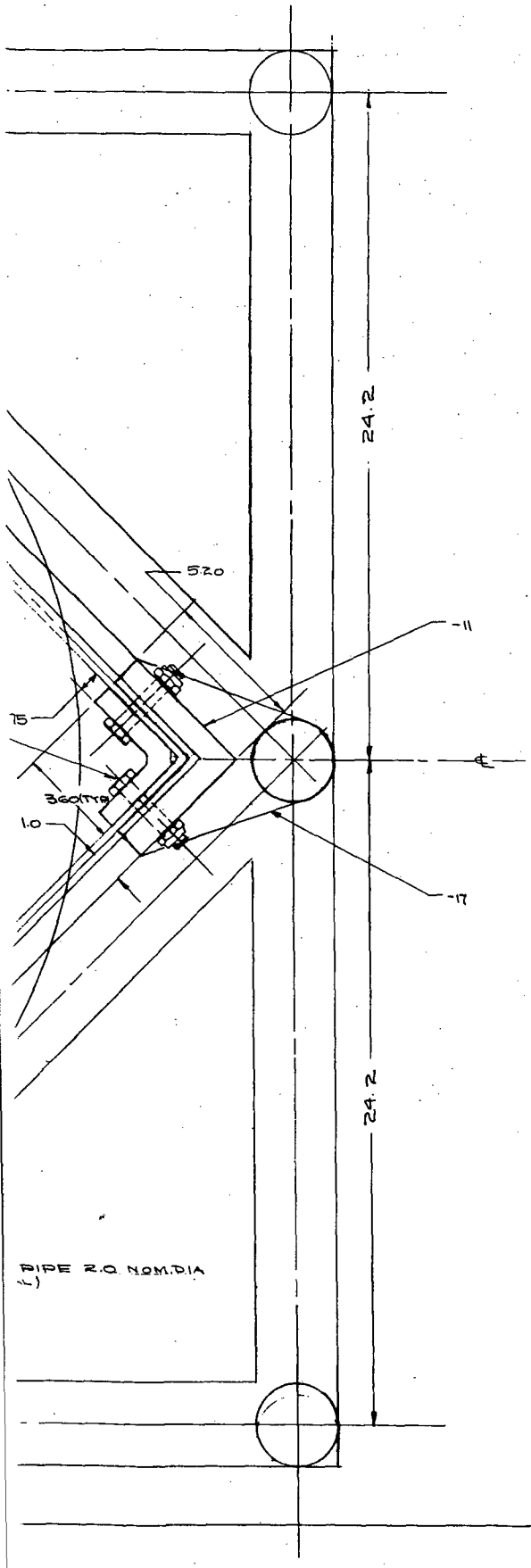

.50
7.25
1.0
5.00
REMOVABLE S
USED WITH THE
TEMPLATE ONLY.
LOCATE INSERT
CUTTING EDGE
BACKUP ℄
FIRING TOOL TEMPL. (REF.)
REMOVABLE SPLICE
LAYUP TOOL TEMPL. (REF.)
BACK-BACKUP ℄
.30 (TYP.)



ABLE SPLICE. TO BE
ITH THE LATUDTOOL
E ONLY.
= INSERT 1/2 IN FROM
NG EDGES.

C-C (1/2 SCALE)

CHG	REVISION	BY



FOR COUNTERCLOCKWISE ROTATION INSTALL BACK-UP PLATES & TEMPLATE OPPOSITE AS SHOWN.

REQUIREMENTS PER ASSEMBLY	DWG. NO.	DASH NO.	PART NAME	MATERIAL
2		-19	FITTING	STEEL 4.0 x 4.0 x 15.5
4		-17	WEB	STEEL .30 x 7.0 x 8.0
2		-15	FITTING	STEEL 4.0 x 6.5 x 15.5
1		-13	FITTING	STEEL 5.6 x 5.6 x 15.5
1		-11	FITTING	STEEL 6.2 x 5.2 x 15.5

MANUFACTURING TOLERANCES ARE UNLESS OTHERWISE NOTED: FRACTIONS ± .031, DECIMALS .X ± .100, .XX ± .030, ANGLES ± 1/2 DEG. ✓ ALL MACHINED SURFACES & AS NOTED EXP MAX 32

MFG'S INSP: [illegible] 1-6-65

VENDOR: [illegible] 1/4/65

PROJECT:

TOOLING: [illegible]

CHECK: [illegible]

STRESS: [illegible]

WELD: [illegible]

PURCH: [illegible]

DRAFTING: [illegible] 1-6-65

MFG'S INSP: [illegible] 1-6-65

FINISH:

THIS DWG DASH NO | NEXT ASSEMBLY | NO. REQ'D

TITLE: SUPPORT STRUCT.- RADOME TEMPLATE

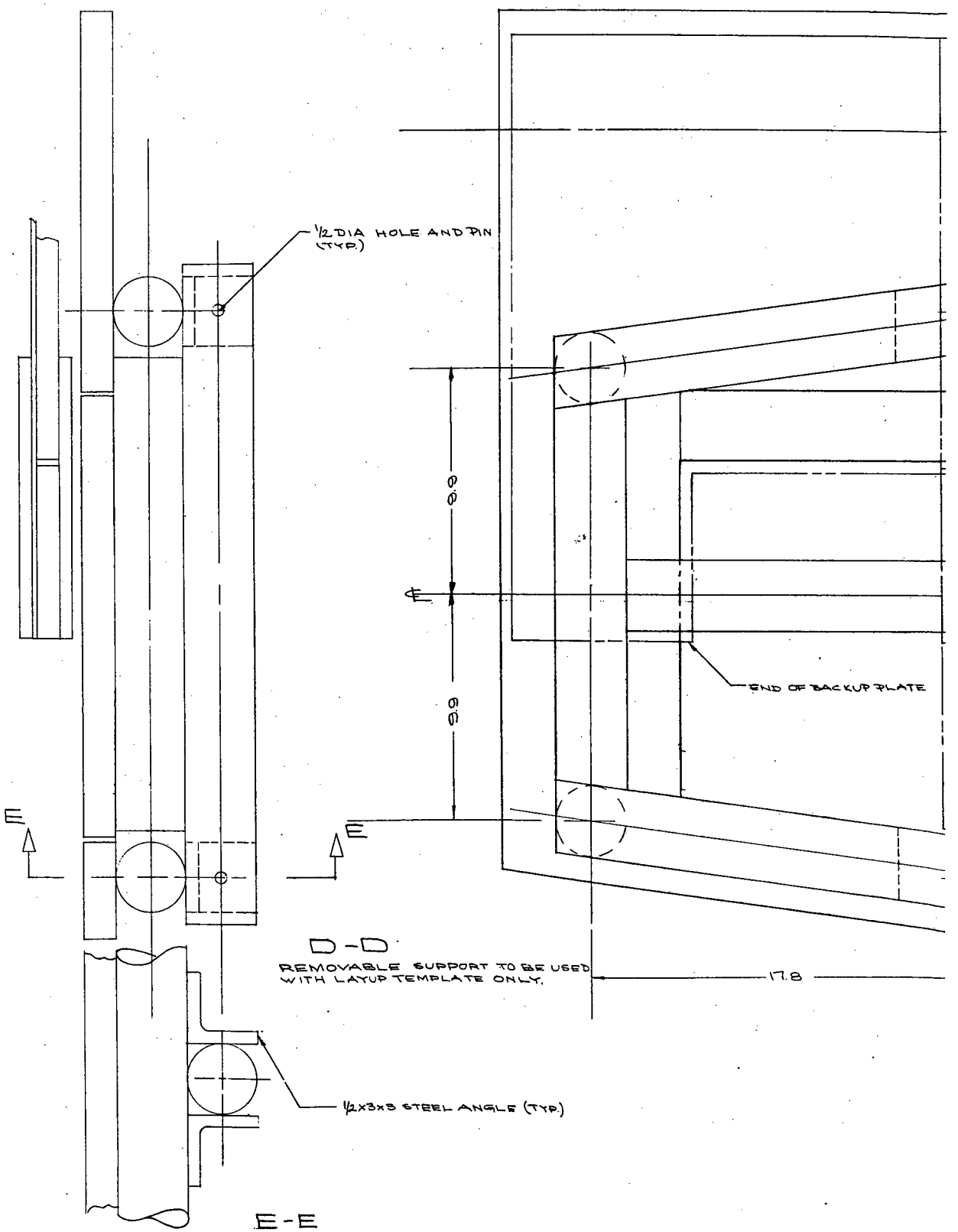
Whittaker Corporation
HARMCO
RESEARCH & DEVELOPMENT DIVISION
3840 Aero Court
San Diego, California 92123

SCALE: HALF | M.S. 339-108

SIZE: D | DWG NO: NR63-152

SHEET 2 OF 3

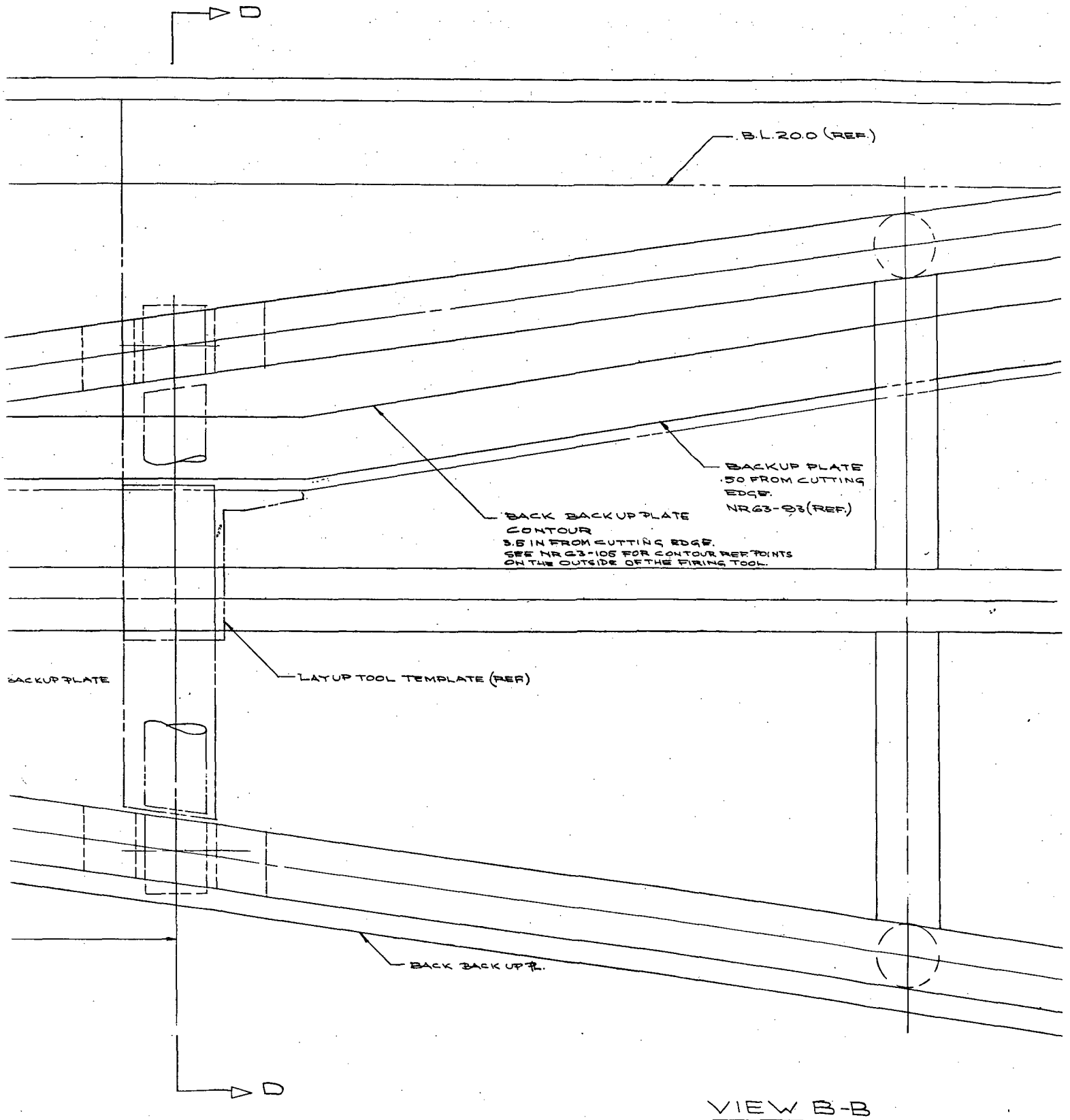
CHANGE LETTER



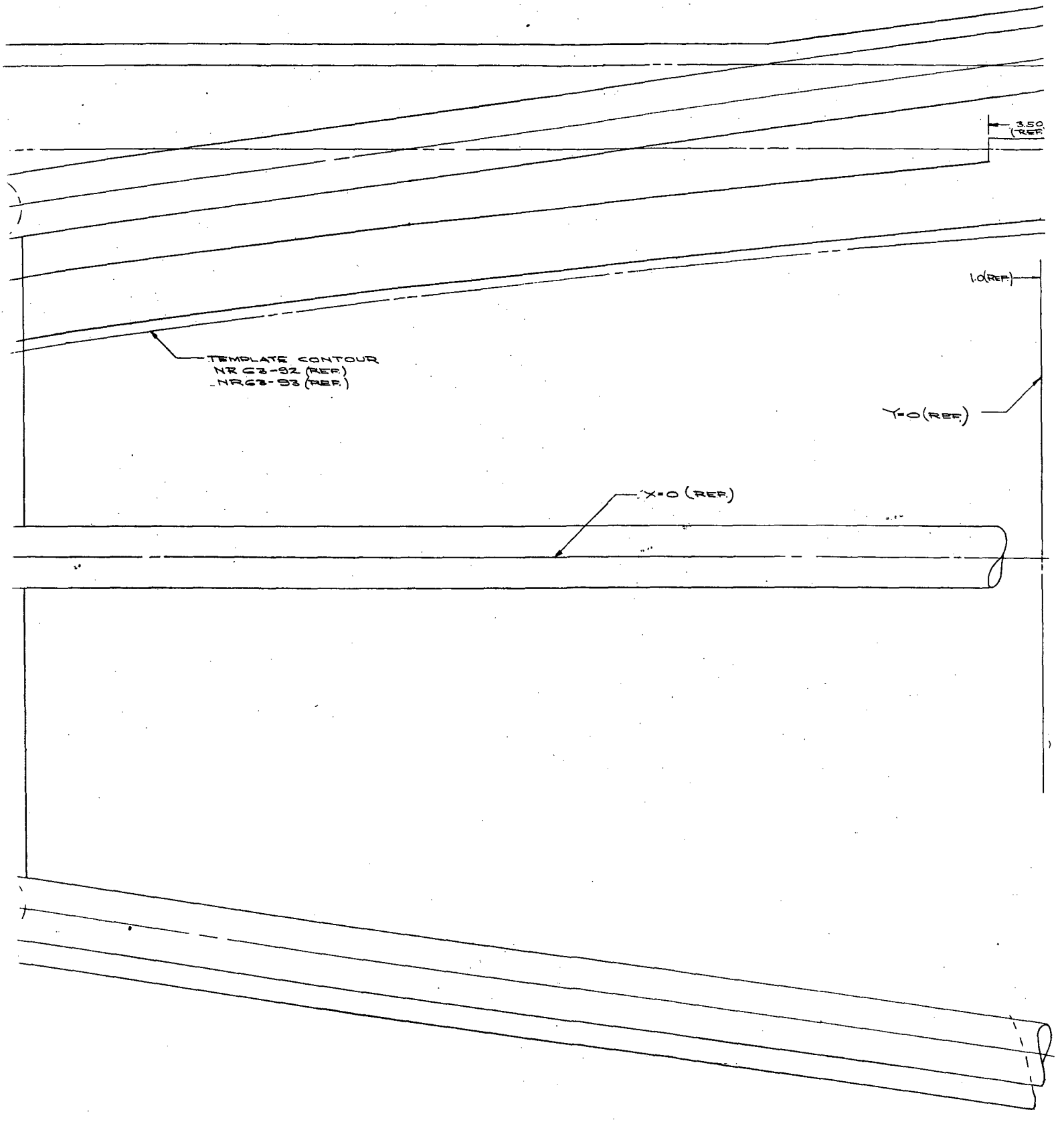
D-D

REMOVABLE SUPPORT TO BE USED WITH LAYUP TEMPLATE ONLY.

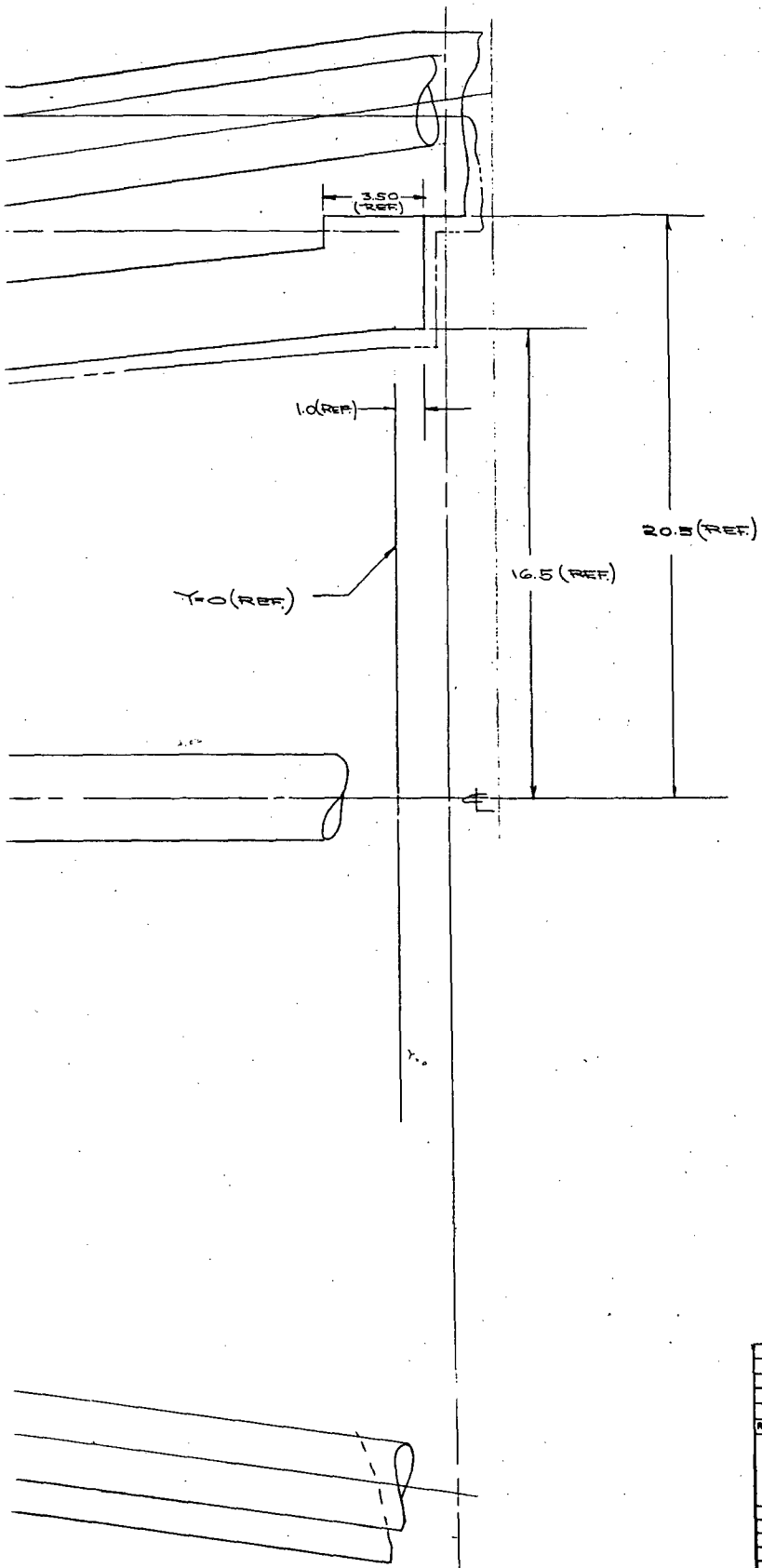
E-E


D
B.L. 20.0 (REF.)
BACKUP PLATE
.50 FROM CUTTING
EDGE.
NR63-93 (REF.)
BACK BACKUP PLATE
CONTOUR
3.5 IN FROM CUTTING EDGE.
SEE NR63-105 FOR CONTOUR REF. POINTS
ON THE OUTSIDE OF THE FIRING TOOL.
BACKUP PLATE
LAYUP TOOL TEMPLATE (REF)
BACK BACK UP PL.
D

VIEW B-B


3.50
(REF.)
1.0(REF.)
TEMPLATE CONTOUR
NRC 3-92 (REF.)
NRC 3-93 (REF.)
Y=0(REF.)
X=0 (REF.)

CHG	REVISION	BY



REQUIREMENTS PER ASSEMBLY	DWG. NO.	DASH NO.	PART NAME
4		-21	ANGLE
-1		OPP SHN	

STEEL ½ x 3.0 x 3.0 x 4.0 LONG

MANUFACTURING TOLERANCES ARE UNLESS OTHERWISE NOTED: FRACTIONS ± .01; DECIMALS .XX ± .005, .XXX ± .003; ANGLES ± ½ DEG. ✓ ALL MACHINED SURFACES TO BE AS NOTED AND MAY BE

NEXT ASSY

FINISH

DRAWN K. Fisher 1/16/67

TRACED [illegible] 1-16-67

CHKD L.L. Gonzalez 1-16-67

ENGR'G [illegible] 1-16-67

APPD [illegible] 1-16-67

Whittaker Corporation
NARMCO
RESEARCH & DEVELOPMENT
DIVISION
3540 Aero Court
San Diego, California 92123

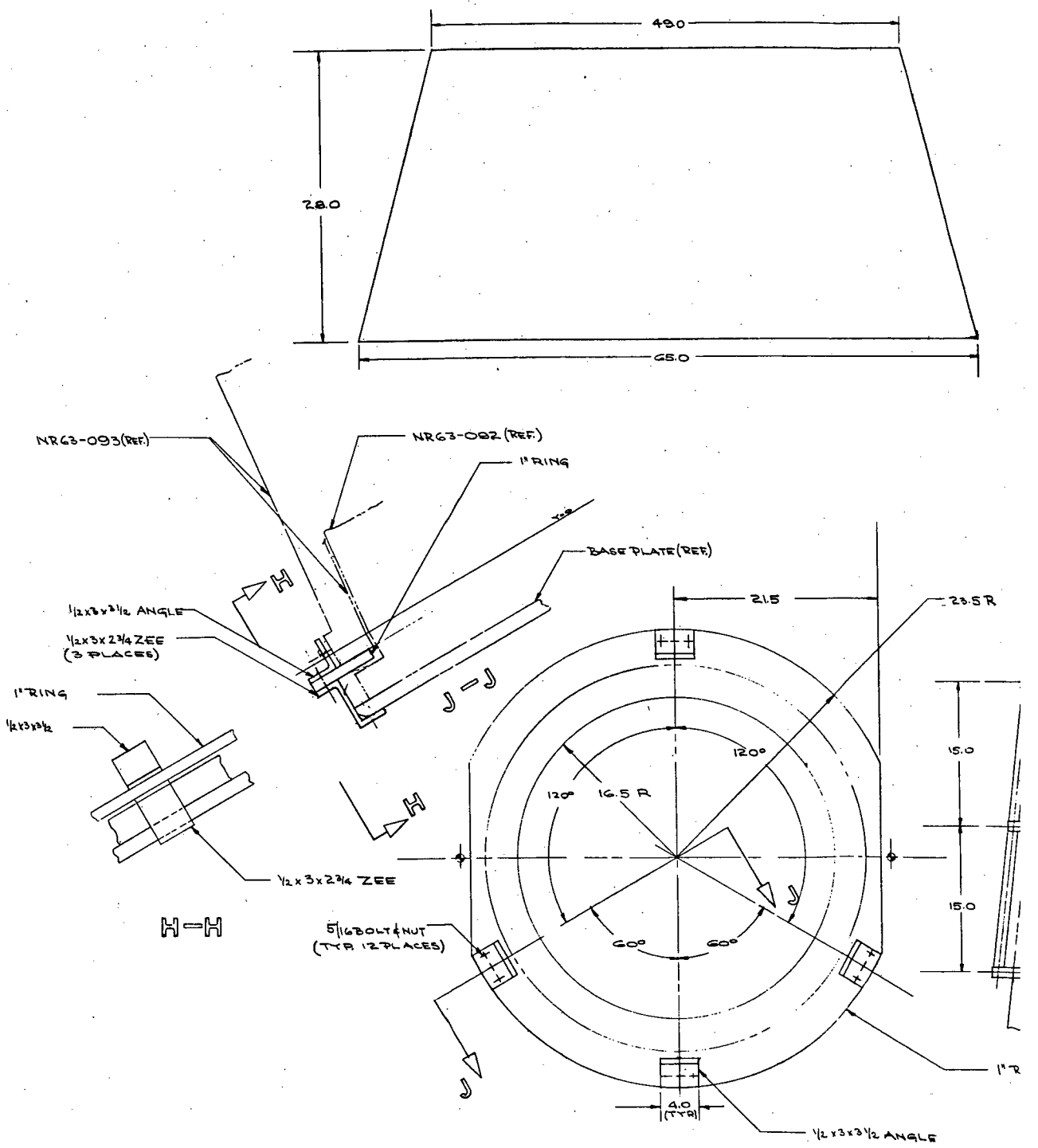
TITLE
SUPPORT STRUCT.
RADOME TEMPL.

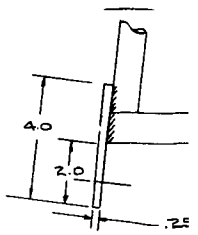
SCALE HALF W.O. 338-10B

DWG NO. NRG3-152

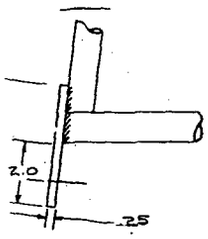
SIZE B SHEET 3 OF 3

THIS WAS DRAWN ON | NEXT ASSEMBLY | NO. REQ'D | CHANGE LETTER

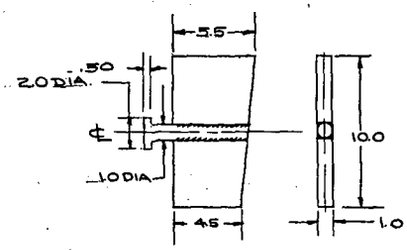

480
280
650
NRG3-093(REF.)
NRG3-082 (REF.)
1" RING
BASE PLATE(REF.)
1/2x3x3 1/2 ANGLE
1/2x3x2 3/4 ZEE
(3 PLACES)
H
J-J
1" RING
1/2x3x3 1/2
H-H
1/2 x 3x2 3/4 ZEE
5/16 BOLT & NUT
(TYP 12 PLACES)
21.5
23.5 R
120°
120°
16.5 R
15.0
15.0
60°
60°
J
J
4.0
(TYP)
1/2 x 3 x 3 1/2 ANGLE
1" R
C C



DETAIL I
1/2 SCALE

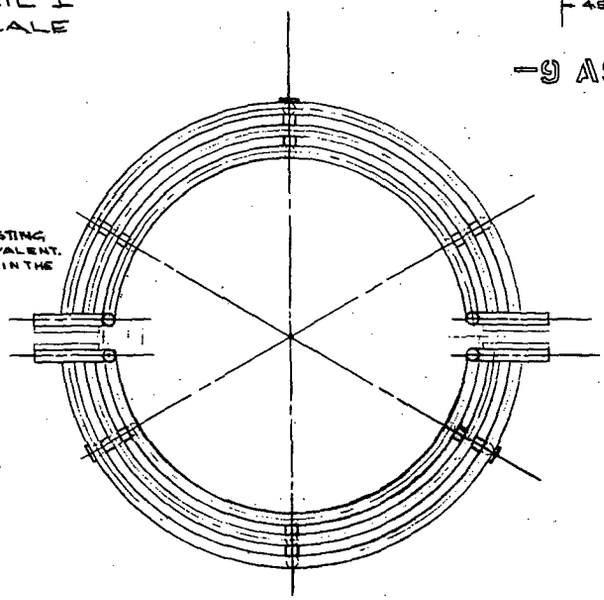


:TAIL I
2 SCALE

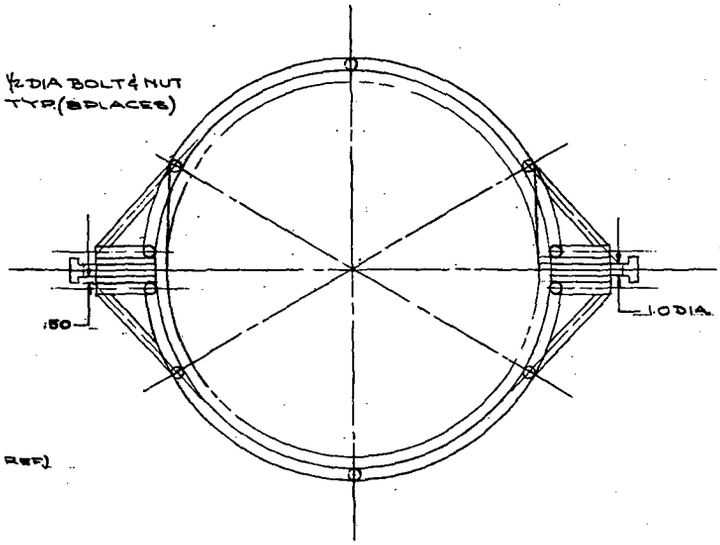


-9 ASSY

RD HOISTING
REQUIVALENT.
VINGS IN THE



A - A



REF)

B—B

REQUIREMENTS PER ASSEMBLY	DWG. NO.	OPP	SHN	PART NAME
3				WIRE ROPE 7/16 DIA STANDARD
3				TURNBUCKLE 1/2 DIA. STEEL
3				WIRE ROPE 7/16 DIA STANDARD
1				CANVAS BELT
3				ZEE SECTION 1/2 x 3 x 2 3/4 STEEL 12.0 LONG
3				ANGLE 1/2 x 3 x 3 STEEL x 12.0" LONG
3				ANGLE 1/2 x 3 x 3 1/2 STEEL x 16.0" LONG
1				TOP-RING 1.0" STEEL PLATE 16.5 DIA.
1				BASERING 1.0" STEEL PLATE 47.0 DIA
1		-13		PIPE ASSY. 1¼" DIA STD ST. PIPE 28 FT. LG.
1		-11		PIPE ASSY. 1¼" DIA STD. ST. PIPE 30 FT. LONG
2		-8		WELD ASSY
-1				

MANUFACTURING TOLERANCES ARE UNLESS OTHERWISE NOTED
FRACTIONS ± .031
DECIMALS .XX ± .020
.XXX ± .005
ANGLES ± 1/2°
√ ALL MACHINED SURFACES 63 AS NOTED REF MIL STD
HEAT TREAT
FINISH

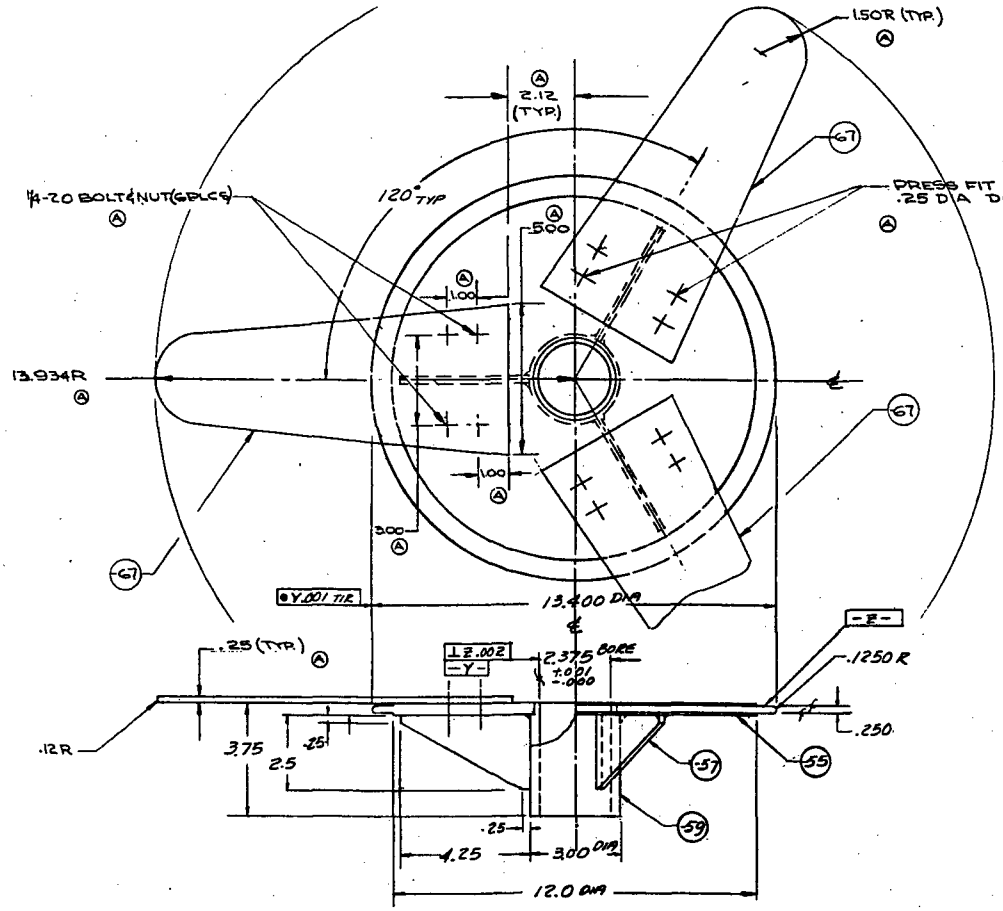
DRAWN [illegible] 5/6
STRESS
CHECKED [illegible]
ENGR [illegible]
PROJECT [illegible]
SUPERV [illegible]

Whittaker CORPORATION
NARMCO
RESEARCH & DEVELOPMENT DIVISION
3540 Aero Court
San Diego, California 92123

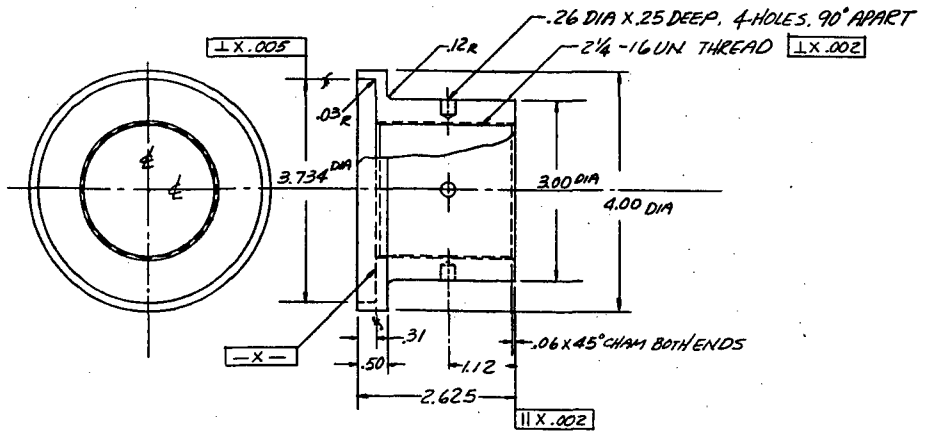
THIS ASSY WAS IN
NEXT ASSEMBLY
NO. REQD

TITLE
HANDLING DEVICE-
RADOME ASSY.

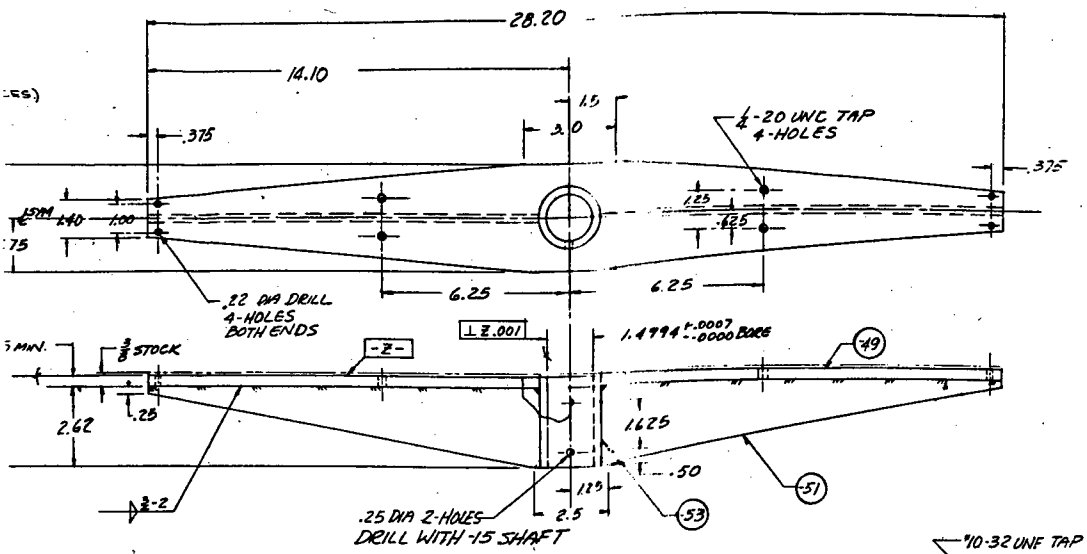
SCALE 1/2" | CONTRACT 338-108
SIZE D | DWG NO NRG3-153
SHEET 1 OF 1



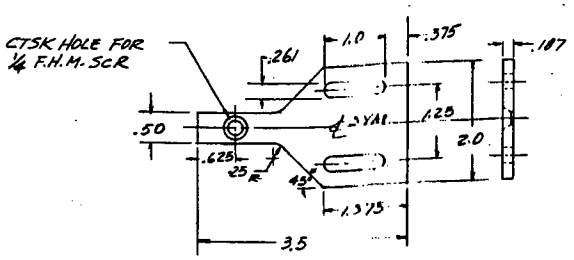
- 7 CENTERING DISC



- 25 ADJ. NUT SCALE: 1/1

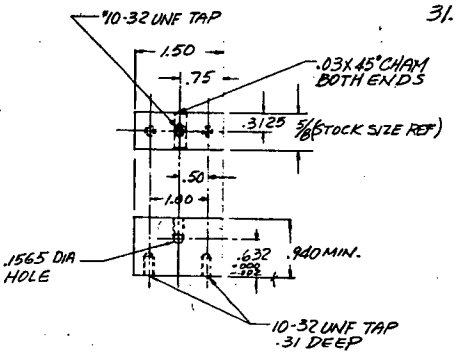


-9 DIAL INDICATOR MOUNTING ARM



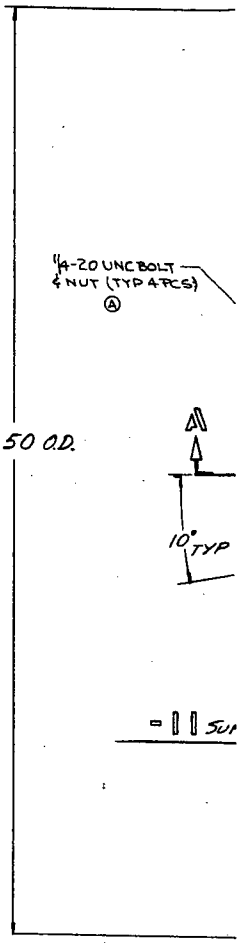
-27 PLATE

SCALE: 1/1

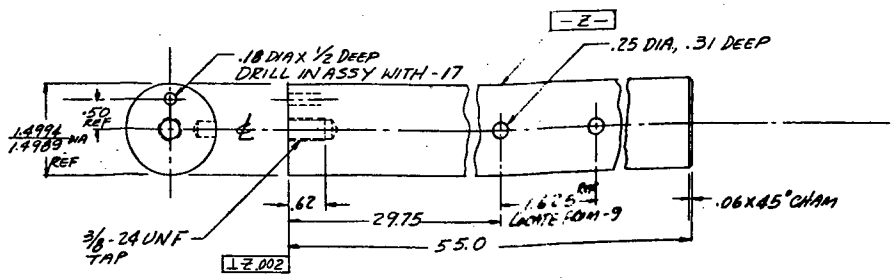


-29 SUPPORT

SCALE: 1/1

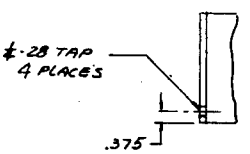


-11 SU

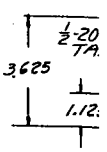


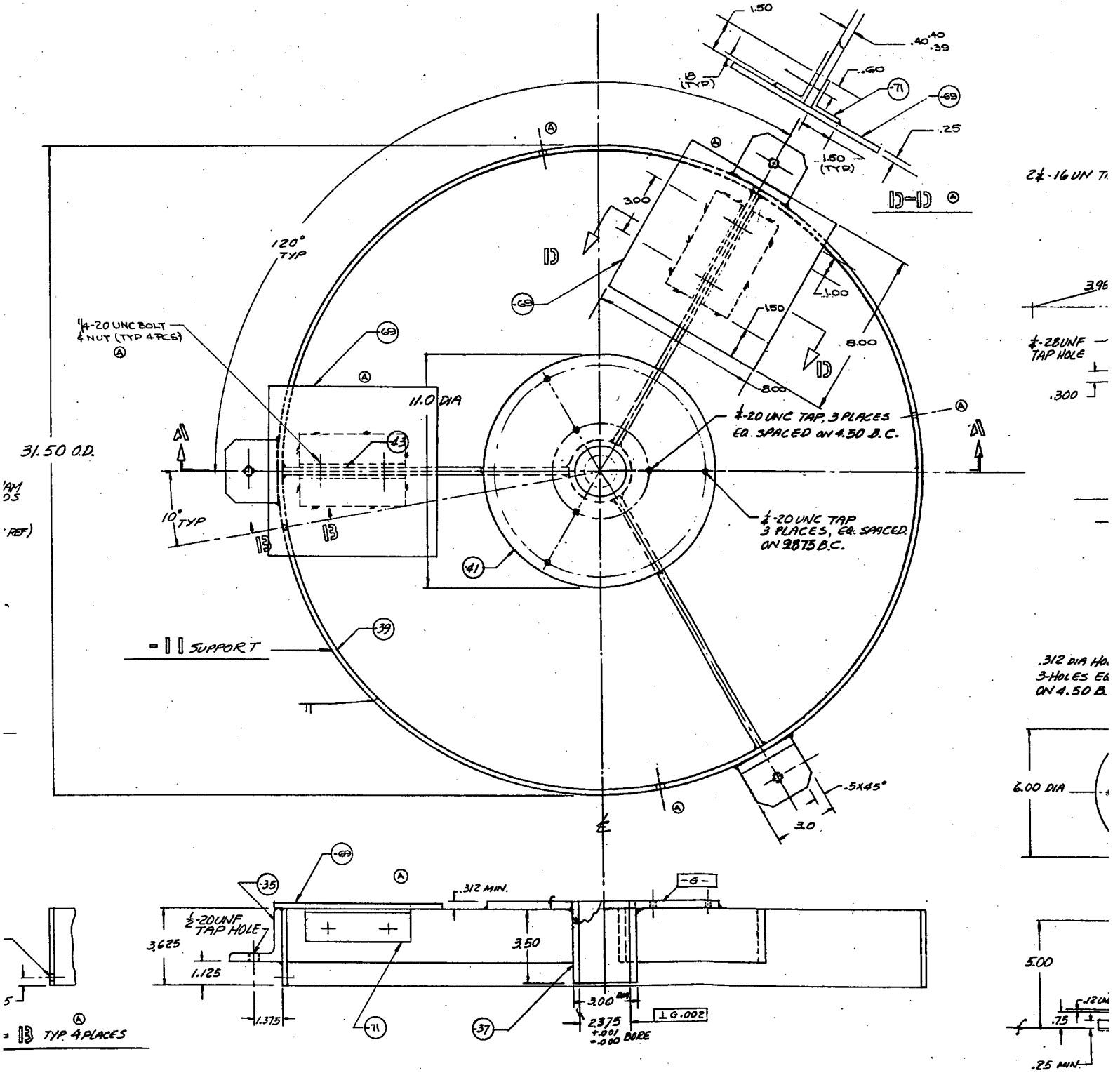
-15 SHAFT SCALE: 1/1

MAKE FROM "THOMPSON IND, INC"
BALL BUSHING SHAFT, CLASS 2"

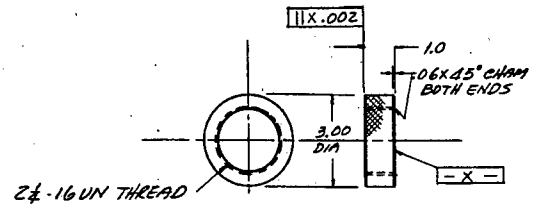


SECTION 13-13 Ⓐ TYP 4 PLACES

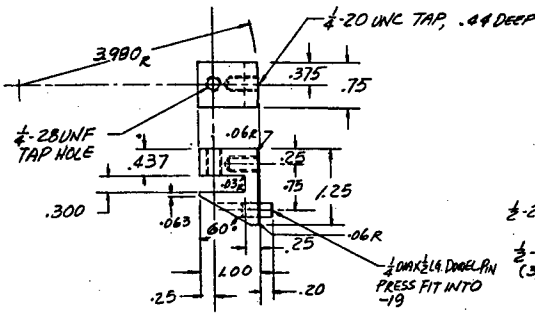



1.50
.40 .39
.60
(71)
(69)
.25
1.50 (TYP)
(13 TYP)
D-D Ⓐ
3.00
120° TYP
(65)
1.00
1.50
8.00
8.00
1/4-20 UNC BOLT & NUT (TYP 4 PCS) Ⓐ
(63)
11.0 DIA
(43)
1/4-20 UNC TAP, 3 PLACES EQ. SPACED ON 4.50 B.C. Ⓐ
31.50 O.D.
10° TYP
1/4-20 UNC TAP 3 PLACES, EQ. SPACED ON 9.875 B.C.
(41)
(39)
= 11 SUPPORT
.5X45°
3.0
(35)
.312 MIN.
-G-
1/2-20UNF TAP HOLE
3.625
1.125
3.50
1.375
(71)
(37)
3.00
2.375 +.001 -.000 BORE
⊥ G.002
= 13 TYP 4 PLACES
2 1/4-16 UN
3.96
1/4-28UNF TAP HOLE
.300
.312 DIA HO
3-HOLES EQ
ON 4.50 B.
6.00 DIA
5.00
.75
.25 MIN

SECTION A-A

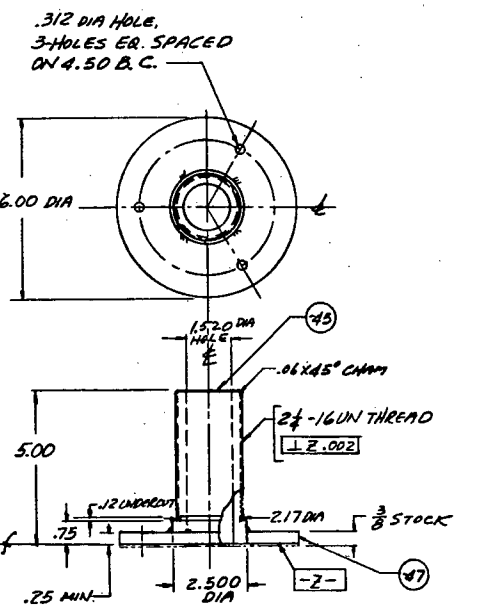


-23 KNURLED NUT

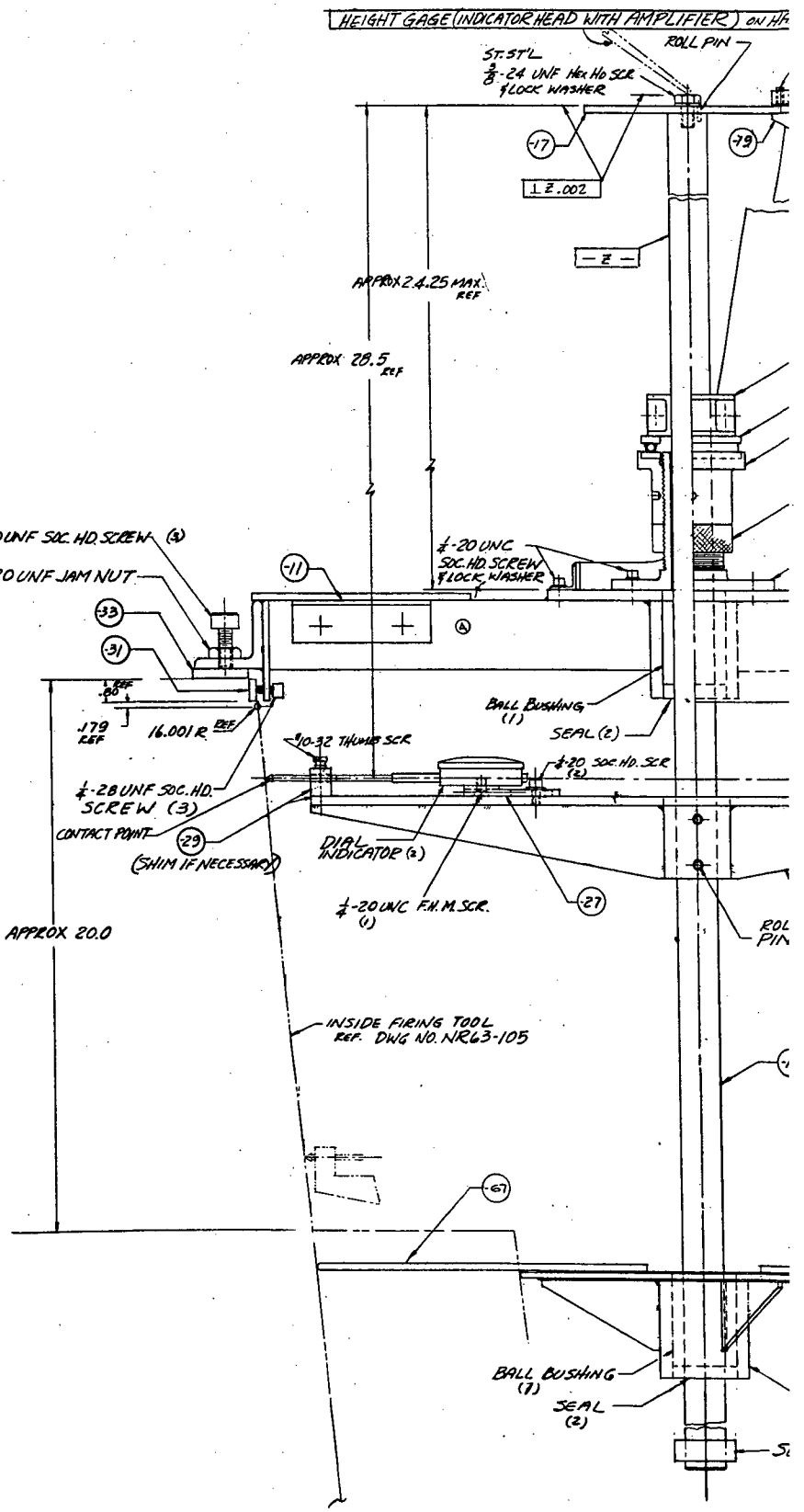


-19 INDEX PLATE CLAMP

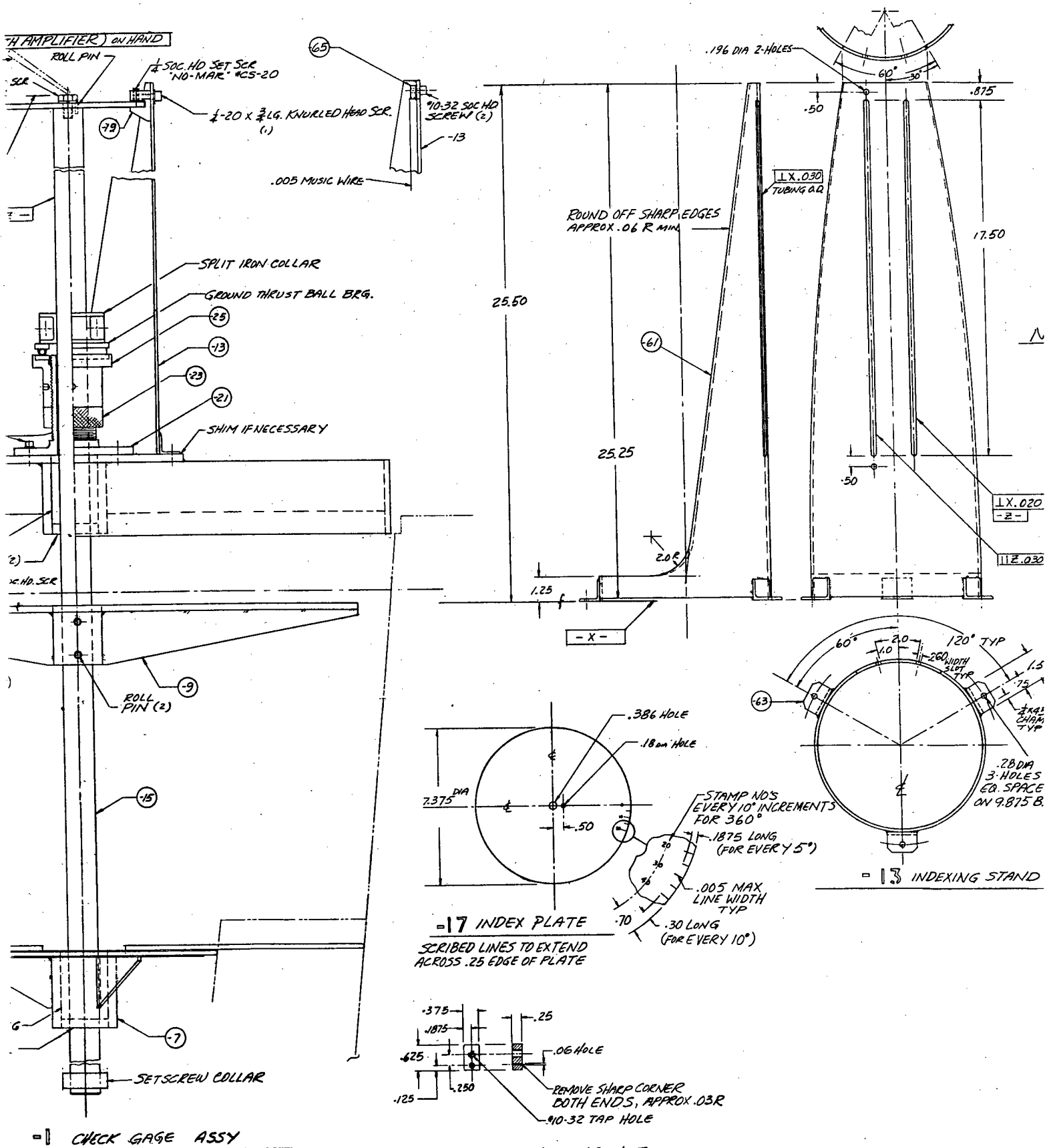
SCALE: 1/1



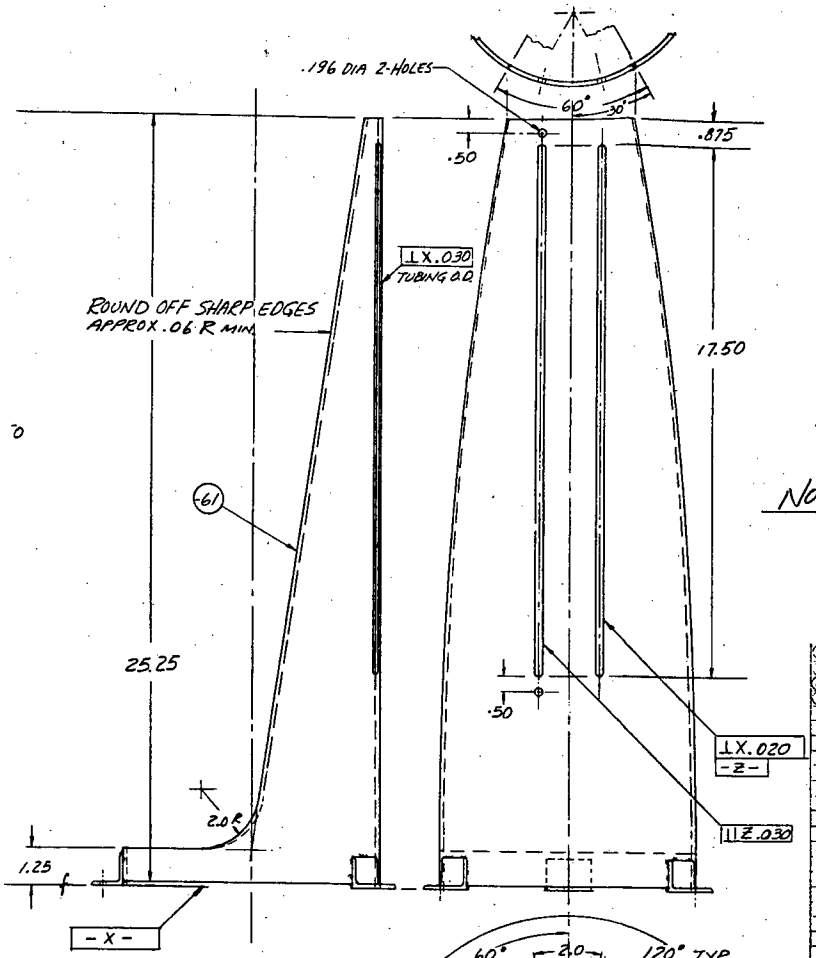
-21 ADJ. SCREW ASSY

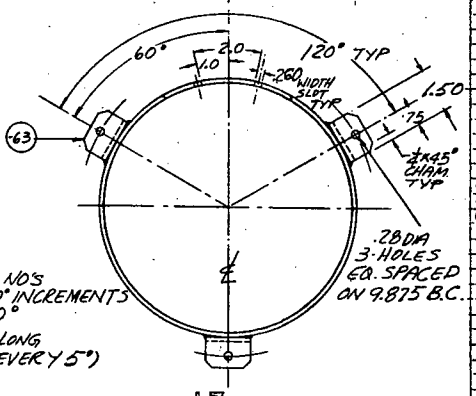


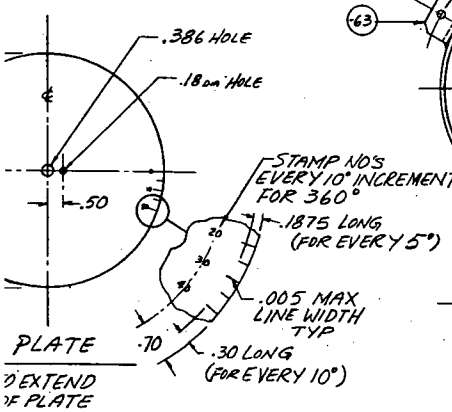
-1 CHECK GI


H AMPLIFIER) on HAND
ROLL PIN
SCR
¼ SOC HD SET SCR "NO-MAR" #CS-20
¼-20 x ¾ LG. KNURLED HEAD SCR. (1)
(79)
(65)
#10-32 SOC HD SCREW (2)
-13
.005 MUSIC WIRE
SPLIT IRON COLLAR
GROUND THRUST BALL BRG.
(25)
(13)
(23)
(21)
SHIM IF NECESSARY
(9)
ROLL PIN (2)
(15)
(7)
SETSCREW COLLAR
-1 CHECK GAGE ASSY
.196 DIA 2-HOLES
60°
30°
.875
.50
1 X.030
TUBING O.D.
ROUND OFF SHARP EDGES APPROX .06 R MIN
17.50
25.50
25.25
(61)
.50
1 X.020
-Z-
11 Z.030
2.0 R
1.25
-X-
.386 HOLE
.188 HOLE
7.375 DIA
.50
STAMP NO'S EVERY 10° INCREMENTS FOR 360°
.1875 LONG (FOR EVERY 5°)
.005 MAX LINE WIDTH TYP
.70
.30 LONG (FOR EVERY 10°)
-17 INDEX PLATE
SCRIBED LINES TO EXTEND ACROSS .25 EDGE OF PLATE
60°
120° TYP
2.0
1.0
.260 WIDTH SLOT TYP
1.5
.75
(63)
.28 DIA 3 HOLES EQ. SPACE ON 9.875 B.
-13 INDEXING STAND
.375
.1875
.625
.125
.250
.25
.06 HOLE
REMOVE SHARP CORNER BOTH ENDS, APPROX .03 R
#10-32 TAP HOLE
-65 WIRE HOLDING NUT
SCALE: 1/1

CHG	REVISION	BY	
A	ADDED LOCATING SCREW KT CENTERING DISK EXTENDED 2 PLATFORMS PROVIDED ADDED -67, 69, -71		1/14/64







PLATE

D EXTEND
F PLATE

-.25

.06 HOLE

REMOVE SHARP CORNER BOTH ENDS, APPROX .03R

#10-32 TAP HOLE

HOLDING NUT

1/1

= 13 INDEXING STAND

3. THIS GAGE SHALL BE PACKAGED IN A WOODEN REUSABLE DISTORTION FREE CONTAINER WITH A HINGED DUST PROOF COVER.

2. ALL METALLIC PARTS SHALL BE STEAM CLEANED AND FLUSHED WITH TRICHLORETHYLENE AFTER WELDING AND MACHINING.

1. ALL WELDED PARTS TO BE CONTINUOUSLY WELDED BY THE HELIARC PROCESS, UNLESS OTHERWISE NOTED.

NOTE:

DASH NO.	OPP SHN	PART NAME	REQUIREMENTS PER ASSEMBLY
		NUT 1/4-20 UNC	
		BOLT 1/4-20 UNC x 1 1/4 LG	
		NUT 1/4-20 UNC	
		BOLT 1/4-20 UNC x 1.0 LG	
		1. DOWEL PIN 1/4 DIA x 1/2 LG	
		2. DIAL INDICATOR "STARRETT" NO. 655-2041, WITH 2 3/8 ROD LENGTH ADDED TO STD LENGTH & ADJUSTABLE BRKT.	
		1/2 CONTACT POINT "7.8 #10 CONTACT POINT FOR DIAL INDICATOR (ABO 11-8)	
		JAM NUT 1/2-20 UNF JAM NUT, ST. ST'L	3
		SCREW 1/2-20 UNF SOC HD SCR x 1 1/2 LG., ST. ST'L	3
		SCREW 1/4-28 SOC. HD. SCR, 3/4 LG. SS ST'L	4
		SEAL "THOMPSON IND. INC." #S-1500	2
		BALL BUSHING "THOMPSON INDUSTRIES INC" #XA-243868, 1 1/2 BORE	2
		2. SPLIT COLLAR SPLIT COLLAR FOR 1 1/2 DIA SHAFT "DODGE MFG. CORP" #SC-24 EQUIV.	
		1. COLLAR SET SCREW COLLAR FOR 1 1/2 DIA SHAFT	
		2. THUMB SCREW #10-32 x 3/4 LG.	
		2. SCREW 1/4-20 UNC FLAT HD M. SCR, 1/2 LG.	
		4. PLAIN WASHER FOR 1/4 SCREW	
		2. ROLL PIN 1/4 DIA x 1/2 LG	
		6. LOCK WASHER FOR 1/4 SCREW	
		10. SCREW 1/4-20 UNC SOC HD SCR 3/4 LG.	
		1. LOCK WASHER FOR 3/8 SCR.	
		1. SCREW 3/8-24 UNF HEX HD CAP SCR. ST. ST'L	
		1. SET SCREW 1/4-28 UNF "HD-HAR" SET SCREW #CS-20 OR EQUIV.	
		1. SCREW #8-20 UNC x 1/4 KNURLED HEAD SCREW	
		2. SCREW #10-32 SOC HD SCR. 9/16 LG.	
		1. ROLL PIN 3/16 DIA x 1/2 LG.	
		√ MUSIC WIRE .005" WIRE x 2" LG	
		1. THRUST BRG 2 1/4 I.D. x 3 3/32 O.D. "BOSTON GEAR" #1029 OR EQUIV.	
		-71 3/16 x 1.6 x 1.6 ANGLE x 5.0 LG.	4
		-69 4 x 8.0 x 8.0 #304 S. ST'L PLATE	2
		-67 4 x 5.0 x 17.0 #304 S. ST'L PLATE	3
		-65 NUT MAKE FROM 1/4 x .375 x .625 S.ST'L PLATE	2
		-63 ANGLE 1.0 x 1.0 x 1/4 x 1.5 LG. #304 S.ST'L	3
		-61 TUBING 8.625 O.D. x .322 WALL x 28.5 LG. #304 S.ST.	1
		-59 TUBING 3.00 O.D. x 2.00 I.D. x 2.0 LG #304 S.ST'L	1
		-57 PLATE 1/4 x 2.5 x 4.3 LG. #304 S.ST'L PLATE	3
		-55 PLATE 3/8 x 14.0 DIA #304 S. ST'L PLATE	1
		-53 TUBING 2.00 O.D. x 1.25 I.D. x 3.0 LG. #304 S.ST'L TUBING	1
		-51 PLATE 1/4 x 2.62 x 13.0 LG #304 ST. ST'L PLATE	2
		-49 PLATE 3/8 x 3.50 x 28.5 LG #304 S.S.T'L PLATE	1
		-47 PLATE 3/4 x 6.3 DIA #304 ST. ST'L PLATE	1
		-45 BAR 2.50 DIA x 5.0 LG #304 S.ST'L ROUND	3
		-43 PLATE 3/8 x 2.5 x 14.0 #304 S. ST'L	1
		-41 PLATE 3/8 x 11.3 DIA #304 S. ST'L	1
		-39 PLATE .250 x 3.625 x 99° LG. TYPE 304 ST. ST'L	1
		-37 TUBING 3.00 O.D. x 2.00 I.D. x 4.0 LG. #304 S.ST'L TUBING	3
		-35 ANGLE 2 1/2 x 2 1/2 x 3/8 x 3.0 LG. #304 S.ST'L ANGLE	3
		-33 PLATE 3/8 x 2.0 SQUARE ST'L PLATE	3
		-31 PLATE 1/4 x 3 1/4 x 1 1/4 ST'L PLATE	2
		-29 BLOCK MAKE FROM 3/8 x 1.0 x 1.50 BRONZE PLATE	2
		-27 PLATE 3/16 THICK x 2.0 x 3.5 304 S.ST'L PLATE	1
		-25 NUT MAKE FROM 4.00 DIA x 3.0 LG #304 ST. ST'L ROUND	1
		-23 JAM NUT MAKE FROM 3.00 DIA x 1.2 LG #304 ST. ST'L ROUND	1
		-21 SCREW ASSY	1
		-19 INDEX PLATE CLAMP. MAKE FROM .75 x 1.00 x 2.25 #304 S.ST'L	1
		-17 INDEX PLATE .250 THICK x 7.375 DIA. TYPE 304 S.ST'L PLATE	1
		-15 SHAFT 1/4 NOMINAL DIA CLASS 2 SHAFT x 55.0 LG. FROM "THOMPSON INDUSTRIES, INC."	1
		-13 INDEXING STAND ASSY	1
		-11 SUPPORT ASSY	1
		-9 DIAL INDICATOR MOUNTING ARM SUB-ASSY	1
		-7 CENTERING DISC ASSY	1
		-5 -3 -1 DWG. NO.	

UNLESS OTHERWISE NOTED TOLERANCES ARE: FRACTIONS ± .031, DECIMALS .XX ± .020, .XXX ± .005, ANGLES ± 1/2° BREAK SHARP EDGES .010 MAX ALL MACHINED SURFACES 125 MAX NOTED REF. WAS 32

MATERIAL — FINISH — NEXT ASSEMBLY — USED ON — NO REQD

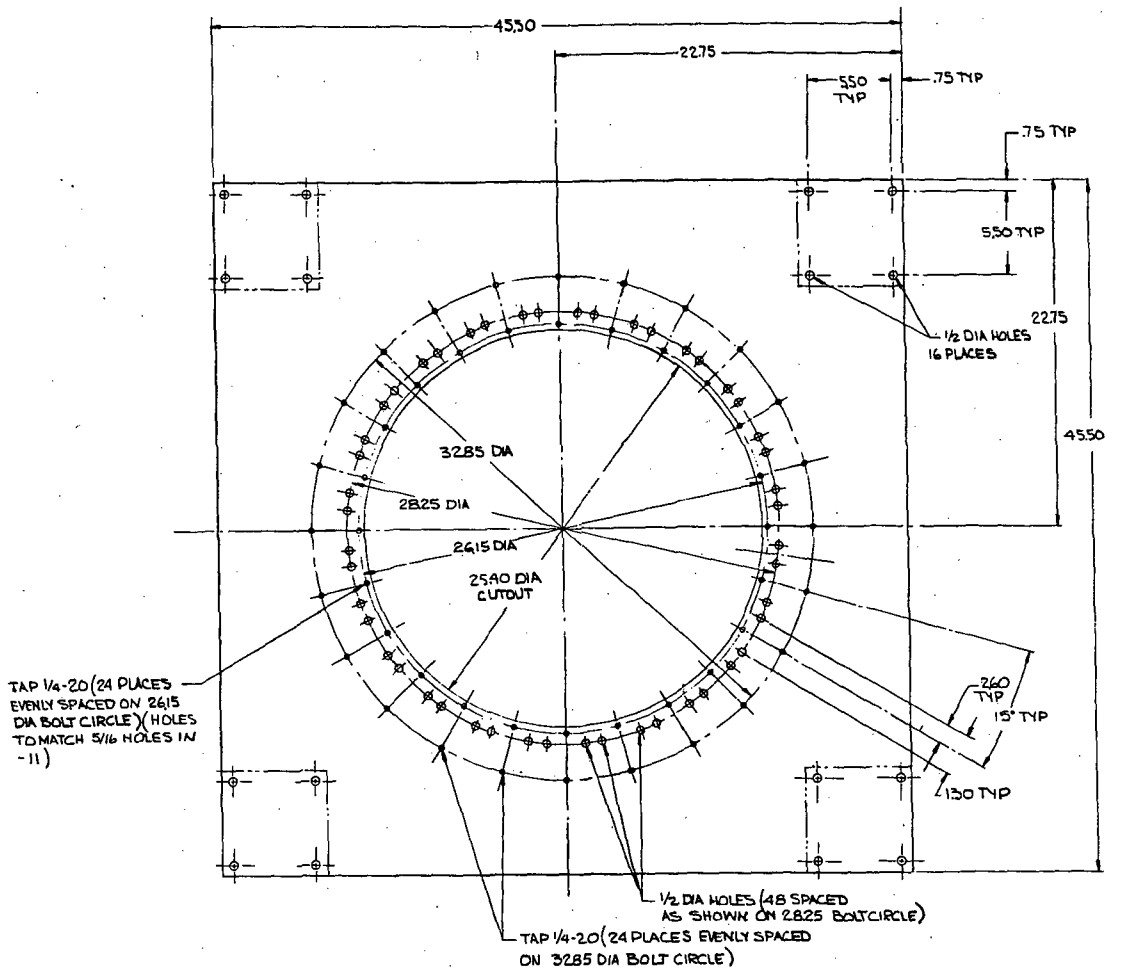
DRAWN BY AG. 1/14/64
STRESS
CHECKED
TOOL ENG.
QUALITY
STRESS
APPROVED
MFG. ENG. 1-18-64

Whittaker CORPORATION
NARMCO RESEARCH & DEVELOPMENT DIVISION
3540 Aero Court
San Diego, California 92123

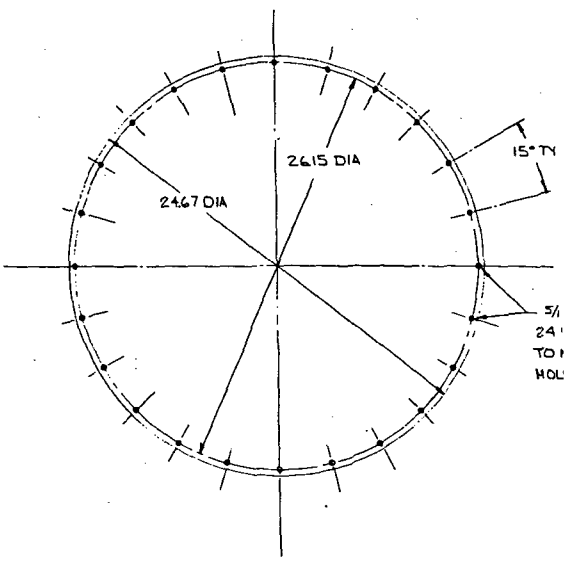
TITLE
CHECK GAGE FOR FIRING TOOL - MOSAIC RADOME

SCALE HALF SIZE — WEIGHT — LBS. — W.O. 538-111

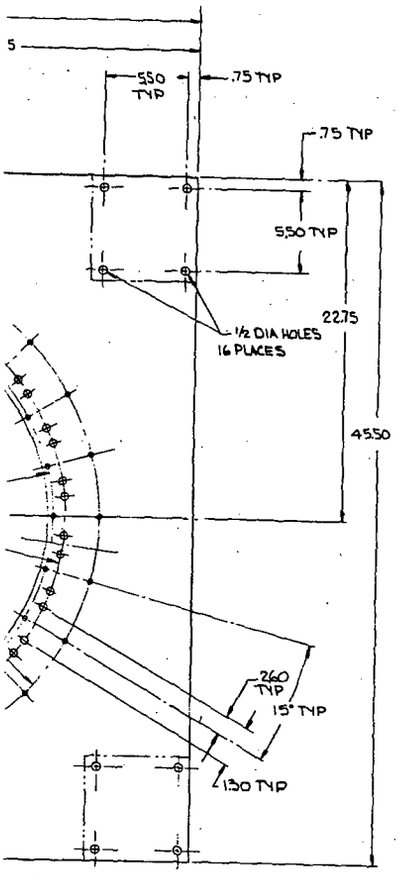
SIZE R — DWG. NO. NR63-157 — CHANGE LETTER A — SHEET 1 OF 1



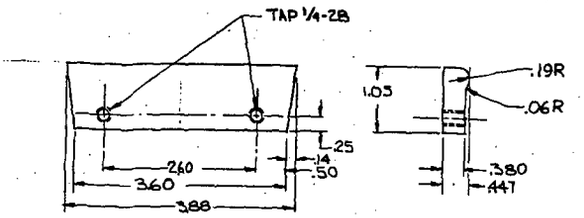
DETAIL - 7 BASE
SCALE 1/4



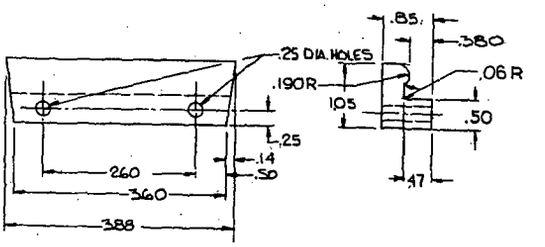
DETAIL - 9 COVER
SCALE 1/4



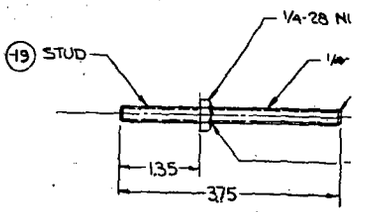
LES (48 SPACED
WN ON 28.25 BOLTCIRCLE)
VLY SPACED
)



DETAIL = 15 SUPPORT
SCALE 1/1

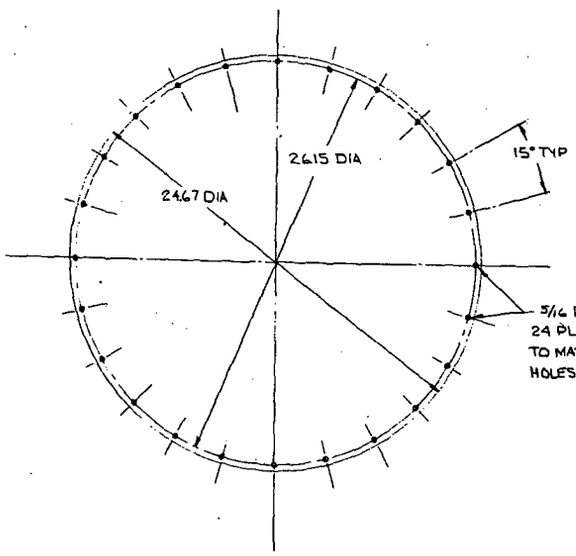


DETAIL = 17 SUPPORT
SCALE 1/1

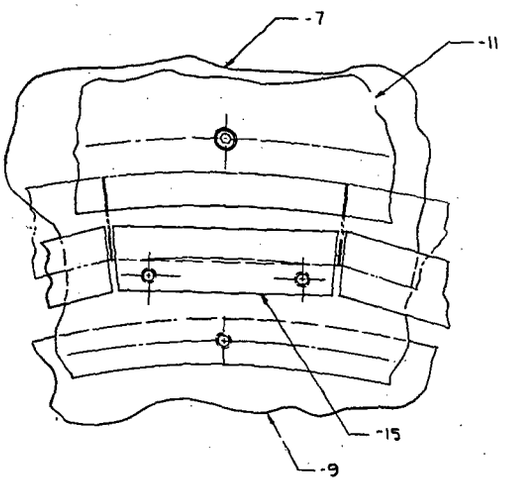


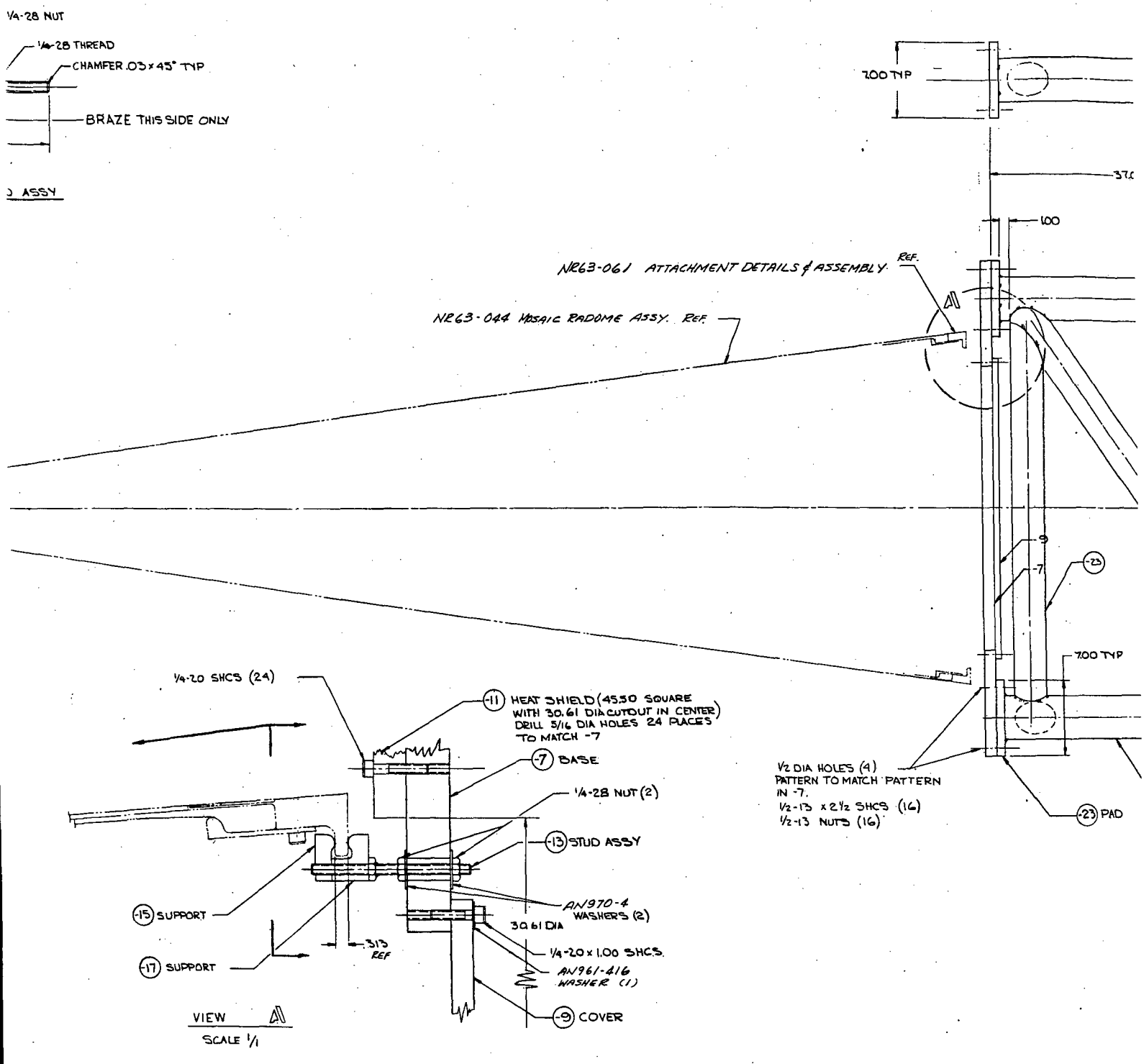
DETAIL = 13 STUD ASSY

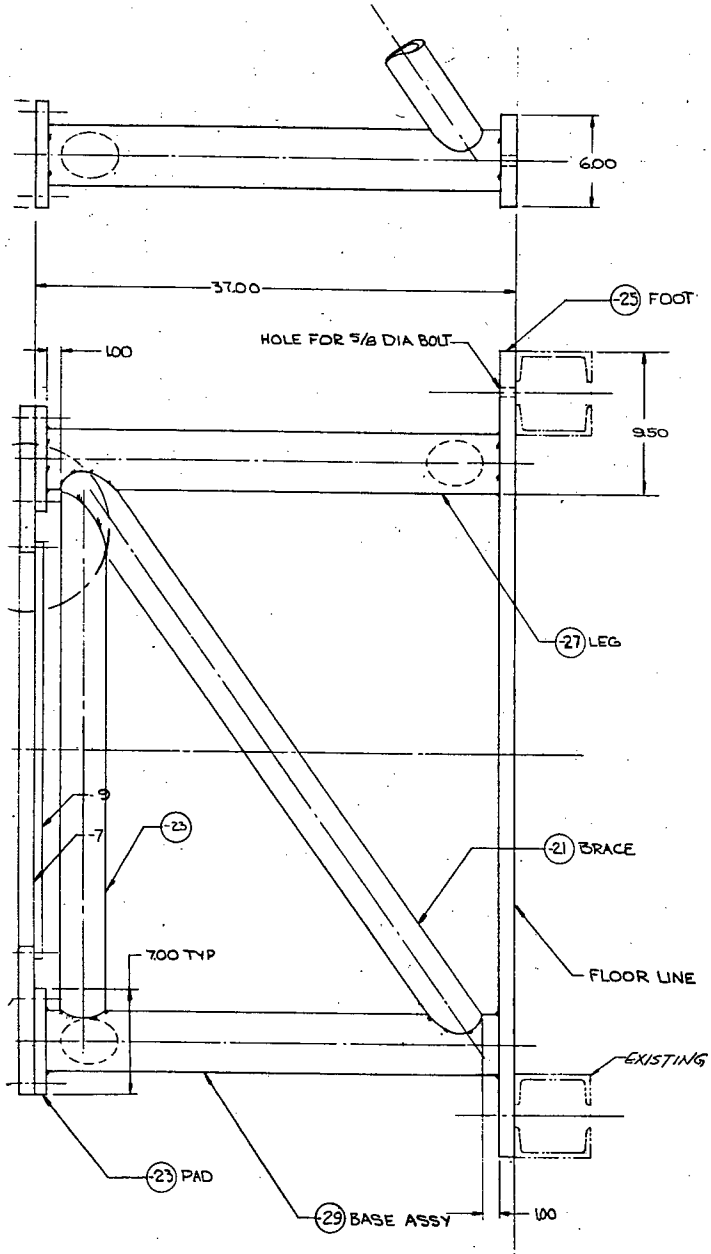




DETAIL = 9 COVER
SCALE ¼




1/4-28 NUT
1/4-28 THREAD
CHAMFER .03 x 45° TYP
BRAZE THIS SIDE ONLY
ASSY
7.00 TYP
NR63-061 ATTACHMENT DETAILS & ASSEMBLY REF.
NR63-044 MOSAIC RADOME ASSY. REF.
-9
-7
-23
7.00 TYP
1/4-20 SHCS (24)
-11 HEAT SHIELD (45.50 SQUARE WITH 30.61 DIA CUTOUT IN CENTER) DRILL 5/16 DIA HOLES 24 PLACES TO MATCH -7
-7 BASE
1/4-28 NUT (2)
-13 STUD ASSY
-15 SUPPORT
AN970-4 WASHERS (2)
30.61 DIA
-17 SUPPORT
.313 REF
1/4-20 x 1.00 SHCS.
AN961-416 WASHER (1)
-9 COVER
VIEW
SCALE 1/1
1/2 DIA HOLES (9) PATTERN TO MATCH PATTERN IN -7.
1/2-13 x 2 1/2 SHCS (16)
1/2-13 NUTS (16)
-23 PAD



DASH NO	PART NAME	
		24 SCREW — 1/2-20 X 1.00 SOC. HD. CAP SC.
		24 SCREW — 1/4-20 X 1.25 SOC. HD CAP SC.
		24 WASHER — AN961-416 OR EQUIV.
		48 WASHER — AN970-4 OR EQUIV.
		1 48 NUT — 1/4-28 HEX. HD. NUT
-29	BASE ASSY	1
-27	LEG	4 — 3 1/2 STD STL PIPE (4.0 O.D. X .226 WALL) X 30 LG
-25	FOOT	2 — 1.0 X 6.0 X .535 HRS
-23	PAD	4 — 3/4 X 7.0 X 10 HRS
-21	BRACE	6 — 2 1/2 STD STL PIPE (2.875 O.D. X .203 WALL) X 47 LG.
-19	STUD	1 — 1/4-28 THREADED STEEL ROD
-17	SUPPORT	.90 X 1.1 X 3.9 KOVAR "A"
-15	SUPPORT	.50 X 1.1 X 3.9 KOVAR "A"
-13	STUD ASSY	48
-11	HEAT SHIELD	3/4 X 45.5 X 45.5 CEMENT ASBESTOS SHEET
-9	COVER	1/2 X 24.7 DIA CEMENT ASBESTOS SHEET
-7	BASE	1 X 45.5 X 45.5 HRS

REQUIREMENTS PER ASSEMBLY — DWG. NO. — -29 -13 NEXT ASSY

MANUFACTURING TOLERANCES ARE UNLESS OTHERWISE NOTED
FRACTIONS ± .031
DECIMALS .XX ± .020, .XXX ± .005
ANGLES ± 1/2 DEG
ALL MACHINED SURFACES & AS NOTED REF. MIL STD

DESIGN — STRESS — PROCESS — TOOLING — CHECK — WEIGHT — APPROVED

HEAT TREAT — FINISH

TITLE
TEST FIXTURE
MOSAIC RADOME

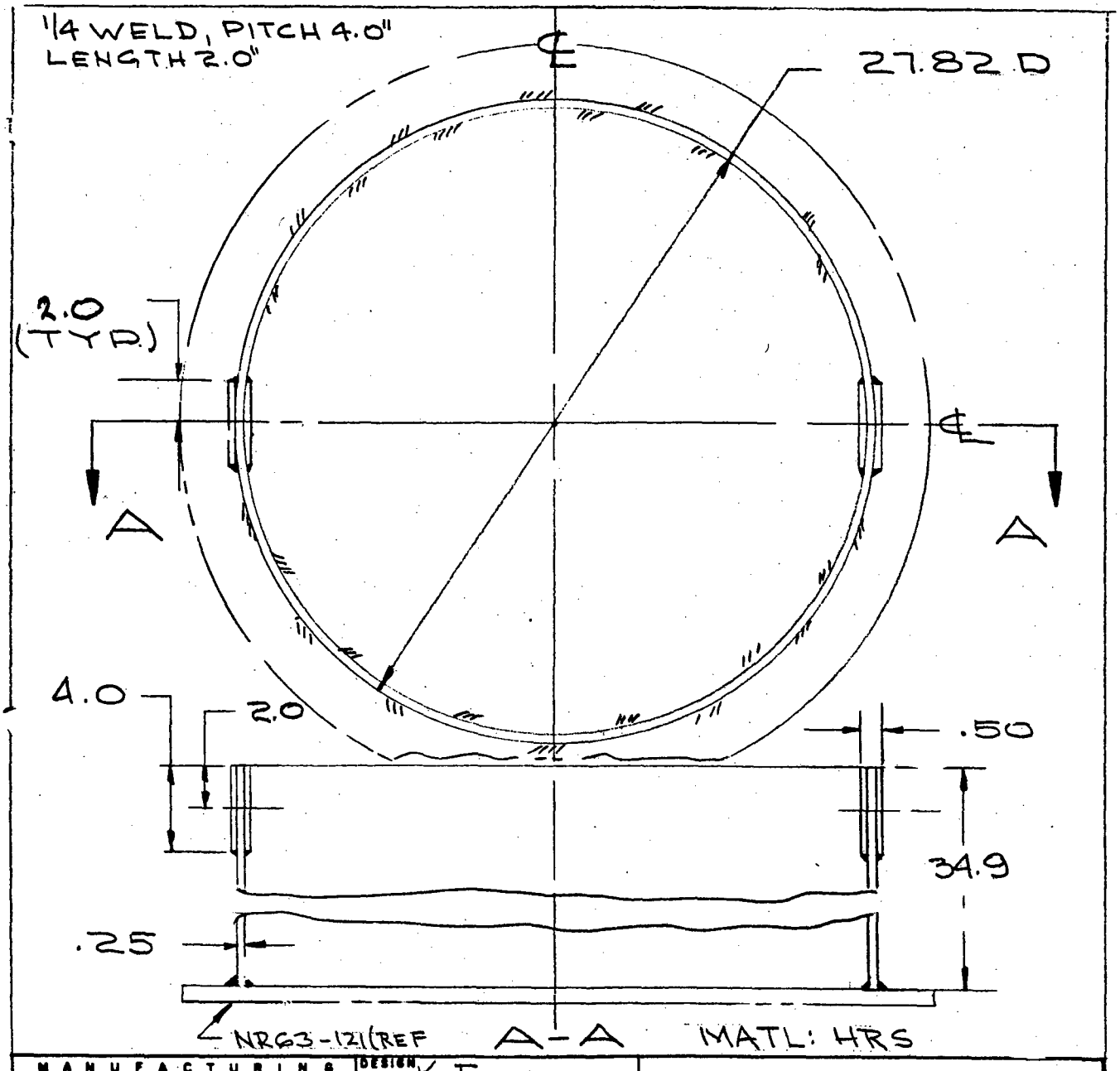
THIS DWG DASH NO — NEXT ASSEMBLY — NO. REQD

NR
NARMCO
RESEARCH & DEVELOPMENT
A DIVISION OF TELEDYNE INDUSTRIES
3540 AERO COURT
SAN DIEGO 23, CALIFORNIA

SCALE FULL & NOTED — M# 398-115

R — DWG NO NR 63-060 — 4/6

SIZE — SHEET 1 OF 1 — ENGINEER LAYOUT



MANUFACTURING TOLERANCES ARE UNLESS OTHERWISE NOTED:
FRACTIONS ± .031
DECIMALS .XX ± .020
.XXX ± .005
ANGLES ± 1/2 DEG.
√ ALL MACHINED SURFACES & AS NOTED REF. NAS 30

HEAT TREAT

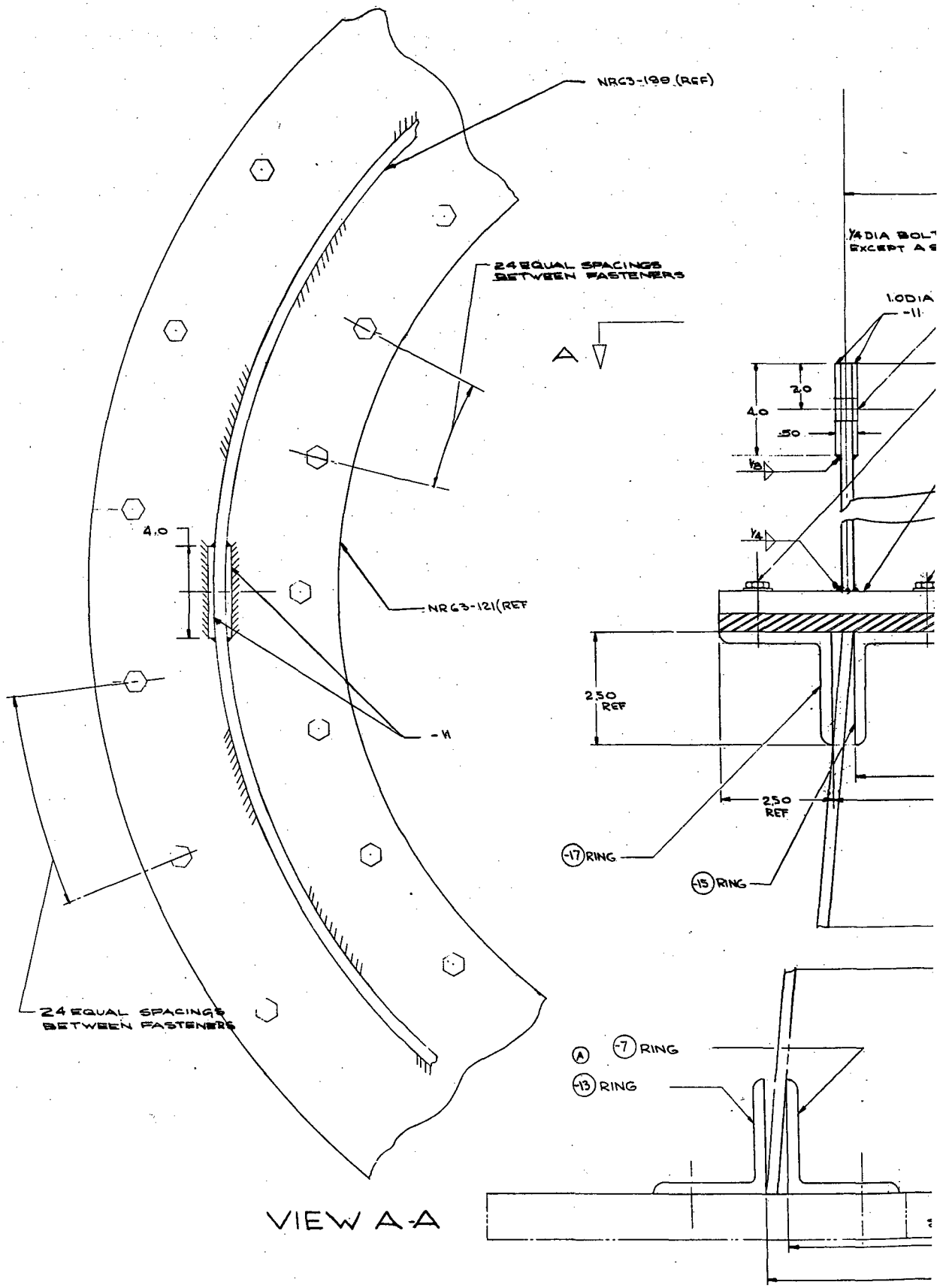
FINISH

DESIGN K. FEHER
STRESS
PROCESS
TOOLING [illegible] 5-18-65
CHECK
WEIGHT
APPROVED [illegible] 5-18-65

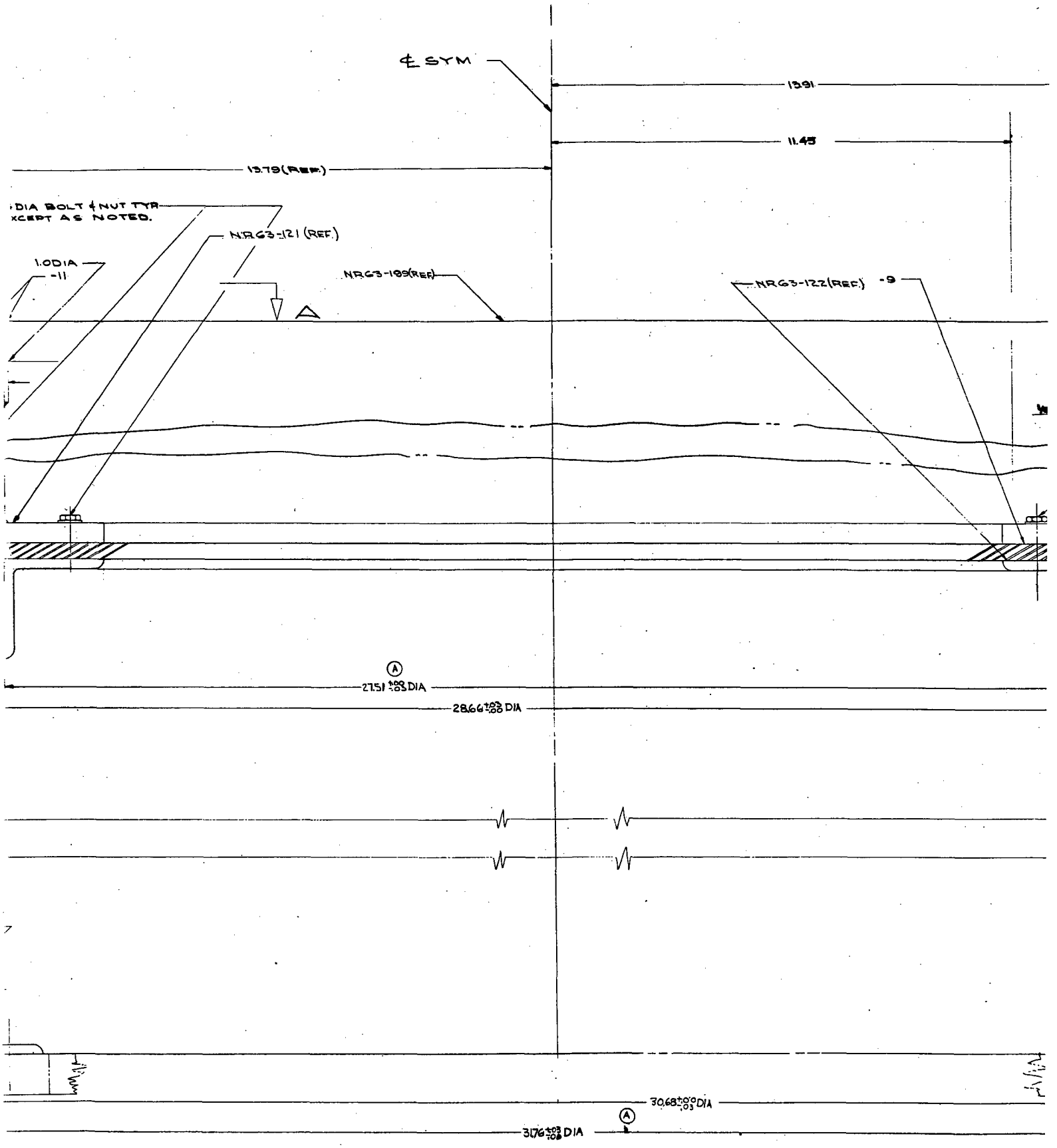
Whittaker CORPORATION
NARMCO
RESEARCH & DEVELOPMENT
DIVISION
•
3540 Aero Court
San Diego, California 92123

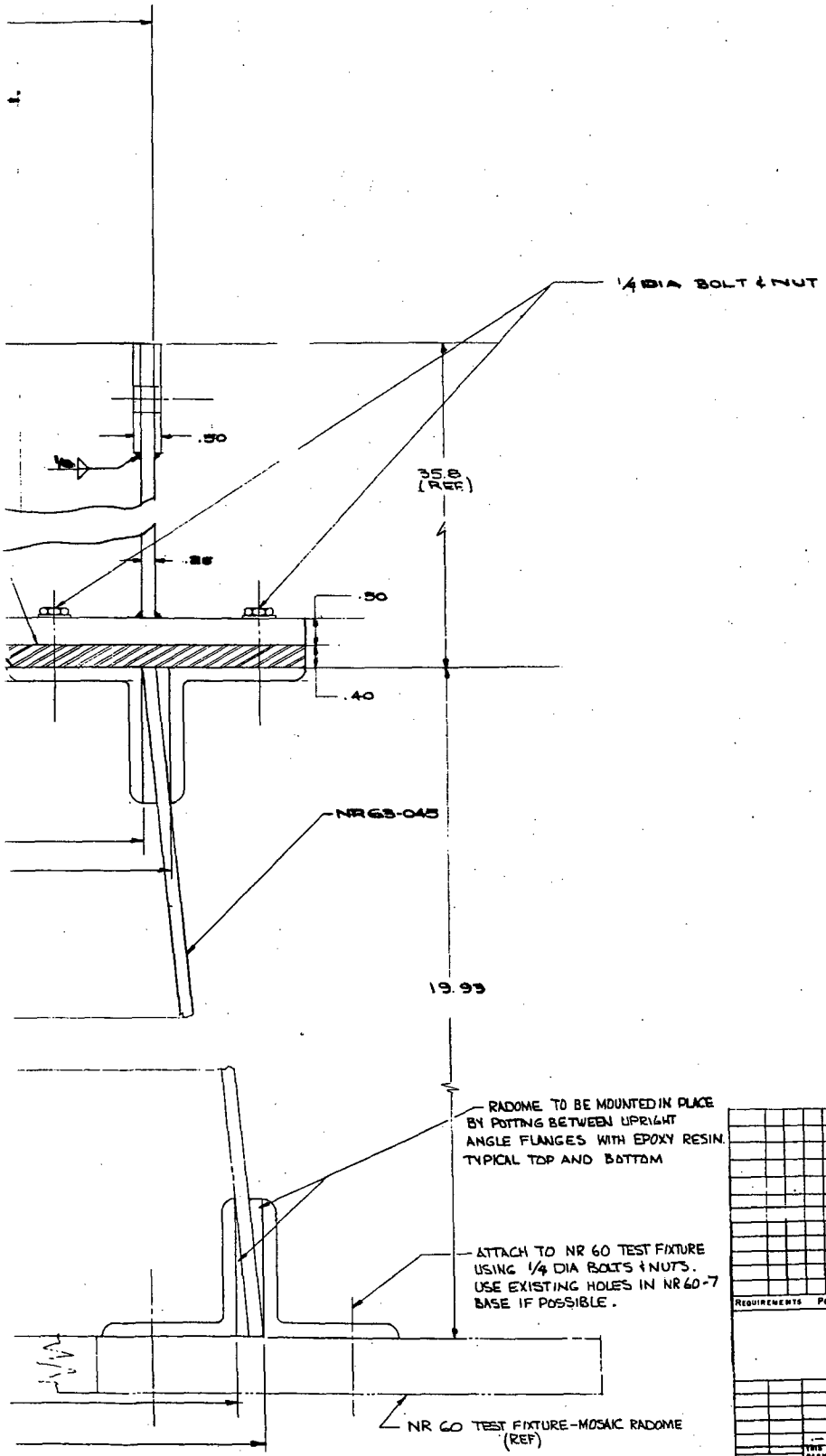
TITLE
LOADING TUBE ASSY
RADOME TEST FIXT.

SCALE NONE
W.O 338-110
DWG. NO. NR63-199
N/R
DWG SIZE
SHEET 1 OF 1
CHANGE LETTER


NRG3-199 (REF)
24 EQUAL SPACINGS BETWEEN FASTENERS
A
4.0
NRG3-121(REF
-11
24 EQUAL SPACINGS BETWEEN FASTENERS
1.0 DIA
-11
2.0
4.0
.50
1/8
1/4
2.50 REF
2.50 REF
-17 RING
-15 RING
A
-7 RING
-13 RING

VIEW A-A


℄ SYM
13.91
11.45
13.79(REF.)
DIA BOLT & NUT TYP
XCEPT AS NOTED.
NRG3-121 (REF.)
1.0DIA
-11
NRG3-199(REF)
NRG3-122(REF.) -9
A
27.51 +.03 -.03 DIA
28.66 +.03 -.03 DIA
30.68 +.00 -.03 DIA
A
31.76 +.03 -.03 DIA



REQUIREMENTS PER ASSEMBLY		DWG. NO.	OPP DASH NO.	SHN	PART NAME
✓	POTTING COMPOUND				EPOXY RESIN
4				-17	RING 1/4 X 2 1/2 x 2 1/2 x 22.6 ALUMINUM STRUCTURAL ANGLE
4				-15	RING 1/8 x 2 1/2 x 2 1/2 x 21.7 ALUMINUM STRUCTURAL ANGLE
1	NR63-190				TUBE
4				-11	DOUBLER STEEL .14 x 4.0 x 4.0
1	NR63-121				PLATE
1				-9	INSERT HARD RUBBER SHEET 65 DUROM
4				-13	RING 1/8 x 2 1/2 x 2 1/2 x 25.0 ALUMINUM STRUCTURAL ANGLE
4				-7	RING 1/4 x 2 1/2 x 2 1/2 x 24.3 ALUMINUM STRUCTURAL ANGLE
-1					

MANUFACTURING TOLERANCES ARE UNLESS OTHERWISE NOTED: FRACTIONS ± .031, DECIMALS .XX ± .020, .XXX ± .005, ANGLES ± 1/2 DEG. ALL MACHINED SURFACES 63 AS NOTED REF MIL STD 10

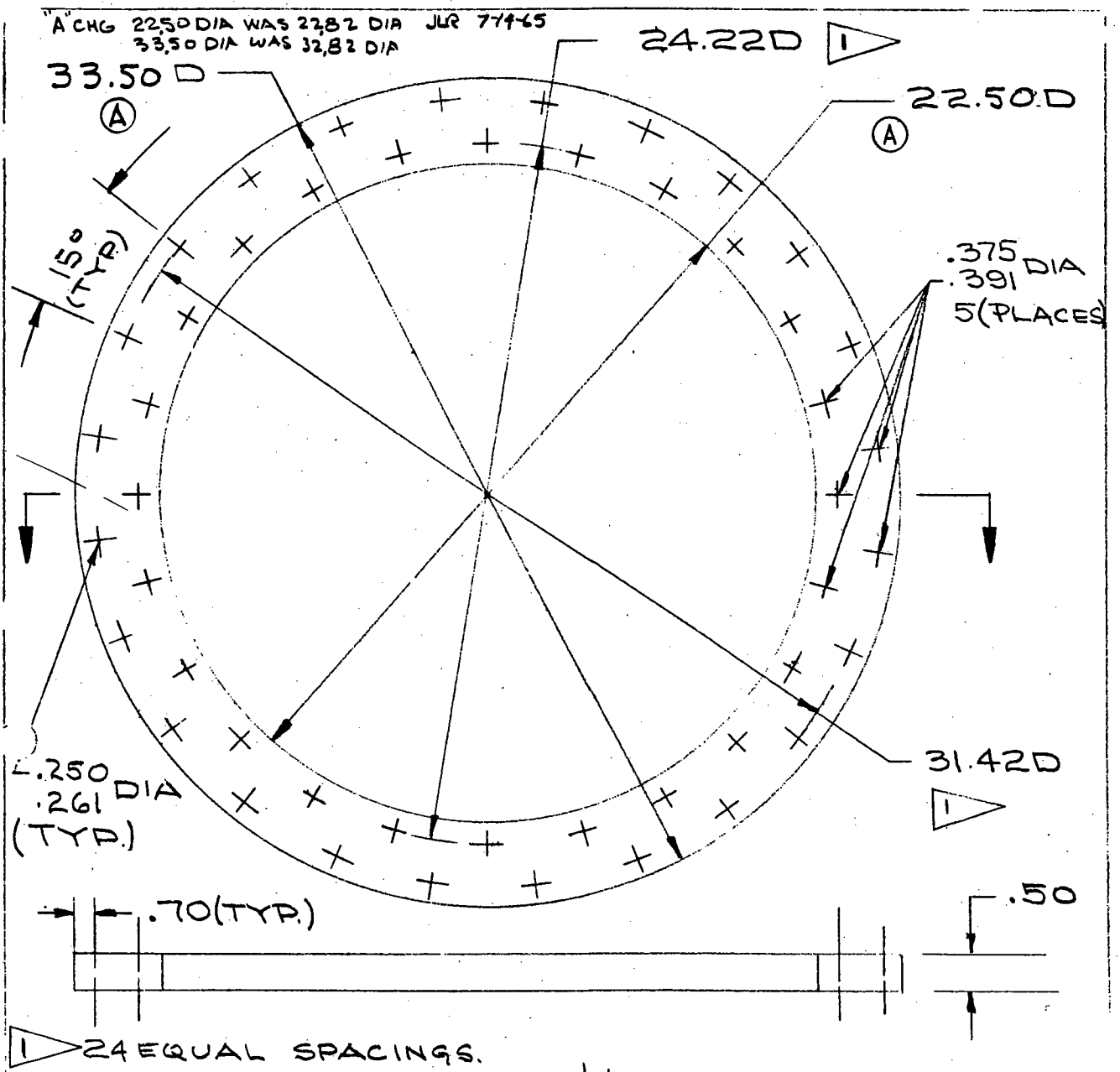
NEXT ASSY | FINISH | TITLE: LOADING FIXTURE MOSAIC RADOME

DESIGN K. Filer 1/9/64 | DRAFTING [illegible] | TRACING [illegible] | CHECK [illegible] | RELEASE [illegible]

Whittaker CORPORATION
NARMCO RESEARCH & DEVELOPMENT DIVISION
3540 Aero Court
San Diego, California 92123

SCALE FULL | MFR'S 538-110 | DWG NO. NR63-120 | REV B | SIZE D | SHEET 1 OF 1

THIS DWG. DASH NO.	NEXT ASSEMBLY	No. REQD.
-1	NR63-185	1

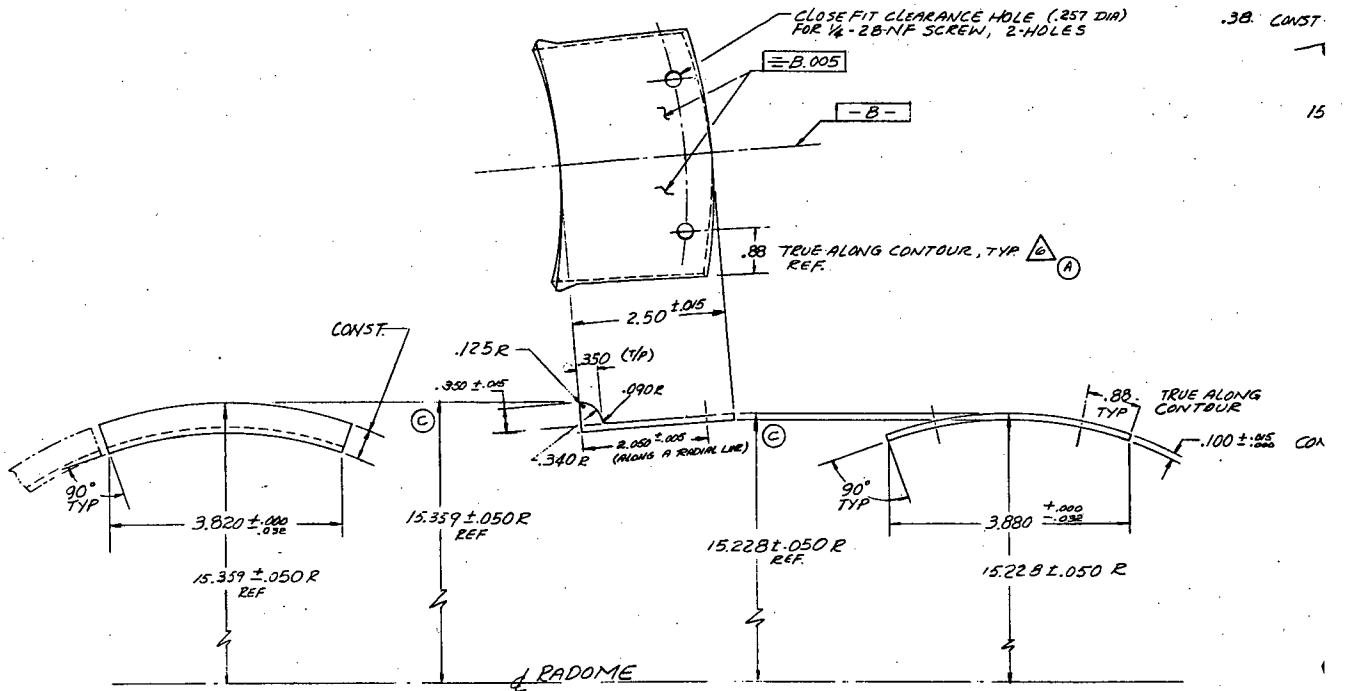


MANUFACTURING TOLERANCES ARE UNLESS OTHERWISE NOTED: FRACTIONS ± .031; DECIMALS .XX ± .020, .XXX ± .005; ANGLES ± 1/2 DEG. ALL MACHINED SURFACES & AS NOTED REF. NAS 30	DESIGN K. FEHER 11/9/64
	STRESS
	PROCESS
	TOOLING M. La Fuf 5-18-65
	CHECK
	WEIGHT
	APPROVED W.M. Jones 5-18-65
HEAT TREAT	
FINISH	

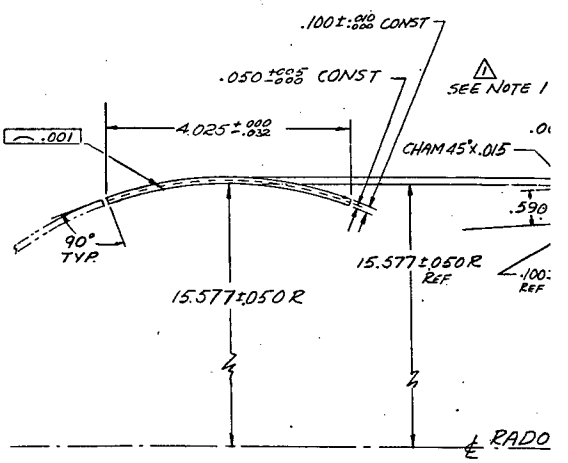
Whittaker CORPORATION
NARMCO
RESEARCH & DEVELOPMENT
DIVISION
3540 Aero Court
San Diego, California 92123

TITLE
SUPPORT PLATE-RADOME LOADING FIXT.

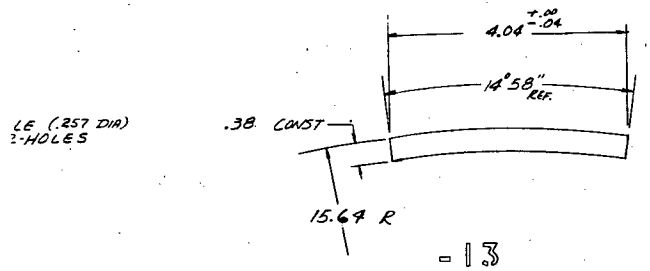
SCALE NONE	W.O 338-110	
DWG. NO. NR63-121		A
DWG SIZE	SHEET 1 OF 1	CHANGE LETTER



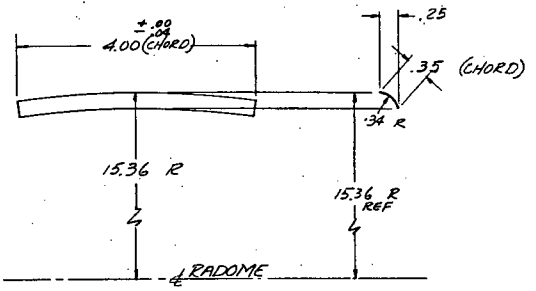
- 7 MAT'L - STAINLESS ST'L, TYPE 17-7PH



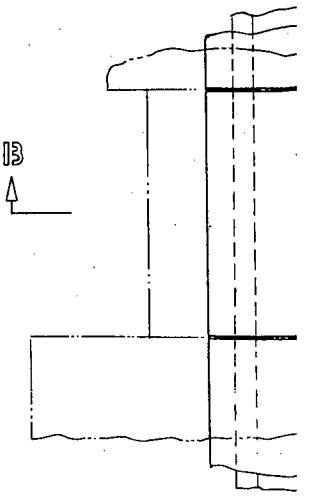
- 9 MAT'L

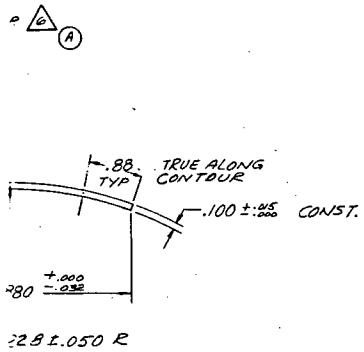


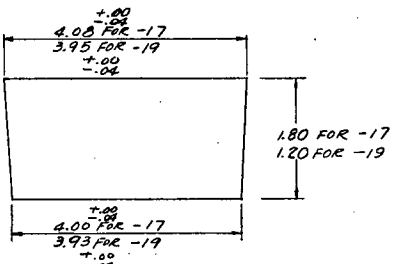
-13



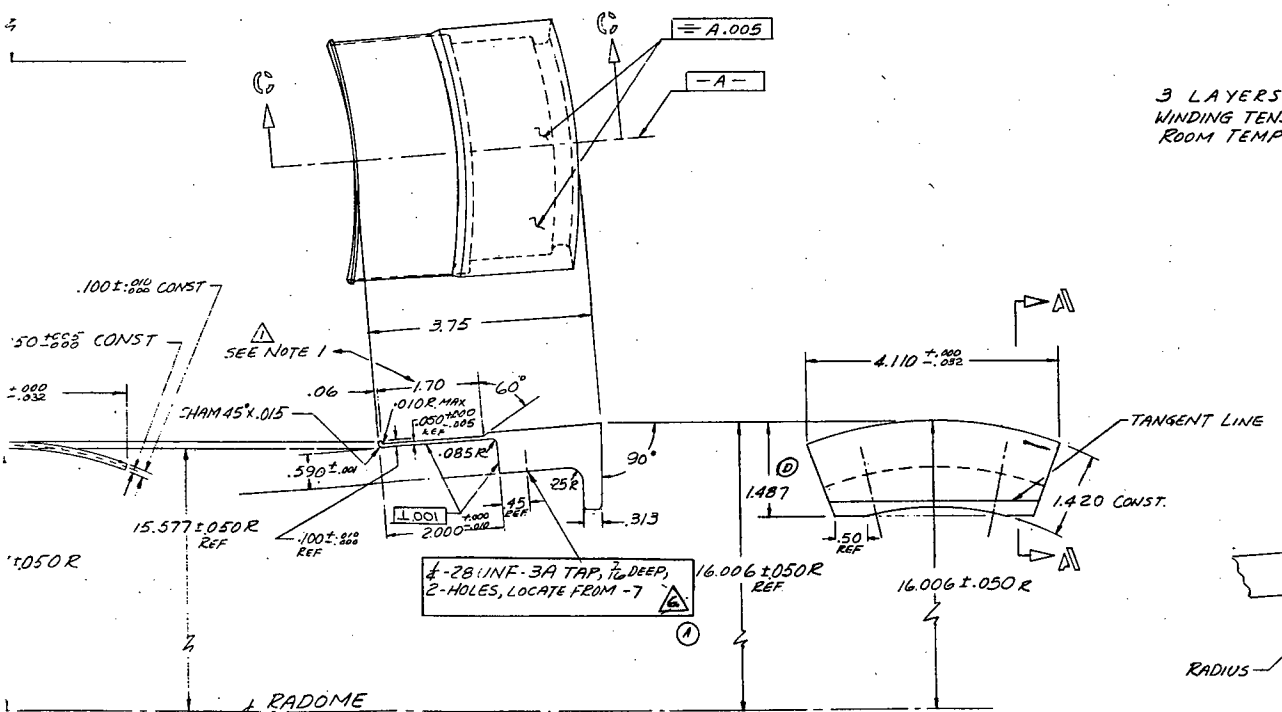
-15





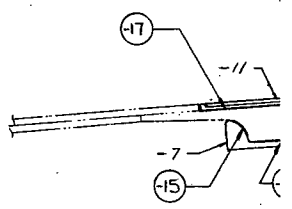


-17 & -19

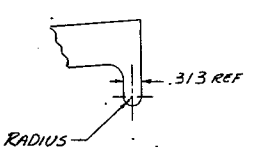


SECTION C - C

3 LAYERS, .020 DIA KOVAR WIRE. WINDING TENSION TO BE 4 LBS. AT AMBIENT ROOM TEMP.



SECTION

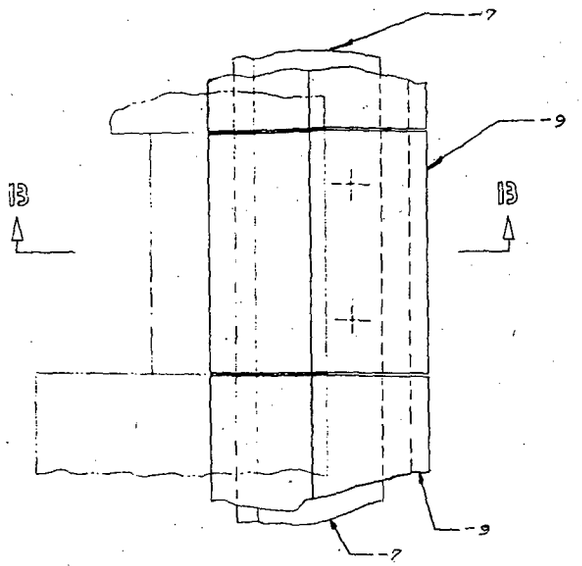


SECTION A - A

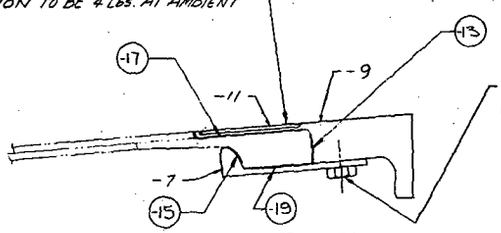
- 9 MAT'L - KOVAR

REV.	REVISION	BY	
A	ADDED NOTE 7 - FINISHED FLUSH ADDED DELTAS TO NOTES 1 ON E/O		
B	REMOVE NOTE 7, GENERAL FINISH TO BE 125 M IN	JLR	
C	DIM. ARROWS EXTENDED B/M, 16-4PH WAS 17-7PH	JY	
D.	DIM 1.487 WAS 1401	JY	

(CHORD)



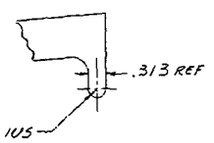
4 YERS, .020 DIA KOVAR WIRE.
IG TENSION TO BE 4 Lbs. AT AMBIENT
TEMP.



SECTION 13 = 13

AN4CH-4 BOLT
(70 - 80 16-INCH WRENCHING TORQUE)

LINE



SECTION A = A

Ref Dwg:

NR63-060 TEST FIXTURE - MOSAIC RADOME.
NR63-044 MOSAIC RADOME ASSY.

NOTES

(A) 6. -7 & -9 MATING PARTS TO BE MATCH DRILLED AND IDENTIFIED

5. PARTS MADE FROM ANNEALED COPPER MUST BE FREE FROM BURRS AND EDGE DEFECTS

(A) 4. PARTS MUST BE IN FULL ANNEALED CONDITION PRIOR TO USE

3. KOVAR "A" (29% NICKEL, 17% COBALT, 54% IRON) MAYBE PURCHASED FROM THE CARBORUNDUM CO. REFRACTORIES DIV., LATROBE PA.

(A) 1. SURFACE ROUGHNESS 40-50 MICRO INCHES, CHEM. MILL FINISH WILL BE ACCEPTABLE AT THIS AREA ONLY.

DASH NO.	PART NAME
	AN4CH-4 BOLT
-9	SHIM .005 THICK ANNEALED COPPER SHEET PER QQ-C-576A
-12	SHIM
-16	SHIM
-13	SHIM .005 THICK ANNEALED COPPER SHEET PER QQ-C-576A
-11	.020 DIA KOVAR A WIRE (APPROX 2200 FT. LG., 3 LAYERS)
-9	OUTER SEGMENT. KOVAR "A"
-7	INNER SEGMENT CRES, TYPE 14-4 PH, MIL-S-25043A

DRAWN 7-25-64
CHECKED G-5-64
ENGR
TRACED
STRESS
WEIGHT
APPROVED
MFG. ENG.

NARMCO
RESEARCH & DEVELOPMENT
SAN DIEGO 37, CALIFORNIA

TITLE: ATTACHMENT DETAILS & ASSEMBLY - MOSAIC RADOME BASE

SCALE: FULL
DWG NO: NR63-061
SIZE: R
SHEET 1 OF 1
REV: C

Distribution List

Contract No. AF 33(657)-10111

Project No. 7-984

Chief
Technical Library
Office of Assistant Secretary of
Defense (R&D)
Room 3E 1065, The Pentagon
Washington 25, D.C.

Commander
Air Force Office of Scientific Research
Washington 25, D.C.
Attn: SREC

Defense Documentation Center (DDC)
for Scientific and Technical Information
Cameron Station
Alexandria, Virginia 22314

AFML (MAG)
Air Force Systems Command
United States Air Force
Wright-Patterson AFB, Ohio

AFML (MAAM)
Air Force Systems Command
United States Air Force
Wright-Patterson AFB, Ohio
Attn: Library

AFML (MATC)(6 copies)
Air Force Systems Command
United States Air Force
Wright-Patterson AFB, Ohio
Attn: Lt. L. E. Stamets

AFML (MAA)(2 copies)
Air Force Systems Command
United States Air Force
Wright-Patterson AFB, Ohio

SEG (SEDCM)
Air Force Systems Command
United States Air Force
Wright-Patterson AFB, Ohio

AFML (MAAE)
Air Force Systems Command
United States Air Force
Wright-Patterson AFB, Ohio

AFAL (AVWE)
Air Force Systems Command
United States Air Force
Wright-Patterson AFB, Ohio
Attn: Mr. Richard Ireland

AFML (MAMC)
Air Force Systems Command
United States Air Force
Wright-Patterson AFB, Ohio

AFML (MAAM)
Air Force Systems Command
United States Air Force
Wright-Patterson AFB, Ohio
Attn: Mr. S. W. Bradstreet

SEG (SEPIE)
Air Force Systems Command
United States Air Force
Wright-Patterson AFB, Ohio

SEG (SEPIR)
Air Force Systems Command
United States Air Force
Wright-Patterson AFB, Ohio

Air University Library
Maxwell AFB, Alabama

AFML (MANC)
Air Force Systems Command
United States Air Force
Wright-Patterson AFB, Ohio

Hq USAF (AFXSAI)
Air Battle Analysis Center
Deputy Director of Plans for War Plans
Directorate of Plans, DCS/P&O
Washington, D.C. 20330

Commanding Officer
US Army Signal Research & Development Laboratory
Fort Monmouth, New Jersey
Attn: Technical Documents Center

Commanding General
Redstone Arsenal
Redstone Arsenal, Alabama
Attn: Technical Library — EC

US Navy
PID-23
17th and Constitution Ave.
Washington, D.C. 20360

Chief
Bureau of Naval Weapons
Washington 25, D.C.
Attn: RAV-321

Chief
Bureau of Naval Weapons
Washington 25, D.C.
Attn: RRMA-31

Chief
Bureau of Ships
Department of the Navy
Washington 25, D.C.
Attn: Code 816-E

Naval Air Engineering Center
Aeronautical Materials Laboratory
Johnsville, Pa.
Attn: M-63-NDR

AFCRL
Air Force Cambridge Research Center
L.G. Hanscom Field
Bedford, Mass.
Attn: Documents Unit, CROOTR-2

AF Development Field Representative
Naval Research Laboratory
Washington 25, D.C.
Attn: Code 1072

Materials Advisory Board
2101 Constitution Avenue
Washington 25, D.C.
Attn: Dr. Jos. Lane

FTD (TDEWP)
Air Force Systems Command
United States Air Force
Wright-Patterson AFB, Ohio

United States Dept. of Interior
Bureau of Mines
College Park, Maryland
Attn: K. M. Smith

A. C. Spark Plug Division
P.O. Box 1002
Flint, Michigan
Attn: Department 32-12

American Lava Corporation
Cherokee Blvd. & Mfg. Road
Chattanooga 5, Tennessee
Attn: Mr. C. V. Tuber

Applied Physics Laboratory
The Johns Hopkins University
Silver Spring, Maryland
Attn: R. O. Robinson

IIT Research Institute
Armour Research Foundation
Technology Center
Metals and Ceramic Research
Chicago 16, Illinois

Bell Aerospace Corporation
Division of Bell Aerospace Corp.
P.O. Box 1
Buffalo 5, New York

The Boeing Company
Aero-Space Division
P.O. Box 3707
Seattle 24, Washington
Attn: Mr. W. M. Sterry
(Interplant Box 28-81)

The Boeing Company
Aero-Space Division
P.O. Box 3707
Seattle 24, Washington
Attn: T. L. Norin
(Antennas & Radomes
Group 2-5463)

The Carborundum Company
Buffalo Avenue
Niagra Falls, New York
Attn: Library 1-2

Coors Porcelain Company
600 9th Street
Golden, Colorado

Corning Glass Works
Corning, New York
Attn: Radome Department

Emerson & Cuming, Inc.
Canton, Mass.
Attn: Eino J. Luoma

Fairchild Stratos Corporation
Missile Division
Hagerstown, Maryland
Attn: Engineering Library

Frenchtown Porcelain Co.
Laboratory-Luks
8th & Harrison Streets
Frenchtown, New Jersey

General Applied Science
Laboratories, Inc.
Merrick and Stewart Avenue
Westbury, L.I., New York
Attn: Library

Georgia Institute of Technology
Atlanta, Georgia
Attn: J. D. Walton
High-Temperature Materials
Branch, Engineering Experiment
Station

Grumman Aircraft Engineering Corporation
Bethpage, L.I., New York
Attn: John Conover
Manufacturing Engineering

Lockheed California Co.
Burbank, California
Attn: E. A. Green
Department 72-25, Building 63-3
Plant A-1

Lockheed Missiles & Space Co.
P.O. Box 504
Sunnyvale, California
Attn: W. A. Kozumplik
Technical Information Center
50-14-Building 201

Martin Company
Aerospace-Baltimore Division
Science-Technology Library, Mail 398
Middle River
Baltimore 3, Maryland

Martin Company
AUTAC, Research Library, A-52
Box 179
Denver 1, Colorado

Melpar Inc.
Fall Church, Virginia
Attn: Dr. J. L. Pentecost

North American Aviation, Inc.
International Airport
Los Angeles 45, California
Attn: Structural Sciences Dept. 282

Northrop Aircraft, Inc.
1001 E. Broadway
Hawthorne, California
Attn: R. R. Nolan, Vice President
Manufacturing

Norton Company
New Bond Street
Worcester 6, Mass.
Attn: Dr. L. Trostel, Jr.

Ohio State University
Columbus 16, Ohio
Attn: Director Antenna Lab.

Mr. Samuel S. Oleesky
9004 Larke Ellen Circle
Los Angeles 35, California

Republic Aviation Corp.
Farmingdale, L.I., New York
Attn: Salvatore Fucci

Republic Aviation Corporation
Farmingdale L.I., New York
Attn: Adolph Kastelowitz, Director
Manufacturing Research

Rutgers, The State University
New Brunswick, New Jersey
Attn: Edward J. Smoke, School
of Ceramics

Shenango China Inc.
New Castle, Pa.
Attn: R. L. Gibson

Stanford Research Institute
Menlo Park, California

US Stoneware Co.
P.O. Box 119
Orville, Ohio
Attn: Alite Division
Engineering Department

Aerospace Industries Association
of America
1725 De Sales Street, N.W.
Washington 6, D.C.
Attn: Mr. S. D. Daniels, Director
of Technical Services

Cornell Aeronautical Laboratory
4455 Genesee Street
Buffalo 21, New York
Attn: H. P. Keichner, Staff
Scientest

Minnesota Mining and Manufacturing Co.
53 Park Avenue
Dayton 19, Ohio
Attn: Robert H. Lamb

Hughes Aircraft Co.
Materials Technology Department
Aerospace Group
Culver City, California

Avco Corporation
Research & Development Division
Metals & Ceramics Research – R-220
Wilmington, Mass.

Liden Laboratories, Inc.
P.O. Box 302
State College, Pa.
Attn: H. P. Kirchner

General Dynamics/Pomona
Pomona, California
Attn: R. L. Hallse
Staff Scientist
Mail Zone 6-76

H. I. Thompson Fiberglass Company
1600 West 135th Street
Gardena, California
Attn: Materials Research Division

Western Gold and Platinum Co.
525 Harbor Blvd.
Belmont, California
Attn: P. W. Smith

Astro-Met Associates Inc.
500 Glendale-Milford Road
Cincinnati 15, Ohio

Scientific & Technical Information Facility
P.O. Box 5700
Bethesda, Maryland 20014
Attn: NASA Representative (2 copies)
(SAK/DL)

Eitel-McCullough, Inc.
San Carlos, California
Attn: Dr. L. Reed

LTV Vought Aeronautics
Dallas, Texas
Attn: W. L. Aves Jr. (2-53431)
Engineering Structures Materials
Applied R&D

Defense Metals Information Center
Battelle Memorial Institute
505 King Avenue
Columbus 1, Ohio

North American Aviation
2000 North Memorial Drive
Department 990
Tulsa, Oklahoma

Northrop Norair
3901 West Broadway
Hawthorne, California 90250
Attn: Technical Information Unit

Fred Baur
Engelhard Industries
113 Astor Street
Newark 14, New Jersey

Unclassified
Security Classification

DOCUMENT CONTROL DATA - R&D

(Security classification of title, body of abstract and indexing annotation must be entered when the overall report is classified)

1. ORIGINATING ACTIVITY (Corporate author)	2a. REPORT SECURITY CLASSIFICATION
Whittaker Corporation Narmco Research & Development Division 3540 Aero Court, San Diego, California 92123	Unclassified
	2b GROUP N/A

3 REPORT TITLE

COMPOSITE CERAMIC RADOME MANUFACTURE BY MOSAIC TECHNIQUES

4. DESCRIPTIVE NOTES *(Type of report and inclusive dates)*

Final Technical Report (1 November 1962 to 5 January 1966)

5. AUTHOR(S) *(Last name, first name, initial)*

Jones, Rodney A.
Barr, Francis A.

6. REPORT DATE	7a. TOTAL NO. OF PAGES	7b. NO. OF REFS
December 1965	484	--

8a. CONTRACT OR GRANT NO.	9a. ORIGINATOR'S REPORT NUMBER(S)
Contract AF 33(657)10111 b. PROJECT NO. MMP Project No. 7-984 c. d.	AFML TR-65-418 9b. OTHER REPORT NO(S) *(Any other numbers that may be assigned this report)*

10. AVAILABILITY/LIMITATION NOTICES

This document is subject to special export controls and each transmittal to foreign governments or to foreign nationals may be made only with prior approval of the Manufacturing Technology Division.

11. SUPPLEMENTARY NOTES	12. SPONSORING MILITARY ACTIVITY
Report on fabrication of large ceramic radomes by mosaic techniques	Air Force Materials Laboratory Research and Technology Division Wright-Patterson AFB, Ohio

13. ABSTRACT

A comprehensive research and development program directed toward the fabrication of large ceramic radomes for operation at 1000°F or above, by ceramic adhesive bonding together of preformed ceramic tile segments, is described. On the basis of state-of-the-art review plus extensive materials selection studies, 99.0% high-density alumina was selected as the radome body material and a magnesium aluminosilicate glass forming composition with a fusion temperature of about 2150°F was selected as the ceramic adhesive. Engineering design, structural investigations, and manufacturing considerations led to the choice of a double layer of staggered, overlapping, trapezoidal tiles for the radome wall construction. The 0.0221 in. thick mosaic tile wall was capped with a monolithic alumina nose cap to form the ogive radome of about 31-in. diameter at the base and of 8-ft height. Fabrication techniques involving use of a differential thermal expansion firing tool concept are described, with details on fused-silica tooling, fabrication, and use. The mosaic full-size radome and radome sections were fabricated and subjected to thermal and structural testing. Test results are correlated with previous detailed thermal and structural analyses. Results show that fabrication of large, high-strength ceramic structures by adhesive bonding mosaic techniques is feasible and provides a means of circumventing some of the serious limitations of conventional ceramic fabrication procedures for large structures. The test results also show that the analytical and design techniques which were developed can be used with reasonable confidence in the design of such composite ceramic structures.

DD FORM 1 JAN 64 1473

Unclassified
Security Classification

14. KEY WORDS	LINK A		LINK B		LINK C	
	ROLE	WT	ROLE	WT	ROLE	WT
Mosaic Radome Ceramic Adhesive Bonding Ceramic or High-Temperature Tooling High-Temperature Parting Agents Radome Thermal Analysis Radome Stress Analysis						

INSTRUCTIONS

1. ORIGINATING ACTIVITY: Enter the name and address of the contractor, subcontractor, grantee, Department of Defense activity or other organization *(corporate author)* issuing the report.

2*a*. REPORT SECURITY CLASSIFICATION: Enter the overall security classification of the report. Indicate whether "Restricted Data" is included. Marking is to be in accordance with appropriate security regulations.

2*b*. GROUP: Automatic downgrading is specified in DoD Directive 5200.10 and Armed Forces Industrial Manual. Enter the group number. Also, when applicable, show that optional markings have been used for Group 3 and Group 4 as authorized.

3. REPORT TITLE: Enter the complete report title in all capital letters. Titles in all cases should be unclassified. If a meaningful title cannot be selected without classification, show title classification in all capitals in parenthesis immediately following the title.

4. DESCRIPTIVE NOTES: If appropriate, enter the type of report, e.g., interim, progress, summary, annual, or final. Give the inclusive dates when a specific reporting period is covered.

5. AUTHOR(S): Enter the name(s) of author(s) as shown on or in the report. Enter last name, first name, middle initial. If military, show rank and branch of service. The name of the principal author is an absolute minimum requirement.

6. REPORT DATE: Enter the date of the report as day, month, year; or month, year. If more than one date appears on the report, use date of publication.

7*a*. TOTAL NUMBER OF PAGES: The total page count should follow normal pagination procedures, i.e., enter the number of pages containing information.

7*b*. NUMBER OF REFERENCES: Enter the total number of references cited in the report.

8*a*. CONTRACT OR GRANT NUMBER: If appropriate, enter the applicable number of the contract or grant under which the report was written.

8*b*, 8*c*, & 8*d*. PROJECT NUMBER: Enter the appropriate military department identification, such as project number, subproject number, system numbers, task number, etc.

9*a*. ORIGINATOR'S REPORT NUMBER(S): Enter the official report number by which the document will be identified and controlled by the originating activity. This number must be unique to this report.

9*b*. OTHER REPORT NUMBER(S): If the report has been assigned any other report numbers *(either by the originator or by the sponsor)*, also enter this number(s).

10. AVAILABILITY/LIMITATION NOTICES: Enter any limitations on further dissemination of the report, other than those imposed by security classification, using standard statements such as:

(1) "Qualified requesters may obtain copies of this report from DDC."

(2) "Foreign announcement and dissemination of this report by DDC is not authorized."

(3) "U. S. Government agencies may obtain copies of this report directly from DDC. Other qualified DDC users shall request through _____."

(4) "U. S. military agencies may obtain copies of this report directly from DDC. Other qualified users shall request through _____."

(5) "All distribution of this report is controlled. Qualified DDC users shall request through _____."

If the report has been furnished to the Office of Technical Services, Department of Commerce, for sale to the public, indicate this fact and enter the price, if known.

11. SUPPLEMENTARY NOTES: Use for additional explanatory notes.

12. SPONSORING MILITARY ACTIVITY: Enter the name of the departmental project office or laboratory sponsoring *(paying for)* the research and development. Include address.

13. ABSTRACT: Enter an abstract giving a brief and factual summary of the document indicative of the report, even though it may also appear elsewhere in the body of the technical report. If additional space is required, a continuation sheet shall be attached.

It is highly desirable that the abstract of classified reports be unclassified. Each paragraph of the abstract shall end with an indication of the military security classification of the information in the paragraph, represented as *(TS)*, *(S)*, *(C)*, or *(U)*.

There is no limitation on the length of the abstract. However, the suggested length is from 150 to 225 words.

14. KEY WORDS: Key words are technically meaningful terms or short phrases that characterize a report and may be used as index entries for cataloging the report. Key words must be selected so that no security classification is required. Identifiers, such as equipment model designation, trade name, military project code name, geographic location, may be used as key words but will be followed by an indication of technical context. The assignment of links, rules, and weights is optional.